Geological and geochemical anatomy of Archaean gneisses from the Vestfold Hills and Rauer Group, East Antarctica

Ian Snape

Thesis submitted for Doctor of Philosophy

University of Edinburgh

1997

Declaration

I declare that the work and results presented in this thesis are my own, except where otherwise acknowledged. This thesis has not been submitted for any other qualification at any other university.

ABSTRACT

Archaean orthogneisses in the Rauer Group and Vestfold Hills have been examined through a combined field, petrological, geochemical and isotopic study in order to document and evaluate regional terrane correlations in the East Prydz Bay region of East Antarctica, and assess models for early Precambrian crustal growth, both regionally and in general terms.

Within the Archaean domain in the Rauer Group, two layered ultramafic-mafic associations, the Torkler-Tango and the Scherbinina Layered Complexes (TTLC & SLC), are hosted in *ca.* 2800 to 3300-3470 Ma Composite Layered Orthogneiss (CLO). The SLC and TTLC are spatially, compositionally and probably temporally separate metaigneous suites. The TTLC is older than *ca.* 2800 Ma CLO intrusive sheets, and geochemical similarities between the TTLC and *ca.* 3300 Ma tonalite-trondhjemite-granite components of the CLO imply that there may be a genetic link between these gneiss units, as both have distinctive arc-like geochemical signatures. The SLC is also cross-cut by *ca.* 2800 Ma CLO components, but SHRIMP U-Pb zircon dating of the complex reveals that it is only marginally older with a crystallization age of 2844 ± 6 Ma. Geochemically, the SLC has very weak arc-like signatures which are attributed to small amounts of crustal contamination (by CLO), and primary geochemical signatures are inferred to have been derived from an E-MORB-like source. A tectonomagmatic setting similar to that deduced for the early Tertiary East Greenland Margin is envisaged as a possible analogue for events at 2844 Ma in the Rauer Group. However, petrogenetic models for the Rauer Group Archaean domain are tentative, because Sr and Nd isotopes indicate that significant open-system behaviour occurred during fluid infiltration associated with a regionally recognised Pan-African (*ca.* 500 Ma) event.

Detailed mapping of intrusive relations that are preserved in Archaean orthogneisses in the Vestfold Hills has allowed a reconstruction of the early high-grade geological history of the terrane. A number of spatially, temporally and compositionally distinct intrusions were emplaced throughout the Crooked Lake magmatic episode between D_1-M_1 and D_2-M_2. The duration of this episode has been precisely defined by SHRIMP U-Pb dating of axial planar leucosomes to 2496.3 ± 0.7 Ma (D_1-M_1) and 2475.3 ± 0.7 Ma (D_2-M_2). The distribution of Crooked Lake Gneiss (CLG) indicates that regional-scale tectonic repetition of major units was local rather than regional, and the amount of strain associated with the main folding and fabric producing event (D_2) is heterogeneous. Geological relationships preserved in low-strain windows show that a previously defined gneiss unit, the Tryne Metavolcanics, is a tectonic intercalation of lithologies rather than a volcanic succession. Low-strain domains also allow recognition of a detailed magmatic event sequence and identification of a

number of relatively undeformed CLG plutons. One of these plutons has two statistically defined zircon age populations; the youngest of these ages (2485.0 ± 1.6 Ma) is interpreted to be the crystallization age of the pluton, whilst the older age (2491.0 ± 1.6 Ma) is considered to reflect inheritance of marginally older CLG protoliths. Although petrogenetic modelling is problematic in the metamorphosed intrusive Vestfold Hills lithologies, the majority of the *ca.* 2500 Ma orthogneisses are interpreted to be subduction-related plutons that formed at the base of a continental volcanic-arc. Unlike the adjacent Rauer Group, correlated Rb/Sr-isotopic relationships and a limited spread of ε_{Nd} imply that significant fluid infiltration and isotopic perturbation associated with the Pan-African event were not important in the evolution of this terrane.

Geological event sequences determined for the Vestfold Hills and Rauer Group differ markedly, and these terranes are considered to have been separate entities at the end of the Archaean. From the available geological and geochemical data, there are no reliable constraints on the timing of terrane juxtaposition, although late amalgamation, possibly at 1000 or 500 Ma, is favoured.

Acknowledgements

A big thanks to my supervisor Simon Harley for help, encouragement, and enthusiasm throughout. Simon has also been excellent company throughout the project, both in Antarctica and Edinburgh. What's more, he cooks a mean freeze-dried chilli con carnage and actually enjoyed Big Sister plum pudding at 2.00 am during a late night sniper polar feeding frenzy. My only complaint is that I have never had anything to complain about!

Thanks also to:

Godfrey Fitton, my second supervisor, for help with XRF and numerous discussions regarding the geochemical and isotopic aspects of this study. Also for taking the trouble to explain to me a few of the mysteries of the hyphen. I still don't grasp the subtleties of the composite adjective versus joining an adverb to an adjective, but now I do at least understand the difference between woolly-mammoth turds and woolly mammoth-turds.

NERC and the Australian Antarctic Division, for generously funding this project. A special thank you to Julian Baldry at NERC for his help with conference and field support, and for granting me three extensions to allow me to go to Baffin and undertake commercial work.

All the staff and expeditioners at the Australian National Antarctic Research Expeditions (ANARE), especially, my fieldie Dave Wyatt, and the Davis Station Chefs, Selwyn and Matt. Also, Vicky, Kirkus and Greenhouse Gasses for putting up with me in Tassie; and finally Damian Gore for lending me the Baird, letting me crash at his field camp, feeding me and for sending me several hundred dirt samples to analyse for him.

At AGSO/ANU/Curtin, Pete Kinny, Lance Black, John Sheraton and Bob Tingey are all thanked for helpful discussions. Bob also lent me all his airphotos for my mapping and Lance very kindly gave me tour of Canberra, shrimped zircons for me, and gave a highly proficient account of the data.

In the department, there are almost too many people to thank and a great many people have helped me in some way. Special thanks, however, must go to the following: Prof Parsons and Mark Hodson for talking to me about feldspars and layered igneous rocks; JED for discussions about geochemistry and for getting me involved in manganism and 'cash for sandstones questions'; Dodie James for help with XRF and discussions of geochem., life, and what it all means; Gordon Waugh, Department Superintendent and accounting/cars/

computers/accidents/field-support fix-it whizz; Mike Hall for thin sections; Yvonne Cooper and team for salvaging my photography; Diana Batey for photography and draughting; John Craven, Chis and Shane for help with computing and printing; Pete Hill, Stuart Kearns and Simon Burgess for efficiently running a user-friendly EPMA service (and especially for coming in at all hours of day and night when It goes wrong).

At SURRC: Rob Ellam, Tony Fallick, Graeme Rogers, Anne, Vinny and Julie are all thanked for their scientific and technical support with getting good numbers from the subtle art of isotope geochemistry, or Voodoo as Vinny calls it.

At Royal Holloway, Nick Walsh is thanked for providing excellent REE analyses at short notice when I finally had to give up on the ICP-MS at SURRC.

For proof-reading: Simon (who read the lot!), Godfrey, Coleen Cole, Sally Brown, Dodie James, Paula McDade, Nic Odling, Kathryn Goodenough, Amanda Voase, Phil Bloor and Claire Bond.

To the Baffin Babes, Coleen and Sally, for making 'Sniper goes to Baffin with two hot chickies' such a humorous and enjoyable experience.

Finally, thanks to all my friends at Edinburgh for making my PhD so much fun. Especially Debbie for her help and support before, during and after Antarctica; Coleen, for being an awake belayer when I fall off, for format-cut-and-paste beyond the call of duty, and for organizing me during the last couple of years; and all those with whom I have enjoyed diving (especially Nic Odling for the ERI and Dunstaffnage experiences), climbing (especially Sharpie, Coleen and James for company and winter benightments) and Taekwondo.

Last but not least, Mum & Dad, for encouragement, financial support, organizing the bank when I was in Antarctica and the Arctic (not an easy task), typing in some of my references, and much more than I can mention here.

Thank you all.

Publications and abstracts

The following papers and abstracts have been written from material presented in this study:

Publications

Harley, S.L., **Snape, I.** & Fitzsimons, I.C.W. 1995. Regional correlations and terrane assembly in East Prydz Bay: evidence from the Rauer Group and Vestfold Hills. *Terra Antarctica.* **2**, 49-60.

Snape, I. & Harley, S.L. 1996. Magmatic History and the high-grade Geological Evolution of the Vestfold Hills, East Antarctica. *Terra Antartica.* **3**, 23-38.

Harley, S.L., **Snape, I.** & Black, L.P. *Accepted.* Age and history of early events in a layered meta-igneous complex, Rauer Group, East Antarctica: evidence for a distinct Archaean terrane. *Precambrian Research.*

Snape, I., Black, L.P. & Harley, S.L. *Accepted.* Refinement of the timing of magmatism and high-grade deformation in the Vestfold Hills, East Antarctica, from new SHRIMP U-Pb zircon geochronology. *Proceedings of the VII International Symposium for Antarctic Earth Sciences,* Siena, Italy, September 1995.

Abstracts

Harley, S.L. & **Snape, I.** 1993. Layered metaigneous complexes: A key to Archaean Terrane correlations between the Rauer Group and Vestfold Hills, East Antarctica. *Abstracts. The Tectonics of East Antarctica,*. Utrecht, October 1993, p. 29-31.

Harley, S.L., **Snape, I.** & Black, L.P. 1995. The Rauer Group: A record of Archaean to Cambrian crustal development and terrane amalgamation in Prydz Bay. *Abstracts. VII International Symposium for Antarctic Earth Sciences,* Siena, September 1995.

Snape, I. & Harley, S.L. 1995. Magmatism, metamorphism and deformation in a rapidly accreted Archaean high-grade terrane, the Vestfold Hills, East Antarctica. *Abstract. VII International Symposium for Antarctic Earth Sciences,* Siena, Italy, September 1995.

Snape, I. & Harley, S.L. 1995. Geological and geochemical evolution of Archaean orthogneisses in Prydz Bay: contrasting magmatic histories in adjacent terranes. *Abstract. VII International Symposium for Antarctic Earth Sciences,* Siena, Italy, September 1995.

Snape, I. & Harley, S.L. 1995. Geological and geochemical constraints on the evolution of reworked Archaean crust in the Proterozoic Rauer Group, East Antarctica. *Abstract. Precambrian 95,* Montreal, Canada, August/September 1995.

Snape, I. & Harley, S.L. 1995. A reassessment of the Archaean geological relationships in the Vestfold Hills, East Antarctica. *Abstract. Precambrian 95,* Montreal, Canada, August/September 1995.

Copies of the main papers (for which there are currently reprints) are provided in the pocket at the rear of the thesis.

Table of Contents

PART 1: INTRODUCTION

Chapter 1
Introduction, objectives and thesis outline

1.1 Introduction 1
1.2 Geological setting: a review of previous work in the East Antarctic Shield 2
1.2.1 Regional correlations and geological evolution 5
1.3 Precambrian Earth evolution: scientific approach and the nature of evidence from high-grade terranes 7
1.3.1 Uniformitarianism 7
1.3.2 Preservation of the oldest rocks 8
1.3.3 Practical problems of geological investigation in the East Antarctic Shield 9
1.4 Methodology 10
1.4.1 An integrated field, petrological, geochemical, and isotopic study 10
1.4.2 Sample selection for detailed study 11
1.4.3 Whole-rock geochemistry 12
1.4.4 General application of isotope analysis to metaigneous rocks 20
1.4.5 The geochemical and isotopic effects of weathering and metamorphism 25
1.5 Study structure and thesis layout 28

PART 2: THE RAUER GROUP

Chapter 2
Geological outline of the Rauer Group

2.1 Introduction and synopsis of Part 2: The Rauer Group 29
2.2 General outline and previous work 29
2.3 Lithology types: spatial and temporal distribution 30
2.3.1 Archaean lithologies in detail 32
2.3.2 Geochemical characteristics of Archaean orthogneisses 35
2.4 Structure 38
2.4.1 The structural scheme of Harley (1987) 38
2.4.2 An expanded structural scheme for the Rauer Group 39
2.5 *P-T-t* evolution and evidence for polymetamorphism 39
2.6 Isotopic studies and geochronology 41
2.6.1 Conventional isotopic data (Sr and Nd) 42
2.6.2 U-Pb zircon geochronology 44
2.7 The Rauer Group: summary, research rationale and objectives 45
2.7.1 Summary: what *is* known of the Archaean domain 46
2.7.3 Objectives and methodology 47

Chapter 3
Field relations of the Archaean domain

3.1 Introduction 49
3.2 The Composite Layered Orthogneiss (CLO) 50
3.2.1 CLO on Scherbinina Island 50
3.3 The Scherbinina Layered Complex (SLC) 51
3.3.1 Relict igneous features 51
3.3.2 The effects of metamorphism and deformation 53
3.3.3 Post-intrusive geological evolution 56
3.4 The Torckler-Tango Layered Complex (TTLC) 65
3.4.1 Relict igneous features 66
3.4.2 The effects of metamorphism and deformation 66
3.5 Summary 76
3.6 Strategy for detailed follow-up work 77

Chapter 4
Petrology of the Scherbinina and Torckler-Tango Layered Complexes

4.1 Introduction 79
4.2 Petrology and mineral chemistry of the Scherbinina Layered Complex (SLC) 80
4.2.1 Outline petrology of the main lithological groups 80
4.2.2 Preservation of igneous textures 83
4.2.3 Retrieval of igneous phase compositions 87
4.2.4 Emplacement temperatures from pyroxene and feldspar thermometry 93
4.2.5 Metamorphic petrology 97
4.2.6 Zircon chemistry 103
4.2.7 Summary and conclusions 106
4.3 Petrology of the early (Archaean) mafic dykes (MD1 & MD2) 107
4.4 Petrology of the Tonalite-Trondhjemite gneisses (TG and TrG) 108
4.4.1 Outline petrography of the Tonalite Gneiss (TG) 108
4.4.2 The Trondhjemite Gneiss (TrG) 108
4.5 Petrology and mineral chemistry of the Torckler-Tango Layered Complex (TTLC) 109
4.5.1 Outline petrology of the complex 109
4.5.2 Mineral chemistry 110
4.5.3 Summary and conclusions for the TTLC 112
4.6 Constraints on the evolution of Archaean mafic rocks in the Rauer Group: Discussion and preliminary conclusions 112

Chapter 5
Geochemistry of the Scherbinina and Torckler-Tango Layered Complexes

5.1 Introduction 115
5.2 Geochemistry of the SLC 115
5.2.1 Principal geochemical characteristics of the complex 115
5.2.2 Major elements 116

5.2.3 Normative compositions 119
5.2.4 Trace and rare-earth elements (REE) 120
5.2.5 Constraints on fractional crystallization from trace elements 126
5.2.6 The role of AFC 129
5.2.7 Preliminary conclusions and working petrogenetic hypotheses 130
5.3 Geochemistry of the Archaean? mafic dykes (EMD) 131
5.3.1 Principal geochemical characteristics 131
5.3.2 Major elements 131
5.3.3 Normative compositions 132
5.3.4 Trace and rare earth elements (REE) 132
5.4 Geochemistry of the TTLC 135
5.4.1 Principal geochemical characteristics 135
5.4.2 An outline of major and trace elements 135
5.4.3 Normative compositions 136
5.4.4 Trace and rare-earth elements (REE) 136
5.4.5 Summary and preliminary conclusions for the TTLC 148
5.5 General summary and conclusions for the SLC, EMD and TTLC 149

Chapter 6
Isotopic evolution of the Archaean Rauer Group

6.1 Introduction 150
6.1.1 Rationale 150
6.2 Oxygen isotope geochemistry of the SLC 151
6.2.1 Results 151
6.2.2 Interpretation and conclusions 152
6.3 U-Pb zircon geochronology 154
6.3.2 Results 154
6.3.4 Discussion and conclusions 158
6.4 Rb-Sr isotopes of the SLC and EMD 159
6.4.1 Results 160
6.4.2 Discussion 162
6.4.3 Summary and conclusions 163
6.5 Sm-Nd isotope geochemistry of the SLC 163
6.5.1 Results 163
6.5.2 Interpretation 165
6.5.3 Discussion of Hypothesis A (AFC) 166
6.5.4 Discussion of Hypothesis B: Metasomatism and isotopic exchange 172
6.5.5 Summary and conclusions 197
6.6 Radiogenic isotope geochemistry for the TTLC 198
6.6.1 Objectives and strategy for the TTLC 198
6.6.2 Rb-Sr isotopes 199
6.6.2 Sm-Nd isotopes 200
6.7 Summary and conclusions 201

Chapter 7

The origin and evolution of the Torckler-Tango and Scherbinina Layered Complexes

7.1 Introduction 204
7.2 A summary and critical appraisal of the SLC, EMD and TTLC 205
7.2.1 Similarities and differences between the SLC, EMD, and TTLC 205
7.3 Constraints on protolith origin 208
7.3.1 Problems associated with 'fingerprinting' source reservoirs and processes 208
7.3.2 Interpretation of source and process: constraints on tectonomagmatic environment 209
7.3.4 Discussion and interpretation from MORB-normalized IE diagrams and TEDDs 215
7.4 Summary, conclusions, and a tentative tectonomagmatic model for the Archaean Rauer Group 221

PART 3: THE VESTFOLD HILLS

Chapter 8

Geological outline of the Vestfold Hills

8.1 Introduction and synopsis of Part 3: The Vestfold Hills 224
8.2 Outline of the geological history 224
8.3 Previous accounts of lithologies and structures 226
8.3.1 Pre-D_1 gneiss suites 227
8.3.2 D_1 deformation and metamorphism (*ca.* 2501 Ma) 228
8.3.3 Post-D_1 to pre-/syn-D_2 gneiss suites 228
8.3.4 D_2 deformation and metamorphism (*ca.* 2487 ± 6 Ma see later discussion). 229
8.3.5 Post-D_2 geological evolution 229
8.4 Geochemical characteristics of the Vestfold Hills orthogneisses: An appraisal of previous results 230
8.4.1 General outline of previous results 230
8.4.2 Principal geochemical characteristics of the main orthogneiss units 230
8.4.3 Geochemical constraints on igneous petrogenesis 232
8.4.5 Overall petrogenetic or tectonomagmatic environment 234
8.4.6 A critique of the Sheraton and Collerson (1984) approach 234
8.5 Isotope studies and geochronology 235
8.5.1 Conventional isotopic data (Sr and Nd isotopes) 235
8.5.2 U-Pb zircon geochronology 236
8.6 Summary, research rationale, objectives and methodology 237
8.6.1 Problems or inconsistencies with previous accounts of the geological evolution 237
8.6.2 Objectives and methodology 241

Chapter 9

Field relations and preliminary petrographic observations from the gneiss complex

9.1 Introduction 243
9.2 Magmatic constraints on geological evolution: the CLG 244
9.2.1 Preserved intrusive features in the CLG 245
9.2.2 An outline of the variety and regional distribution of CLG magma types 245

9.2.3 Relative chronology of Crooked Lake magmatism 251
9.2.4 Relationship of Crooked Lake intrusives to the D_2-M_2 event 254
9.3 Status and regional distribution of gneiss lithologies: constraints on the amount of tectonic repetition 255
9.3.1 Lithological constraints on the amount of tectonic repetition 255
9.3.2 Structural constraints on the amount of tectonic repetition 257
9.3.3 Extrapolation into the southern region 257
9.4 Geological evidence from low-strain windows 260
9.4.1 The status of the Tryne Metavolcanics 260
9.4.2 The relationship between the Mossel Gneiss and the EMG 263
9.4.3 The Chelnok Paragneiss: Evidence for a tectonothermal history prior to the *ca.* 2500 Ma events? 267
9.5 Further observations regarding the metamorphic history 270
9.5.1 An outline of the problems 270
9.5.2 Currently unanswered questions regarding the metamorphic evolution of the Vestfold Hills 270
9.6 Discussion and conclusions 275
9.7 Strategy for detailed analytical work from a revised geological framework 278

Chapter 10
Refinement of the timing of magmatism, metamorphism and deformation from U-Pb zircon dating

10.1 Introduction 279
10.2 Rationale for further geochronology 279
10.2.1 Problems related to the timing of magmatism, metamorphism and deformation 280
10.3 Sample selection for refined geochronology 280
10.3.1 Detailed field relations of samples (see Figure 10.1 for sample locations) 281
10.4 U-Pb isotope geochronology 285
10.4.1 Analytical and data treatment procedures 286
10.4.2 Isotopic results 287
10.5 Discussion: interpretation of zircon geochronology 291
10.5.1 The age of D_1-M_1 and the origin of the Mossel Gneiss 291
10.5.2 The age of the LAS (CLG) pluton: constraints on AFC and tectonic repetition 291
10.5.3 The age of D_2-M_2 and the relationship of CLG lithologies to deformation 292
10.6 Summary and conclusions 292

Chapter 11
Geochemical and isotopic evolution of the Vestfold Hills orthogneisses

11.1 Introduction 293
11.1.1 Sample selection for geochemical and isotopic analysis 293
11.1.2 Approach and technical difficulties 294
11.2 Geochemical characteristics of the main orthogneiss lithologies 294
11.2.1 Overview of the principal orthogneiss lithologies 294
11.2.2 Principal geochemical characteristics 295

11.3 The Crooked Lake Gneiss in detail 302
11.3.1 Geochemical character of field-defined suites 302
11.3.3 Summary and discussion 311
11.3.4 Preliminary constraints on fractional crystallization from major- and trace-element bivariate diagrams 313
11.4 REE and Spidergrams 314
11.4.1 REE Results 314
11.4.2 Spidergrams 314
11.4.3 Trace-element discrimination diagrams (TEDDs) 316
11.4.4 Discussion and interpretation of REE and spidergrams 318
11.5 Oxygen isotopes 319
11.5.1 Results 320
11.5.2 Discussion and interpretation 321
11.6 Rb-Sr isotopes 321
11.6.1 Results 322
11.6.2 Discussion and interpretation 322
11.6.3 Summary of conclusions 330
11.7 Sm-Nd isotopes 330
11.7.1 Results 332
11.7.2 Discussion and interpretation 332
11.7.4 Summary of conclusions 336
11.8 Summary, discussion and conclusions 337
11.8.1 Summary of geochemical and isotopic results 337
11.8.2 Problems that concern a geochemical classification scheme for the CLG 338
11.3.3 Problems with modelling protolith petrogenesis in detail: this study and previous attempts 338
11.8.4 Steps towards an integrated petrogenetic and tectonomagmatic model for the Vestfold Hills orthogneisses 340

Chapter 12
Summary, discussion, and implications for the geological evolution of the Vestfold Hills

12.1 Introduction 347
12.2 Summary and discussion of lithological and structural revisions 347
12.2.1 Pre-D_1 gneiss suites 347
12.2.2 D_1-M_1 (Section 9.4) 348
12.2.3 Post-D_1 to pre/syn-D_2 gneiss suites 349
12.2.4 D_2-M_2 (Section 9.3) 350
12.3 Summary and discussion of the geochemical evolution of the Vestfold Hills orthogneisses 353
12.3.1 Summary of the geochemistry of the principal orthogneisses (Sections 11.3 & 11.8.2) 353
12.4 Summary and discussion of isotope studies and geochronology 355
12.4.1 A critique of previous Sr and Nd isotopes from the results of this study

(Sections 11.6 & 11.7) 355
12.4.2 Further constraints on the age of orthogneisses and high-grade deformation events from U-Pb zircon geochronology (Chapter 10) 358
12.5 A summary of the origin and evolution of the Vestfold Hills gneiss complex 359
12.5.1 Previously unanswered questions and further constraints from this study 359
12.5.2 Summary of the geological evolution of the Vestfold Hills 361

PART 4: SYNTHESIS

Chapter 13
Discussion, conclusions and wider context

13.1 Introduction: discussion, conclusions and wider context 362
13.2 Magmatism, crustal accretion and terrane assembly in East Prydz Bay 362
13.2.1 Refined Archaean geological histories in East Prydz Bay 362
13.2.2 Magmatism in the Rauer Group 362
13.2.3 Magmatism in the Vestfold Hills 365
13.2.4 Timing of terrane assembly in East Prydz Bay 365
13.3 Wider implications 370
13.3.1 Archaean magmatism and the growth of continental crust 370
13.3.2 Constraints on the behaviour of trace elements and radiogenic isotopes during metamorphism 375
13.4 An appraisal of the scientific approach adopted in this study and suggestions for further research 381
13.4.1 An appraisal of the rationale and scientific approach adopted in this study 381
13.4.2 Suggestions for further regional study 382
13.5 Concluding statement 386

Part 1:

Introduction

Chapter 1

Introduction, objectives and thesis outline

1.1 Introduction

Our understanding of the Precambrian geological evolution of Antarctica has improved dramatically in the last 25 years (see reviews by Oliver *et al.*, 1983; Thompson *et al.*, 1991; Tingey, 1991), and research in Antarctica has led to advances of major international significance in a wide range of areas. Notable progress has been made in the study of plate tectonics, through recognition of the pivotal role of Antarctica in continental reconstructions (*e.g.* Moores, 1991; Dalziel, 1992); magmatic processes, for example the geochemical evolution of Proterozoic dyke swarms (*e.g.* Collerson & Sheraton, 1986); and in metamorphic petrology, such as the recognition of ultra-high temperature (UHT) metamorphism in the Napier Complex (see reviews by Harley, 1989; Harley & Hensen, 1990). However, the growth of Precambrian continental crust in the East Antarctic Shield, as elsewhere, is controversial; particularly with respect to the significance of subduction-related magmatic accretion in the Archaean. Geochemical and isotopic studies of Archaean high-grade terranes clearly have an important bearing on this issue. However, there are considerable difficulties associated with working in ancient high-grade terranes. Problems range from the philosophical, regarding the suitability of plate-tectonic processes as an analogue for Precambrian Earth evolution; to the practical, in that all the Earth's oldest rocks are moderately to highly deformed and have polymetamorphic histories. The practical difficulties associated with the geological analysis of high-grade terranes also presents problems for pre-Gondwana terrane correlations. In the East Antarctic Shield, juxtaposed Archaean and Proterozoic terranes have long been recognised, but there is considerable uncertainty regarding the relationships between these regions, the significance of reworking, and the nature and timing of terrane correlations. These problems are well exemplified by the East Prydz Bay region, where there has been considerable debate regarding the geological evolution of the Rauer Group and Vestfold Hills. Recent tectonic models advocate that the largely Proterozoic Rauer Group comprises the reworked southern margin of the Archaean Vestfold Hills terrane, where Archaean crustal fragments have been tectonically interleaved with more dominant juvenile Proterozoic crustal additions.

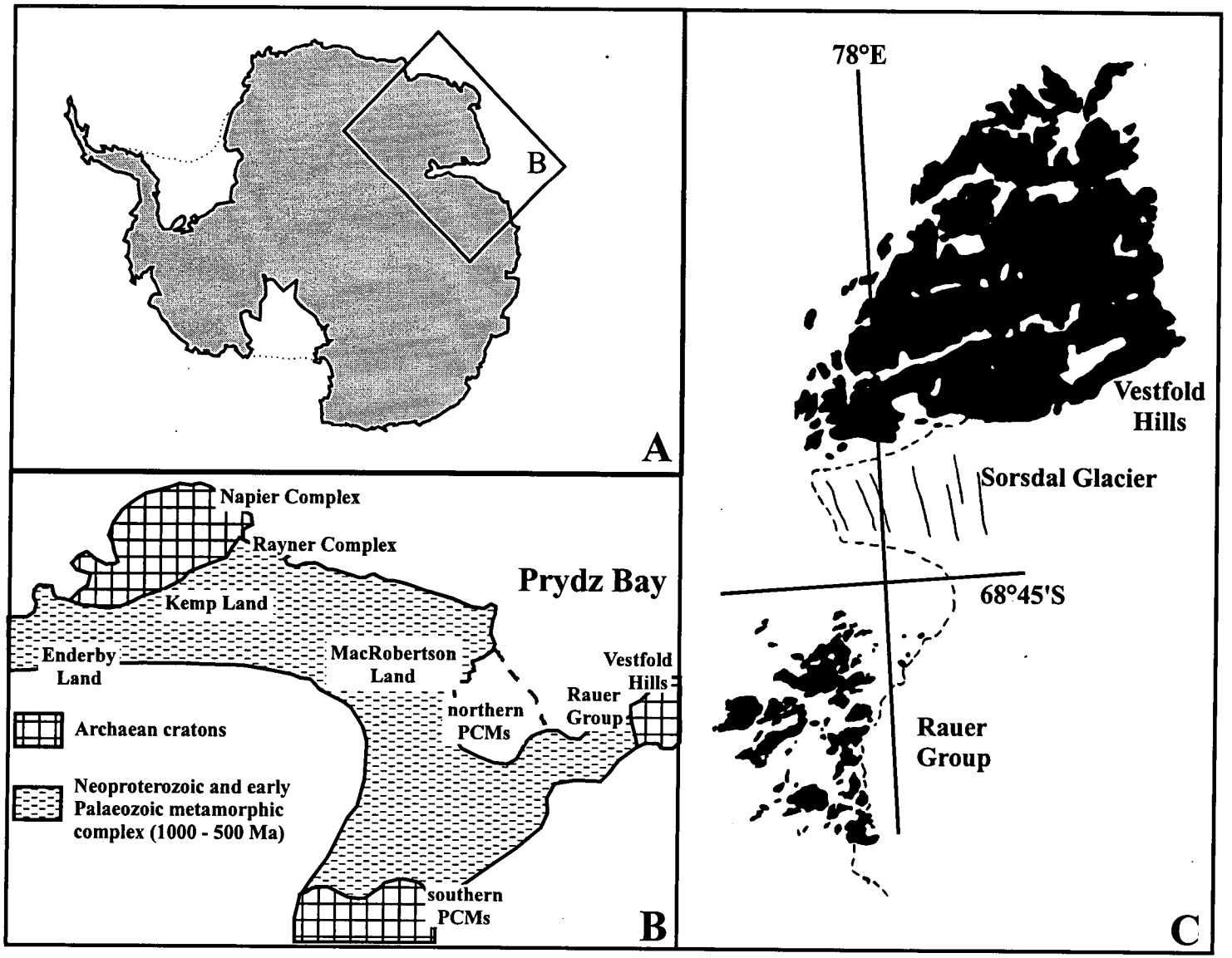

Figure 1.1 Geographical outline of Antarctica showing the location of Prydz Bay in the context of the East Antarctic Shield.

By studying the geological and geochemical anatomy of Archaean orthogneisses in the Rauer Group and Vestfold Hills, focusing on the relationships between magmatism, metamorphism and deformation, this study aims to help establish the scale and importance of well-dated events in the region. From this basis, regional terrane correlations and models of Precambrian crustal growth in the East Prydz Bay region can be assessed.

However, to understand the project design in detail, it is first necessary to examine the relationship between the Rauer Group and Vestfold Hills in the context of the East Antarctic Shield (Section 1.2). An overview of some of the relevant and currently debated topics in Precambrian geology is also pertinent, therefore a brief outline of some of the problems that are particular to the study of *Precambrian Earth evolution* are described in the following section (Section 1.3). The rationale for the scientific approach adopted in the study, or the *methodology*, is presented in Section 1.4, whilst an overview of the *thesis outline* is included in the final section in this chapter (Section 1.5).

1.2 Geological setting: a review of previous work in the East Antarctic Shield

The East Antarctic Shield is dominantly composed of Precambrian rocks, comprising a number of Archaean cratonic nuclei separated by an extensive Neoproterozoic to early Palaeozoic (1000 & 500 Ma) high-grade metamorphic complex (Figure 1.1b). The major Archaean blocks occur in the Napier Complex, southern Prince Charles Mountains (PCMs) and the Vestfold Hills, and are adjacent to an apparently continuous mobile belt that extends from the Rayner Complex of Enderby and Kemp Lands, through the northern PCMs of MacRobertson Land, to the southern Prydz Bay region of Princess Elizabeth Land (Figure 1.1b, Sheraton & Collerson, 1983; James & Tingey, 1983).

The relatively stable Archaean cratons consist of structurally interleaved ortho- and paragneiss sequences that typically preserve evidence of varied and prolonged geological histories. A number of common features have been identified, and a number of authors have suggested that they all shared a broadly similar tectonometamorphic history (*e.g.* James & Tingey, 1983). The first recognisable structures are usually rootless intrafolial folds (F_1). These were refolded or attenuated by a second deformation (D_2-F_2) that produced similar recumbent to reclined, tight to isoclinal folding, often associated with syn-tectonic and/or axial planar felsic melts. A final high-grade deformation event (D_3) that resulted in both

open warping of previous structures and attenuation in upright high-grade shear zones is also typical (*cf.* Parker *et al.*, 1983; James & Tingey, 1983; Harley, 1989).

The *ca.* 3000-2800 Ma Napier Complex of Enderby Land includes the oldest recognised crustal rocks in East Antarctica (3870 Ma, Black *et al.*, 1986a & b; 3800 Ma, Harley & Black, 1997). The geological relationships preserved in this region are thought to be the product of a complex and exceptionally high-grade metamorphic Archaean history (Ellis, 1980; Sheraton *et al.*, 1982, 1987; Harley, 1983, 1985; Harley *et al.*, 1993; Harley & Black, 1997). Major tectonothermal events are thought to have occurred at ~3000 Ma, ~2800 Ma, ~2500 Ma and at about 2500-2400 Ma (Black & James, 1983; Harley & Black, 1987, 1997; Sheraton *et al.*, 1987; Tingey, 1991). A similar lengthy history was also proposed for the Vestfold Hills by Collerson *et al.* (1983), who inferred a *ca.* 3000 Ma early high-grade metamorphic and deformational event (D_1-M_1), and a later intense D_2-M_2 granulite event at *ca.* 2500-2400 Ma that was closely followed by open warping (D_3-F_3) immediately prior to cratonization (Collerson *et al.*, 1983; Oliver *et al.*, 1982; Parker *et al.*, 1983).

After the last high-grade metamorphic event, all the Archaean cratons in Antarctica appear to have deformed in a passive manner by repeated dyke intrusion and relatively localised brittle-ductile deformation during the Proterozoic (James & Tingey, 1983; Sheraton *et al.*, 1987; Passchier *et al.*, 1991). Reworking appears to be of limited extent and only occurred around the margins of some of these cratons, such as minor refolding on the edges of the Napier Complex and Vestfold Hills (*e.g.* Sheraton *et al.*, 1980, 1984; Tingey, 1982), and formation of retrograde shear zones in the Napier Complex (Sandiford, 1985; Harley, 1985).

In contrast to the Archaean blocks, the Proterozoic mobile belt is believed to reflect new crustal accretion associated with a major high-grade 'Grenvillian' (*ca.* 1000 Ma) event that generally only involved relatively minor reworking of Archaean crust (Sheraton *et al.*, 1984; Black *et al.*, 1987; Harley, 1987). The Proterozoic crust does not contain abundant mafic dykes, although a number of mafic dyke generations have been recognised in some areas of the mobile belt. These mafic dykes are typically recrystallized and highly deformed, or have been transposed into parallelism with the regional *ca.* 1000 Ma gneissic layering (Sheraton *et al.*, 1987; Harley, 1987; Sims *et al.*, 1994).

The effects of the Proterozoic event(s) in East Antarctica were clearly quite complex and protracted. Nevertheless, an approximate 1000 Ma age has been reported from throughout East Antarctica, from Dronning Maud Land and the Rayner Complex (Shibata *et al.*, 1986; Black *et al.*, 1987) to the northern PCMs (Tingey, 1982) and the Rauer Group (Tingey,

1982; Sheraton *et al.*, 1984; Kinny *et al.*, 1993). Events at this time are typically associated with upper amphibolite- to granulite-facies metamorphism, often with intense folding or ductile deformation (*e.g.* James & Tingey, 1983; Harley & Hensen, 1990). Similar high-grade events have been reported on other continents at about this time (see reviews by Harley & Hensen, 1990; Harley, 1992; Davidson, 1995).

The last regional high-grade geological event in East Antarctica occurred at about 500 Ma, implying an association with Pan-African events. The extent, grade and significance of this event is currently the subject of considerable debate. In some areas, such as the Brattstrand Bluffs - Larsemann Hills - Bolingen Islands areas in Prydz Bay, *P-T* conditions reached granulite grade (*e.g.* Zhao *et al.*, 1992, 1995; Hensen & Zhou, 1995). In other areas, such as the Rauer Group, it *appears* to be more locally restricted, with a low- to medium-grade metamorphic overprint that is usually associated with brittle shear-zones and pegmatite emplacement (*e.g.* Harley *et al.*, 1992). Although *ca.* 500 Ma magmatism appears to have been relatively limited (*e.g.* Tingey 1982, Sheraton *et al.*, 1993), at least in the East Prydz Bay area, there was extensive resetting of U-Pb isotopic systems at this time (*e.g.* Kinny *et al.*, 1993). The magnitude and full implications of this pervasive tectonothermal event are, however, largely unknown at present (*cf.* Harley, 1988).

1.2.1 Regional correlations and geological evolution

One of the most frustrating problems encountered in reconstructing the regional geological evolution of any area is the discontinuous nature of rock outcrop. This problem is particularly acute in Antarctica where major geological changes, or even terrane boundaries, generally occur beneath glaciers or the ice sheet (*cf.* Tingey, 1991). Nevertheless, a number of authors, based on a variety of observations, have postulated tentative correlations that range from defining coeval or cogenetic lithologies on a local scale (*e.g.* for the Vestfold Hills, Figure 1c, Sheraton & Collerson, 1984), to correlating dyke suites between the Archaean cratons (*e.g.* Collerson *et al.*, 1983; Sheraton & Collerson, 1983), or proposing that Archaean cratons and younger dykes extend into adjacent areas of the Proterozoic mobile belt (*e.g.* Sheraton *et al.*, 1984; 1993; Tingey 1982; Sims *et al.*, 1994).

However, recent geochronological studies using high precision U-Pb dating of zircons, have forced a reinterpretation of the geological history for many regions within the East Antarctic Shield (*e.g.* Black *et al.*, 1991a; Black *et al.*, 1993; Kinny *et al.*, 1993). Earlier attempts to constrain the age of a variety of lithologies and subsequent tectonothermal events commonly produced imprecise or even erroneous ages. This is largely the result of

attempting to apply isotopic systems that are easily reset during high-grade metamorphism (especially Rb-Sr or K-Rb systems) or, as Black *et al.* (1991a) demonstrated for the Vestfold Hills, where unrelated samples have been combined together in order to provide a sufficient spread of points to define an 'isochron'. Hence, there is a need to reassess many simple or provisional correlations between or even within terranes.

Largely stemming from a revised chronostratigraphy for the Vestfold Hills (Black *et al.*, 1991a), and new geochronological results for the Rauer Group (Kinny *et al.*, 1993), this study aims to further constrain the igneous, metamorphic and early structural history of Archaean orthogneisses in these two adjacent high-grade terranes. In their study of the Vestfold Hills orthogneisses, Black *et al.* (1991a) demonstrated that varied magma suites were emplaced and deformed in a rapid crust-forming episode during a *ca.* 50 Ma period at the end of the Archaean. In the broadest sense these constraints offer a unique opportunity to examine crustal accretion processes at this crucial time in the Earth's history (*cf.* Kröner 1985, 1991; Windley, 1981; 1995), but they also emphasise the need for a re-examination of the geological evolution of the region (discussed in detail in Chapter 8).

Recent studies in the Rauer Group and Vestfold Hills by a joint Melbourne-Utrecht team have attempted to correlate a relatively clear Proterozoic event sequence deduced for the Vestfold Block, consisting of mylonite, ultramylonite and pseudotachylite development punctuated by multiple dyke emplacement (Passchier *et al.*, 1991), with similar features in the Rauer Group, even though these features were subsequently intensely deformed by the *ca.* 1000 Ma event in the latter region (Dirks *et al.*, 1993, 1994; Sims *et al.*, 1994). Earlier work, based mainly on broad lithological similarities between the orthogneisses of the two areas and the presence of deformed Vestfold Hills-like mafic dykes in the Rauer Group, led some authors (*e.g.* Sheraton & Collerson, 1983) to suggest that the gneisses of the two areas might correlate directly. Later studies, however, have tended to highlight the considerable differences between the two terranes and recognise that for much of their history they possibly evolved quite differently (Black *et al.*, 1991a; Kinny *et al.*, 1993).

Early studies estimated that the extent of reworked Archaean crust in the Rauer Group is relatively minor (*e.g.* Sheraton *et al.*, 1984; Harley, 1987), and that most rocks represent juvenile crustal additions emplaced during the Proterozoic at about 1000 Ma. In contrast, Kinny *et al.* (1993) inferred that up to 50% of the rocks may be Archaean in age, with extensive orthogneiss suites being of either 3270 Ma or 2800 Ma age. Although these ages indicate that there are Archaean components in both the Rauer Group and adjacent Vestfold Hills, there is no evidence to support a correlation between the Archaean gneissic

components in these two regions. Whilst it is commonly held that the two terranes share a similar history sometime prior to or during the *ca.* 1000 Ma event (*e.g.* Collerson *et al.*, 1983; Black *et al.*, 1991a, b; Kinny *et al.*, 1993; Sims *et al.*, 1994), the exact timing of terrane juxtaposition is not yet known. Whether a link between the Vestfold Block and Rauer Group existed in the Archaean is an important question. Inherited *ca.* 2800 Ma zircon populations in the felsic gneisses of the Vestfold Hills which are thought to reflect an older, deeper, source region (Black *et al.*, 1991a), and the presence of undated pre-2526 Ma mafic and paragneiss units, are an indication that there may be a connection with at least some gneisses of similar relative age in the Rauer Group. The status of 2800 Ma rocks in the Vestfold Hills is undefined at present, but clearly the potential link with the Rauer Group merits consideration. Hence, a detailed examination of all the possible correlatives between Archaean components in the these two terranes is imperative, because a separate-terranes hypothesis for the two regions may have important implications for continental reconstructions (Black *et al.* 1991a; Moores, 1991; Dalziel, 1991, 1992; Sheraton *et al.*, 1993). At a more regional level, the timing of Vestfold Hills-Rauer Group juxtaposition influences process-oriented models that concern the geological evolution of the area (*e.g.* tectonic and thermal reactivation of mobile belts, Dirks & Wilson, 1995). However, testing existing models or establishing new hypotheses requires rigorous and detailed comparisons with between terranes, focusing on magmatic, metamorphic and deformational events of Archaean, Grenvillian (*ca.* 1100-1000 Ma) and Pan-African (*ca.* 600-500 Ma) age.

1.3 Precambrian Earth evolution: scientific approach and the nature of evidence from high-grade terranes

1.3.1 Uniformitarianism

The principle of uniformitarianism - that the present is the key to the past - is regarded by many as the fundamental tenet of geology. However, it is also generally accepted that the principle becomes proportionally weaker when applied further back in the Earth's early history. As Hall & Hughes (1993) noted, the earliest-formed rocks cannot have developed in precisely the same way as those in modern magmatic, sedimentary or metamorphic provinces. The problem is, what alternative is there? The observations that we can make from modern geological provinces lead to testable models that can be analysed, refined or refuted. This process of scientific enquiry is less easily pursued in the study of Precambrian Earth evolution. Changing the parameters of models derived to explain modern geological processes, or *modified analogues*, is one valid approach that can be tested theoretically or experimentally. For example, recent work has investigated the nature of thermal regimes in

modern subduction zones (*e.g.* Peacock *et al.*, 1994). By changing the parameters in these models to more closely reflect Archaean geothermal gradients, it has been possible to formulate models that can account for differences in the geochemistry of Archaean subduction-related magmas (*e.g.* Martin, 1986; Defant & Drummond, 1990). Other variations on the plate-tectonic theme perhaps require a greater departure from uniformitarian principles (*e.g.* Park, 1995), and there is considerable debate as to when or even if uniformitarianism principles can be applied to the interpretation of Precambrian suites (*cf.* Kerr, 1985, Kröner, 1984; Meissner, 1983; Windley, 1993; Burke, 1995).

Although it is recognised that uniformitarian principles are less robust when applied to Archaean suites, in practice, a uniformitarian approach has been adopted throughout this study. *If* geological, geochemical or isotopic parameters appear similar to those from modern geological provinces, then I have assumed that modern plate-tectonic processes *probably* are valid analogues.

The problems associated with interpretation of the Archaean geological record are not only philosophical, however, and there are two main practical problems that influence or bias the interpretation of the Earth's early history. The first problem concerns the preservation potential of ancient suites, because some rock types or associations are more likely to be preserved than others. The second problem stems from the observation that most of the direct evidence of early Earth evolution comes from rocks that have been metamorphosed and tectonically dismembered. To some extent, both of these problems have shaped the direction of this study, and are worthy of further discussion at this stage.

1.3.2 Preservation of the oldest rocks

Our understanding of early Earth evolution, as derived directly from the geological record, comes mostly from granite-greenstone belts or high-grade gneiss terranes (see Windley, 1995), and all the Earth's very early history (4.0-3.6 Ga) is contained in high-grade gneiss terranes that have been reworked during younger orogenic events (Nutman *et al.*, 1993).

Some of the specific problems that are associated with the nature of evidence that is preserved in high-grade terranes include:

- ***Deducing relative event sequences.*** High-grade deformation often results in extensive transposition of originally discordant relationships.

- ***Defining cogenetic suites.*** Transposition often hinders recognition of suites that are related spatially, temporally or through a common protolith-forming processes.

- ***Event correlation between regions.*** Magmatic, metamorphic and deformational events may be diachronous, have different phases that relate to one 'event', or events in different regions may co-incidentally share the same age but be genetically unrelated. All these aspects are particularly difficult to assess in high-grade terranes.

- ***Metamorphic recrystallization.*** Metamorphism often overprints primary phases and textural information, and even then, peak metamorphic assemblages or compositions are only rarely preserved.

- ***Open-system chemical exchange during metamorphism or deformation.*** Element mobility during metamorphism and/or deformation is well-documented. Associated changes range from minor to major effects, but the implications may be profound for models of protolith-forming processes.

These practical problems have shaped the direction or methodology of this study, and are discussed at length in the following chapters. Additional problems that are peculiar to work in Antarctica are described in the next section (Section 1.3.3), and a methodology that is designed to accommodate or minimise some of these 'problem' aspects is outlined in the following section (Section 1.4).

1.3.3 Practical problems of geological investigation in the East Antarctic Shield

Exposure

Approximately 99% of Antarctica is covered by ice; a situation that is clearly not conducive to direct regional correlations. Bedrock exposure is restricted to a few coastal oases, such as the Vestfold Hills and Bunger Hills (*e.g.* Pickard, 1986); remote mountain ranges, such as the PCMs; and isolated nunatacks, such as Mt. Brown (see Tingey, 1991, figure 1.1). Major breaks in geology often coincide with glaciers, and as with palinspastic reconstructions for the Arctic (*e.g.* Harland *et al.*, 1992; Friend *et al.*, 1997), are a convenient cover for proposed terrane boundaries. Outcrop mapping is only really possible for a short summer season, and the outcrop pattern varies from season to season depending upon snow distribution.

However, having noted the difficulties, the generally excellent exposure in snow- and ice-free areas is one major advantage of working in Antarctica. Bedrock exposure is up to 90 % in some areas, such as the eastern Vestfold Hills. Another important feature is that erosion rates are often very fast, which means that most exposed rocks are extremely fresh.

Rock types

The East Antarctic Shield almost entirely comprises medium- to high-grade gneisses. There are no granite-greenstone belts and very few unmetamorphosed sedimentary sequences (Tingey, 1991). The principal rock types are felsic orthogneisses, paragneiss sequences, deformed metaplutonic ultramafic-mafic centres, deformed mafic dykes, and post-deformational mafic dykes and granites. In the East Prydz Bay region, orthogneisses dominate in the Vestfold Hills and Rauer Group, whilst paragneisses dominate in the Larsemann Hills - Bolingen Islands - Brattstrand Bluffs areas, although both broad rock types are represented throughout and occur as tectonically interleaved gneiss associations.

1.4 Methodology

1.4.1 An integrated field, petrological, geochemical, and isotopic study

Previous geological studies in the Vestfold Hills and Rauer Group are either of a reconnaissance nature (*e.g.* Sheraton *et al.*, 1984), or have focused in detail on certain aspects of the geology (*e.g.* the metamorphic studies of Harley and co-workers). This study has a broad remit in that it encompasses all the previous work that has considered the origin and evolution of the Archaean gneisses in the two regions. However, in order to achieve the greatest understanding of the early geological history, selected suites have been studied in considerable detail.

The scientific methodology partly stems from previous studies in the region, either following previous lines of enquiry or examining aspects that have not yet been studied, but it also reflects the problems of working in high-grade terranes that were outlined in the previous section (Section 1.3). In common with many such studies, the basis for laboratory analysis lies in fieldwork. The approach adopted here is predominantly field and geochemically oriented, and although some petrographic aspects are described in detail, regional petrographic descriptions are not a major component of this study. Although mineral and microtextural analysis is an important aspect of the analysis of high-grade terranes, a greater understanding of protolith-forming processes can be attained *at a regional scale* through the application of whole-rock geochemical and isotopic investigation.

Rather than focus on one specific technique (*e.g.* O isotopes, whole-rock geochemistry, REE, or petrography), a combined approach has been adopted. The main focus has been on chemical systems that are *not* prone to change during metamorphism and that can be readily applied to a wide range of rock types. The study of major and trace elements combined with radiogenic isotopes is particularly powerful because each technique relates to different aspects of the whole-rock system (*i.e.* the sample). For example, major and trace elements behave differently during partial melting and fractional crystallization and considerable variations can be produced by such processes. By contrast, radiogenic isotopes are not normally fractionated by partial melting or fractional crystallization. Sr- and Nd-isotope systems are particularly useful because although they behave differently during igneous petrogenesis and metamorphism. They also have similar long-lived decay schemes, and are therefore of key importance in deducing Precambrian Earth evolution. When combined with stable isotopes and whole-rock geochemistry, radiogenic isotopes may provide considerable insight into the nature of protolith-forming processes and post-crystallization mobility associated with metamorphism.

1.4.2 Sample selection for detailed study

Although all the main gneiss suites described in the regional context of the Rauer Group and Vestfold Hills were sampled during the course of this study, only selected suites are described and discussed in detail. An extensive range of felsic orthogneisses and paragneisses has been collected from both the Rauer Group and Vestfold Hills. Many have been analysed geochemically, but very few are discussed in this study (the analyses have been included in Appendix 2). This is because the generally high-strain state of felsic rocks means that individual samples are often not easily characterised as belonging to well-defined suites. Instead, the main focus is on ultramafic - mafic - intermediate suites that can be recognised as being cogenetic based on field relations. This approach has both advantages and disadvantages. Hall & Hughes (1993, p.626) succinctly explained the main advantage of studying mafic magmatic rocks, noting that 'compared to granitic intrusions, the style of mafic magmatic rocks readily reflects the environment in which they formed. Gabbros, pillowed laves and mafic dykes commonly retain their distinctive features even in areas of high deformation and metamorphism'. They also noted the main difficulty of studying the intrusive mafic components of these suites (Hall & Hughes, p.629), that 'the parental magma compositions of such intrusions are difficult to decipher'.

The following sections outline some of the advantages and disadvantages that are inherent in studying plutonic rocks, and provides a brief overview of the theoretical applications of the techniques employed in this study.

1.4.3 Whole-rock geochemistry

The interpretation of whole-rock geochemistry from plutonic rocks is at best a hazardous process. Most plutonic rocks, other than those that are demonstrably quenched liquids, are probably best regarded in the broadest sense as being cumulates. Irvine (1987, p.461-462) provides a useful definition of the term 'cumulate':

> 'Cumulate. An igneous rock characterised by a cumulus framework of touching mineral crystals or grains that have evidently been formed and concentrated by processes of crystallization differentiation. The fractionated crystals are called cumulus crystals. They typically are subhedral to euhedral, and they are generally cemented together by a texturally later generation of postcumulus materials that appear to have crystallized (or recrystallized) from the interstices of the cumulus framework. The solidification stage during which the cumulus crystals are formed is called the primary or cumulus stage; the processes involved in the solidification of the intercumulus liquid are termed post cumulus processes.'

This definition provides the first clue as to why whole-rock chemistry is difficult to apply to cumulates. Although it might seem obvious, any analysis will represent a combination of cumulus crystals and postcumulus materials, therefore any attempt to interpret the nature of the fractionation process must account for the inclusion in the analysis of both fractionated products and the crystals (or their later replacement products) that may have been responsible for the fractionation process.

In the literature, the problems that are peculiar to whole-rock analysis of cumulates have been addressed in a number of ways. Two end-member scenarios illustrate some of the different approaches; most workers usually adopt one or other. In the first approach, elements are plotted on variation diagrams, and trends are interpreted as if the analyses were liquids. Usually a number of key variations or element ratios diagnostic of magmatic processes or, missing out the magmatic processes stage altogether, diagnostic of tectonic setting, are used to infer something of the petrogenetic history of a rock. Examples of this situation include Van Calsteren (1978) for the Palaeozoic Cabo Ortegal complex (NW Spain), Olsen *et al.* (1983) for the Concord gabbro-syenite complex (USA), Munksgarrd *et al.* (1992) for the northern PCMs, Sheraton *et al.* (1993) for the Bunger Hills (East Antarctica), and Muir *et al.* (1994) for the Rhinns complex (Scotland).

The other end-member approach essentially ignores whole-rock major and trace elements altogether, presumably on the grounds that a detailed understanding of the mechanisms that produce cumulates are better achieved via fieldwork, isotopic analysis, theoretical studies or, most commonly, by studying textures and mineral chemistry. Studies of major significance that have adopted this approach include Wager & Brown (1968), McBirney (1975, 1987), McBirney & Noyes (1979), Martin & Nokes (1988) and Sparks *et al.* (1993).

Unfortunately, metamorphosed cumulates such as those collected in this study preserve little mineralogical of textural information that can be used to unravel the origin and evolution of the East Prydz Bay layered complexes. Nevertheless, whole-rock geochemistry *may* provide valuable insights into the origin of mafic plutonic suites, provided that certain limitations are appreciated. A number of workers have adopted such an approach by considering the interpretation of whole-rock geochemistry in the context of cumulate processes (*e.g.* Wilson *et al.*, 1987; Weibe, 1993; Le Roex *et al.*, 1996; Arnason *et al.*, 1997), and a similar approach has been adopted in this study.

The cumulate system

The principal limitation to whole-rock geochemistry in the study of cumulates arises because cumulate rock suites cannot be modelled as a series of liquids related by a liquid-line of descent. Unlike crystal fractionation models that assume crystal-liquid equilibrium and efficient removal of fractionating crystals from the residual melt, in their simplest form cumulates represent aspects of both the residue and fractionated liquid products. Unfortunately, from the whole-rock geochemistry viewpoint, this process is dynamic and chemical exchange occurs at scales greater than sample-sized systems. For example, Petersen (1987) and others have established that melts move through crystal piles (the crystal mesh) before finally crystallizing. Petersen (1987 p. 505) describes a simple model whereby 'solidification contraction leads to flow of solute-enriched liquid in a direction opposite to the direction of the main growth, solute-rich liquids accumulate along the margins of the magma chamber and give rise to a marginal inverse compositional zonation'. A similar general model was proposed for Skaergaard by McBirney & Noyes (1979), whereby most crystallization took place in an advancing front of solidification against the floor, walls, and roof where crystals nucleated and grew in a static boundary layer. Later modifications to such models, such as 'constitutional zone refining' (McBirney, 1987) also emphasize the importance of *in situ* crystallization and the involvement of trapped liquid compositions. Such ideas were advanced upon by Langmuir (1989) in a theoretical

consideration of the effects of *in situ* crystallization, who further emphasised the importance of trapped liquids in determining the bulk composition of cumulate sequences. These models have a number of possible implications for the interpretation of whole-rock geochemistry, which are perhaps best discussed in the context of studies that have examined the whole-rock geochemistry of relatively recent cumulates that are unmetamorphosed.

In their study of the Okenyenya sub-volcanic ring complex (Namibia), Le Roex *et al.* (1996) found that major-element and compatible-element variations often reflect various amounts of accumulation. For example, elements such as Al will largely reflect the modal abundance of feldspar. Similarly, trace elements that are compatible in early formed cumulus phases, such as Ni and Cr in olivine and orthopyroxene, and Ba and Sr in feldspars, will be strongly controlled by modal mineral abundances. However, Le Roex *et al.* (1996) also noted that many incompatible elements and especially incompatible-element ratios, still have a strong link between the primary liquid composition and the present whole-rock geochemistry. The overall geochemical variations shown by the Okenyenya complex were interpreted by Le Roex *et al.* (1996, p. 665) to have resulted from a complex interplay between *in situ* crystallization with variable expulsion of interstitial melt, recharge by variably contaminated magmas, and re-equilibration of primocrysts with trapped interstitial melt. Nevertheless, they observed that many incompatible trace elements have good inter-element correlations, and that there are only minor differences between incompatible trace-element patterns for chilled margin samples and cumulates. In terms of a general approach, Le Roex *et al.* (1996, p. 665) concluded that by considering the more pronounced geochemical and mineralogical variations, plutonic chemistry would allow some insight into the genetic processes that may have acted on the magma, and that there is a link between cumulate whole-rock geochemistry and 'different melting environments in the mantle'.

Similarly, in a study of the Pleasant Bay layered gabbro-diorite intrusion (USA), Weibe (1993) also considered the affects of cumulate processes on geochemistry. Weibe (1993 p.476) noted that 'a genetic relationship between the gabbroic cumulate layers and the mafic liquids represented in the dykes and chilled margins is indicated by their similar abundances of compatible trace-elements and the similar abundances and ratios of the incompatible trace-elements'. Nevertheless, he also noted that intrusive whole-rock geochemistry may be strongly affected by the accumulation of crystals, and that concentrations of trace elements that have high K_d values for certain elements, such as Ba in alkali feldspar, Zr in zircon, and P in apatite, may be strongly affected by accumulation of these phases.

In their study of the Kruuse Fjord gabbro complex (East Greenland), Arnason *et al.* (1997) also found a comparable link between gabbros-ultramafic rocks and associated quenched-liquid marginal suites. They noted that many major-element and trace-element concentrations were not appreciably different between cumulates and quenched margin suites, although abundances of REE were slightly depleted in the cumulate as a consequence of olivine, plagioclase and clinopyroxene accumulations.

In practical or general terms, the observations (outlined above) made by Weibe (1993), Le Roex *et al.* (1996) and Arnason *et al.* (1997), can be related to theoretical, empirical and field-based models of cumulate genesis. The main implication from such models is that incompatible and compatible elements may not be well-correlated because they are effectively from different parts of the cumulate whole-rock system. Many major elements and compatible elements will be quickly incorporated into the crystal mesh, whereas incompatible elements and volatiles will move through this mesh until advancing crystallization and fluid-dynamic conditions dictate that the liquid becomes trapped. This is one of the reasons that incompatible-element variations are not often directly correlated with major-element based indices of differentiation. In a simplistic way, the major elements and compatible elements may often appear to be decoupled from the incompatible elements. However, there are also good theoretical reasons why many elements do correlate, and this relates to the nature of the trapped-liquid component.

From a theoretical basis, the importance of the trapped liquid for determining incompatible trace-element abundances can be explained by considering simple mass balance and crystal fractionation models. During cumulus-mineral growth, the concentration of an element in the crystal is probably governed by a model that lies somewhere between equilibrium and fractional crystallization (*cf.* Langmuir, 1989, and see review in Rollinson, 1993). Except at very low values of melt fraction (*F*, *i.e.* the final residual liquid), the concentration of many incompatible elements in the major cumulus phases of basaltic systems, such as olivine, plagioclase, orthopyroxene and to a lesser extent clinopyroxene, will be very low compared to that in the residual liquid. Therefore, when residual liquids become trapped, a major component of the whole-rock incompatible-element budget is contained in this volumetrically minor component. In practical terms, this means that there is often a strong link between the incompatible-element signatures of primary liquid compositions and those of cumulates, particularly for incompatible elements and normalized incompatible-element patterns. Within-suite variations, however, might be expected to reflect dilution, by the inclusion of cumulus phases that have low incompatible-element abundances, or alternatively elements may have been fractionated as the melt moved through the crystal

mesh. This means that bulk distribution coefficients (D values) for incompatible elements will in effect equal the sum of the mineral-melt distribution coefficients (K_d values) for all cumulus minerals that interacted with the melt prior to 'trapping'.

Although the somewhat pragmatic approach outlined above is probably an oversimplification, and there are bound to be uncertainties and exceptions, it does explain the commonly observed link between cumulate geochemistry and liquid compositions, but also stresses the potential for highly variable behaviour for selected element groups depending upon the early crystallization history. Some of the further implications regarding this are discussed below for the major-element and trace-element subsystems, and the problems inherent in the interpretation of whole-rock cumulate chemistry is a topic that is referred to throughout this study.

Norms

The use and application of norms in studying orthogneisses in Precambrian high-grade terranes is variable. Although possibly the most widely used textbook on *Igneous Petrogenesis* dismisses norms in two sentences, on the grounds that they 'have little intrinsic value in the description of the geochemical characteristics of igneous rocks within a modern petrogenetic framework' (Wilson, 1989, p.7-8), norms do receive some attention in this study. However, a number of factors that relate to problems with the interpretation of whole-rock geochemistry in cumulates (outlined above), are also applicable. These problems, and others that relate to norm calculations in high-grade suites and their general applicability are briefly outlined below:

- ***Problems relating to the cumulate record.*** The main limiting factor regarding normative application to cumulates is that most empirical or experimental studies are concerned with the liquid-line of descent. This cannot be assumed for norms that have been calculated from cumulates, and their interpretation is not straightforward because usually more than one fractionating phase can be expected in any given suite of cogenetic rocks.

- ***Sensitivity to major-element mobility.*** Norm calculations are particularly sensitive to major-element mobility. Although all major elements are linked through a constant sum relationship, mobility of relatively minor constituents, such as K or Na, may have little effect on other major elements, but can have a proportionally much larger effect on normative compositions. This is partly because feldspars are calculated early on the normative procedure (see Cox *et al.*, 1979). Other effects, such as secondary carbonate veining can also influence the norm.

- ***Sensitivity to the estimation of Fe^{2+}/Fe^{3+}.*** This parameter is difficult to measure even in fresh rocks and the measured Fe^{2+}/Fe^{3+} is unlikely to faithfully record that of the protolith in the high-grade gneisses investigated in this study (*cf.* McNaughton & Wilson, 1983).

- ***Sensitivity to estimates for volatiles (e.g. H_2O and CO_2).*** As above, such species are difficult to measure, probably do not reflect the volatile content of the protolith, but may influence the norm calculation.

- ***Choice of normative procedure.*** CIPW norms are the most commonly cited convention, but other algorithms are also used (*e.g.* Elthon, 1983). Falloon *et al.* (1988) and Rollinson (1993) illustrate some of the advantages and disadvantages of the different procedures. In this study, the CIPW norm is used throughout because it is the most widely used and is also directly comparable with previous work in the region (*e.g.* Sheraton & Collerson, 1984).

- ***Extrapolation to experimental systems.*** There are number of problems associated with using normative compositions for phase diagram construction. A number of authors (*e.g.* Presnall *et al.*, 1979; Falloon *et al.*, 1988; Rollinson, 1993) noted that apparent trends or inflections can be induced by analytical or computational difficulties associated with CIPW norms. Other problems include; (i) difficulties of extrapolating between experimental systems and cumulate compositions; (ii) problems associated with predicting the effects of minor components (*e.g.* Na in the CMAS system); (iii) most projections yield the best results if there is some independent constraint on the fractionating assemblage, because 'for a projection to be useful in interpreting crystal-liquid equilibria, it must be made from a phase which is present in the melt, for otherwise the observed trends are meaningless' (Rollinson, 1993, p. 93); (iv) spurious trends can be induced from oblique projections (Rollinson, 1993).

It is primarily for these reasons that extensive use of normative compositions or phase diagrams has not been undertaken in this study[1].

Mantle- or MORB-normalized incompatible trace-element diagrams (spidergrams)

The 'primitive mantle' (PM) is an estimate the composition of the mantle before the continental crust formed (Rollinson, 1993). Mantle-derived suites are commonly compared

[1]The polybaric CMAS system of O'Hara (1968), and the projections of Grove *et al.* (1982) and Thompson *et al.* (1984), were plotted in an exploratory examination of the data, but quantitative or even particularly informative results were not obtained.

with this theoretical reservoir and are presented on log-normalized multi-element plots, with elements arranged in order of increasing compatibility with respect to a small percentage melt of the mantle. In this study, the PM values of McDonough *et al.* (1995) are used (Appendix 3).

MORB-normalized diagrams are considered more suitable for evolved basalts, andesites and crustal rocks (Rollinson, 1993). The 'average' composition of MORB is used as a comparison, although the plotting order is the subject of considerable debate (*e.g.* Pearce, 1983; Bevin *et al.*, 1984; Saunders & Tarney, 1984; Wilson, 1989; McCulloch & Gamble, 1991; Rollinson, 1993). The original plotting order of Pearce (1983) is based on two parameters. The first is ionic potential (ionic charge/ionic radius), which is used as a measure of element mobility in aqueous fluids. Elements with low (<3) and high (>12) ionic potentials are considered mobile and those with intermediate values are generally immobile. The second parameter is the element *D*-values for small degree partial melts of a garnet lherzolite. Elements are ordered so that mobile elements are placed on the left in order of increasing incompatibility, and the immobile elements are arranged from right to left in order of increasing compatibility.

The plotting order used in this study follows these basic principles, but slightly changes the order of Pearce (1983). Changes are made because Hf and Ta have not been analysed as they require expensive INAA. Also, because Nb and the other HFSE are of key importance in the identification of subduction signatures (see Pearce, 1983; Sun & McDonough, 1989; and see references in Chapters 5, 7 & 11), additional immobile elements have been added to the plotting order to monitor Nb and the HFSE relative to average MORB. Additionally, Nb has been placed between La and Ce, rather than between Th or LILE that are commonly thought to be mobile during metamorphism. Although the choice of plotting order will obviously influence the pattern to some extent, the important point is how variations compare with N-MORB. To this effect, the position of the HFSE relative to other elements has either been preserved in the original order suggested by Pearce (1983), or elements have been chosen to favour a null-hypothesis approach. For example, subduction-related basalts generally have less enriched MORB-normalized LREE relative to LILE, hence inserting Nb between La and Ce could potentially increase Nb/Nb* (described in Chapter 5), that is to decrease the measure of the Nb anomaly and the subduction signature. These features are discussed further in Chapters 5, 7 and 11.

Trace-element discrimination diagrams (TEDDs)

The use of trace-element discrimination diagrams (TEDDs) has become popular as a means to quickly identify magmatic processes or tectonomagmatic settings that produced ancient igneous rocks. Generally, the better schemes divide groups of rocks based on sound petrogenetic argument and from a large empirical dataset derived from modern rocks that formed in well-known tectonic settings. There are a number of advantages and disadvantages to associated with using such diagrams, some of which are outlined below. The disadvantages listed here are used to negate the use of some of the many diagrams without troubling to plot them up.

<u>The main advantage of using TEDDs</u>

- Most TEDDs are quick and easy to plot and are a graphical comparison with a large, modern, empirically-derived geochemical dataset.

<u>Some of the specific disadvantages of using TEDDs</u>

- (i) The petrogenetic models which form the basis of TEDDs may be inapplicable when applied to ancient rocks (discussed in Section 1.3.1). This is particularly true for the Archaean, and factors such as different geothermal gradients or mantle composition may influence the interpretation of some TEDDs.

- (ii) Most discrimination diagrams are not strictly applicable to cumulate rocks because absolute concentrations will be affected by dilution. This should not, however, affect the relative proportions plotted on triangular diagrams (Rollinson, 1993).

- (iii) Related to (ii) above, many diagrams are highly sensitive to cumulus processes. This is particularly acute for major elements and strongly compatible trace-elements (discussed further above). Incompatible-element ratios, by comparison, may not change appreciably by fractional crystallization in the magma chamber.

- (iv) It is often not easy to analyse some of the diagnostic elements, such as Ta or Hf.

- (v) Applying discrimination diagrams to metamorphosed rocks may lead to spurious results due to element mobility. This problem is generally less acute in relatively anhydrous granulite rocks, providing there was no melting, but TEDDs that include LILE elements (*e.g.* LILE mobility is described by Rollinson & Windley, 1980a and Rudnick *et al.*, 1985) or H_2O should be avoided or treated with caution.

- (vi) Finally, TEDDs that use complex discriminant functions should be avoided. Although perhaps something of a personal prejudice, such diagrams often have 'fields' that are difficult to reproduce

and the calculations that are involved render intuitive understanding of the underlying petrogenetic mechanisms problematic.

From the list described above, it is apparent that there are several problems with applying TEDDs to ancient metamorphosed cumulates. Nevertheless, it is worth considering those discrimination diagrams that are not likely to be strongly influenced by these problems. A useful review of the TEDDs that are most commonly applied to determine the tectonic setting of basalts is provided by Rollinson (1993), and Table 1.1 is largely compiled from table 5.1 in Rollinson (1993). Those TEDDs that will not be considered further are indicated by Roman numerals and refer to the list above.

From Table 1.1 there are only 9 discrimination diagrams that have not been rejected and of those remaining only 7 trace elements are used (P, Mn, Ti, Y, Zr, Nb, La).

Table 1.1 A list of possible TEDDs, largely compiled from Rollinson (1993), that *might* be applicable to the Rauer Group and Vestfold Hills orthogneisses. The last discriminant, Nb/Y-Zr/Y is from Fitton *et al.* (in press.). The 'Reject?' column refers to discriminants not to be pursued at this stage for reasons stated in the text. All other TEDDs are references in Rollinson (1993) and are described and assessed in the text (Chapters 7 & 11).

Discriminant	**Reject?**	**Discriminant**	**Reject?**
Ti-Zr	II	Ti-V	II
Ti-Zr-Sr	III	K_2O-H_2O	IV, V
La-Y-Nb	✓	Ti-Zr-Y	✓
Cr/Y	III	Zr/Y-Zr	✓
Cr-Ce/Sr	III	Zr/Y-Ti/Y	✓
TiO_2-Y/Nb	III? ✓	Ti/Y-Nb/Y	✓
FeO-MgO-Al_2O_3	III	K_2O/Yb-Ta/Yb	IV, V
Ti-Zr-Y-Sr DF	III, VI	MnO-TiO_2-P_2O_5	✓
Zr-Nb-Y	✓	K_2O-TiO_2-P_2O_5	V
Th-Hf-Ta	IV	Nb/Y-Zr/Y	✓

1.4.4 General application of isotope analysis to metaigneous rocks

Oxygen-isotope geochemistry

The application of whole-rock oxygen isotopes to orthogneisses may potentially elucidate processes of crust formation in rocks that have remained closed to oxygen-isotope exchange since crystallization. Alternatively they may provide an insight into the nature of late- to

post-crystallization processes. Essentially, the oxygen-isotope composition of metaigneous rocks reflects three main processes:

- ***(i) Magma generation,*** with oxygen isotope signatures largely inherited from the source region, with possible minor modification by the extraction and transport process (McNaughton & Wilson, 1983; Chivas *et al.*, 1982; Fourcade *et al.*, 1994).

- ***(ii) Fractional crystallization and/or assimilation.*** In high-temperature systems the $^{18}O/^{16}O$ fractionation between minerals and melt is very small. Consequently, fractional crystallization can produce only small variations in $\delta^{18}O$. Typical increases during fractional crystallization are of the order 0.03-0.04 ‰ per % SiO_2 (*e.g.* Matsuhisha, 1979; Woodhead *et al.*, 1987; Fourcade *et al.*, 1994). In contrast, assimilation of crust (or any other reservoir) that has a significantly different oxygen-isotope composition will strongly influence the ratio of the magma.

- ***(iii) Late- to post-crystallization processes.*** Large variations in $\delta^{18}O$ can arise from late-stage hydrothermal activity associated with the final stages of pluton crystallization. Perhaps the best example is the Skaergaard intrusion, where the main complex has an isotopic range of +10 to -5 ‰ (Taylor & Forester, 1979). A similar range of isotopic values were reported for the gabbros from the Tertiary centres of Skye and Rum (Forester & Taylor, 1977; Greenwood *et al.*, 1992). Alternatively, $\delta^{18}O$ can be changed by fluid-flow a long time after crystallization either during regional metamorphism or through contact metamorphism associated with later intrusions (Valley *et al.*, 1984; Barnicoat & Cartwright, 1995, 1997).

General application of combined radiogenic isotopes

Sr and Nd isotopes are potentially useful systems for studying the geological evolution of metaigneous rocks. Both systems have long half lives (4.88×10^{10} y. for ^{87}Rb and 1.06×10^{11} y. for ^{147}Sm), and are therefore suitable for studying Precambrian rocks. Although both isotopic systems are long-lived they are complementary because they are geochemically quite different.

Sm and Nd are very similar LREE and are therefore only weakly fractionated by normal fractional crystallization processes. Generally, Sm (the parent isotope of the decay series) is the slightly more compatible element leading to progressively lower Sm/Nd in more evolved rocks. The similar ionic size and charge (Sm^{3+} = 1.04 Å, Nd^{3+} = 1.08 Å) means that it is difficult to fractionate $^{147}Sm/^{144}Nd$ during metamorphism and both elements are generally immobile under many conditions of crustal metamorphism.

By contrast, Rb and Sr are relatively different elements. Rb is a group IA LILE (Rb^{1+} = 1.48 Å) whereas Sr is a group IIA LFSE (Sr^{2+} = 1.13 Å) which has a lower ionic radius and

higher charge. Rb (the parent) is generally strongly incompatible during fractional crystallization whereas Sr is moderately incompatible except where plagioclase is a fractionating phase (K_{dSr} for Plag ~2), when it may be compatible. These differences mean that evolved rocks generally have higher Rb/Sr and that Sr is generally less mobile than Rb. Rb is known to be mobile under some (if not most) metamorphic conditions. Some of the controls on element mobility are discussed further below and in Chapters 5, 6, 7, and 11.

Rb-Sr isotopes: methodology and calculation of geochemical parameters

The analytical techniques and associated errors used to determine Sr-isotopic ratios are described in Appendix 1. The results and calculated parameters (outlined below) are included in the text in the relevant section.

Rb-Sr dating

Given a sufficient spread of Rb/Sr and providing that the system remains closed to both Rb and Sr, then the isotopic decay scheme of:

$$^{87}_{37}\mathrm{Rb} \rightarrow ^{87}_{38}\mathrm{Sr} + B^{-} \text{ (negative beta emission)} \qquad [1.1]$$

is capable of defining the crystallization age of a suite of cogenetic rocks. Since it is difficult to precisely measure the isotopic concentration in a sample, isotopic ratios are normally determined and for the Rb-Sr system the ratio of radiogenic ^{87}Sr is related to ^{86}Sr by the equation:

$$\left(\frac{^{87}\mathrm{Sr}}{^{86}\mathrm{Sr}}\right)_m = \left(\frac{^{87}\mathrm{Sr}}{^{86}\mathrm{Sr}}\right)_i + \left(\frac{^{87}\mathrm{Rb}}{^{86}\mathrm{Sr}}\right)_m \left(e^{\lambda t} - 1\right) \qquad [1.2]$$

where ***m*** denotes measured ratios, ***i*** is the initial ratio, λ is the decay constant in units of reciprocal years ($\lambda = 1.42 \times 10^{-11}\ y^{-1}$). This equation defines a straight line with an intercept corresponding to the initial Sr ratio (I_{Sr}), and where the age, ***t***, is calculated from:

$$t = \frac{1}{\lambda}\ln(m+1) \qquad [1.3]$$

Sr isotopes in petrogenesis

Since primary melting and fractional crystallization processes do not fractionate $^{87}Sr/^{86}Sr$, initial Sr ratio (I_{Sr}) is of petrogenetic importance and may provide information about source regions, assimilation-fractional crystallization (AFC) processes, or possibly subsequent metamorphic isotopic and elemental mobility. It is possible to calculate the I_{Sr} of a suite of

cogenetic rocks from the intercept on an Rb-Sr isochron diagram, or alternatively from the crystallization age as determined by independent means:

$$(I_{Sr}) = \left(\frac{^{87}Sr}{^{86}Sr}\right)_m - \left(\frac{^{87}Rb}{^{86}Sr}\right)\left(e^{\lambda.t} - 1\right) \qquad [1.4]$$

In this case, *t*, the time elapsed in years, is determined by zircon U-Pb geochronology[2].

Sr model ages and the epsilon-Sr parameter (ε_{Sr})

Given the present day $^{87}Rb/^{86}Sr$ and $^{87}Sr/^{86}Sr$, it is sometimes possible to estimate the time that such a rock could have differentiated from a hypothetical reservoir. There are a large number of assumptions involved in this approach, (see Faure, 1986), the most important being the condition of closed-system isotopic evolution and the choice of reservoir model. In common with Nd model ages (described below), such calculations are complicated by differences between models. For Sr, the problem is perhaps worse because there is disagreement regarding the present day and past values of the Bulk Silicate Earth (BSE), although there is a general consensus of the value of BSE at the time of Earth formation (see Faure, 1986). Values for BSE used in this study are after McCulloch & Black (1984) and correspond to $^{87}Sr/^{86}Sr = 0.69897$ at 4.6 Ga as derived from the *Basaltic Achondrite Best Estimate* (BABI).

Despite the assumptions and uncertainties, initial $^{87}Sr/^{86}Sr$ can be compared relative to a time-integrated BSE uniform reservoir to yield a model age by:

$$t = \frac{1}{\lambda} \ln \frac{\left(\frac{^{87}Sr}{^{86}Sr}\right)_m - \left(\frac{^{87}Sr}{^{86}Sr}\right)_{BSE}}{\left(\frac{^{87}Rb}{^{86}Sr}\right)_m - \left(\frac{^{87}Rb}{^{86}Sr}\right)_{BSE}} \qquad [1.5]$$

Similarly, the I_{Sr} calculated for the time of crystallization according to [1.5] can be compared with a time integrated $^{87}Sr/^{86}Sr$ reservoir model ages and, to be consistent with the epsilon notation used for Nd (ε_{Nd} described below), epsilon Sr (ε_{Sr}) is defined by:

---

[2]U-Pb zircon ages are used because there is greater precision and accuracy than conventional isochron techniques, and because apparent ages from isochrons, pseudoisochrons or errorchrons can be older or younger than the crystallization age given certain circumstances (discussed further in Chapter 6).

$$\varepsilon_{Sr} = \left[\frac{\left(\frac{^{87}Sr}{^{86}Sr}\right)_i}{\left(\frac{^{87}Sr}{^{86}Sr}\right)_{BSE}} - 1 \right] \times 10^4 \qquad [1.6]$$

Sm-Nd dating

The method of Sm-Nd dating is similar to that described for Rb-Sr (above), except that Equations 1.1 and 1.2 become (respectively):

$$^{147}_{62}Sm \rightarrow ^{143}_{60}Nd + \alpha \text{ (alpha decay)} \qquad [1.7]$$

$$\left(\frac{^{143}Nd}{^{144}Nd}\right)_m = \left(\frac{^{143}Nd}{^{144}Nd}\right)_i + \left(\frac{^{147}Sm}{^{144}Nd}\right)_m \left(e^{\lambda.t} - 1\right) \qquad [1.8]$$

The Sm-Nd isochron age is calculated as for [1.3], where the half life, λ, is 6.54×10^{-12} y^{-1}.

Nd isotopes in petrogenesis

As with Sr isotopes, Nd-isotope ratios are not normally fractionated by partial melting or fractional crystallization, and initial Nd ratios may yield important information about source regions and AFC processes. Initial $^{143}Nd/^{144}Nd$ can be defined directly from the intercept on an isochron diagram, but are more accurately defined by the method of Fletcher & Rosman (1983). In common with Sr isotopes (described above), it is also possible to calculate the initial $^{143}Nd/^{144}Nd$ relative to the crystallization age of the suite, as determined by more accurate means, by the equation:

$$(I_{Nd}) = \left(\frac{^{143}Nd}{^{144}Nd}\right)_m - \left(\frac{^{147}Sm}{^{144}Nd}\right)\left(e^{\lambda.t} - 1\right) \qquad [1.9]$$

Nd model ages and the epsilon-Nd parameter (ε_{Nd})

For Nd isotopes, two model reservoirs are commonly quoted. $^{143}Nd/^{144}Nd$ are usually compared relative to a Chondritic Uniform Reservoir (CHUR) model, and ε_{Nd} is defined by:

$$\varepsilon_{Nd} = \left[\frac{\left(\frac{^{143}Nd}{^{144}Nd}\right)_i}{\left(\frac{^{143}Nd}{^{144}Nd}\right)_{CHUR}} - 1 \right] \times 10^4 \qquad [1.10]$$

CHUR parameters used in this study are taken as $^{147}Sm/^{144}Nd = 0.1967$ and $^{143}Nd/^{144}Nd = 0.512638$ for the present day (Jacobsen & Wasserberg, 1980; Goldstein *et al.*, 1984), and reflect normalization of $^{146}Nd/^{144}Nd = 0.7219$ (see Faure, 1986). The second most commonly described reservoir is 'depleted mantle' (DM), which can be compared directly with CHUR through the epsilon notation [1.10]. The present value of DM is ~ +10 epsilon units. Although estimates for time-integrated DM evolution vary widely (see review in Rollinson, 1993), the preferred model in this study assumes a linear reservoir evolution since core-mantle differentiation, and is defined by a present-day DM that has $^{147}Sm/^{144}Nd = 0.2137$ and $^{143}Nd/^{144}Nd = 0.51315$ (Peucat *et al.*, 1988).

As described above for Sr model ages, Nd model ages can be calculated relative to either CHUR or DM, and are defined by:

$$t = \frac{1}{\lambda} \ln \frac{\left(\frac{^{143}Nd}{^{144}Nd}\right)_m - \left(\frac{^{143}Nd}{^{144}Nd}\right)_{CHUR}}{\left(\frac{^{147}Sm}{^{144}Nd}\right)_m - \left(\frac{^{147}Sm}{^{144}Nd}\right)_{CHUR}} \qquad [1.11]$$

In Chapter 6, time-dependent perturbation of the Nd-isotope system is discussed at considerable length. Forward and backward calculations utilize the observation that ^{147}Sm decay to ^{143}Nd only results in a trivial change to $^{147}Sm/^{144}Nd$, and $^{147}Sm/^{144}Nd$ is treated as being constant unless modified directly by Sm or Nd mobility. Forward modelling calculations can be derived by re-arranging [Equation 1.9].

1.4.5 The geochemical and isotopic effects of weathering and metamorphism

The effects of weathering

Most basement rocks in the Rauer Group and Vestfold Hills are extremely fresh. Erosion rates are relatively fast, with isostatic rebound and strong winds culminating in aeolian transport of weathered material from the near-icecap environment into the southern ocean. Therefore weathering profiles are often shallow. Nevertheless, there are regional variations. In the western Vestfold Hills and in depressions in the Rauer Group, salt weathering has had a marked effect on the landscape, and weathered rock can extend down to several cm. Ultramafic-mafic compositions are particularly prone to weathering in such areas, and many such outcrops are not suitable for geochemical studies.

Loss on ignition (LOI) is often quoted as a crude index of weathering (*e.g.* Davidson & Harmon, 1989; Chen *et al.*, 1990; Fourcade *et al.*, 1994[3]), and values for basalts are commonly of the order 1-2 wt.% LOI. Values for samples discussed in this study are *all* <1 % LOI, and most are <0.5% LOI, indicating that most are extremely fresh. Therefore, the effects of weathering are not considered further in this study.

The geochemical and isotopic effects of metamorphism and deformation

Open-system geochemical and isotopic exchange during high-grade metamorphism or granulite-amphibolite retrogression is a subject of considerable debate (*e.g.* McNaughton & Wilson, 1983; Longstaffe & Schwarcz, 1977; Rollinson & Windley, 1980a & b; Rollinson, 1983, 1987, 1996; Rudnick *et al.*, 1985; Stahle, 1987; Ague, 1991; Cohen *et al.*, 1991; Burton *et al.*, 1994; Fowler *et al.*, 1995; Barnicoat & Cartwright, 1997; and many others).

In these studies, a number of criteria have been applied to assess the extent of mobility, the most common of which are:

- ***Textural and structural evidence for low strain and isochemical metamorphism.*** In common with other studies (*e.g.* Rollinson, 1987; Luais & Hawkesworth, 1994), samples selected in this study are from areas where late deformation and migmatisation have had minimal effect. Most of the suites examined in detail in this study retain abundant evidence of their igneous parentage (*e.g.* primary minerals, textures, and graded layering). Such suites were chosen in the belief that the main geochemical trends are most likely to be primary in these areas. However, these primary features and the assumption of isochemical metamorphism are described and assessed further throughout the text.

- ***Correlation between immobile elements.*** One approach is select elements that are known to be relatively immobile during metamorphism and fluid transport (*cf.* Rollinson, 1987; Kim & Jacobi, 1996). A suite of cogenetic samples *may* be expected to show coherent trends on major- and trace-element variation diagrams, whereas such trends may be disrupted in the event of element mobility (*cf.* Rollinson, 1987, p. 346). A similar qualitative approach has been adopted in this study. However, there are significant problems with this approach which include: (i) decoupled behaviour between major- or compatible elements and incompatible elements (see above, Section 1.4.2, and *cf.* Kim & Jacobi, 1996); (ii) elements that have been mobilized may be related during the mobilization event (*e.g.* K & Rb or the REE, *cf.* Patchett, 1993).

---

[3]Fourcade *et al.* (1993) and others have noted the importance of weathering on geochemistry. In particular they noted that ultramafic-mafic compositions weather more than felsic rocks. They found a very strong correlation between LOI, Mg and $\delta^{18}O$, with compositions that have LOI > ~1% being adversely affected. They suggested a weathering correction for such rocks. This has not been applied in this study, because all analysed rocks have LOI < 1%.

- ***Alteration indices.*** Complex 'alteration indices' (*e.g.* Hashiguchi *et al.*, 1983) have not been applied in this study because it is often difficult to ascertain how such indices vary by crystal fractionation/accumulation processes, or even how they elucidate which elements have been mobile.

The approaches adopted to distinguish open-system exchange for isotopes are variable. Modern interpretations of Sr isotopes in high-grade terranes have tended to conclude that at least some disturbance has occurred. This is either evident as a scatter on isochron diagrams, or because model ages are highly variable. Nd isotopes, by contrast, are generally regarded as being immobile under most conditions of metamorphism, except during migmatisation. The degree of correlation (MSWD, see Appendix 1 for definition) on an isochron diagram is commonly cited as evidence for or against open-systems mobility. MSWDs greater than about 1 or 2 are often considered suspect, although some authors attach geochronological significance to suites that have values significantly higher (*e.g.* Stern & Hanson, 1993, MSWD = 1.8; Vrevsky *et al.*, 1996 MSWD = 3.6; Collerson *et al.*, 1983, MSWDs = 1.9 - 83.8), and for suites that have a limited range of Sm/Nd (see also Appendix 1). These approaches are assessed at length in Chapters 6 and 13.

General methodology adopted in this study

The geochemical approach adopted in this study has been primarily designed to elucidate protolith-forming processes, and in common with most studies in high-grade terranes, the aforementioned geochemical criteria have been applied to exclude metasomatically altered samples or groups of mobile elements. For the isotopes, a 'look-and-see' approach has been adopted. This study provides the first conventional isotopic investigation in the region that is independently constrained from field relations and U-Pb zircon geochronology, therefore breadth of coverage was considered more important than a very detailed study of any particular unit. This approach is addressed at various stages throughout the study and is critically assessed in the *Conclusions* (Chapter 13).

Wherever possible, cogenetic samples were chosen to represent the full compositional range within a given suite. In the field, low-strain rocks were chosen for geochemistry or geochronology to avoid possible inclusion of tectonic mixtures, and also because such rocks are less foliated, have better preserved primary features, and are the least altered (both metamorphically and through weathering). Later, the choice of samples was further refined on the basis of petrographic and geochemical character. Criteria for excluding samples for detailed analysis (on the grounds that they may be altered through metamorphism or weathering) included extensive retrograde-mineral development, or geochemical outliers

that are markedly different from other samples in the suite for no obvious petrogenetic reason (*i.e.* 'fliers'). However, it is significant that such 'fliers' are rare.

1.5 Study structure and thesis layout

The structure of the research undertaken during the course of this study was largely determined by *specific objectives* that are detailed in the Chapter 2 for the Rauer Group and Chapter 8 for the Vestfold Hills. Rather than artificially group the various areas of research by techniques, such as field relations or geochemistry, the Rauer Group and the Vestfold Hills are treated as separate studies to a large extent. This is partly because a different emphasis was appropriate in each terrane. The overall layout of the thesis reflects this, and it has been separated into four parts.

Part One comprises this chapter, which was written to provide an overview of the wider context to the study and an outline of the some of the approaches that have been taken.

Part Two details work undertaken in the Rauer Group, and comprises six chapters (Chapters 2-7) which are divided into *geological outline*, *field relations*, *petrography*, *geochemistry*, and *isotopes*, with a *synthesis* chapter at the end that provides a discussion of the origin and evolution of the Rauer Group Archaean domain. Part Two focuses on minor sub-areas in the Rauer Group and is biased towards geochemistry and isotopes because background geology is reasonably well established (see Chapter 2 and Harley, 1987) and because this study presents the first detailed geochemical investigation of the Rauer Group.

Part Three documents work undertaken in the Vestfold Hills. It has a similar format to Part Two, and comprises 5 chapters (8-12) which have been divided into *geological outline*, *field relations*, *U-Pb- zircon geochronology*, *geochemistry and isotopes*, and a *final synthesis* chapter that discusses and summarises the advances that have been made in the Vestfold Hills. Compared with Part Two, less emphasis is placed on the geochemistry and isotopes because their interpretation of the data is relatively straightforward. More emphasis is placed on the field relations which reflects the much greater time needed to regionally map the northern Vestfold Hills.

The final part of the thesis, **Part Four**, comprises one chapter which provides a discussion and summary of parts two and three in a wider context, and relates back to the background that has been established in this chapter.

Part 2:

The Rauer Group

Chapter 2

Geological outline of the Rauer Group

2.1 Introduction and synopsis of Part 2: The Rauer Group

In this chapter I briefly review previous work in the Rauer Group to provide a background to the research rationale and objectives in this terrane. Emphasis is placed on published accounts of the Archaean lithologies, since the overall aim of my work in the Rauer Group is to document the early event history and understand the tectonomagmatic processes involved in Archaean crust-formation. By using a process-oriented approach the objective is to ascertain if the ancient domains in the Rauer Group are essentially reworked Vestfold Hills-type crust, or whether they are unrelated Archaean suites.

The overall structure of **Part 2: The Rauer Group**, reflects the objectives and methodology adopted in this terrane; these are outlined at the end of this chapter (Section 2.7.3). The following chapter (Chapter 3), provides a description and discussion of new field observations made during the 1992/93 and 1993/94 field seasons. These observations are augmented by a detailed petrological and mineral chemical study (Chapter 4), and taken together this information provides a comprehensive geological framework from which to interpret geochemical and isotopic data, presented in the following chapters (Chapters 5-7). The final chapter in the Rauer Group section, Chapter 7, discusses and concludes what is now known about Archaean crust-formation in the Rauer Group.

2.2 General outline and previous work

The Rauer Group comprises 10 major and numerous smaller islands or promontories on the Prydz Bay coast totalling approximately 300 km^2 in area (see Figure 2.1). The group is situated 15 km south of the Vestfold Hills, separated by the Sϕrsdal Glacier, and lies 40 km north from the Brattstrand Bluffs and Svenner Islands, separated by sea or seasonal ice.

The first comprehensive account of the geological evolution of the Rauer Group was by Harley (1987), who described and defined the main lithological units and established a generally accepted deformational sequence and metamorphic framework. Subsequent work has essentially refined, modified and expanded this scheme (*e.g.* Harley & Fitzsimons,

1991; Kinny *et al.*, 1993; Sims *et al.*, 1994), demonstrating that this part of the East Antarctic Precambrian shield preserves a complicated and lengthy magmatic, deformational and metamorphic history.

Geological relationships and geochronology indicate that the Rauer Group is a composite terrain comprising Archaean protoliths structurally interleaved on a local scale with younger mid-Proterozoic crustal additions (Sheraton *et al.*, 1984; Kinny *et al.*, 1994). The Archaean gneisses record a polymetamorphic history, preserving evidence for at least two major peaks of granulite facies metamorphism that both appear to have terminated in near-isothermal decompression *P-T* paths (Harley, 1987, 1988; Harley & Fitzsimons, 1991). In contrast, rocks of Mid Proterozoic age are thought to mainly reflect deformation and granulite facies metamorphism in a major event at *ca.* 1000 Ma (Harley, 1987; Harley & Fitzsimons, 1991; Kinny *et al.*, 1993). In addition to Archaean and Proterozoic high-grade metamorphic and deformational episodes, the Rauer Group also records the effects of a later tectonothermal event at *ca.* 500 Ma. This later event is generally considered to have been the first major rehydration of the terrane, resulting in local isotopic resetting and an upper greenschist facies overprint (Harley, 1987; Kinny *et al.*, 1993; Harley & Fitzsimons, 1995; Harley, Snape & Fitzsimons, 1995). However, there is current debate as to whether events at *ca.* 500 Ma also progressed at high-grade, with the greenschist overprint being only a late expression of this event (*e.g.* Ren *et al.*, 1992; Henson & Zhou, 1995). The nature of the *ca.* 500 Ma event in the Rauer Group is important because it has implications for regional and global correlations and because it influences the interpretation of metamorphic *P-T-t* paths in this terrane. This debate will be considered further in the discussion sections (Chapters 7 & 13).

2.3 Lithology types: spatial and temporal distribution

Rauer Group lithologies are both temporally and compositionally diverse (*cf.* Harley, 1987, Harley *et al.*, 1992), but have been subdivided into four broad associations (Figure 2.1) by Harley & Fitzsimons (1991), comprising:

- ***Association 1.*** Young granitic to dioritic orthogneisses, sometimes preserving igneous features, that were emplaced near to 1000 Ma (Kinny *et al.*, 1993).

- ***Association 2.*** Layered paragneisses, comprising Fe-rich pelites and semipelites, quartzites, leucogneiss, impure calc-silicates and minor mafic granulite.

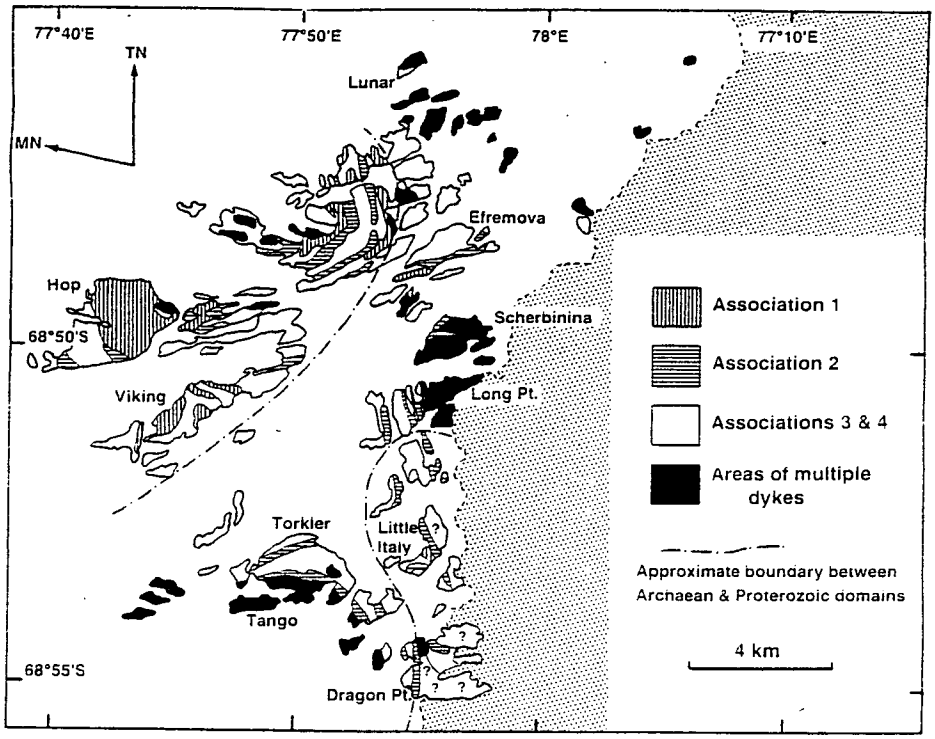

Figure 2.1 Lithological distribution of gneiss associations in the Rauer Group (after Harley & Fitzsimons, 1991). Areas of multiple dykes also correspond to Associations 3 & 4. Note also that the age boundary is highly schematic.

- ***Association 3.*** Homogeneous orthogneiss of granitic to tonalitic composition, some of which may have Archaean protolith ages.

- ***Association 4.*** Composite Layered Orthogneisses (CLO) of predominantly felsic and mafic granulite of *probable* Archaean age. The CLO often containing migmatitic features and early foliations, and are commonly associated with marbles and metapelite lenses.

In addition, Harley and co-workers (*e.g.* Harley *et al.*, 1992; Harley & Fitzsimons, 1995; Harley *et al.*, 1995) noted that relict layered mafic-ultramafic complexes occur with the oldest associations (Associations 3 & 4) and that these associations are dissected by multiple mafic dyke suites. The younger lithologies (Associations 1 & 2) contain less mafic dykes than the Archaean rocks which commonly have 6 or more generations. In general, dykes appear to be most abundant in the NE Rauer Group where they locally constitute up to 60 % of the outcrop on some islands (*e.g.* Dyke and Neptune Islands; see also Sims *et al.*, 1994).

2.3.1 Archaean lithologies in detail

Rocks of Archaean age occur predominantly on islands and promontories on the eastern side of the Rauer Group, where they are often structurally interleaved with younger lithologies. Sheraton *et al.* (1984) and Harley (1987) originally estimated the amount of Archaean crust to be relatively minor (~10 %), although rocks of this age are now thought to constitute as much as 50 % (Kinny *et al.*, 1993; Harley & Fitzsimons, 1991; Harley, Snape & Fitzsimons, 1995). The detailed account presented below describes rock-types or associations that are thought to be part of the Archaean domain based largely on structural and geological criteria. Despite a limited number of geochronology sites there is also spatial correlation between the field-defined Archaean domain and the chronology sites of Sheraton *et al.* (1984) and Kinny *et al.* (1993).

Although Harley & Fitzsimons (1991) divided the Archaean domain into two groups of lithological associations (Associations 3 & 4) further distinctions are made here for the purposes of discussion in later sections. It is useful to divide the Archaean domain into four main groups of lithologies comprising:

- ***Composite Layered Orthogneiss (CLO),*** corresponding to Association 4 of Harley & Fitzsimons (1991).

- ***Homogeneous Felsic Orthogneiss,*** corresponding to Association 3 of Harley & Fitzsimons (1991).

- ***Paragneiss sequences.*** There are two chemically distinct paragneiss sequences, the Fe-rich Torckler Paragneiss[1] and the Mg-rich Mather Paragneiss.

- ***Layered meta-igneous complexes.*** There are two distinct layered complexes, the fine-grained, generally granular, Torckler-Tango Layered Complex (TTLC), and the coarse-grained Scherbinina Layered Complex (SLC).

The Composite Layered Orthogneiss (CLO)

CLO is the most abundant rock type or lithological association. It comprises interlayered felsic and mafic protoliths and essentially equates to the well-layered variants of the orthopyroxene-quartz-feldspar and garnet-quartz-feldspar gneisses of Sheraton & Collerson (1983). It is also broadly similar in composition to the Archaean Mossel Gneiss in the

[1] Renamed according to the recommendations of Ricci *et al.* (1993).

adjacent Vestfold Hills terrane (Sheraton & Collerson, 1983; 1984). Harley (1987) described the CLO as being well layered on 10-cm to 2-m scales and as being locally migmatitic (*cf.* Harley, 1987, figures 2a & 2b) with discordant leucosomes preserved in low-strain areas. Such lithological and structural heterogeneity led Harley (1987, p.178-179) to sub-divide the CLO into 3 components:

- ***(i) a mafic component***, comprising 10-40 % CLO locally, occurring as lenses, boudins, layers or irregular schlieren of mafic granulite containing two pyroxenes, plagioclase, ilmenite ± hornblende. These mafic layers retain an internal foliation that is sometimes cross-cut by fine-scale felsic veinlets. Such veinlets feed into or coalesce with larger felsic layers, corresponding to component (ii) below.

- ***(ii) a felsic- to intermediate- gneiss component*** of broadly granodioritic to tonalitic composition comprising 5-10 % orthopyroxene, 40 % plagioclase, 5-20 % quartz, 5 % biotite and sometimes garnet (<5 %) and alkali feldspar ± ilmenite, apatite, zircon and monazite. These layers preserve a moderate foliation and layering defined by orthopyroxene- (± garnet) rich layers. This sublithology is closely associated with the mafic component (i). This relationship, in conjunction with diffuse margins and the fine-scale veining, is taken to indicate derivation of the felsic compositions by partial melting of the enclosed mafics (at least in part).

- ***(iii) a leucocratic garnet absent quartzo-feldspathic component.*** These components occur as layers that are coarse-grained and sometimes discordant to components (i) and (ii) (*cf.* Harley 1987, figure 2b), although they often have a weak biotite foliation.

All sublithologies within the CLO have been folded by relatively late open to close folds (F_4 of Harley, 1987; Section 2.4 below) which locally produced an axial-planar biotite foliation that is usually markedly discordant to earlier layering and to foliations. The early foliation is best preserved in component (ii) although mafic layers preserve traces of even older structures that were refolded prior to formation of the compositional layering and foliation in the CLO.

Homogeneous Felsic Orthogneiss

This lithology is abundant throughout the central and southern Rauer Group where it is interlayered with older and younger gneisses. Intrusive contacts with the CLO, SLC and the TTLC have been observed (see Sections 2.2 & 2.3.3) although the distinction between the homogeneous felsic components in the CLO is often difficult to determine where highly strained (*cf.* Harley, 1987). Since there has been little precise dating and because a number of probably separate suites are similar in appearance, the Homogeneous Felsic Orthogneisses are divided into two broad groups:

- ***(i) Tonalitic Gneiss (TG).*** The most abundant lithology comprises orthopyroxene and/or clinopyroxene granites (*s.l.*) with tonalite being the dominant composition overall. This suite is observed to intrude CLO, SLC and TTLC and is therefore an important intrusive chronological marker. In their geochronology study, Kinny *et al.* (1993) correlated two examples of this suite, from Torckler Island and Short Point (see Harley, Snape & Black, in press, figure 2, for locations), on the basis of petrography, age (*ca.* 2800 Ma, described further in Section 2.6) and chemical composition[2]. Field relations and petrographic details of this suite are presented in Chapters 3 & 4, with geochemical, isotopic and petrogenetic information considered in the following chapters (Chapters 5-7).

- ***(ii) Dragon Point Orthogneiss (age unknown).*** Corresponding to the KOG suite of Harley (1987) the Dragon Point orthogneiss is abundant on Dragon Point and also crops out in a belt from Babe Ruth Island to Long Point. The age of this suite is unknown at present and for this reason these gneisses were not incorporated into the scheme of Harley & Fitzsimons (1991) outlined above, but were described separately as the Dragon Point orthogneiss (Harley *et al.*, 1992). Nevertheless, since this suite contains a number of refolded fabrics, and has abundant (deformed) mafic dykes, the Dragon Point Orthogneiss may be Archaean in age, hence a brief description is included here.

  Typical mineralogy comprises K-feldspar-quartz-orthopyroxene-plagioclase-biotite-ilmenite with garnet present locally. Plagioclase is usually more abundant than K-feldspar, therefore these rocks can be described as enderbites (hypersthene tonalites). Aggregates of ferromagnesian phases define a foliation which is axial planar to tight upright folds. These features were subsequently refolded into open flexures by late deformation (see Section 2.4 below).

Archaean paragneisses

Within Associations 3 and 4 of Harley & Fitzsimons (1991) are relatively minor metasediments. These comprise Fe-rich psammites and pelites (Torckler Island Paragneiss), calc-silicates and marbles, and rare high-Mg pelites (Mather Paragneiss). Although these compositions provide important metamorphic and geochronologic information (referred to in later sections) they are of limited use geochemically and are not thought to have been involved in orthogneiss protolith petrogenesis (see Chapters 5-7), hence they are not described in detail here.

---

[2]Kinny *et al.* (1993) dated a second sample from Short Point that is petrographically and chemically similar to the TG above, but they found this sample to be much older (3269 ± 9 Ma). Although this probably corresponds to one of the components of the CLO (outlined above), similarities with the younger suites make any rigorous distinction difficult to apply, hence the rather general scheme presented here.

Layered metaigneous complexes

The presence of metaigneous layered complexes in the Rauer Group, as distinct from mafic components within layered mafic and felsic gneiss, was first noted by Harley (1987). Two relict igneous intrusions can be distinguished, the Scherbinina and Torckler-Tango Layered Complexes (SLC and TTLC, respectively).

- ***The SLC*** occurs in the NE Rauer Group. The main outcrop occurs on a *ca.* 250 x 500 m peninsula on the eastern margin of Scherbinina Island, although minor boudins and strongly deformed layers occur elsewhere on Scherbinina Island, and on Long and Short Points. The SLC is distinguished from the TTLC primarily on the basis of mineralogy and texture. It comprises an assemblage of clinopyroxene - orthopyroxene - plagioclase - Fe-Ti oxide ± hornblende ± biotite and, although recrystallized at mineral scales, retains a coarse-grained intergranular to subophitic texture.

- ***The TTLC*** occurs in the SW Rauer Group and crops out as a series of elongate mega-boudins (20 - 150 m long) traceable over a strike length of 7 km from Babe Ruth Island, through Torckler and Tango Islands, to D.H. Green Isle. The complex retains a number of igneous features, including graded modal layering and bronzite phenocrysts. In general, however, the complex has been pervasively recrystallized to clinopyroxene-orthopyroxene-plagioclase granulite with a medium-grained granoblastic to lobate textures.

The only published accounts of these complexes are by Harley and co-workers (Harley, 1987; Harley & Fitzsimons, 1991; 1995; Harley *et al.*, 1992) who essentially noted their occurrence and distribution. There are no published chemical or mineralogical analyses. One of the objectives of this study is to document the field relations and geochemistry of these intrusions in detail in order to constrain protolith petrogenesis and their subsequent evolution. A comprehensive account of the field relations, petrography and geochemistry of the TTLC and SLC is presented in the following five chapters (Chapters 3-5).

2.3.2 Geochemical characteristics of Archaean orthogneisses

A brief review of published geochemical data for Archaean orthogneisses from the Rauer Group is presented here, since previous work is integrated into this study in later sections. The published geochemical database for the Archaean domain is small: there are only analyses for 13 samples, for which there are whole-rock, trace- element and/or REE-data.

The Sheraton et al. (1984) dataset

This dataset comprises two samples for which there are Nd- and Sr-isotope data. On the basis of Archaean Nd model ages (Section 2.6) I have retained these two analyses in the combined dataset compiled here (Table 2.1). Sheraton *et al.* (1984) also included two

'average' analyses from a total of 18 samples that they consider to be Archaean. The justification for assigning these gneisses to the Archaean domain is not stated, therefore, in the absence of isotopic data, and in view of the geological complexity outlined in the previous section (Section 2.3.1), these analyses will not be considered further.

Table 2.1 A compilation of published whole-rock geochemistry for Archaean orthogneisses from the Rauer Group. These samples are thought to be representative of >2800 Ma Archaean Felsic crust in the Rauer Group. Sample no. 81285120 was dated at 3269 ± 9 Ma by Kinny *et al.* (1993).

sample number:	81285120	81285143
SiO_2	74.10	69.80
TiO_2	0.51	0.80
Al_2O_3	12.05	13.02
Fe_2O_3	1.06	2.00
FeO	1.21	2.28
Mn	0.05	0.08
MgO	0.54	0.68
CaO	1.49	1.73
Na_2O	3.56	3.65
K_2O	5.14	5.00
P_2O_5	0.10	0.15
H_2O+	0.48	0.34
H_2O-		
CO_2		
rest	0.20	0.27
Total	100.49	99.80

	81285120	81285143
Ba	746	950
Li	4	5
Rb	140	125
Sr	86	80
Pb	7	12
Th	2	9
U	0.5	0.5
Zr	375	529
Nb	17	22
Y	45	63
La	43	70
Ce	72	121
Nd	38	59
Sc	3	5
V	12	20
Cr	6	15
Ni	6	7
Cu	11	18
Zn	23	71
Ga	13	15
As	0.5	0.5
Be	2	3

Note: all AGSO numbers in this study from this point forward are prefixed by #, *e.g.* 81285120 = #5120 and 81285143 = #5143.

The Harley et al. (1992) dataset

This is the largest (reliable) geochemical dataset for the Rauer Group, comprising 9 whole-rock major-element and trace-element and REE analyses for granitic orthogneisses from the Archaean domain. All are I-type granites in the classification of Chappell & White (1974) and Chappell (1977), and are typically metaluminous with molecular A/CNK ratios ($Al_2O_3/CaO+Na_2O+K_2O$) < 1.1 (Harley *et al.*, 1992). Silica variation diagrams for these 9 samples have a considerable scatter for most elements (diagrams not included here). With increasing SiO_2 there are broad linear trends of decreasing Al_2O_3, MgO and CaO, and increasing Na_2O and K_2O, but there is a wide scatter for most trace elements, especially Y, Rb, Sr, Nb and Zr. Nevertheless, on the basis of variations in REE abundances from 9 samples, Harley *et al.* (1992) distinguished 3 geochemical groups (Figure 2.2):

- ***Group 1: Depleted and fractionated.*** On the basis of mineral abundance and bulk rock composition this group comprises trondhjemites, tonalites and granites (TTG). REE patterns are steeply inclined with strong HREE depletion and a strong positive Eu anomaly. Ce/Yb_N (Ce/Y normalised to Chondrite) are high (~36), with correspondingly high K/Rb (up to 2500) and Ti/Y.

- ***Group 2: Undepleted and unfractionated tonalites.*** This suite correlates with homogeneous granitic components within the CLO (?) outlined above and is characterized by high REE abundances with a relatively flat profile, low Ce/Yb_N (~5), K/Rb and Ti/Y, and no Eu anomaly.

- ***Group 3: Undepleted and fractionated.*** These are charnockitic (?) to A-type granites that correspond to or include the Dragon Point orthogneiss (?). REE are undepleted, with high HREE abundances (~10 x Chondrite), and are strongly fractionated as represented by high Ce/Yb_N (~35).

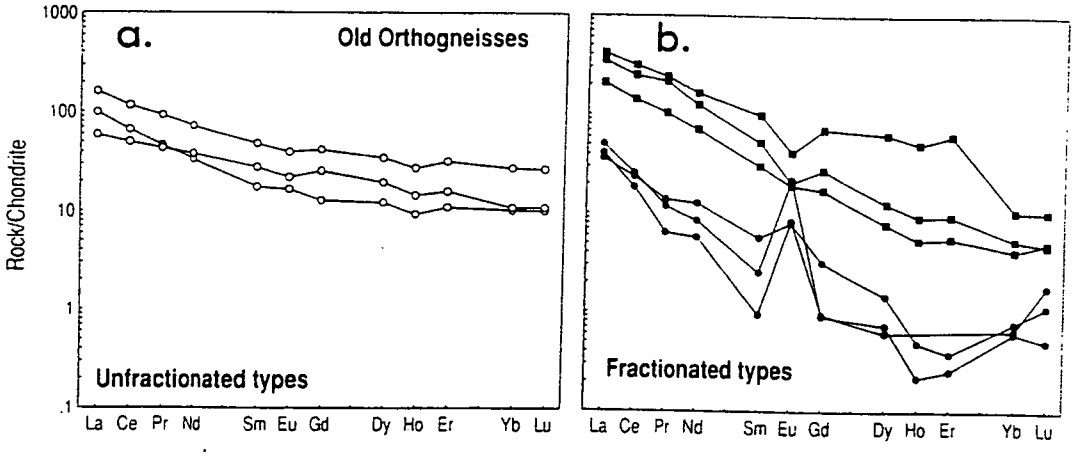

Figure 2.2 Chondrite normalised REE patterns for Archaean felsic orthogneisses from the Rauer Group. Group 1 are depleted and fractionated; Group 2 are undepleted and unfractionated; Group 3 are undepleted and fractionated (after Harley *et al.*, 1992).

The Kinny et al. (1993) dataset

In the course of their zircon geochronology study, Kinny *et al.* (1993) presented whole-rock major-element and trace-element data for an additional two Archaean felsic orthogneiss samples. Both are homogeneous orthopyroxene-bearing granitic gneisses. One is from Torckler Island and the other is from Short Point. In addition they also dated a sample from the Sheraton *et al.* (1984) dataset that has Archaean Nd model ages (see Section 2.6). Since these three samples are the only ones that have precisely constrained U-Pb zircon ages they are the most useful. Further reference to these samples will be made in later sections with respect to constraining the geological history of the Archaean domain (Chapters 3-6) and in terms of orthogneiss petrogenesis (Chapters 5-7).

Geochemical synopsis

In a preliminary appraisal of the Archaean orthogneiss geochemistry, Harley *et al.* (1992) suggested that the depleted, highly-fractionated orthogneisses (Group 1) reflect an origin through high-pressure hydrous melting of a garnet- ± amphibole-bearing source. The relatively high abundances of REE in Groups 2 & 3, by comparison, were considered to have originated from dry melting of felsic to intermediate granulite crust, with fractionation of plagioclase responsible for intrasuite variation (Harley *et al.*, 1992). However, from the limited number of geochemical analyses it is not possible to conclude with any certainty if the groups defined either on the basis of field observations (Section 3.3.1) or on geochemical grounds are related to each other in age or petrogenetic origin. It is clear though that Archaean felsic orthogneisses preserve a diversity of protolith signatures that were produced by a variety of magmatic processes. The nature of magma petrogenesis is considered further in later sections (Chapters 5-7) and ultimately an attempt is made to integrate the data from the various datasets into an evolving tectonomagmatic framework for the Archaean Rauer Group (Chapter 7).

2.4 Structure

Lithological divisions are largely based on a combination of distinctive association or composition and according to relative age as defined by cross-cutting structural relationships. Harley (1987) noted five major deformation events (D_1-D_5) which are of regional extent, and it this scheme that provides the structural framework to the outline presented below.

2.4.1 The structural scheme of Harley (1987)

The earliest structural and fabric relationships (D_1 & D_2) are preserved as relict features in mafic and paragneiss rafts within Proterozoic felsic orthogneisses. These comprise layer-parallel S_1 fabrics in mafic granulite, a later hornblende-defined S_2 fabric, and rare close to isoclinal folds (F_2). These features were all truncated and refolded by D_3, resulting in close to isoclinal major folds. This D_3 event was considered by Harley (1987) to be the main folding event responsible for inter-layering felsic orthogneiss with older mafic granulite, paragneiss and Composite Layered Gneisses. Further high-grade deformation (D_4) reoriented earlier structures, producing steeply SE plunging open to close folds (F_4). This deformation event produced macroscopic layering of E-W orientation with steep southward dips in the north and west outcrops, but with a dominantly northerly strike dipping east and west in coastal outcrops. In contrast to the pervasive ductile early deformations (D_1-D_4), the

final regional event (D_5) is associated with localized fluid infiltration characterized by steeply-dipping shear zones, pegmatite emplacement, and a spatially limited upper greenschist facies overprint (Harley, 1987).

2.4.2 An expanded structural scheme for the Rauer Group

Since the first detailed account of the structural evolution of the Rauer Group (Harley, 1987), Harley and co-workers (*e.g.* Harley & Fitzsimons, 1991; Harley *et al.*, 1992; 1995) and Sims *et al.* (1994) have recognised that the event termed D_3 probably includes a number of discrete and temporally unrelated deformations, and that S_3 is probably a combination of sub-concordant, strongly transposed foliations that both pre-date and post-date the intrusion of multiple generations of mafic dyke suites. Sims *et al.* (1994) expand upon the Harley (1987) scheme in detail, concentrating on the development of gneissic layering relative to dyke emplacement in the northern Rauer Group. Their relative chronology of events has been correlated with previous work and integrated with the available geochronology in the *Conclusions* section of this study (Table 13.1, see also Section 2.6). The geological history presented here has been condensed and describes only events, or deformation episodes, that are of regional significance. For example, dykes 12-14 and deformations D_6-D_8 of Sims *et al.* (1994) are all tentatively regarded as features associated with the *ca.* 1000 Ma event, whilst Pegmatite 4, the brittle-ductile shearing and the retrograde overprint (D_9-D_{11}, Sims *et al.*, 1994) will be referred to (also tentatively) as belonging to the *ca.* 500 Ma, or Pan African, event.

A summary of the Archaean to early Palaeozoic geological evolution is presented in Table 13.1 (Chapter 13) to allow discussion of the timing of terrane juxtaposition between the Rauer Group and Vestfold Hills (*e.g.* Collerson *et al.*, 1983; Sims *et al.*, 1993), but is not repeated in this section. Aspects of the event sequence and the significance of the *ca.* 500 and 1000 Ma events are referred to in more detail in the next chapter (Chapter 3) where geological evolution of the Scherbinina Layered Complex is described, and in the conclusion sections (Chapter 13) when discussing proposed terrane correlations between the Rauer Group and the Vestfold Hills.

2.5 *P-T-t* evolution and evidence for polymetamorphism

The metamorphic evolution of the Rauer Group is demonstrably long and polycyclic in character but, in common with many high-grade terrains, only fragments of this history are preserved. At least two unrelated granulite facies peak events are inferred for the Archaean

and Neoproterozoic (Figure 2.3, Harley, 1987; Harley & Fitzsimons, 1991; Harley *et al.*, 1992).

Metamorphic conditions during the *ca.* 1000 Ma event are best recorded by younger lithologies (< 1400 Ma, Sheraton *et al.*, 1984) which bear no record of the Archaean events in the Rauer Group; these include the Fe-rich metapelites and associated paragneisses (Filla Paragneiss) and the *ca.* 1030 Ma granitic to dioritic orthogneiss (Hop Island Orthogneiss; Harley & Fitzsimons, 1991; Harley *et al.*, 1992; Kinny *et al.*, 1993). These lithologies record maximum *P-T* estimates of 7 - 9 kbar and 840 ± 30 °C, with peak metamorphic conditions terminating in near-isothermal decompression of ~2 kbar at minimum temperatures of about 800 °C (Harley, 1988; Harley & Fitzsimons, 1991; Harley & Buick, 1992).

Although it is recognised that a complete Proterozoic metamorphic *P-T-t* path has not been preserved in all the rocks (*cf.* Harley, 1987, figure 10), with any possible pre-peak metamorphic assemblage overprinted by the subsequent *ca.* 1000 Ma maximum, evidence for more extreme granulite (Archaean ?) conditions has been locally preserved in some

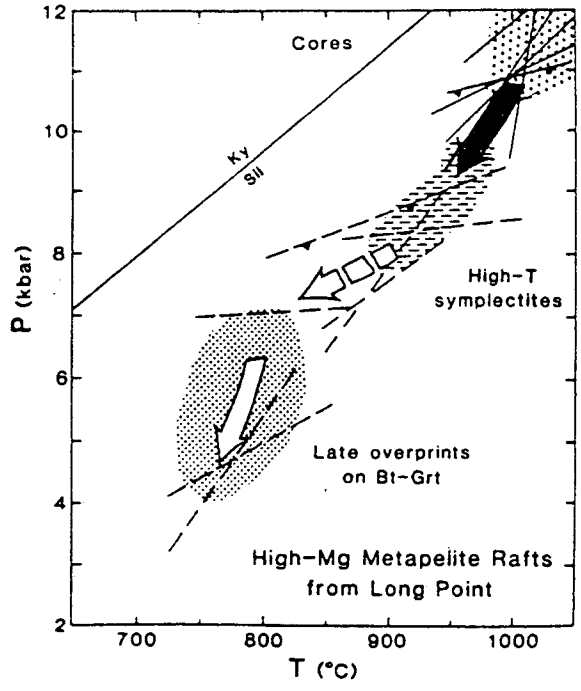

Figure 2.3 *P-T* estimates for the high-*T* decompression path (filled arrows) and later overprint (open arrow) on the Long Point metapelites. Estimates (dashed and barred lines) are based on a range of thermobarometers, and define the shaded *P-T* areas related to peak conditions (large dots), initial high-*T* decompression (dashes) and later, *ca.* 1000 Ma, overprints (small dots) (after Harley *et al.* 1992).

relatively old lithologies. Mg-metapelite rafts (Mather Paragneiss) contained within felsic orthogneiss of Archaean age (Kinny *et al.*, 1993) record maximum *P-T* conditions of 10-12 kbar and 1000-1050 °C. These extreme granulite conditions are constrained by garnet-orthopyroxene thermobarometry (Harley & Fitzsimons, 1991) and are consistent with the high-grade conditions predicted for coexisting aluminous orthopyroxene - sillimanite - garnet (Mg_{70}) and aluminous orthopyroxene - sillimanite - quartz assemblages (Harley *et al.*, 1992). Later reaction textures, involving the production of sapphirine, orthopyroxene, and cordierite define an initial decompression path to 8 kbar at temperatures of 900 °C (see Figure 2.3; Harley & Fitzsimons, 1991).

2.6 Isotopic studies and geochronology

The first isotopic study in the Rauer Group was by Arriens (unpublished data quoted in Tingey 1981; 1982 and elsewhere, see below) who reported a Rb-Sr isochron age of about 1000 Ma for felsic gneisses from Filla Island. This age was interpreted by Tingey (1981; 1982) and Sheraton *et al.* (1984) to represent the time of regional metamorphism in the Rauer Group. The significance of the *ca.* 1000 Ma age obtained by Arriens was confirmed in broad terms by the more comprehensive isotopic studies of Sheraton *et al.* (1984) and Kinny *et al.* (1993).

Based on Nd_{CHUR} and Nd_{DM} model ages, Sheraton *et al.* (1984) constrained most gneisses in the Rauer Group to be of Meso- to Neoproterozoic age, with *ca.* 1600 - 1800 Ma crust-formation ages. They also identified two felsic orthogneisses with Archaean model ages (see Section 2.3.2 above), thereby providing the first isotopic indication that the Rauer Group contains reworked Archaean crust. It is also significant that their isotopic data do not directly support a *ca.* 1000 Ma age for metamorphism, but they did find evidence for perturbation of isotope systems by a *ca.* 500 Ma event (see also Section 2.7).

Conventional isotopic systems (*e.g.* Tingey, 1981; Sheraton *et al.*, 1984) appear to identify regional tectonothermal events of Archaean (3800-3900 Ma), Proterozoic (*ca.* 1000 Ma) and Phanerozoic (*ca.* 500 Ma) age. Surprisingly, given the regional nature of the Sheraton *et al.* (1984) study (see below, and also discussion in Chapter 6), these ages are broadly confirmed by much more precise U-Pb zircon geochronology. In their zircon study, Kinny *et al.* (1993) obtained crust (protolith) formation ages of *ca.* 3270, 2800 and 1000 Ma. From structural and cross-cutting relationships, Kinny *et al.* (1993) constrained the age of the main high-

grade event to *ca.* 1000 Ma and found that igneous zircons in the both Archaean and Proterozoic protoliths were variably reset at *ca.* 500 Ma. The cause of Pb-loss at that time was attributed by Kinny *et al.*, (1993) to fluid-infiltration via post-deformational (high-grade deformations, see Section 2.4) pegmatite emplacement. In support of this model, a *ca.* 500 Ma crystallization age was obtained from one of the pegmatites (Kinny *et al.*, 1993).

Despite the apparent consistency between different isotopic techniques, the significance of the various tectonothermal events that occurred in the Rauer Group is currently a matter of considerable debate (see below). In order to critically appraise the published isotopic data, a compilation and detailed overview of the published isotopic work is presented here. These data are referred to in detail in later sections (*e.g.* Chapter 6).

2.6.1 Conventional isotopic data (Sr and Nd)

For the unpublished Rb-Sr data from Filla Island (Arriens, first quoted in Tingey, 1981), there appears to be some confusion over the details of the data and/or the regression. Tingey (1981) quoted 1073 ± 101 Ma, Sheraton & Collerson (1983) quoted 1073 ± 111 Ma, Sheraton *et al.* (1984) quoted 1050 ± 109 Ma, apparently correcting for the Steiger & Jäger (1977) decay constant, Collerson & Sheraton (1986) quoted 1106 ± 114 Ma, Tingey (1991) quoted Collerson & Sheraton (1986) and Kinny *et al.* (1993) quoted 1050 ± 110 Ma!

Problems probably arise from using different decay schemes and/or regression techniques. For the sake of simplicity, the Arriens age will be referred to in this study as *ca.* 1000 Ma. Although the actual data is unpublished, this 'age of high-grade metamorphism' has been cited as the primary evidence that there was a high-grade metamorphic event in the Rauer Group at *ca.* 1000 Ma (*e.g.* Harley, 1987). It has also been cited as the age of metamorphic retrogression in the SW Vestfold Hills (*e.g.* Collerson & Sheraton, 1986). However, despite its apparent importance, the *ca.* 1000 Ma Rb-Sr age was not replicated by the study of Sheraton *et al.* (1984), although they admit that their samples were not strictly collected with precise geochronology in mind (Sheraton *et al.*, 1984, p.174) as they sampled gneisses in a 200 km transect across the Prydz Bay coastline.

In their isotopic study, Sheraton *et al.* (1984) analysed 16 samples for Sr isotopes from the Rauer Group and selected 5 of these for Nd isotopic analysis. Primarily because their sampling strategy was one of terrane scale isotopic mapping, they were unable to define convincing isochrons for any of their suites from the Rauer Group. Nevertheless, Sheraton *et al.* (1984) argued that their model ages are of geological significance and that most

gneisses from the Rauer Group tend to have crust-formation ages between ~1600 and 1800 Ma (Tables 2.2 & 2.3). They also noted that two samples have much older Sr_{BSE} (3890 & 3970 Ma) and Nd_{CHUR} (3220 & 3520 Ma) or Nd_{DM} (3450 & 3750 Ma) model ages.

Sheraton *et al.* (1984) concluded that there is only a very minor Archaean gneiss component in the Rauer Group, and that most of the terrane comprises middle Proterozoic crust. Although of apparently minor extent, they further tentatively (?) suggested that there might

Table 2.2 A compilation of the Sr-isotopic data for the Rauer Group, from the Sheraton *et al.* (1984) database.

Sample	Location	Rock Type	Rb (ppm)	Sr (ppm)	$^{87}Rb/^{86}Sr$	$^{87}Sr/^{86}Sr$	BSE (Ma)
5103	Filla Island	Orthogneiss	29.58	489.6	0.1744	0.70704	1880
5115	SE Rauer Group	Orthogneiss	89.56	99.47	2.612	0.75706	1390
5119	E of Torckler Island	Orthogneiss	86.89	486.2	0.5164	0.71522	1710
5120	**E Rauer Group**	**Orthogneiss**	**140.1**	**85.85**	**4.838**	**0.98059**	**3970**
5124	Hop Island	Orthogneiss	42.3	776.9	0.1573	0.71192	6770
5125	Hop Island	Orthogneiss	189	38605	1.415	0.73164	1420
5127	E of Hop Island	Orthogneiss	85.7	490.1	0.5054	0.71796	2200
5131	S of Hop Island	Orthogneiss	103.8	462	0.6493	0.71823	1680
5133	Torckler Island	Orthogneiss	82.26	397.5	0.5979	0.71448	1340
5143	**NE Rauer Group**	**Orthogneiss**	**124.9**	**79.87**	**4.628**	**0.9626**	**3890**
5104	Filla Island	Paragneiss	78.93	160.2	1.425	0.72887	1260
5114	SE Rauer Group	Paragneiss	172.2	134.7	3.717	0.77611	1370
5118	E of Torckler Island	Paragneiss	241.3	90.48	6.943	0.86227	1600
5123	Hop Island	Paragneiss	213.2	287.7	2.149	0.75161	1580
5128	E of Hop Island	Paragneiss	102.6	555.1	0.5342	0.71809	2060
5134	Torckler Island	Paragneiss	190	142.6	3.881	0.8009	1760

Table 2.3 A compilation of the Nd isotopic data for the Rauer Group, from the Sheraton *et al.* (1984) database.

Sample	Location	Rock Type	Sm (ppm)	Nd (ppm)	$^{147}Sm/^{144}Nd$	$^{143}Nd/^{144}Nd$	Error (2σ)	T_{CHUR} (Ma)	T_{DM} (Ma)
5103	Filla Island	Orthogneiss	7.48	32.71	0.1384	0.511392	24	1160	1820
5115	SE Rauer Group	Orthogneiss	25.67	130.61	0.1189	0.511191	20	1260	1770
5120	**E Rauer Group**	**Orthogneiss**	**7.86**	**37.46**	**0.1269**	**0.510188**	**16**	**3570**	**3750**
5143	**NE Rauer Group**	**Orthogneiss**	**10.82**	**53.37**	**0.1226**	**0.510257**	**28**	**3220**	**3450**
5128	E of Hop Island	Paragneiss	4.67	34.41	0.0820	0.510816	26	1350	1700

be a link between Archaean orthogneisses in the Rauer Group and similar aged rocks from Enderby Land (discussed further in Chapter 13).

2.6.2 U-Pb zircon geochronology

The zircon U-Pb geochronology study by Kinny *et al.* (1993) has redefined the chronology of events in the Rauer Group, indicating that there were major crust-forming magmatic episodes at *ca.* 3270, 2800 and 1000 Ma, and that as much as 50 % of the currently exposed crust is Archaean. The extensive influence of the *ca.* 500 Ma event is also apparent from their data, as all the samples from the Rauer Group appear to have suffered some degree of Pb-loss at that time.

Table 2.4 A compilation of zircon data for the Rauer Group (from Kinny *et al.*, 1993). Age in brackets denotes inherited zircons.

Sample	Description	Structural position	Age (Ma) ± 2σ	Age of Pb loss
5120	Granitic Orthogneiss	pre-D_3	3269 ± 9	
TI13	Granitic Orthogneiss	pre-D_3	2810 ± 14	488 ± 3
SP12	Granitic Orthogneiss	pre-D_3	2801 ± 6	540 ± 19
TI14	Cpx-qtz-plag-Paragneiss	pre-D_3	(3267 ± 17, 2850 ± 50)	
FI02	Leuconorite melt phase	post-D_2	1057 + 22/-10	
FI04	Granitic Orthogneiss	pre-D_3	1027 ± 27	515 ± 54
HI08	Qtz monzodioritic Gneiss	pre-D_3	1000 +51/-37	490 ± 105
FI05	Garnet Leucogneiss	D_3-D_4	998 ± 18	
FI06	Garnet Leucogneiss	late D_4	1004 ± 52	548 ± 26
FI03	Sheared pegmatite	syn-D_5	500 ±12	
HI07	Lamprophyre dyke	post-D_5	(2455 ± 32, 1000-500)	

The relatively precise zircon ages reported by Kinny *et al.* (1993) provide an important geochronological framework that enables a reinterpretation of previous work (*e.g.* Sheraton *et al.*, 1984) and to a certain extent directs the course of further study. Table 2.4 is a summary of all the currently published zircon ages for the Rauer Group, and includes inherited zircon ages in orthogneisses (contamination and/or source), provenance ages in the paragneisses, and metamorphic or Pb-loss ages associated with the *ca.* 500 Ma event. The distribution of this zircon data is referred to in later sections (*e.g.* Chapters 6 & 13) and since data for the Archaean samples are utilised further in later geochemistry and isotope sections (Chapters 5-7), a detailed summary of the three key Archaean orthogneisses is included here. The following account is summarised from Kinny *et al.* (1993).

- ***Short Point orthogneiss SP12.*** This is an orthopyroxene and clinopyroxene-bearing granitic gneiss that was sampled near one of the sites defined by Sheraton *et al.* (1984) as having Archaean Nd model ages. This sample has a simple zircon population comprising subhedral igneous grains. Spot analyses yielded concordant to near concordant isotopic compositions corresponding to a protolith emplacement age of 2801 ± 6 Ma, but with a lower intercept of 540 ± 19 Ma corresponding to the age of Pb-loss. The whole-rock Nd_{CHUR} age for this sample is *ca.* 2990 Ma.

- ***Torckler Island orthogneiss TI13.*** This is a clinopyroxene-bearing granitic gneiss that closely resembles SP12 in appearance and chemical composition. Zircons from this sample are variable in form but are generally equant to subhedral in form. Ages essentially define a bimodal population, some grains range between concordant at about 2800 Ma and discordant at about 500 Ma, the other population is concordant at 500 Ma. Overall, upper and lower intercepts are 2810 ± 14 and 488 ± 3 Ma, representing protolith crystallization and Pb-loss ages respectively. The Nd_{CHUR} age for this sample is *ca.* 3000 Ma

- ***Short Point orthogneiss #5120.*** This sample was originally collected by Sheraton *et al.* (1984) and was distinguished as being Archaean in age on the basis of Nd_{CHUR} model age (3570 Ma). This sample is petrographically and chemically similar to SP12 above and is also a clinopyroxene- and orthopyroxene-bearing granitic gneiss. Zircons from this sample are morphologically variable and include prismatically faceted grains and unzoned, rounded to subhedral, grains. The majority of analyses define a discordance line with an upper intercept 3269 ± 9 Ma and a poorly defined lower intercept at 350 ± 150 Ma. Additional analyses that do not fall on the main discordance line appear to have been affected by an intermediate Pb-loss event, presumably at *ca.* 2800 Ma. The 3269 ± 9 age is therefore considered a likely minimum age for this protolith and the actual crystallization age may be nearer to the oldest $^{207}Pb/^{206}Pb$ age at 3292 ± 20 Ma.

2.7 The Rauer Group: summary, research rationale and objectives

It is obvious from the geological outline described above that the Rauer Group is a complex polycyclic high-grade terrain that was geologically active from at least the mid-Archaean to the Cambrian. Some aspects of the geological evolution have been studied in detail; the most notable are accounts of the metamorphic history documented by Harley and co-workers (*e.g.* Harley, 1987; 1988; Harley & Fitzsimons, 1991; Harley & Buick, 1992). Additionally, a comprehensive structural framework has also emerged (Harley, 1987; Sims *et al.*, 1994) which, when combined with precise U-Pb zircon geochronology (Kinny *et al.*, 1993), goes some way towards defining a relative and absolute chronology of events for the Rauer Group. However, accounts of the earliest evolution of the terrane are still fragmentary and little is known about the magmatic and structural evolution during the Archaean.

2.7.1 Summary: what *is* known of the Archaean domain

Lithologies and U-Pb zircon geochronology

Within the Archaean domain, four lithological associations have been distinguished: (i) Composite Layered Orthogneisses; (ii) Homogeneous Felsic Orthogneisses; (iii) Fe-rich and Mg-rich paragneisses and (iv) Layered meta-igneous complexes. Relatively precise protolith ages have been determined for components of the CLO (*ca.* 3270 Ma), the Homogeneous felsic orthogneisses (*ca.* 2800 Ma), and there are *ca.* 2800 - 3270 Ma provenance ages for the Fe-rich paragneisses (Torckler Paragneiss). However, much of the Archaean domain is only loosely defined, based on structural criteria or by lithological association, and there are no isotopic data for either the high-Mg paragneisses or the layered meta-igneous complexes.

Geochemistry and conventional isotopic studies

For orthogneisses from the Archaean domain, published geochemical and petrogenetic studies are of a preliminary nature. Conventional isotopic work in the Rauer Group is limited to the regional Sr and Nd model-age mapping of Sheraton *et al.* (1984). This study was completed before later work had established a lithological-structural or geochronological framework. Although their data distinguished between Proterozoic and Archaean protoliths, attempts at constraining processes of crustal growth were hampered by poor (independent) geochronology. Similarly, Harley *et al.* (1992) distinguished between groups of felsic orthogneiss on the basis of chemical characteristics, but they were unable to constrain if the gneisses are related in age or petrogenetic origin. Problems with early studies largely reflect geological complexity in the Rauer Group. Moreover, the deformed nature of contacts between gneiss units means that potentially related suites are difficult to define because temporally and possibly genetically diverse lithologies were juxtaposed by progressive episodes of high-grade deformation.

Structure and metamorphism

The structural and metamorphic evolution in the Rauer Group during the Archaean is not well constrained at present. This is largely because it is difficult to relate rock types that are suitable for dating (*e.g.* felsic orthogneisses) to those more suited to microtextural fabric analysis or quantitative thermobarometry (*e.g.* high-Mg metapelites). Nevertheless there are two lines of evidence that indicate there was an Archaean tectonothermal history in the Rauer Group: (i) early fabrics preserved in mafic layers of the CLO suggest an Archaean deformational history and (ii) *P-T* estimates from the Mather Paragneiss record significantly higher-grade conditions than reported from any of the younger lithologies. However,

because there is only limited geochronology it is not possible to constrain the nature or significance of Archaean tectonothermal events in the Rauer Group.

2.7.3 Objectives and methodology

My work in the Rauer Group can be considered in terms of specific objectives and wider objectives. Wider objectives are essentially aimed towards:

- Understanding the petrogenetic history of individual orthogneiss suites.
- Comparing Archaean gneiss suites in the Rauer Group with those in the adjacent Vestfold Hills craton and with other Archaean terranes in the EAS in order to assess the timing of terrane amalgamation.
- Relating magmatism to a tectono-magmatic framework for the Rauer Group and the East Prydz Bay region in general.

In order to achieve these wider objectives, however, it was first important to define specific objectives and establish a methodology. Specific objectives are:

- Distinguish between Archaean and Proterozoic lithologies and structures in the field.
- Identify gneiss suites that preserve primary relationships (*i.e.* intrusive contacts) to enable reconstruction of a geological event sequence for the Archaean domain.
- Identify orthogneiss suites that are most likely to retain protolith characteristics and geochemistry (see Section 1.4).
- Relate mineral, whole-rock and isotopic chemistry to modern-day analogues with a view to extrapolation to models of Archaean crustal growth in the Rauer Group (assumptions inherent in this approach are discussed in Section 1.4 & Chapter 13).

The methodology adopted to accomplish these specific objectives can be broken down into four phases: *fieldwork, petrography and mineral chemistry, geochemical and isotopic analysis*, and *data integration*.

Fieldwork

The main fieldwork objective in the Rauer Group was focused on low-strain areas. In practical terms this involved constraining the nature of contacts between the SLC and TTLC with adjacent gneisses, and relating internal and external intrusive phases and structures to the regional scheme already established for the Rauer Group. Detailed field observations of relict igneous features are then to be used to define which lithologies are most likely to be petrogenetically related, thereby providing independent constraint on magmatic processes (*cf.* Section 1.4).

Petrography and mineral chemistry

Petrographic observations and mineral-chemical data are designed to: (i) examine and document relict igneous phases and textures with a view to assessing magma petrogenesis; (ii) relate the development of metamorphic assemblages to the *P-T* framework established for other lithologies, (*i.e.* is it possible to determine if the SLC and/or TTLC share the same *P-T* history as the rest of the Rauer Group?) (iii) assess petrographically whether there is evidence for open-system chemical behaviour, that is, does gneiss geochemistry still faithfully reflect the chemistry of the protolith ?

Geochemical and isotopic analysis

In common with many geochemical studies in high-grade terranes, the purpose of undertaking whole-rock and isotopic analysis of orthogneisses is to elucidate the processes involved in protolith formation. In brief, the most important petrogenetic processes can be thought of in terms of a sequence of events involving: melt extraction from a source region(s); magma - host-rock interaction during ascent and/or emplacement, with or without fractionation; *in situ* fractionation in the magma-chamber; and finally, post-crystallization modification (either by late-stage magmatic alteration or unrelated metamorphism).

Data integration

This phase essentially ties together the data from the first three phases. From this basis, previous accounts of the Archaean domain are re-evaluated and the specific and wider objectives outlined above are addressed.

Each of the phases outlined above are reflected in the following chapters (Chapters 3 - 7).

3.2 The Composite Layered Orthogneiss (CLO)

The general distribution and character of the CLO was outlined in the previous chapter (Section 2.3.1) and only new field observations are reported here. The CLO is abundant throughout Scherbinina Island, Split Island and the Long Point area (see Harley, Snape & Black, in press, figure 2) but does not crop out in the immediate proximity of the TTLC. Therefore, the description of the CLO presented here is restricted to the Scherbinina Island area.

3.2.1 CLO on Scherbinina Island

Outcrops of CLO on Scherbinina Island are correlated with similar lithologies of Archaean age on Short Point (Sheraton *et al.*, 1984; Kinny *et al.*, 1993; Harley, Snape & Black, in press; see figure 2). Gneissic layering on the Scherbinina Island defines a late (post high-grade fabric development) km-scale open fold with an ESE trending axial plane. Outcrops to the NW are often garnet bearing, and there are relatively few cross-cutting mafic dykes, whereas to the SE, near the layered complex, layered migmatitic and homogeneous felsic gneisses contain less garnet and are cut by numerous deformed mafic dykes. These mafic dykes have granulite assemblages and were multiply deformed prior to regional warping. All the dykes noted adjacent to the SLC cross cut isoclinally folded fragments of complex that are now preserved as highly attenuated boudins in the CLO/Homogeneous Felsic Orthogneiss.

The CLO crops out immediately adjacent to the SLC in two locations; on the SE tip of the SLC Peninsula and on the NE margin of the complex (Figure 3.1). Contacts between the two units are tectonic, but more commonly they are separated by Homogenous Felsic Orthogneiss. However, the 'homogeneous' prefix for this gneiss is a relative term to distinguish it from the more heterogeneous migmatitic and layered CLO. The Homogenous Felsic Orthogneiss in this area comprises at least three components; a tonalitic gneiss (TG), a trondhjemitic gneiss (TrG) and a coarse-grained granitic gneiss. These collectively form a 'group' of gneisses (tonalite-trondhjemite-granite gneisses or 'TTG') that all post date the SLC. Since, they all have different relative crystallization ages they will be described further in the context of the post-SLC geological evolution (Section 3.3.3).

Chapter 3

Field relations of the Archaean domain

3.1 Introduction

Outcrop-scale geological mapping and detailed observations made during the 1992/93 and 1994/95 ANARE field seasons confirm that variably interlayered Homogeneous Felsic Orthogneiss and Composite Layered Orthogneiss (CLO) are the most abundant constituents of the Archaean domain. These lithological associations surround the two layered meta-igneous complexes (Scherbinina and Torckler-Tango Layered Complexes; SLC and TTLC respectively) and the two Archaean paragneiss units (Torckler and Mather Paragneisses) that are described in outline in Chapter 2.

In this chapter, I describe the relationships between these Archaean components, document the geological character of the main orthogneiss units, and define event sequences where possible. The layered complexes have been studied in most detail because they are the most geologically diverse and, since they are relatively undeformed, they retain evidence of the earliest events in the terrane. No new observations are reported here with respect to the paragneiss units and they are not considered further.

Within this chapter the TTLC and the SLC are described separately. Since the two complexes do not crop out together, and because they differ in appearance and chemistry, they are assumed to be unrelated in the first instance. The CLO is described first as a background to the younger units. It is also worth stating at this stage that the observed relationship between the SLC and CLO is entirely tectonic and that neither suite has diagnostic xenolith relationships that can be used to constrain their relative age. The CLO does not occur adjacent to the TTLC and their mutual relationship is also unclear. The other major lithological association in the Archaean domain, the Homogeneous Felsic Orthogneiss, is described in the context of an intrusive suite that cross-cuts the other three units.

3.3 The Scherbinina Layered Complex (SLC)

3.3.1 Relict igneous features

The SLC is a coarse-grained layered igneous complex that largely escaped the effects of penetrative high-grade deformation prevalent elsewhere in the Rauer Group. As a consequence of strain partitioning, the SLC as a whole can be thought of in terms of low-strain areas, where relict igneous features are well-preserved, separated by high-strain zones (HSZs) where intrusive relationships, magmatic textures and primary mineralogy have been overprinted by successive deformations and fabrics (*cf.* Sims *et al.*, 1994).

In low-strain areas, intergranular (Figure 3.2), sub-ophitic, spotted or 'oikocrystic' (Figure 3.3) and pegmatoidal comb textures (Figure 3.4) are preserved on surfaces that are perpendicular to a steeply ESE-plunging mineral-elongation lineation. In addition to these relict igneous textures, there are a variety of larger-scale magmatic features. Perhaps the most striking of these features, given the high-grade deformational history in the Rauer Group, is the preservation of primary compositional layering, which occurs on decimetre to 10-metre scales (Figure 3.5). Individual layers commonly grade from melagabbros and gabbros to leucocratic ferrodiorites, with compositional changes defined by modal variations in orthopyroxene, clinopyroxene, plagioclase and Fe-Ti oxides. In addition, there are less common extreme differentiates including ultramafic cumulates, leucocratic coarse-grained to pegmatitic ferrodiorites, and relatively rare late-stage oxide veins and patches.

Ultramafic compositions, including hornblendite and websterite, occur on the NE and SW flanks of the main gabbroic body (see Figure 3.1). Although these outcrops are intruded by TG sheets (Section 3.3.3 below), their precise relationship to the main complex is not clear because contacts are either tectonic or not exposed. Nevertheless, finely layered pyroxenites and oikocrystic (Figure 3.3) variants that occur as dismembered layers and pods within the main SLC gabbro are clearly cogenetic with the complex.

Within-suite intrusive relationships indicate that the more felsic compositions were emplaced late in the crystallization sequence. Individual layers contain cognate ultramafic xenoliths and are truncated by late-stage leucocratic and pegmatoidal varieties (*e.g.* Figure 3.4). Rare decimetre- to metre-scale oxide veins and patches cross-cut igneous layering but are contained within the complex. Some of these contain metamorphic garnet and all are enriched in quartz, opaques, apatite and zircon. These veins and patches predate all the

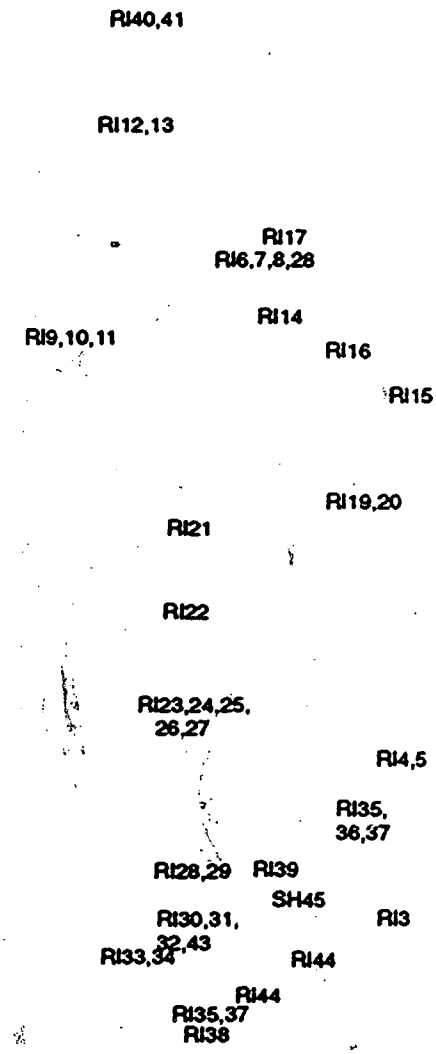

Figure 3.1 Lithological map of the Scherbinina Layered Complex and surrounding gneisses. Overlay sheet shows sample locations (locality: Scherbinina Island).

Scherbinina Layered Complex

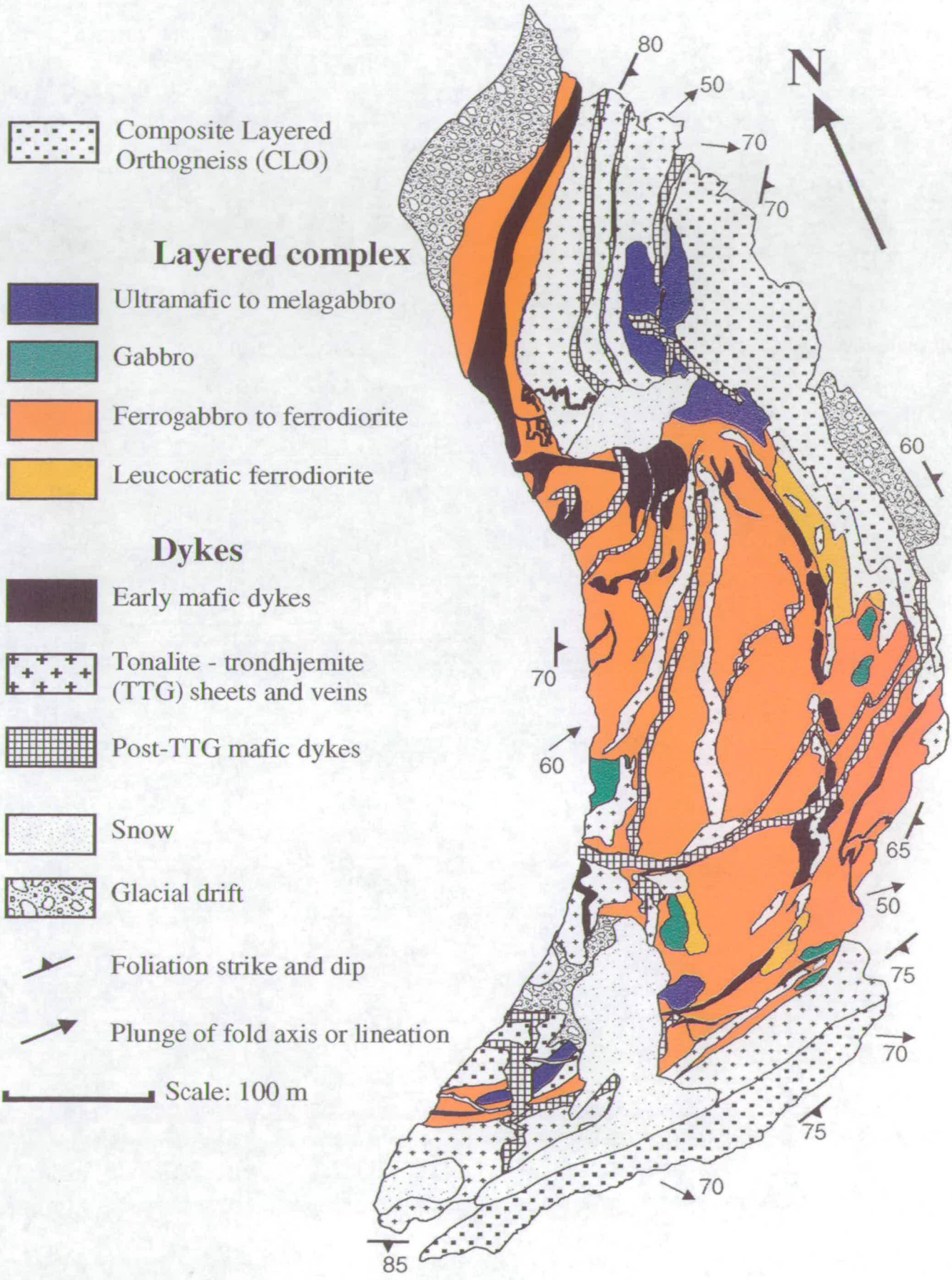

deformations, the mafic dyke suites, and the TG (Section 3.3.3 below), and are interpreted to be sites where residual fractionated liquids crystallized. Both the oxide veins and patches and the finely layered pyroxenites are inferred to be co-magmatic on the basis of gradational contacts and because there are compositional and textural gradients between rock types. This interpretation is further supported by petrographic observations (Chapter 4) and geochemical similarities between these rock types and the main body of the complex (Chapter 5). These field observations are particularly important because the 'extreme' differentiates help constrain the age and petrogenetic history of the complex. One example of the garnet-zircon oxide patches has been studied for zircon U-Pb geochronology by SHRIMP to determine the crystallization age of the SLC (Chapter 6), whilst the conventional isotope characteristics of the ultramafic to melagabbroic rocks elucidates important aspects of magma petrogenesis and post-crystallization geochemical processes (Chapter 6).

3.3.2 The effects of metamorphism and deformation

High-grade metamorphism and deformation produced physical and chemical changes to the SLC at all scales. Microscale recrystallization of primary phases and textures is described in the next chapter (Chapter 4), and the possibility of geochemical or isotopic changes (metasomatism and isotopic perturbation) are discussed in Chapter 6. However, a number of important hand-specimen to outcrop-scale affects are also apparent:

- ***Metamorphic fabric development.*** Fabric development in response to high-grade folding and shear is variable and tends to be partitioned into narrow, metre-scale, HSZs. Much of the SLC at the type location is of generally low strain, where foliation development is weak if discernible at all, although most rocks have a steeply-plunging mineral-aggregate lineation. Where more strongly deformed in HSZs, the SLC develops a strong foliation, defined by biotite and amphibole, and a steeply ESE plunging mineral elongation lineation defined by individual grains and elongate aggregates or lenses of amphibole and pyroxene. Intrusive relationships with multiply deformed mafic dykes and the TG suite indicate that fabrics in the SLC are composite and formed by successive high-grade deformations.

- ***Folding.*** Outcrop- to meso-scale deformation resulted in multiple folding episodes and reactivation of HSZs (*cf.* Sims *et al.*, 1994). In the main body of the SLC, some individual layers were isoclinally folded prior to intrusion of mafic dykes and TG sheets (Figure 3.7). However, decimetre-scale graded modal layering defines way-up to the E and SE for the complex as a whole, so that despite local isoclinal to tight folding, most of the complex is right way up and is not isoclinally folded on a scale similar to that of the exposed body (100 m-scales). Nevertheless, smaller fragments of the complex are isoclinally folded on large scales (10-100 m-scales) outwith the complex (see Figure 3.1), and dismembered folds and boudinaged pods of the SLC occur elsewhere on Scherbinina and nearby islands to the SW.

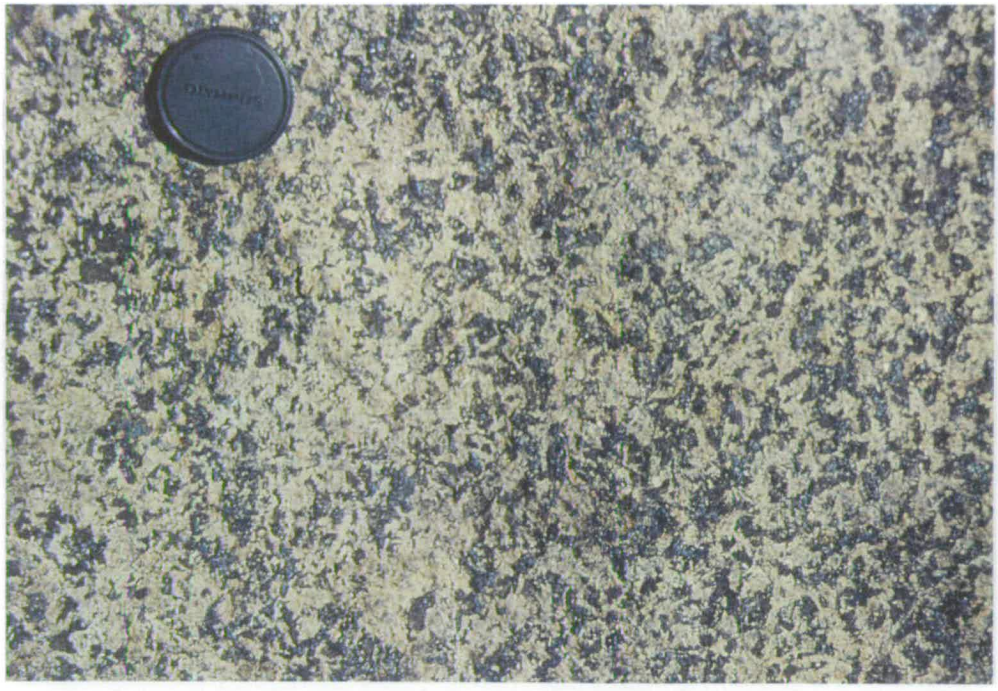

Figure 3.2 SLC gabbro with a coarse-grained intergranular texture preserved in an area of low strain (locality: central Scherbinina Peninsula; lens cap for scale is 50 mm wide).

Figure 3.3 Oikocrystic cumulate texture in SLC melagabbro. Light patches are plagioclase-dominated areas, dark areas are clinopyroxene- and orthopyroxene-rich areas (locality: central Scherbinina Peninsula; notebook for scale is 12 x 20 cm).

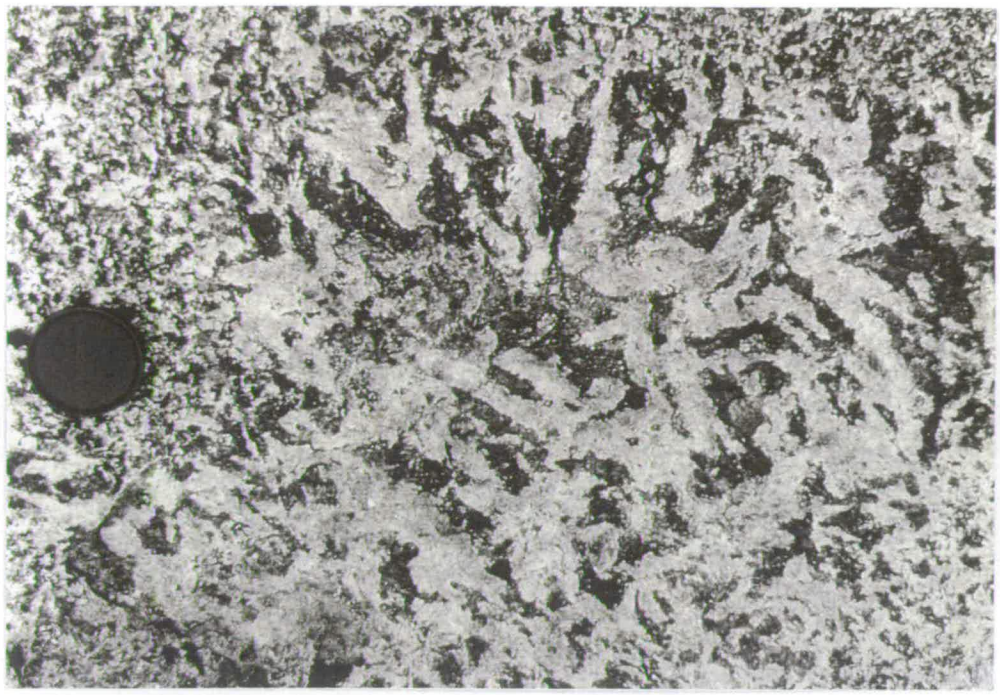

Figure 3.4 Felsic pegmatoidal comb texture defined by plagioclase and intergrown and/or exsolved magnetite and ilmenite. Note that pegmatite texture is gradational with the more usual equigranular gabbro host (locality: central Scherbinina Peninsula; lens cap for scale is 50 mm wide).

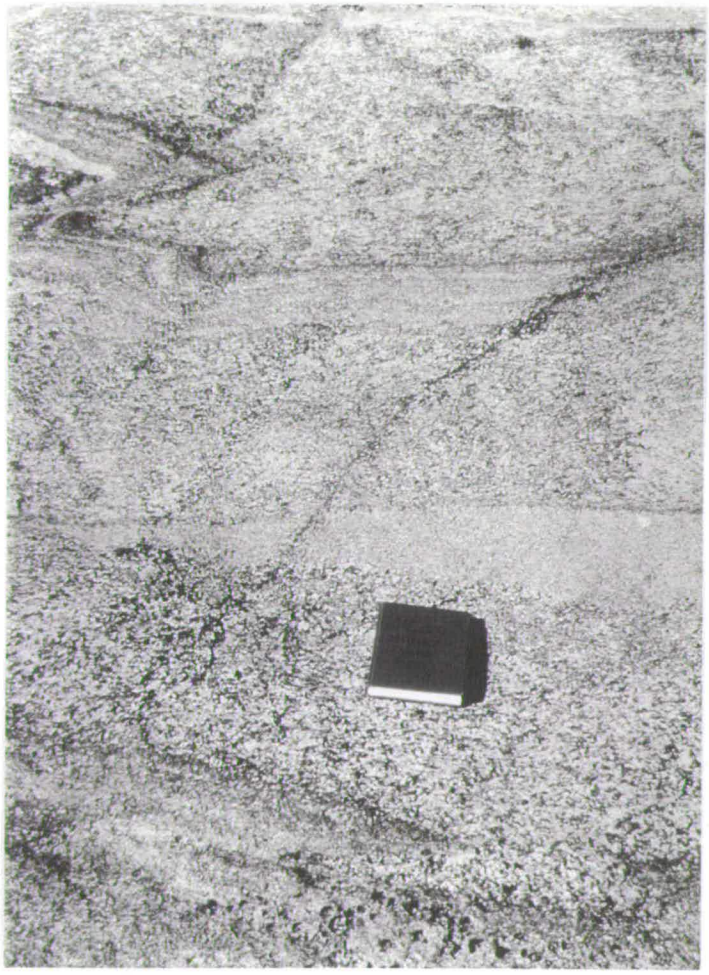

Figure 3.5 Graded modal layering in the SLC. Way-up is to the ESE (locality: central Scherbinina Peninsula; notebook for scale is 12 x 20 cm).

3.3.3 Post-intrusive geological evolution

The relatively competent coarse-grained nature of the SLC ensured that it largely escaped the pervasive effects of the younger high-grade deformations, and many early high-grade structures and relationships are still recognisable. In the main complex there is evidence for a protracted sequence of deformation events punctuated by intrusion of mafic and felsic dykes. This allows the definition of a detailed event history for the area that can be compared with histories deduced for other localities in the region, especially the adjacent Vestfold Hills. A summary of this event sequence, including the older CLO, is presented in Table 3.1 and described in more detail below. Sample localities are shown on an overlay to Figure 3.1, whilst detailed field relations and key locaties within the SLC complex are described in figure captions for brevity.

Table 3.1 Summary of events in the Archaean domain of the Rauer Group

CLO protolith formation	SLC protolith formation (intrusion into CLO?)	TTLC protolith formation, (intrusion into CLO?)
D_1 folding	D_1 folding	D_1 folding
D_2 folding	D_2 folding	D_2 folding
Intrusion of Homogeneous Felsic Orthogneiss tonalitic component (TG). CLO, SLC and TTLC juxtaposed by this time.		
Polyphase high-grade deformation punctuated by intrusion of mafic dykes.		Polyphase high-grade deformation but *no* mafic dykes. Geographic coincidence or genetic reason?
All lithologies co-deformed by D_6 SLC and D_7 SLC regional folding events. These events are correlated with structures on Filla Island dated at *ca.* 1000 Ma by Kinny *et al.* (1993)		
All lithologies transected by *ca.* 500 Ma pegmatites and planar deformation structures. Evidence for local rehydration and/or metasomatism of all lithologies by this event.		

Early deformation (D_1)[1] of the SLC

Igneous layering is folded into close to isoclinal folds with 0.2- to 3-metre amplitudes and wavelengths. Fold-axes and lineations plunge at about 60° to 120/140° and are attenuated and truncated against later fold structures and local HSZs in which planar fabrics are developed. It is not apparent whether this deformation phase is of regional extent; if it is

[1]'D' numbers (D_{1-n}) in this section refer to deformation episodes deduced from the SLC; they do not necessarily correspond to D numbers described by other workers for the terrane. A synthesis is given in Chapter 13, Table 13.1.

then it is possible that it correlates with the first recognised fabric in the CLO (see Figure 3.12 below).

Early mafic dykes (MD1)

A number of petrographically and geochemically distinct suites intruded into the SLC before intrusion of the TG (a distinctive chronological marker described below). Of these suites, an ultramafic (hornblendite) dyke and numerous pale-grey dykes (Fe-tholeiites) cross-cut D_1 folds but were then deformed by a further deformation (D_2 below) prior to TG intrusion.

Early deformation (D_2)

This deformation is defined by open to close folding of primary layering and MD1 dykes in the SLC. Felsic segregations formed in some MD1 dykes at this time. As with D_1, it is not possible to ascertain if this event was of regional extent, but it is possible that it correlates with the second fabric recognised in the CLO.

Early mafic dykes (MD2)

At least one suite of mafic dykes cross-cuts F_2 folds in MD1 mafic dykes, but are in turn cross-cut by TG sheets. Some dykes cross-cut folded segregations or veins in MD1 dykes (Figure 3.8). A further group of spotted (oikocrystic?) mafic dykes and a single high-Mg mafic dyke are constrained to have intruded by this time, but their relative position in the MD1-MD2 sequence is uncertain.

Early deformation (D_3)

This deformation phase resulted in an intensification of D_2 structures, shearing along dyke margins and development of HSZs in the SLC.

Felsic magmatism (TG)

Felsic sheets of Tonalitic Gneiss (TG) cross-cut the SLC (Figure 3.9), CLO, at least 4 suites of mafic dykes (MD1 & MD2) and 2 deformations (D_1 and D_2) in both SLC and CLO. Where TG intrude SLC, there is evidence to indicate that assimilation was locally important. To the north of the complex, in an area dominated by pyroxenite to hornblendite ultramafic rocks and early mafic dykes, injection of TG resulted in formation of a breccia in which felsic melts reacted with host gneisses (Figure 3.10). Xenoliths and wall zones of

Figure 3.6 Close fold defined by primary layering in the SLC gabbro (locality: central Scherbinina Peninsula; lens cap for scale is 50 mm wide).

Figure 3.7 Isoclinally folded modal layering in the SLC is parallel to a co-deformed pale grey mafic dyke, seen at the top RHS of the photo, that contains deformed felsic segregations (*cf.* Figure 3.8). The isoclinally folded SLC, the mafic dyke and the folded segregations were all intruded by a further dyke, that is itself deformed. All lithologies have granulite assemblages (locality: N central Scherbinina Peninsula; hammer for scale is 60 cm long).

Figure 3.8 Close folds defined by early mafic dyke (MD1) and felsic segregations were subsequently intruded by a second generation of early mafic dykes (MD2) after melting/leucosome formation and folding (D_2). Both dykes are pale grey plagioclase + two pyroxene granulites (locality: N central Scherbinina Peninsula; lens cap for scale is 50 mm wide).

Figure 3.9 Intrusive TG sheets cross-cutting the SLC gabbro (locality: N central Scherbinina Peninsula looking south; hammer for scale is 1.2m long).

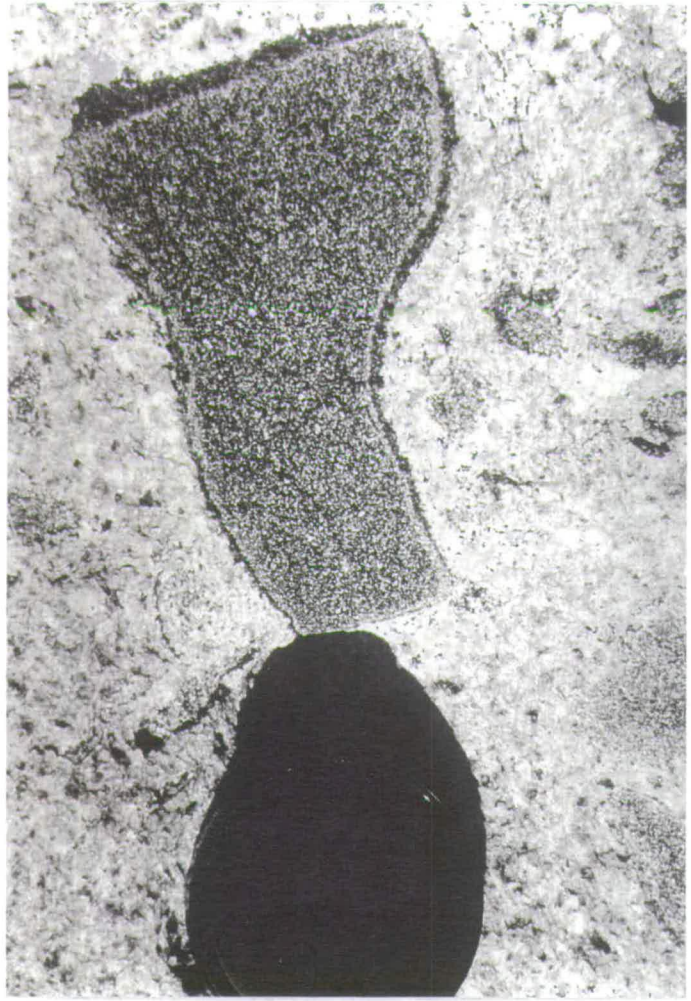

Figure 3.10 Intrusive breccia of SLC gabbro-ultramafic and early mafic dykes invaded by tonalite (TG). Angular fragments of mafic gneiss often have bleached margins reflecting the removal of amphibole by reaction with the intrusive tonalite melt and the interface between the two lithologies is commonly marked by a clinopyroxene selvage. These features indicate assimilation associated with crystallization (AFC) of the tonalite (locality: NE Scherbinina Peninsula; lens cap for scale is 50 mm wide).

Figure 3.11 Relict SLC pod in Homogeneous Felsic Gneiss (TG + TrG) on the margin in the main complex. SLC gabbro and the deformed early mafic dyke both have a pronounced fabric that is truncated at the margin with the tonalite (intrusive contact). This tonalite sheet intrudes along the margin between the CLO and the main body of the complex and in this region it has abundant partial-melt (?) patches of trondhjemite (Figure 3.13 was taken nearby; locality: SE Scherbinina Peninsula; lens cap for scale is 50 mm wide).

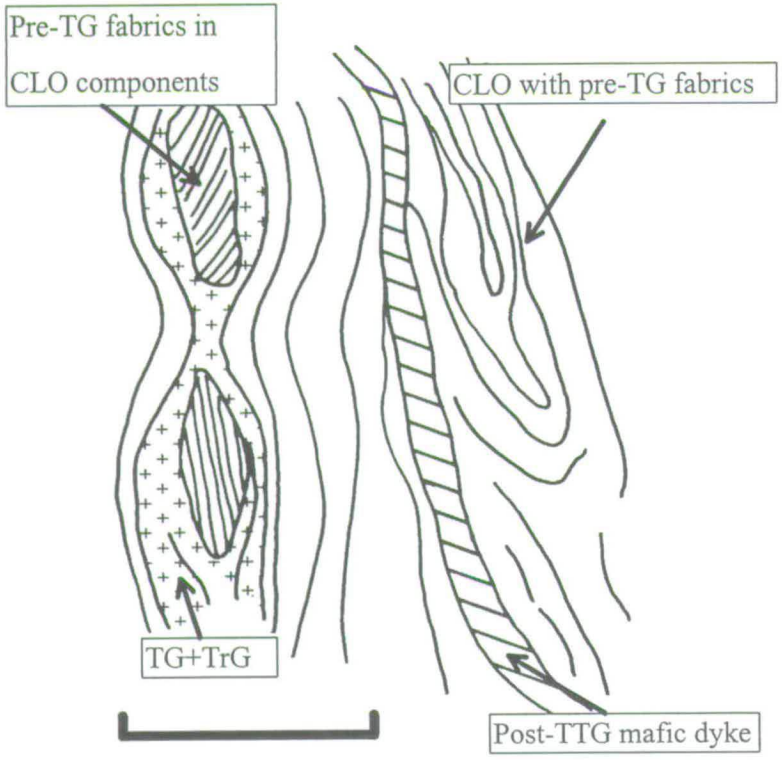

Figure 3.12 Field sketch of typical geological relations on the margin of the main SLC body. CLO contains rootless isoclines defined by mafic layers and also has early fabrics that are preserved in boudins. These structure are cross-cut by intrusive TG sheets and veins. These lithologies were all deformed together prior to intrusion by mafic dykes, which were in turn deformed by later deformation phases (locality: SE Scherbinina Peninsula; scale bar is 1 m).

Figure 3.13 Leucocratic (trondhjemitic) partial-melt (?) patches (TrG) in tonalite host (TG). Interconnected to elongate patches are folded within the TG sheet (locality: SE Scherbinina Peninsula; width of foreground is 2 m).

mafic gneiss have bleached margins adjacent to granular tonalite, reflecting the loss of amphibole. These margins and rinds of clinopyroxene aggregates on the xenoliths are interpreted to have formed by assimilation accompanying crystallization (AFC). Clinopyroxene is typically absent from the tonalites away from these margins, which instead has orthopyroxene (*ca.* 5-10 %) as its principal mafic phase.

In the SLC, the main gabbroic body, early mafic dykes, and HSZs with well-defined planar fabrics and granulite-grade assemblages, are all cut by the TG (Figure 3.11). These felsic intrusives mainly intruded as near-planar NS-trending sheets, but they were subsequently deformed and intruded by younger mafic dykes. Similar cross-cutting features to those found in the main complex, can be found in CLO lithologies on the SE tip of Scherbinina Island, further to the SW on the eastern half of Long Point and Short Point, and on islands further NE including Split and Dyke Islands (*e.g.* Harley & Fitzsimons, 1991; Harley *et al.*, 1992; Sims *et al.*, 1994). In these areas, TG[2] that cross-cuts the CLO clearly post-dates early structures (Figure 3.12), but is co-deformed with the latter gneiss suite along with younger metabasite dykes. Such relationships are considered to be characteristic of the Archaean component in the Rauer Group.

Deformation (D_4)

HSZs related to or focused along TG resulted in high-grade shearing and orthopyroxene fabric development in the tonalite.

Partial melting of the TG

TG sheets were locally remobilised, presumably by *in situ* partial melting, to produce trondhjemitic patches (TrG) or segregations (Figure 3.13). These podiform and lensoid patches interrupt orthopyroxene-bearing fabrics in TG and locally invaded adjacent gneisses (SLC, CLO and mafic dykes).

Regional deformation (D_5)

This regional event folded the SLC/CLO and intrusive TG. Elongate to interconnected TrG melt seggregations in TG are also folded and both the tonalite and trondhjemite share a common garnet-biotite fabric (Figure 3.14) that post dates the melting/remobilization event

---

[2]Note that the TG described here forms one component of the Homogeneous Felsic Orthogneiss. All the TG are thought to have formed in a single magmatic episode (*ca.* 2800, see Chapters 2 & 6), whereas the Homogeneous Felsic Orthogneiss is a catch-all term to distinguish a group of felsic intrusives that cross-cuts CLO and SLC lithologies, but that are possible composite in age.

described above. Existing high-strain zones were reactivated and accentuated by this deformation.

Post-TG mafic dykes (MD3)

At least two mafic dyke sets were emplaced in the D_5-D_6 structural interval. These dykes cross-cut fold closures (rootless isoclines) and fabrics in the TG/TrG association and also clearly truncate the SLC/CLO boundary.

Regional deformation (D_6)

These structures are defined by the near-coaxial refolding of D_5 and S_5 to give isoclinal refolds. Mafic dykes that cross-cut folds and garnet-biotite fabrics in the TG and TrG (MD3) were pervasively refolded during this pervasive deformation. D_6 structures are the first of the post-TG deformations that can be correlated with the *ca.* 1000 Ma event (Kinny *et al.*, 1993) with some degree of confidence.

Post-TG mafic dykes (MD4)

Two or more sets of dykes were emplaced that cross-cut D_6 fold structures in the CLO, SLC and TG/TrG associations and MD3 mafic dykes. A 2 m wide example of this suite intrudes across the width of the SLC and passes into the CLO/HFG association on the eastern side of the complex. Here it is deflected towards the north (sinistral offset) as later D_7 structures (described below) increase in intensity.

Partial melting

Local remobilization of the TG/TrG association produced coarse-grained granitic partial melts and pegmatites. Local intrusion of adjacent gneisses, including MD4.

Regional deformation (D_7)

Open to moderate folding of all early structures, mafic dykes (MD1-4) and felsic sheets into broad large-scale folds. These structures control the overall form surface of the Rauer Group and correspond to the D_4 and D_6 (or D_7) deformations of Harley *et al.* (1987) and Sims *et al.* (1994) respectively. Syn-tectonic aplites on Filla Island thought to correspond to this deformation phase have been dated by Kinny *et al.* (1993) at *ca.* 1000 Ma.

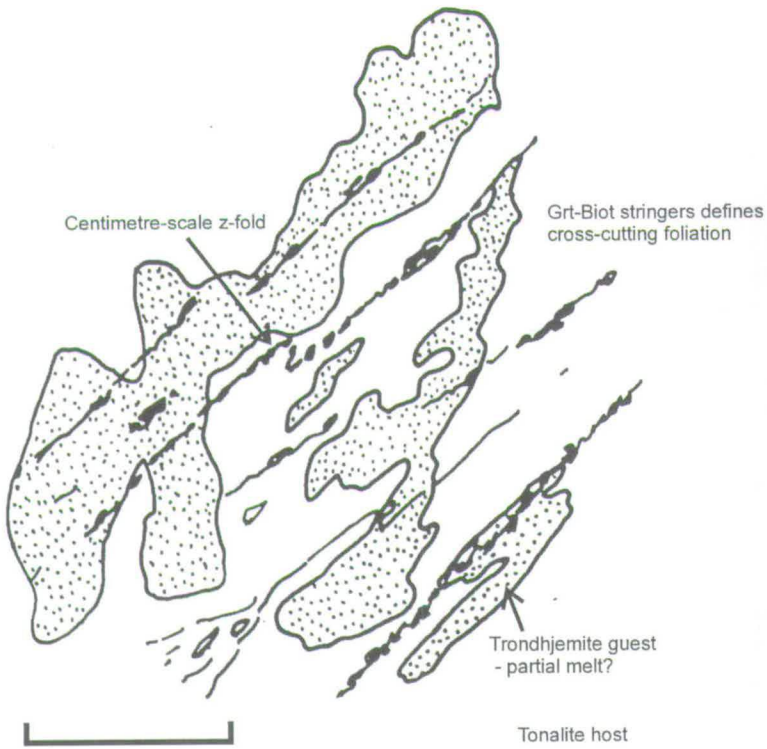

Figure 3.14 Field sketch of garnet-biotite fabric in Homogeneous Felsic Gneiss. The foliation is defined by stringers of garnet and biotite that pass into the trondhjemite from the tonalite. The trondhjemite patches cross cut an orthopyroxene fabric in the tonalite but share the garnet - biotite fabric indicating the sequence: TG intrusion - deformation - partial melting - deformation (D_5) followed by mafic dyke intrusion (locality: SW Scherbinina Peninsula; scale bar is 25 cm).

Figure 3.15 Xenolith of SLC (?) gabbro enclosed in *ca.* 2800 Ma Tonalite Gneiss on Tango Island (locality: central Tango Island; chisel for scale is 15 cm long).

Rehydration and regional deformation (D_8)

D_8 is characterised by localised deformation, rehydration and pegmatite emplacement. Planar mylonite-granitic pegmatite associations that are 10 to 20 cm in thickness cross-cut the SLC and all surrounding high-grade gneisses at an outcrop spacing of 10 m to greater than 40 m. Often the felsic gneisses within 50 cm of the pegmatite sheets are altered to a grey colour, indicating rehydration and/or metasomatism (see also Chapter 6).

One large example of a retrograde shear zone occurs on the northern flank of the SLC, where a topographic depression marks the location of the shear zone and a later brittle fault. In this zone, SLC fabrics, dykes, CLO and TG are all transposed. Granulite assemblages are altered to epidote-chlorite-actinolite-carbonate (greenschist), and epidote quartz veins cut the transposed (composite) foliation. This shear-zone is cut by one of the pegmatites mentioned above, but from the intimate relationship between mylonites, pegmatitites and shear zones, it is likely that all these features occurred at about the same time.

3.4 The Torckler-Tango Layered Complex (TTLC)

The TTLC crops out in the SW Rauer Group where it occurs as a series of elongate mega-boudins that are typically 20 - 150 m long. The largest and least deformed boudins occur on Torckler, Tango and DH Green Islands, although other minor outcrops also occur on Babe Ruth and Pete's Islands. These mafic - ultramafic bodies are enclosed within and are locally intruded by homogeneous felsic orthogneiss (*e.g.* Figure 3.16) similar to sample TI13 from Torckler Island, dated at 2810 ± 14 Ma by Kinny *et al.* (1993; see section 3.6.2).

In contrast with the coarse-grained SLC, the TTLC is mostly an equigranular medium-grained two-pyroxene granulite, although some of the most basic compositions are orthopyroxene-phyric. Compositions within individual boudins or layers range from websterite to leucogabbro, with changes defined entirely by the modal abundances of clinopyroxene, orthopyroxene and plagioclase. There are also other important macroscale differences between the two complexes, most notably that the TTLC was not intruded by mafic dykes. However, the presence of a rare (there is only one!) SLC xenolith in the Homogeneous Felsic Gneiss (TG?) near to the TTLC on Tango Island (Figure 3.15), and the similarity between this felsic gneiss and the TG on Scherbinina Island, indicates that these two metaigneous complexes were both part of the Archaean Rauer Group domain by 2800 Ma. Certainly, both complexes appear to have experienced the same late deformation episodes, and in common with the SLC outlined above, the TTLC was folded and refolded prior to felsic orthogneiss intrusion at *ca.* 2800 Ma.

Although clearly affected by multiple regional deformation episodes, the competency contrast between the TTLC and the surrounding homogeneous felsic orthogneiss has led to pronounced strain partitioning between the two lithologies. The felsic orthogneiss has accommodated most of the deformation and it commonly has a strong foliation, whereas the TTLC behaved much more rigidly, tending to boudinage rather than flow. Such strain partitioning has enabled the boudins to retain many of their primary igneous protolith features and the TTLC can now be regarded as a series of low-strain lenses.

3.4.1 Relict igneous features

Despite being folded, refolded (Figures 3.16 - 3.18) and boudinaged, the TTLC retains a variety of primary igneous features including graded and cross-stratified layering. Individual layers are often compositionally graded on scales from 5 cm to 2 metres (Figures 3.19 - 3.21) and are defined by orthopyroxene, clinopyroxene and plagioclase in varying proportions. Metamorphic hornblende is minor and tends to be restricted to the more deformed ultramafic horizons. Layers are commonly cross-stratified or repeated rhythmically on centimetre- to decimetre-scales. These layering features are typical of layered igneous complexes (see Upton, 1987 and other references in Parsons, 1987) and are clearly *not* the product of metamorphism or deformation.

The ultramafic layers preserve the most abrupt and contrasting compositional changes with clinopyroxenite and orthopyroxenite layers alternating on a cm-scale, although they are sometimes graded. One facies of ultramafic composition is porphyritic and contains cm-sized, deformed, bronzite phenocrysts (Figure 3.22) in a medium-grained groundmass of granoblastic orthopyroxene and clinopyroxene.

3.4.2 The effects of metamorphism and deformation

In contrast to the SLC, where coarse-grained relict igneous textures and primary igneous phases are variably preserved, the TTLC was almost entirely recrystallized to a medium-grained granoblastic to lobate granulite. Although foliation or fabric development is generally minimal, recrystallized graded and rhythmic layering defines isoclinal and refolded folds with 5 - 50 m wavelengths (*e.g.* Figures 3.16 & 3.17) These fold structures are locally truncated by thrust or detachment surfaces (*cf.* Upton, 1987) and a variety of leucocratic felsic veins or narrow sheets (*e.g.* Figure 3.17). Although such features cross-cut

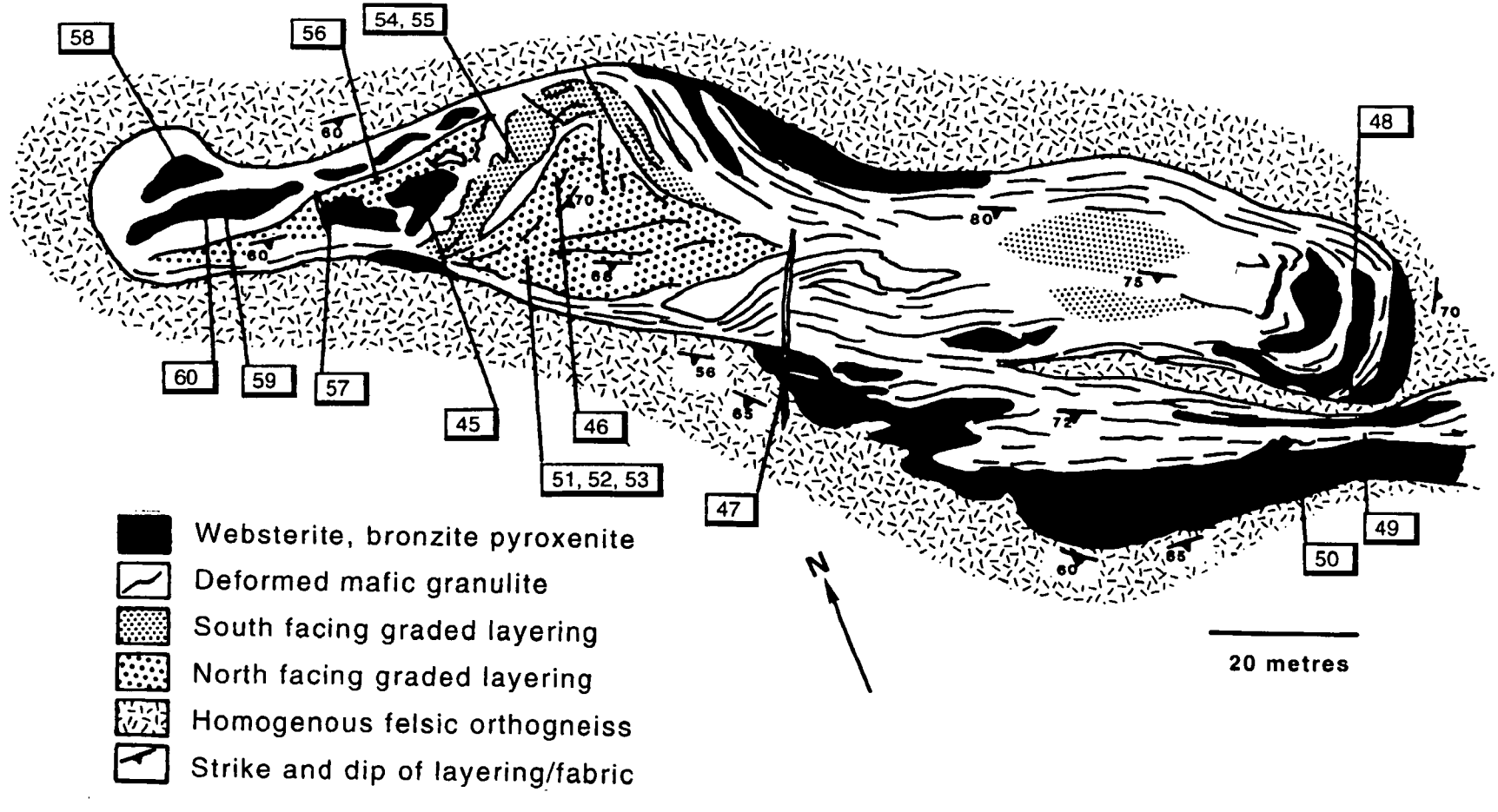

Figure 3.15 Outcrop sketch map of the TTLC at Green Isle showing the inrusive contacts with the Homogeneous felsic orthogneiss. Sample localities are shown in bold boxes and are prefixed RI/tear/## (locality: central DH Green Isle).

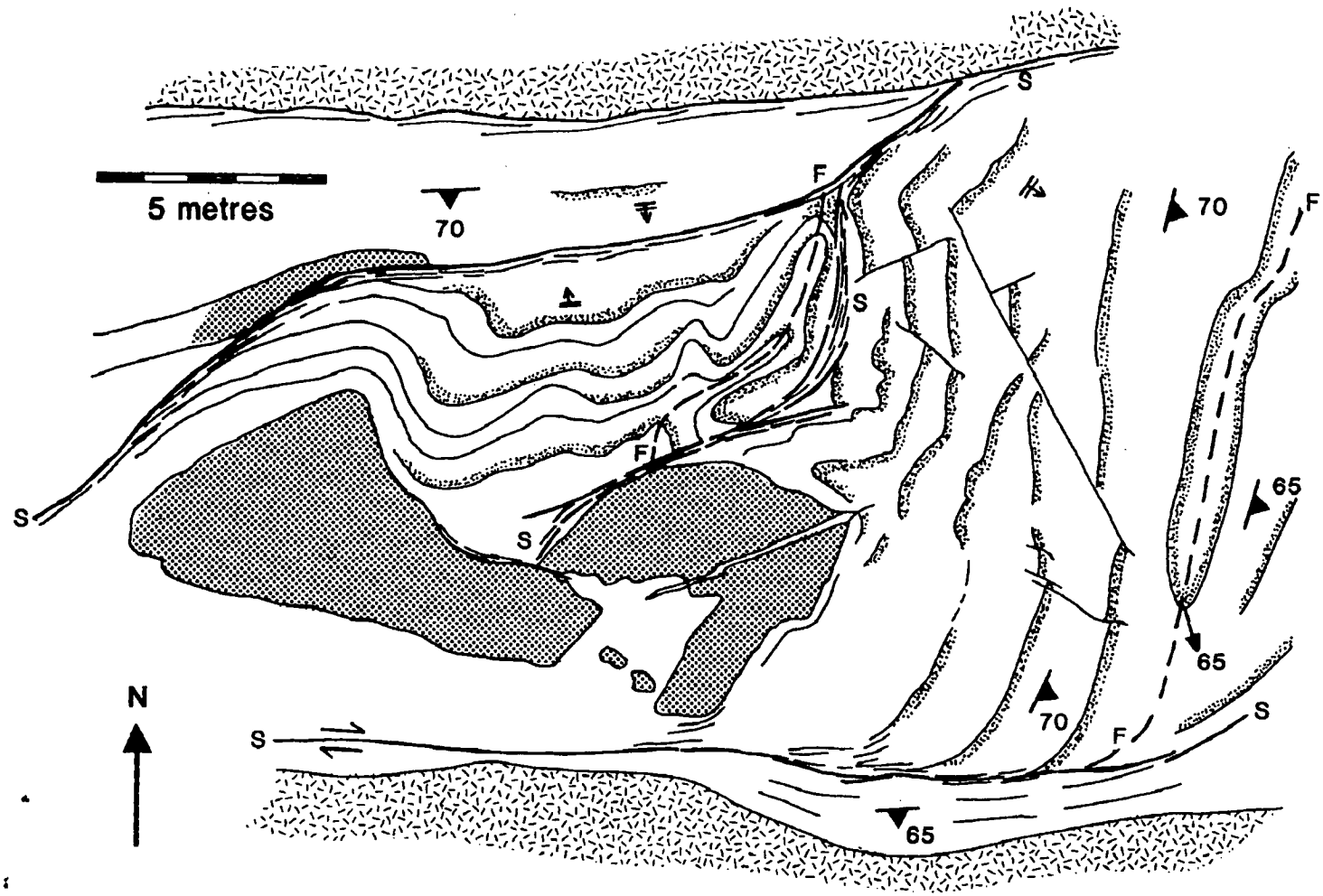

Figure 3.17 A detailed field sketch of the TTLC at Green Isle. Note refolded isoclines and internal thrust or detachment surfaces that are contained within the boudins (after Harley & Fitzsimons, 1995; locality: central DH Green Isle between samples 46 and 57 on Figure 3.16.)

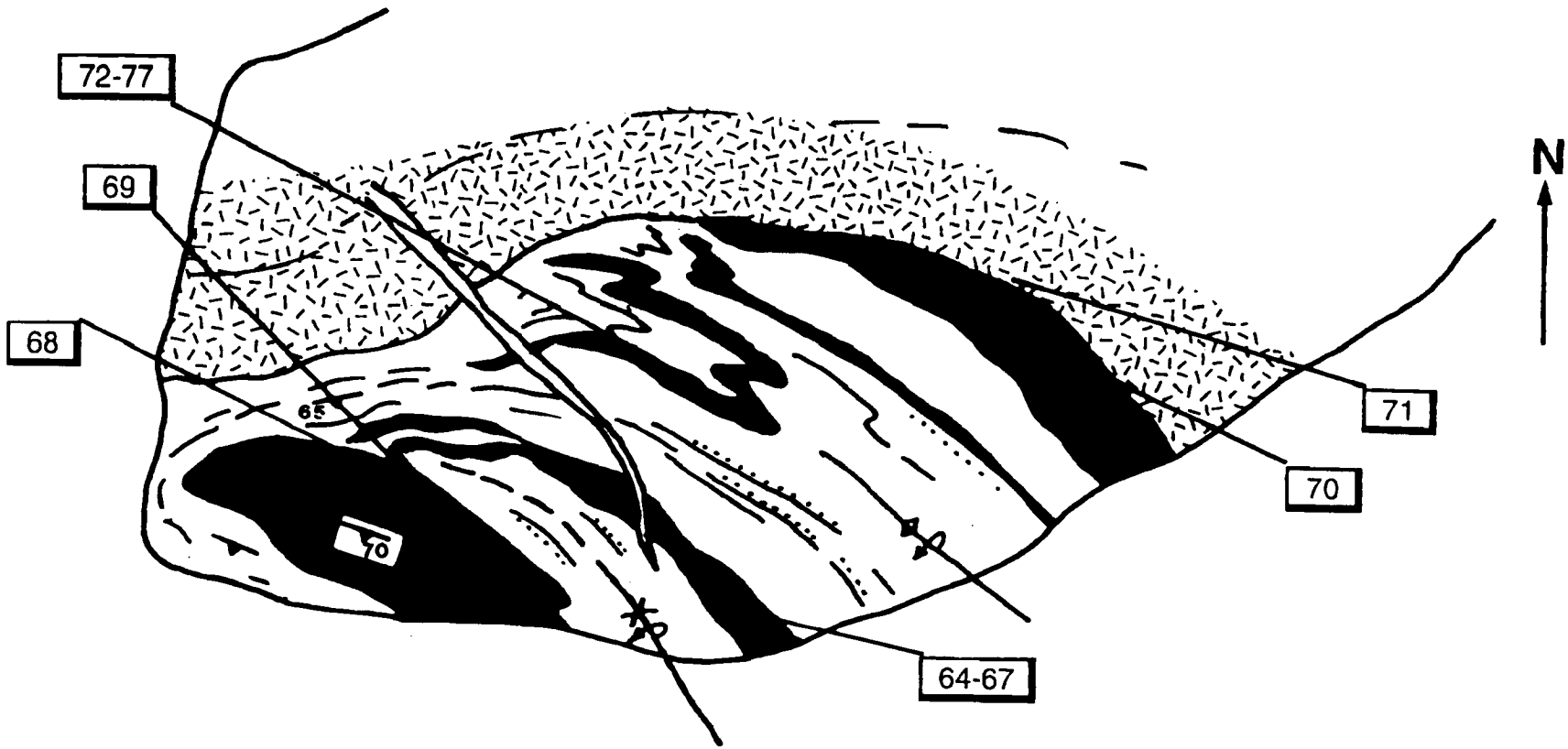

Figure 3.18 Outcrop sketch map of the TTLC at Torkler Island. The overall structure of the boudin is of a steeply plunging antiformal synclline. Sample localities are also shown and are prefixed RI/year/## (locality: SW Torkler Island).

Figure 3.19 Close, metre-scale, folded mafic layer in the TTLC (locality: central DH Green Isle; Vegemite jar for scale is 10 x 7 cm).

Figure 3.20 Decimetre-scale graded modal layering in the TTLC. Note: (i) layers are right way up and are offset by small normal extensional faults. The relatively competent mafic layers deformed by 'brittle' failure whilst the more leucocratic interlayers deformed by solid-state flow; (ii) The relatively undeformed features in the lower part of the photo pass into a high-strain zone towards the top (locality: E side of Tango Island in the detailed section on Figure 3.21; Pencil for scale is 16 cm long).

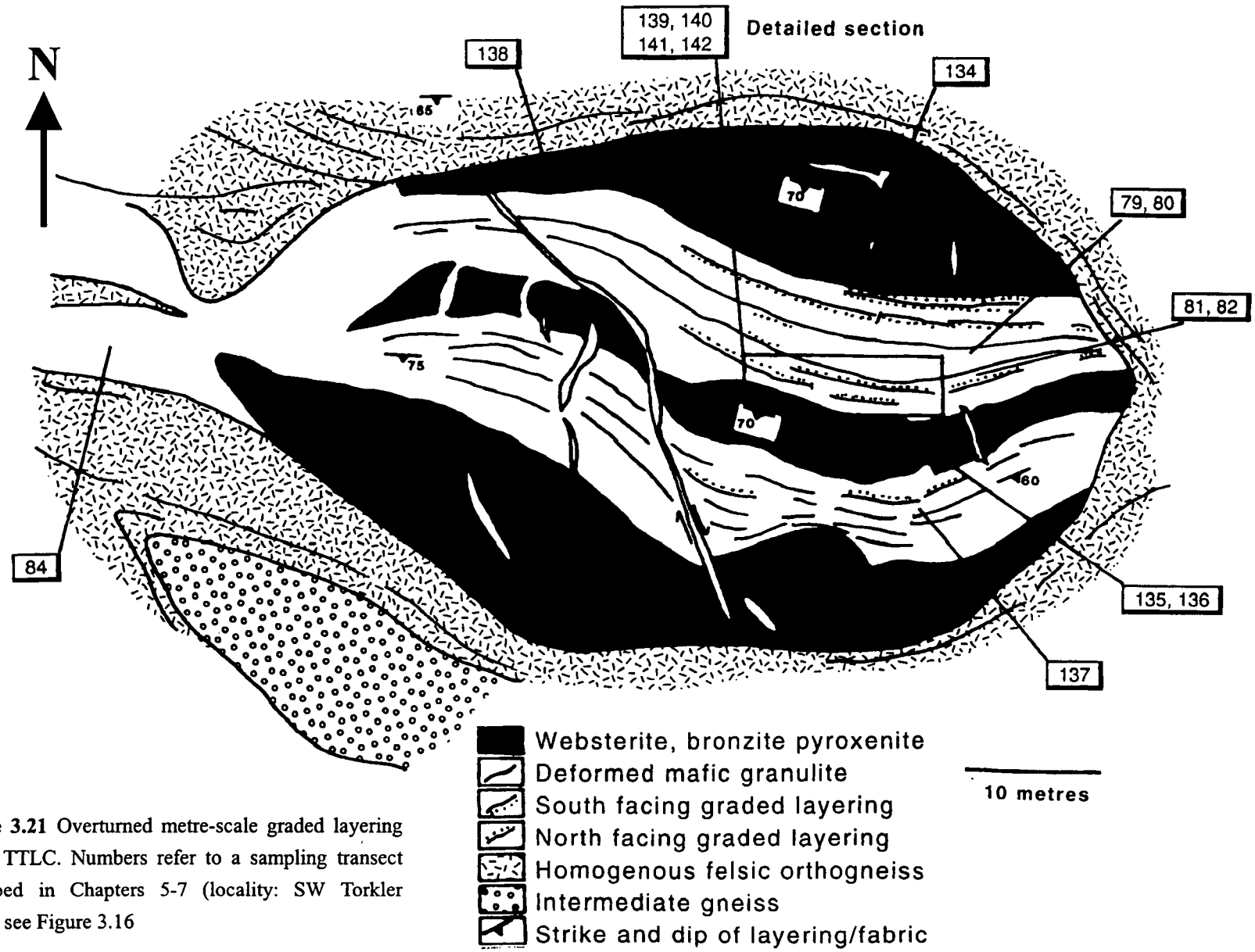

Figure 3.21 Overturned metre-scale graded layering in the TTLC. Numbers refer to a sampling transect described in Chapters 5-7 (locality: SW Torkler Island, see Figure 3.16

Figure 3.22 Bronzite-phyric layer in the TTLC. Euhedral bronzite phenocrysts are commonly 1-2 cm long (locality: central DH Green Isle; scale bar is 20 cm).

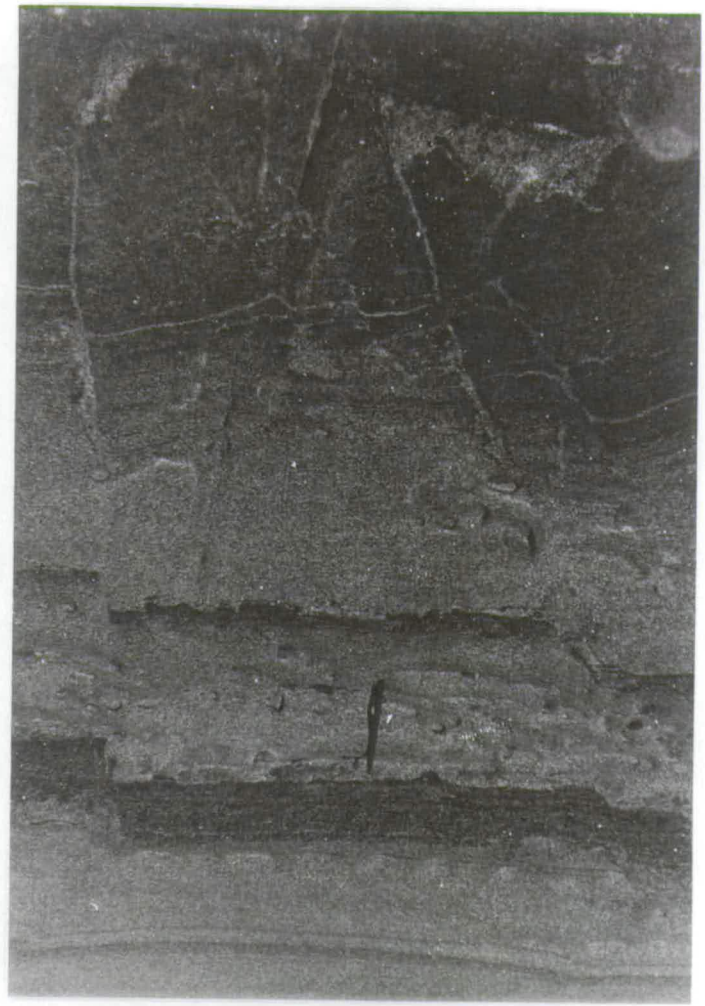

Figure 3.23 Normal extensional faults in TTLC. Note that some fault planes are picked out by small veins of leucosome (locality: within the detailed section shown on Figure 3.21; pen for scale is 15 cm long).

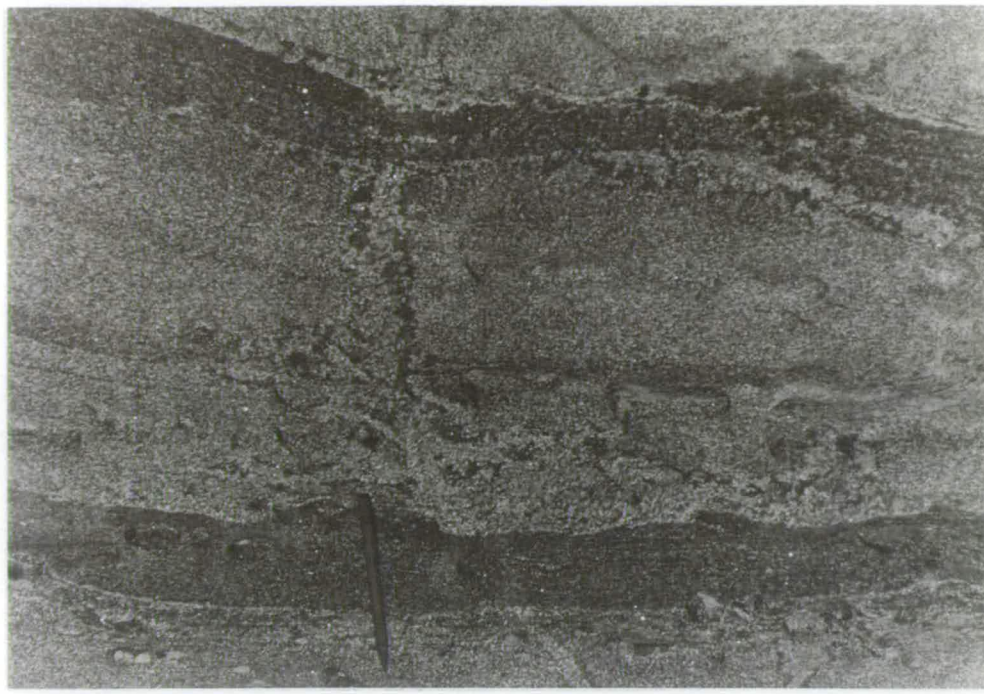

Figure 3.24 Branches of leucosome passing from bottom to top through decimetre-scale graded modal layering in the TTLC. Note (i) melts appear to permeate through horizons of mafic composition, but presumably broke through the ultramafic horizon at a fracture controlled location away from the plane of the outcrop shown here; (ii) some melt has ponded beneath the relatively impermeable upper ultramafic horizon whilst minor amounts also moved along the mafic/ultramafic interface above the lower layer (locality: within the detailed section shown on Figure 3.21; pen for scale is 15 cm long).

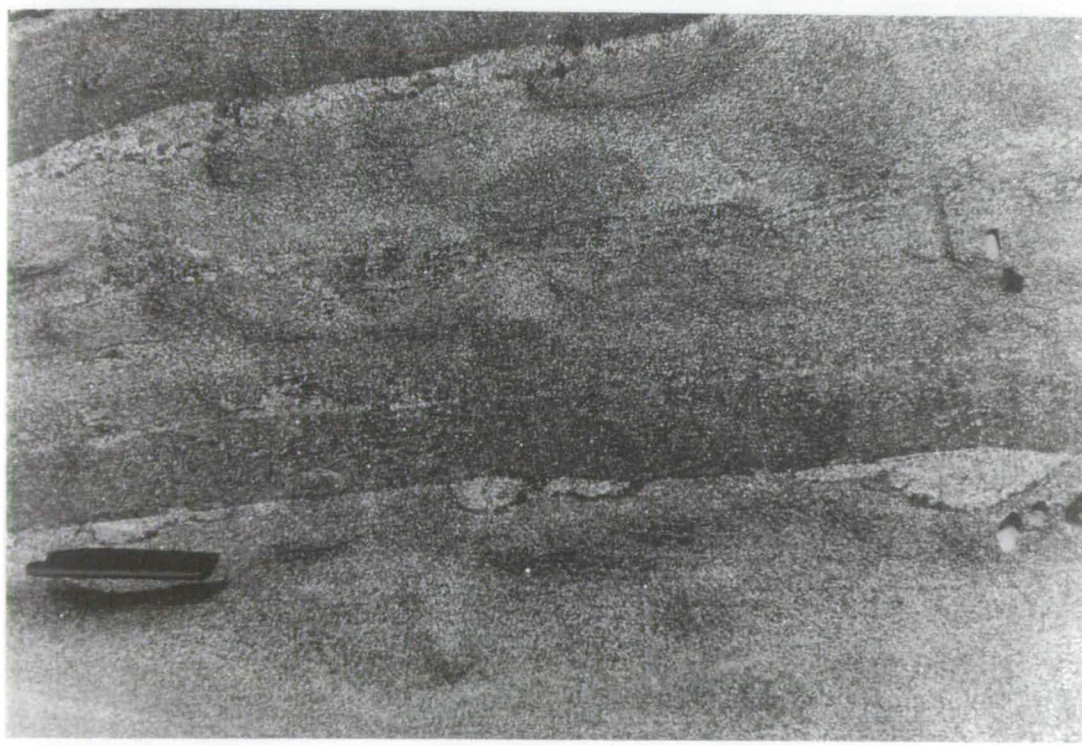

Figure 3.25 Channel structures define melt conduits at the interface between ultramafic and mafic layers. The geometry of the conduit on the RHS of the photo indicates that melt moved perpendicular and upwards relative to the plane of the outcrop. These geopetal structures indicate that melt generation occurred when these graded layers were right way-up, and hence could predate folding (locality: within the detailed section shown on Figure 3.21; pen for scale is 15 cm long).

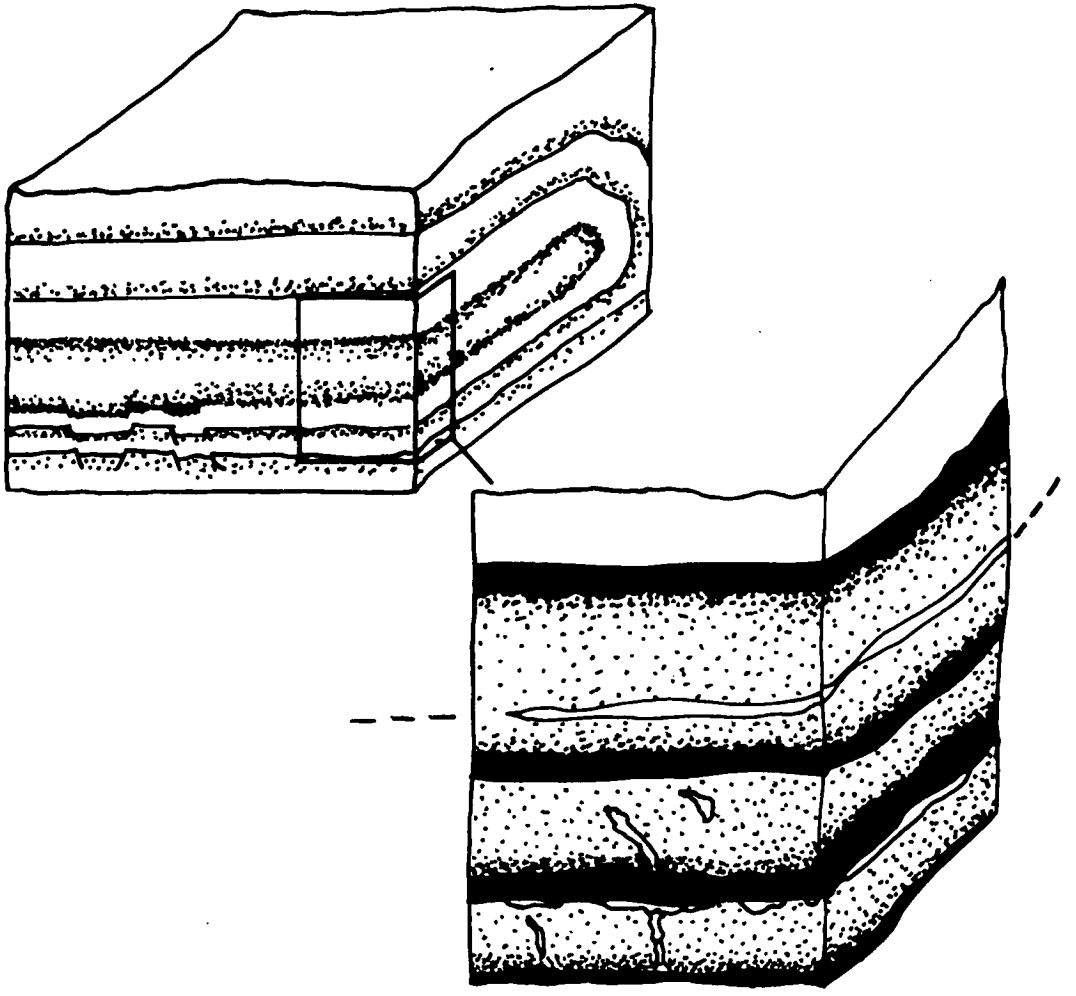

Figure 3.26 Schematic block diagram of the detailed section shown on Figure 3.21, showing the relationship of the isoclinal fold, axial planar leucosome and minor leucosome that is perpendicular to the axial plane (*e.g.* Figure 3.23; locality: Tango Island).

primary layering and early fold structures, they terminate within the TTLC boudins and do not extend into the surrounding Homogeneous Felsic Orthogneiss. On the basis of such relations, two phases of folding and a variety of localized internal deformation features are inferred to have affected the TTLC prior to intrusion of Homogeneous Felsic Orthogneiss which, on the basis of correlation with felsic gneisses dated in the region by Kinny *et al.* (1993), is infered to have occurred at *ca.* 2800 Ma.

The effects of internal deformation are most spectacularly developed on Tango Island where a recumbent isocline (see Harley, Snape & Black, 1995) is preserved in a large boudin on the NE side of the island. Internal deformation structures vary between plastic and brittle depending on bulk composition. Competent mafic-ultramafic layers have deformed by brittle, normal or listric, extensional faults (Figure 3.23), whereas leucogabbroic interlayers deformed by ductile flow. Brittle structures commonly terminate in these interlayers but reappear in adjacent mafic-ultramafic horizons.

Features similar to those depicted in Figures 3.17 and 3.23 have been noted in largely undeformed layered igneous complexes (*e.g.* Upton, 1987) where they are thought to have formed by localized ductile deformation at a time when igneous layers were only partly crystalline. Similarly, the occurrence of slump folds is well-documented from the layered complex of Rum and felsic veins are commonly observed to back-intrude mafic complexes. Such discordant felsic intrusives are interpreted to have formed by the redistribution of residual melts during a late magmatic phase (*e.g.* Marshall & Sparks, 1984; Lanyon *et al.* 1993).

However, the origin and timing of the fault development and melt intrusion in the TTLC is problematic. *Prima facie* evidence that faulting and melt injection occurred *before* folding in the late magmatic stage is not present. Although the upper overturned limb of the isocline does contain inverted graded layers (assuming that layering was initially 'normal'), the fault structures described above are not observed. It is also unfortunate that the felsic veins, whilst often discordant to primary layering, are discontinuous and cannot be traced directly across the axial region of the fold.

Nevertheless, there is circumstantial evidence that faulting and melt injection probably occurred *synchronously or after* folding and significantly after crystallization. Narrow felsic veins are markedly discordant to primary layering in the limbs of the fold, but are often virtually parallel to layering and are axial planar to first (?) generation folds in the core of the isocline. Regardless of orientation, none of the veins cross-cut the tectonic contact

between the boudin and surrounding homogeneous felsic orthogneiss and they are not found in the latter. On balance it is likely that the felsic melts and extensional structures developed either synchronously with or during the late-stages of folding. This scenario is the most plausible because it accounts for melt veins that are perpendicular and those that are parallel to the axial plane of the fold. The more extensively developed perpendicular variety can be explained because the limbs of the isocline would have responded by locally extending as the overall deformation within the boudin evolved from folding, to flattening and extension, and then boudinage.

Following from the interpretation that melt injection occurred synchronously to late in the folding history, it is reasonable to interpret the intrusive features as geopetal structures. Figures 3.24 and 3.25 illustrate how melt appears to have easily migrated upwards through leucogabbroic layers, but appears to have ponded beneath more competent or impermeable mafic horizons. The passage of melt across such layers is restricted to areas of inherent weakness, such as faults, or to local well-defined areas of melt break through. It is interesting to speculate that ovoid to elongate leucosome patches apparent in sections exposed perpendicular to the fold axis, probably represent conduits where melt flowed in channels along the interface between mafic and leucogabbroic layers. This interpretation has been summarized schematically in Figure 3.26.

If the interpretation that felsic veins contained within the TTLC are syntectonic leucosome is correct, then there are a number of potentially important implications:

- Dating the leucosome would directly constrain the timing of the earliest deformation event thus far identified in the Rauer Group.

- Interpretation of protolith chemistry in terms of igneous parentage *in this area* might be significantly flawed, since the leucosome could be of local derivation (Discussed further in Chapters 5-7).

3.5 Summary

The Archaean domain in the Rauer Group is dominantly composed of 4 orthogneiss suites that enclose two minor Archaean paragneiss units. A geological event sequence has been deduced for each of the orthogneiss suites and is summarised in Table 3.1. Direct correlations between structures in individual gneiss units is problematic in any gneiss terrane, but is particularly difficult in a terrane as complex as the Rauer Group.

Nevertheless, some degree of consistency is emerging and it is apparent from fieldwork that the three oldest crustal components, the CLO, SLC and TTLC, all underwent two phases of folding prior to intrusion of TG protolith. Following emplacement of TG protoliths, all 4 orthogneisses were co-deformed by a series of events between *ca.* 2800 - 500 Ma.

3.6 Strategy for detailed follow-up work

Although the CLO and Homogeneous Felsic Orthogneiss are the most abundant gneiss components in the Rauer Group, they are not ideally suited to detailed geochemical study. This is because:

- CLO and Homogeneous Felsic Orthogneiss are usually highly strained, hence relationships and primary features are largely overprinted.
- CLO and Homogeneous Felsic Orthogneiss are composite gneiss associations where individual constituents (*e.g.* felsic and mafic compositions) are potentially unrelated
- Many protolith components have undergone partial melting and therefore probably do not faithfully preserve geochemical signatures that reflect initial crustal-growth processes.

For these reasons only a limited amount of time is devoted to the CLO and HFG lithologies in this study, although a representative selection (~40 samples) of these lithologies has been collected from throughout the Archaean domain.

The two remaining orthogneiss components, the layered meta-igneous complexes, can potentially tell us much about Archaean crustal growth in the Rauer Group. As these complexes are relatively competent mafic bodies, they retain primary igneous features that may independently constrain magma petrogenesis, and they are also less susceptible to melting during metamorphism. Moreover, both complexes have a range of compositions that are clearly genetically related and that can, theoretically, be used to geochemically model magma petrogenesis by inverse modelling techniques. There are, however, two significant drawbacks that are briefly described and assessed below:

(i) The complexes were recrystallized to granulite assemblages and, from the available isotopic evidence, there was at least one major fluid-infiltration event. Although these events are potentially capable of altering protolith chemistry, any likely affects can be assessed from the geochemical data so this need not be an excluding factor. In order to minimise any potential influences associated with metamorphism or, more importantly,

metasomatism, samples were selected from within low-strain areas away from HSZs, pegmatites and younger intrusions.

(ii) Our understanding of whole-rock chemistry as applied to cumulate rocks is limited (discussed further in Chapter 1). Cumulates are complex systems that are conceptually more difficult to deal with than lavas. Nevertheless, most of the samples selected for detailed study are from the layered complexes because, on balance, the potential advantages of a co-magmatic suite outweigh the disadvantages.

For each of the layered complexes, approximately 40 samples were taken for further study. In addition, a selection of mafic dykes from the SLC were sampled. In the first instance these dykes are divided on field criteria into early (Archaean) mafic dykes (MD1 & MD2) that intruded before the TG suite, and mafic dykes that intruded after the TG suite (MD3 and MD4). As with the main gneiss components, there are advantages and disadvantages of studying mafic dykes. The main advantage is that they are mafic rocks that more-or-less approximate to liquid compositions, hence they are easier to deal with than the cumulates. The main disadvantage is that none of the dykes can be assumed to be strictly related petrogenetically (*cf.* Hanson, 1989), especially when many of them are known to have intruded at different times. However, largely for the purpose of comparing the dykes with the SLC, and for comparison with the Proterozoic dykes in the adjacent Vestfold Hill, representative samples of the different dyke suites have been taken.

Chapter 4

Petrology of the Scherbinina and Torckler-Tango Layered Complexes

4.1 Introduction

The petrology and mineral chemistry of the layered complexes provides important independent information that can be used in conjunction with whole rock chemistry to constrain protolith petrogenesis. Additionally, metamorphic textures and phases retain at least a partial record of the *P-T*-fluid history of the rocks which in turn provides an insight into the chemical and isotopic evolution of the suites during the high-grade events. The main aim of this chapter is to document preserved magmatic mineralogy and textural criteria, and then assess to what extent primary chemistry has been retained. Given ideal assemblages, bulk compositions, and reaction textures, such an approach is capable of constraining a number of aspects of the magmatic and metamorphic evolution of these rocks, such as magma crystallization temperature, oxygen fugacity, emplacement pressure, and peak *P-T* conditions during the later high-grade events. In reality only fragments of this history are preserved and the techniques that are commonly applied to metaigneous rocks need carefully assessing before any petrogenetic or thermobarometric conditions can be deduced. A brief assessment of the suitability or practicality of alternative approaches to the thermobarometry techniques used here is included in the relevant sections (4.2.4 and 4.2.5).

Most of this chapter is devoted to the SLC since this is the most lithologically diverse comagmatic suite and because of it's key role in defining the structural evolution of the Rauer Group. A less detailed account of the TTLC is presented because this complex is mineralogically quite restricted. A brief account of the Tonalite Gneiss (TG) and early (Archaean?) mafic dykes (EMD) is also included here because they are considered further in later chapters, primarily in the context of 'crustal evolution and terrane assembly in East Prydz Bay' (Chapter 13).

4.2 Petrology and mineral chemistry of the Scherbinina Layered Complex (SLC)

4.2.1 Outline petrology of the main lithological groups

In the field the SLC is a distinctive coarse-grained gabbro that has variably preserved igneous textures in sections perpendicular to the regional mineral elongation lineation. Compositionally, the complex has been arbitrarily divided into ultramafic websterites, melanocratic gabbros (melagabbros), intermediate gabbros, and leucocratic ferrodiorites. In addition there are a variety of late-stage intrusions including minor Fe-Ti oxide[1]- and sulphide-rich veins, and Fe-Ti oxide ± quartz ± garnet pegmatites. Decimetre- to metre-scale gradations between the main lithological types and the late-stage intrusions implies that all are related by fractional crystallization processes and therefore comprise a compositionally varied comagmatic suite.

Ultramafic websterites and amphibole websterites

This lithological division is broadly defined by having less than 10 % feldspar, but is otherwise compositionally and texturally varied. This variability reflects initial bulk composition, size of primary phases and textures, and the degree to which the rocks were recrystallized and deformed. Some layered websterites that are unequivocally part of the complex (*e.g.* RI108) have alternate layers of bright green chrome diopside, orthopyroxene, with lesser amounts of phlogopite, sulphides, apatite and secondary hornblende. Large orthopyroxene and clinopyroxene phenocrysts, typically 2-3 cm in length, are still recognizable in hand specimen but microscopically have been internally recrystallized to a granoblastic two pyroxene texture where individual phenocrysts are replaced by mineral domains dominated by one or other pyroxene type. One remarkable example of this rock type [GR 198 612] has been deformed into a kink band where individual orthopyroxenes are deformed and sharply folded at right angles.

More commonly, rocks of this composition are dominated by orthopyroxene and hornblende with appreciable amounts of Fe-Ti oxide. They occasionally have large (1 cm) ragged primary orthopyroxenes that are partly replaced by metamorphic amphibole (*cf.* Section 4.2.2 and Figure 4.1). Most orthopyroxenes are generally pleochroic pink to colourless, have

[1]BEI reveals that magnetite and ilmenite are usually intergrown reflecting exsolution and/or oxidation-exsolution processes.

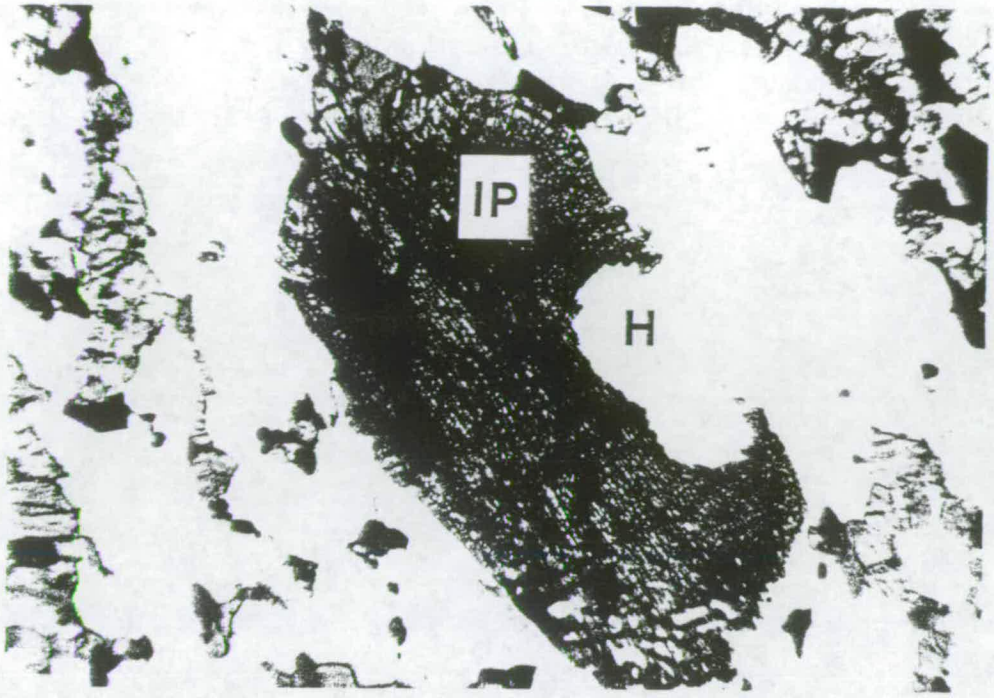

Figure 4.1 Photomicrograph of large primary pigeonite now exsolved on a fine scale into an intergrowth of Cpx and Opx. The margin is ragged and is partly replaced by Hbl and Plag. IP indicates igneous pyroxene, H indicates a hole in the slide. The groundmass is predominantly Plag, Cpx, Opx and Hbl (field of view is 3 mm across).

a medium-grained granoblastic to lobate texture, and hence are not igneous. Hornblendes are typically elongate, pale green, and generally larger than the orthopyroxenes.

A third variety of the ultramafics appears to be later in age than the main complex (see Section 4.3). It comprises Hbl > Cpx > Opx, with minor biotite and only accessory (~1-3 %) Fe-Ti oxides. All phases appear to be metamorphic and biotite was the last phase to form. This rock type is interpreted to be a dyke as field evidence indicates that it intruded after the formation of primary compositional layering. The dyke (RI38) possibly has a magmatic composition, but it is unclear if it represents a highly altered metabasite that has undergone partial melting. There are coarse plagioclase-quartz 'sweats' or patches that could be melts, but these have not been studied in detail and their status and age is uncertain.

Melagabbros (mafic gabbros)

These are coarse-grained and are distinguished from the ultramafics and leucocratic varieties by having 10-30 % plagioclase. They comprise either intergranular or oikocrystic (spotted) varieties although in detail relict textures are recrystallized to medium-grained

granoblastic to elongate mosaics of orthopyroxene, hornblende, clinopyroxene and plagioclase with lesser amounts of Fe-Ti oxide and accessory phases. Nevertheless, variations in modal abundance define regular cm-scale textural domains that are defined by plagioclase- or ferromagnesian-rich aggregates. These sometimes occur as spheroidal to elongate felsic patches that probably correspond to primary feldspar aggregates (chadacrysts) enclosed by poikilitic clinopyroxene (oikocrystic), and are defined by a clinopyroxene- and orthopyroxene-rich framework (*cf.* Mathieson, 1987). The clots comprise approximately 40-60 % plagioclase, with the remainder made up of clinopyroxene, orthopyroxene and hornblende.

Intermediate gabbros

These make up the bulk of the complex and constitute the average composition of individual layers. They do not have oikocrystic textures but, as with the more mafic varieties, coarse partly recrystallized textural domains are common. Modal proportions of the main phases are variable but are generally in the order Plag > Hbl > Cpx ≅ Opx > Fe-Ti oxides, with relict feldspar sometimes present. Additional phases include accessory apatite and zircon and minor late biotite. Recognizable relict phases (pyroxene & feldspar) are common and locally constitute up to 30 % of the rock (see also Section 4.2.2). Occasionally mm-scale primary layering, defined by partially replaced pyroxenes, is preserved. Such fine-scale primary layering is usually truncated at a shallow angle by a later tectonic fabric defined by hornblende or more rarely biotite.

Leucocratic ferrodiorites and felsic pegmatites

These comprise only a small percentage of the complex (< 5 %). Modal proportions are generally Plag >> Hbl ≅ Cpx ≅ Opx ≅ Fe-Ti oxides > ternary feldspar > Qtz, with minor apatite, biotite and zircon. The pegmatoidal varieties have abundant plagioclase and Fe-Ti oxides and locally have minor garnets. The coarse textural arrangement of the pegmatites is essentially igneous but has been recrystallized on intra- and inter-grain scales. Ternary feldspar and partially-replaced magmatic pyroxenes are common. The garnets are clearly metamorphic and are separated from metamorphic orthopyroxene by plagioclase moats. Accessory zircon, apatite and chalcopyrite constitute up to 5 %.

Late-stage oxide- and sulphide-rich patches and veins

Field relations indicate that these rocks types represent the last phase of activity in the complex prior to the high-grade deformation events. Sulphide-rich patches and veins are

very rare and constitute less than 1 % of the complex. They dominantly comprise pyrite and chalcopyrite with minor pyrrhotite. These rocks are of limited petrogenetic value and have not been considered further. The oxide-rich patches, by contrast, proved to be of crucial importance as they contain abundant large euhedral zircons that were ultimately used to date the complex (Detailed in Sections 4.2.6 & Chapter 6). The patches have locally variable assemblages but generally comprise Mag/Ilm, Grt, Plag, Opx, Qtz, zircon, chalcopyrite, pyrite, pyrrhotite and allanite (rare). The oxides are disseminated throughout whilst Grt-Opx-Plag-Qtz occur as coronites where garnet is separated from orthopyroxene and quartz by plagioclase moats. Large zircons and small plagioclase laths are sometimes contained within metamorphic garnets. Details of zircon morphology and garnet-bearing assemblages are given below in Sections 4.2.2 and 4.2.5 respectively.

4.2.2 Preservation of igneous textures

Many of the gabbros, especially those without a strong foliation/lineation, preserve coarse-grained igneous textures and relict mineral phases. These are less commonly found in more mafic compositions and tend to be best preserved in low strain areas in the complex away from shear zones. Although recrystallized extensively at the microscopic scale, intergranular, sub-ophitic and weakly porphyritic textures (Figure 4.1) are recognizable in coarse domains of 1 cm or greater. Such textures are distinguished by the overall distribution of (metamorphic) ferromagnesian minerals and feldspar and the partially recrystallized vestiges of primary phases. A number of relict igneous phases are still recognizable, the most abundant being exsolved pyroxene and feldspar, with less common apatite, zircon, magnetite and ilmenite. These primary phases are distinguished from later metamorphic generations largely on the basis of morphological, textural and cross-cutting criteria. These features are described more fully below for the pyroxenes, feldspars and zircons.

Igneous pyroxenes

Relict pyroxenes are the most easily identified igneous phase that can be distinguished in thin section. They range in size from about 2 mm to 1 cm and sometimes still retain their euhedral shape (Figure 4.1). Around the margins they are often recrystallized to a fine- to medium-grained polygonal mosaic of Opx, Cpx, Hbl and Plag, whilst internally the pyroxenes are characterised by sieve and patch replacement by hornblende which is superimposed on irregular lamellae of Opx and Cpx. Although the Hbl preferentially exploits Cpx lamellae (Figure 4.2 & 4.3) it is discordant overall and is clearly a late feature.

Unlike the igneous feldspars described below, the exsolution lamellae are not strictly crystallographically oriented and commonly bifurcate or taper to a point (*cf.* Figures 4.2 & 4.3 with Robinson, 1980; figures 33 & 34). Despite this morphological irregularity, the Opx-Cpx lamellae are attributed to exsolution from originally sub-calcic compositions. Lamellae are uniformly developed within the mm-scale domains chosen for reintegration (described in next section) and, importantly, there is no coarsening towards grain margins.

Igneous feldspars

Relict igneous feldspars have only been recognised in the more evolved rock types and are most common in the leucocratic ferrodiorites. They can be distinguished from secondary feldspars by the presence of regular exsolution lamellae comprising orthoclase in host plagioclase. Exsolution textures are variable. They include small (*ca.* 5μm) blebs or discontinuous stringlets; fine lamellae that are usually parallel and often display two or three distinct orientations (Figure 4.4); and well-developed, coarse (10-40 μm), euhedral to subhedral lozenge shaped forms (Figure 4.5). Such exsolved textures commonly define regular zones or core regions that are typically surrounded by more homogeneous plagioclase mantles (Figures 4.5). Core regions are entirely free from inclusions whereas the plagioclase rims contain polyphase inclusions. Primary plagioclase and alkali feldspar has not been identified on either textural or compositional grounds in any of the rocks from the main SLC intrusion (plagioclase enclosed within garnet in RI15 might be the exception).

Igneous zircons

Zircons in this rock are coarse (100-600 μm), euhedral, and mostly preserve the simple first order prismatic and pyramidal faces typical of crystallisation from a melt phase (Figure 4.6). Rare grains are botryoidal or ragged. Cathodoluminescence (CL) and backscattered electron imagery (BEI) of the prismatic zircons reveals two distinct types of compositional variation in all grains. Fine-scale regular magmatic oscillatory can be seen in CL in the core regions of some grains and there is a corresponding general growth zoning from core to rim that is revealed by BEI. These primary features are overprinted by irregular to cuspate regions that are both bright and dark in BEI and that occur mainly near grain rims. The latter zones are also focused along annealed fractures that traverse zircon cores. These features are discussed in more detail in Section 4.2.6 where the zircon chemistry is described.

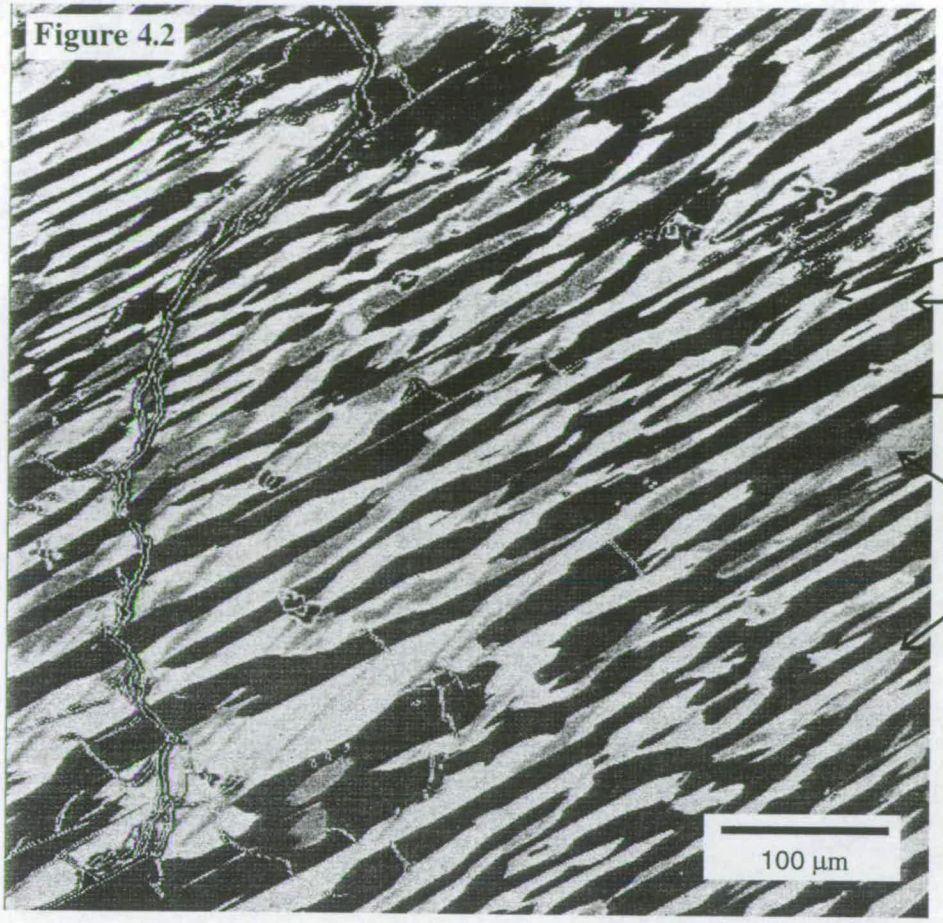

Figure 4.2 BEI of exsolved and partly replaced pigeonite. Opx, Cpx and Hbl are indicted. Note the Hbl referentially exploits Cpx and is discordant to the Cpx-Opx intergrowths.

Figure 4.3 Schematic representation of Figure 4.2. Square denotes typical areas used in modal reintegration.

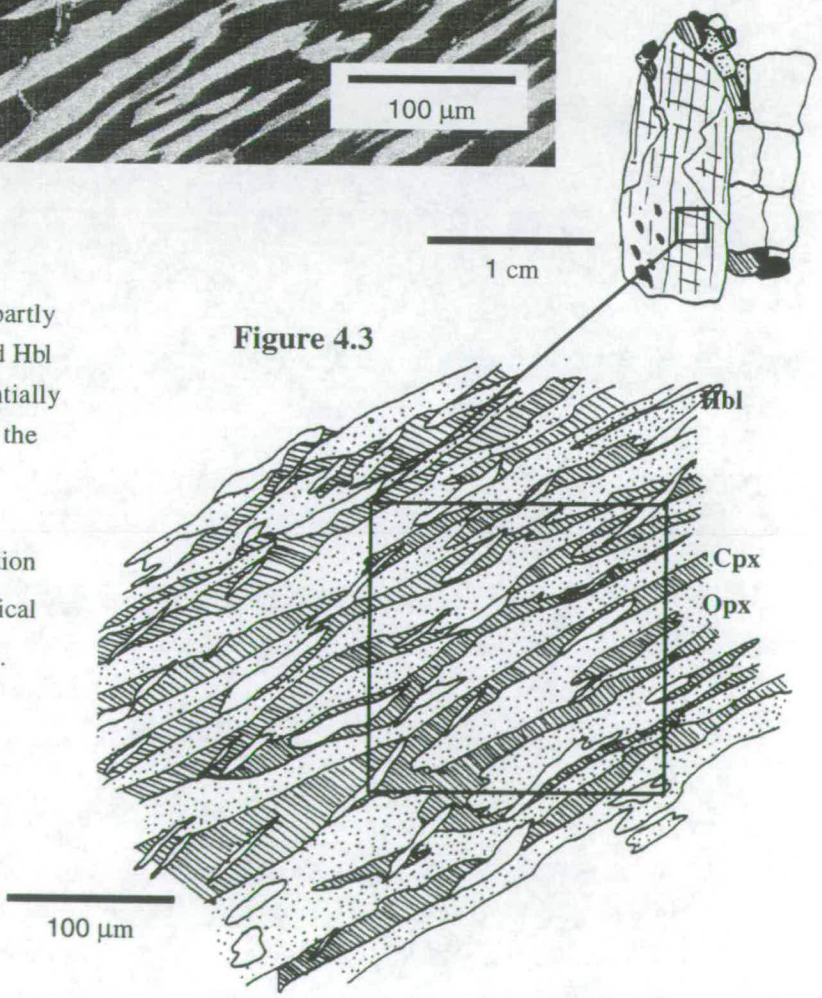

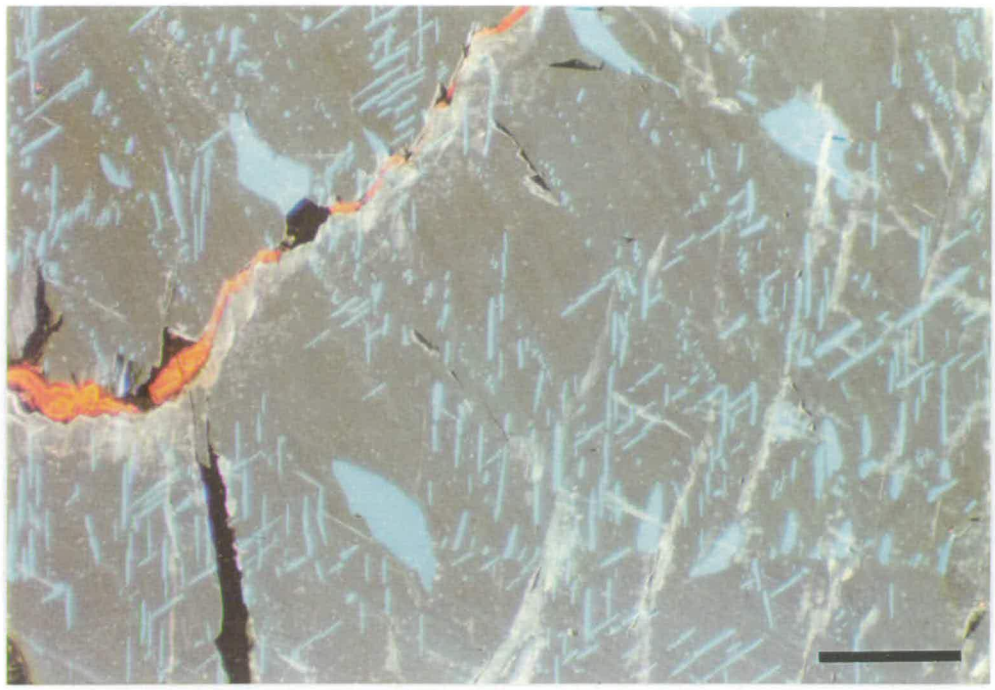

Figure 4.4 CL photomicrograph of exsolution textures in relict ternary feldspars. The light blue is orthoclase and the dark green-blue is plagioclase. The orange-red vein is minor late calcite replacement (scale bar is ~200 μm).

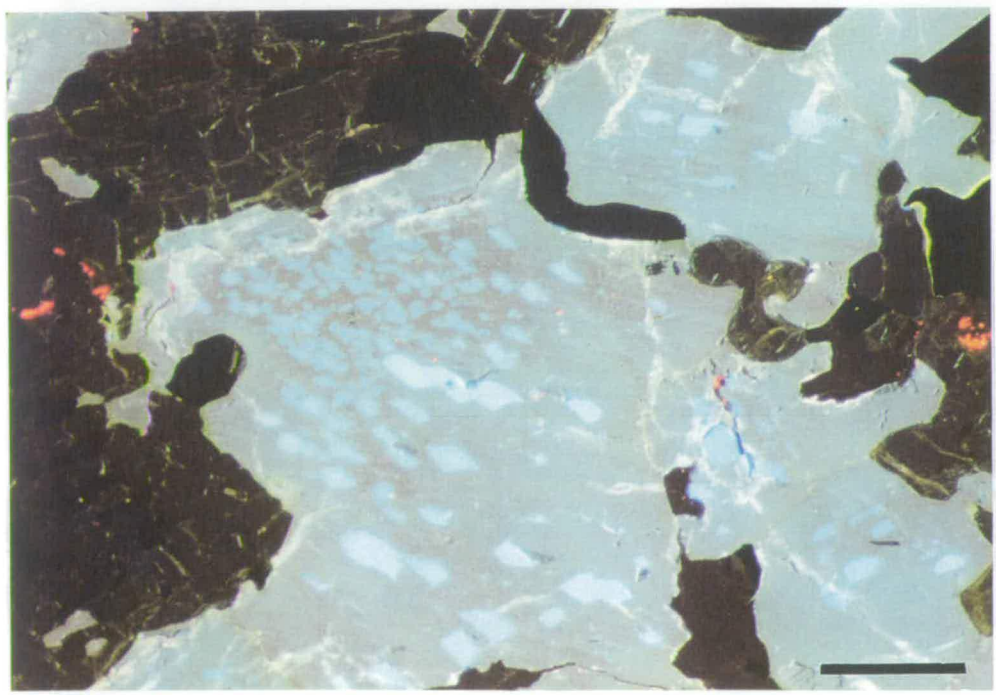

Figure 4.5 Regular exsolution lamellae in relict ternary feldspar. These coarse lozenge-shaped orthoclase exsolution forms are common in evolved SLC compositions. Dark brown minerals are Cpx-Opx; the black minerals are Mag/Ilm intergrowths; the minor orange-red patches are late carbonate (scale bar is ~400 μm).

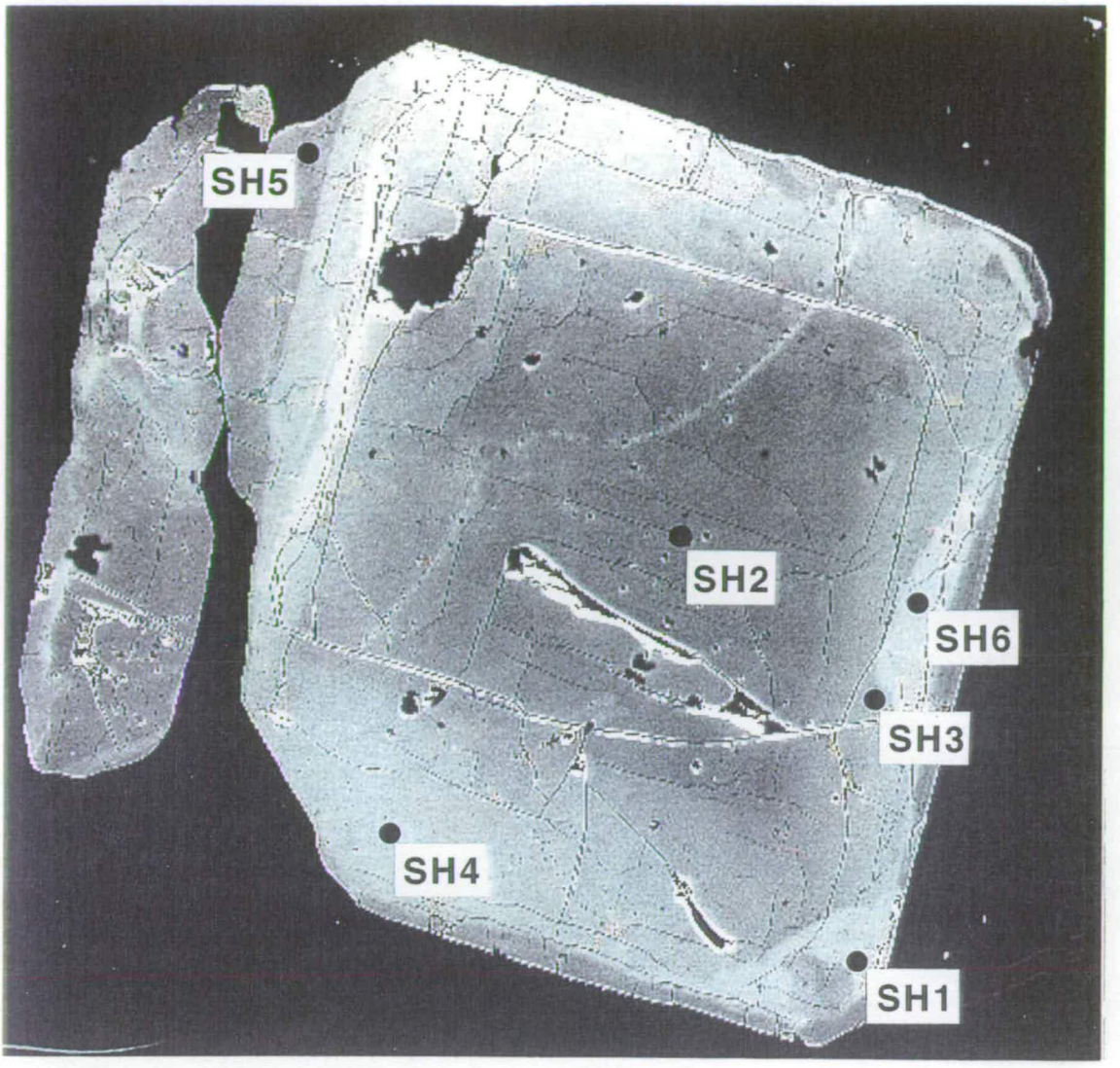

Figure 4.6 BEI of a typical coarse, euhedral magmatic zircon (zircon 8) from RI15. Note the regular zoning rimward to brighter BEI shade, and the irregular cuspate regions (bright and dark in BEI) near the grain rims. The chemical variations that cause of this features are discussed in the text (zircon is ~600 μm across). This figure corresponds to figure 8a in Harley, Snape & Black (in press).

4.2.3 Retrieval of igneous phase compositions

Techniques and assumptions

In an attempt to reconstruct primary phase compositions, the largest and least altered grains were studied in detail by electron microprobe. The approach involves analysing coherent (*s.l.*) domains that are recognizable as being of igneous origin on textural grounds. The modal proportions of host and guest within the exsolved domain were estimated by BEI processing and then each phase was analysed for the major elements. This allows a reintegrated original bulk composition to be calculated.

A number of assumptions are inherent in this approach, any one of which could potentially influence the reintegrated composition. The most important assumptions relate to the scale of open system chemical mobility. Individual grains, or at least texturally recognizable parts of grains, should have remained closed chemical systems during cooling, metamorphism and deformation.

The first important assumption concerns the scale of diffusion during exsolution. So-called granule exsolution occurs when exsolved material migrates to form discrete grains at or near the edges of the original host (*e.g.* Lindsley & Anderson, 1983; Lindsley, 1983; Fuhrman & Lindsley, 1988). Although it is often difficult to determine chemically whether such migration has occurred, textural evidence often indicates which grains have been affected and to what extent. In order to minimise this possibility, domains were selected away from grain margins in areas that have regular exsolution textures (*e.g.* Figures 4.3 & 4.5).

For the feldspars, the condition of isochemical exsolution appears justified on textural grounds. For the pyroxenes this condition is not strictly attained because even the least altered pyroxenes have a small amount of hornblende replacement. A further assumption is therefore required: that most of the major element components of the hornblende are derived from the pyroxene and that Al, K, Na and the hydrous components are either very small[2] overall or were derived externally. Textural criteria suggest that hornblende largely formed at the expense Cpx and therefore the alkali and hydrous components are attributed to selective transport by fluids during metamorphism sometime after exsolution.

Clearly, the aforementioned assumptions suggest caution when viewing the final compositional and thermometry data. Nevertheless, steps were taken to minimise possible errors. Within individual grains, a series of areas were selected to avoid grain margins, microscale cracks, inclusions, and areas with patch replacement (*i.e.* more extensive) hornblende. Modal estimates for each of the phases were made using the BEI processing on the Cameca electron microprobe. This was commonly repeated for a number of areas within each grain to obtain average modal proportions for each phase. Individual lamellae were then analysed several times by electron probe micro-analysis (EPMA, see Appendix 1 for operating conditions), and several lamellae in each host grain were analysed in this way. The technique used to acquire the data is shown schematically in Figure 4.3. Compositional

[2]Since the amount of Hbl is effectively quite small and the non-pyroxene quadrilateral components are less than 2 mol. % (described in the next section), the Hbl has been included in the reintegration procedure.

data for all phases (Kspar, Plag, Cpx, Opx & Hbl) were usually very similar both within grains and between samples. Modal estimates were more variable but were usually within about 5 % of each other.

Pyroxene compositions

In total, 4 pyroxene grains were analysed by EPMA, 2 grains from RI19 and 2 grains from RI21. From a total of approximately 100 spot analyses, the average compositions for each phase in each grain is presented in Table 4.1. The results for each grain are similar. The orthopyroxene lamellae have compositions of about En_{44} with only a 1-2 % Wo component and the clinopyroxenes (augite) have compositions of about $Wo_{46}Fs_{32}En_{22}$. However, in order to reintegrate these compositions it is first necessary to recast the Hbl components. Since all three phases have very similar densities (~3.2), mixing is proportional to the modal abundance. Hornblende is relatively minor, usually comprising less than 20 %, hence the distribution of Mg, Ca and Fe is thought to closely reflect primary composition of the reintegrated grain.

Reintegrated pyroxene compositions listed in Table 4.1 and Figure 4.7 lie in the pigeonite field of the pyroxene quadrilateral (Morimoto, 1988), with end-member compositions that range between $Fs_{45}En_{40}Wo_{15}$ and $Fs_{39}En_{39}Wo_{22}$. Table 4.1 details average pyroxene compositions and calculated primary compositions from modal estimates (BEI processing). This compositional data is used in Section 4.2.4 for semi-quantitative thermometry to determine a minimum crystallization temperature for the SLC, and at the very least demonstrates that some of the thermal history prior to metamorphism is preserved.

A rigorous examination of pyroxenes from different bulk compositions to determine crystallization temperatures for the range of magma types, has not been undertaken because (i) time was not available given the broad nature of this study (ii) it is possible that subtle changes in pyroxene composition, and hence temperature estimates, are likely to be outweighed by the uncertainties and assumptions inherent in the approach.

Feldspar compositions

In order to minimise possible errors resulting from the exsolution process or later recrystallization, exsolved areas near grain boundaries, the core to rim transition, and feldspars with irregular or obvious granule exsolution, were avoided. Fortunately the feldspars are easier to deal with than the pyroxenes because the exsolved domains do not have a later overprint. This is restricted instead to neoblast plagioclase growth around the

Table 4.1 Average reintegrated pyroxene compositions. Since densities of these phases are all very similar, mixing is ~ proportional to abundances. Note also that Fe^{2+}/Fe^{3+} has not been estimated or corrected for the temperature calculation. * denotes calculations from Lindsley & Anderson (1983)

	RI19PX1				RI19PX3			
	Opx	Cpx	Hbl	Pig	Opx	Cpx	Hbl	Pig
SiO_2	49.78	51.11	40.20	49.13	49.63	49.42	40.22	48.00
TiO_2	0.08	0.17	2.55	0.54	0.10	0.40	2.32	0.77
Al_2O_3	0.63	1.26	11.39	2.76	0.76	2.18	10.73	3.79
Cr_2O_3	0.00	0.01	0.01	0.01	0.01	0.00	0.01	0.01
MnO	0.74	0.32	0.16	0.49	0.67	0.24	0.14	0.43
FeO	31.98	12.77	19.98	23.21	32.85	13.39	19.62	24.64
MgO	15.18	11.17	7.78	12.58	14.65	10.75	7.86	12.06
NiO	0.05	0.03	0.04	0.04	0.06	0.03	0.04	0.04
CaO	0.64	22.33	11.69	10.51	0.60	21.25	12.18	9.32
Na_2O	0.02	0.35	1.60	0.42	0.00	0.42	1.58	0.53
K_2O	0.01	0.01	1.67	0.30	0.00	0.12	1.39	0.40
Total	**99.10**	**99.52**	**97.09**	**100.00**	**99.34**	**98.19**	**96.08**	**100.00**
Modes	*0.47*	*0.36*	*0.17*		*0.48*	*0.27*	*0.25*	
Wo	0.01	0.47	0.30	0.23	0.01	0.46	0.31	0.21
En	0.45	0.32	0.20	0.38	0.44	0.32	0.20	0.37
Fs	0.53	0.21	0.51	0.39	0.55	0.22	0.49	0.42
Wo*	0.01	0.45		0.25	0.01	0.43		0.23
En*	0.46	0.35		0.37	0.44	0.36		0.36
Fs*	0.53	0.20		0.38	0.54	0.22		0.41
X_{Fe}				**0.50**				**0.53**

	RI21PX1				RI21PX2			
	Opx	Cpx	Hbl	Pig.	Opx	Cpx	Hbl	Pig.
SiO_2	49.49	50.78	40.46	48.59	49.76	49.72	40.32	47.95
TiO_2	0.10	0.20	2.60	0.70	0.10	0.58	2.58	0.86
Al_2O_3	0.71	1.40	11.05	3.28	0.69	2.99	11.19	3.97
Cr_2O_3	0.00	0.00	0.00	0.00	0.00	0.00	0.00	0.00
MnO	0.65	0.25	0.12	0.42	0.65	0.22	0.14	0.43
FeO	32.50	13.11	19.81	24.48	32.57	13.83	20.33	25.54
MgO	14.61	10.98	7.61	12.19	14.66	10.77	7.60	12.12
NiO	0.00	0.00	0.00	0.00	0.00	0.00	0.00	0.00
CaO	0.69	22.07	11.91	9.48	0.66	20.64	11.55	8.06
Na_2O	0.02	0.36	1.58	0.47	0.00	0.53	1.60	0.54
K_2O	0.01	0.03	1.60	0.38	0.01	0.28	1.66	0.50
Total	**98.78**	**99.18**	**96.76**	**99.99**	**99.12**	**99.56**	**96.97**	**99.99**
Modes	*0.49*	*0.29*	*0.22*		*0.52*	*0.23*	*0.25*	
Wo	0.02	0.46	0.30	0.21	0.02	0.44	0.29	0.18
En	0.44	0.32	0.19	0.37	0.44	0.32	0.19	0.38
Fs	0.55	0.22	0.50	0.42	0.55	0.23	0.51	0.44
Wo*	0.02	0.45		0.23	0.02	0.42		0.21
En*	0.44	0.34		0.36	0.44	0.35		0.36
Fs*	0.54	0.21		0.41	0.54	0.23		0.43
X_{Fe}				**0.53**				**0.54**

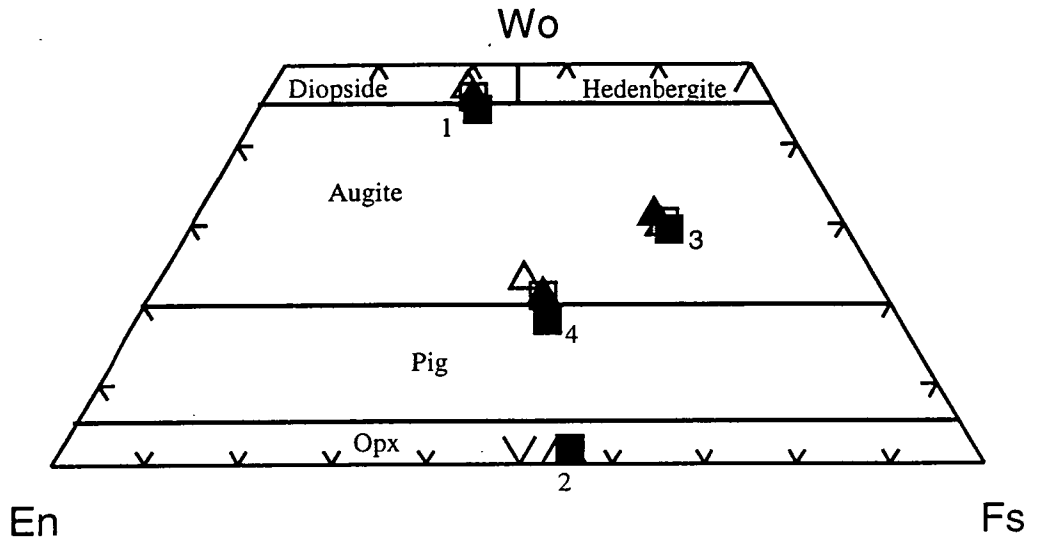

Figure 4.7 Reintegrated pyroxene compositions. Compositions of Opx and Cpx exsolution lamellae are shown. Hbl has been recast into ideal end-member pyroxenes and is also shown. The reintegrated bulk composition has been calculated from the modes. Note that most reintegrated bulk compositions are quite similar. Different symbols refer to the 4 samples summarized in Table 4.1. (1) are average Cpx analyses; (2) are average Opx analyses; (3) are Hbl compositions calculated as pyroxene endmembers; (4) are reintegrated Hbl analyses. Note that reintegrated compositions straddle the Pig - augite (sub-calcic augite) fields and near to the Cpx - Opx tie line.

margin. It is also worth noting that the feldspars are very fresh and appear to have largely escaped the effects of low-grade alteration.

Areas with regular exsolution textures comprise a core region of 20-35 % orthoclase ($Or_{88}Ab_{11}An_1$ - $Or_{96}Ab_4An_0$) in host andesine plagioclase ($Ab_{67}An_{31}Or_2$ - $Ab_{61}An_{37}Or_2$). Chemically the host plagioclase is fairly homogeneous within each core region, although there are steep chemical gradients immediately adjacent to exsolved orthoclase (described below). Neoblast overgrowths are compositionally distinct. They are strongly zoned from compositions similar to those in the core regions, to higher Ca and Al, and lower Si and Na away from the core. K shows a slight decrease.

Detailed chemical profiles across large exsolved orthoclase blebs reveals a symmetrical increase in Al and Ca in host plagioclase adjacent to the orthoclase, with a corresponding decrease in Si and Na (Figures 4.8) beginning *ca.* 14 μm from the boundary. K remains constant. There is a much less pronounced complimentary gradient in the orthoclase blebs. Kay (1978) described similar characteristics from ternary feldspars in anorthosites from the Larminie Range in the Adirondacks and argues that they are consistent with exsolution of

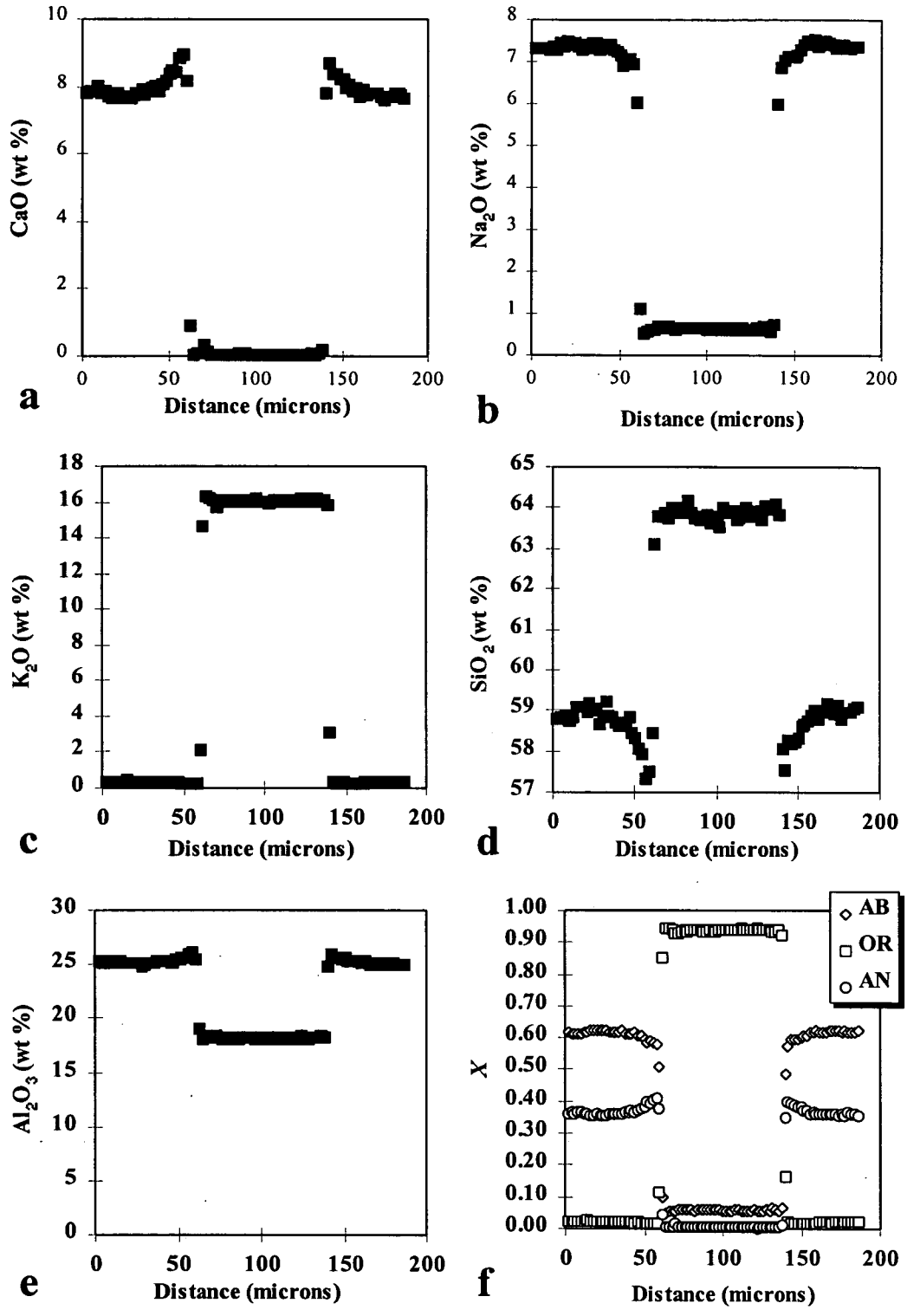

Figure 4.8 EPMA traverse across host plagioclase-guest orthoclase exsolution features. Analyses were performed at 5 *n*A in spot mode at 2 μm intervals.

orthoclase from an originally homogeneous host rather than syn- or post magmatic alteration. Kay (1978) further suggested that an exsolution origin by nucleation and diffusion is most likely. This involves in-migration of Na and Si coupled with expulsion of Al and Ca from the bleb area, with the chemical profile produced because the rate of Al-Si diffusion is slow. It is worth noting that the mesoperthite textures studied here are much larger than the Adirondacks specimens described by Kay (1978) and there is a correspondingly much further displaced chemical profile in the plagioclase host.

Despite micron-scale chemical complexity, the majority of exsolved core regions are of sufficiently coarse grain-size and regular texture to provide estimates of primary composition. When exsolved host/guest are reintegrated they indicate that primary feldspars were strongly ternary mesoperthites ranging in composition from $Or_{20}An_{25}Ab_{25}$ to $Or_{34}An_{25}Ab_{41}$ (Table 4.2). The significance of such ternary compositions and the variability between samples is discussed towards the end of the next section.

4.2.4 Emplacement temperatures from pyroxene and feldspar thermometry

Pyroxene temperature estimates

Three types of thermometers have been applied to igneous or high-temperature metamorphic rocks (Lindsley, 1983), these are:

- ***Single pyroxene*** thermometers derived from the Ca content of Cpx, Opx or pigeonite (Pig). These provide minimum temperature estimates.
- ***Two-pyroxene*** thermometers derived either from the Ca contents of coexisting Cpx-Opx, Cpx-Pig and Pig-Opx or Fe-Mg exchange between Cpx-Opx pairs.
- ***Three-pyroxene*** thermometers defined by coexisting Cpx-Opx-Pig, a condition that will occur at a unique temperature for a given bulk composition.

Of the possible assemblages (hence thermometers) outlined above, the SLC has only coexisting *metamorphic* Cpx and Opx, which will be discussed below. It is not known whether the igneous pigeonite coexists with either primary Cpx or Opx. All the primary pyroxenes present in RI19 and RI21, and studied by BEI (about a dozen in total), were pigeonites, so it is probable that pigeonite was the only stable pyroxene in these Fe-enriched rocks. A thorough examination of more Mg-rich bulk compositions might reveal coexisting Pig-Cpx pairs, but for reasons of time, this has not yet been undertaken.

Nevertheless, the composition of primary pigeonite can provide an estimation of the minimum crystallization temperatures for the most differentiated (and presumably coolest)

Table 4.2 Average analyses of exsolved mesoperthites from the SLC. Mesoperthite bulk compositions have been estimated from modal abundances and chemical compositions of host plagioclase and guest orthoclase.

	RI19.1		RI19.2		RI19.3		RI19.4		RI21.1		RI21.2	
	Plag	Kspar	Plag	Kspar	Plag	Kspar	Plag	Kspar	Plag	Kspar	Plag	Kspar
SiO_2	59.27	64.08	59.40	64.01	60.42	64.54	59.99	64.38	58.30	64.16	58.85	63.72
Al_2O_3	25.32	18.40	24.93	18.55	24.58	18.42	24.97	18.49	25.53	18.33	25.53	18.45
FeO	0.12	0.05	0.13	0.05	0.13	0.08	0.14	0.02	0.29	0.04	0.36	0.03
MgO	0.03	0.01	0.01	0.01	0.02	0.01	0.02	0.01	0.09	0.00	0.06	0.01
CaO	7.32	0.07	7.02	0.23	6.59	0.06	6.94	0.08	7.86	0.09	7.68	0.07
Na_2O	7.48	0.85	7.72	1.23	7.75	0.61	7.68	0.70	6.97	0.64	7.01	0.70
K_2O	0.25	15.18	0.19	14.64	0.28	15.63	0.24	15.48	0.24	15.80	0.33	15.49
Total	**99.82**	**98.69**	**99.45**	**98.78**	**99.82**	**99.33**	**100.07**	**99.20**	**99.27**	**99.07**	**99.81**	**98.47**
Si	2.65	2.99	2.67	2.98	2.70	2.99	2.68	2.99	2.63	2.99	2.64	2.99
Al	1.34	1.01	1.32	1.02	1.29	1.01	1.31	1.01	1.36	1.01	1.35	1.02
Fe	0.00	0.00	0.01	0.00	0.00	0.00	0.01	0.00	0.01	0.00	0.01	0.00
Mg	0.00	0.00	0.00	0.00	0.00	0.00	0.00	0.00	0.01	0.00	0.00	0.00
Ca	0.35	0.00	0.34	0.01	0.32	0.00	0.33	0.00	0.38	0.00	0.37	0.00
Na	0.65	0.08	0.67	0.11	0.67	0.05	0.66	0.06	0.61	0.06	0.61	0.06
K	0.01	0.90	0.01	0.87	0.02	0.92	0.01	0.92	0.01	0.94	0.02	0.93
Total	**5.01**	**4.99**	**5.01**	**5.00**	**5.00**	**4.99**	**5.01**	**4.99**	**5.01**	**5.00**	**5.00**	**5.00**
N.B. Totals for Kspar are all ~0.4 wt% higher because BaO has not been included												
Ab	**0.64**	**0.08**	**0.66**	**0.11**	**0.67**	**0.06**	**0.66**	**0.06**	**0.61**	**0.06**	**0.61**	**0.06**
Or	**0.01**	**0.92**	**0.01**	**0.88**	**0.02**	**0.94**	**0.01**	**0.93**	**0.01**	**0.94**	**0.02**	**0.93**
An	**0.35**	**0.00**	**0.33**	**0.01**	**0.31**	**0.00**	**0.33**	**0.00**	**0.38**	**0.00**	**0.37**	**0.00**
	n=6	n=6	n=4	n=5	n=10	n=4	n=5	n=8	n=4	n=5	n=3	n=5
Modes	69.60	30.40	70.87	29.13	80.63	19.37	74.05	25.95	64.43	35.57	66.17	33.83
	Ternary X		**Ternary X**		**Ternary X**		**Ternary X**		**Ternary X**		**Ternary X**	
	Ab	**0.47**	Ab	**0.50**	Ab	**0.55**	Ab	**0.41**	Ab	**0.41**	Ab	**0.43**
	Or	**0.29**	Or	**0.26**	Or	**0.20**	Or	**0.34**	Or	**0.34**	Or	**0.33**
	An	**0.24**	An	**0.24**	An	**0.25**	An	**0.25**	An	**0.25**	An	**0.25**

rocks of the SLC. There are a number of calibrations (*e.g.* Ross & Huebner, 1979) available for the minimum stability of pigeonites with similar bulk compositions to those calculated for the SLC pigeonites. The most widely applied thermometers, however, are those presented in Lindsley and Anderson (1983) and Lindsley (1983). Data for RI19 and RI21

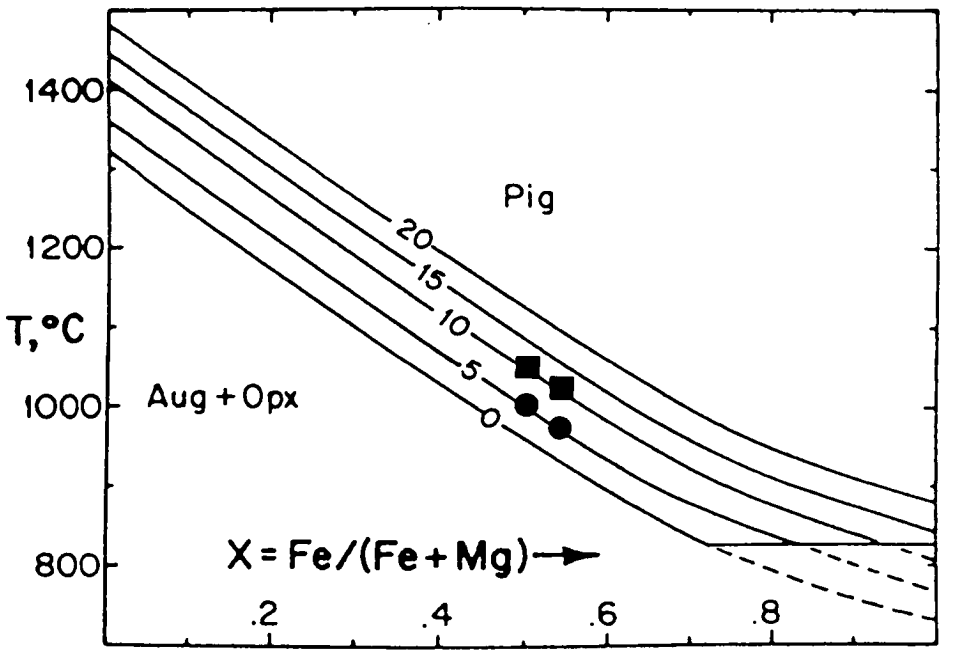

Figure 4.9 *T-X* diagram showing the minimum stability of pigeonites as a function of X_{Fe}. The position of the reintegrated SLC pigeonites are shown on the diagram. The *T-X* diagram is from Lindsley (1983) after Lindsley & Andersen (1983). The SLC pigeonites are shown at 5 and 10 kbar (different symbols) in this diagram, although quantitative independent assessment of emplacement pressure has not been made.

are shown on Figure 4.9 (after Lindsley, 1983) which provides minimum temperature estimates for 5, 10, 15 and 20 kbar. Reintegrated pigeonites have X_{Fe}[3] values of 0.50-0.54 which correspond to minimum temperatures of ~960-1000 °C at an assumed pressure of 5 kbar, and ~1020-1060 °C at 10 kbar.

Feldspar temperature estimates

Most feldspar thermometry utilizes the composition of coexisting feldspars, which is strongly a function of temperature and is only weakly influenced by pressure. In the ternary feldspar system there is complete solid solution (at high temperature) for the Ab-Or and Ab-An binaries, but only limited solid solution between An and Or. The limiting factor is the critical temperature of the ternary feldspar solvus. For coexisting ternary feldspar pairs the distribution of components between phases can be used to estimate the temperature of formation (see review by Fuhrman & Lindsley, 1988). However, for hypersolvus rocks with only one feldspar, the solvus provides a minimum constraint on the temperature of formation (*e.g.* Rollinson, 1982) in a manner similar to that described for pigeonite above.

---

[3] $X_{Fe}=Fe^{2+}/Fe^{2+}+Mg^{2+}$

As with the coexisting pyroxenes in RI19 & RI21, the compositions of coexisting orthoclase and plagioclase relate to *metamorphic* conditions and do not record igneous or even peak metamorphic temperatures and instead reflect a closure temperature, or the temperature of the last fluid infiltration event (*e.g.* reviews by Fuhrman & Lindsley, 1988; Brown & Parsons, 1994). Nevertheless, they are shown on Figure 4.10 which also indicates the reintegrated bulk compositions of primary feldspars and the positions of the 1000 and 1100 °C isotherms at pressures of 5 and 10 kbar. Of the six reintegrated compositions from RI19 and RI21, three are very similar in composition and cluster at about $Ab_{41}Or_{34}An_{25}$. This corresponds to minimum temperature estimates of ~1150 °C at 5 kbar or slightly lower temperatures if the pressure was nearer to 10 kbar[4]. Lower pressure conditions (*e.g.* 1 kbar) yield unreasonably high temperatures for these rocks in excess of 1250 °C.

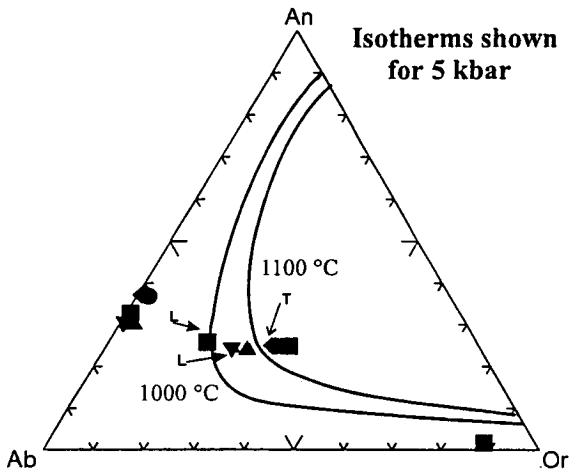

Figure 4.10 Ternary feldspar diagram showing the compositions of exsolved mesoperthites from the SLC and the position of the 1000 and 1100 °C isotherms at pressures of 5 and 10 kbar from the calibration of Fuhrman & Lindsley (1988). The compositional divide between mesoperthite and perthite is approximately after Deer, *et al.* (1992). Also shown for comparison are strongly ternary compositions from the Lewisian (Rollinson, 1982) and the Tigalak Intrusion, Labrador (Weibe & Wild, 1983).

The samples studied here are generally from the most evolved compositions and would presumably have been relatively low-temperature crystallization products. Perhaps the most similar intrusion to the SLC in terms of bulk composition is the Skaergaard Layered

[4] Temperature estimates were calculated for a variety of assumed pressures using the Solvecalc 1.0 program (Nekvasil & Wen, year unknown). A number of calibrations were examined, but the Fuhrman & Lindsley (1988) calibrations for ternary compositions are generally regarded as being the most reliable (Parsons, 1996, pers. comm.).

Complex in Greenland. It is certainly the most extensively studied Fe-tholeiite intrusion in the world. Comparison with crystallization temperatures from relatively late differentiates from Skaergaard with similar X_{Mg} values to those studied here would be in the region 1050-1150 °C (see Lindsley, 1983), but certainly not as high as 1250 °C. Hence there is some justification for assigning relatively high pressures (~5-10 kbar) to these thermometers, which in turn reduces these temperature estimates to plausible values.

The other three reintegrated compositions are less ternary in composition and would yield lower minimum temperatures, however, it is likely that these grains have suffered small amounts of granule exsolution from the original host. In effect this has resulted in the reintegrated compositions tracking towards progressively more plagioclase rich compositions as orthoclase blebs coalesced and mobilized to form discrete K-feldspar grains. There is textural evidence for this locally and, although such areas were avoided in the reintegration procedure, it is not possible to guarantee that such mobilization did not occur prior to analysis.

4.2.5 Metamorphic petrology

Outline petrology

The relict mineral, chemical and textural features reflecting the igneous parentage of the SLC (described above) are moderately to largely overprinted by metamorphic assemblages developed in one or more of the high-grade tectonothermal events that occurred in the Rauer Group (see Section 2.5). As a consequence, the SLC is metamorphosed to granulite facies assemblages typified by two-pyroxene + plagioclase mafic granulites with variable hornblende + biotite contents. Garnet-bearing pyroxene granulite is also present, both in the Fe-rich differentiates of the SLC and intrusive mafic dykes.

Despite widespread evidence for fluid-related isotopic disturbance to zircon systematics (*e.g.* previous section and Kinny *et al.*, 1993), there is little textural or mineralogical evidence for low grade retrogression in the main body of the layered complex (although see discussion in the next chapter). Grain boundaries are usually granoblastic to lobate within irregular relict textural domains (Section 4.2.1). The most ubiquitous phase associated with low grade retrogression is biotite, which occur as oriented grains parallel to the main composite foliation. It is more abundant in areas of higher relative strain especially within shear zones. Carbonate is another common but very minor late alteration phase comprising less than 1 %. CL reveals that it is restricted to small veins (micron-scale) in some but not all rocks (*e.g.* Figure 4.5). Rarely hornblende is replaced by fibrous actinolite although this

only occurs in some rocks and constitutes less than 1 % of the amphibole in even the most altered rock studies here.

More widespread development of assemblages including actinolite, chlorite and epidote, reflecting retrogression at upper greenschist to lower amphibolite conditions, are restricted to late planar shear zones adjacent to the complex (see also Harley, 1987). These features will not be considered further here. Instead focus is limited to the more widespread granulite assemblages that characterise the complex.

Choosing appropriate thermobarometers

A description of the most common metamorphic overprinting relationships involving Opx, Cpx and Hbl has been outlined in the previous sections. For estimating metamorphic conditions, however, these assemblages are of little use. Pyroxene thermometry, for example, is prone to retrograde Fe-Mg exchange down to temperatures as low as 600 °C in slowly cooled or polymetamorphic granulites (see reviews by Essene, 1989, and Harley, 1989). It is also sensitive to small analytical errors because the solvus curve is very steep at metamorphic temperatures. A more thorough approach involves the distribution of Ca between coexisting Ca-rich and Ca-poor pyroxenes in the quadrilateral system En-Di-Fs-Hd as developed by Lindsley & Anderson (1983) and Lindsley (1983), amongst others. Such thermometers are still far from adequate for granulite thermometry. Lindsley (1983) attributes this to a variety of possible reasons that include: inadequate reintegration of exsolved material, high alumina contents, and a low blocking temperature of perhaps only 550 °C; or as Robinson (1980, p. 446) puts it: because the crystal structure of clinopyroxene and orthopyroxene are very similar there are 'rampant possibilities for development of metastability and for recrystallization during cooling..'.

Other thermobarometers have similar problems. There has been some application of the magnetite-ilmenite thermometer (*e.g.* Buddington & Lindsley; 1964; Anderson & Lindsley, 1988), but reintegrated oxide exsolution lamellae only occasionally recapture peak metamorphic or igneous temperatures in slowly cooled or reworked terranes (Essene, 1989). Moreover, the thermometer is highly sensitive to changes in oxygen fugacity and many of the SLC samples studied here have complex oxy-exsolution textures (*e.g.* trellis structures) and therefore such thermometers are not pursued further.

By far the most useful pressure and temperature dependant assemblages present in the SLC are those involving garnet. Garnet-bearing assemblages occur as local patches or veins

within the SLC and comprise Grt-Plag-Opx-Mag/Ilm ± Hbl ± Qtz with minor late biotite and accessory phases. Textures are granular to weakly lobate, dominated by coarse anhedral garnets separated from Opx and Qtz (where present) by plagioclase moats (Figure 4.11). This indicates the simplified reaction:

Grt + Qtz = Opx + Plag

progressing towards the right with either decreasing pressure or increasing temperature (*cf.* Bohlen *et al.*, 1983; Harley, 1988; Essene, 1989). Textures such as Opx-Mag/Ilm intergrowths adjacent to hornblende and orthopyroxene mantles around magnetite suggest that magnetite and hornblende are also involved in the garnet breakdown reactions in some rocks.

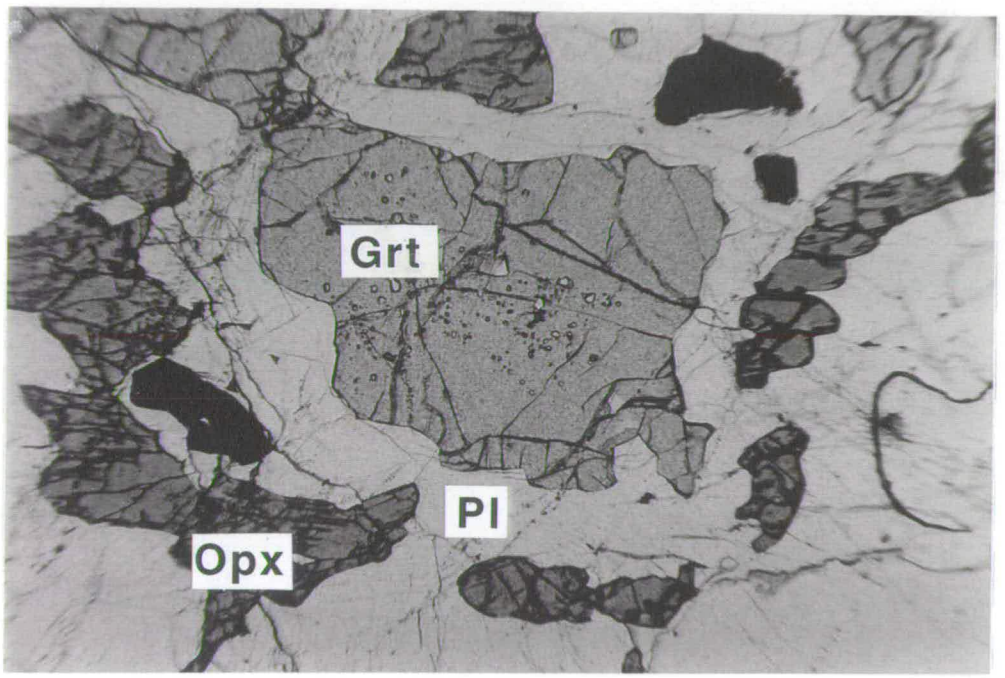

Figure 4.11 Photomicrograph of Grt separated from Qtz by a layered corona of Plag and Opx. Sample RI15, Fe-rich late-stage differentiate of the SLC (field of view is 7 mm across).

Mineral chemistry of garnet-bearing assemblages

Two samples of garnet-bearing SLC granulites (RI15 and RI30) have been selected for thermobarometry. These differ in that RI15 is quartz-bearing whereas RI30 is quartz-absent, with abundant Hbl and appreciable biotite. Mineral chemical and thermobarometric data are summarised in Tables 4.3 and 4.4 respectively. Mineral analyses were obtained on a

Cameca-Camebax electron microprobe at the University of Edinburgh. Operating conditions and examples of analytical precision are included in Appendix 1. The results presented in Table 4.3 are the distillation of many electron probe analyses, involving multiple analyses of individual cores and rims from adjacent phases and, in many cases, core to rim traverses.

Garnets are Fe-rich, with typical compositions $Alm_{62}Prp_{13}Grs_{14}Sps_5And_6$ (RI15) and $Alm_{60}Prp_{22}Grs_{10}Sps_3And_5$ (RI30). Compositional zoning is minor apart from near the rims, where X_{Mg} and Grs decrease while Sps and Alm increase. Orthopyroxene grains are homogeneous with X_{Mg} of 37 and 52 in RI15 and RI30 respectively. Alumina contents in orthopyroxenes in RI15 are near 0.8 wt% whereas those in RI30 contain 1.8 wt% Al_2O_3. Plagioclase exhibits minor compositional zoning from An_{45} - An_{38} between garnet and orthopyroxene, with most of the zonation to higher An occurring immediately adjacent to the garnet.

Thermobarometry from garnet-bearing assemblages

Temperatures ascribed to the formation of orthopyroxene + plagioclase in equilibrium with garnet have been calculated using garnet-orthopyroxene Fe-Mg distribution thermometers (Harley, 1984a; Lee & Ganguly, 1988; Carswell & Harley, 1989) for pressures in the range 5-10 kbar. Estimates (8 kbar) obtained using small garnet core compositions range from 930-919 °C (Lee & Ganguly, 1988) to 812-787 °C (Carswell & Harley, 1989) and 771-743 °C (Harley, 1984a) for RI30 and RI15 respectively. Estimates based on garnet rims are in the ranges 877 - 968 °C, 764 - 833 °C and 723-787 °C for the three thermometers. Temperatures of 800 °C are calculated using the garnet-hornblende thermometer of Graham and Powell (1984). On the basis of these results a temperature of 800 °C is assumed for the formation of the corona textures.

Pressure estimates for the formation of the orthopyroxene-plagioclase assemblages have been obtained using garnet-orthopyroxene Al_2O_3 barometry (Harley & Green, 1982; Harley, 1984b) and garnet-orthopyroxene-plagioclase-quartz barometers (Bohlen *et al.*, 1983; Newton & Perkins, 1982; Essene, 1989). The garnet-orthopyroxene Al_2O_3 barometer is subject to large uncertainties in these samples because of the low Al_2O_3 contents in orthopyroxene and high Alm + Sps in garnet (Harley, 1984c). For RI15, the Harley and Green (1982) method converges with the Harley (1984b) calibration at *ca.* 7 kbar and 700°C, and pressure estimates would be higher (by 2-4 kbar) at 750 and 800 °C respectively.

Table 4.3 Average analyses for Grt-Opx-Plag±Qtz rocks (RI15 & RI30) from the SLC.

	RI30					RI15					
	Opx	Grt rim	Grt core	Plag	Hbl	small Grt	Opx (i)	Plag	Opx (ii)	large Grt core	large Grt rim
SiO_2	49.81	37.47	37.28	54.49	40.30	37.03	48.58	57.34	48.51	37.22	36.96
TiO_2	0.04	0.03	0.05	0.02	1.97	0.05	0.02	0.02	0.03	0.07	0.03
Al_2O_3	2.02	20.49	20.60	28.18	12.50	20.25	0.88	25.49	0.93	20.02	19.97
Cr_2O_3	n.d	n.d	0.01	n.d	0.02	0.02	n.d	n.d	n.d	n.d	0.01
Fe_2O_3	n.c	1.33	1.31	n.c	n.c	1.31	n.c	n.c	n.c	1.89	1.74
FeO	28.76	26.60	26.35	0.22	18.38	28.22	36.15	0.17	36.23	26.74	28.09
MnO	0.84	2.25	1.90	0.00	0.27	2.45	1.10	n.d	1.05	1.36	2.41
MgO	17.36	5.37	5.82	0.03	8.47	3.07	11.72	0.01	11.79	3.65	3.36
NiO	0.03	0.02	0.00	n.d	0.05	n.d	n.d	n.d	n.d	n.d	n.d
CaO	0.46	5.45	5.90	11.06	10.95	6.93	0.98	8.64	0.86	8.43	6.64
Na_2O	0.04	0.02	0.01	5.28	1.61	0.00	0.03	6.58	0.00	0.00	0.00
K_2O	0.00	0.00	0.00	0.19	1.73	0.00	0.00	0.42	0.00	0.00	0.00
Total	**99.35**	**99.06**	**99.25**	**99.49**	**96.23**	**99.33**	**99.46**	**98.68**	**99.40**	**99.37**	**99.21**
Si	1.94	2.98	2.96	2.47	6.25	2.98	1.96	2.61	1.96	2.98	2.98
Ti	0.00	0.00	0.00	0.00	0.23	0.00	0.00	0.00	0.00	0.00	0.00
Al	0.09	1.92	1.93	1.51	2.28	1.92	0.04	1.37	0.04	1.89	1.90
Fe^{3+}	n.c	0.08	0.08	n.c	n.c	0.08	n.c	n.c	n.c	0.11	0.11
Fe^{2+}	0.93	1.77	1.75	0.00	2.38	1.90	1.22	0.00	1.23	1.79	1.89
Mn	0.03	0.15	0.13	n.d	0.04	0.17	0.04	0.00	0.04	0.09	0.16
Mg	1.01	0.64	0.69	0.00	1.96	0.37	0.71	0.00	0.71	0.44	0.40
Ca	0.02	0.46	0.50	0.54	1.82	0.60	0.04	0.42	0.04	0.72	0.57
Na	0.00	0.00	0.00	0.47	0.48	0.00	0.00	0.58	0.00	0.00	0.00
K	0.00	0.00	0.00	0.01	0.34	0.00	0.00	0.02	0.00	0.00	0.00
Total	**4.02**	**8.02**	**8.04**	**5.01**	**15.79**	**8.02**	**4.02**	**5.01**	**4.02**	**8.02**	**8.02**
	per 6 O	per 12 O	per 12 O	per 8 O	per 23 O	per 12 O	per 6 O	per 8 O	per 6 O	per 12 O	per 12 O

RI30 shows pressure convergence only at temperatures less than 700 °C (P = 3-4 kbar) if rim garnet compositions affected by Fe-Mg exchange are used, and yields a pressure of 5 kbar when garnet cores are used in the calculations. Application of the Fitzsimons and Harley (1994) retrieval method for an assumed temperature of 800 °C for corona formation produces pressure estimates of 11.5 ± 3 and 8.8 ± 1.5 kbar for RI15 and RI30 respectively. Garnet-orthopyroxene-plagioclase-quartz barometers are inherently more reliable for these Fe-Ca rich rocks than Al_2O_3 barometry, for reasons discussed in Fitzsimons and Harley (1994). Of the available barometers, those that rely on calibrations in the Fe end-member system are more suitable here as activities do not require extrapolation to high dilution (*e.g.* of pyrope component). Nevertheless, garnet activity-composition relations will influence the pressures obtained. The FAGS barometer of Bohlen *et al.* (1983) yields pressures (at 800 °C) of 7.2 and 7.7 kbar for RI15 and RI30 respectively. The equivalent reaction as presented

Table 4.4 Summary of thermobarometric data for RI30 & RI15 from the SLC.

	RI30		RI15		
Compositional data	**Grt core-Opx**	**Grt rim-Opx**	**sm Grt-Opx**	**Grt core-Opx**	**Grt rim-Opx**
Grt X_{Mg}	0.283	0.264	0.162	0.196	0.176
Grt X_{Py}	0.225	0.210	0.121	0.143	0.133
Grt X_{Gr}	0.163	0.154	0.197	0.238	0.189
Grt X_{Sp}	0.042	0.050	0.055	0.030	0.054
Opx X_{Mg}	0.521	0.521	0.366	0.367	0.367
Opx X_{Al}	0.045	0.045	0.021	0.022	0.022
Hbl X_{Mg}	0.451	-	-	-	-
Hbl $X_{Mg\#}$	0.532	-	-	-	-
Plag X_{an}	0.530	0.530	0.410	0.410	0.410
Fe-Mg K_d values					
K_d Opx-Grt	2.75	3.03	2.98	2.39	2.72
K_d Hbl-Grt	2.11	-	-	-	-
T(°C) at 8 kbar					
$T_{Harley, 1984}$	772	721	743	881	787
$T_{Lee \& Ganguly, 1988}$	931	875	919	1077	968
$T_{Carswell \& Harley, 1989}$	813	763	787	921	8.33
$T_{Graham \& Powell, 1984}$	800	-	-	-	-
P (kbar) at 800°C					
$P_{Harley \& Green, 1982}$	8.8	8.9	12.2	11.6	12.3
$P_{Harley, 1984}$	5.9	3.6	6.6	12.1	8.6
$P_{Fitzsimons \& Harley, 1995}$	7.7	7.3	-	-	-
$P_{Newton \& Perkins, 1982}$	8.3	7.6	7.7	9.9	8.5
PFAGS$_{Essene, 1989}$	7.8-8.5	7.8	8.0	8.2-8.6	8.0
PFAGS$_{Bohlen \textit{ et al.}, 1990}$	7.7	7.6	7.2	7.2	7.1
$P_{Thermocalc, Holland \& Powell, 1990}$	7.2-7.9	7.2	-	7.1	-

in the calibration by Essene (1989) yields pressures in the range 7.8 - 8.8 kbar depending upon the choice of garnet activity model. Pressures estimated for the FAGS reaction using THERMOCALC (Holland & Powell, 1990; Powell & Holland, 1988; version 90/3) coupled with ideal component activities for garnet and orthopyroxene are in the same range. For comparison, the Mg end-member calibration by Newton and Perkins (1982) yields higher pressures (9.7-8.3 kbar). The preferred pressure of corona formation in these rocks (at 800 °C) is 8 ± 1 kbar; pressures relevant to the formation of Grt + Qtz + Opx in the higher-T granulite metamorphic peak would have been greater than this.

Comparison with adjacent areas in the Rauer Group

The preferred P-T conditions of corona formation in the SLC mafic granulites, 8 ± 1 kbar and 800 °C, are consistent with previous P-T estimates for the post-peak decompressional

history in the Rauer Group as deduced from calc-silicates, metapelites, metabasites and felsic to intermediate orthogneisses (Harley, 1988; Harley & Fitzsimons, 1991; Harley *et al.*, 1992). These similarities, in reaction texture and calculated *P-T* conditions, indicate that the SLC shared the same metamorphic evolution as the more regionally extensive gneiss associations described by Harley & Fitzsimons (1991).

4.2.6 Zircon chemistry

Igneous growth zoning vs. fluid related alteration

One large zircon from RI15 (Zircon 8; see Figure 4.6) was analysed using SIMS at the University of Edinburgh by Nick Post (visiting from University of NSW, Australia). The results are presented in Table 4.5 and the operating procedure and conditions are described in Appendix 1. SIMS analysis for Hf, U, Th and REE reveals that, in broad terms, both cores and rims are moderately to strongly enriched in HREE with respect to LREE (chondrite normalized), and they have pronounced positive Ce and negative Eu anomalies (Figure 4.12). In detail, the core region is variable but is chemically distinct from the rim by having higher abundances of all the REE. The rims are also different by having depleted MREE relative to the cores. Areas that are bright in BEI (see Figure 4.6) also have much higher U/Th ratios and generally have a higher positive Ce anomaly (Ce/Ce*) but with a much less pronounced negative Eu anomaly (Eu/Eu*).

The inner region within this zircon represents growth during the magmatic stage which is reflected in regular oscillatory zoning (observable under CL in particular) and a gradual overall change in chemistry from the core towards the rim. Those portions of the rim that are bright in BEI or that have distinctive cuspate textures that cross-cut the magmatic zoning, are interpreted to be associated with small-scale metasomatism controlled in part by fluid access along fractures. Most of these fractures are now annealed and can only be seen using BEI.

Recognition that the zircons are internally complex is clearly important for geochronological work. Cores and rims such as this one have been studied by SHRIMP to constrain the crystallization age of the complex and the timing of fluid infiltration. The results, discussion and detailed interpretation of the regional implications is presented in Harley, Snape and Black (in press). A brief account is included in Chapter 6 in the conjunction with the isotopic evolution of the complex.

Table 4.5 (a) SIMS analysis of zircon 8 (RI15).

	Description	La	Ce	Pr	Nd	Sm	Eu	Gd	Tb	Dy	Ho	Yb	Lu
SH1	Zir 8 High cuspate edge	0.14	6.95	0.08	0.95	0.98	0.13	4.43	2.81	38.56	16.71	243.40	68.46
SH2	Zir 8 Low core	0.21	7.51	0.16	2.62	5.75	0.95	30.59	9.56	114.00	38.14	258.70	56.84
SH3	Zir 8 Transition zone	0.19	13.09	0.27	2.78	5.14	0.75	27.55	9.61	120.30	44.66	401.80	97.12
SH4	Zir 8 Transition zone	0.10	23.14	0.19	3.99	6.72	0.93	43.91	16.77	218.20	79.18	662.50	149.30
SH5	Zir 8 Transition zone	0.04	7.71	0.03	0.41	0.54	0.32	5.28	2.34	23.56	7.16	52.82	11.22
SH6	Zir 8 High cuspate edge	0.04	4.33	0.01	0.16	0.26	0.08	1.40	1.21	18.44	8.82	155.10	48.67

b). Indices of REE fractionation between core and rim

	Hf	Th	U	Eu/Eu*	Sm/Nd	MREE*	U/Th
SH1	18670	82	1317	0.189	1.02	1.68	15.99
SH2	11650	65	91	0.22	2.20	4.51	1.40
SH3	16240	170	894	0.19	1.85	2.99	5.26
SH4	15900	346	702	0.16	1.69	3.24	2.03
SH5	12260	51	99	0.56	1.31	2.25	1.94
SH6	15640	41	1021	0.39	1.58	1.32	25.06

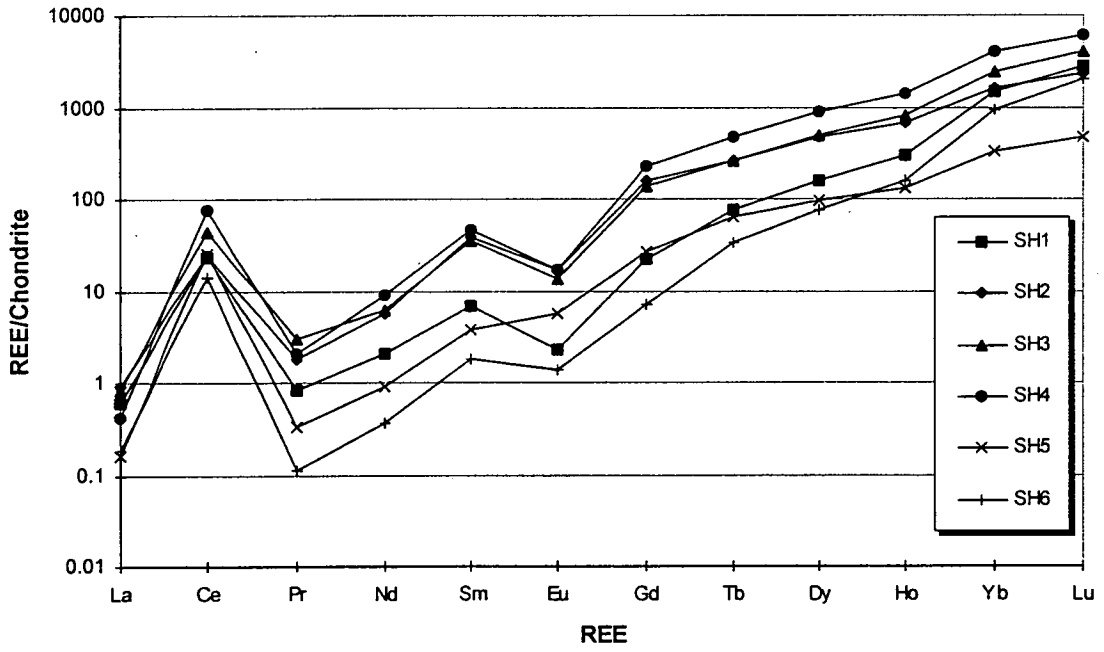

Figure 4.12 Chondrite-normalized REE analyses for zircon 8(RI15). Location of ion probe analysis points are shown on Figure 4.6. Note that rims are depleted in MREE relative to the core.

Although some studies (*e.g.* Hinton & Upton, 1991) have used the REE abundance of primary phases to calculate the REE composition of the melt (given known mineral/melt distribution coefficients), this has not been attempted here because sample RI15 is clearly an extreme late-stage differentiate (see Chapter 5). Nevertheless, the relative difference between core and rim does contain information regarding the distribution and behaviour of the REE during metamorphism. The chemical exchange required to produce the rims in zircon 8 occurred as the zircon attempted to re-equilibrate with the fluid and the metamorphic assemblage that was present during the infiltration event. From the limited ion probe analyses available for RI15 it is not possible to quantify the extent of metasomatism associated with this process. However, the relative difference between core and rim implies that there was trace-element and REE-mobility during metamorphic retrogression, and that the fluid responsible was capable of fractionating closely related elements (*e.g.* Sm/Nd) and altering phases that are commonly regarded as being relatively inert during metamorphism. Clearly this has important implications for the geochemical and isotopic evolution of the SLC and other less well-studied gneisses in the Rauer Group.

Implications for open-system chemical behaviour

Largely for the purposes of dating, zircons from RI15 and RI43 have been studied in considerable detail by CL, BEI, SHRIMP and to a lesser extent SIMS ion probe. Perhaps the most striking observation from studying these zircons is the extent to which igneous grains have been chemically and isotopically modified by fluid interaction during metamorphism.

The chemical character of the zircon rim for Zircon 8 as described above, includes a relative enrichment of the LREE/MREE with respect to the core as seen by lower Sm/Nd. However, given that overall change in LREE/MREE is accomplished by a relative depletion of the MREE rather than enrichment of the LREE, and from the textural features shown on Figure 4.6, it is apparent that these rims are not overgrowths. Instead, they are interpreted as reaction zones that interacted most with fluids during retrogression. From the relative depletion in MREE from this zircon, it is apparent that the fluid was reactive with respect to REE, and was capable of dissolving, fractionating, complexing, and transporting REE. This has important implications for the interpretation of protolith chemistry.

Although REE and their isotopes are traditionally regarded as being the most robust chemical criteria used to study protolith signatures from high-grade rocks, a number of recent studies have demonstrated that high temperature fluids are capable of forming REE complexes (*e.g.* Wood, 1990a; 1990b; Phillipott & Selverstone, 1991; Gammons *et al.*,

1996; Pan & Fleet, 1996). In particular, fluoride, chloride and carbonate ligands are now known to be able to hold and transport appreciable trace and REE in solution.

Although the samples chosen for study within the SLC were selected from the least deformed and consequently the least retrogressed rocks, there is evidence that minor metasomatic alteration affected a variety of compositions to some extent. Apart from minor late biotite and amphibole development that is attributed to rehydration, some apatites retain evidence of late-stage fluid interaction. CL reveals that they have similar core-rim relationships as those seen in the zircons. Apatite is a ubiquitous phase in the SLC and occurs in a most compositions, although is very minor or rare in the most basic rock types. Whilst a study of the chemistry of the apatites proved to be beyond the scope of this project, the presence of optically and hence chemically distinct rims as revealed by CL further raises the possibility that much of the SLC experienced some degree of trace and REE metasomatism. On the basis of geochemical and isotopic criteria discussed in the next chapter, the magnitude or actual amount of metasomatic alteration is probably very limited. Nevertheless, even minor REE metasomatism has profound implications for the behaviour and evolution of long lived radiogenic isotopes, especially for the Nd system.

4.2.7 Summary and conclusions

The SLC is a remarkable gneissic component in the Rauer Group that contains mineralogical and textural vestiges of it's protolith despite extensive and protracted polyphase high-grade reworking. Relict textures and primary mineralogy record at least a some of the early thermal history of the complex. Although thermometry is severely restricted by the nature of the phases involved, minimum estimates for crystallization temperature (at 5-10 kbars) of ~1000-1050 °C have been retrieved from igneous pigeonites, whilst higher minimum temperatures of ~1100-1150 °C have been estimated from igneous mesoperthites. Unfortunately, there are no independent geobarometers, but on geological grounds and from the feldspar thermometry, it is likely that the SLC was emplaced at depth in the crust.

Field evidence combined with textural and mineralogical observations further indicates that SLC subsequently underwent a series of high-grade deformational and metamorphic episodes. This resulted in the widespread development of Opx-Cpx-Plag ± Hbl assemblages in the main complex and the more restricted development of Grt + Qtz assemblages in the most Fe-rich lithologies. Although there is no record of peak metamorphic conditions, thermobarometry thought to reflect pressures and temperatures relevant to the onset of

garnet corona formation indicate that the SLC underwent post peak near isothermal decompression through *P-T* conditions of at about 800 °C and 8 ± 1 kbar. These results are consistent with *P-T* estimates from similar textures elsewhere in this part of the Rauer Group and confirm that the SLC and the surrounding Archaean domain shared the same metamorphic history that many of the younger (Proterozoic) lithologies enjoyed. Although field relations between the SLC and CLG are largely tectonic, the similarity in *P-T* history when taken in conjunction with geochemical and isotopic evidence presented in the next chapter, further confirm that the SLC intruded into what is now considered the Archaean domain of the Rauer Group. Expressed differently, the SLC was not an allochthonous terrane with a distinct tectonic and metamorphic history that was tectonically incorporated into the other Archaean crustal during one of the later tectonic episodes (*e.g.* 1000 Ma or 500 Ma events).

Finally, detailed petrographic and mineral chemical analysis of zircons from an important late differentiate within the main complex (RI15), provides some evidence to suggest that trace and REE were mobile during the late retrograde event. Thus, it is possible that the SLC and other gneissic protolith experienced *minor* whole-rock chemical disturbance and isotopic perturbation at this time. The nature and scale of these secondary processes and the extent to which the SLC chemistry reflects that of the protolith is discussed in the next chapter.

4.3 Petrology of the early (Archaean) mafic dykes (MD1 & MD2)

The deformed mafic dykes that are contained within the SLC (Section 3.3.3) all have similar mineral assemblages comprising Plag-Opx ± Hbl > Mag/Ilm >Biotite > Apatite. They are dominated by medium-grained irregular polygonal to polygonal-lobate textures. Elongate mineral shapes tend to dominate in relatively high-strain areas, and hornblende and biotite become more abundant. The main mineral associations are consistent with granulite facies metamorphism, however, the assemblages are not suitable for quantitative thermobarometry for reasons described in Section 4.2.5.

Unlike the SLC, there is no obvious relict major mineralogy, presumably because the dykes are generally finer grained. However, coarse-grained relict textural domains are sometimes preserved, the most spectacular being oikocrystic textures that developed in some dykes (EMD oikocrystic dykes; see Chapter 3). Such textural domains are generally too large to study petrographically. Nevertheless, smaller analogous domains of about 1 cm in width are

defined by large, almost skeletal, inter-connecting and optically continuous clinopyroxene(s) that enclose plagioclases. It is likely that these were originally igneous ophitic or sub-ophitic textures that have since been recrystallized at grain boundaries.

Although 3 distinct generations of mafic dykes can be recognised in the field (described in Chapter 3), it is unlikely that detailed petrography will add significantly to those distinctions. The relative difference in colour index between pale grey and dark grey dykes is accounted for entirely by variations in the abundance of ferromagnesian versus quartzofeldspathic constituents (only minor Qtz).

4.4 Petrology of the Tonalite-Trondhjemite gneisses (TG and TrG)

4.4.1 Outline petrography of the Tonalite Gneiss (TG)

The Tonalite gneiss (TG) is coarse-grained (2-5 mm) and mainly comprises Plag (~60 %), and Qtz (~20 %) with lesser Opx, Ilm, Biot, Grt and accessory zircon and monazite. Textures are dominated by an irregular granoblastic to subhedral Plag-Qtz texture, although Opx and Grt - Biot trails define a weak foliation in some samples. In general the Plag-Qtz texture is strongly strained and is characterised by extensive intracrystalline deformation features and local grain boundary recrystallization. Plagioclases commonly show kinking, undulose extinction, deformation twinning and have sutured grain boundaries. Microfracturing of plagioclase is common and fractures are often filled with carbonate and sericite. Quartz grains have sutured boundaries with plagioclase and are ubiquitously recrystallized into high angle subgrains, some of which are now undulose. Orthopyroxene occurs as altered pink-green polygonal to lobate grains, but is also locally altered to fine carbonate, mica, chlorite and opaques which is attributed to late-stage retrogression (Harley, Snape & Black, in press).

Zircons

The zircons in TG samples are complex and comprise two main textural populations:

- ***Type I.*** Clear, elongated multifaceted grains.
- ***Type II.*** Complex zircons with elongate cores that are often cracked and broken, surrounded by broad rims with rounded terminations.

Type I zircons and the rims of Type II zircons are attributed to metamorphic growth. Elongate cores in the Type II zircons have oscillatory zoning and are therefore thought to be of igneous origin. The isotopic data from one of the TG rocks (SH45) is detailed in Harley, Snape & Black (in press) and is outlined in Chapter 6.

4.4.2 The Trondhjemite Gneiss (TrG)

The TrG comprise ~95 % Qtz and antiperthitic to mesoperthitic alkali feldspar, forming seriate to lobate granoblastic textures with a typical grainsize of 0.1 - 1 mm. Feldspars have extensive string and filament perthite textures, now weakly deformed and partially altered to sericite in places. Minor ferromagnesian phases also occur, and include brown-red Hbl and rare Opx and Ilm.

4.5 Petrology and mineral chemistry of the Torckler-Tango Layered Complex (TTLC)

4.5.1 Outline petrology of the complex

Compared with the SLC, the TTLC is mineralogically and texturally simple. Most of the complex has a medium-grained granoblastic to lobate texture defined predominantly by metamorphic Opx, Cpx and Plag with very minor Hbl, Qtz, Mag/Ilm and apatite. Bulk compositional differences within individual layers and throughout the complex as a whole are defined almost entirely by variations in the abundance of Cpx, Opx and Plag.

The only exception to an otherwise monotonous mineralogy and texture is a relatively uncommon porphyritic ultramafic variety that contains large euhedral orthopyroxenes set in a more typical granoblastic groundmass. When separated from the groundmass, individual Opx crystals are up to 1.5 cm long and are either flat euhedral prisms or, occasionally, weakly folded single crystals. On morphological grounds it is likely that these are relict igneous grains.

Overall there is little obvious textural or mineralogical information that relates either to protolith formation or subsequent metamorphism. Opx, Cpx and Plag occur throughout with no significant overprinting relationships. Where Hbl becomes locally abundant (10-15 %) it appears to be concentrated in narrow layers with no obvious orientation with respect to the primary layering. Hornblende sometimes occurs as poikiloblasts enclosing Cpx, Opx and

Plag indicating formation later than the main two-pyroxene assemblage, probably related to fluid infiltration along fractures during retrogression.

For reasons discussed in Section 4.2.5, the assemblages described above for the TTLC are of little use for thermobarometry. Nevertheless a preliminary study of mineral compositions has been undertaken to establish whether there is any composition difference between primary orthopyroxenes and those of the recrystallized groundmass. Metamorphic Cpx, Opx and Plag have also been analysed within layers to see if any cryptic variation has been preserved.

4.5.2 Mineral chemistry

Primary orthopyroxenes

The primary orthopyroxenes described above are difficult to study adequately in thin section or by EPMA because they are very large (*ca.* 1cm). However, where euhedral phenocrysts can be distinguished from later Opx and Cpx, they have a variety of exsolution features. Exsolution lamellae are generally only weakly developed, but granule exsolution of clinopyroxene has resulted in small discrete grains forming in the interiors of some grains. Because these exsolution features are coarse grained, it is not possible to reintegrate the compositions using the reintegration technique described in Section 4.2 for the SLC. However, one individual grain proved large enough to analyse by XRF (Table 4.6).

Table 4.6 XRF analysis of Opx phenocryst.

	TTLC Opx	normalized to 100%	cations per 6 O
SiO_2	54.71	54.92	1.94
TiO_2	0.13	0.13	0.00
Al_2O_3	1.43	1.44	0.03
Cr_2O_3	na	na	0.00
Fe_2O_3	13.13		
(FeO)	(11.82)	(11.86)	(0.35)
MnO	0.25	0.25	0.01
MgO	27.97	28.08	1.48
NiO	na	na	0.00
CaO	2.60	2.61	0.10
Na_2O	0.25	0.25	0.01
K_2O	0.08	0.08	0.00
P_2O_5	0.01	0.01	
LOI%	0.37	0.37	
Total	**99.61**	**100.00**	**3.92**
	for FeO		

This grain was taken from DH Green Isle [GR 870 550] by extracting it out of a relatively crumbly groundmass in the field. The sample was about 1.5 cm long and had euhedral terminations, with no obvious inclusions, fractures or overgrowths. The single grain was crushed into a fine powder in an agate pestle and mortar before ignition at 1100 °C to convert any Fe^{3+} to Fe^{2+}. It was then fused at 1100 °C following the method described in Appendix 1. It is worth noting that the analysis has a high total (100.93). This is attributed to incomplete or even partial conversion of Fe^{2+} to Fe^{3+} during ignition. Assuming that much of the Fe at the fusion stage was ferrous, there would be a slight underestimate of the amount of flux required resulting in a small overall higher total. On this basis, the Fe measured as Fe_2O_3 was then converted to the equivalent FeO (resolving the analysis total to near 100%) prior to estimation of the proportion of Fe^{3+} on stochiometric grounds following Lindsley & Anderson (1983) and Lindsley (1983). Since the amount of Al is very small, less than the deficiency in the tetrahedral site, Fe^{3+} is taken as Fe^{3+} = 2-Si-Al(IV), where all the measured Al is attributed to the tetrahedral site. This provides at least an estimation of the amount of Fe^{3+}, which is very small as would be expected (0.03 Fe^{3+} cations per 6 oxygens).

The phenocryst has end-member compositions of ~$En_{77}Fs_{18}Wo_5$ which is higher in Mg and Ca than the groundmass (described below). This result was expected and the higher Ca reflects equilibration at high magmatic temperatures. Although there are a number of assumptions inherent in the procedure adopted here, including the treatment of Fe^{3+} and the relative imprecision of estimating temperatures from single pyroxenes, calculated minimum temperatures are in the region 1250 - 1300 °C at 5 and 10 kbar respectively (Lindsley, 1983).

Estimating temperatures from the single pyroxenes is not as precise as from two or three pyroxene assemblages, nonetheless, it does provide a temperature estimate. Given that the TTLC is such an Mg-rich complex it is perhaps not surprising to retrieve such high temperatures.

Metamorphic Opx-Cpx-Plag assemblages

Individual graded layers commonly have bulk-rock compositional gradients preserved over distances of 10s of centimetres (see Section 3.4). In detail this is almost entirely defined by variations in modal abundance. Sequential samples from one individual layer (RI79) have been studied in detail by EPMA. Modal variations from the base of the layer to the top range from Opx + Cpx (~85 % in total) + Plag (~15 %) to Opx + Cpx (~40 % in total) + Plag (~60 %). Opx and Cpx compositions are constant throughout with compositions of

$En_{77\pm0.8}Fs_{22\pm0.6}Wo_{1\pm0.2}$ and $En_{44\pm0.5}Fs_{8\pm0.3}Wo_{48\pm0.2}$ respectively. Plagioclase compositions, however, are variable and there is a sharp compositional divide between the top and the middle of the layer. Basal and middle plagioclases have very uniform compositions at $An_{53\pm1.0}Ab_{45\pm1.0}Or_{2\pm0.4}$, whereas plagioclases in the upper part of the layer are again uniform but with compositions of about $An_{60\pm1.0}Ab_{38\pm1.0}Or_{2\pm0.1}$.

This compositional variation in plagioclase within layers presumably reflects a higher Ca/Na bulk composition in the upper part of the layer. It is possible that this reflects the differentiation mechanism that produced the layering. Normal layering would be characterised by a decreasing Ca to Na ratio, but reverse zoning is common in igneous layers where early formed plagioclase either floated or crystallized from the top downwards. However, a detailed discussion of the possible mechanisms of igneous layering is beyond the scope of this project, although it is considered a little further in the next chapter.

4.5.3 Summary and conclusions for the TTLC

The TTLC was almost entirely recrystallized to a simple granulite assemblage and texture comprising Opx, Cpx and Plag. Retrograde hornblende and biotite are minor and are only locally developed. Despite an almost monotonous mineralogy, a relative rare cumulus rich horizon has abundant relict primary orthopyroxenes. Although these have internally recrystallized, a single whole-grain analysis by XRF provides an estimate of the primary composition. Based on the Ca content in the orthopyroxene, minimum temperature estimates for the onset of Opx crystallization are in the region of 1250-1300 °C at 5 and 10 kbar respectively. The compositional data for this orthopyroxene is referred to in relation to whole-rock geochemistry and an interpretation of the crystal fractionation history of the complex (Chapters 5 & 7).

4.6 Constraints on the evolution of Archaean mafic rocks in the Rauer Group: Discussion and preliminary conclusions

The petrographic features described in this chapter for the main Archaean mafic rocks in the Rauer Group (SLC, TTLC & EMD) are similar in that all have granulite facies assemblages dominated by Cpx, Opx and Plag. None of the rocks studied here contain olivine or pseudomorphs that could be replacement products after olivine. This does not mean that olivine was never present, but rather if it was initially present then it has subsequently reacted to the metamorphic assemblage described above.

Having noted the main similarity between these rocks, there are significant differences especially between the two layered complexes. The main contrast relates to primary protolith bulk composition and grainsize, but there are also differences in the development of late-stage hydrous minerals attributed to fluid infiltration and retrogression. A number of these differences are highlighted below.

The SLC is coarse-grained and retains abundant relict igneous textures and partly recrystallized primary phases. By contrast, the TTLC is generally finer-grained and relict igneous features are restricted to relatively rare phenocrysts (Opx). The EMD are also finer-grained than the host SLC. Nevertheless primary textures have survived recrystallization and repeated deformation in some dykes, although relict mineralogy has not been identified in this study.

The SLC is mineralogically quite diverse when compared with the TTLC and EMD. It comprises relict igneous vestiges largely overprinted by granulite assemblages dominated by Cpx-Opx-Plag ± Hbl (age uncertain), and then later by biotite. The EMD also have these retrograde hydrous minerals superimposed on a two-pyroxene + plagioclase assemblage. The TTLC, by contrast, has only minor hornblende and biotite that are locally restricted. This is attributed to differences in bulk composition and the extent of fluid infiltration rather than variation in metamorphic grade or history.

None of the mafic rocks studied here proved to be particularly suitable for quantitative thermobarometry, and only limited constraints can be placed *P-T* conditions relevant to protolith emplacement. Nevertheless, qualitative assessment of feldspar thermometry and geological criteria described in the next section implies (tentatively) that the layered complexes were not shallow level intrusions but were emplaced at depth in the crust. On this basis magmatic crystallization temperatures for relatively evolved Fe-rich differentiates of the SLC provide minimum temperature estimates of 960-1000 °C and 1020-1060 °C, at 5 and 10 kbar respectively, from reintegrated primary pigeonites. Higher, and possibly more reliable, minimum temperature estimates in the region 1050-1150 °C for the same pressures were obtained from reintegrated strongly ternary mesoperthites. Although not directly comparable with the thermometry results from the SLC, a minimum temperature estimate for the onset of orthopyroxene crystallization in the high-Mg TTLC lies in the region of 1250 - 1300 °C.

Whilst the preserved igneous features in the layered complexes do not comprehensively constrain the thermal evolution of Rauer Group mafic protolith prior to metamorphism, they

do illustrate that vestiges of primary mineralogy and mineral chemistry are retained in these multiply deformed polymetamorphic rocks. Furthermore, such observations provide independent constraints on the fractional crystallization histories of the complexes, and the petrological accounts described in this chapter will be integrated into discussions concerning the nature of protolith petrogenesis in the following chapter.

Although neither of the layered complexes preserve peak metamorphic assemblages (at least in terms of phase chemistry), extreme differentiates of the SLC have garnet reaction textures consistent with isothermal decompression. Thermobarometry from these rocks constrains *P-T* conditions at the onset of corona formation to ~800 °C and 8 ± 1 kbar, which are similar to values from elsewhere in the Rauer Group. This observation is important because it confirms that the SLC and the Archaean domain shared the same metamorphic history as recorded by the younger Proterozoic gneiss associations.

In conjunction with the detailed isotopic study presented in the next chapter and in Harley, Snape & Black (submitted), zircons from one of the SLC late differentiates have been studied in detail. Textural, mineral-chemical, and isotopic observations indicate that the igneous zircon cores (2840 Ma) have isotopically reset rims (~500 Ma) that were produced by interaction with a fluid during metamorphism (see Chapter 6). A relative depletion of MREE with respect to LREE in the zircons implies that the fluid was capable of dissolving, fractionating and transporting REE on at least the intermineral scale. This has important implications for relating trace-element and REE signatures to protolith petrogenesis and could seriously bias the interpretation of Sr and Nd isotopes. However the presence of delicate primary textures and mineralogy, as defined by small-scale variations in major element chemistry, implies that element mobility was relatively minor or was possibly restricted to certain element species and/or bulk compositions.

Chapter 5

Geochemistry of the Scherbinina and Torckler-Tango Layered Complexes

5.1 Introduction

This chapter documents an outline and comparison of the geochemistry of the Scherbinina and Torckler-Tango Layered Complexes (SLC & TTLC). A brief account of the Archaean mafic dykes (EMD as described in Chapter 3) is also included. The rationale for undertaking whole-rock geochemistry for each of these suites is described in a general context in Chapter 1 (Section 1.4.3), and more specifically in the context of the Rauer Group in Chapter 3. In brief, the objectives are:

- To provide documentation of the geochemistry of previously undescribed mafic gneiss suites in the Rauer Group that are of Archaean age.
- To provide an account of these gneisses in order to establish whether they could be reworked equivalents of Archaean crust in the adjacent Vestfold Hills.
- To provide a geochemical framework within which to consider or interpret stable- and radiogenic-isotope data.
- To establish, if possible, the petrogenetic histories of the different mafic gneiss suites in the Rauer Group.

Interpretations of the data are limited to working hypotheses, primarily to provide a background to the isotope study described in Chapter 6. Constraints from both geochemical and isotopic datasets are integrated with field and petrographic observations in the final chapter (Chapter 7) in Part 2.

5.2 Geochemistry of the SLC

5.2.1 Principal geochemical characteristics of the complex

The SLC is a differentiated Fe-rich tholeiite with ***mg***-numbers that vary from 77 to 22. In general the complex is characterised by a trend towards Fe-enrichment (Figure 5.1),

although there is a slight inflection towards evolved alkali compositions. On the basis of field observations and geochemical criteria, samples collected from the complex have been divided into two groups. The first group defines a coherent trend on most inter-element variation diagrams (*e.g.* ***mg*** *vs.* Cr & Ni; Zr *vs.* Nb and other incompatible elements). It comprises 17 samples and represents the bulk of the layered complex. This group is referred to as the 'Main Trend' (SLC MT). The second group of 10 samples consists of extreme differentiates and 2 metasomatically altered rocks. The 2 altered samples (SH11 & SH14) are from near Petes Isle (outside the main complex) and have patch leucosomes and distinctive chemistry. Sample RI15 is an extreme differentiate and is the garnet-oxide pegmatite described in detail with respect to metamorphic studies and zircon dating in Sections 4.2.6 and 6.3. Sample SH79 is also an oxide-rich patch. These samples will not be considered further in this section. The remaining 6 extreme differentiates are distinguished from the SLC MT and are described further below.

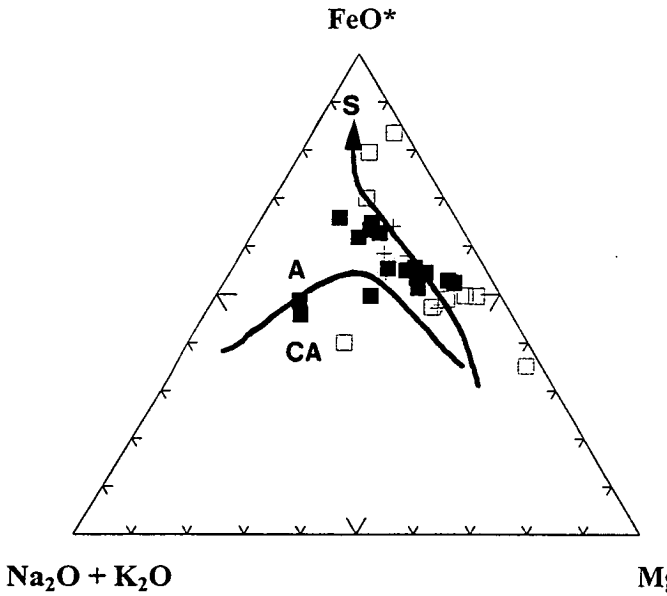

Figure 5.1 Igneous AFM diagram for the SLC. Filled squares are the 'Main Trend' (n=17), open squares are extreme differentiates or highly altered rocks, and crosses are EMD described in Section 5.3. The calc-alkaline/tholeiite division is after Irvine & Baragar (1971), Skaergaard trend is after Wager & Brown (1967).

5.2.2 Major elements

Description

The SLC MT is characterised by high $Fe_2O_{3(t)}$ (8.3-20.5 wt%), and relatively low ***mg*** (~60-28) and CaO (5.1-7.6 wt%). Using ***mg*** as a crude index of differentiation, MgO decreases from 14.3 to 2.6 wt%, whilst $Fe_2O_{3(t)}$ shows a general decreasing trend. However, some of the most differentiated samples have high $Fe_2O_{3(t)}$ (15-20 wt%) which results in very low

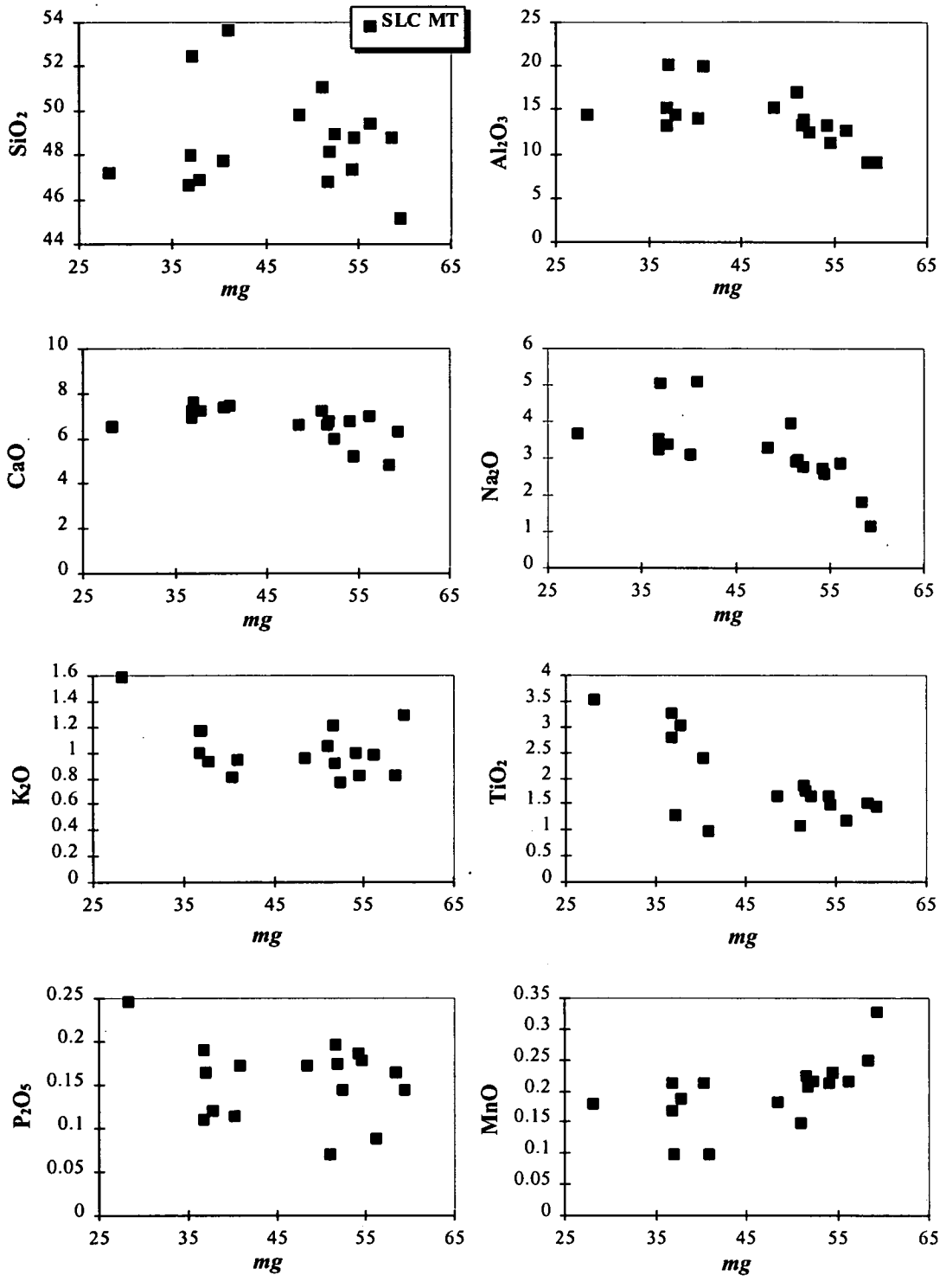

Figure 5.2 Selected major elements plotted against *mg*. Data are for the SLC MT only

mg-numbers for these samples. Many major elements show a weak inflection at about ***mg*** 48 (Figure 5.2). For example: CaO increases to about this point and then decreases; Al_2O_3 initially increases and then remains roughly constant; Na_2O increases overall but less strongly between ***mg*** 48 and 22. MnO is not well correlated with ***mg*** but generally decreases. There are only poorly defined correlations for SiO_2, K_2O, P_2O_5 and TiO_2, although a few low-***mg*** rocks with high $Fe_2O_{3(t)}$ also have very high Ti, which presumably reflects the greater abundance of ilmenite and magnetite in these samples.

Interpretation

Taken in conjunction with the field relations and petrographic observations described in the previous chapters, coherent major-element correlations imply that the SLC has not been significantly affected by major-element metasomatism. The sample that plots well into the calc-alkaline field in Figure 5.1 is obviously highly altered; it contains patch leucosomes and was included in the dataset to illustrate the effects of metasomatism. Most of the remaining samples are thought to be related to each other by crystal fractionation processes. The samples excluded from the main trend are websterites (Cpx + Opx 'accumulations') or late-stage differentiates (enriched in Fe-Ti oxides).

The geochemical features described above are dominated by Fe-enrichment relative to MgO. Such trends are characteristic of large, apparently closed-system, intrusions such as Skaergaard and are usually attributed to suppressed magnetite fractionation as a consequence of crystallization along an oxygen buffer (see Wilson, 1993, and references therein). The late onset of magnetite and/or ilmenite fractionation is consistent with petrographic and trace-element geochemical observations for the SLC (described further below).

Trends showing increasing CaO, Na_2O and Al_2O_3 down to about ***mg*** 48 are consistent with magmatic differentiation dominated by fractionation/accumulation of combinations of clinopyroxene, orthopyroxene ± olivine. Figure 5.3 illustrates that CaO enrichment is less than would be predicted for fractionation of orthopyroxene or olivine alone and indicates that a calcic ferromagnesian phase (*i.e.* Cpx or Pig) is likely to have been an essential cumulus mineral. Extensive fractionation of Ca-plagioclase at this early stage can be excluded because Al_2O_3 would decrease with falling ***mg*** (or MgO). For compositions more evolved than ***mg*** 48 (MgO < 8 wt%), however, plagioclase probably was important, as seen by the inflections and relative decreases in CaO, Na_2O and Al_2O_3 below ***mg*** 48. Note that

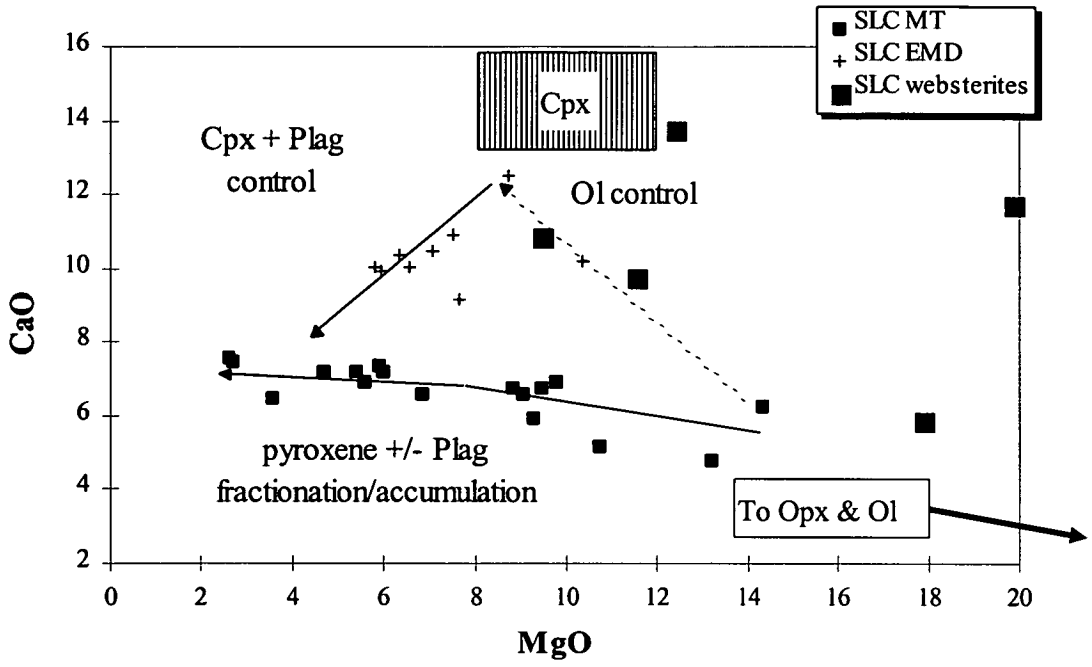

Figure 5.3 Plot of CaO *vs.* MgO for the SLC MT, EMD (described in Section 5.3) and websterites associated with the SLC. Also shown for comparison is the low-pressure fractionation trend initially dominated by olivine and then clinopyroxene and plagioclase typical of continental tholeiites (Ol → Ol+Plag → Ol+Plag+Cpx; *cf.* Wilson, 1989, figure 10.12). The SLC MT control 'line' can be explained by crystal fractionation/accumulation of orthopyroxene, clinopyroxene, and late plagioclase. Residual products are mixtures that vary between orthopyroxenites and clinopyroxenites. Olivine has not been found in any of the SLC rocks, but its presence cannot be excluded on geochemical grounds.

there is no constraint on the presence or absence of olivine on the basis of major element-variation diagrams, and it is very difficult to distinguish between the affects of orthopyroxene and olivine control (discussed further below). The elements P_2O_5, K_2O, and TiO_2 are considered in the context of trace elements.

5.2.3 Normative compositions

Normative mineralogy for the SLC does not contain *Q* or *Ne* and has roughly equal proportions of *Hy*, *Di* and *Ol* corresponding to silica saturated basalts or olivine tholeiites (*cf.* Thompson, 1984). For *Hy*, *Di* and *Ol* there are poor positive correlations with ***mg***. There is a very strong negative correlation between ***mg*** and *Ab*, reflecting increasing Na_2O in low-***mg*** samples. *An* has a marked inflection at about ***mg*** 48, which mirrors the inflection in Al_2O_3 and CaO (see Figure 5.2). *Or* remains roughly constant.

5.2.4 Trace and rare-earth elements (REE)

Trace elements, as described here, refers to those elements analysed by XRF (Appendix 2) and usually includes the high-abundance REE (La, Ce & Nd). 'REE' are also used more specifically to refer to the lanthanide series La to Lu, which in this study were mainly analysed by ICP-AES (Appendix 3).

Description of trace-element behaviour

The behaviour of the trace elements during fractional crystallization is considered by a first-order subdivision into compatible and incompatible elements. For compatible elements, such as Ni and Cr, there is a strong positive correlation with ***mg*** which, as might be expected, reflects the sharp decrease in MgO (Figure 5.4). Sc also generally decreases with ***mg***. Cu appears to increase throughout, although high concentrations are restricted to the Fe- and Ti-rich samples described above. Overall there is only a weak correlation between ***mg*** and the incompatible trace elements. Nevertheless, there are strong correlations between many LILE, HFSE and REE. For example, trace elements such as Ce, Nb, Nd, Zr, Y and P are all positively correlated with Zr or Nb (see Figure 5.9, discussed further below).

Rare-earth elements (REE)

REE patterns for the SLC are moderately enriched[1] relative to chondrite and have fractionated[1] patterns with average $(Ce/Yb)_N \sim 4.2$. The SLC also has similar patterns across a wide compositional range. Data for 9 samples are shown in Figure 5.5. These data represent the compositional range ***mg*** 78 (RI108) to ***mg*** 28 (RI19). Across this range there is only a poor correlation of REE concentrations with ***mg*** and, although concentrations vary by almost an order of magnitude, there is only slight fractionation of LREE/HREE (Figure 5.6).

Spidergrams

A large number of different normalizing factors are currently in use by different authors (as reviewed by Rollinson, 1993). Two sets of normalising values are used here to illustrate trace-element characteristics of the SLC: primitive mantle (PM) values are after

---

[1] 'Enriched' in this context refers to trace-element abundances relative to normalizing composition (*e.g.* Chondrite, PM, N-MORB). 'Fractionated' refers to the shape of the pattern relative to normalizing composition and implies element fractionation by a non-specific process (*e.g.* crystal fractionation, partial melting, assimilation).

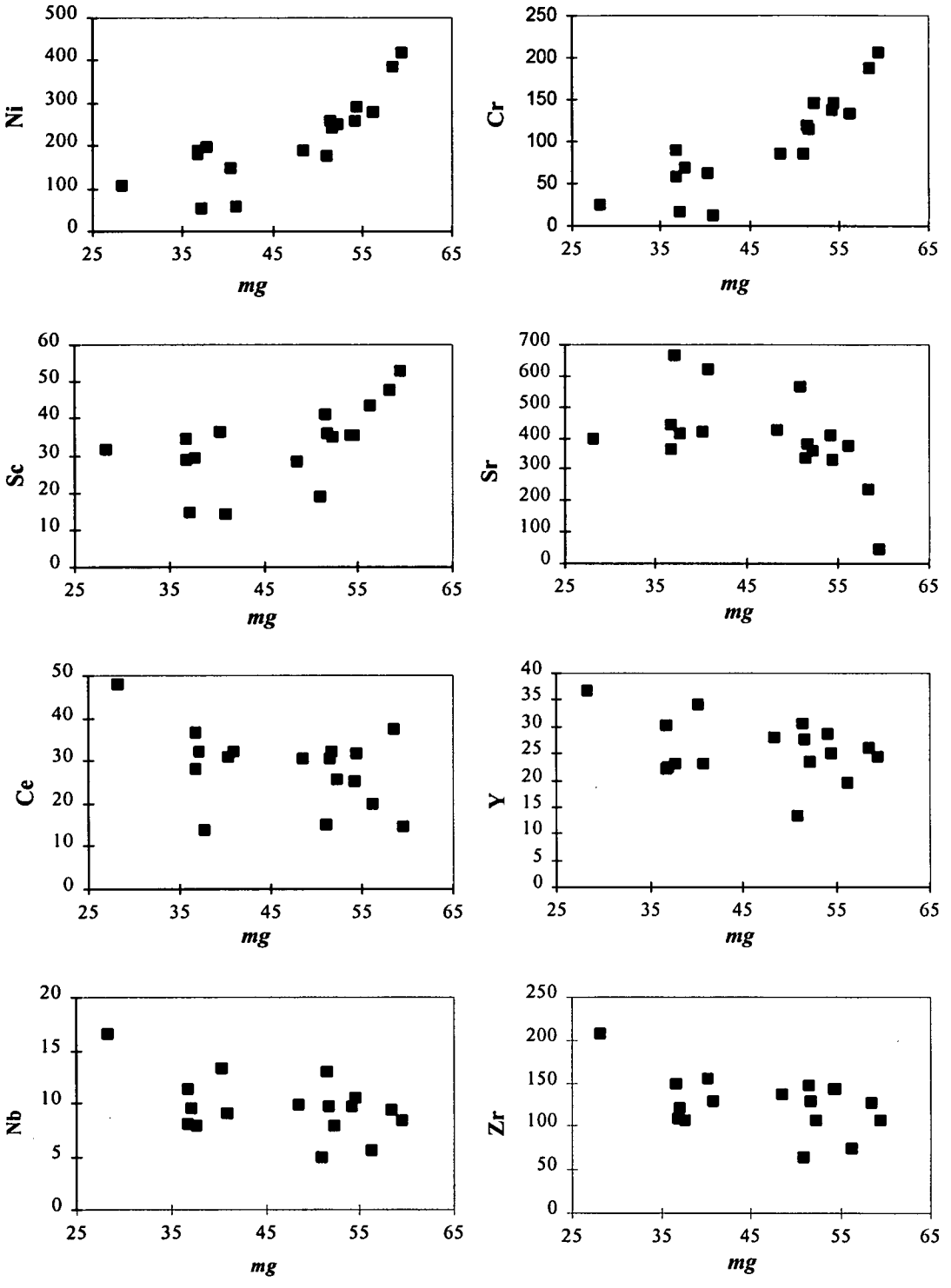

Figure 5.4 Selected trace-element variations *vs. mg* for the SLC MT. The 6 extreme differentiates plot away from the trends defined on these diagrams. Most are pyroxenites with very high Cr, Ni and *mg*.

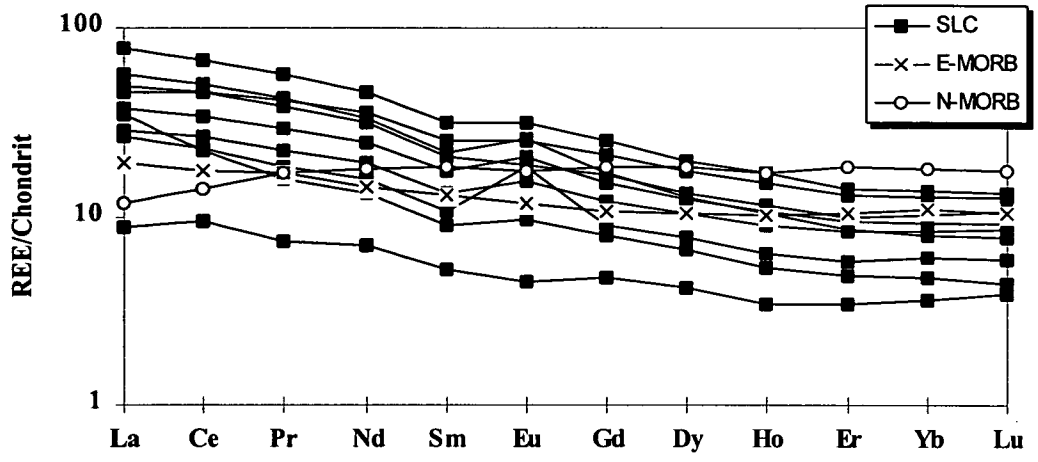

Figure 5.5 REE data for the SLC normalized to chondrite (Nakamura, 1974). E- and N-MORB MORB (after Sun & McDonough, 1989) are shown for comparison.

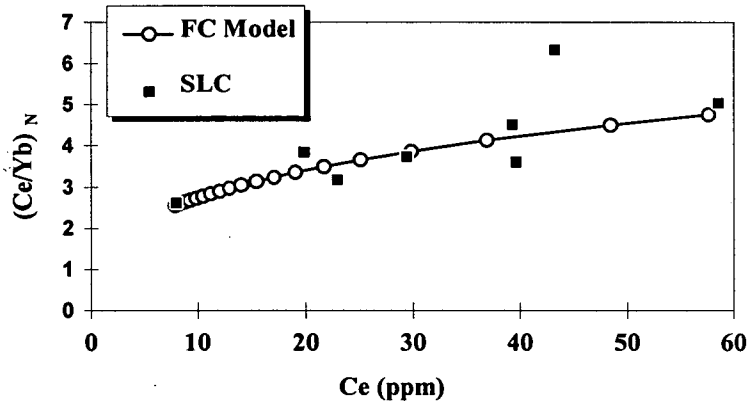

Figure 5.6 $(Ce/Yb)_N$ *vs.* Yb for the SLC showing a slight fractionation with increasing concentrations across the compositional range ***mg*** 78 - 28. Fractional crystallization model (FC) is for D_{Ce}=0.05 & D_{Yb}=0.2 (F=1-0.15).

McDonough & Sun (1995), and N-MORB are after Sun & McDonough (1989). Reasons for choosing these values as opposed to others are outlined in Chapter 1.

Figure 5.7 illustrates PM-normalized trace-element variations for the SLC[2]. Note that many immobile elements (Nb, Zr, Y, *etc.* of Pearce, 1983) have similar patterns to E-MORB but have slightly higher abundances, whereas the more mobile elements, especially Pb, Th and K, are substantially enriched relative to E-MORB (discussed further in Chapter 7). Also, the LILE and LREE are slightly fractionated with respect to the HREE and Y by comparison with the E-MORB pattern.

[2] Only those samples with full REE analyses have been included in this plot.

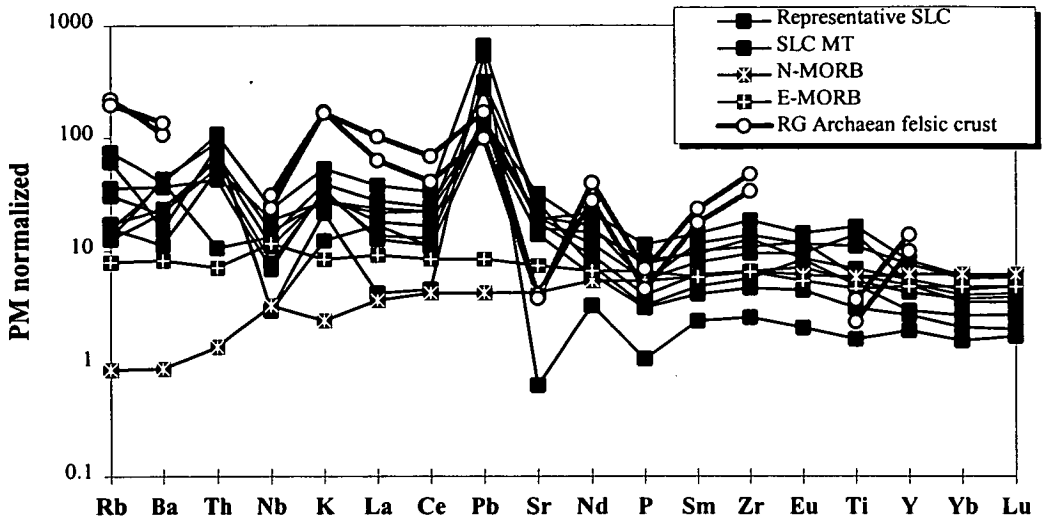

Figure 5.7 PM normalized (after McDonough & Sun, 1995) PM-normalized trace-element variations for the SLC. Representatives of Rauer Group Archaean felsic crust are also shown because they are potential assimilants (data from Sheraton *et al.*, 1984). E-MORB and N-MORB (Sun & McDonough, 1989) are shown for comparison.

Interpretation and steps towards a working hypothesis

Constraints on protolith petrogenesis and metasomatism

Assuming derivation from an E-MORB source, for the purposes of discussion, the observed SLC trace-element patterns could reflect one or more of the following processes:

- Lower or more variable degrees of partial melting than average E-MORB.
- Closed-system magmatic differentiation involving combinations of crystal settling, fractional crystallization, *in situ* crystallization or some other related mechanism.
- Assimilation of continental crust, either before or during magmatic differentiation.
- Metamorphic redistribution of trace elements.

Distinguishing between these processes is likely to be difficult for any suite of rocks, but it is particularly problematic for metamorphosed cumulates, especially when quenched or primary liquid compositions are not known. Nevertheless, a number of constraints can be placed on protolith petrogenesis and the possible influences of later metamorphic disturbance.

Partial melting

The nature and extent of partial melting is the most difficult aspect to constrain in the study of the SLC rocks. In lavas or quickly cooled igneous rocks that might approximate liquid compositions, it is sometimes possible to elucidate these processes from the relationships between compatible and incompatible trace elements (*e.g.* Hanson, 1989; Pearce & Parkinson, 1993; Fitton *et al.*, in press; and many others). However, in cumulate rocks, elements that are compatible in mantle phases are also strongly compatible in the fractionating/accumulating assemblage, as described above. This means that the concentration of an element such as Sc, for instance, is largely a measure of the amount of primary clinopyroxene and orthopyroxene that is included in the rock, and as such Sc does not relate directly to the extent of melting. For this reason, emphasis is placed on the behaviour of incompatible trace elements and, in particular, incompatible trace-element ratios.

There is no guarantee that the SLC geochemical trends described here are related by a single melt-extraction event. However, the sampling strategy concentrated on graded layers or units that have gradual rather than abrupt contacts and all samples are from within a relatively restricted part of the complex at the type locality. Furthermore, the SLC is similar to Skaergaard (the type example of closed-system fractional crystallization) in a number of respects, especially the Fe-enrichment trend (see above). It is probable, therefore, that the suite studied here was emplaced as a single magma batch and that subsequent differentiation occurred in an essentially closed system.

Closed system magmatic differentiation

Observations from petrography and interpretation of major-element chemical trends highlight the importance of plagioclase, clinopyroxene, orthopyroxene ± olivine in the fractionating/accumulating assemblage. Incompatible trace-element covariations support some of these observations and have the added advantage that they can potentially reveal the nature of mantle source regions or additional processes such as AFC. Unlike major or compatible elements, incompatible trace elements (IE) are essentially excluded from the early-formed cumulus framework and therefore IE dominantly reflect the composition of the trapped intercumulus liquid. Such liquid compositions are influenced by the removal of early formed phases, or in the case of *in situ* crystallization, interaction with a crystal mush up to the point at which the liquid is no longer mobile at small scales (*cf.* Paster *et al.*, 1974; Wilson *et al.*, 1987; McBirney, 1987; Langmuir, 1989). This has a number of important consequences for interpreting incompatible trace-element signatures.

As long as the whole-rock system (sample) is not a site of early accumulation for an IE-rich phase (*e.g.* monazite, zircon, apatite), then the IE abundance will be predominantly that of the trapped liquid because the cumulus framework will have very low concentrations of these elements until the last of the liquid crystallizes[3]. Therefore, provided that closely related trace elements are not appreciably fractionated from each other by interaction with the crystal framework, the ratios of these elements will be very similar to those of the primary magma, and hence the source (*e.g.* Sun & McDonough, 1989; Arnason *et al.*, 1997).

Incompatible trace-element variations are considered further in the next section in terms of fractional crystallization by application of an inverse modelling approach.

Assimilation

Constraining the amount of crustal assimilation on the basis of trace elements alone is difficult and most workers rely heavily on combined isotope and trace-element modelling (*e.g.* Gray *et al.*, 1981; Wilson *et al.*, 1987; Galán *et al.*, 1996; *cf.* Roberts & Clemens, 1995). The next chapter considers the isotopic evidence for assimilation but demonstrates that it is not possible to ascertain if this was an important process. This issue is referred to again in the next section and in the final chapter (Ch 7) in Part 2.

Metasomatism

Detailed quantification of trace-element mobility is not possible from the SLC dataset. A commonly-used qualitative disciminant for mobility, however, is the degree of correlation on trace-element covariation diagrams (*e.g.* Collerson *et al.*, 1991; Murton *et al.*, 1992; Kin & Jacobi, 1997). Since most trace elements are well correlated with each other in the SLC dataset, including elements that might be expected to behave differently during metasomatism (*e.g.* Y *vs.* Nb) it is likely that IE are not significantly different from those of the protolith. Exceptions appear to be restricted to LILE which have considerably more scatter that other IE. On this basis most trace elements are regarded as being immobile on the scale of sampling in the following discussion, but the problem of mobility is considered further by reference to the isotope study described in the next chapter.

---

[3] It is likely that as the trapped liquid begins to crystallize, IE increase to the point that concentrations are sufficient for the late crystallization of accessory phases where such elements are essential structural constituents (in the sense of Sun & Hanson, 1975). It is also possible that IE concentrations greatly increase in the early formed phases by residual melt/crystal mesh exchange (*e.g.* Barnes, 1986) and it is for this reason that trace-element concentrations in cumulus phases in layered complexes probably do not faithfully record the IE concentration of the magma from which they initially formed in a straight-forward way.

5.2.5 Constraints on fractional crystallization from trace elements

Trace-element ratios and application of inverse trace-element modelling is described here to demonstrate that fractional crystallization could produce many of the observed IE variations that characterise the SLC.

Background

Where fractional crystallization is considered to be the dominant differentiation mechanism, trace-element enrichment or depletion is governed by the well-known Rayleigh equation (*e.g.* Allègre & Minster, 1978):

$$C_L/C_o = F^{(D-1)} \qquad [5.1]$$

where, C_L is the trace element concentration in the evolving liquid, C_o is the concentration in the primary magma, F is the fraction of remaining liquid, and D is the bulk distribution coefficient.

Although this equation is usually used in forward modelling calculations of liquid evolution for a specified assemblage with inferred K_d values (*e.g.* Sheraton & Collerson, 1984), it is also possible to estimate the bulk distribution coefficient (D) for elements where a compositional range is known to be related by Rayleigh fractionation. Allègre *et al.* (1977) demonstrated that the slope of a data array on a log-log plot of a moderately incompatible element against a highly incompatible element will be approximately equal to 1-D, and for a compatible element plotted against a highly incompatible element will be approximately equal to D-1.

Assumptions and results

There are a number of assumptions inherent in this approach, the first being the suitability of the Rayleigh model. From the discussion in Sections 1.4.2 & 5.2.4, it is likely that the mechanism that controlled trace-element fractionation for the SLC MT *approximated* a Rayleigh function. The second assumption is one of a closed system magma chamber, hence calculated D values are for fractional crystallization and not for variable degrees of partial melting. The third main assumption concerns the choice of abscissa element, which should be perfectly or nearly perfectly incompatible (*i.e.* $D \cong 0$). For the SLC MT, of those elements that are not likely to be mobile during metamorphism, Nb appears to have behaved the most incompatibly relative to other elements analysed by XRF (following Hanson,

1989). However, while D_{Nb} is very small, it is not 0 and it should be appreciated that any estimated D values that approach Nb will be slight under-estimations (although the difference is probably not within the precision of the technique).

Hanson (1989) illustrated a theoretical application of the inverse modelling approach, based on combined CE and IE relationships, that is capable of constraining a number of key aspects of the partial melting and fractional crystallization history of a comagmatic suite. However, as described in previous sections, CE and IE are not often well correlated and probably represent quite different parts of the cumulate whole-rock system. Hence, it is not possible to estimate absolute D values from compatible elements. Nevertheless, it is possible to determine relative compatibility of these elements by considering variations in CE ratios with respect to ***mg*** or decreasing CE concentrations.

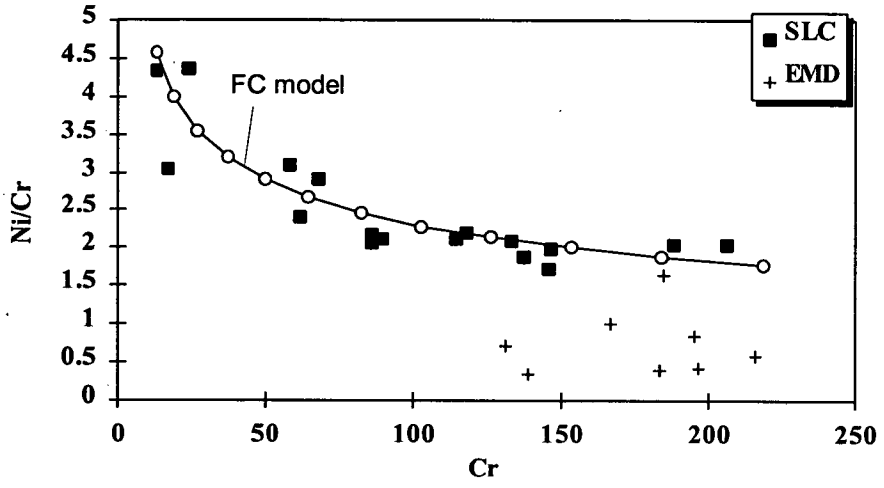

Figure 5.8 Ni/Cr *vs.* Cr for the SLC (see text for details of model)

Figure 5.8 illustrates the relationship between Ni and Cr for the SLC. In this case D_{Ni} is slightly less than D_{Cr} as seen by the increase in Ni/Cr *vs.* Cr (or ***mg***, the results are similar). Note that the Ni-Cr ratio changes according to an exponential (Rayleigh) relationship. The EMD and a simple theoretical fractional crystallization model ('FC Model' defined by Eq. 5.1) are also shown for comparison. The model assumes starting compositions of Ni = 480 ppm; Cr = 300 ppm; F = 0.9-0.35; D_{Cr} = 3; D_{Ni} = 2. A similar approach has been applied to the other CE resulting in a compatibility order:

$$D_V \sim D_{Mn} < D_{Sc} << D_{Ni} < D_{Cr}$$

For the IE, calculations have been restricted to those elements that are thought to be related by a function approximating fractional behaviour as the residual magma evolved with

respect to the cumulate pile, and that have a reasonably strong correlation with Nb. It should be appreciated that, given the assumptions described above, these D values are probably semi- quantitative at best. Nevertheless the first encouraging conclusion is that calculated D values are plausible igneous bulk distribution coefficients. Figure 5.9 illustrates the results graphically, and the estimated D values are shown on the graphs. For these IE, the order or compatibility appears to be:

$$D_{Nb} < D_{Nd} = D_P < D_{Zr} < D_{Ce} < D_Y = (D_{Ti}?)$$

Note that D values for most elements are higher than can be explained by combinations of olivine or plagioclase alone. Sr initially increases with Nb (not shown on graphs, *cf.* Figure 5.4d), but there is an inflection which is consistent with Sr becoming compatible as a consequence of plagioclase fractionation. Appreciable early magnetite or ilmenite fractionation is unlikely since this would lead to much higher D values for Ti relative to Y. Similarly, apatite must have been a late crystallizing phase because D_P (and D_{LREE}) are low. However, IE fractionation dominated by clinopyroxene/pigeonite could explain much of the observed data.

Qualitatively, D values determined for the SLC MT are probably better than order of magnitude estimates. The roles of orthopyroxene, plagioclase and olivine are difficult to assess. Since Ni is only slightly less compatible than Cr (Figure 5.8), it is probable that orthopyroxene and/or olivine were fractionating phases, otherwise Cr would be much more compatible than Ni ($K_{dCpx/Cr} \approx 10 \times K_{dCpx/Ni}$). This is difficult to assess further because independently estimated D values of Cr and Ni for Opx, Cpx, Pig and Ol in basaltic systems are highly variable (*e.g.* Wilson, 1989, figure A1; Rollinson, 1993, table 4.1, and others). Moreover, because clinopyroxene and/or pigeonite have appreciably higher K_d values for most IE than olivine, plagioclase or orthopyroxene, the contribution of the latter minerals to overall bulk distribution coefficients would be masked by the contribution of clinopyroxene and/or pigeonite.

To summarize, compatible- and incompatible-element variation diagrams are consistent with a fractional or *in situ* crystallization magmatic differentiation mechanism. Early fractionation of IE was dominated by clinopyroxene and/or pigeonite and orthopyroxene. Plagioclase was an important but relatively late fractionating phase. Apatite, magnetite and/or ilmenite were unlikely to have been early cumulus phases. Unfortunately, the role of olivine cannot be established on trace-element grounds.

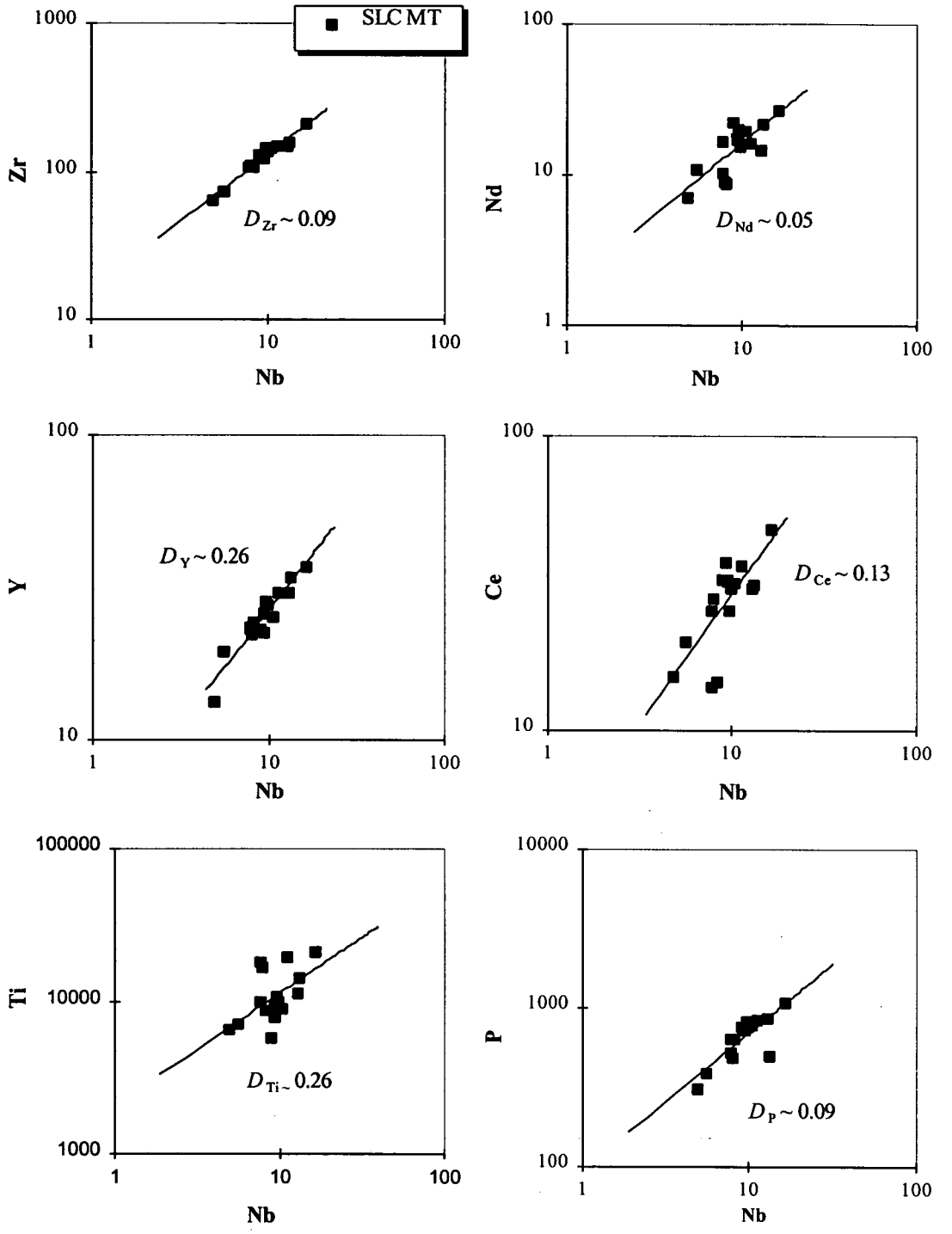

Figure 5.9 Logarithmic plots of incompatible elements *vs.* Nb. Solid lines are used to estimate bulk distribution coefficients.

5.2.6 The role of AFC

The spidergram patterns illustrated in Figures 5.5 & 5.7 are characterised by progressively more fractionated and enriched patterns with a number of positive or negative anomalies

relative to a reference E-MORB or PM source (discussed further in Chapter 7). Some of these features may be related to LILE mobility. However, as Figure 5.7 illustrates, there are possible contaminants with spidergram patterns which could also generate these anomalies. Samples #5120 and #5143 are thought to be representative of the Composite Layered Orthogneisss in the Rauer Group (see Section 2.3.2) and if assimilated into a primary magma, the generally much higher IE abundances characteristic of felsic crust could easily displace the IE patterns from an E-MORB-like signature towards the observed patterns of the SLC MT (discussed further in Chapter 7).

Note also that for many 'immobile' incompatible trace elements the effects of AFC are very similar to those predicted by fractional crystallization involving clinopyroxene (*i.e.* higher LREE/HREE), and it is not easy to distinguish between these two processes on trace-element grounds. This is one reason why a detailed interpretation of trace-element signatures is reserved until after discussion of the isotope geochemistry in the next chapter. Isotope geochemistry can potentially discriminate between fractional crystallization, assimilation, and post-emplacement geochemical perturbation, although for the SLC, the results are not straightforward.

5.2.7 Preliminary conclusions and working petrogenetic hypotheses

Major- and trace-element compositional variations within the SLC are consistent with fractionation/accumulation dominated by clinopyroxene/pigeonite, orthopyroxene and plagioclase. Unaltered ultramafic cumulates are websterites and although olivine would be stable in these plagioclase-absent assemblages, none of the SLC rocks have relict olivine or obvious olivine replacement products. Unfortunately major- and trace-element chemistry cannot resolve whether olivine was involved in the petrogenesis of the complex or not.

Comparison of spidergram patterns with a number of potential mantle source 'reservoirs' indicates that the SLC is most similar to E-MORB in character. Variations from source patterns may reflect slightly smaller degrees of partial melting than average E-MORB, but could equally reflect fractional crystallization and/or assimilation processes. Unfortunately, the relative contribution of these latter two processes cannot easily be distinguished on the basis of trace elements alone (discussed further in Chapter 7).

Finally, coherent major-, trace- and REE patterns that are consistent with 'expected' igneous differentiation process imply that large-scale metasomatism did not affect these rocks. However, poor correlations for LILE relative to ***mg***, REE or HFSE, suggests that the LILE

might be significantly modified. Such a pattern of LILE mobility is a characteristic of high-grade terranes described by many workers (*e.g.* Tarney & Windley, 1977; Rollinson & Windley, 1980; Sheraton & Collerson, 1984).

The next chapter critically examines the isotope geochemistry of the SLC and all the available data are integrated into a tentative tectono-magmatic framework in the final chapter (Chapter 7) in Part 2.

5.3 Geochemistry of the Archaean? mafic dykes (EMD)

A preliminary geochemical account of the early mafic dykes (EMD) that are contained within the SLC is given here, largely to compare the chemistry with the host layered complex. A large number of mafic dykes, of all the relative ages described in Chapter 3, have been geochemically analysed and the data are included in Appendix 2. The post-tonalite mafic dykes (PTMD) of probable Proterozoic age are not, however, described in detail in this thesis even though data are included in the appendix as part of the general Prydz Bay catalogue.

5.3.1 Principal geochemical characteristics

Most of the EMD are Fe-tholeiites, although one sample (SH70) is a high-Mg tholeiite. Compositionally, the dykes are broadly similar to the host complex, and are characterised by Fe-enrichment (see Figure 5.1), low ***mg***, and moderately fractionated and enriched trace-element patterns relative to PM. There are, however, a number of significant differences that are not directly attributed to the contrasting cumulate origin of the SLC.

5.3.2 Major elements

Compared with the SLC, the EMD have a similar range of ***mg***, SiO_2, $Fe_2O_{3(t)}$ and MgO, but have distinctly higher CaO. Of particular interest, CaO decreases sharply with decreasing ***mg*** (or MgO). Figure 5.3 (in Section 5.2.1) shows the compositions of the EMD compared with the SLC and compositional trends typical of most continental tholeiites. The single high-Mg sample (SH70) plots on the olivine control line, and all the other samples lie along a compositional liquid line of descent dominated by clinopyroxene with possible plagioclase fractionation. On this basis, and in common with continental tholeiites in general, it is likely that most EMD have undergone extensive (low pressure) fractionation of olivine with minor clinopyroxene and plagioclase. This is clearly quite different to the SLC, where

clinopyroxene or pigeonite is considered to be the dominant fractionating phase (possible reasons for this contrast are considered in Chapter 7).

5.3.3 Normative compositions

Most of the EMD have similar normative mineralogies to the SLC. All the dykes except RI5 have varying proportions of *Ol*, *Di* and *Hy*, and are broadly classified as olivine tholeiites. RI5 is slightly *Q* normative (does not contain *Ol*) and is closer in composition to a quartz tholeiite. Compared with the SLC, the EMD have higher *Di* and more variable *Hy* and *Ol*. *An* and *Ab* are in the same range as the SLC, but *Or* is slightly lower.

5.3.4 Trace and rare earth elements (REE)

Trace elements

Although all the EMD might be related by a common fractional crystallization history, there is no reason to suppose that any of the dykes are strictly comagmatic, and therefore trace-element modelling between dykes is inappropriate. Overall, trace-element characteristics are quite similar to the SLC but there are a number of important differences. Compared with the SLC, the EMD have higher Cr but lower Ni concentrations, and low but variable Ni/Cr ($\approx 0.7 \pm 0.6$) compared with higher Ni/Cr (≈ 2.5) for the main complex (see Figure 5.8). Most IE are also generally less enriched and less fractionated as typified by slightly lower LILE/HFSE and LREE/HREE (see Figure 5.10; described further below).

Rare earth elements

REE patterns for the EMD are enriched and slightly fractionated relative to chondrite with average (Ce/Yb)N of about 2.5. The patterns are appreciably flatter than the SLC although abundances are broadly similar (Figure 5.11).

Spidergrams

Spidergram patterns for the EMD are similar to the SLC and E-MORB (Figure 5.12). In common with the main complex, LILE are variable indicating that these elements were probably mobile during metamorphism. Most of the remaining elements, especially REE & HFSE, have similar patterns to E-MORB, although there are slight differences in concentrations.

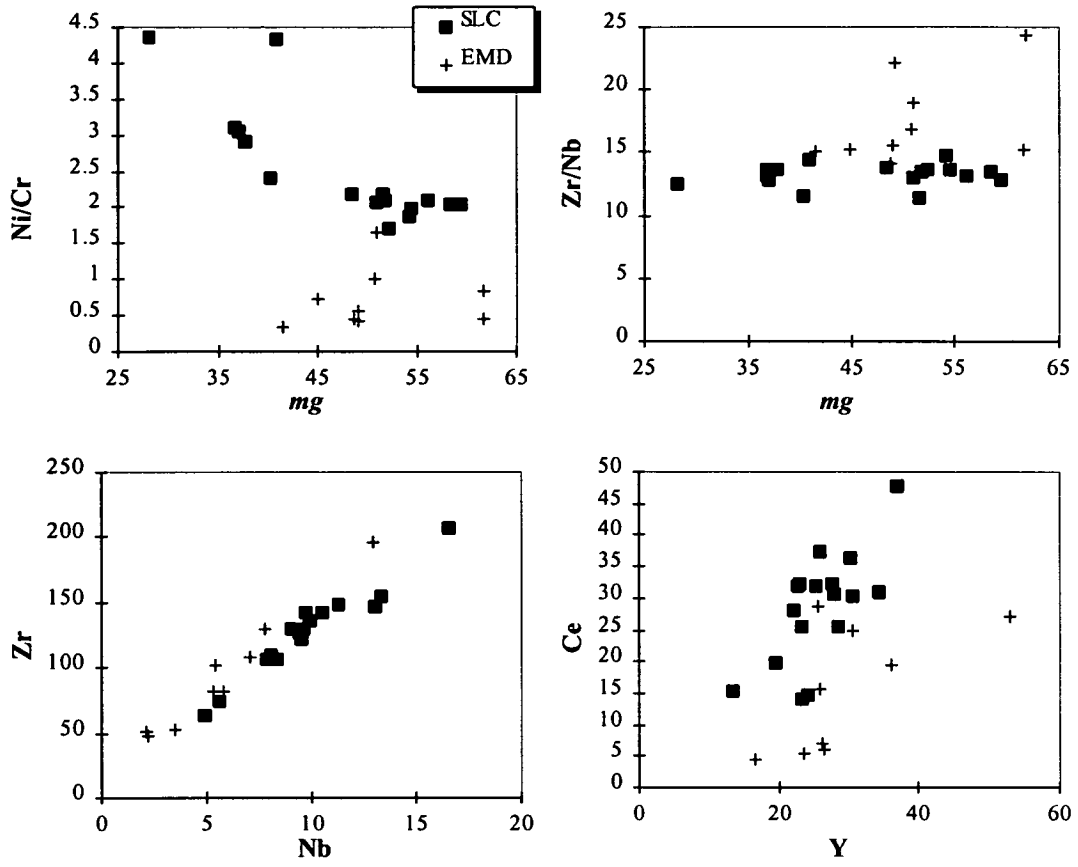

Figure 5.10 Selected trace-element variation diagrams for the EMD highlighting differences with the SLC. Ni/Cr *vs. mg*; Zr/Nb *vs. mg*; Zr *vs.* Nb; Ce *vs.* Y.

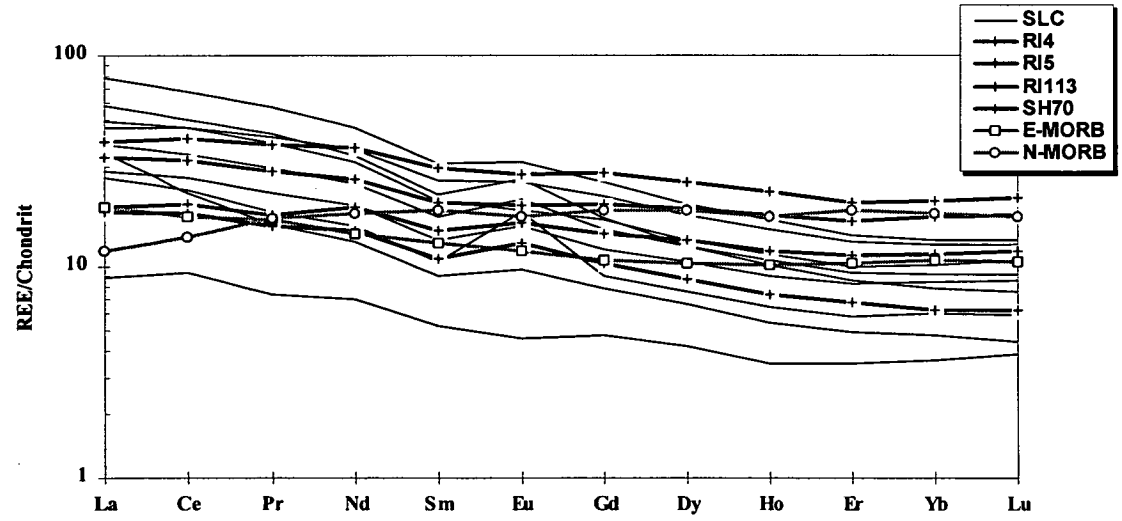

Figure 5.11 Chondrite-normalized REE patterns for the EMD. The SLC, E-MORB and N-MORB (Sun & McDonough, 1989) are shown for comparison.

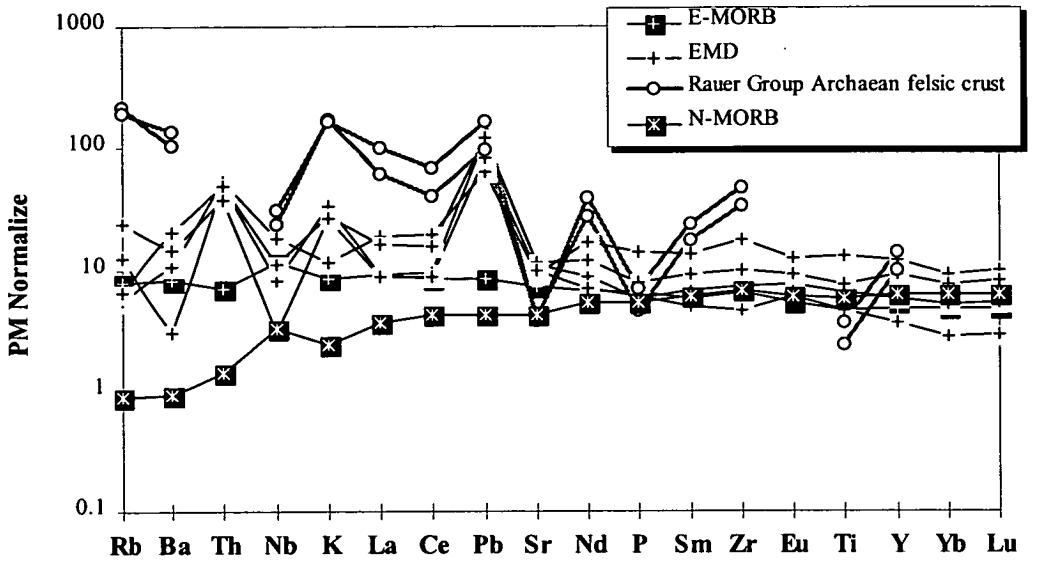

Figure 5.12 PM-normalized abundances for the EMD. Representatives of the Rauer Group Archaean felsic crust (#5120 & #5143), E-MORB and N-MORB are shown for comparison.

Comparison with the SLC and preliminary interpretation

Although the EMD and SLC datasets are not directly comparable (because the SLC is a cumulate body), REE, trace-element ratios, and spidergram patterns are consistent with derivation from *broadly* similar source regions but with primary melts following different fractional crystallization paths. Petrogenetic deductions made from major elements and compatible elements (*e.g.* Ni/Cr), imply that the EMD have undergone extensive olivine fractionation with only minor involvement of clinopyroxene and plagioclase. In detail, however, there are differences between the SLC and EMD, such as variable IE ratios (Figure 5.10) and less fractionated REE profiles (Figure 5.11), that are more likely to reflect mantle source characteristics or partial-melting processes. However, as with the SLC, it is difficult to ascertain if there has been significant assimilation of the surrounding crust. High concentrations of LILE elements could be produced by crustal contamination, but because these elements are likely to be mobile (*e.g.* Tarney & Windley, 1977; Rollinson & Windley, 1980), they cannot be relied upon to constrain this process.

Further similarities and differences between the SLC and EMD are considered in Chapter 7, after discussion of the isotope data.

5.4 Geochemistry of the TTLC

5.4.1 Principal geochemical characteristics

Overall the TTLC is characterised by relatively high SiO_2 (48-55 (Av. 53) wt%), CaO (5-15 wt%) and MgO (2-25 wt%), but with correspondingly low $Fe_2O_{3(t)}$ (4-12 wt%), resulting in very high ***mg***-numbers (86.6 - 45.5). Trace-element concentrations are highly variable. Elements that are compatible in major mantle phases are generally high (*e.g.* Ni up to 1100 ppm; Cr up to 3360 ppm), while incompatible-element concentrations are generally very low (*e.g.* Nb < 5 ppm; Zr < 90 ppm). Geochemical variation diagrams (Figures 5.13-5.14) are typified by inter-element relationships that are broadly consistent with magmatic differentiation.

Three loosely defined geochemical groups can been recognised and the complex has been divided into:

- ***Group (i),*** comprising high ***mg*** rocks that have low alumina contents (*e.g.* Figure 5.13b; n=18). These correspond to the melanocratic layers or the basal parts of layers (see Chapter 3 for field description).

- ***Group (ii),*** comprising moderately high ***mg*** rocks that have high alumina contents (*e.g.* Figure 5.13b). These correspond to leucocratic layers or the tops of layers (n=10). Elements other than Al_2O_3 that have a strong affinity with plagioclase, such as Na_2O and Sr are also markedly higher in this group (*e.g.* Figures 5.13f & 5.14c).

- ***Group (iii),*** comprising low ***mg*** rocks with anomalous major- and trace-element chemistry (*e.g.* Figures 5.13b & h; n=5). The origin of this group is less immediately apparent but is considered further below.

5.4.2 An outline of major and trace elements

For most major and trace elements, Groups (i) and (ii) appear to be intimately related and have coherent inter-element trends. The compositional relations between samples and groups has been examined by using ***mg***-number as an index of differentiation. Overall, Groups (i) and (ii) have geochemical trends towards more evolved samples (lower ***mg***) that are characterised by *decreasing* SiO_2, MgO and $Fe_2O_{3(t)}$, with corresponding increases in Al_2O_3, Na_2O and K_2O (Figure 5.13). CaO initially increases from 5 wt% up to about 15 wt% at ***mg*** 82 before slightly decreasing.

Many trace-element bivariate diagrams have a sharp inflection at about ***mg*** 82, with TiO_2, MnO, P_2O_5, Zr, Y and possibly Sc all showing marked inflections. Ni and Cr decrease consistently with falling ***mg***, although there is a compositional break between the groups with Group (i) having higher values for both elements. Other elements, such as Rb, Pb, and LREE, do not show systematic variations with ***mg***.

An interesting feature of the relationship between Group (i) and Group (ii) is that the composition gap that defines the two groups and the point of inflection described above for some trace elements occurs at different ***mg*** values. Elements with a strong affinity for plagioclase, such as Al, Na and Sr are clearly much higher in the more leucocratic layers, although other trace elements, such as Y, are effectively being decoupled from the process responsible for the differences between the two groups. This will be discussed further in the next section.

Group (iii) comprises only 5 rocks that have been distinguished because they are anomalous with respect to the main suite (Groups (i) and (ii)). Although Group (iii) has low SiO_2 and high $Fe_2O_{3(t)}$ (hence low ***mg*** values), abundances of MgO, CaO and Na_2O and some minor elements are similar to Groups (i) and (ii). However, Group (iii) has anomalously high TiO_2, V, Zr, P_2O_5, MnO, Th and Y. Three of the samples also have very high Ni (> 980 ppm). It is interesting to note that many of the elements that are high in Group (iii) correspond to those elements in Groups (i) and (ii) that have marked inflections with decreasing abundances associated with increasing differentiation. It is tempting to relate these features to a causative mechanism, with one possible explanation being that Group (iii) rocks contain a high proportion of cumulus accessory phases such as spinel and/or apatite.

5.4.3 Normative compositions

The TTLC is dominated by normative *Hy-Di-Ab* mineralogies and some compositions are weakly *Ol* or *Q* normative. Compositionally many of the TTLC rocks plot near to the *Di-En-Ab* plane of the Yoder & Tilley (1962) normative basalt tetrahedron and are perhaps best described as hypersthene tholeiites.

5.4.4 Trace and rare-earth elements (REE)

Trace elements

The TTLC is characterised by high abundances of elements that are compatible in typical major mantle phases, but has very low IE concentrations. Although some trace elements are

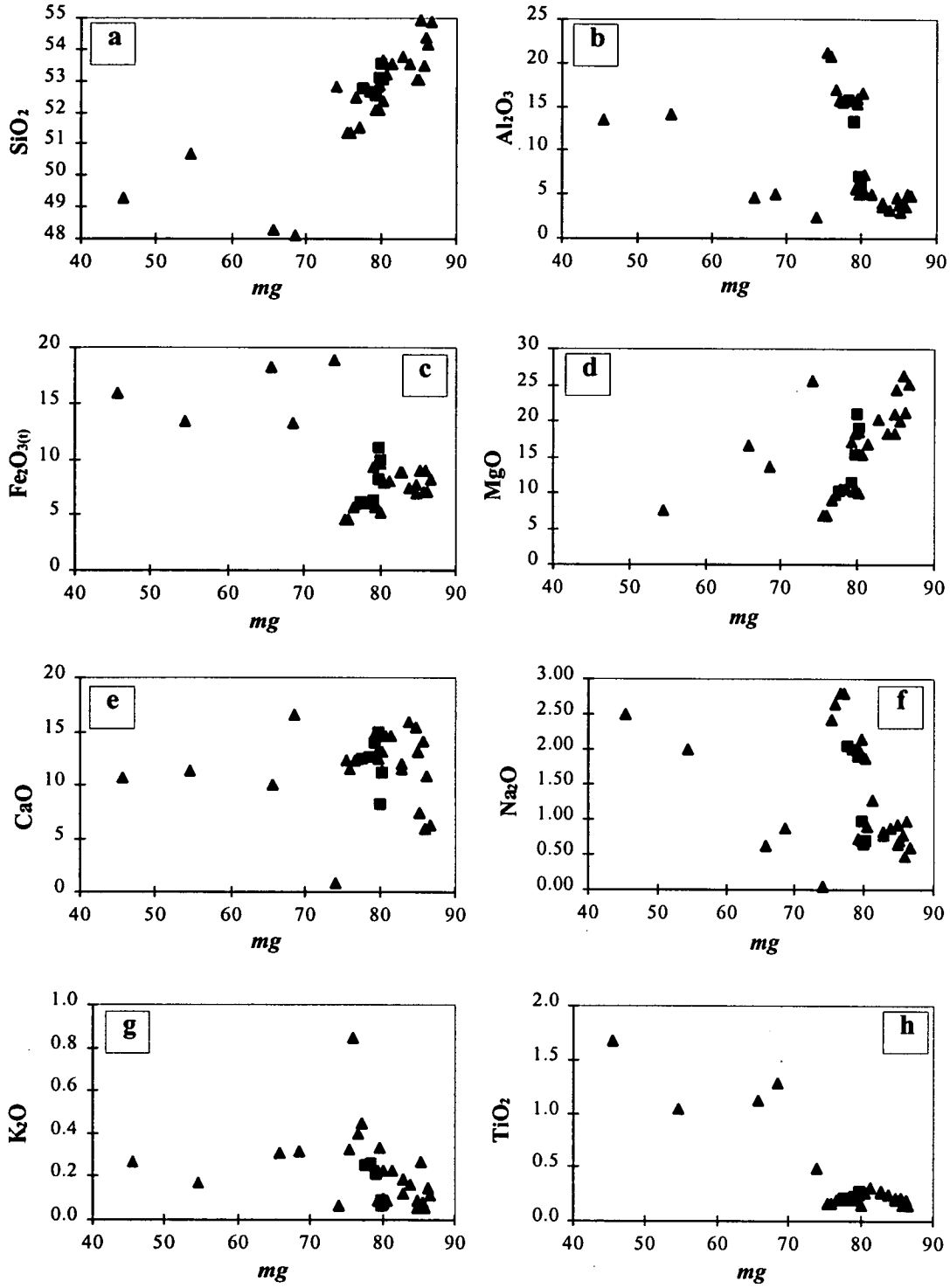

Figure 5.13 Selected major-element variation diagrams for the TTLC (a-h). Square symbols represent a traverse across a single graded layer.

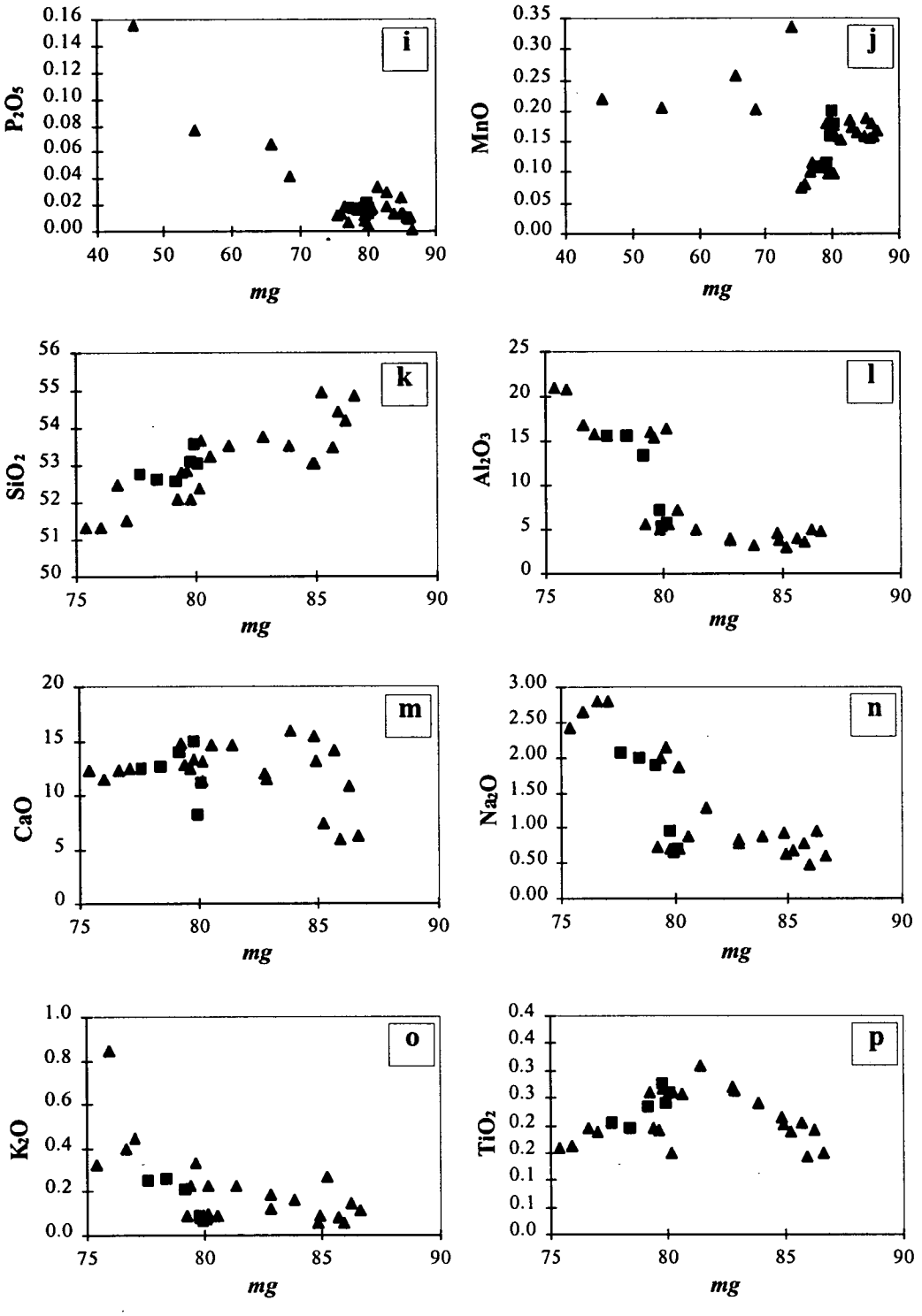

Figure 5.13 cont. Selected major-element variation diagrams for the TTLC (i-p). Square symbols represent a traverse across a single graded layer.

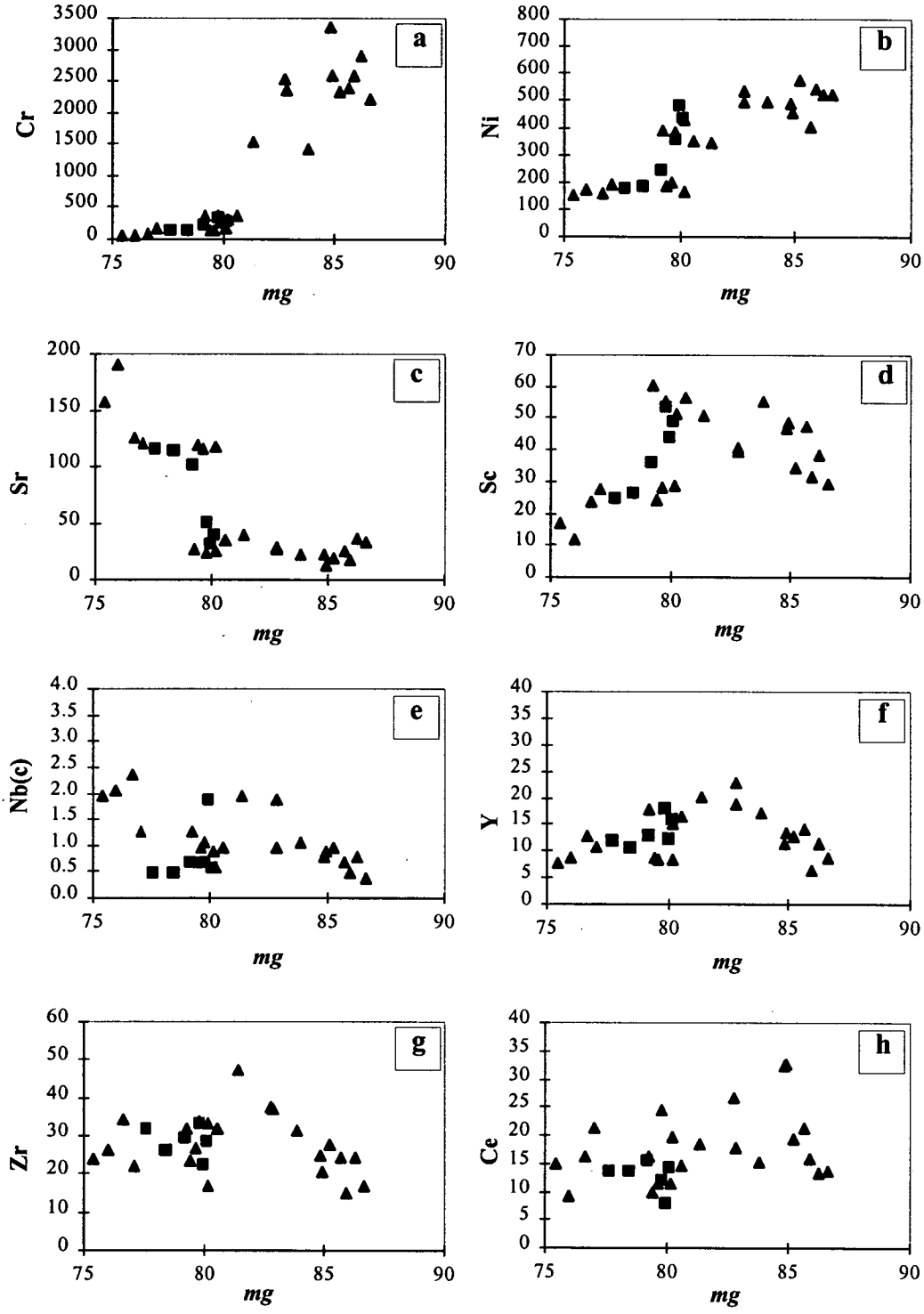

Figure 5.14 Selected trace-element variation diagrams for the TTLC (Groups (i) - (ii) **only**). Square symbols represent a traverse across a single graded layer.

reasonably well-correlated with ***mg*** (*e.g.* Cr, Ni & Zn; Figure 5.14), or have marked inflections with ***mg*** (*e.g.* Y & Nb), most IE covariations are not well-correlated. By contrast with the SLC, for example, elements such as Zr, Nb, P_2O_5, Y and TiO_2 are not strongly related (Figure 5.15).

As described in previous sections, CE/IE are likely to be variable as they have been strongly influenced by the fractionation-accumulation process, whereas IE ratios might be independent of this process to some extent. Such ratios for the TTLC, however, are variable in their behaviour. For example, although Zr/Y and Ti/Y are relatively constant, ratios involving Nb are highly variable (*e.g.* Zr/Nb = 12.0-66.6; Y/Nb = 3.9-26.4). Even though Nb concentrations are often less than 2 ppm in the TTLC, variability in Nb is not attributed to analytical uncertainty (this is discussed further in Chapter 7). It seems most likely that such large variations in ratios reflect petrogenetic or alteration processes as described for the SLC in section 5.2.4. The relative influence of these processes (*viz.* partial melting, fractional crystallization, assimilation, metasomatism) is assessed further below.

REE

Only 4 rocks have been analysed for REE from the TTLC (Figure 5.16); RI56 & RI63 are from group (I) and RI47 & RI59 are from group (ii). For these samples, MREE to HREE (Gd-Lu) are flat or possibly slightly concave up, and are only moderately enriched relative to chondrite (3-10 x chondrite). There are small positive and negative Eu anomalies corresponding to the abundance of plagioclase. LREE (La-Sm) patterns are moderately fractionated relative to chondrite with $(La/Sm)_N = 2.2\text{-}4.7$, and have variable shapes (Figure 5.16). These features are considered further below.

Spidergrams

PM-normalized abundance patterns are presented in Figure 5.17 for the four rocks[1] for which ICP-AES REE data are available. There are number of important features to note from Figure 5.17, that are referred to in following sections and chapter 7:

- HREE and Y have parallel flat patterns.
- Most LILE are highly variable.

[1] PM-normalized IE patterns for all the TTLC are similar to these 4 samples.

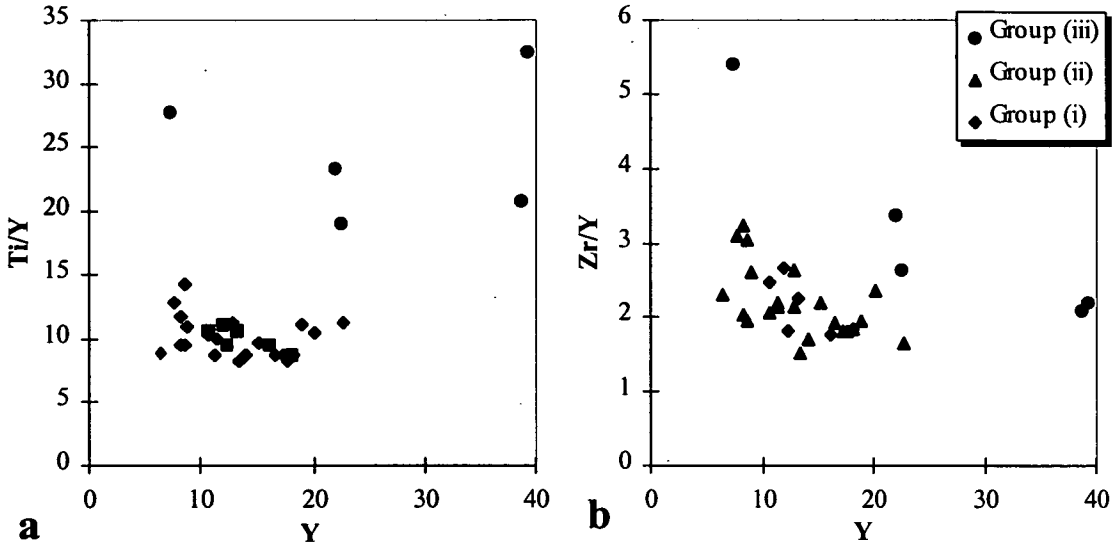

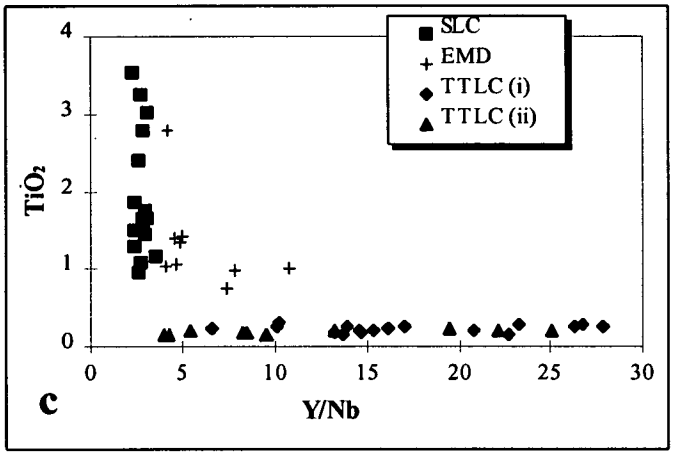

Figure 5.15 An illustration of the variations in trace-element ratios for the TTLC. (a) Zr/Y decreases slightly with Y implying that $D_{Zr}>D_{Y}$. (b) Ti/Y is relatively constant implying similar *D*-values. (c) is a trace-element discrimination diagram after Floyd & Winchester (1975) which will be discussed further in Chapter 7.

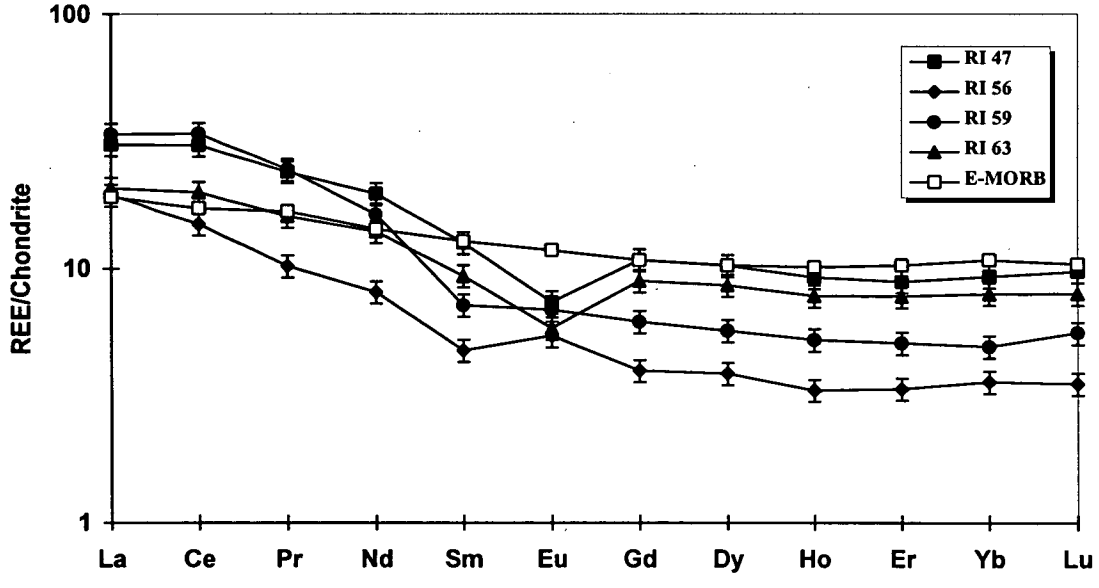

Figure 5.16 Chondrite-normalized REE patterns for the TTLC (Nakamura, 1974). E-MORB values of Sun & McDonough (1989) are shown for comparison.

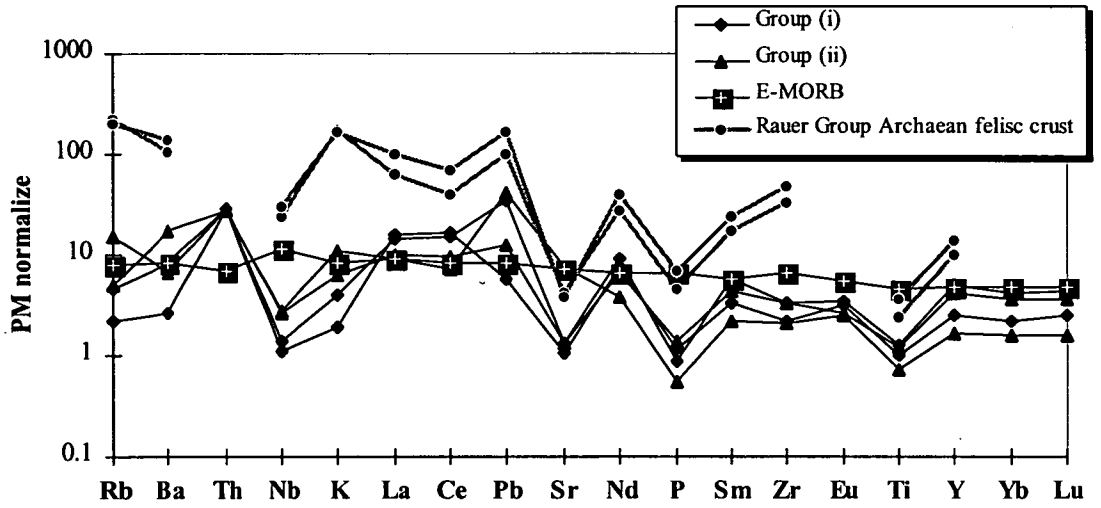

Figure 5.17 PM normalized spidergram for the TTLC (McDonough & Sun, 1995). E-MORB is shown for comparison (Sun & McDonough, 1989).

- There are pronounced negative anomalies for Ti, P and Nb (Nb would still be negative if placed between the 'immobile' elements La and Ce, see discussion in Section 1.4.2).

- Three of the four samples have negative Sr anomalies, which includes plagioclase-rich RI63 from Group (ii).

Comparison with the SLC and a preliminary interpretation

The TTLC differs markedly from the SLC and EMD. Although all these gneiss suites comprise two-pyroxene + plagioclase granulite assemblages with minor hornblende, there are marked differences in bulk composition. The TTLC is a high-Mg layered complex that was clearly derived from a relatively high degree partial melt from a mantle source. This resulted in low IE concentrations throughout the suite irrespective of fractionation/accumulation processes.

Major-element chemistry, dominated by high MgO and relatively high SiO_2, and trace-element signatures dominated by high CE concentrations, very low IE concentrations, negative HFSE anomalies, and flat HREE but fractionated LREE patterns, are all characteristics typical of boninites (*e.g.* Cape Vogel, Papua New Guinea, and other examples cited in Hickey & Frey, 1982). It is therefore tempting to infer a boninite origin for the TTLC. However, there are fundamental differences between the TTLC and boninite magmas. Perhaps most importantly, the TTLC is an intrusive (cumulate) layered complex whereas boninites more closely approximate liquids (although some of those described by Hickey & Frey (1982), are highly porphyritic). Nevertheless, spidergram patterns and, more

importantly, closely related IE ratios are unlike either the SLC or EMD. This could reflect differences in crystal fractionation/accumulation history, source character, extent of crustal contamination, or degree of open-system metasomatic exchange (see SLC section above). If the dominant processes are primary (magmatic), than the comparison with boninite magma series warrants close attention, since the TTLC may represent the intrusive equivalent of this magma type. Each of these potential processes are briefly assessed below in order to provide a background to the isotope geochemistry and synthesis chapters to follow (Chapters 6 & 7).

Fractional crystallization/accumulation processes

The presence of bronzite phenocrysts in some ultramafic rocks (*e.g.* Section 4.5.2) and the observed major-element variations are consistent with magmatic differentiation dominated by fractionation/accumulation of orthopyroxene at an early stage. As with the SLC, it is difficult to implicate olivine on the basis of major-element or trace-element variations, but given the high-*Hy* and low-*Ol* normative mineralogy, olivine is unlikely to have been an important phase. Moreover, a trend of decreasing SiO_2 with decreasing ***mg*** implies orthopyroxene rather than olivine control. This is because orthopyroxene has high SiO_2 (*e.g.* bronzite phenocrysts described in Section 4.5.2 have ~54.9 wt%) relative to olivine. Fractionation/accumulation of clinopyroxene, plagioclase and possibly minor spinel/magnetite is also likely. Inflections in some variation diagrams for trace elements *vs.* ***mg*** may relate to early plagioclase accumulation in the upper parts of layers (flotation?) and/or reflect the role of clinopyroxene as a fractionating phase. Inflections in Ti and Y *vs.* ***mg***, for example, might reflect dilution as a consequence of plagioclase flotation, coupled with increasing D_Y and D_{Ti} as a consequence of clinopyroxene fractionation (possibly with minor spinel/magnetite). Alternatively, in a simple layer-scale closed system, it is possible that IE were concentrated towards a 'middle zone' (*cf.* the chamber-scale evolution of Skaergaard, reviewed in Wilson, 1993) by advancing crystallization from above (plagioclase) and below (pyroxenes).

However, poor correlations between IE precludes further or more rigorous constraints on the fractionating assemblage by inverse-modelling techniques. There are a number of possible reasons why these elements might not correlate well. The most likely are outlined in the sections below, but one possibility that needs to be addressed in this section is that IE patterns and ratios are strongly controlled by the fractionation/ accumulation process.

It is possible that IE abundances and ratios do not relate closely to the 'trapped liquid' assumption described in Sections 1.4.4 & 5.2.4, but instead more closely reflect the

chemistry of the cumulus framework. However, there are a number of arguments against this hypothesis. For example, if IE in the high ***mg*** Group (i) rocks were to reflect orthopyroxene-dominated accumulation they would be expected to have higher $(Nb)_N$ than other modes since K_{dNb} is at least an order of magnitude greater for orthopyroxene than the other possible major phases, olivine or clinopyroxene (see Kelemen *et al.*, 1993; Rollinson, 1993, table 4.1). Conversely, K_{dY} is much less for orthopyroxene than clinopyroxene, which would be consistent with higher modal abundances of clinopyroxene in mid-layer compositions, but Nb and Y both have inflections with respect to ***mg*** (*cf.* also Nd & Zr). Furthermore, the TTLC has similar spidergram patterns for significantly different assemblages and modes. Although fractionation/accumulation of plagioclase may explain positive and negative Sr anomalies, negative Ti, P and Nb are less easily accounted for by this process. Since all rock compositions from ultrabasic to leucogabbros have similar negative anomalies, there is no complementary 'reservoir' that can account for these features by closed-system fractionation. Even the anomalous Group (iii) rocks with high P and Ti have similar IE patterns (negative anomalies) to Groups (i) and (ii) because they have relatively high concentrations for all IE.

Alternatively, if it is assumed that IE patterns of the cumulates reflect the residue from open system magmatic processes, whereby erupted compositions have high Ti, P and Nb, the cumulus phases would all need to have concentrations (hence *D*-values) for Ti, P and Nb appreciably less than neighbouring elements such as Nd, La, Ce and Zr (assuming that many other elements are 'suspect'/mobile). Although K_d values for possible primary cumulus phases are likely to be dependent to some extent on *P-T-X* conditions particular to the TTLC, it is unlikely that they would be significantly different to published values for basaltic systems (*e.g.* Irving & Frey, 1984; Wilson, 1989, figure A1; Kelemen *et al.*, 1993; Rollinson, 1993, table 4.1). Hence, none of the possible fractionating phases described above would have pronounced negative Ti, P and Nb anomalies relative to Nd, La, Ce, Zr.

To conclude, therefore, it is most likely that the *IE patterns* and at least some *IE ratios* most closely reflect processes other than *in situ* fractionation/accumulation.

Source characteristics versus assimilation

Quantifying the degree of partial melting directly from these cumulate rocks is not possible because, as described for the SLC, compatible elements are dominantly controlled by the fractionation/accumulation process (although qualitatively it is likely that the extent of partial melting was large). Nevertheless, it is possible that trace-element ratios and

spidergram patterns reflect source region and hence magma generation process, although it is only possible to be sure of this if the effects of secondary mobility and crustal assimilation can be distinguished.

Although assimilation and metasomatism are fundamentally different processes, protolith bulk composition prior to crust/fluid interaction has a similar influence on both. Compared with the SLC, EMD, and basalts in general, the TTLC has high CE but very low IE abundances. It is well established that, in normal circumstances, to accomplish large displacements in elemental abundances as a consequence of assimilation, the concentration of the element in the assimilant must be significantly higher than in the uncontaminated magma (*e.g.* DePaolo & Wasserberg, 1979; DePaolo, 1981; Powell, 1984). For the TTLC this means that most major and compatible elements will be largely unaffected by contamination of felsic crust (except by dilution).

The exception for major elements would be SiO_2, the dominant component in the Rauer Group Archaean felsic gneisses. Perhaps this explains the high SiO_2 of the TTLC? The consequences of such assimilation have been assessed by Gray *et al.* (1981) who demonstrated the trace element and isotopic affects of mixing large amounts (~25 %) of felsic crust into a basic layered intrusion (the Kalka Layered Complex, central Australia). Interestingly, they argued that the assimilation of SiO_2-rich crust led to the prevalence of orthopyroxene in the fractionating assemblage (Gray *et al.*, 1981, cite experimental work of Irvine, 1975, in support of this), which possibly has some similarity with the TTLC.

By contrast with most major and compatible elements, the very low IE abundances of the TTLC would have been chemically susceptible to assimilation by highly IE enriched felsic crust (discussed at length in the next chapter), much more so than the SLC or EMD. This tendency to acquire a crustal IE signature would have been further enhanced by the very high intrusion temperature of the TTLC suite, even relative to other (Fe-rich) basalt compositions. In this respect the TTLC would be similar to many komatiites in its thermal behaviour (*cf.* Arndt, 1986; Arndt & Jenner, 1986).

Similarly, during fluid infiltration metasomatism, the CE will be largely unaffected. These elements will be strongly linked to major elements and major phases and will be relatively unaffected by low time-integrated fluid fluxes that only have low CE concentrations. By contrast, IE that have concentrations at the 1-10 ppm level in the protolith (Appendix 2) will, in effect, be much more susceptible to large changes as a consequence of

metasomatism by interaction with a crustally equilibrated fluid (mechanisms, processes and the influence of bulk compositions are described further in Chapters 6 & 13) .

Compared with the SLC, the bulk composition characteristics described above imply that the TTLC is likely to be much more sensitive to both assimilation *and* metasomatism. These processes are assessed further in the next two chapters. However, at this stage it is worth highlighting a few trace-element characteristics.

Chondrite-normalized REE patterns and PM-normalized spidergram patterns shown in Figures 5.15 and 5.16 respectively illustrate that LILE are variable with respect to each other and relative to HFSE and REE. In detail the LREE are also moderately variable; less so than the LILE but more so than the HREE. These features suggest caution when examining relationships between elements with a view to *detailed* interpretation of protolith petrogenesis (*e.g.* least squares modelling). However, the *overall* chemical variations are sufficiently consistent for a variety of mineralogies to be able establish some general characteristics of the protolith, which in turn may constrain possible assimilation and/or source characteristics. Unfortunately, it is very difficult to unravel the relative contributions of these two processes on trace-element grounds alone. Nevertheless, two end-member petrogenetic scenarios can be considered or posed as 'working' hypotheses: IE dominated by assimilation (Hypothesis A), or inherited from source (Hypothesis S).

Hypothesis S

If element mobility during metamorphism was minimal and the amount of assimilation of felsic crust was also small, IE ratios and normalized patterns would dominantly reflect mantle source characteristics. Given high LILE/HFSE and LREE/HFSE, as evident from pronounced negative Nb, Ti and P anomalies, subduction-related magmatism would be strongly implicated. In many respects the TTLC has similar spidergram patterns to many island-arc volcanics (*e.g.* Sunda Arc, Stolz *et al.*, 1990; Aleutians, Yogodzinski *et al.*, 1994; and especially the Cape Vogel boninites, Hickey & Frey, 1982).

Hypothesis A

Alternatively, if assimilation was important, given the very low IE abundances for the TTLC, spidergram patterns would very quickly assume the characteristics of those elements that have high concentrations in the crust. Figure 5.18 illustrates an abbreviated spidergram for the elements that are likely to be least mobile during metamorphism. This shows the

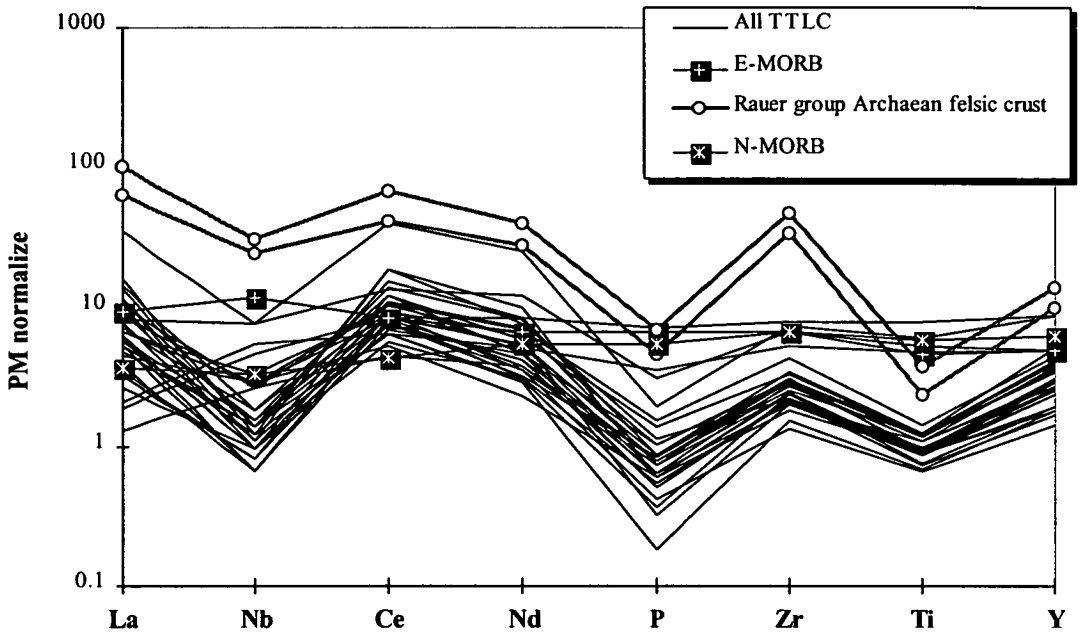

Figure 5.18 Illustrates the composition of the TTLC normalized to PM (after McDonough & Sun, 1995). Representative assimilants (#5120 & 5143) and E-MORB and N-MORB (after Sun & McDonough, 1989) are shown for comparison.

relationship between LREE/HFSE and Y^2/HFSE for the TTLC and the most likely crustal assimilants in the Rauer Group (#5120 & #5143). Average E-MORB and N-MORB (Sun & McDonough, 1989) are shown for comparison. Since the crust is strongly enriched in IE relative to the TTLC any assimilation would have a marked affect on the protolith signature (this will be discussed further in Chapter 7).

5.4.5 Summary and preliminary conclusions for the TTLC

On major- and trace-element grounds the TTLC is perhaps best considered as the intrusive equivalent of a boninite (*cf.* Hickey & Frey, 1982, and references therein). However, detailed comparison with this rock type is complicated by the intrusive nature of the complex and possibly the effects of metamorphism. *In detail* it is possible that IE signatures have been modified by metasomatism processes, although *in general* spidergram patterns and many IE ratios (except LILE) are probably not too dissimilar from those of the protolith. If this is the case, it is most likely that IE features reflect source components (including crustal contaminant), and are not the product of fractionation/accumulation processes.

[2] Y is chosen because it can be measured precisely by XRF and behaves in similar manner to HREE.

5.5 General summary and conclusions for the SLC, EMD and TTLC

The three major mafic gneiss units in the Rauer Group (SLC, EMD & TTLC) are all broadly tholeiitic in composition, although they have distinct major- and trace-element characteristics within this general classification. For each of the three suites, a number of petrogenetic processes including closed-system magmatic differentiation, partial melting from a variety of mantle source compositions, and open-system crustal contamination and metasomatism have been discussed. Incompatible-element signatures are considered to be most diagnostic of mantle source composition and/or crustal assimilation. IE ratios, and spidergram patterns for the Fe-rich SLC and EMD are consistent with derivation from an E-MORB-like source, with primary melts modified by fractionation and/or assimilation. The Mg-rich TTLC differs from the SLC and EMD in its major- and trace-element character. Perhaps most noticeably spidergram patterns have pronounced Nb, Ti and P anomalies. This might be a feature inherited from the mantle source region or the processes involved in melting; alternatively, it could be an artefact of assimilation of Rauer Group felsic crust. Unfortunately, low IE concentrations imply that the TTLC would also be relatively prone to open-system exchange by both assimilation or metasomatism. Such low concentrations, and generally poor correlations between many IE, indicate that some degree of metamorphic disturbance *is* likely to have been important, more so than for the SLC or EMD. However, a final synthesis regarding the origin and evolution of the SLC, EMD and TTLC is reserved until after isotopic data are presented and assessed in the next chapter.

Chapter 6

Isotopic evolution of the Archaean Rauer Group

6.1 Introduction

6.1.1 Rationale

An integrated study combining precise U-Pb zircon dating with whole-rock stable and radiogenic isotopes is potentially the most powerful way of constraining the timing and nature of protolith petrogenesis, as well as identifying and accounting for secondary geochemical effects related to metamorphism in the polyphase Rauer Group. Given the terrane-scale remit of this study, and because of the time and expense involved in isotopic work, it was only possible to acquire a limited isotopic data set for the Rauer Group. The overall objective for detailed chemical analysis was to strike a balance between regional coverage and more detailed work within individual suites. The former is important because very little isotopic work has been undertaken in the Rauer Group and the current database is insufficient to compare with adjacent Archaean regions. The latter aspect is important to enable characterisation of intrasuite variations in order to understand protolith petrogenesis and its subsequent geochemical and isotopic evolution.

The previous three chapters illustrate some of the remarkable igneous features preserved in the Scherbinina and Torckler-Tango complexes (SLC & TTLC). Despite a protracted polydeformational history, the SLC retains more of its igneous protolith character than the TTLC. The SLC is also crucial to understanding the tectonic evolution of the Rauer Group. For these reasons, and because it was possible to constrain the crystallization age of the complex by precise U-Pb zircon dating, the SLC has been studied in more detail than either the TTLC or the early mafic dykes (EMD). Nevertheless, a pilot Nd-isotope study of these other Archaean mafic gneiss units has been undertaken in order to provide some regional coverage of the Rauer Group.

The SLC is described first because the isotope systematics are more complex than for the TTLC. The Nd-isotope ratios, in particular, are unusual and a variety of possible models for the SLC are described in some detail. This is partly to illustrate the processes that were unlikely to have been important, but also because certain aspects of the various 'rejected'

models are integrated into the final synthesis. A number of the conclusions for the SLC are then directly applicable to the TTLC and EMD.

The last section in this chapter outlines the wider implications for the geochemical evolution of the Archaean domain in the Rauer Group. A final integrated account of the geochemical evolution of these orthogneiss suites, combing petrographic observations, geochemistry and the isotope data, is presented in Chapter 7.

6.1.2 Sample selection

Sample selection in the field was primarily aimed towards collecting samples suitable for constraining protolith petrogenesis through a combined geochemical and isotopic study. Following many other workers in similar high-grade terranes (*e.g.* Collerson *et al.*, 1983; Kerr & Fryer 1994; Stern & Hanson, 1991), large samples (5-20 kg) were chosen from a wide range of bulk compositions. It was hoped that such large samples would evolve as chemically and isotopically closed systems at the whole-rock scale, at least for the immobile trace elements and the Nd-isotope system.

Specific samples were selected for isotopic analysis on geochemical grounds from a large geochemical dataset (*cf.* Dodson, 1982). The criteria used to select these samples reflects a balance between avoiding obvious extreme differentiates or altered rocks, whilst selecting a wide range of comagmatic bulk compositions that are hopefully related by crystal-fractionation processes. The suitability of this approach is reassessed at the end of this chapter and in Chapter 13.

6.2 Oxygen isotope geochemistry of the SLC

A rationale for the application of oxygen isotopes to metaplutonic rocks has been outlined in Section 1.4.4 and a description of the methodology and analytical techniques is presented in Appendix 1. This section details the results for the SLC and provides an interpretation of the data.

6.2.1 Results

Oxygen-isotope ratios have been measured on representative samples from bulk compositions that range from websterite to differentiated leucocratic ferrodiorite. Throughout this compositional range the SLC has restricted $\delta^{18}O$ values from 5.7 to 6.7 ‰

Table 6.1 Oxygen-isotope ratios for the SLC Main Trend and EMD.

No.	Suite	Description	mg	$^{18}O_{(1)}$	$^{18}O_{(2)}$	^{18}O	
RI10	SLC	Main Trend	50.99	6.71		6.7	
RI11	SLC	Main Trend	37.73	5.95	6.19	6.1	
RI19	SLC	Main Trend	28.15	5.69	5.67	5.7	
RI22	SLC	Main Trend	31.08	6.20		6.2	
RI23	SLC	Main Trend	54.5	6.02	5.84	5.9	
RI30	SLC	Main Trend	40.29	6.26		6.3	
RI33	SLC	Main Trend	56.22	5.97		6.0	
RI35	SLC	UM SLC High Ni	63.66	5.77		5.8	
RI108	SLC	UM High MgO + CaO	72.99	6.50	6.26	6.4	
RI113	RG EMD	Early Fe-Tholeiite	43.64	6.39		6.4	
SH70	RG EMD	Early Mg-Tholeiite	61.77	6.32		6.3	
						Av.	St. Dev.
						6.1	0.3

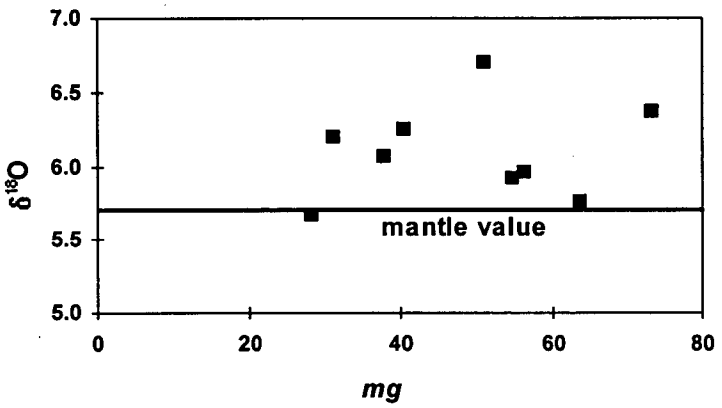

Figure 6.1 Plot of $\delta^{18}O$ *vs.* ***mg*** for the SLC. Mantle value is shown for comparison by solid line.

(Table 6.1), with an average of 6.1 ± 0.3 ‰. Using ***mg*** as a simple index of differentiation, there is no systematic variation in $\delta^{18}O$ for the dataset as a whole (Figure 6.1).

6.2.2 Interpretation and conclusions

The limited range of oxygen-isotope compositions for the SLC are only slightly higher than the mantle value of ~5.7 ‰ (Taylor, 1980). Since the SLC is thought to be derived primarily from the mantle on other geochemical grounds, these results preclude significant interaction

with different oxygen-isotope reservoirs. Overall there is a restricted range of $\delta^{18}O$ for a variety of bulk compositions, 6 of the 9 analyses are *possibly* correlated with ***mg***. For ***mg*** values from ~63.7 to 30.1 these 6 analyses vary from 5.8 to 6.3 ‰. An increase of ~0.5 ‰ would be expected across this compositional range through fractional crystallization processes (*e.g.* Chivas *et al.*, 1982; Fourcade *et al.*, 1994). Although the oxygen-isotope data do not directly elucidate the petrogenesis of these rocks further, a number of important processes that commonly affect metaplutonic rocks can be ruled out.

Possible consequences of large amounts of assimilation

It is unlikely that there was large-scale assimilation of the surrounding felsic crust or Archaean high-Mg pelites (see Chapter 2) because this would probably have resulted in higher $\delta^{18}O$. Although oxygen-isotope data are not available for the most likely assimilants (*e.g.* #5120 & #5134), on petrological and geochemical grounds they would have relatively high $\delta^{18}O$ (*e.g.* Faure, 1986, figure 25.4 & Rollinson, 1993, figure 7.6).

Possible consequences of hydrothermal alteration

Most high-level plutons are associated with hydrothermal systems during the late stages of their evolution, which commonly results in a large range of oxygen isotope compositions (*e.g.* Forester & Taylor, 1977; Norton & Taylor, 1979; Taylor & Forester, 1979; Solomon & Taylor, 1991; Greenwood *et al.*, 1992). The samples studied here were taken from throughout the complex and are unlikely to have interacted with such fluids given their homogeneity. Although there is evidence for limited late-stage fluid infiltration on petrological grounds (see Chapter 4), and from radiogenic isotopes (Sections 6.4 & 6.5 below), regional fluid infiltration is not capable of homogenising isotopic compositions at the scale of the complex except if very large degrees of fluid-rock interaction were involved (*cf.* McNaughton & Wilson, 1983; Gruau *et al.*, 1992). Although it possible that mantle-derived fluids with $\delta^{18}O$ of ~5.7 could have homogenised isotopic compositions during metamorphism (*e.g.* the 500 Ma rehydration event), this would seem fortuitous given that a mantle value would be expected for unaltered rocks of this composition. Moreover, in their study of the calc-silicate paragneisses on Little Italy Island (SW Rauer Group), Cartwright *et al.* (1997) found evidence for large variations in $\delta^{18}O$ across relatively small length scales (1-10 cm), which implies that the degree or scale of oxygen-isotope homogenisation was relatively small in this terrain. Also, if there was large-scale interaction with an externally-derived fluid, it is most likely that there would be a range of $\delta^{18}O$, especially to values lower than mantle (*e.g.* Nutman *et al.*, 1989). Finally, if there were large amounts of fluid-rock interaction, it is likely that delicate magmatic textures, primary mineralogy and the largely

anhydrous granulite assemblages described in the previous chapter, would not have been preserved as they are.

In conclusion, oxygen isotope compositions for the SLC are most consistent with derivation from a mantle source with little subsequent modification either during emplacement or by later fluid infiltration.

6.3 U-Pb zircon geochronology

A full account of the U-Pb zircon geochronology for the SLC and cross-cutting tonalitic gneiss is presented in Harley, Snape & Black (in press). A copy is included in the pocket at the rear of the thesis. Two of the three samples chosen for dating were amongst those rocks selected for detailed petrographic, geochemical and conventional isotopic study during the course of this study, however, since LP Black wrote most of the account of the zircon geochronology, only a brief description is given here. The following is largely a summary of the results from Harley, Snape & Black (in press).

6.3.1 Samples and methods

Three samples from within the SLC area were selected for analysis. Two of these (RI43, RI15) were sampled from the more felsic parts of the layered magmatic complex whilst one sample (SH45) was obtained from a cross-cutting homogeneous tonalitic orthogneiss sheet representative of the TG (see Figure 3.9). The respective sample sites are located on Figure 3.1, and petrographic descriptions are outlined in Chapter 4.

Zircons were extracted from the disaggregated rock samples using standard heavy liquid and magnetic separation techniques and mounted in epoxy discs which were polished and gold-coated prior to ion microprobe analysis. U-Pb analyses were carried out by LP Black using the SHRIMP II ion microprobe at the Australian National University, Canberra, following the standard techniques described by Compston *et al.* (1984) and Williams *et al.* (1984). A full account of the analytical techniques is presented in Appendix 1.

6.3.2 Results

All isotopic data for these zircon analyses are plotted on conventional U-Pb concordia diagrams in Figures 6.2a to d. Uncertainties on all ages reported below are quoted at the 2σ level. Analytical results are presented in Harley, Snape & Black (in press).

SLC pegmatoidal ferrodiorite (RI43)

On the basis of morphology virtually all of the zircons in the analysed sample (95 %) is of metamorphic origin, including unusual botryoidal varieties. The presence of 3-4 old grains in the analysed population (14 grains; Figure 6.2a) reflects a sampling bias as distinct old grains were preferentially targeted. Multifaceted equant grains of metamorphic type define an age grouping at 511 ± 10 Ma. The five significantly older (Archaean) analyses are too broadly scattered to define any individual event age with confidence. The analyses might be indicative of an event near 2800 Ma, an age established from previous work in the Rauer Group (Kinny *et al.*, 1993) and the new data from the other SLC sample in this study, but whether the grains are older and then reset at or near 2800 Ma is not clear. The scatter in discordant analyses indicates that these grains suffered considerable radiogenic Pb-loss at time(s) other than 511 ± 10 Ma.

SLC garnet-bearing quartz-oxide vein (RI15)

Zircons in this rock have been described in Chapter 4 (Section 4.2.3) and are considered to have crystallized from a melt phase.

All but three of the 30 SHRIMP U-Pb analyses approximate a chord with concordia intercepts at 459 ± 21 Ma and 2829 ± 35 Ma (Figure 6.2b). Although the upper intercept defines a realistic age for crystallization of the euhedral prismatic grains, the high MSWD of 20 for this population indicates significant scatter in the isotopic analyses. The best-fit straight line obtained by the omission of the seven most discrepant analyses in this population yields concordia intercept ages of 2844 ± 6 Ma for zircon crystallization and 512 ± 12 Ma for variable isotopic resetting (Figure 6.2b). A second event slightly younger than 2840 Ma is suggested by the data obtained for grain 100.1, a zircon with a low Th/U ratio (0.14). This has been omitted from the regressed fit described above because the position of this analysis relative to the others in the zircon population cannot be accounted for in a simple 2-stage model.

The three discrepant old analyses in RI15 all come from one grain (grain 11) that was analysed at five points. Analyses 11.5 and 11.6 lie on a discordia between the origin and an upper concordia intercept at 3100-3200 Ma. Point 11.5 has 15% reverse discordance, a feature that cannot in this case be attributed to high U-content (*cf.* Black *et al.*, 1991a) as the measured U is only 199 ppm. Analysis 11.1 plots between analyses 11.5 and 11.6 and the main discordia. This, therefore, may represent a mixture of inherited *ca.* 3130 Ma zircon

Figure 6.2 (a) $^{207}Pb/^{235}U$ - $^{206}Pb/^{238}U$ concordia diagram for zircons from pegmatitic ferrodiorite RI43 from the Scherbinina Layered Complex. The 5 discordant old grains are suggestive of an event near 2800 Ma but do not allow definition of any precise age. The 8 concordant zircon analyses are from multifaceted equant grains and define an age grouping at 511 ± 10 ma (2σ).

Figure 6.2 (b) $^{207}Pb/^{235}U$ - $^{206}Pb/^{238}U$ concordia diagram for zircons from garnet-oxide segregation RI15, with all data from each analytical session included. The best-fit straight line gives concordia intercept ages of 2844 ± 6 Ma for zircon crystallization and 512 ± 12 Ma for variable isotopic resetting. Open error polygons are analyses from an anomalously old (3100-3200 Ma), probably inherited grain.

Figure 6.2 (c) $^{207}Pb/^{235}U$ - $^{206}Pb/^{238}U$ concordia diagram for zircons from metamorphosed tonalitic orthogneiss SH45, sampled from a felsic sheet that cuts the SLC and its early mafic dykes. The oldest zircons are near-concordant and define a discordia with an upper intercept of 3470 ± 12 Ma and a lower intercept of 528 ± 12 Ma. All Archaean ages are from cracked elongate cores. Clearer rounded overgrowth rims have only been analysed at one spot, which gives the concordant 2550 Ma data point. The discordant data spread between 3470 Ma and 2000 Ma suggest that there was more than one age of Archaean zircon growth in this sample. The intrusive tonalite sheet has to be younger than 2844 Ma, the age of the SLC that it cuts.

Figure 6.2 (d) $^{207}Pb/^{235}U$ - $^{206}Pb/^{238}U$ concordia diagram for equant multifaceted zircons from pegmatitic ferrodiorite RI43 and the tonalitic gneiss SH45. in each of these rocks the *ca.* 520 Ma zircons are essentially concordant. A pooled age of 519 ± 8 Ma is obtained combining the data from both samples.

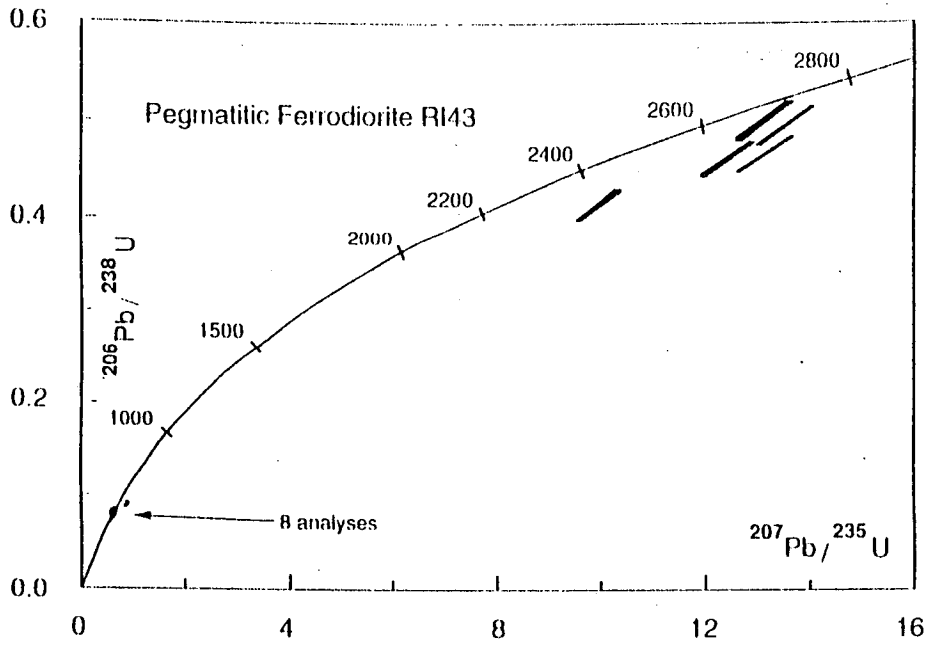
Pegmatitic Ferrodiorite RI43
$^{206}Pb/^{238}U$
$^{207}Pb/^{235}U$
8 analyses
1000
1500
2000
2200
2400
2600
2800
0.0
0.2
0.4
0.6
0
4
8
12
16

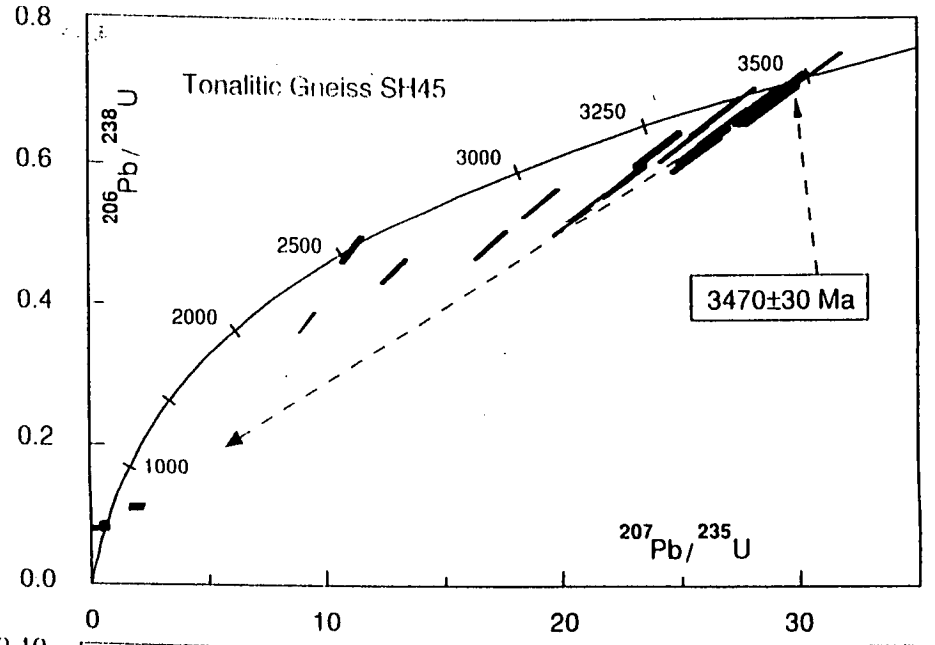
Tonalitic Gneiss SH45
$^{206}Pb/^{238}U$
$^{207}Pb/^{235}U$
3470±30 Ma
1000
2000
2500
3000
3250
3500
0.0
0.2
0.4
0.6
0.8
0
10
20
30

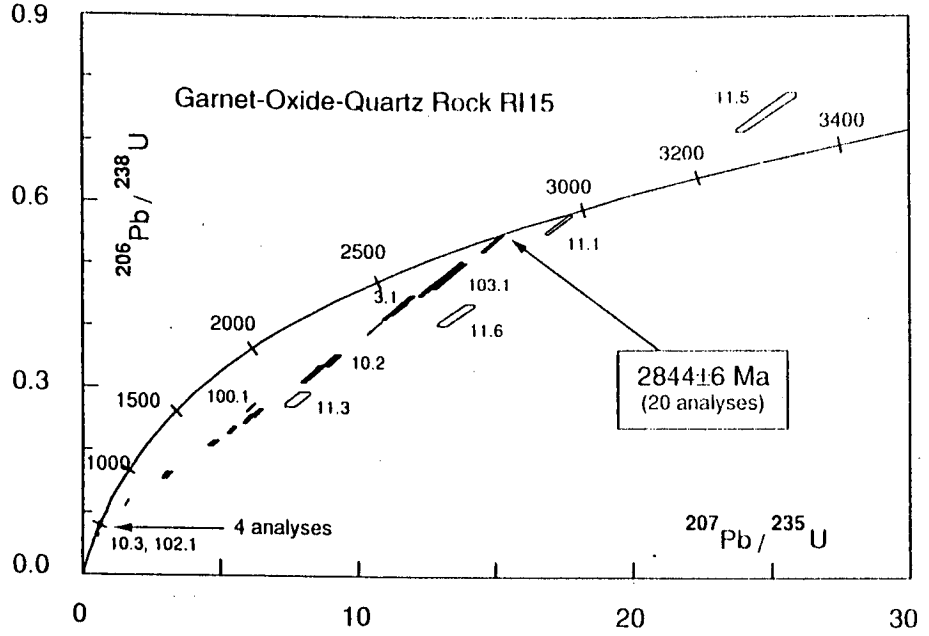
Garnet-Oxide-Quartz Rock RI15
$^{206}Pb/^{238}U$
$^{207}Pb/^{235}U$
2844±6 Ma
(20 analyses)
4 analyses
10.3, 102.1
3.1
103.1
11.6
10.2
11.3
100.1
11.1
11.5
1000
1500
2000
2500
3000
3200
3400
0.0
0.3
0.6
0.9
0
10
20
30

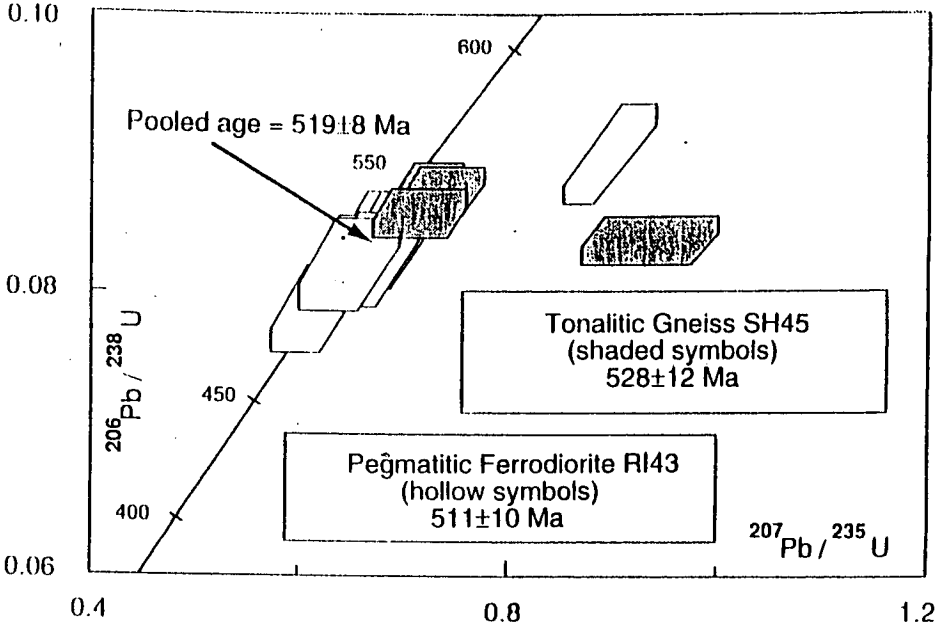
Pooled age = 519±8 Ma
Tonalitic Gneiss SH45
(shaded symbols)
528±12 Ma
Pegmatitic Ferrodiorite RI43
(hollow symbols)
511±10 Ma
$^{206}Pb/^{238}U$
$^{207}Pb/^{235}U$
400
450
550
600
0.06
0.08
0.10
0.4
0.8
1.2

and 2840 Ma magmatic zircon. Analysis 11.4, from a BEI bright zone in this grain, is of about the same age as the remaining 26 analyses forming the principal zircon population.

Two zircon grains displaying the distinctive trace-element compositional variations as described in Section 4.2.3 were selected to monitor any correlation between chemistry and isotopic systematics (grains 10 and 13). Three analyses were made on grain 10, most of which is typical magmatic zircon and yields old ages (10.1 and 10.2). An overgrowth at the tip of this grain, other analyses near the end or the edges of grains, yield ages near 500 Ma.

Tonalitic Orthogneiss (SH45)

This tonalitic orthogneiss clearly cuts the SLC and is part of the suite of homogeneous TG that also cut the CLO unit. The analysed zircons in this sample form a complex array with at least two and probably three age populations (Figure 6.2c). Four analysed grains yield an age of 528 ± 12 Ma, indistinguishable from the age of late metamorphic grains in RI43 (511 ± 10 Ma) and the young components of the zircons in RI15 (512 ± 12 Ma) (Figure 6.2d). The young analyses were derived from clear, elongated, multifaceted grains that comprise approximately half of the zircon population. Older (Archaean) zircon components have also been strongly affected by isotopic equilibration at 500 Ma.

All of the Archaean ages for this sample were derived from elongate cores that are enclosed by broad rims with rounded terminations. Although some cores preserve relatively euhedral boundaries with their rims, most have been rounded. In these cores euhedral oscillatory zoning is observed and despite considerable isotopic complexity, the overall pattern is consistent with crystallization at *ca.* 3500 Ma followed by subsequent episodes of Pb loss and, possibly, new zircon growth. The timing of the secondary episodes is not well constrained by the data, though the isotopic array is consistent with both Archaean and early Palaeozoic perturbations.

Scatter in the isotopic array limits the derivation of a precise age for the Archaean zircons in this sample. As most of the analyses plot below concordia they require extrapolation from their present-day compositions to derive their original crystallization age, and two methods of extrapolation are possible. The first is to regress a line from the origin through the analyses to concordia, equivalent to deriving ages from $^{207}Pb/^{206}Pb$. This procedure assumes that any Pb-loss occurred only in recent times, which is not likely given the independent evidence for an isotopic event at 500 Ma. Nevertheless, by using only data that lie on or near concordia it is possible to minimise the bias introduced by any non-zero age Pb-loss.

Based on this approach seven of the analyses with $^{207}Pb/^{206}Pb$ fairly close to each other (MSWD = 10) can be combined to yield an age of 3465 ± 12 Ma for the crystallization of original zircon cores.

The alternative and more rigorous way of treating the data is to use a regression which is independent of assumptions on the timing of Pb-loss events. There is a better cohesion of analyses to such a regression, because 15 analyses have a comparable MSWD (12) to the 7 analyses used above for determination of the weighted mean $^{207}Pb/^{206}Pb$ age. The resultant upper intercept age is 3470 ± 30 Ma.

The agreement between the different methods of age calculation for the oldest grains in the tonalitic gneiss gives considerable credence to the 3470 Ma age, and the more conservative 3470 ± 30 Ma estimate derived with fewer assumptions and from a larger number of analyses is adopted as the age of crystallization age of the zircons. This is either related to the primary age of this orthogneiss or to the age of a coherent suite of grains inherited from earlier source rocks, an important issue to be addressed in the discussion below.

6.3.4 Discussion and conclusions

Age of the SLC

Magmatic zircons from sample RI15 define a crystallization age of 2844 ± 6 Ma (2σ) for the Scherbinina Layered Complex. This age estimate is consistent with the isotopic results obtained from the ferrodiorite, RI43. Although both are of broadly late Archaean age, the SLC is older than the felsic orthogneisses dated by Kinny *et al.* (1993) from Short Point and Torckler Island (2801 ± 6 & 2810 ± 14 Ma respectively).

Age of the homogeneous tonalitic orthogneiss

The best-fit age of 3470 ± 30 Ma for the Archaean zircon population in the tonalitic orthogneiss SH45 cannot represent the age of the tonalite itself as this rock clearly cuts the SLC and at least three generations of deformed mafic dykes. However, the tonalite does not preserve any analysed magmatic zircon populations that cluster at ages younger than 2844 Ma, the age of the SLC. The 500 Ma zircons in the tonalite are indistinguishable in age from those in the geologically earlier SLC rocks and are not magmatic in habit. Hence, the present data do not allow the intrusive age of the tonalite to be defined. This rather negative result is, however, balanced by the following features of the zircon data that have a bearing on arguments about the post-Archaean history of the region:

- The scatter in the U-Pb array suggests a late Archaean history for the TG suite. Based on the previous studies of Archaean felsic orthogneisses from the Rauer Group (Kinny *et al.*, 1993), combined with the new data available on the SLC rocks, rounding of the zircon cores and formation of overgrowths are most likely to have occurred at 2800 Ma. This would place the early dyking and deformation events that pre-date the TG but affect the SLC in the 2840-2800 Ma interval.

- There is no evidence in the zircon populations for any Proterozoic ages, and hence no argument for intrusion of these TG sheets either at 1000 Ma or in the 1700-1300 Ma time interval (discussed further in Section 13.2.4), the latter period being that separating the principal dyking events in the nearby Vestfold Hills.

- The TG bear no isotopic similarity to the younger felsic orthogneiss suites in the Rauer Group. The latter rocks have been dated by Kinny *et al.* (1993) at 1030-1000 Ma and preserve only mid- to late-Proterozoic Sm-Nd model ages.

- The TG are isotopically distinct from compositionally similar tonalitic gneisses that form a large part of the Vestfold Hills and were emplaced in that region at only *ca.* 2500 Ma (Black *et al.*, 1991a; this study, Chapter 10).

Inheritance and possible age of the Composite Layered Orthogneiss (CLO)

The 3470 ± 30 Ma age obtained for zircons in the tonalitic gneiss must be inherited from older felsic source material and very little new zircon can have crystallized from the tonalite itself. It is most likely that this tonalite and its inherited zircons were derived during partial melting of the CLO unit that forms a major component of the Archaean basement in the Rauer Group. Rounding and rimming of the inherited zircons could have occurred either during tonalite formation or in metamorphic events that had already affected the CLG. Unfortunately, the limited extent of zircon inheritance identified in the SLC does not directly constrain the age of the basement into which it intruded at 2840 Ma, but an age of 3470 ± 30 Ma is taken as an upper limit.

6.4 Rb-Sr isotopes of the SLC and EMD

Sr-isotopic data have been successfully determined for 7 samples from the SLC MT and for 4 samples of the enclosed Early (Archaean?) Mafic dykes (EMD). Data for the EMD are described here partly for brevity, and also because the range of values and interpretation of the data is the same for both the layered complex and the dykes. If the *ca.* 2800 Ma age estimate for the TG is correct (Section 6.3.4), the age of the protolith used to calculate ε_{Sr}

for the EMD will be approximately the same as the SLC (up to 40 m.y. younger). An outline of the methodology and rationale is presented in Chapter 1; analytical techniques and errors are described in Appendix 1; the analyses and calculated isotopic parameters are compiled in Table 6.2.

6.4.1 Results

The SLC MT has very low Rb/Sr and of the samples for which $^{87}Rb/^{86}Sr$ and $^{87}Sr/^{86}Sr$ have been successfully determined, there is a restricted range between about 0.02 and 0.12 corresponding to $^{87}Rb/^{86}Sr$ of 0.043 and 0.339 respectively. On an isochron diagram there is no correlation between $^{87}Rb/^{86}Sr$ and $^{87}Sr/^{86}Sr$ for the SLC MT (Figure 6.3). Although most samples have a restricted $^{87}Sr/^{86}Sr$ range between about 0.704024 and 0.711860, one sample (RI 30) has a very high ratio of 0.741646 ± 28. Calculated ε_{Sr} for the SLC MT and the EMD vary markedly between -158 and 544 (discussed below).

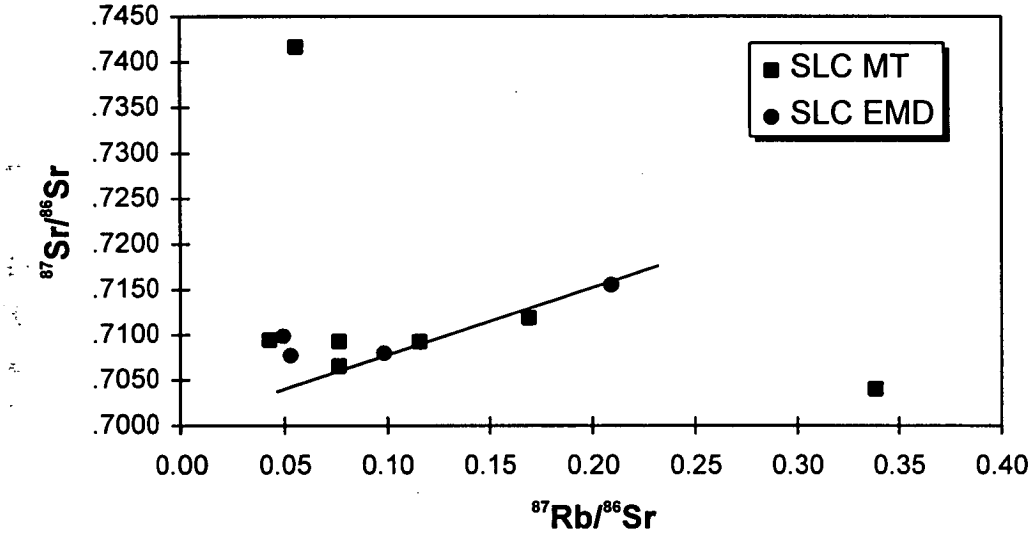

Figure 6.3 Rb-Sr Isochron diagram for the SLC MT and EMD showing that there is no correlation between $^{87}Rb/^{86}Sr$ and $^{87}Sr/^{86}Sr$ (note very restricted range of low $^{87}Rb/^{86}Sr$). The 5 most closely correlated SLC samples (excluding the two obvious outliers) define an errorchron implying an age greater than the age of the earth, with a MSWD >16,000. Similarly, the five most correlated samples from the combined SLC MT and EMD datasets (shown by the trendline) define an implausibly old age of 4.43 ± 0.86 Ga., although the MSWD is somewhat lower at about 8.

Table 6.2 Rb-Sr isotopic data for the SLC. Parameters used in the calculations are described in Chapter 1 (Section 1.4.4).

Sample	Suite	Sr (ppm)	Rb (ppm)	Rb/Sr	$^{87}Rb/^{86}Sr$	$^{87}Sr/^{86}Sr$	Err (2σ)	I_{Sr} at 2.84	$\varepsilon_{Sr2.84}$	T_{BSE} (Ma)
RI10	SLC MT	562.9	22.5	0.0400	0.1157	.709206	21	.704446	46.26	9.65×10^{9}
RI11	SLC MT	413.3	10.9	0.0264	0.0763	.709239	28	.706098	69.83	-5.21×10^{10}
RI19	SLC MT	399.9	46.8	0.1170	0.3385	.704024	22	.690095	-158.40	-1.88×10^{8}
RI22	SLC MT	665.2	9.8	0.0147	0.0426	.709427	36	.707673	92.28	-8.33×10^{9}
RI23	SLC MT	332.1	19.4	0.0584	0.1691	.711860	31	.704902	52.76	5.76×10^{9}
RI30	SLC MT	417.9	8	0.0191	0.0556	.741646	28	.739359	544.17	∞
RI33	SLC MT	375.4	9.9	0.0264	0.0763	.706522	39	.703382	31.09	-1.65×10^{10}
RI35	SLC MT	294.9	8.3	0.0281	Isotopic ratio failed					
RI108	SLC MT	13.6	38.5	2.8309	Isotopic ratio failed due to Rb contamination					
RI4	SLC MD	229.8	7.8	0.0339	0.0982	.707942	24	.703901	38.48	1.55×10^{10}
RI5	SLC MD	190.9	3.5	0.0183	0.0530	.707703	26	.705520	61.58	-6.95×10^{9}
RI113	SLC MD	240.7	4.1	0.0170	0.0493	.709829	37	.707800	94.10	-1.09×10^{10}
SH70	SLC MD	205.1	14.8	0.0722	0.2089	.715492	40	.706894	81.17	5.88×10^{9}

6.4.2 Discussion

Overall, the Sr-isotopic character of the SLC MT and the EMD cannot be explained by fractional crystallization. A number of possible processes could have produced the observed data, *all* of which would have involved either selective or limited open-system isotopic or trace-element exchange rather than homogenisation at the scale of the complex. Complete homogenisation of $^{87}Sr/^{86}Sr$ can be ruled out because the data would define a well-correlated but younger isochron (possibly of 1000 or 500 Ma age).

The earliest open-system processes that could have operated would have been crustal assimilation or hydrothermal alteration. Textural evidence and the oxygen isotope data discussed in the previous section imply that pervasive fluid-rock interaction was not extensive, certainly not on the scale that many modern shallow-level layered complexes have experienced. AFC processes, by contrast, could potentially influence both $^{87}Rb/^{87}Sr$ and $^{87}Sr/^{86}Sr$ across a wide compositional range. Although such a model is considered in the next section with respect to Nd-isotope characteristics, the Sr data are less readily explained by AFC processes. Whereas the Nd composition of the most likely assimilant is isotopically distinct and present in higher concentrations (Section 6.5.3), Sr abundances in the country rock are very low when compared with the SLC (see Section 2.3.2) and therefore the potential for producing evolved (high) $^{87}Sr/^{86}Sr$ compositions (*e.g.* RI30) by assimilation is much less (*e.g.* Powell, 1984). Furthermore, the overall very low Rb/Sr values for the SLC and EMD are inconsistent with assimilation of a high Rb contaminant such as samples #5120 and #5134 (Table 2.1).

The most plausible interpretation is that $^{87}Rb/^{86}Sr$ and/or the isotopic ratio was perturbed a long time after protolith crystallization. Rb and other LILE are known to be amongst the most mobile elements during metamorphism (*e.g.* Weaver & Tarney, 1981) and therefore secondary fractionation of $^{87}Rb/^{86}Sr$ is to be expected given the polymetamorphic history of the Rauer Group. Although it is difficult to compare Rb/Sr values between granulites, since the ratio will vary to some extent according to protolith bulk composition, the relatively low values for the SLC are similar to estimates of the 'average' lower continental crust (Weaver & Tarney, 1984), which is thought to reflect a depleted reservoir in terms of Rb and other LILE. In detail, however, the degree of Rb depletion or even enrichment within a suite of rocks is likely to be highly heterogeneous.

For example, sample RI30, possibly had a much higher initial Rb/Sr but Rb was presumably then depleted relative to Sr. Whereas 5 other samples have similar $^{87}Sr/^{86}Sr$ over a range of

$^{87}Rb/^{86}Sr$ values, which is consistent with isotopic evolution at low $^{87}Rb/^{86}Sr$. Another sample (RI19), however, has a relatively high $^{87}Rb/^{86}Sr$ (accounted for by relatively high Rb, not low Sr) but low $^{87}Sr/^{86}Sr$, a feature that may be related to late stage biotite growth (and hence Rb enrichment) in this rock (RI19 has appreciable biotite).

6.4.3 Summary and conclusions

Preliminary Sr-isotope data for the SLC do not constrain the age of the protolith or the timing of any of the metamorphic events that affected the Rauer Group. Isotopic homogenisation did *not* occur at the scale of sampling (up to 100s of metres scale) although the Sr-isotopic system was pervasively altered during metamorphism. It is likely that the main cause of isotopic disturbance was depletion of Rb relative to Sr in some rocks, probably associated with LILE mobility. A possible depletion mechanism for relatively evolved compositions might be related to the involvement of potassium-bearing feldspar in breakdown reactions (see Section 4.2.3). By contrast, one sample is enriched in Rb, presumably associated with late-stage biotite development associated with the *ca.* 500 Ma rehydration event.

6.5 Sm-Nd isotope geochemistry of the SLC

Nd-isotope data have been successfully determined for 9 samples from the layered complex. An outline of the methodology and rationale, including choice of reservoir parameters (*e.g.* CHUR and DM), is presented in Chapter 1; analytical techniques and errors are described in Appendix 1; the analyses and calculated isotopic parameters discussed in the text are compiled in Table 6.3.

6.5.1 Results

The SLC has a relatively restricted range of $^{147}Sm/^{144}Nd$ values from 0.1317 to 0.1541. These are not strongly correlated with $^{143}Nd/^{144}Nd$ (Figure 6.4), but if there is a correlation it is **negative**. This relationship precludes a direct age estimate from the Nd data. However, since the time of crystallization is known independently from zircon U-Pb dating (2840 Ma; see Section 6.3), this rather surprising result can be considered further in terms of the epsilon notation. Figure 6.5 represents the same data in terms of ε_{Nd}. Note that there is a large spread in calculated ε_{Nd} spanning almost 24 epsilon units, with samples ranging from 13.0 to -10.6.

Table 6.3 Nd-isotope data and calculated model parameters for the SLC.

Sample	*mg*	$^{143}Nd/^{144}Nd_{(m)}$	Err (2σ)	$^{147}Sm/^{144}Nd$	Err (2σ)	$^{143}Nd/^{144}Nd_{(i)}$	$\varepsilon_{Nd2.84}$	Err (2σ)	T_{CHUR} (Ga)	T_{CHUR} (2σ) (Ga)	T_{DM} (Ga)	T_{DM} (2σ)
RI10	51.0	0.511580	5	0.1418	0.0000	0.508921	-0.57	0.10	2.92	0.014	3.23	0.011
RI11	37.70	0.511658	6	0.1489	0.0002	0.508866	-1.66	0.03	3.10	0.004	3.40	0.002
RI19	28.2	0.511460	7	0.1445	0.0007	0.508751	-3.92	0.11	3.41	0.023	3.61	0.020
RI22	31.1	0.512083	6	0.1317	0.0000	0.509614	13.04	0.12	1.30	0.014	1.91	0.011
RI23	54.5	0.511954	6	0.1455	0.0009	0.509227	5.43	0.22	2.03	0.018	2.58	0.021
RI30	40.3	0.511320	5	0.1530	0.0015	0.508451	-9.81	0.45	4.55	0.132	4.46	0.094
RI33	56.2	0.511284	12	0.1534	0.0009	0.508409	-10.64	0.10	4.70	0.056	4.57	0.039
RI35	63.7	0.511235	6	0.1482	0.0005	0.508457	-9.70	0.05	4.36	0.021	4.33	0.016
RI108	73.0	0.511649	6	0.1541	0.0000	0.508760	-3.75	0.12	3.51	0.021	3.72	0.015

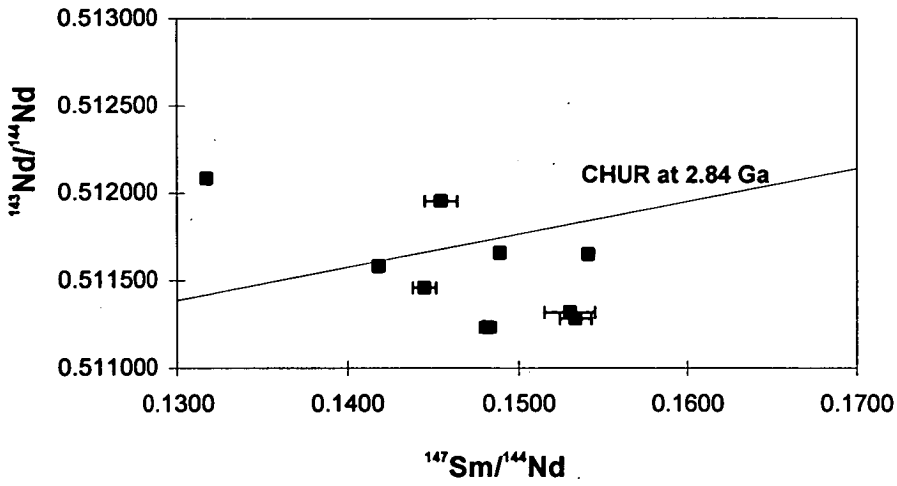

Figure 6.4 Sm-Nd isochron diagram for the SLC. A reference isochron for CHUR at 2840 Ma is shown for comparison. Note that no three samples define isochrons even for different initial ratios or ages.

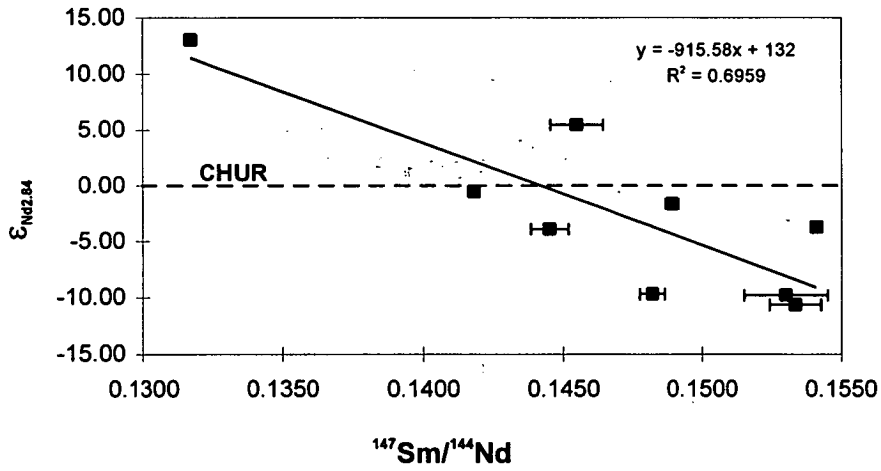

Figure 6.5 The same data as in Figure 6.4 expressed as ε_{Nd} relative to CHUR. Note that there is a broadly defined negative correlation between $^{147}Sm/^{144}Nd$ and ε_{Nd}.

6.5.2 Interpretation

The SLC rocks described here are all considered to be members of a cogenetic suite (on field, petrographic and geochemical grounds), therefore the isotopic characteristics depicted in Figure 6.5 must represent a mixing array. Since 7 out of the 9 samples have negative ε_{Nd}, the role of assimilation entailing isotopically-evolved early Archaean crust must be considered. This is the most obvious model capable of producing a negatively-oriented array with ε_{Nd} values less than CHUR. In the following discussion and figures, this model will be

referred to as 'Hypothesis A'. If such a scenario was responsible for the highly varied ε_{Nd}, then assimilation must have occurred late in the fractional crystallization history because $^{143}Nd/^{144}Nd$ was unable to homogenise within the complex. Such a situation is not uncommon and so-called assimilation-fractional crystallization (AFC) phenomena are well documented in the literature (*e.g.* DePaolo, 1981; Stewart & DePaolo, 1987).

The other general model that must be considered involves open-system exchange during metamorphism. This model will be referred to as 'Hypothesis B'. In the general case such a metasomatic model involves changing $^{147}Sm/^{144}Nd$ and/or $^{143}Nd/^{144}Nd$. Since none of the data points in Figure 6.4 define an isochron (of any age), this model requires disequilibrium at the scale of the complex to be dominant otherwise the data would define an isochron, albeit with a different initial isotopic ratio than the protolith. Unlike the AFC models mentioned above, open-system behaviour Sm-Nd isotopes is generally considered unlikely except in unusual circumstances, and Nd-isotope ratios are thought by many to be amongst the most robust during metamorphism (*e.g.* Patchett, 1989; Cohen *et al.*, 1991; Bowring & Housh, 1995). However, I consider that this is the most viable model that can explain the isotopic character of the SLC (for reasons given below).

Since many isotope geochemists assume that whole-rock Nd isotopes are not significantly mobile during high-grade metamorphism (*e.g.* Collerson *et al.*, 1991; Bennett *et al.*, 1993; Kerr & Fryer, 1994), Hypothesis A will be rigorously examined first to establish whether AFC processes could have produced the observed isotopic array. The following discussion of isotopic modelling is extensive, and those not interested in the detailed arguements regarding mechanisms are invited to proceed directly to Section 6.5.5 where the conclusions are summarized. In addition, Table 6.5 is provided below as a guide to the discussion.

6.5.3 Discussion of Hypothesis A (AFC)

From field relations and on geochemical grounds the most likely contaminants for the SLC at the time of intrusion would have been the surrounding crust (CLO, described in Chapters 2 & 3). For a contaminant to change magma composition appreciably, it must be isotopically distinct and have significantly higher concentrations of the contaminating elements (*e.g.* DePaolo, 1981; Powell, 1984; Faure, 1986). At the time of SLC intrusion (2840 Ma), the Archaean components of the CLO would have had evolved Nd-isotopic compositions ε_{Nd}[1] = -6.7 and -3.8, for samples #5120 and #5143 respectively. The present

[1] Isotopic data for #5120 and #5143 are from Sheraton *et al.* (1984). Their published data is presented in Table 2.1, but for the purposes of comparison and modelling in this thesis, their $^{143}Nd/^{144}Nd$ values

day (after assimilation in this model) range of Nd concentrations for the SLC[2] is between 4.59 ppm for ultramafic cumulate RI108 and 26.92 ppm for differentiated ferrodiorite RI 19. By contrast, the most likely assimilant(s) have higher Nd concentrations of between 1.4 and 11.6 times the Nd concentration of the SLC, depending on the bulk composition of the complex. Therefore, given such a significantly large contrast between the SLC and surrounding gneisses, it is important to consider AFC as a viable isotopic-mixing process.

Table 6.5 An overview of the discussion regarding the Nd-isotope evolution of the SLC. This table summarizes various models that are presented to discuss the negative ε_{Nd}-$^{147}Sm/^{144}Nd$ and $/^{143}Nd/^{144}Nd$ - $^{147}Sm/^{144}Nd$ arrays shown on Figures 6.4 & 6.5.

Model	Process	Comment
Hypothesis A -tested for different assimilants	Assimilation of RG felsic crust	Rauer Group felsic crust at 2840 not sufficiently evolved to account for $\varepsilon_{Nd} < \sim -6.0$. This model would also require derivation from an ultradepleted mantle source.
Hypothesis B	Metamorphic disturbance to the Sm-Nd system	The only reasonable interpretation of the SLC data.
B1	Secondary fractionation of $^{147}Sm/^{144}Nd$	Amount of secondary fractionation required is not petrologically feasible. Negative ε_{Nd} array, but cannot explain the negative isochron diagram
B1a	Internal exchange	
B1b	External exchange	
B2	Direct exchange of $^{143}Nd/^{144}Nd$	All isochrons would 'rotate' towards a younger isochron in a reservoir-exchange model.
B2a	Internal exchange	
B2b	External exchange	
B3	Petrological, geochemical and spatial constraints	Metamorphic recrystallization was not the underlying mechanism that resulted in isotopic disturbance. Instead, the spatial distribution of adjacent units with respect to the fluid flow pathway was the key factor.

have been normalized to $^{146}Nd/^{144}Nd = 0.7219$ by multiplying the measured $^{143}Nd/^{144}Nd$ by a factor of 0.512638/0.511836 to correct for inter-laboratory differences (see Faure, 1986, p.209 for details).

[2] Of those samples studied for Nd isotopes and where isotope-dilution data are available for Nd concentrations.

General assimilation models

There is considerable scatter in the Nd data for the SLC and therefore it is not practical to invert the AFC equations derived by DePaolo (1981) and others to attempt to directly quantify AFC models (*e.g.* Powell, 1984). Nevertheless, it is useful to consider a series of hypothetical models, in this case to demonstrate that simple mixing (in the sense of Faure, 1986) or AFC could produce the geometry of the SLC isotopic array (negative), but that these models could not produce the required spread of ε_{Nd} (24 epsilon units). However, a number of conceptual constraints and geochemical assumptions first need to be addressed.

It is not possible to constrain the primary composition of the magma, either in terms of ε_{Nd} or Nd concentration. However, because the overall geochemical features of the complex cannot be explained by intracrustal melting (see Section 5.5.2), derivation from a mantle source can be assumed. As most rocks range from about DM (excluding RI22 with ε_{Nd} = 13.04) to more isotopically evolved compositions, derivation from a time-integrated DM source corresponding to ε_{Nd} = 3.8 at 2840 Ma has been assumed for the purpose of the following theoretical models.

Choice of mixing model

Mixing models fall into two main categories: simple two-component mixing models and complex AFC models. Neither model is capable of fully describing the behaviour of Nd-isotopes for the SLC, but both models are capable of illustrating certain aspects of the process. Simple two-component mixing models for Nd concentrations and Nd-isotopes (*e.g.* DePaolo & Wasserberg, 1979) are of the form:

$$C_{hyb} = X_m \cdot C_m + (1-X_m) \cdot C_a \qquad [6.1]$$

$$\varepsilon_{Nd(hyb)} = \frac{X_a \cdot C_{Nd(a)} \cdot \varepsilon_{Nd(a)} + (1-X_a) \cdot C_{Nd(m)} \cdot \varepsilon_{Nd(m)}}{X_a \cdot C_{Nd(a)} \cdot + (1-X_a) \cdot C_{Nd(m)}} \qquad [6.2]$$

where hyb refers to the hybrid composition after mixing; X is the weight fraction of a, the assimilant, and m, the magma (where $X_a + X_m = 1$), and C is the concentration of Nd in either the magma or the assimilant.

For given magma and assimilant compositions, this model describes a simple hyperbolic function between two end-members for different degrees of mixing. This does not account

for the effects of fractional crystallization or accumulation on Nd concentration (fractional crystallization will not affect $^{143}Nd/^{144}Nd$). DePaolo (1981) has demonstrated that this simple model will differ radically where bulk distribution values are anything other than unity, and since D_{Nd} is likely to be <<1, this is an important factor to consider. To overcome this difficulty, DePaolo (1981) developed a series of equations that account for variable rates of assimilation relative to fractional crystallization and also allows for different D values. However, the equations are difficult to apply to the SLC dataset because many of the variables, especially initial magma composition, are not known. Furthermore, the inherent problems of constraining the relative roles of fractionating and accumulating assemblages in cumulates (described in Sections 1.4.3) makes whole-rock geochemical data difficult to integrate into the AFC equations. In particular, it is not clear how the chemistry of a trapped liquid evolving through a cumulus pile, as in the *in situ* fractionation model of Langmuir (1989) for example, could be accommodated.

Given the inherent complexity of the AFC models, a variation on the simple two-component mixing model will be used here to illustrate the possible behaviour of the SLC during both AFC and open-system metasomatic exchange. To account for variations in Sm/Nd by fractional crystallization, all the fractionation is assumed to have occurred before assimilation. Such a situation is not entirely untenable, since most assimilation must have occurred after the point at which magma was able to communicate efficiently on at least 10s of metre scales, otherwise $^{143}Nd/^{144}Nd$ would have homogenised[3]. To do this, a differentiated magma body with an initial isotopic ratio corresponding to a time-integrated DM value (ε_{Nd} ~3.8 at 2840 Ma), and a range of $^{147}Sm/^{144}Nd$ and Nd concentrations slightly greater than the present range of the SLC, is assumed. Although there is a reasonable correlation between $^{147}Sm/^{144}Nd$ and ε_{Nd}, there is only a poorly defined relationship between ε_{Nd} and Nd concentration (or 1/Nd) for the SLC. Nevertheless, for these theoretical models, a normal relationship whereby higher $^{147}Sm/^{144}Nd$ correlates with lower Nd concentrations is assumed. Simple mixture modelling has then be applied to a number of different starting compositions, as illustrated in Figure 6.6.

[3] The length- and time-scales of chemical and isotopic homogenisation within a differentiating magma chamber and between cumulus minerals and trapped liquid is poorly understood at present. However, Barnes (1986) has shown that reaction between trapped liquid and cumulus minerals is profound and can result in a great deal of chemical and isotopic homogenisation at the cm- to m-scales.

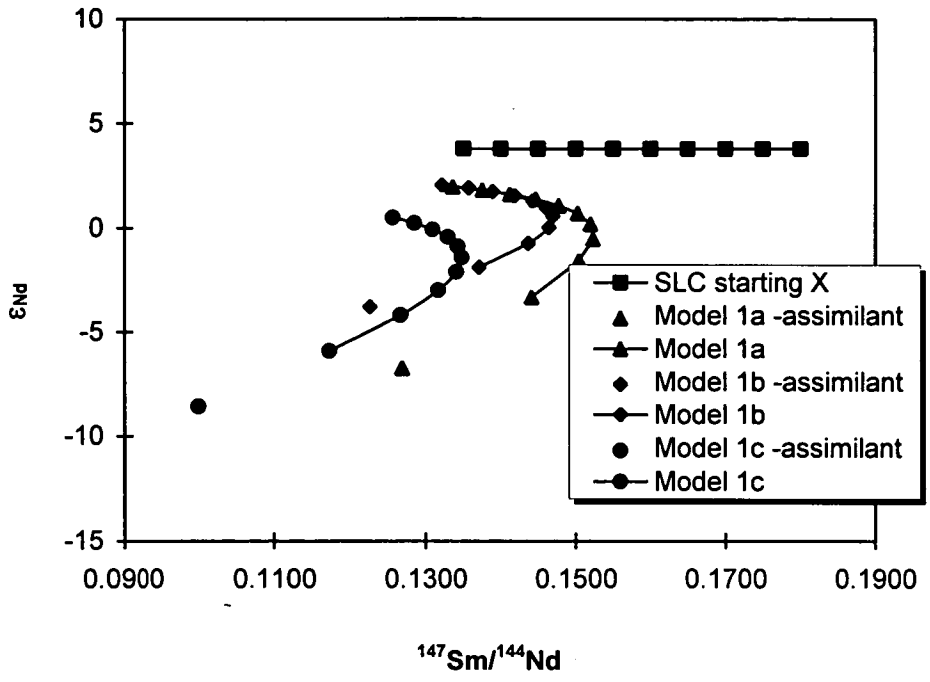

Figure 6.6 Hypothetical model A1 (assimilation) for the isotopic evolution of the 'SLC' given an initial DM Nd-isotope ratio and a range of initial Nd concentrations and Sm/Nd. The model is for a fixed amount of contamination (10 %) of 'SLC' by 3 potential wallrock compositions (see text). Three representative assimilants have been chosen; Model 1a corresponds to #5120; Model 1b corresponds to #5134; and Model 1c is the most isotopically evolved and chemically potent crust that could reasonably be expected to occur in the Rauer Group. The general form of the mixing line illustrates that it is relatively easy to produce a negatively correlated ε_{Nd} *vs.* $^{147}Sm/^{144}Nd$ array from an initially homogeneous source with positive ε_{Nd}.

Results for simple mixture modelling

Three models (A1a, b & c) have been calculated for different assimilants, each with 10 % assimilation. The first two assimilants, #5120 and #5134 (see Table 2.1), are from Sheraton *et al.* (1984). It is likely that they are representative of the early Archaean felsic rocks in the Rauer Group and presumably correspond to the undepleted fractionated old orthogneisses of Harley *et al.* (1992) as described in Section 2.3.2 An additional hypothetical assimilant has also been included (model A1c). This sample has been included in order to provide a maximum limit on the most chemically and isotopically potent assimilant and represents the most isotopically evolved rock type that could reasonably be expected to occur in the Rauer Group. It is based loosely on samples #722 and #625 of the old orthogneisses described above (Harley *et al.*, 1992). Although real isotopic data have not been determined for either of these samples, they are the most undepleted fractionated samples in the Harley *et al.* (1992) dataset (see Section 2.3.2). To maximise the assimilation potential of this hypothetical rock type, the four following extreme chemical and isotopic values from the

old orthogneisses have been combined: (i) the lowest measured Sm/Nd ratio, to produce the fastest evolution towards negative ε_{Nd}; (ii) the most undepleted old orthogneiss, resulting in the highest Nd concentration for maximum mixing effect; (iii) the oldest realistic age for the model based on the available U-Pb zircon dating (3470 Ma; see Section 6.3), to maximise the time available for isotopic evolution prior to SLC intrusion; (iv) derivation from a CHUR source, since a DM source would have a higher ε_{Nd}. These combined characteristics equate to a minimum (most evolved) ε_{Nd} isotopic composition of ~-8.5 at 2840 Ma (model A1c).

It is immediately apparent from all the models that given a reasonable ratio of assimilant to magma (~10%), a restricted range of Sm/Nd with a negative trend of ε_{Nd} similar to the present SLC is possible. However, although there is a general tendency for the low abundance rocks (with high ***mg*** and high $^{147}Sm/^{144}Nd$) to become proportionally more negative in terms of ε_{Nd}, *none* of the possible assimilants in the Rauer Group at 2840 Ma are sufficiently evolved to produce SLC rocks with ε_{Nd} as low as -10. Even for very large amounts of contamination (and field relations, geochemistry and oxygen isotopes indicate that there could not have been a great deal of assimilation) the range of ε_{Nd} with values <-10 to >3.8 could not have been produced by any of the assimilants used in the simple models examined here.

Different model parameters and complex AFC models

The model described above was only run for a very limited number of conditions, primarily to illustrate that contamination could potentially produce the geometry of the isotopic mixing array, but cannot explain the observed spread in ε_{Nd} for the SLC. A somewhat better fit could possibly obtained for the intermediate ε_{Nd} values, for the range between the assumed DM protolith source and negative epsilon values down to about -6, by modifying the model parameters or possibly by using the AFC models of DePaolo (1981). For example, the degree of assimilation is likely to be strongly temperature dependant, therefore more basic bulk compositions (*i.e.* highest initial Sm/Nd) could potentially assimilate more crust than cooler compositions. If different mixing ratios were chosen to reflect this factor, then the lowest Sm/Nd rocks would have values nearer to DM, as observed in the real dataset. The problem remains, however, that no geologically feasible parameter changes or even application of more complex AFC models can explain ε_{Nd} values that are higher than the source or lower than the most isotopically evolved potential assimilant (*e.g.* see DePaolo, 1981, figs. 3 & 4 for constraints on AFC models).

Metamorphic perturbation of Nd-isotope systematics can, however, more readily explain all the observed data for the SLC. To illustrate this, the same basic model described for assimilation is used, but with one important difference - time.

6.5.4 Discussion of Hypothesis B: Metasomatism and isotopic exchange

General arguments for and against Nd-isotope mobility during metamorphism or metasomatism

Although resetting of Nd isotopes at an intermineral scale during high-grade metamorphism is well documented (*e.g.* Futa, 1981; McCulloch & Black, 1984; Burton & O'Nions, 1991), many workers assume that the scale of isotopic perturbation for the Nd system during metamorphism is less than the size of a typical sample. Hence, the model-age geochronology approach (*e.g.* Borg & DePaolo, 1994; Kerr & Fryer, 1994) and the more general application of Nd isotopes to the petrogenetic studies of high-grade metamorphic Precambrian rocks (*e.g.* Bowring *et al.*, 1989; Collerson *et al.*, 1991; Muir *et al.*, 1994;), have only very rarely been specifically tested to ensure that there has not been Nd-isotope perturbation. Notable exceptions include Black and co-workers (*e.g.* McCulloch & Black, 1984; Black & McCulloch, 1987; Black, 1988) and Gruau and co-workers (*e.g.* Gruau *et al.*, 1992; 1996).

A number of criteria are commonly cited as evidence against metamorphic disturbance. For example, Cohen *et al.* (1991) for the Lewisian, and Bowring & Housh (1995) for the Slave Province, argued that because juxtaposed mafic and felsic layers have distinctly different isotopic characteristics (*i.e.* ε_{Nd} values), they did not isotopically homogenise and therefore Nd movement was restricted to less than the metre-scale. However, this need not be the case since individual layers have different mineral assemblages which are capable of internally buffering chemical and isotopic systems to different extents during infiltration metasomatism (discussed further below). Another often-cited discriminant that apparently mitigates against Nd mobilisation, is the retention of coherent trace-element patterns (*e.g.* Collerson *et al.*, 1991). Using such criteria for discerning open-system behaviour in the Nd system is tenuous for two reasons. Firstly, REE and especially Sm/Nd will tend to have a systematic interdependence during igneous petrogenesis and metasomatic processes, so that Sm/Nd are likely to be broadly related (correlated) whatever the underlying mechanism. The second problem concerns the sensitivity of the Nd system to even small changes (undetectable on most element-element or multi-element plots) in Sm/Nd ratio a long time after crystallization (*cf.* Patchett, 1989). For relatively young rocks, ε_{Nd} or model-age calculations will not be significantly influenced by metasomatism even if there are quite

large changes to $^{147}Sm/^{144}Nd$ after crystallization. This is not the case for very old rocks that were subsequently metamorphosed or metasomatized a long time after formation (*e.g.* the SLC). In a perceptive theoretical study of the effects of metasomatism on Nd-isotope systematics, Rosing (1990) showed that for very old rocks, even a small change (5-10 %) in $^{147}Sm/^{144}Nd$ a significant time after crystallization can induce changes of up to 4 epsilon units. Building on the ideas expressed in Rosing's paper, Gruau *et al.* (1996) demonstrated that the Garbenschiefer amphibolite unit, a suite of orthogneisses within the >3700 Ma Isua Supracrustal belt of Greenland, have variations in ε_{Nd} between -1 and 5 that were produced by small degrees of metasomatism during a reworking event at about 2900 Ma.

An outline of the possible mechanisms of open system isotopic behaviour

A series of models are described below to illustrate a number of theoretical scenarios, partly based on ideas presented in Rosing (1990) and Gruau *et al.* (1996), that could explain the apparent isotopic contrast between juxtaposed mafic and felsic gneisses in general (*e.g.* Bowring & Housh, 1995) and, more specifically, between the evolved ferrodiorites and the ultramafic cumulates of the SLC. The models are probably a gross over-simplification of the real situation. Nevertheless, they are an attempt to apply a simple mixing model to a range of geologically plausible situations. Suggestions for how combined geochemical and isotopic modelling in high-grade terrains in general could be improved are discussed later in the conclusions chapter (Part 4). This section merely illustrates that given the long and complex geological history of the Rauer Group, relatively little perturbation is required to drastically alter the ε_{Nd} parameter. Unfortunately, a rigorous process-orientated approach is beyond the scope of this thesis and the current dataset.

Three variations of a simple metasomatism model are outlined below. The first general model (Hypothesis B1) considers changes in Sm/Nd at 500 Ma for a range of hypothetical SLC compositions ($^{147}Sm/^{144}Nd$ and Nd concentrations). This sort of model is the simplest conceptually and has been described in the literature (*e.g.* McCulloch & Black, 1984; Rosing, 1990; Gruau *et al.*, 1996). It is likely that the isotopic effects of changing $^{147}Sm/^{144}Nd$ have been studied for a number of reasons.

- It is relatively easy to predict the outcome of theoretical changes in the ratio.
- A decrease in the ratio is the only realistic mechanism that can produce crustal rocks that have ε_{Nd} values that are significantly higher than DM, without resorting to ultradepleted early Archaean mantle models (*vis.* Collerson *et al.*, 1991; Bennett *et al.*, 1993, Bowring *et al.*, 1995).

- Relatively large changes in ε_{Nd} can be produced by only small changes in $^{147}Sm/^{144}Nd$ if disturbance to the system occurred a long time after crust formation. Two end-member variations of this hypothesis are possible, either internal exchange within the SLC (Model B1a), or external exchange with the surrounding gneisses (Model B1b).

The second general model (Hypothesis B2) attempts to integrate a degree of isotopic perturbation with the change in Sm/Nd. As far as I am aware, no quantitative work has been done on this to date. A number of workers have considered the effects of metasomatism for the Sr system involving changes to both $^{87}Sr/^{86}Sr$ and Rb/Sr (*e.g.* Van Breeman & Dallmeyer, 1984; Cliff, 1985; Bickle & Chapman, 1990), but there are no thorough accounts of documented changes in Nd-isotope ratios. As with the first hypothesis, two overall variants are possible, involving either partial internal exchange (Model B2a) or a degree of external exchange (Model B2b).

The third model (Hypothesis B3) attempts to qualitatively integrate petrological, geochemical and spatial constraints into the first two models. Again, very little (no?) work has been done on the petrological controls of isotopic resetting (for radiogenic isotopes), although important recent work by Wood (1990a, 1990b), Gammons *et al.* (1996), Pan & Fleet (1996) and Gruau *et al.* (1992; 1996) have made significant advances in our understanding of the possibilities, if not the underlying mechanisms.

The consequences of secondary fractionation of $^{147}Sm/^{144}Nd$ (Models B1a & b)

Figure 6.7 illustrates the closed-system ε_{Nd}-time evolution diagram for a hypothetical layered complex that has a range of $^{147}Sm/^{144}Nd$ between 0.1350 and 0.1800. All compositions within the suite evolve towards progressively more negative ε_{Nd} with time according to their initial $^{147}Sm/^{144}Nd$. However, relatively small changes in $^{147}Sm/^{144}Nd$ a long time after protolith formation ($>10^9$ years), as shown in Figure 6.8, are capable of producing a large discrepancy between the original ε_{Nd} and calculated apparent values of this parameter.

The potential for such large changes to ε_{Nd} as a consequence of secondary Sm/Nd fractionation have been quantified by McCulloch and Black (1984), Rosing (1990) and Gruau *et al.* (1996). Expressing the epsilon parameter of Equation 1.10 in a different form, the ε_{Nd} for a time t in the past is *approximated* by (modified from the above references):

$$\varepsilon_{Nd(t)} = \varepsilon_{Nd(0)} - f^{Sm/Nd} \cdot Q \cdot t \qquad [6.3]$$

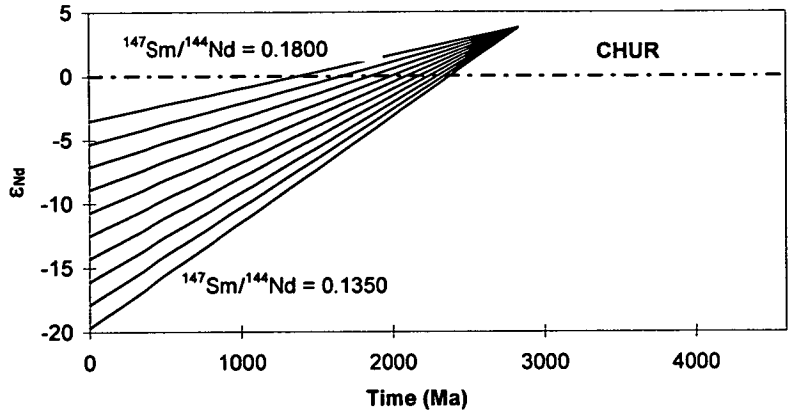

Figure 6.7 Closed system evolution from a DM source for a realistic range of $^{147}Sm/^{144}Nd$ similar to the SLC.

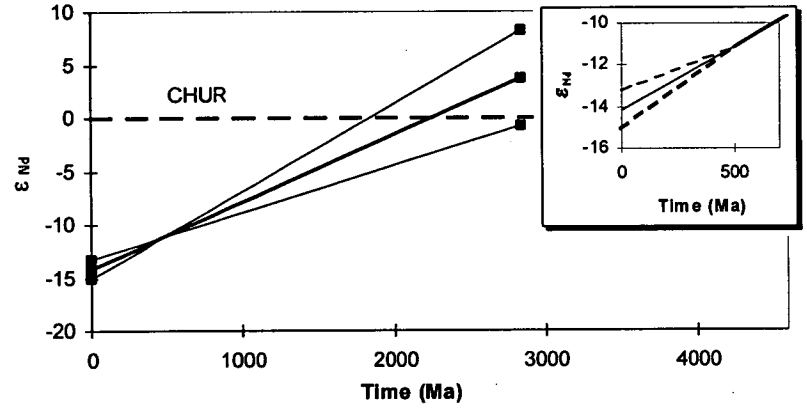

Figure 6.8 An illustration of the profound effects that secondary Sm/Nd fractionation can have on apparent ε_{Nd} values. An intermediate $^{147}Sm/^{144}Nd$ value of 0.1550 is shown evolving until 500 Ma, with +10 % and -10 % secondary fractionation of the original ratio. The inset details the effects to isotopic evolution at 500 Ma, resulting in changes of $\Delta\varepsilon_{Nd(0)}$ of ~1, but this propagates to $\Delta\varepsilon_{Nd(t)}$ of about 4.5 at 2840 Ma ($\Delta\varepsilon_{Nd}$ is defined below).

Where $\varepsilon_{Nd(0)}$ is the ε_{Nd} today as defined in [1.10],

$f^{Sm/Nd} = (^{147}Sm/^{144}Nd)_{sample}/ (^{147}Sm/^{144}Nd)_{CHUR} - 1$,

$Q = (10^4 . \lambda . (^{147}Sm/^{144}Nd)_{CHUR})/(^{143}Nd/^{144}Nd)_{CHUR}$,

and t = protolith age in millions of years.

Following from this, the deviation between the calculated apparent $\varepsilon_{Nd(app)}$ and the original $\varepsilon_{Nd(true)}$ values are given by:

$$\Delta\varepsilon_{Nd(t)} = \Delta^{147}Sm/^{144}Nd . Q . K . (t - t_{(met)}) \qquad [6.4]$$

where $\Delta\varepsilon_{Nd}$ is the difference between the real and apparent values expressed in epsilon units ($\varepsilon_{Nd(app)} = \varepsilon_{Nd(true)} - \Delta\varepsilon_{Nd}$); $\Delta^{147}Sm/^{144}Nd$ is the relative variation in $^{147}Sm/^{144}Nd$ brought about by perturbation at the time of metamorphism $t_{(met)}$; t is the age of the protolith[4] determined by independent means; and K is the ratio between protolith and chondritic $^{147}Sm/^{144}Nd$. An additional variation introduced in this study is $\Delta\varepsilon_{(t\,met)}$, which is the direct change in ε_{Nd} at the time of metamorphism. This will be used in later sections. Also, for simplicity and to allow direct correlation with Figures 6.4 and 6.5, $^{147}Sm/^{144}Nd$ has been retained in the models and graphs rather than $f^{Sm/Nd}$.

In Figures 6.8 & 6.9 an intermediate $^{147}Sm/^{144}Nd$ value of 0.1550 was chosen, with a $\Delta^{147}Sm/^{144}Nd$ of +10 % and -10 %, resulting in $\Delta\varepsilon$ values of $\sim \pm 4.5$. Although such variations could explain the ε_{Nd} variations in the Garbenschiefer amphibolite unit (spanning 6 epsilon units; Gruau *et al.*, 1996), it is apparent that much higher degrees of secondary Sm/Nd fractionation would be required to account for the SLC data.

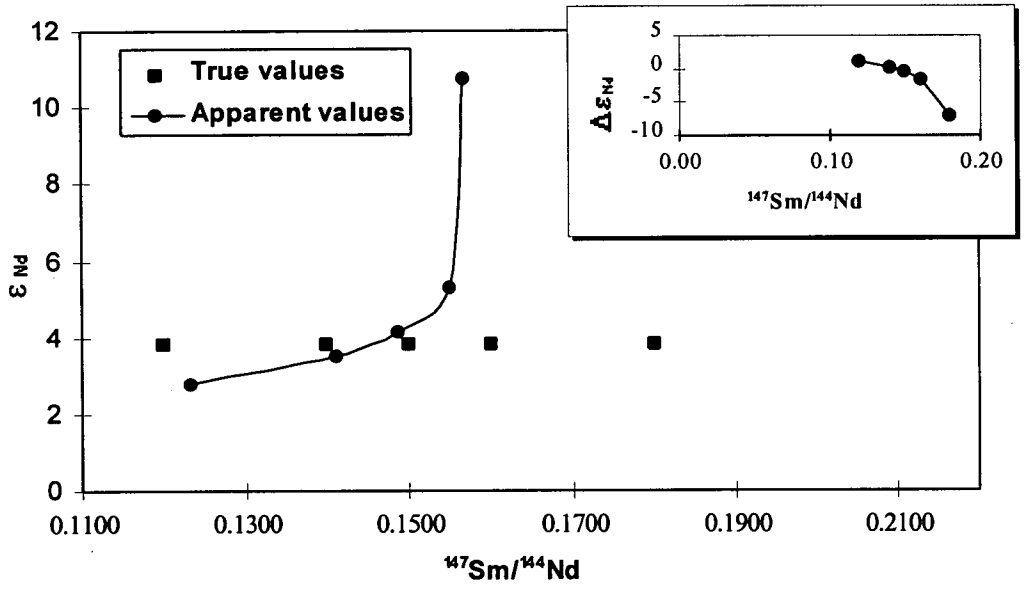

Figure 6.9 Model B1a An illustration of the possible changes in ε_{Nd} by internal redistribution of Sm/Nd for a hypothetical DM-derived 'SLC' protolith (true values). The model is based on binary mixing of Sm and Nd with an 'average' SLC composition (apparent values). Inset shows that $\Delta\varepsilon_{Nd}$ is largest for compositions with high initial Sm/Nd, which in this model would correspond to low Sm and Nd concentrations. Note that the overall apparent changes are in the opposite sense to the real SLC data.

[4]For simplicity, t denotes the age of the protolith, $t_{(met)}$, is used to distinguish the age of metamorphism/metasomatism, and t_0, is used to denote the present day.

Further consideration of the redistribution of Sm/Nd for the SLC, ignoring possible mineralogical controls for the moment, is described by reference to simple models that illustrate the effect of secondary fractionation by net internal redistribution (Model B1a), and by interaction with an externally derived LREE enriched fluid (Model B1b).

Model B1a assumes a high degree (20 %) of bulk mixing (X_a = 0.2) of end-member compositions with an 'average' composition for the complex compiled from Appendix 2 and Table 6.3. A range of starting compositions slightly greater than the present SLC is used for the model, which assumes a net re-equilibration of end members by mixing with an average composition of ~16 ppm Nd and $^{147}Sm/^{144}Nd$ of 0.1450. As with the assimilation models described earlier (Hypothesis A), the choice of starting compositions is biased to emphasise that low abundance rocks are effectively prone to larger changes in $^{147}Sm/^{144}Nd$ (discussed further below), and hence larger $\Delta\varepsilon_{Nd}$ (*e.g.* Figure 6.9 inset). In this simple mixing model, such a bias means that high abundance, low $^{147}Sm/^{144}Nd$ rocks only change $^{147}Sm/^{144}Nd$ by +2.8 %, whereas low abundance high $^{147}Sm/^{144}Nd$ change by 12.9 %. It is apparent that bulk compositions with high $^{147}Sm/^{144}Nd$ have $-\Delta\varepsilon_{Nd}$ and consequently have higher apparent ε_{Nd}, which is not the case for the SLC dataset (*cf.* Figure 6.5).

A variation of this model can be used to consider the effects metasomatism by an externally-buffered fluid (Model B1b). Given the high Nd concentrations and LREE-enriched nature of the surrounding crust (see Model A1), it is likely that an externally-buffered infiltrating fluid would have low Sm/Nd values (less than the present value for the SLC). Given similar degrees of mixing to model B1a (or any amount), this metasomatism model could only result in higher apparent ε_{Nd} (since the results are similar to model B1a, the graphs are not included here). The only way that the majority of the SLC samples could have evolved to lower apparent ε_{Nd} by secondary fractionation of $^{147}Sm/^{144}Nd$ alone, would be through interaction with a LREE-depleted fluid. However, such a fluid would be unlikely to persist without interacting with the extremely fractionated LREE-enriched CLO, or even the SLC. Even if such a fluid did interact with the SLC, the relative degree of mixing according to Equation 6.2 would need be very large for ratios for the high $^{147}Sm/^{144}Nd$ compositions of most of the SLC. Moreover, the high apparent ε_{Nd} samples (RI22 & RI23) would also be affected and they would therefore have had an increased $^{147}Sm/^{144}Nd$ but decreased apparent ε_{Nd}. For these reasons, such a fluid is considered unlikely.

Overall, changes in $^{147}Sm/^{144}Nd$ by secondary fractionation as defined in Hypothesis B1 cannot explain the observed data for the SLC. Interaction with an externally-buffered fluid would probably result in higher apparent ε_{Nd}, whereas net internal redistribution of

$^{147}Sm/^{144}Nd$ would require large $\Delta^{147}Sm/^{144}Nd$ to affect a wide range of bulk compositions. For example, by rearranging Equation 6.4, the range of $\Delta^{147}Sm/^{144}Nd$ needed to return the SLC to DM values is between 23.5 and -31.5 % with an average of -18.1 %, if the single anomalously high sample (RI22) is excluded. However, given the similar geochemical nature of the LREE and the geological, geochemical and isotopic features described in the previous sections, such large-scale LREE disturbance is highly unlikely. For such changes to take place a significant degree of $^{143}Nd/^{144}Nd$ resetting would be expected and the data would at least approximate a positive linear correlation on an isochron diagram. Moreover, contemporaneous large-scale major- and trace-element mobility would be inevitable, and the textural features described for the complex would not have been preserved as they are. Clearly, the processes that controlled isotopic perturbation for the SLC were more complex than simple secondary fractionation of Sm/Nd. In particular, a mechanism is required that is capable of explaining how some low $^{147}Sm/^{144}Nd$ rocks that have high positive ε_{Nd}, whereas the majority of intermediate or high $^{147}Sm/^{144}Nd$ rocks have very negative ε_{Nd}.

Bulk compositional reasons for systematic isotopic resetting

Although the studies of Black & McCulloch (1984) and Gruau *et al.* (1996) and others are important in that they demonstrate that time-integrated secondary fractionation of Sm/Nd can significantly alter apparent ε_{Nd} values, the model has a number of over-simplifications. For brevity a number of key problems are outlined in point form below:

- In their study of Sm/Nd redistribution, Gruau *et al.* (1996) emphasised the obvious relationship between $\Delta\varepsilon$ and $\Delta^{147}Sm/^{144}Nd$ in terms of percentage changes to the ratio. However, the absolute change in Sm/Nd are also important. For example, a 10 % change will have a much greater effect on Sm/Nd values near to CHUR, than more evolved samples with lower Sm/Nd. For the same *percentage* increase for a range of $^{147}Sm/^{144}Nd$, relatively high values of $^{147}Sm/^{144}Nd$ will have proportionally larger $\Delta\varepsilon_{Nd}$. This is because the production of radiogenic ^{143}Nd is dependant upon the amount of ^{147}Sm (*e.g.* Equation 1.7). Therefore the K term in Equation 6.4 increases with higher $^{147}Sm/^{144}Nd$.

- The model described by Gruau *et al.* (1996) and others (*e.g.* Hypothesis B1) relies only on changes in Sm/Nd and does not take into account initial bulk composition or the mechanism by which the ratio is changed. Obviously, the respective concentrations of Nd and/or Sm must change. If this is accomplished by Nd loss from the system, then there need not be any direct change to isotopic compositions at the time of metamorphism. However, if there is a gain in Nd it would almost certainly have a different isotopic ratio (given that small original variations in $^{147}Sm/^{144}Nd$ would lead to different samples evolving along separate trajectories from 2.84 to 0.5 Ga; *cf.* Figure 6.7), and mass balance would lead to a direct change in $^{143}Nd/^{144}Nd$ according to the simple mixing model described earlier [6.2]. Hence, those rocks with low original Nd

concentrations are effectively prone to isotopic resetting by Nd gain in a simple model involving exchange between two Nd-isotope reservoirs.

- If the potential for isotopic resetting is bulk composition dependent, and the usual pattern of igneous differentiation for Sm and Nd leads to evolved rocks with progressively higher Nd concentrations and $^{147}Sm/^{144}Nd$ (*e.g.* Faure, 1996, table 12.1 & figure 12.1), then low abundance, high $^{147}Sm/^{144}Nd$ rocks will be prone to net Nd gain with more evolved $^{143}Nd/^{144}Nd$ isotopic compositions (*e.g.* Figure 6.9). This is because relatively differentiated members of a suite will evolve to proportionally more negative ε_{Nd} with time. However, for the reverse situation where relatively evolved rocks change due to metamorphism/metasomatism, bulk composition is likely to have a profoundly different influence. Net gain of Nd is less likely if the surrounding rocks have significantly lower Nd (and Sm) abundances. Nevertheless, the potential for secondary fractionation of $^{147}Sm/^{144}Nd$ is still possible and could be accomplished by loss of Nd and/or Sm, which will be largely controlled by the bulk distribution coefficients for these elements with respect to the fluid ($D_{solid\text{-}fluid}$).

The following discussion illustrates some of the possible consequences of the aforementioned points, again by reference to simple theoretical models.

Change in $^{147}Sm/^{144}Nd$ and $^{143}Nd/^{144}Nd$ by metasomatism (Models B2a & b)

Although a number of studies have attempted to explain variable ε_{Nd} for apparently cogenetic suites on the basis of secondary Sm/Nd fractionation alone (*e.g.* McCulloch & Black, 1984; Rosing, 1990; Gruau *et al.*, 1996; and the discussion of Hypothesis B1), for the reasons outlined in 1-3 above, it is highly likely that changes in REE would be accompanied by direct perturbation of Nd isotopes, certainly for relatively low-abundance rocks. However, there is also another end-member scenario not considered in detail in the aforementioned studies. This involves partial direct isotopic perturbation with little or no Sm/Nd variation.

Fluid-enhanced diffusion of $^{143}Nd/^{144}Nd$

Although isotopic diffusion distances between solids are typically up to cm-scales for metamorphic time-scales, diffusion distances in a fluid phase may reach 10s of metres (*e.g.* Bickle & McKenzie, 1987). Therefore the possibility for direct resetting of $^{143}Nd/^{144}Nd$ is significant in any isotopically heterogeneous gneiss terrain if such a fluid medium is present during metamorphism. Complete homogenisation of $^{143}Nd/^{144}Nd$ for the SLC, however, clearly did not happen as $^{143}Nd/^{144}Nd$ and $^{147}Sm/^{144}Nd$ do not define a young isochron age. Nevertheless, disequilibrium conditions might be expected, and Figure 6.10 illustrates the simplest scenario of systematic partial re-equilibration of isotopic compositions by internal redistribution of $^{143}Nd/^{144}Nd$ only. Since Sm and Nd concentrations (and hence ratio)

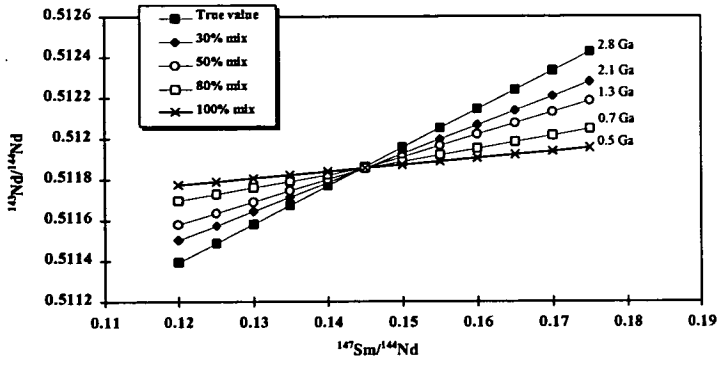

Figure 6.10 The theoretical effects of partial Nd-isotope re-equilibration of $^{143}Nd/^{144}Nd$ by internal exchange.

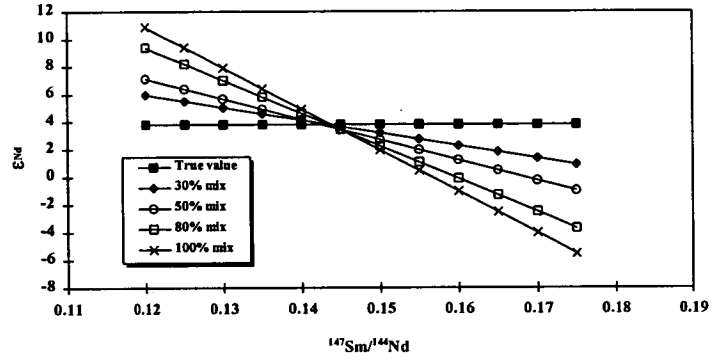

Figure 6.11 The theoretical effects of partial Nd-isotope re-equilibration of $^{143}Nd/^{144}Nd$ by internal exchange. The effects are expressed in terms of ε_{Nd}.

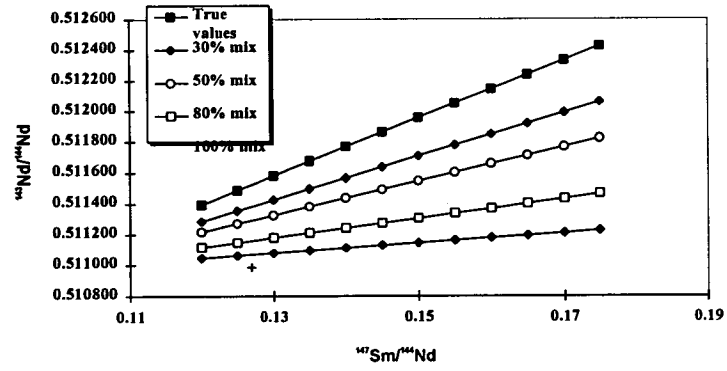

Figure 6.12 The theoretical effects of partial Nd-isotope re-equilibration of $^{143}Nd/^{144}Nd$ by external exchange with a fluid that has equilibrated with Rauer Group felsic crust (CLO).

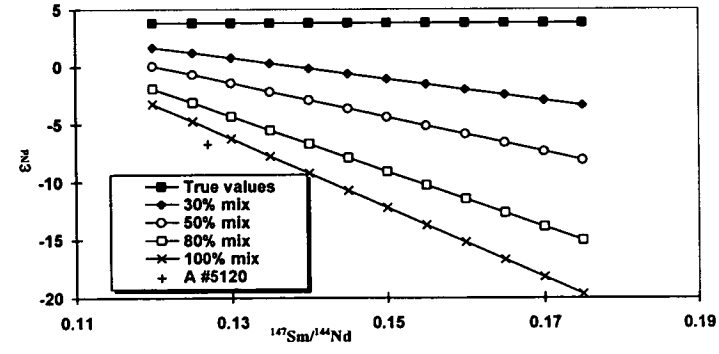

Figure 6.13 The theoretical effects of partial Nd-isotope re-equilibration of $^{143}Nd/^{144}Nd$ by external exchange with a fluid that has equilibrated with Rauer Group felsic crust (CLO). The effects are expressed in terms of ε_{Nd}.

remain fixed, the model is effectively equivalent to partial internal isotopic redistribution controlled by fluid-enhanced diffusion.

This model produces a suitable negative array of ε_{Nd} *vs.* $^{143}Nd/^{144}Nd$ (Figure 6.11), however, the measured isotopic ratios would define a positive correlation (isochron) proportional to the amount of mixing and the age of metamorphism. Figure 6.10 illustrates an isochron diagram for systematic models involving: (i) closed system evolution (no resetting); (ii -iv) partial isotopic resetting corresponding to 20, 50 and 80 % internal homogenisation; and (v) the effects of complete homogenisation (100 % mixing). Note that the 2.84 Ma starting isochron rotates about the 'average' composition towards a 500 Ma isochron for complete homogenisation. A similar situation is described by Montigny and Faure (1969) for the Rb-Sr system, where the age of metamorphism is defined by a largely reset whole-rock isochron. Faure (1986) mentions other examples of Rb-Sr isochron ages that are intermediate between the time of protolith formation and metamorphism. Clearly such models cannot explain the SLC data (*e.g.* Figures 6.4 & 6.5). A possible variation of the model is to consider partial re-equilibration with an external reservoir (Figures 6.12 & 6.13). Given the likely external source characteristics described earlier, partial isotopic homogenisation without secondary fractionation of Sm/Nd would still produce a positive correlation on an isochron diagram, and although there would be a negative ε_{Nd} array at 2840 Ma, all rocks would be displaced to negative values (Figure 6.13).

Given that neither direct isotopic perturbation or secondary fractionation of $^{147}Sm/^{144}Nd$ can account for the SLC isotopic array in isolation, the question becomes 'could a hybrid model involving both mechanisms must be responsible for the large spread in ε_{Nd} observed for the complex?'

There are a number of possible scenarios that could plausibly combine a degree of Sm and Nd mobility with isotopic resetting. As with the previous models there are two main possibilities, involving either partial internal redistribution of Sm/Nd and $^{143}Nd/^{144}Nd$, or external exchange. The following discussion first considers direct changes to $^{143}Nd/^{144}Nd$ by Nd mobility *only* (*i.e.* Nd mixing related to Nd concentration displacements, as described earlier), for both internal and external exchange. Next, the possible influence of fluid enhanced diffusion or advective transport of isotopic compositions are qualitatively assessed. The rationale for this is discussed further below.

Internal and external exchange by direct mixing

The possible effects of partial internal homogenisation linked to a redistribution of Sm and Nd can be evaluated by what could be described as the 'limited Nd-gain model'. In this model, changes in $^{143}Nd/^{144}Nd$ at the time of metamorphism (*i.e.* $\Delta\varepsilon_{Nd(tmet)}$) are only attributed to direct mixing of Nd compositions. Since low $^{147}Sm/^{144}Nd$ tend to have high Nd concentrations, then they are more likely to change ratio by net Nd loss and as a consequence will not directly change isotopic composition. In contrast, high $^{147}Sm/^{144}Nd$ rocks gain evolved Nd according to simple mixing (Equation 6.2).

The results for this type of model indicate that $\Delta\varepsilon_{Nd}$ is strongly controlled by the $\Delta^{147}Sm/^{144}Nd$ term in Equation 6.4. This leads to a slight decrease in apparent $\Delta\varepsilon_{Nd}$ for Sm/Nd rocks that are less than average, and progressively higher $\Delta\varepsilon_{Nd}$ for ratios that are greater than average. This is because in those rocks that are subject to direct[1] $\Delta\varepsilon_{Nd(tmet)}$, (*i.e.*

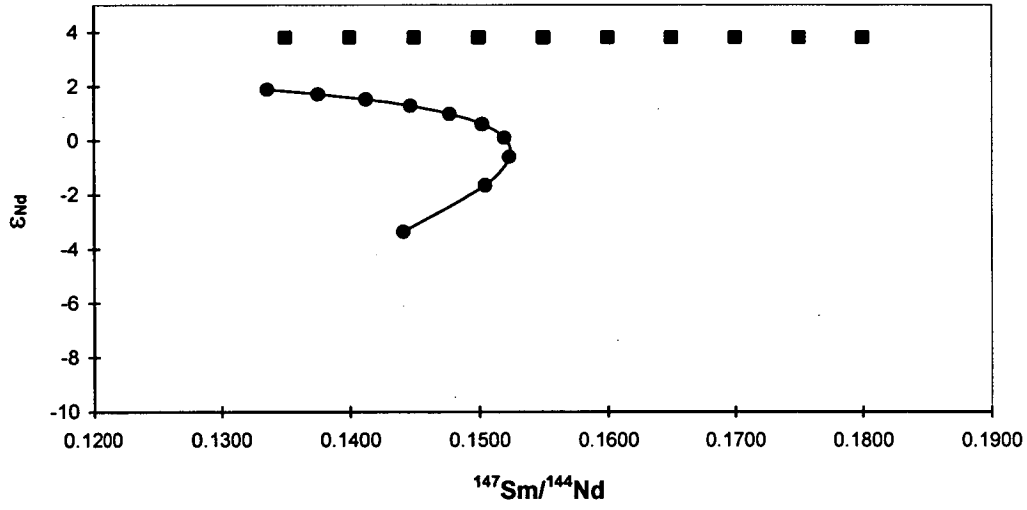

Figure 6.14 shows the results for interaction with an externally-buffered fluid. The parameters are the same as model B1a, and in this case, Nd-isotope resetting involving a direct change in isotopic composition at t_{met} = 500 Ma whereby the compositions with the lowest Nd abundance are the most influenced by fluid infiltration. Calculated ε_{Nd} at 2840 Ma are shown assuming equal mixing where $\Delta^{147}Sm/^{144}Nd$ is proportional to $\Delta\varepsilon_{Nd(tmet)}$. Although the model can easily produce a negative εNd array, $\Delta\varepsilon_{Nd}$ in high abundance samples is only controlled by $\Delta^{147}Sm/^{144}Nd$ resulting in a lower value of apparent ε_{Nd}. Furthermore, whilst low-abundance samples with high $^{147}Sm/^{144}Nd$ exchange with more evolved $^{143}Nd/^{144}Nd$ at 500 Ma, there is a counterproductive $\Delta^{147}Sm/^{144}Nd$ that offsets this direct change during the back-calculation procedure. This means that, proportionally, only a small decrease in apparent ε_{Nd} is possible by this model.

[1] Direct in this case means that most $\Delta\varepsilon_{Nd}$ is induced at the time of metamorphism, rather than via secondary fractionation of $^{147}Sm/^{144}Nd$ and the back-calculation proceedure.

low Nd concentrations) the direction of change is offset and even outweighed by the time-integrated $^{147}Sm/^{144}Nd$ increase (figures not included here).

For the external exchange models, however, a broadly negative ε_{Nd} array would be produced if partial homogenisation occurred by interaction with an externally-buffered fluid (Figure 6.14; model parameters are described in the figure caption). This is largely because the difference in ε_{Nd} between protolith and surrounding crust at 500 Ma is larger than the difference in Sm and Nd concentration (proportionally much more so than in the AFC models described earlier). Although this model illustrates an important feature of contrasting ε_{Nd} evolution with time for different initial $^{147}Sm/^{144}Nd$ compositions (referred to again in later discussion), it still has important differences with the real SLC data. This is partly because $\Delta\varepsilon_{Nd}$ relies on the cross-over effect described in Figure 6.7 to produce a negative ε_{Nd} array (which results in an overall positive trend of $^{143}Nd/^{144}Nd$ today), and as with all models that involve simple mixing with evolved crust, *all* ε_{Nd} values become progressively more negative.

Rationale for decoupled $\Delta^{147}Sm/^{144}Nd$ and $^{143}Nd/^{144}Nd$ mobility

Although the simple 'reservoir-interaction' models described above illustrate that small changes to Sm/Nd coupled with limited direct isotopic perturbation can produce a negative ε_{Nd} array, the displacement of concentration profiles can behave much differently to the movement of isotopic fronts during metasomatism. In their study of Sr-isotope behaviour during fluid infiltration in the Hercynian Trois Seigneurs Massif, Bickle & Chapman (1990) found that trace-element profiles generally move much more slowly than corresponding isotopic compositions (discussed further below). This is because trace-element mobility is intrinsically linked to mineralogy (stability/instability) and bulk composition, and is therefore rate-limited by slow-moving major elements; whereas the rate by which isotopic changes are propagated depends on diffusivity which is controlled by $D_{solid\text{-}fluid}$ for Nd, in addition to fluid flux and porosity.

Enhanced $^{143}Nd/^{144}Nd$ mobility relative to $^{147}Sm/^{144}Nd$

In an attempt to qualitatively integrate the difference in length scales between trace-element and isotopic profiles, a further refinement can be made to the metasomatism model described above by creating a significant difference between the proportion of low ε_{Nd} exchanged with the protolith and the change in $^{147}Sm/^{144}Nd$. For the internal redistribution model, this effectively means that apparent ε_{Nd} are produced by combinations of different proportions of $\Delta\varepsilon_{Nd(tmet)}$ and $\Delta^{147}Sm/^{144}Nd$. However, this means that apparent ε_{Nd} are

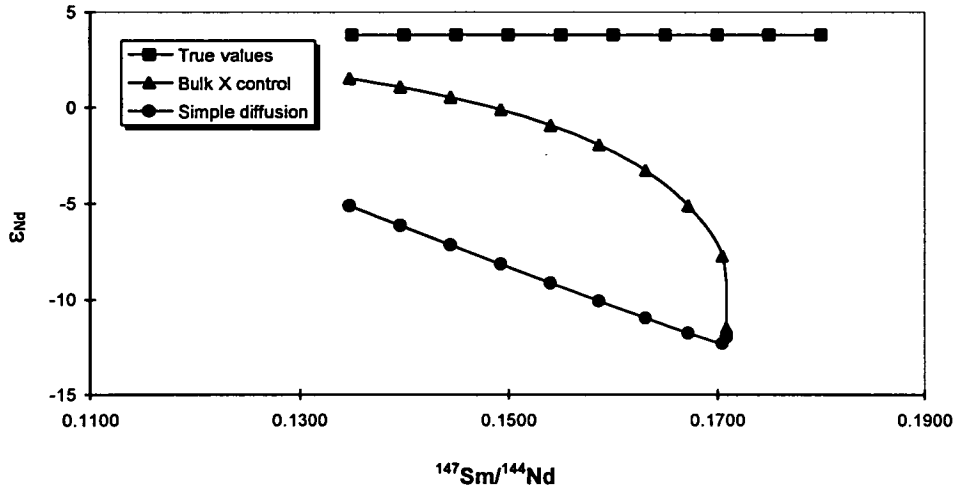

Figure 6.15 As with Models B2a, the effective mixing is bulk-composition dependant, with only small $\Delta^{147}Sm/^{144}Nd$ affecting relatively high Nd abundances. The maximum percentage change in $^{147}Sm/^{144}Nd$ in this model is only ~ 7 %, with a direct change in ε_{Nd} at 500 Ma of between -3 and -18 epsilon units.

confined to intermediate values between the two end-member models. Briefly, either the ε_{Nd} array is positive when $\Delta^{147}Sm/^{144}Nd$ is dominant, or it is negative when $\Delta\varepsilon_{Nd(t\text{met})}$ is dominant. In common with the end-member models described earlier, the problem remains that as the ε_{Nd} array becomes a progressively more negative, so the present day $^{143}Nd/^{144}Nd$ becomes positive on an isochron diagram.

Similarly, for the external-exchange model, an arbitrary difference can be introduced to account for the greater transport distances of isotopic compositions when compared to concentration profiles. Depending upon how the mechanism of isotopic transport is modelled, for example by considering simple diffusion unrelated to bulk composition or by having the isotopic profile related to Nd concentrations (Figure 6.15), broadly negative ε_{Nd} arrays can be produced fairly readily. However, the same problems encountered with previous models remain: (i) it is difficult to explain strongly positive ε_{Nd} rocks; (ii) the respective changes in $\Delta^{147}Sm/^{144}Nd$ are counteractive to a certain extent; (iii) (most importantly), it is difficult to produce the present day measured values of $^{147}Sm/^{144}Nd$ *vs.* $^{143}Nd/^{144}Nd$, and negative ε_{Nd} arrays are largely produced by the 'cross-over effect' (*e.g.* Figure 6.7 inset).

Interim summary and steps towards a realistic petrologic model

From the lengthy discussion above regarding different 'reservoir' exchange models, it is clear that systematic exchanges of this type cannot adequately account for the observed SLC Nd-isotope data. Many of the models described above were deliberately weighted from the outset, within the confines of geological plausibility, to produce a relatively large negative ε_{Nd} array. Two possibilities remain: either the process of isotopic perturbation is largely random, and the negative ε_{Nd} array shown in Figure 6.5 is not geologically or statistically meaningful, or the array does not reflect simple open-system behaviour governed by 'reservoir-scale' exchanges.

At this point it is pertinent to reconsider the original geological and isotopic relationships for the suite, in particular, the relationship between whole-rock chemistry, isotopic composition, mineralogy, and the spatial distribution of samples as a whole. The main aim of the models described above are to explore possible mechanisms that could produce a negative array between ε_{Nd} and $^{147}Sm/^{144}Nd$. But is this relationship geologically or statistically valid? If it is, then it is important to establish whether the independent variable ($^{147}Sm/^{144}Nd$) is the *cause* of the array or a secondary feature, with the relationship more closely controlled by a different but possibly related variable.

A discussion of what would constitute a statistically valid correlation for $^{147}Sm/^{144}Nd$ *vs.* $^{143}Nd/^{144}Nd$ either today or at any time in the past is fraught with assumptions. A summary of the pitfalls of the common denominator effect are given in Rollinson (1993), who cites Dodson (1982) as an example of why simple ratio correlation in isotope geology ***is*** valid. Essentially, this is because isotopic ratios are measured independently and can only be modified in a limited number of ways, primarily by radioactive decay. However, the statistical assumptions in the case of the SLC dataset are peculiar. An artefact of measuring isotopes in very old rocks is that positive correlations on isochrons generally improve with time. This is because the spread in y values (*e.g.* $^{143}Nd/^{144}Nd$) increases with the time-dependant production of daughter isotope. However, for a negative correlation produced by isotopic disturbance, as monitored by a correlation coefficient (r) for example, the degree of correlation will decrease from the time of perturbation until the slope of the line becomes positive again with time (in about $\sim 6 \times 10^9$ years for the SLC!), from which point the correlation will again improve. For example, the present day correlation coefficient $(r)^2$ for

---

[2] Although there are a number of assumptions involved that might not strictly apply to this dataset, especially regarding the distribution of data points and the influence of outliers, the Pearson-product moment correlation is used here. There are two reasons why the test is used here in preference to a

$^{147}Sm/^{144}Nd$ *vs.* $^{143}Nd/^{144}Nd$ for the SLC is statistically valid at better than the 95 % confidence level, whereas the correlations at the time of metamorphism (500 Ma) and protolith emplacement (2840 Ma) were significant at better than the 99 % and 99.9 % confidence levels respectively.

Given that understanding the mechanism of isotopic disturbance is the objective of this discussion, further statistical considerations will be calculated for ε_{Nd} values at 500 Ma, the most likely age of disturbance. For the 9 data points on Figure 6.5, there is a correlation coefficient (r) of -0.71 for the relationship between ε_{Nd} and $^{147}Sm/^{144}Nd$, which for 7 degrees of freedom (n-2) is statistically significant at the 99 % confidence level. Since, a *positive* trend would normally be expected, this relationship is clearly very strong. However, there are a number of factors that control the independent variable of an isochron plot, and measured $^{147}Sm/^{144}Nd$ is a product of two main processes. Most importantly, this ratio would have been controlled by the sum of all the different aspects of protolith petrogenesis as reflected in the primary mineral assemblage. However, it could also have changed during fluid infiltration, which will be controlled by the interaction of a variety of metasomatic variables, such as the fluid-rock ratio, fluid composition and the mineral assemblage. The influence of mineralogy *could* be particularly important when metamorphic reaction takes place in the presence of the fluid in response to changes in *P-T-X* (where *X* includes fluid composition) conditions (*e.g.* Ferry, 1980; Rumble, 1989) or as a consequence of deformation (*e.g.* Condie & Sinha, 1996). This raises two fundamentally important questions: where do REE reside in the SLC and how did these phases behave during metamorphism or fluid-infiltration metasomatism?

Distribution and behaviour of REE in metamorphic rocks

Of the few studies that have considered the possibility of Nd-isotope mobility, most attempt to explain variations in apparent ε_{Nd} by reference to reservoir-exchange models as described in the previous section (*e.g.* McCulloch & Black, 1984; Gruau *et al.*, 1996). Although a few studies have acknowledged that variations in mineral assemblage or modal distribution can influence the stability or instability of whole-rock or outcrop-scale radiogenic-isotopic systems during metamorphism, the underlying mechanisms have not been examined in detail for different rock types or assemblages.

'rank' test: (i) The correlation is strongly controlled by the highly positive ε_{Nd} value, which **could** be strongly controlled by the mineralogy of this particular rock, and (ii) Excel® can quickly provide a correlation matrix for a large dataset by this method.

In their study of isotopic perturbation in the Garbenschiefer unit, Gruau *et al.* (1996) found no correlation between ε_{Nd} and mineralogy, and as such they were unable to find a causative mechanism to explain the metasomatism process and concluded that the distribution of ε_{Nd} values appeared random. However, they did suggest that metamorphic segregation led to amphibole and plagioclase modal variations, and that the major-element redistribution necessary for this recystallization was important. They state that 'in such a context, the mobility of the LREE could easily bring about a fractionation of a few percent in $^{147}Sm/^{144}Nd$ (Gruau *et al.*, 1996, p.233)'. By contrast, in an earlier study of metakomatiites from Finland, Gruau *et al.* (1992) were able to relate variations in ε_{Nd} to modal composition which they advocate controlled secondary fractionation of $^{147}Sm/^{144}Nd$. The studies have two important differences. The Garbenschiefer amphibolite is an example of where disequilibrium isotopic conditions were dominant at outcrop scales, whereas the Finland komatiite[3] re-equilibrated completely at outcrop scales. This contrasting behaviour is primarily related to differences in bulk composition and the extent of retrogression (discussed further in Part 4, Chapter 13). Apart from these observations (as far as I am aware), no studies to date have systematically examined the influence of mineral stability or reaction on the behaviour of the radiogenic isotopes during metamorphism. A number of studies have considered the influence of bulk composition and reaction on major-element mobility (*e.g.* Ferry, 1980; Winchester & Max, 1984; Ague, 1991; Selverstone *et al.*, 1991; Ferry & Dipple, 1991), however, little has been done to constrain the behaviour of trace elements and REE. Linking reaction progress theory (*e.g.* Ferry, 1980 and others) to radiogenic-isotope systems is likely to prove an important step in metamorphic geochemistry.

Having noted the overall paucity of information regarding mineralogical controls on whole-rock isotopic disturbance, a number of studies have considered the residence of trace elements and REE in metamorphic rocks (*e.g.* Futa, 1981; Grauch, 1989; Watt & Harley, 1993; Condie & Sinha, 1996; Gruau *et al.* 1996; Pan & Fleet, 1996; Ayres & Harris, 1997). Disequilibrium trace-element and isotopic behaviour during crustal anatexis has recently been well documented by a number of authors (*e.g.* Sawyer, 1991; Watt & Harley, 1993; Nabelek & Glascock, 1995; Johannes *et al.*, 1995; Ayres & Harris, 1997) and there are a number of important conceptual similarities between these studies and the metasomatism process. Of particular importance is the residence of REE. For pelitic or granitic (*s.l.*)

---

[3] The Finland metakomatiite has Nd concentrations typically <5 ppm and is dominated by an equilibrium greenschist facies assemblage comprising amphibole ± chlorite ± Plag. Very large amounts of fluid infiltration affected these rocks.

protolith and melt compositions, it is apparent that a major proportion of the REE reside in accessory phases (*e.g.* Watt & Harley, 1993; Bea, 1996; Ayres & Harris, 1997). For the LREE (*i.e.* Sm & Nd), monazite is the most important host, followed by apatite, and these phases can contain almost all the LREE budget of these bulk rock compositions. However, compared with granites and pelites, the SLC differs significantly in bulk composition and REE concentrations, and most of the complex has sufficiently low REE to inhibit the crystallization of accessory phases where REE are essential structural constituents. Therefore, the bulk of REE will be hosted in major phases and apatite (+ rare zircon in some rocks). Differences in modal abundance and the response of these minerals during fluid infiltration provides a petrological basis from which to reconsider the SLC Nd-isotope data. The behaviour of minerals with respect to fluid infiltration also adds a further dimension to the earlier discussion regarding the correlation between ε_{Nd} and Sm/Nd.

Some comments on the relationships between bulk composition, mineralogy, $^{147}Sm/^{144}Nd$ and ε_{Nd}

Bulk compositional variations in the SLC are defined by modal variations in the ferromagnesian minerals orthopyroxene, clinopyroxene, hornblende and biotite, and the quartzofeldspathic minerals plagioclase, and to a lesser extent potassium feldspar and quartz. Accessory apatite occurs throughout, but is more abundant in leucocratic rocks. Zircon also possibly occurs in these rocks in very small quantities. Quantifying the modal mineralogy of these very coarse-grained, foliated and lineated rocks would be very difficult. It would be even more difficult to define the total distribution of the REE. Nevertheless, qualitatively there is an important correlation between the $^{147}Sm/^{144}Nd$, ε_{Nd} and mineral modes. The most negative ε_{Nd} (high $^{147}Sm/^{144}Nd$) rocks are dominated by clinopyroxene, hornblende and orthopyroxene, whilst the two positive ε_{Nd} (low $^{147}Sm/^{144}Nd$) rocks have abundant plagioclase with only minor ferromagnesian phases. This relationship is well exemplified by a correlation matrix for major elements, trace elements and normative compositions (for ε_{Nd} at t=500 Ma; Table 6.5).

In this table there are two main groups of strongly correlated variables: (i) a strong positive correlation between $^{147}Sm/^{144}Nd$ and *Di*, with associated positive correlations for elements or normative minerals that are related to clinopyroxene (*e.g.* Sc); and (ii), negative correlations between $^{147}Sm/^{144}Nd$, *An*, *Ab,* and elements or normative minerals that are associated with plagioclase (*e.g.* Sr).

The normative mineralogy is an approximation of the primary anhydrous mineral assemblage estimated on the basis of whole-rock major element chemical analysis. Values for *Di*, in this case, are a measure of the diopside that could have formed in the SLC. This would correspond most closely to clinopyroxene in the protolith. Textural evidence indicates that hornblende is largely a replacement product after clinopyroxene (*e.g.* Figures 4.2 & 4.3), and mineral-chemical considerations suggest that hornblende is most closely related to hydrated clinopyroxene. Therefore, *Di* is a measure of both clinopyroxene and hornblende in the metamorphosed rocks of the SLC.

Table 6.5 Part of a correlation matrix for the SLC examining the statistical relationship between $^{147}Sm/^{144}Nd$, ε_{Nd} and other chemical variables at the time of metasomatism. There are very high r-values for a number of important variables involving $^{147}Sm/^{144}Nd$, ε_{Nd} and normative *Di*.

	mg	**SiO_2**	**Al_2O_3**	**Fe_2O_3**	**MgO**	**CaO**	**Na_2O**	**K_2O**	**TiO_2**	**MnO**	**P_2O_5**
$^{147}Sm/^{144}Nd$	0.46	-0.42	**-0.71**	**0.70**	0.55	-0.40	-0.72	-0.45	-0.04	**0.88**	-0.47
$\varepsilon_{Nd0.5}$	-0.19	**0.62**	0.35	-0.56	-0.26	-0.05	0.39	0.26	-0.06	-0.49	0.34
	LOI%	**Nb**	**Zr**	**Y**	**Sr**	**Rb**	**Th**	**Pb**	**Ba**	**Sc**	**Zn**
$^{147}Sm/^{144}Nd$	-0.05	-0.23	-0.26	-0.10	**-0.75**	0.05	0.53	-0.49	**-0.71**	**0.59**	**0.65**
$\varepsilon_{Nd0.5}$	-0.13	0.12	0.16	0.00	0.33	0.06	-0.48	0.05	0.14	-0.54	-0.35
	Cu	**Ni**	**Cr**	**Ce**	**La**	**V**	***Or***	***Ab***	***An***	***Di***	***Hy***
$^{147}Sm/^{144}Nd$	0.44	0.45	0.42	-0.40	-0.32	0.31	-0.45	**-0.72**	**-0.68**	**0.81**	0.56
$\varepsilon_{Nd0.5}$	-0.10	-0.18	0.01	0.16	0.11	-0.25	0.25	0.39	0.30	**-0.88**	0.02
	Ol	***Mt***	***Il***	***Ap***	**$^{143}Nd/^{144}$ Nd**		**Sm**	**Nd**	**$^{147}Sm/^{144}Nd$**		
$^{147}Sm/^{144}Nd$	0.17	-0.03	-0.04	0.36	**-0.67**		-0.28	-0.38	-		
$\varepsilon_{Nd0.5}$	-0.47	-0.06	-0.06	0.09	-		0.17	0.25	**-0.71**		

From these considerations, it is likely that $^{147}Sm/^{144}Nd$ in the protolith was strongly influenced by the modal abundance of clinopyroxene if metamorphism was isochemical. This would have resulted in high ratios in clinopyroxene-dominated cumulates, whereas low $^{147}Sm/^{144}Nd$ would reflect a decreased abundance of clinopyroxene, offset by the greater abundance of plagioclase in the more evolved rocks, as shown by the antithetic relationship between *Di* and *An* + *Ab*.

It is possible that there are particularly strong correlation coefficients between $^{147}Sm/^{144}Nd$, ε_{Nd} and *Di* for a number of petrographic, chemical, and isotopic reasons. These relationships can be considered by reference to three crucial questions:

- 1. Does the modal abundance of the major phases control the relative values of $^{147}Sm/^{144}Nd$ and, if it does, is this a primary or secondary feature?

- 2. If mineralogy does control $^{147}Sm/^{144}Nd$, does it also control the negative array between $^{147}Sm/^{144}Nd$ and ε_{Nd}?

- 3. If modal abundance does not control ε_{Nd}, why are there strong negative correlations between ε_{Nd} and *Di* (and other indices of differentiation), and between $^{147}Sm/^{144}Nd$ and ε_{Nd} (especially when isotopic decay of ^{147}Sm to ^{143}Nd should normally produce a positive trend)?

These questions are fundamental to understanding the process and scale of open-system isotopic exchange in the SLC. In a wider context, they are important because these relationships (correlations) can help to establish to what extent chemical criteria, especially coherent trace-element trends, reflect protolith petrogenesis or systematic control by fluid infiltration metasomatism. Understanding the cause and effect relationships between the geological and chemical variables for the SLC forms the basis of the following discussion. This discussion and the final synthesis draws heavily on key aspects from the 'rejected' reservoir-type models described earlier.

Evidence for decoupled $^{147}Sm/^{144}Nd$ and $^{143}Nd/^{144}Nd$ mobility

Given the strong correlations between ε_{Nd}, bulk composition and mineralogy for the SLC described above, it is possible to reconsider certain components of the open-system isotopic exchange models as described in the general context of Hypothesis B. Figure 6.16 shows the calculated ε_{Nd} parameters for the SLC at 500 Ma, compared with a hypothetical layered complex derived from a CHUR source that has evolved from 2840 to 500 Ma as a series of closed isotopic whole-rock systems. The arrows labelled $\Delta\varepsilon_{Nd(tmet)}$ and $\Delta^{147}Sm/^{144}Nd$ illustrate the end-member changes that would have been required to produce the isotopic characteristics of samples RI22 and RI35 from an initial CHUR-source evolution trajectory. This could be accomplished by internal redistribution dominated by $\Delta^{147}Sm/^{144}Nd$, fluid enhanced diffusion or advection of $^{143}Nd/^{144}Nd$ ($\Delta\varepsilon_{Nd(tmet)}$), or combinations of both. Similar open-system isotope-exchange vectors could be inserted for each of the samples, with a different sense of change for sample groups depending whether they are more or less evolved than the hypothetical CHUR-derived suite.

<u>The relative importance of $\Delta^{147}Sm/^{144}Nd$</u>

It is apparent from Figure 6.16 that the direction of secondary fractionation ($\Delta^{147}Sm/^{144}Nd$) is opposite for low *Di* and high *Di* bulk compositions. However, given the contrasting K_d values for REE in plagioclase as opposed to clinopyroxene & hornblende (*e.g.* McCulloch

& Black, 1984; Faure, 1986, table 12.2; Grauch, 1989; Gruau *et al.*, 1992), such changes would be in the correct direction if Sm and Nd were redistributed in the presence of a fluid and partitioned according to their predicted *D*-values for these whole-rock assemblages. This implies that the mineralogy could have strongly controlled the direction and magnitude of the $\Delta^{147}Sm/^{144}Nd$ term. However, the problem with this is that internal redistribution purely by $\Delta^{147}Sm/^{144}Nd$ would need to be very large for some samples. So much so that there would have to be a complete reversal of the relationship between normative mineralogy and $^{147}Sm/^{144}Nd$ during the protolith to metamorphite transformation. For such a model to apply, the relatively plagioclase rich protolith (high *An* + *Ab* & low ***mg***) would have had to have higher primary $^{147}Sm/^{144}Nd$ than the clinopyroxene-rich protolith (high *Di* & high ***mg***). Such a situation is highly unlikely from what is known of the distribution coefficients and corresponding REE patterns for these minerals (*e.g.* McCulloch & Black, 1984; Faure, 1986, table 12.2; Gruau *et al.*, 1992).

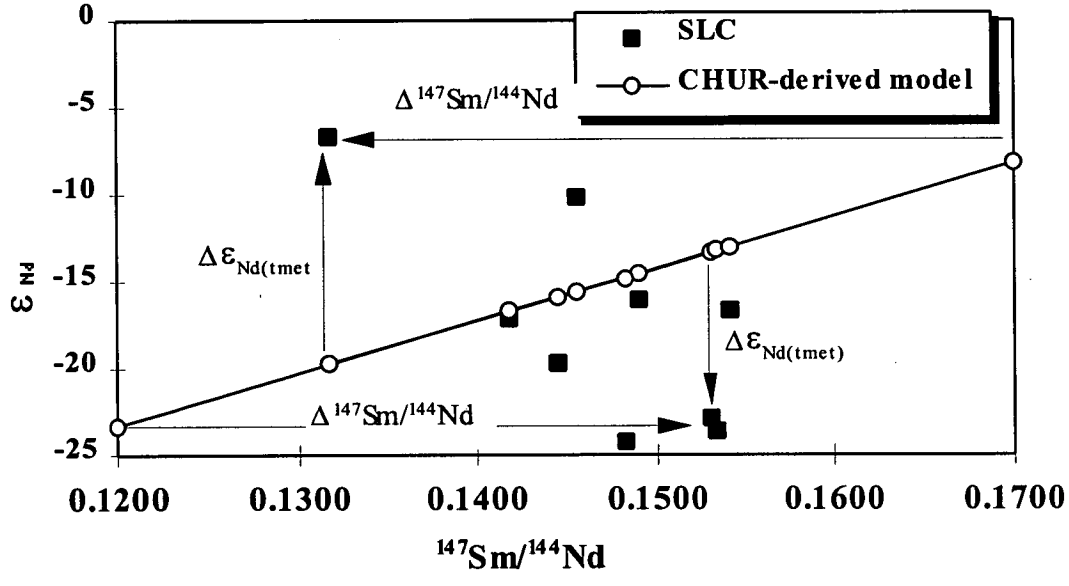

Figure 6.16 Figure illustrating the relative importance of the $\Delta^{147}Sm/^{144}Nd$ and $\Delta^{143}Nd/^{144}Nd$ terms. A CHUR derived model is calculated assuming $\Delta^{147}/^{144}Sm$ only. Note the complete reversal of bulk compositions: the pyroxenites would require very low initial $^{147}Sm/^{144}Nd$, and the plagioclase-bearing leucocratic suites would require very high $^{147}Sm/^{144}Nd$.

Any involvement of clinopyroxene, orthopyroxene or plagioclase during fractional crystallization/accumulation would lead to a relative enrichment in LREE/MREE (hence lower Sm/Nd values) in the more evolved rocks. Different degrees or successive batches of melt extraction could produce a temporal evolution in $^{147}Sm/^{144}Nd$, but there is no obvious reason why this should be correlated with major-element chemistry and mineralogy because

the most significant bulk compositional differences are within gradational layers or units, not between them (see Chapter 3). The only way that *in situ* differentiation could lead to LREE depletion in these gabbroic compositions, would be if REE in the evolving intercumulus liquid were strongly influenced by a LREE-enriched phase that has $K_{dREE>>1}$ and with $K_{dSm<Nd}$, such as apatite (*e.g.* see Faure, 1986; table 12.2). Apatite is present in a variety of SLC compositions, however, it was unlikely to have been an early-formed cumulus or fractionating phase (see Chapter 5). This is illustrated by strong positive correlations between Zr (or Nb) and Y, and a positive corelation between P_2O_5 and REE. There is also a poorly defined antithetic relationship between P_2O_5 and $^{147}Sm/^{144}Nd$, and the highest Nd rocks generally have the lowest Sm/Nd values (*e.g.* RI22 *vs.* RI35).

In conclusion, by far the most plausible explanation for the fractionation of Sm and Nd within the SLC is that the REE patterns shown in Figure 6.5 **are** largely primary features (see Chapter 5). The reason that $^{147}Sm/^{144}Nd$ is strongly correlated with mineralogy (*e.g. Di*), is because REE were fractionated in the magma chamber according to the bulk distribution coefficients of the early-formed minerals during normal fractional-crystallization processes (*cf.* Faure, 1986; table 12.1 & figure 12.1). However, even though the predicted $D_{solid\text{-}fluid}$ values for Sm and Nd in plagioclase- or clinopyroxene-rich rocks would favour $\Delta^{147}Sm/^{144}Nd$ in the directions indicated by Figure 6.16, it is highly unlikely that the ultramafic-mafic protoliths would have originally evolved towards the significantly LREE-depleted compositions needed to account for the very large $\Delta^{147}Sm/^{144}Nd$ required by this end-member model.

In answer to questions 1 and 2 posed in the previous section; modal abundance *does* control $^{147}Sm/^{144}Nd$, and the range of ratios is essentially a primary feature. However, mineralogy *does not* control $\Delta\varepsilon_{Nd}$ or apparent ε_{Nd} values *directly* via the $\Delta^{147}Sm/^{144}Nd$ term in equation 6.4.

The reasons why large values of $\Delta^{147}Sm/^{144}Nd$ are difficult to achieve, and why $^{143}Nd/^{144}Nd$ are likely to be much more responsive during fluid infiltration are discussed in the next section.

<u>The relative importance of $^{143}Nd/^{144}Nd$</u>

The second end-member model outlined in Figure 6.16 is open-system behaviour governed entirely by $\Delta\varepsilon_{Nd(t\text{met})}$. The following discussion builds upon some of the processes described in the earlier section regarding hybrid models. The most important point is that direct mobility of isotopic compositions by fluid-related diffusion or advection is likely to occur

over greater distances than the displacement of concentration profiles (*e.g.* $\Delta^{147}Sm/^{144}Nd$[4]). Key factors that will influence the advection or diffusion distance of an isotopic front and the net exchange (magnitude of $\Delta\varepsilon_{Nd(tmet)}$), are values of time-integrated fluid flux, diffusivity, $D_{solid\text{-}fluid}$ for Nd, and the relative isotopic variability between different rock units in the path of the fluid. Most of these factors are the same as described in Figures 6.10 - 6.13 for isotopic resetting without $\Delta^{147}Sm/^{144}Nd$. The only important difference is the *spatial distribution of isotopically distinct units*, because this will strongly control the 'isotopic potential' between adjacent isotopic systems during fluid infiltration. In this context 'isotopic potential' refers to the relative difference in isotopic composition between adjacent whole-rock systems. The isotopic potential and time-integrated fluid flux are more important to consider than the somewhat arbitrary 'fluid-rock ratio' described by some authors (*e.g.* Gruau *et al.*, 1992). As noted by Spear (1993, p.687), this is because fluid-rock ratios are calculated assuming that 'the infiltrating fluid is an end-member composition, regardless of the equilibrium composition of the rock being infiltrated, and it is very unlikely that a fluid will not equilibrate continuously with its surroundings at the temperatures of metamorphism'. Given that a 'significant' amount of fluid equilibration will occur over relatively short distances, the spatial distribution of isotopically distinct whole-rock systems (high isotopic potentials) with respect to the direction of fluid movement will be *the* crucial factor in determining the direction and magnitude of $\Delta\varepsilon_{Nd(tmet)}$ for each whole-rock system (*i.e.* sample).

A schematic summary of the importance of some of these effects are shown on Figure 6.17. The data for the SLC are currently insufficient to attempt detailed modelling regarding advection distance of isotopic reaction fronts as described by Bickle & McKenzie (1987) and translated by Skelton (1992) and Skelton *et al.* (1996). Nevertheless, the qualitative observations depicted in Figure 6.17 are relevant to the isotopic evolution of the SLC and other high-grade terrains that have experienced retrogression associated with fluid-infiltration (Oliver, 1996, argued that *all* high-grade terrains fall into this category!).

Returning to Figure 6.16, the $\Delta\varepsilon_{Nd(tmet)}$ vector can be reassessed in terms of local-scale $^{143}Nd/^{144}Nd$ mobility. For a suite of rocks with a moderate range of primary $^{147}Sm/^{144}Nd$ (*e.g.* 0.1300 - 0.1600), an overall spread of ε_{Nd} at 500 Ma would be of the order of 15 epsilon units. Theoretically, intermediate $^{147}Sm/^{144}Nd$ values could be displaced to either

[4] This might not be so for the Rb-Sr system because Rb and the LILE are orders or magnitude more mobile that Sr in most circumstances. Sm & Nd, however, are generally much more immobile than Rb and are difficult to fractionate.

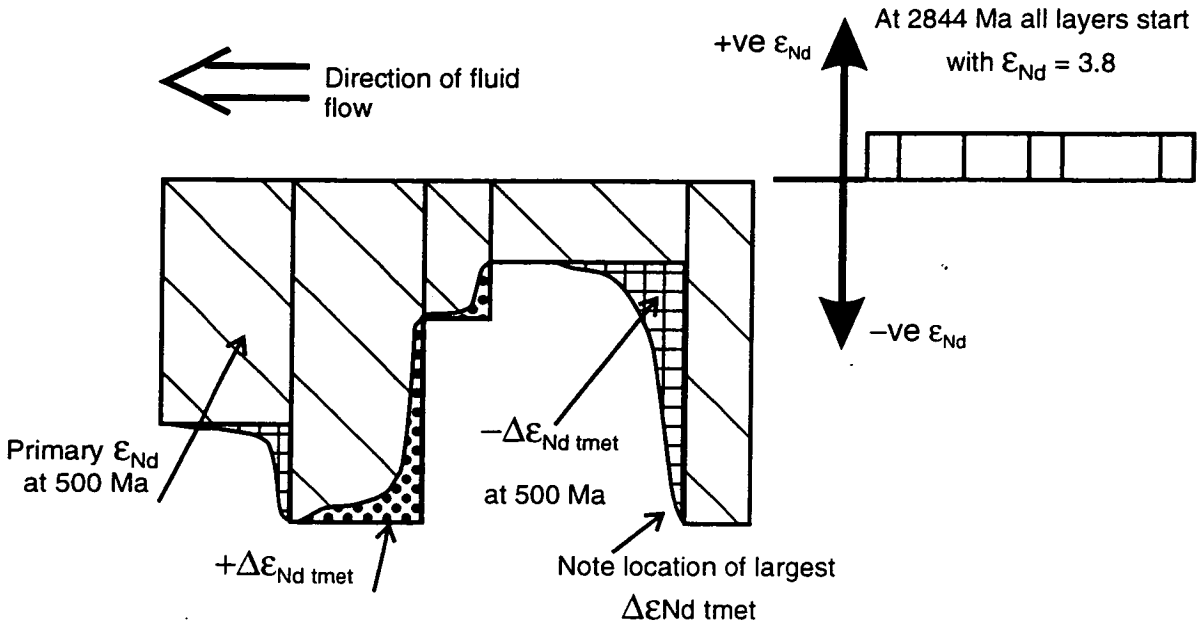

Figure 6.17 Schematic representation of Nd-isotope profiles associated with fluid infiltration in the Rauer Group at 500 Ma. The key feature is that rocks with low $^{147}Sm/^{144}Nd$ (low *Di*) that evolve to very negative ε_{Nd} values with time are effectively only prone to large $\Delta\varepsilon_{Nd(tmet)}$ in one direction, to higher values. the converse is true for rocks with high $^{147}Sm/^{144}Nd$ (high *Di*).

higher or lower $\Delta\varepsilon_{Nd}$, but extreme ratios would be most influenced by significantly different isotopic compositions.

Two well-characterized end-member compositions illustrate the importance of this exchange mechanism. The strongly positive ε_{Nd} sample (RI22) has the largest normative *An* +*Ab*, the lowest *Di* and $^{147}Sm/^{144}Nd$, and its present distribution within the complex is ~ 1 metre from a melagabbroic body with high $^{147}Sm/^{144}Nd$. These features suggest that this whole-rock system would be subject to a large positive $\Delta\varepsilon_{Nd(tmet)}$ by fluid-enhanced diffusion or advection-controlled exchange with less evolved neighbours. Furthermore, because it is one of the most evolved compositions in terms of $^{147}Sm/^{144}Nd$ and ε_{Nd}, it would only be prone to large $\Delta\varepsilon_{Nd}$ in one sense, to positive $\Delta\varepsilon_{Nd(tmet)}$, which when propagated to the crystallization age (Equations 1.9 & 1.10) results in apparent ε_{Nd} that is much greater than CHUR.

By contrast, sample RI35 has high normative *Di*, high $^{147}Sm/^{144}Nd$, and a correspondingly low *An* + *Ab*. It occurs as a large (~5 m^2) pyroxenite pod surrounded by more leucocratic SLC compositions. These features suggest that this whole-rock system would be subject to

negative $\Delta\varepsilon_{Nd(tmet)}$. In a similar way that RI22 is only likely to change strongly in one direction, samples with high $^{147}Sm/^{144}Nd$, such as RI35, would not be strongly influenced by rock types that have similar $^{147}Sm/^{144}Nd$ (hence $^{143}Nd/^{144}Nd$; *cf.* Figure 6.17). In effect, they would only be isotopically susceptible to negative $\Delta\varepsilon_{Nd(tmet)}$.

Returning to the third question posed in the earlier section, there is a link between mineralogy and ε_{Nd}, but it is a third-order relationship. Mineralogy ultimately controlled the primary distribution of $^{147}Sm/^{144}Nd$, which in turn governed the isotopic evolution trajectory for individual whole-rock systems with time (for 2340 Ma). In a heterogeneous isotopic terrane, this effectively created a situation where high or low $^{147}Sm/^{144}Nd$ rocks have the largest isotopic potentials and are, in turn, only prone to large changes away from their own end-member compositions. Hence the statistically valid negative correlation between *Di* and ε_{Nd}.

A re-examination of the field relations

Clearly there is a need to re-examine the field relations and sampling strategy adopted here, both in terms of sample selection in the field for the SLC as a whole, and the rationale for selecting samples for detailed analysis on the basis of geochemistry. Table 6.6 summarises the field relations for each of the samples analysed for Nd isotopes. A number of criteria were considered when selecting samples which introduced a strong sampling bias aimed at recovering igneous protolith chemistry. The most important consequences of this sampling strategy relate to the proximity of samples to adjacent rock types of high isotopic potential (local isotopic sinks).

Most of the samples described in Chapter 5 were sampled >0.5 m from moderately different SLC bulk compositions (as seen in modal abundances), >5 m from mafic dykes (greater distances from the large late mafic dykes), and at a minimum distance of 5-10 metres from intrusive TG sheets. Although these observations introduce further complexity into the open-system model, they also provide constraints on the length-scale of chemical and isotopic movement within the complex and explain the overall bias in the data towards negative apparent ε_{Nd}.

There are two inter-related reasons why a significant number of samples have low ε_{Nd} values. A number of such samples were collected from an area approximately 5-10 metres from a metre-scale high-grade shear zone/TG sheet. The TG are usually intimately related to these ductile structures (see Chapter 3), and it is apparent that metre-wide shear zones commonly developed as a consequence of the ductility contrast between tonalite and SLC.

Isotopically, these zones represent areas of high isotopic potential because they contain a distinct isotopic sink (the TG with low ε_{Nd}) and would also have had relatively high time-integrated fluid fluxes. Therefore, it is possible that intrusive TG sheets and associated high-grade SZs influenced the isotopic composition of SLC at distances greater than 5 metres during retrogression.

Table 6.6 Summary of field characteristics for the SLC Nd-isotope dataset. Field relations are described in relation to other bulk compositions which could potentially have evolved as distinct isotopic sinks.

Sample	$\Delta\varepsilon_{Nd}$ req'd	Field setting
RI10	-0.43	Foliated SLC *ca.* 1 m from UM pod; >10m from tonalite.
RI11	-1.50	Relatively undeformed coarse-grained SLC surrounded by SLC of similar composition.
RI19	-3.75	Layered part of complex near margin (<15 m), between TTG shear zone and margin.
RI22	+13.09	Relatively felsic SLC; *ca.* 1 m from mafic SLC.
RI23	+5.54	Slightly higher colour index than above, sampled nearby.
RI30	-9.60	Relatively felsic but with high Di. (Low colour index because of high normative Opx+Ol).
RI33	-10.42	>1 m < 10 m from tonalite,~1 m away from a SZ.
RI35	-9.50	UM gabbro >1 m but <10m from TTG.
RI108	-3.57	UM Cpx-rich pod <5 m wide contained within intermediate SLC.

These observations and those summarized in Table 6.6 can be used to constrain the relative displacement distances for Nd-isotopic fronts and REE profiles.

Constraints on the scale of $^{143}Nd/^{144}Nd$ mobility

As demonstrated in the earlier discussion and Figures 6.10 - 6.13, if internal isotopic homogenisation occurred on outcrop scales (10-200 m), there would be a positive correlation on an isochron diagram (described for the TTLC in the next section). Alternatively, if redistribution occurred at <1 metre scales, as concluded by Cohen *et al.* (1992) and (most) others, I wouldn't need to discuss any of this section at all. Unfortunately, it is most likely that $^{143}Nd/^{144}Nd$ mobility occurred on the 1-10 metre-scale in the SLC - the same scale as the sampling strategy adopted here.

Constraints on REE mobility

The relative contribution of $\Delta^{147}Sm/^{144}Nd$ to either of the samples described in detail above (RI35 & RI22), or indeed any of the SLC MT, cannot be directly determined. Although secondary fractionation is considered here to be a minor contribution, it is possible that

there were small changes in Sm/Nd and other REE. If an average $^{147}Sm/^{144}Nd$ value of 0.1450 for the complex as a whole is taken, and assuming that during *in situ* fractionation or accumulation only 'normal' trends of LREE enrichment were possible, most samples could only have changed by <5 %. Even samples at the extreme end of the $^{147}Sm/^{144}Nd$ range (*e.g.* RI22 & RI35) could only have changed by < 10%. These are probably quite realistic upper estimates for the extent of secondary fractionation for samples collected from this complex. The implications for REE and trace-element signatures can be qualitatively assessed on this basis, and are summarized below in point form.

- The widespread Nd-isotopic disturbance in the SLC suggests caution when viewing any of the major-element, trace-element or REE data. However, for the REE at least, it is likely that the degree of secondary fractionation is small, and is probably about the same as the analytical uncertainty inherent in the ICP-AES technique (~10%).

- Given that many bivariate major- and trace-element variation diagrams (Chapter 5) are very strongly correlated, it is likely that most elements other than the highly incompatible LILE were *not* significantly altered during metamorphism. However, because metasomatism could have *systematically* altered protolith chemistry thereby introducing trends on such diagrams, as described earlier in this discussion, once again the data should be treated with caution. As a further general point regarding the trace-element characteristics of the SLC a whole, the models described at this beginning of this discussion that consider the effects of simple mixing become relevant for the displacement of concentration profiles. In brief, evolved rocks with high trace-element or REE concentrations are less susceptible to large metasomatic changes on mass-balance grounds than are low-abundance samples. This is a feature that is exemplified by reference to the TTLC in Section 6.6 below.

6.5.5 Summary and conclusions

Nd-isotope data for the SLC define a negative trend on an isochron diagram that cannot be explained by fractional crystallization or assimilation processes. ε_{Nd} calculated for each sample on the basis of an independently-constrained crystallization age of 2840 Ma indicates that the complex has a range of Nd-isotopic compositions that spans almost 24 epsilon units. This very large spread of values is attributed to open-system isotopic exchange during the 500 Ma metamorphic event that affected the Rauer Group.

Although many isotope geochemists assume that Nd is not normally mobile at scales greater than large samples (*i.e.* dm scales), a number of studies have found evidence for disturbance to the Nd system during metamorphism (*e.g.* Black & co-workers and Gruau & co-workers). They attributed this to secondary fractionation of Sm/Nd, but were unable to constrain the

underlying petrological or chemical mechanism that ultimately controlled changes in apparent ε_{Nd}.

However, the Nd-isotope data obtained for the SLC cannot be explained by secondary fractionation of Sm/Nd, and direct redistribution of $^{143}Nd/^{144}Nd$ isotopes is favoured instead. An important factor is the length of time involved between crust accretion and fluid-related retrograde metamorphism. The main factor that was responsible for the large spread in ε_{Nd} and a negative $^{147}Sm/^{144}Nd$ *vs.* ε_{Nd} array was the spatial distribution of different bulk compositions during fluid infiltration. During the 2340 m.y. period between protolith formation and isotopic disturbance, adjacent isotopic systems evolved to very different isotopic compositions. In effect, these became sinks of high isotopic potential that were capable of isotopic exchange during metamorphism.

The results from this study are remarkable in that very large shifts in ε_{Nd} appear to have been possible *without* associated major-element, trace-element of REE metasomatism. Isotopic perturbation appears to have been possible largely by fluid enhanced diffusion and/or advection.

A re-examination of the field relations indicates that isotopic transport distances for Nd isotopes in the SLC were of the order 1-10 metres, and that large-scale isotopic homogenisation did not occur. Although minor displacement of concentration profiles and $^{147}Sm/^{144}Nd$ *may* have occurred, it is likely that the distances and hence degree of change were up to several orders of magnitude less than the corresponding isotopic displacement.

The implications of this study for the geochemical evolution of the SLC are described at the end of this chapter and are addressed in the next chapter where petrographic, geochemical and isotopic data are integrated into a regional synthesis. The wider implications of this study regarding the behaviour of Nd isotopes during metamorphism in other Archaean high-grade terranes, are discussed in the final chapter (Part 4).

6.6 Radiogenic isotope geochemistry for the TTLC

6.6.1 Objectives and strategy for the TTLC

Largely because of the financial and time limitations associated with radiogenic isotope measurement, only a pilot study of the TTLC has been undertaken. Four samples have been analysed for Sr- and Nd-isotope ratios. The results for Nd are quite poor, although they are

Table 6.7 Sr- and Nd-isotope data and calculated parameters for the TTLC.

Sample	RI47	RI56	RI59	RI63
Sr (ppm)	27.4	157.0	22.1	28.3
Rb (ppm)	2.9	3.2	1.4	9.6
Rb/Sr	0.1058	0.0204	0.0633	0.3392
$^{87}Rb/^{86}Sr$	0.3064	0.0590	0.1833	0.9885
$^{87}Sr/^{86}Sr$	.713799	0.714821	0.707877	0.781048
Err (2 SE)	31	33	84	47
I_{Sr} at 2.84	0.701190	0.712393	0.700334	0.740369
$\varepsilon_{Sr2.84}$	-0.2	159.6	-12.8	558.8
T_{BSE}	2.84×10^9	-3.47×10^{10}	2.24×10^9	5.71×10^9
$^{143}Nd/^{144}Nd$	0.511705	0.511665	0.511582	0.511554
Err (2σ)	14	12	16	14
$^{147}Sm/^{144}Nd$	0.1392	0.1244	0.0995	0.1413
Err (2σ)	0.0051	0.0000	0.0000	0.0102
$\varepsilon_{Nd2.84}$	2.84	7.50	15.05	-0.89
Err (2σ)	1.61	0.24	0.31	3.50
T_{CHUR}	2.46×10^9	2.04×10^9	1.65×10^9	2.96×10^9
T_{DM}	2.87×10^9	2.46×10^9	2.04×10^9	3.26×10^9

tantalising all the same. All the results and calculated parameters are summarized below in Table 6.7.

6.6.2 Rb-Sr isotopes

From the arguments developed for the SLC regarding the possible mechanisms for open-system isotopic exchange during the 500 Ma event, it is not surprising to find that the Rb-Sr system in the TTLC was disturbed. The TTLC is generally finer-grained than the SLC and concentrations of the incompatible-elements are significantly lower than either the SLC or more importantly, than the surrounding felsic orthogneisses (TG).

Although there are only 4 Sr-isotope ratio analyses, it is readily apparent that they do not define an isochron of any age (Figure 6.18). Moreover, calculated model ages for two samples, RI 56 & RI 63 are respectively younger and older than the age of the earth. The other two samples yield Precambrian model ages, but it is unlikely that these ages are of chronological significance.

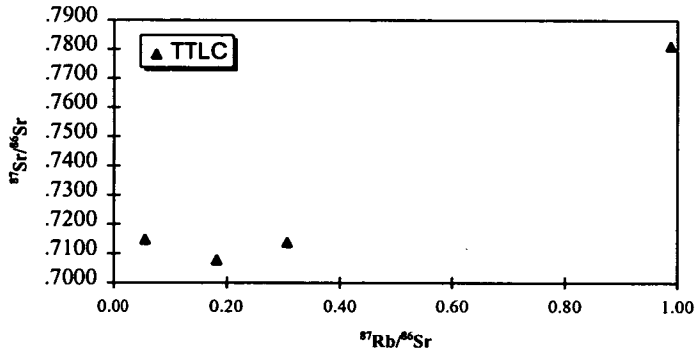

Figure 6.18 Rb-Sr isochron diagram for the TTLC. Note that all samples have low Rb/Sr and that the datapoints do not define an isochron/errorchron of any age (even two-point 'isochrons', calculations not shown).

6.6.2 Sm-Nd isotopes

Only four samples of the TTLC have been analysed for Nd-isotope ratios. The precision for two samples (RI 56 & RI 59) is excellent (Table 6.8), but unfortunately results for the other two samples (RI 47 & RI 63) are less impressive because they have relatively large analytical errors for $^{147}Sm/^{144}Nd$. The error on this ratio stems from the Sm determination (see Appendix 1), and is particularly acute for sample RI 63. This sample failed twice using the isotope dilution technique, and the Sm abundance has been determined by ICP-AES (corrected to ID data).

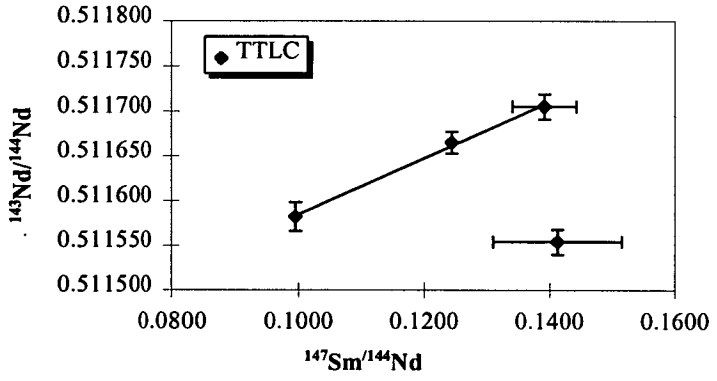

Figure 6.19 Sm-Nd isochron diagram for the TTLC. Note that there is a restricted range of Sm/Nd. The sample that does not correlate with the others was determined by ICP-AES and therefore is not strictly comparable with the other samples.

Results

Of the four data points (Figure 6.19), three points lie on an 'isochron' that defines a whole-rock age of 485 ± 93 Ma (MSWD 0.4). The fourth sample, RI 63, is clearly distinct from the others. It is possible that this is because Sm/Nd in this sample was determined by ICP-AES and not ID-MS.

Although there is a very low MSWD for the three samples, this can in part be attributed to the relatively large error in $^{147}Sm/^{144}Nd$ for sample RI 47, and also because there are a limited number of samples. Hence, such a three point isochron should be treated with caution. Nevertheless, the *ca.* 500 Ma age corresponds to an important metamorphic event in the region and is the most likely event to be associated with isotopic resetting (see previous discussion, section 6.5). The retrieval of this age is surely more than coincidence.

Discussion and conclusions

The Sr- and Nd-isotope data for the TTLC are similar to the SLC in that they do not retain protolith signatures and were clearly disturbed during metamorphism. This result is perhaps not surprising for the Sr-system, but as with the SLC, the degree of Nd-isotope mobility is significantly greater than expected. *If* the Sm-Nd data for the TTLC do reflect isotopic re-equilibration at *ca.* 500 Ma, the length-scale of homogenisation was potentially more than 10 metres (discussed further below).

6.7 Summary and conclusions

The isotopic character of the Archaean Rauer Group is dominated by variable mobilisation and partial resetting during the 500 Ma fluid-infiltration event. Oxygen-isotope ratios appear to be least perturbed and $\delta^{18}O$ values for the SLC are very close to estimates of the mantle reservoir and are interpreted to approximately equate to those of the protolith. U-Pb zircon systems, however, was variably reset at *ca.* 500 Ma. Large igneous zircons in a late-stage differentiate of the SLC have core regions that retain Archaean crystallization ages of *ca.* 2844 ± 6 Ma. Irregular rims around such cores have variably reset ages that are either discordant between 2844 ± 6 Ma and *ca.* 500 Ma, or are concordant at about 500 Ma. Similarly, Sr- and Nd-isotope systems were variably reset at this time. Perhaps not surprisingly, the Rb-Sr system was pervasively perturbed and measured Sr-isotope ratios or calculated model parameters do not reflect those of protoliths. The Sm-Nd system, by comparison, is usually regarded as being amongst the most robust during crustal metamorphism. Large samples were collected from the SLC, EMD and TTLC that might normally be expected to retain isotopic compositions not too dissimilar to their protolith precursors. However, the SLC (and EMD) have a range of ε_{Nd} that vary between 13.0 and -10.6, spanning almost 24 epsilon units. This remarkable range of isotopic compositions occurs within an area that is less than 200 x 500 m^2 and is more variable than the ε_{Nd} values reported for most Archaean cratons. It is even more remarkable that such profound disturbance to the system appears to have occurred by mobility of $^{143}Nd/^{144}Nd$ (at length-

scales of 1 to 10 m), but without significant REE metasomatism, and it is most likely that $^{147}Sm/^{144}Nd$ and REE patterns for the SLC (Figure 5.5) are not significantly different from those of the protolith.

The lengthy discussion in Section 6.5 demonstrates that assimilation of older crust is not a viable mechanism capable of explaining the observed ε_{Nd} *vs.* $^{147}Sm/^{144}Nd$ isotopic array, although some degree of crustal contamination cannot be ruled out. Since most recent accounts of Nd-isotope behaviour in Archaean high-grade terranes have not been specifically tested for closed system isotopic evolution, a large number of possible open-system processes are considered in detail in this study. Of the few published studies that concluded that the Nd-system *is* prone to perturbation during metamorphism, all have attempted to explain open-system behaviour in terms of reservoir-type exchanges dominated by secondary fractionation of $^{147}Sm/^{144}Nd$ (*e.g.* Black and co-workers & Gruau and co-workers). However, from the arguements developed to explain the SLC data, and from what is known from other studies about the relative advection/diffusion distances of isotopic compositions *versus* concentration profiles during fluid infiltration, it is likely that the dominant mechanism involves mobility of $^{143}Nd/^{144}Nd$ ($\Delta\varepsilon_{Nd/met}$) instead. Open-system Nd-isotope exchange via a mechanism similar to that established for oxygen-isotope front movement is envisaged as a suitable process-analogue.

For the TTLC, preliminary Nd-isotope results tentatively imply homogenisation of $^{143}Nd/^{144}Nd$ at *ca.* 500 Ma. However, because this high-Mg complex has much lower REE concentrations and variable LREE patterns, some degree of secondary fractionation of $^{147}Sm/^{144}Nd$ is also likely. These bulk compositional features, the generally finer-grained nature of this complex, and an overall lack of relict mineralogy or textures compared with the SLC, possibly rendered the TTLC much more susceptible to isotopic perturbation and ultimately to homogenisation. It is possible that isotopic disequilibrium dominates in the SLC because of the partial preservation of igneous mineralogy and coarse-grained textures with relict phases, especially relatively inert accessory phases, possibly inhibiting complete homogenisation even at small-scales. However, further analyses of well-characterised samples from both complexes are required to confirm these observations and to develop these ideas further.

As a final concluding comment, there are two key factors that determined the behaviour of the various isotopic systems during the 500 Ma fluid-infiltration event. This first was the primary bulk composition and relationship of individual samples relative to surrounding gneisses at 1- to 10 metre-scales during fluid infiltration. The second factor was the length

of time between protolith formation and fluid infiltration. For the Sm-Nd system in the SLC, small primary differences in $^{147}Sm/^{144}Nd$ enabled adjacent whole-rock systems to evolve along different Nd-isotope evolution trajectories for 2300 m.y. from 2840 Ma to 500 Ma. These adjacent areas therefore evolved into markedly different sinks with high isotopic potential. Enhanced fluid activity at 500 Ma enabled communication of $^{143}Nd/^{144}Nd$ between these sinks with profound results when back-calculated to the age of crystallization as determined by the U-Pb zircon technique. It is likely that similar spatial and temporal variables influenced the behaviour of the Rb-Sr system at 500 Ma. However, because LILE (hence Rb) are highly mobile during metamorphism, much more than Sr, $^{87}Rb/^{86}Sr$ are probably not even close to their protolith values. By comparison with the radiogenic-isotope systems, oxygen-isotope ratios are not altered by time-dependent parent-daughter isotope decay schemes. Assuming that the SLC oxygen-isotope ratios were mobile to some extent, it is likely that they would only have exchanged with adjacent SLC whole-rock systems, given the qualitative textural observations for relatively low time-integrated fluid fluxes. Hence, $\delta^{18}O$ values for the SLC are probably not much different to those of the protolith.

The observations and conclusions presented in this chapter are developed further in the next chapter that considers possible models for the petrogenetic evolution of the Archaean Rauer Group. The wider implications from the study are discussed in the final chapter, in Part 4.

Chapter 7

The origin and evolution of the Torckler-Tango and Scherbinina Layered Complexes

7.1 Introduction

Detailed accounts of the geological and geochemical evolution of the Scherbinina Layered Complex (SLC), Early Mafic Dykes (EMD) and Torckler-Tango Layered Complex (TTLC) are described in Chapters 3 to 6. The *specific objectives* outlined in Chapter 2 have been described according to the originally proposed phases of study, and comprise *fieldwork*, *petrography and mineral chemistry*, and *geochemistry and isotopic analysis*. The final phase of study in the Rauer Group, *data integration*, is described in this chapter.

The following section (Section 7.2) summarises what advances have been made in the Rauer Group during the course of this study by comparing the SLC, EMD and TTLC. Section 7.2 also outlines a discussion of some of the implications for protolith petrogenesis. The following section (Section 7.3) reassess the *working hypotheses* proposed in Chapter 5 incorporating the conclusions from the isotope study described in Chapter 6. In brief, I noted in Chapter 5 that the SLC and EMD are similar to E-MORB, although features such as more enriched LILE and LREE, and negative Nb anomalies could be attributed to a number of processes. The TTLC, by contrast, is geochemically distinct and appears to share many of the features that are characteristic of modern boninites. However, many diagnostic trace-element characteristics are similar to the Rauer Group felsic crust and as noted in Chapter 5, it is difficult to distinguish between the effects of crustal contamination and source enrichment on trace-element grounds alone. Since the main conclusion from Chapter 6 was that Nd and Sr isotopes were significantly perturbed during metamorphism, in section 7.3 I outline further attempts to distinguish between the two main enrichment models, crustal contamination and source enrichment, without the use of radiogenic isotopes.

The final section in this chapter (Section 7.4) discusses and concludes what can reasonably be deduced about the origin and evolution of the SLC, EMD and TTLC. In this section I also propose a tentative testable tectonomagmatic model that may explain the origin and evolution of the Archaean Rauer Group. However, it should be appreciated that many of the

conclusions presented here are based on a number of fundamental assumptions regarding the interpretation of trace-element signatures in metamorphosed cumulates (discussed in Chapter 1). For these reasons, all the models proposed here should be viewed as tentative rather than definitive.

7.2 A summary and critical appraisal of the SLC, EMD and TTLC

7.2.1 Similarities and differences between the SLC, EMD, and TTLC

The SLC, EMD, and TTLC have a number of important similarities and differences. These similarities and differences primarily relate to bulk composition, which in turn influenced the way that protoliths responded mechanically and chemically during metamorphism and deformation. Since the manner in which protoliths behave during metamorphism and deformation potentially affects interpretations of origin and chemical evolution, a review of the similarities and differences of the SLC, EMD and TTLC is presented here.

The similarities include:

- ***Relict igneous features.*** The SLC, TTLC and EMD all retain relict igneous features.

- ***Response to deformation.*** During high-grade deformation, the layered complexes behaved as competent components relative to the surrounding felsic orthogneisses. This means that the complexes tended to boudinage rather than flow, and the finite strain within boudins is typically much less than in the surrounding areas. Therefore, the complexes can now be viewed as low-strain windows that retain a much more comprehensive record of the geological evolution of the Rauer Group than can be deduced from the surrounding gneisses. EMD that are contained within the SLC also enjoyed enhanced preservation, although originally discordant dyke relationships within the Scherbinina Island mega-boudin become progressively transposed toward the margins of the complex.

- ***Mineralogy.*** The SLC, EMD, and TTLC all have assemblages that dominantly comprise Cpx - Plag - Opx - Mt/Ilm - Apatite ± Hbl ± Biot ± accessory phases. The SLC also has minor Kspar ± Grt, and some EMD also have minor Grt (not the samples studied geochemically).

- ***Age.*** The SLC, EMD, and TTLC are thought to be of Archaean age based directly on U-Pb zircon dating or, indirectly, from cross-cutting relationships and extrapolation from dated lithologies.

- ***Deformation history.*** The SLC and TTLC experienced two major folding episodes (F_1 & F_2) prior to intrusion by tonalitic gneisses at *ca.* 2800 Ma. Some EMD intruded after F_1 but before F_2, others intruded after F_2 but before intrusion of the *ca.* 2800 Ma tonalite. All Archaean mafic gneiss units are inferred to have experienced a common deformation and metamorphic history

after intrusion of the *ca.* 2800 Ma tonalites, although regional variations in metamorphic grade or deformation intensity were likely (*e.g.* Harley, 1988; Sims *et al.*, 1994).

Important differences include:

- ***Bulk composition.*** The SLC and EMD are Fe-rich and have moderate compatible-element (CE[1]) abundances and enriched incompatible-element (IE) abundances relative to MORB, whereas the TTLC is a high-Mg suite that has high CE but very low IE abundances.

- ***Texture, mineralogy and mineralogical response to metamorphism and deformation.*** Although both complexes have been recrystallized at grain scales, the much coarser-grained SLC has relict textural domains that define pigeonite, ternary feldspar, and cm-scale subophitic and intergranular textures. The TTLC is medium grained and is almost entirely recrystallized to a granoblastic to lobate Cpx - Opx - Plag texture. Preservation of primary mineralogy in the TTLC is confined to relatively uncommon bronzite phenocrysts that are preserved in some websterite horizons.

- ***Geochemical and isotopic response to metamorphism.*** Most major element and trace elements are probably not too dissimilar from those of the protolith for all three suites (SLC, EMD & TTLC). The exceptions appear to be confined to the LILE which appear to have been variably redistributed during metamorphism. However, the degree of open-system behaviour is different between the SLC and TTLC. For example, very low abundances of Nb in the TTLC mean that even a small addition of Nb during fluid infiltration may have had a very large effect on Nb concentrations and especially ratios involving Nb. Differences are attributed to bulk composition and grainsize. Similar fluid interaction with the SLC or EMD would have proportionally much less influence because fluid composition would have been buffered to a greater extent. The bulk compositional tendency to acquire elements by net transfer from surrounding rocks would have been assisted by the generally finer-grained nature of the TTLC because finer-grained rocks effectively have a larger surface area that is capable of reacting with a fluid. Differences in bulk composition and grain size also influenced the relative degree or length-scale of Nd-isotope resetting. For instance, the SLC has partially reset Nd isotopes at length-scales of 1-10 metres; whereas Nd isotopes appear to have completely homogenised in the TTLC at similar or greater length-scales during the *ca.* 500 Ma fluid infiltration event.

- ***Crystal fractionation histories.*** The SLC and EMD are both Fe-tholeiites, but have chemical differences that may be partly explained by different fractionation paths. The importance of pyroxene (orthopyroxene + pigeonite and/or augite) fractionation in the SLC is apparent from geochemical variation diagrams and petrographic observations. The presence of primary olivine in the SLC or any of the mafic rocks in the Rauer Group cannot be determined conclusively from the data presented in this study. However, the absence of olivine in ultramafic compositions in the SLC implies that it probably was not a major early-formed cumulus phase. The EMD, by contrast, appear to lie on a common fractional crystallization path that may have been produced by early

[1] Compatible and incompatible in this context loosely refers to D-values > or < 1 (respectively) for a typical garnet lherzolite.

fractional crystallization of olivine followed by plagioclase + clinopyroxene. In this respect the EMD are similar to most continental tholeiites. Petrographic observations, semi-quantitative thermobarometry, circumstantial evidence from oxygen isotopes, and the interpretation that pyroxenes were the dominant fractionating phases rather than olivine, all imply that the SLC was emplaced at considerable depth, probably in the middle to lower crust. The EMD, by analogy with continental tholeiite fractionation trends described from elsewhere (*e.g.* Wilson, 1989), appear to have been modified by low-pressure fractionation. By contrast with both the SLC and EMD, the high-Mg, high CE abundances and low IE abundances that characterise the TTLC imply derivation by large degree partial melting of a mantle source[2]. Crystal fractionation dominated by early orthopyroxene formation is indicated by the presence of abundant bronzite phenocrysts in some basal websterite layers. Early plagioclase formation, possibly accumulating by flotation to the tops of layers, is indicated by the distribution of major element and trace elements within layers. Clinopyroxene probably entered relatively late. As with the SLC, the absence or presence of olivine cannot be established for certain, although high normative *Hy,* low normative *Ol*, and a trend of decreasing SiO_2 with falling ***mg***, all strongly indicate the predominance of orthopyroxene fractionation rather than olivine.

Limitations to interpreting the nature of protolith geochemistry

There are two main limitations that restrict the use of whole-rock geochemistry to constraining the nature of protolith forming processes in the suites examined in this study. The first limitation concerns the cumulate nature of the SLC and TTLC and, as described in Chapters 1 and 5, geochemical techniques that assume liquid compositions should be viewed critically. The second limitation concerns element mobility during metamorphism, which is difficult to establish in a regional geochemical study without specifically designing a strategy to determine which elements are mobile and on what scale mobility takes place. Geochemical signatures from the SLC are probably more robust than in the TTLC although, qualitatively at least, most elements appear to be broadly coherent for both suites. Nevertheless, interpretations or techniques that rely heavily upon isochemical metamorphism should be avoided or viewed critically.

The most important discovery from this study is that Nd isotopes did not evolve as closed systems even though the SLC, EMD, and TTLC samples all have dominantly anhydrous assemblages and relatively well-preserved igneous features compared with *most* Archaean orthogneisses (*e.g.* Bennett *et al.*, 1993; Bowring & Housh, 1995). Therefore, initial Nd-isotope ratios in the Rauer Group cannot be interpreted in terms of protolith petrogenesis

[2] High-***mg***, CE and low IE when compared with the SLC are for similar modal mineralogies. It is unlikely that these differences are entirely due to cumulate processes, and differences in the composition of primary liquids is implied.

(*cf.* Sheraton *et al.*, 1984), and it is likely that the same caveat applies to many other polymetamorphic orthogneisses (discussed in a wider context in Chapter 13).

The next section documents my attempts to constrain protolith petrogenesis on the basis of all the aforementioned *similarities*, *differences* and *limitations*.

7.3 Constraints on protolith origin

Major- and trace-element characteristics of the SLC, EMD, and TTLC are quite distinct despite similar modal (metamorphic) mineralogies. These chemical differences are thought to reflect separate magmatic histories, involving variables such as source composition, melt-generation processes, crystal fractionation paths and element mobility. The latter two variables were reviewed in the previous section, and are discussed at length in Chapters 3 to 6. The next two sections discuss possible source reservoirs and melting processes that may have been involved in the production of the SLC, EMD, and TTLC. The models are kept simple, and detailed calculations of partial-melting histories, possible residual mineralogies, cumulate-liquid ratios, or melt-migration pathways, are not considered in this study because the rock types involved do not lend themselves to such modelling.

7.3.1 Problems associated with 'fingerprinting' source reservoirs and processes

One of the *wider objectives* (Chapters 1 & 2) of this study is to ascertain whether Archaean mafic suites in the Rauer Group are reworked equivalents of Archaean crust in the adjacent Vestfold Hills. However, observations from modern magmatic centres indicate that many unrelated mafic suites are broadly similar in chemistry or undergo common fractionation histories (*e.g.* Paraná and Columbia River Continental Flood Basalts (CFBs), Cox, 1980). Conversely, markedly different rocks types can be produced in the same tectonomagmatic setting or event, even within the same volcanic centre, (*e.g.* tholeiite - calc-alkaline - high-K calc-alkaline & shoshonite lavas of the Aeolian Arc; Francalanci, 1993). Therefore, the approach adopted in this study has been process-oriented wherever possible. Although, as described above, the main difficulty with this approach is that relatively similar geochemical signatures can be produced by different processes (*e.g.* the similarity between island-arc volcanics and CFBs, Thompson *et al.*, 1983). These problems are readily apparent when comparing the SLC, EMD and TTLC. Nevertheless, *if* the relatively local effects of crystal fractionation/accumulation, assimilation, and metamorphism can be distinguished from more fundamental source signatures, then there may be a much more robust means to determine which suites, if any, are related.

A number of observations of the chemistry are similar for all three suites, such as LREE and LILE enrichment relative to HREE and HFSE. The main difficulty is determining where the enrichment process took place: in the continental crust through assimilation or metasomatism; in the mantle wedge above a subduction zone; or directly from subcontinental lithosphere (also ultimately subduction derived). These problems are well recognised and are not unique to this study, and were considered by Thompson *et al.* (1983, p. 173) who posed two questions:

- How may continental flood basalts (CFB) be discriminated from the products of subduction-related magmatism?

- Is it easy to distinguish chemically between CFB and subduction-related basalts?

The answer to question 2 proved relatively straightforward; it is *extremely* hard to tell the two groups apart. This observation is particularly true when LILE, and Sr and Nd isotopes cannot be relied upon to distinguish between reservoirs such as the continental crust and the subcontinental lithosphere (*cf.* Hawkesworth & Norry, 1983, and references therein). Consequently, the answer to the first question is rather more involved and provides the topic of the following discussion.

7.3.2 Interpretation of source and process: constraints on tectonomagmatic environment

In order to assess the origin and evolution of the Rauer Group mafic rocks further, modified MORB-normalized incompatible-element (IE) diagrams for the SLC, EMD and TTLC are presented in Figure 7.1a-c. Trace-element characteristics are then considered further by examination of various trace-element discrimination diagrams (TEDDs) that are thought to be relatively robust to the potentially spurious effects of cumulate processes and element mobility (as described in Section 1.4.3). The rationale for the approach adopted here is described in Chapter 1 and is largely based on the assumption that IE abundances may change by crystal fractionation and accumulation, but IE ratios (*e.g.* MORB-normalized IE patterns) will largely reflect those of the trapped liquid and may (with care) elucidate the source or melt-generation process.

A brief description and interpretation of MORB-normalized IE diagrams and TEDDs

- ***MORB-normalized incompatible element diagrams (Figure 7.1a-c).*** A key feature of the SLC, EMD, and TTLC is enrichment in LREE and LILE relative to HREE and HFSE. The SLC differs from the EMD in the degree of enrichment in LREE and LILE. Most elements in the SLC plot between E-MORB and the Rauer Group felsic crust, although it is interesting to note that both SLC and EMD have very high Th and Pb concentrations.

- ***Zr/Y - Ti/Y (Figure 7.2).*** The SLC, EMD, TTLC and representatives of the Rauer Group felsic crust plot in the *plate-margin basalts* group. East Greenland (#KF13A) plots close to the dykes and near to the majority of the SLC MT. High Ti/Y for some SLC rocks probably relate to ilmenite accumulation (see Section 1.4.3). TTLC plots in a tight cluster well-within the *plate-margin basalts* field and away from the crust.

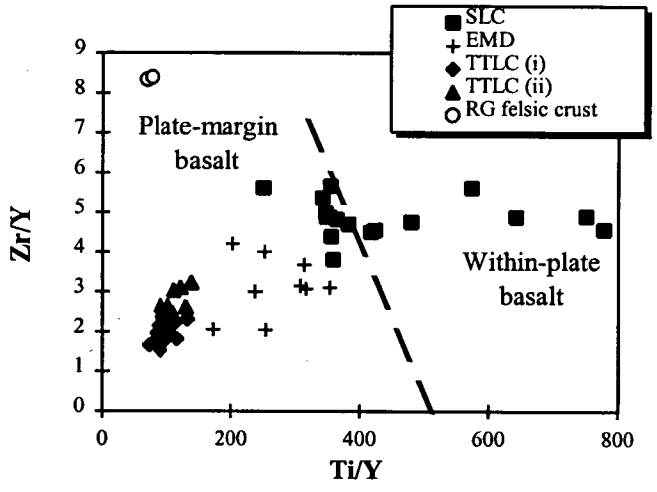

Figure 7.2 Zr/Y - Ti/Y TEDD for basalts showing the fields of *within-plate basalts* and *plate-margin basalts* (after Pearce & Gale, 1977)

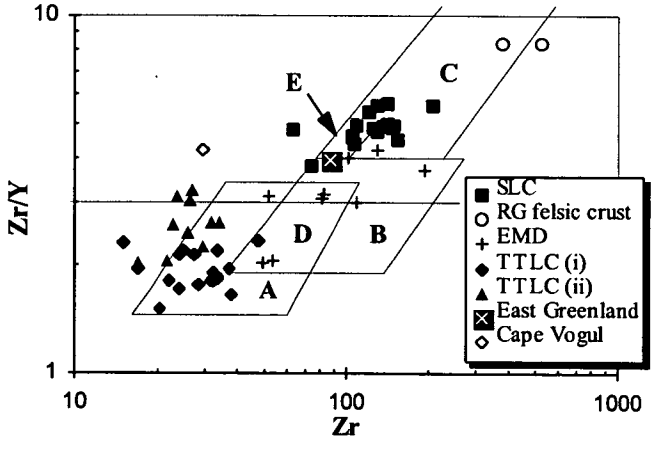

Figure 7.3 Zr/Y - Zr TEDD for basalts. A = *volcanic-arc basalts*; B = *MORB*; C = *within-plate basalts*; D = *MORB + volcanic-arc basalts*; E = *MORB + within-plate basalts* (after Pearce & Norry, 1979). The Zr/Y - Y TEDD has also been used to discriminate between *continental arc* (high Zr & Zr/Y) and *oceanic arc* (low Zr & Zr/Y). The divide is at Zr/Y = 3 (shown).

- ***Zr/Y - Zr (Figure 7.3).*** The SLC straddles the *within plate basalts* and *within plate basalts* + MORB fields. East Greenland (KF13A) plots near to the SLC but closer to MORB. EMD are more similar to the *volcanic-arc basalts + MORB* fields. The TTLC are mainly within the volcanic arc basalts field. Cape Vogul and many other boninites are not well characterised by this TEDD, and plot towards high Zr.

- ***Zr/Y - Zr (after Pearce, 1983, not shown fully on figure).*** SLC, EMD and East Greenland (#KF13A; Arnason *et al.*, 1997) all plot in the *continental-arc basalts* field (which overlaps with the *within-plate basalts* field above). These are distinct from the TTLC which plots mostly in the *oceanic-arc basalts* field. The location of East Greenland straddles the *within-plate basalts* and the *MORB + within-plate basalts* fields in Figure 7.3. In the Pearce (1983) variant (not shown), #KF13A plots as a continental arc basalt showing that Zr/Y - Zr variations do not effectively discriminate between *arc* and *within-plate* extensional settings.

- ***Ti - Y/Nb (see Figure 5.14c).*** The SLC and EMD have constant Y/Nb and broadly correspond to the *continental tholeiite* field. The TTLC has very low Ti, highly variable Y/Nb, but is consistent with derivation from a HFSE-depleted *MORB* source. Nb mobility probably resulted in low Nb/Y for some samples.

- ***Zr - Nb - Y (Figure 7.4).*** The SLC plots in the *within-plate tholeiite + volcanic-arc basalts* field. The EMD plots more towards the *N-MORB + volcanic-arc basalts* field. The TTLC plots firmly in the *N-MORB + volcanic-arc basalts* field.

- ***Y - La - Nb (Figure 7.5).*** The SLC defines an array between *weakly enriched E-MORB* and continental crust. The EMD plots between *E-MORB* and *continental basalts*. Most TTLC samples plot in the *volcanic-arc tholeiite* field although there is a broad spread towards crust which may be assimilation or, more likely, minor LREE and Nb mobility.

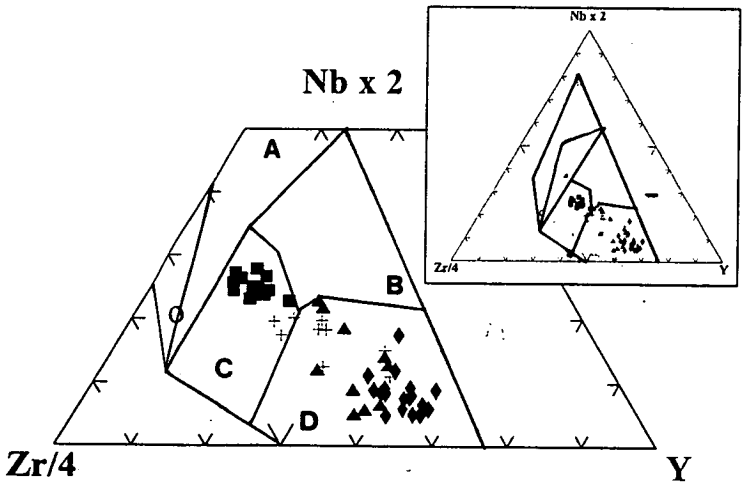

Figure 7.4 Zr - Nb -Y TEDD for basalts. A = *within-plate basalts*; B = *E-MORB*; C = *within-plate tholeiites*; D = *N-MORB + volcanic-arc basalts* (after Meschede, 1986).

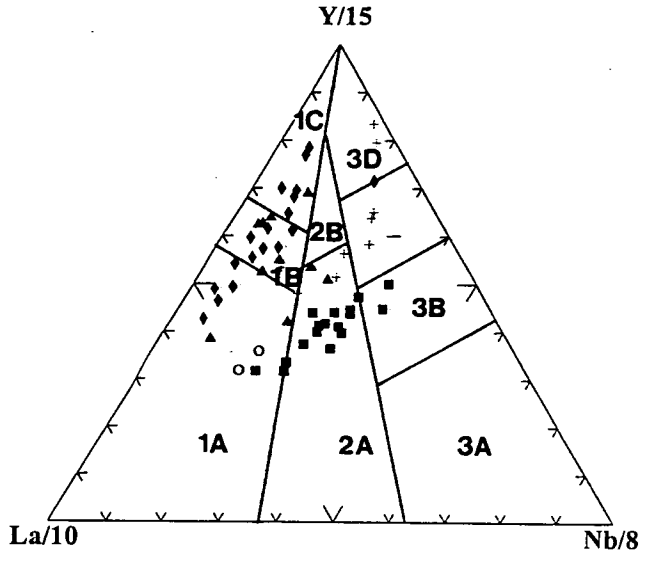

Figure 7.5 La - Y - Nb TEDD for basalts. 1A = *calc-alkali basalts*; 1B = *transitional* between 1A and 1C; 2A = *continental basalts*; 2B = *back-arc basin basalts*; 3A = alkali basalts from *intra-continental rift*; 3B = *E-MORB*; 3C = *weakly enriched E-MORB*; 3D = *N-MORB* (after Cabinis & Lecolle, 1989).

- ***Zr - Ti - Y (Figure 7.6).*** The SLC broadly corresponds to the *within-plate* field but extends to high Ti (see Zr/Y - Ti/Y above). The EMD are more *MORB*-like. The TTLC does not plot within the template and is clearly affected by extreme Ti depletion.

- ***MnO - TiO_2 - P_2O_5 (Figure 7.7).*** The SLC has a wide scatter on this plot, but as with most of the EMD, broadly plots in the *island-arc tholeiite + MORB* fields. This diagram does not distinguish between island-arc basalts and continental tholeiites, but generally CFB plot between *MORB* and *island-arc tholeiites*. The TTLC plots firmly in the *boninite* field. Although MnO is potentially controlled by orthopyroxene accumulation, it is encouraging to note that all compositions, including the plagioclase-rich leucocratic layers, form a tight cluster.

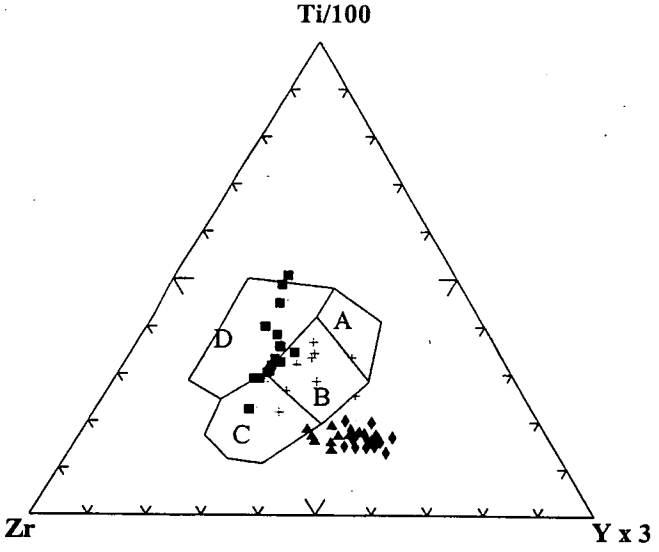

Figure 7.6 Ti - Zr - Y TEDD for basalts. A = *island-arc tholeiites*; B = *MORB + island-arc tholeiites + calc-alkali basalts*; C = *calc-alkali basalts*; D = *within-plate basalts* (after Pearce & Cann, 1973).

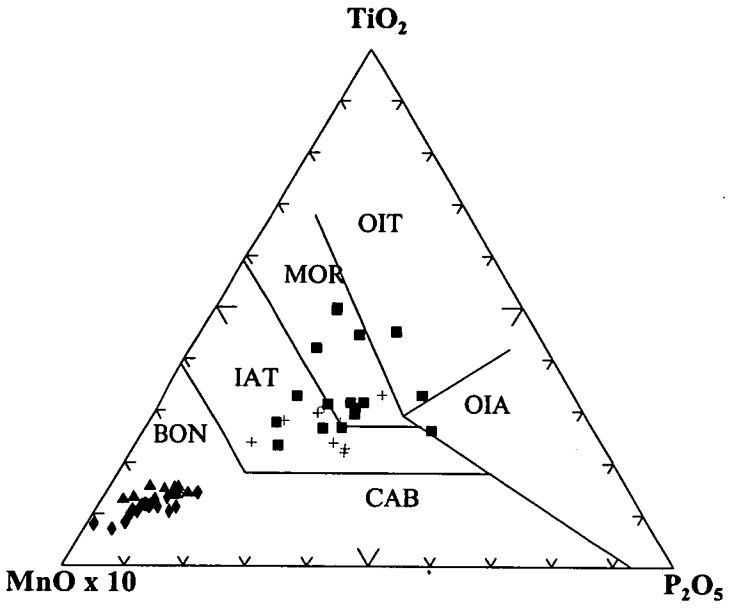

Figure 7.7 MnO - TiO_2 - P_2O_5 TEDD for basalts. OIT = *ocean-island tholeiite* or *seamount tholeiite*; IAT = *island-arc tholeiite*; OIA = *ocean-island alkali basalt*; CAB = *island-arc calc-alkaline basalt*; BON = *boninite*, which occupies the Mn-rich part of the CAB field (after Mullen, 1983).

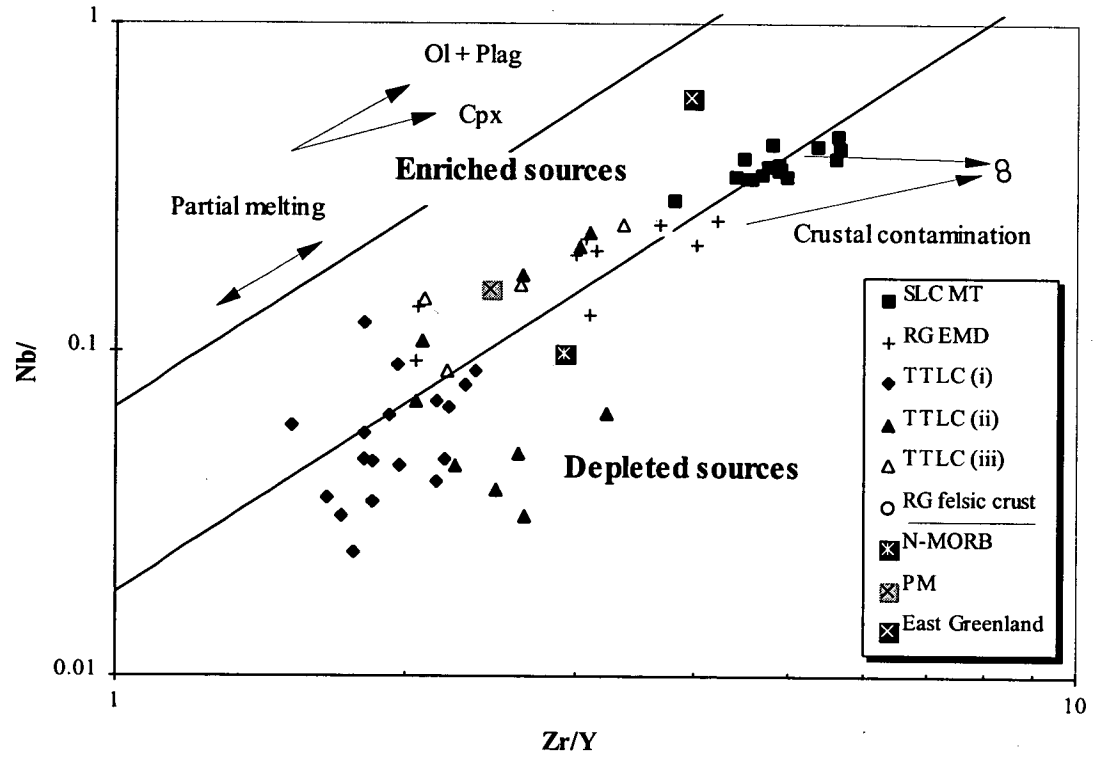

Figure 7.8 Nb/Y - Zr/Y TEDD for basalts. The parallel lines define the upper and lower bounds of the Iceland array and are thought to bracket E-MORB that are derived by melting mantle that is directly influenced by the Iceland plume. Other plume-related suites, such as most OIB, also plot within the parallel lines. Depleted sources, by contrast, have lower Nb/Y - Zr/Y variables and include N-MORB and volcanic-arc basalts. The Rauer Group felsic crust is typical of Archaean crust in terms of Nb/Y - Zr/Y variables (after Fitton *et al.*, in press; N-MORB and PM are after Sun & McDonough, 1989; East Greenland representative is #KF13A from Arnason *et al.*, 1997).

- *Nb/Y - Zr/Y.* The SLC forms an array between *E-MORB source* and the Rauer Group felsic crust. As described in Chapters 5 and 6, it is difficult to distinguish between the effects of Cpx fractionation and assimilation in the SLC. Note that East Greenland (#KF13A) also plots within the *E-MORB source* parallel lines. The EMD form a broad array between *E-MORB source* and crust. Note that the TTLC have a large scatter but that most samples are from *depleted MORB source*. The scatter is outside analytical precision and the variability is considered to be real (see Appendix 1 & discussed further in Section 7.4.3 below). TTLC samples that plot in the *E-MORB source* field are thought to have gained Nb relative to Zr during metamorphism, and most of the high-Nb samples are from within a few metres of felsic gneiss. This diagram does not distinguish between MORB and volcanic arc basalts but it does distinguish between *enriched* and *depleted* sources. Most volcanic arc basalts are primarily derived from depleted sources and therefore plot near to N-MORB. An important feature of this diagram is that the effects of crustal contamination can be distinguished by an array towards high Zr/Y in the *depleted source* field. However, it is not possible to derive *enriched source* signatures by mixing a magma from a *depleted source* with crust.

7.3.4 Discussion and interpretation from MORB-normalized IE diagrams and TEDDs

The SLC

The involvement of felsic crust in the evolution of the SLC is indicated by a number of TEDDs (*e.g.* Figures 7.4, 7.5 & 7.8) and also possibly by the MORB-normalized IE diagram (Figure 7.1a). However, constraining the involvement of crust directly has proved extremely difficult, and Nd and Sr isotopes proved to have been significantly altered during metamorphism. In an effort to ascertain what effects crustal contamination may have had, a simple geochemical model was constructed based on binary mixing, or rather unmixing. By rearranging Equation 6.1 it is possible to predict the concentration of an element in a melt prior to mixing (*i.e.* solve [6.1] for C_m). The main difficulty with the model concerns the bulk composition of the SLC.

To date, no gabbros of the SLC have been found that appear to represent quenched primary liquids. Moreover, the complex has been tectonically dismembered such that it is no longer possible to estimate the bulk composition directly, not that this has ever proved easy even where well-exposed intrusions have had a relatively simple post-emplacement history (*e.g.* Skaergaard, Wager & Brown, 1968). Nevertheless, for the purposes of the model presented here, the closest estimate for the bulk composition of the complex is taken to be the average of the SLC MT. This assumes a closed-system evolution for the complex and does not allow for extensive IE-enriched eruptives. There are a number of extreme differentiates, both

ultramafic cumulates and IE enriched pegmatites, but these are not included in the 'average' calculation.

In Figure 7.9, elements are arranged in order of increasing abundance of normalized E-MORB. The two representative Rauer Group felsic samples (#5120 & #5143) have been plotted with the 'average' SLC. Note that the SLC lies between E-MORB and this crust for most elements. The results of bulk subtraction of ~ 15% crust from the SLC are also shown. Note that the subtraction of felsic crust reduces the pattern of the SLC to one that is very similar to that of E-MORB. Excellent agreement is achieved for all elements except Ti, Sr, Th, Pb and Ba (shown by arrows on Figure 7.9). Of those elements that do not match well, Sr is strongly influenced by plagioclase fractionation/accumulation (see Section 1.4.2). Ti is presumably enriched by the late onset of ilmenite crystallization, and ilmenite accumulation is thought to have led to very high Ti in some samples (see Section 4.2 & Figure 3.4). It is possible that Th, Ba and Pb were mobile during metamorphism. Most immobile elements agree very well with this simple model, and surprisingly, so does K and Rb. Although the absolute percentage of mixing is probably not very well constrained because of uncertainties regarding the ratio of cumulus phases to trapped liquid and the assumption of closed-system evolution, 15 % is not unrealistic. The important point to note is that a modest degree of crustal contamination can readily explain the enriched[3] and fractionated LILE, LREE and small negative HFSE anomalies.

In conclusion, the SLC is interpreted to have originated from an *enriched plume source*, and the intrusion is thought to have been associated with CFB-type magmatism. The SLC intruded into older components of the Rauer Group Archaean domain (described further below), at which time the complex acquired some of the geochemical character of that crust through assimilation. A tectonomagmatic setting similar to the East Greenland early Tertiary igneous province is envisaged as a possible modern day analogue for events at 2840 Ma in the Rauer Group.

The EMD

REE patterns and IE ratios, especially those involving Nb, Zr and Y, indicate that the EMD and SLC were derived from mantle reservoirs that had different source characteristics. One possible explanation is that the dykes were derived from a mantle source that previously

[3] Enriched and fractionated are defined in Chapter 5.

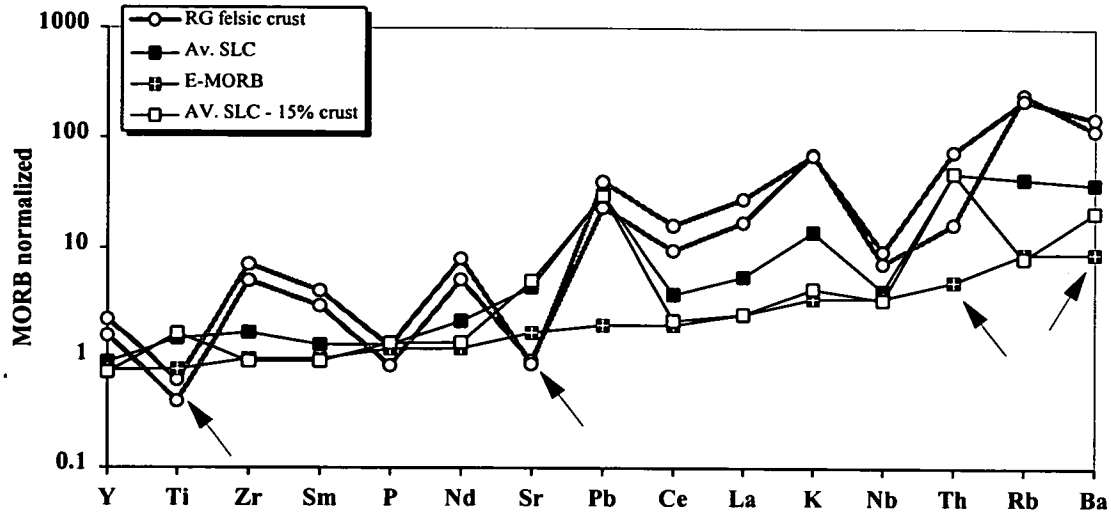

Figure 7.9 MORB-normalized IE diagram showing the effects of subtracting crust from the SLC. A crude estimate of the bulk composition of the complex has been estimated from the average composition of the SLC. The primary liquid has then been calculated by the bulk removal of 15% of the Rauer Group felsic crust (average of #5120 & #5143 of Sheraton *et al.*, 1984). This results in a primary melt that is very similar to E-MORB in composition, except for the elements indicated by arrows (discussed in the text).

had melt extracted (*e.g.* extraction of the SLC). Successive melting of an E-MORB source would lead to magmas with lower Nb/Y and Zr/Y (although not leaving the parallel lines on Figure 7.8), and would also produce low-abundance incompatible-element patterns. However, given that the EMD have flatter IE patterns than the SLC, and generally have less pronounced Nb and P anomalies, it is likely that the EMD may be less contaminated than the main complex. If this is the case, some of the dykes may reflect melting of a source that is transitional between enriched and depleted MORB sources (*i.e.* they are more N-MORB-like). Such a transitional character is further suggested by the distinct location of the EMD on a number of TEDDs (*e.g.* Figures 7.3, 7.4, 7.5, 7.6 & 7.8) which all imply that the EMD are more MORB-like in character. Finally, a model that relates the EMD to the SLC would make geological sense as intrusion of the SLC at 2840 Ma was followed by repeated dyke emplacement (EMD) for at least the next 40 m.y. (see Section 6.3). By analogy with the temporal evolution of the East Greenland margin, the SLC and EMD may represent a similar transition from CFB-related magmatism directly associated with a plume, to more oceanic magmatism as continental break-up progressed (*e.g.* Larsen *et al.*, 1992; Fitton *et al.*, in press).

The TTLC

The TTLC is spatially unrelated to the SLC and is clearly chemically distinct. Although

troughs and peaks of the MORB-normalized IE patterns for the TTLC and Rauer Group Archaean felsic crust match very closely, the origin of the similarity is not immediately apparent. This is an important aspect that the isotope study (Chapter 6) was unable to reconcile and the patterns shown on Figure 7.1c could be the result of mantle processes, crustal assimilation, or metasomatic alteration.

Reset Nd isotopes indicate that metamorphic disturbance was isotopically pervasive, and Sr isotopes and highly variable Nb/Y and Nb/Zr indicates that LILE and possibly Nb were also mobile to some extent. However, petrographic observations and coherent geochemical signatures for a wide range of bulk compositions imply (but do not confirm) that broad geochemical patterns are probably not too dissimilar from those of the protolith. Therefore the effect of metamorphism on most trace elements is considered to be relatively minor in extent (discussed further in Chapter 13).

The involvement of crustal contamination is also very difficult to determine. This is not a problem that is unique to this study, and the role of crustal contamination in the evolution of 'siliceous high-Mg basalts' (SHMB) is currently a matter of considerable debate (*cf.* Arndt & Jenner, 1986; Sun *et al.*, 1989; Seitz & Keays, 1997, for crustal contamination; and Hamlyn & Keays, 1986; Hatton & Sharpe, 1985; Redman & Keays, 1985, Hall & Hughes, 1993, against crustal contamination). Although it is not possible to thoroughly review the origin of SHMB here, there are a number of important aspects from other studies that are relevant to the TTLC.

- SHMB have been found in both continental and oceanic settings,
- SHMB commonly have negative HFSE anomalies,
- SHMB have a range of IE abundances,
- SHMB range from aphyric dykes that presumably approximate quenched melts (*e.g.* Sun *et al.*, 1989; Hall & Hughes, 1987; 1993), to highly porphyritic lavas and dykes (*e.g.* Hickey & Frey, 1982; Hamlyn & Keays, 1986) and cumulates (*e.g.* Seitz & Keays, 1997),
- two main modes of origin have been proposed to account for SHMB; either derivation through boninite-forming processes (*i.e.* subduction related; boninites as defined by Crawford *et al.*, 1989), or through crustal contamination of komatiites (see references above).

A crustal setting cannot be assumed for the TTLC; the complex does have negative HFSE anomalies and IE abundances that are at the high end of the boninite range (*s.s.*), but are

possibly lower than many continental SHMB (*e.g.* Vestfold Hills Norite complex, Seitz & Keays, 1997). *Although abundance comparisons cannot be strictly applied to the cumulate TTLC*, Seitz & Keays (1997) found that the IE abundances of the cumulate portions of the norite were not appreciably different to those in the aphyric portions of the complex. Hence, it is possible that IE abundances of the TTLC are largely governed by the amount of trapped liquid in the system, and low IE concentrations may well be representative of the primary liquid. However, regarding the crucial question of a crust *versus* source origin for the negative HFSE anomalies, the low IE abundances and high intrusion temperature for the TTLC (*e.g.* Section 4.5.2) would tend to imply that large amounts of crustal contamination are theoretically possible (see also Huppert *et al.*, 1984). In order to distinguish between these origins further, a simple mixing calculation has been attempted in a manner similar to that described above for the SLC.

Rocks that might represent primary liquid compositions have not been identified in the TTLC. Therefore, any attempts at mass balance calculations rely upon a number of assumptions and are hindered by the effects of fractionation and accumulation and, most importantly, the possibility of open-system behaviour (*i.e.* separation of magma from the residual cumulate pile). However, *if* the average composition of the complex is taken as a very crude approximation of the primary liquid composition, simple bulk mixing of representative Rauer Group Archaean felsic crust (#5120 & #5134) cannot have exceeded 5 %, otherwise the abundance of many *immobile* incompatible elements such as Ce, Zr, Nb (?) and Y would all have been less than zero in the primary melt. Expressed differently, the mass of incompatible elements in only ~5 % felsic crust is more than the corresponding concentration of many elements in the TTLC. Perhaps more importantly, the depth of the HFSE anomalies (HFSE/HFSE*) is greater in the TTLC than in the crust (Table 7.1), therefore binary mixing of crust cannot produce the observed anomalies.

Other lines of evidence also suggest that large amounts of crustal contamination did not take place. For example, there is no direct textural evidence within the complex for assimilation, whereas in other documented examples where large amounts of assimilation are thought to have occurred (*e.g.* Kalka, Gray *et al.*, 1981), there is abundant evidence in the form of xenoliths and crustal pendants.

An alternative interpretation to a primary or source origin for the geochemical features of the TTLC, is that they are in some way related to the accumulation process. However, as described in Chapter 5, accumulations of orthopyroxene would be expected to produce positive Nb anomalies relative to La and Ce (*cf.* Keleman *et al.*, 1990; 1993, and others).

Table 7.1 Results of binary mixing calculations for the TTLC. HFSE/HFSE* (*e.g.* Nb/Nb*) are calculated from the geometric mean of MORB-normalised compositions relative to position of the Nb, P and Ti on Figure 7.1c; see also enclosed Abbreviations Card). The results are for bulk mixing (Equation 6.1) of PM with 10, 30 and 60 % crust. Note that HFSE/HFSE* for the TTLC are lower than those of the crust, implying that simple binary mixing cannot produce the depth of the negative anomalies observed for the TTLC (see Appendix 1 for details of analytical procedures and discussion of errors). As a general point, accumulation would result in a tendency for Opx- and/or Cpx-rich compositions to acquire *positive* Nb and Ti anomalies (*i.e.* HFSE/HFSE* > 1.0).

	TTLC av.	Av. crust	PM + 10%	PM + 30%	PM + 60%
Nb/Nb*	0.36	0.39	0.46	0.41	0.39
P/P*	0.01	0.16	0.32	0.21	0.17
Ti/Ti*	<0.01	0.14	0.37	0.22	0.16

Moreover, if accumulation was the cause of the distinctive TTLC patterns (*i.e.* Figure 7.1c), the websterites would be HREE enriched relative to the LREE, and there would still be no explanation for the observed similarity in incompatible-element patterns for both websterites and leucocratic plagioclase-rich cumulates (see Figure 5.15).

All of the aforementioned general considerations render a contamination model for the origin of the HFSE anomalies highly unlikely. They also imply that whilst cumulate formation may influence the abundance of trace elements, largely by dilution, it is likely that IE ratios and patterns must reflect the composition of the primary liquid to some degree. Although it is difficult to establish for certain, the most likely interpretation is the simplest one: that the bulk composition of the complex does approximate that of the primary liquid, at least to within one order of magnitude, and the presence of HFSE anomalies is primary and not a consequence of crustal contamination. Therefore a suitable model is required that can account for the geochemical character of the complex. The most geochemically similar modern analogue is associated with island-arc magmatism, where large degree partial melts have been extracted from peridotite that has been depleted by a previous melt extraction event (*e.g.* Hickey & Frey, 1982; Hawkesworth *et al.*, 1993). Negative HFSE anomalies, such as those observed for the TTLC, are commonly interpreted to have resulted from preferential enrichment in LILE and LREE either by a slab-derived fluid (*e.g.* Hawkesworth *et al.* 1991; Stolper & Newman, 1994) or a slab-derived small-degree partial melt (*e.g.* Yogodinski, 1994). The possibility of HFSE retention in residual accessory phases has also been proposed (*e.g.* Foley & Wheller, 1990), although it is considered an unlikely explanation for large degree partial melts (*e.g.* Hickey & Frey, 1982).

In conclusion, the TTLC is interpreted to be an intrusive that is akin to a boninite. Although it is important to emphasise that the *cumulate* TTLC *cannot be compared directly with a boninite*, because boninites are *lavas* that are formally defined and classified on the basis of major elements (Crawford *et al.*, 1989), a number of similarities imply that the TTLC protolith possibly formed in a similar manner to modern boninites. The role of crustal contamination is *not* considered to have been a major factor in the evolution of the TTLC, and the reason that the TTLC has similar incompatible-element patterns to the Rauer Group felsic crust is that both were formed in a similar way, by island-arc magmatism (*cf.* Kim & Jacobi, 1996). Whilst the age of the TTLC is not yet known, it is possible that the complex is as old as the *ca.* 3300-3500 Ma felsic orthogneisses. An intrusive boninite of such antiquity would be an exciting discovery, although much work remains to be done to confirm the origin and evolution of this complex (discussed further in Chapter 13).

7.4 Summary, conclusions, and a tentative tectonomagmatic model for the Archaean Rauer Group

Interpretation of incompatible trace-element signatures indicates that the TTLC was derived from a depleted mantle source that had experienced one or more previous melt extraction events. Strong negative Nb, P and Ti anomalies are interpreted to be the result of preferential enrichment in LILE and LREE that were ultimately derived from a subducted slab in an island arc. The very presence of such a mafic complex in the present crust would suggest formation in a tectonic regime that was favourable to preservation, such as an arc. Moreover, since all modern *in situ* boninites occur in fore-arc regions (see Kim & Jacobi, 1996, and references therein), a forearc setting for the TTLC is possible.

The presence of *ca.* 3500 Ma inherited zircons in the SLC indicates that the complex intruded into *ca.* 3300-3500 Ma arc-derived crust that may already have contained the TTLC. On the basis of a single SLC xenolith in tonalite adjacent to the TTLC (*ca.* 100 m away), and because of regional correlations of *ca.* 2800 Ma tonalite, it is apparent that the Composite Layered Orthogneiss (CLO), TTLC, and SLC were juxtaposed by 2800 Ma. The Tonalite Gneiss, as described in Chapter 3, effectively stitched together these three ancient gneiss components. Events in the interval 2840 - 2800 Ma are interpreted to be related to plume-related rifting in a similar setting to the East Greenland margin during the early Tertiary. The SLC and EMD are considered to be rift-related and ultimately derived from an enriched mantle source. Minor similarities with the TTLC, the Rauer Group felsic crust, and

arcs in general, can be explained by contamination by much older arc-derived felsic crust. Later intrusion of mafic dykes (EMD) with MORB-like chemistry is a feature typical of many Phanerozoic continental dyke-swarms that are attributed to continental break-up. The chemical differences between the SLC and EMD are relatively minor and can be explained by differences in conditions of melt generation. The EMD appear to reflect a transition from an enriched plume-related source to one that is more MORB-like. Such a temporal transition is characteristic of the early Tertiary East Greenland margin and the geochemical evolution of the North Atlantic Tertiary igneous province in general (*e.g.* Larsen *et al.*, 1992; Fitton *et al.*, in press). It is also probable that less enriched LILE (?), LREE, and relatively weak negative Nb anomalies reflect less crustal contamination than that experienced by the SLC. Thermal considerations would support such a contention (*e.g.* Huppert & Sparks, 1984).

Although the origin and evolution of the Tonalite Gneiss suite has not been examined in detail in this study, it is apparent from the abundance of inherited zircons that the suite was dominantly derived by intracrustal melting of the *ca.* 3300-3500 Ma Composite Layered Orthogneiss (CLO). Evidence for local derivation or interaction between the TG and CLO was documented by Harley (1987), although the conditions and circumstances of melt generation have yet to be studied in detail.

The geological history of the Rauer Group after the *ca.* 2800 Ma event(s) is at least as complex as that deduced for the Archaean. A complicated series of high-grade deformation events punctuated by mafic and felsic intrusions (dykes, plutons, sheets and localised remelting of felsic rocks) affected the Rauer Group between 2800 Ma and prior to *ca.* 1050 Ma (see Chapters 2 & 3). It is apparent that at *ca.* 1000 Ma, there was a major tectonothermal episode that produced abundant juvenile crustal additions, and tectonically interleaved the Archaean domain with younger Proterozoic gneisses (Harley, 1987; Kinny *et al.*, 1993; Kinny pers. comm.). At some time in the Proterozoic, a suite of paragneisses (Filla Paragneisses) were incorporated into the otherwise orthogneiss-dominated Rauer Group terrane. All of these components (Archaean and Proterozoic units) were metamorphosed and deformed in the lower crust at about 1000 Ma prior to rapid exhumation (*e.g.* Harley, 1988; Kinny *et al.*, 1993; Harley *et al.*, 1996).

The final event of regional significance appears to have occurred at *ca.* 500 Ma. Although interpreted by Harley (1987) and Kinny *et al.* (1993) to be of lower grade than the *ca.* 1000 Ma event, characterised by upper greenschist- to lower amphibolite-facies assemblages, the *ca.* 500 Ma event had a profound influence on isotopic systems in the terrane. Events between 2800 Ma and 500 Ma appear to have had little influence on zircon systematics, and

metamorphic conditions during the *ca.* 1000 Ma event are regarded as progressing under relatively fluid-absent conditions (*e.g.* Harley & Buick, 1992). The 500 Ma event, however, is interpreted to have been the first significant rehydration of the terrane. At this time zircons were variably reset as evidenced by the abundance of 500 Ma metamorphic zircons or variably reset older grains (*e.g.* this study, Chapter 6). In addition, it is apparent from this study that Sr- and Nd-isotope systems were significantly perturbed at 500 Ma.

Arguably the most important contribution made during the course of this investigation, is the discovery that Nd isotopes in the Rauer Group were highly perturbed during metamorphism. The amount of open-system behaviour required to explain the spread in Nd-isotope compositions is surprising considering that there are abundant relict igneous features, which appear to include bulk geochemistry and REE patterns (*i.e.* Sm/Nd). The implications for previous interpretations of Nd isotopes in terms of protolith petrogenesis and crustal growth models in the Rauer Group, and indeed other polymetamorphic high-grade terranes, is profound.

Many of the conclusions described in this chapter are tentative or speculative and much work remains to be done to confirm, refine or refute the hypotheses put forward in this study. Areas of key importance regarding models for the origin and evolution of the layered complexes concern the interpretation of whole-rock geochemical signatures in plutonic rocks and the effects of element and isotopic mobility. A number of suggestions as to how this may be achieved are outlined in *suggestions for further research* in Chapter 13 (Part 4).

Part 3:

The Vestfold Hills

Chapter 8

Geological outline of the Vestfold Hills

8.1 Introduction and synopsis of Part 3: The Vestfold Hills

This chapter documents and outlines a review of previous work in the Vestfold Hills to provide a background to the research rationale and objectives in this terrane. Towards the end of this chapter, a series of questions are posed that highlight the need for further research, especially fieldwork, in the terrane. Although the wider objective in the Vestfold Hills is to understand the petrogenesis of the various gneiss lithologies within the context of the magmatism and crustal accretion in East Prydz Bay (and globally), in practice most of the work described in Part 3 concentrates on refining and establishing a sound geological framework.

The overall structure of **Part 3: The Vestfold Hills**, reflects the objectives and methodology adopted in this terrane; these are outlined at the end of this chapter (Section 8.6.2) after a review of previous work. Chapter 9 provides a description and discussion of new field observations made during the 1992/93 and 1993/94 field seasons. These observations define a more complete geological event sequence than has been previously recognized in the terrane. Key elements from this geological history proved to be syn-deformational leucosomes which are used to precisely constrain the magmatic, metamorphic and deformational event sequence by U-Pb zircon dating, and are described in the following chapter (Chapter 10). Chapter 11 re-examines the geochemical and conventional isotopic characteristics of the Vestfold Hills within the context of a robust geological and chronological framework. The final chapter in Part 4 (Chapter 12), discusses and concludes what is now known about Archaean crust formation in the Vestfold Hills.

8.2 Outline of the geological history

The first mapping in the Vestfold Hills was undertaken by McLeod *et al.* (1966), who described three distinct E-W trending gneissic units which they, and subsequent workers (*e.g.* Oliver *et al.*, 1982; Collerson *et al.*, 1983; Sheraton & Collerson, 1984), interpreted to be structurally interleaved and tectonically repeated throughout the area. Field and petrographic descriptions of the dominant gneissic lithologies (*e.g.* Oliver *et al.*, 1982;

Collerson *et al.*, 1983; Sheraton & Collerson, 1984) all broadly agree on a three-fold lithological division, with Collerson *et al.* (1983) modifying the earlier schemes and introducing subsequently accepted (*e.g.* Passchier *et al.*, 1991; Black *et al.*, 1991a) formal names for the main lithological types (Figure. 8.1). The Chelnok Paragneiss[1] and Mossel and Crooked Lake orthogneisses occur in broadly E-W trending bands throughout the terrane, where individual suites have been considered to be tectonically repeated by steeply plunging km-scale F_2 folds (*e.g.* Oliver *et al.*, 1982; Parker *et al.*, 1983; Collerson *et al.*, 1983). Collerson *et al.* (1983) also introduced a further lithological division, the Tryne Metavolcanics, a compositionally diverse succession occurring on southern Long Peninsula and near Rybnaya Bay. In addition to the four main lithologies formally defined by Collerson *et al.* (1983), Black *et al.* (1991a) and Harley (1993) introduced two minor units, these are respectively: the 'syn-deformational (D_2)' Grace Lake Granodiorite, and the Taynaya Paragneiss.

The first geochronological study in the terrane was by Collerson *et al.* (1983), who presented several Rb-Sr and Sm-Nd isochrons for the three main orthogneiss units and suggested that there were two temporally distinct crust-forming events. The Mossel Gneiss and Tryne Metavolcanics were thought to have crystallized and then subsequently been deformed and metamorphosed at about 3000 Ma, with the younger Crooked Lake Gneiss (CLG) emplaced and deformed under similar conditions at about 2500 to 2400 Ma. However, the zircon U-Pb study of Black *et al.* (1991a) demonstrated that this interpretation was incorrect, and instead most of the magmatic and high-grade deformational activity occurred in a *ca.* 50 m.y. period at the end of the Archaean. The first phase of magmatism produced Mossel Gneiss protolith and lasted from at least 2526 ± 6 Ma to 2501 ± 4 Ma, closely followed by intrusion of CLG suites between 2501 ± 4 Ma to 2484 ± 6 Ma. These relatively precise crystallization ages constrain the age of D_1-M_1 to about 2501 Ma. Black *et al.* (1991a) also identified another minor unit in the north, the Grace Lake Granodiorite. They dated two spatially separate granodiorites and obtained ages of 2489 ± 8 Ma and 2481 ± 14 Ma. Based on field evidence, Black *et al.* (1991a) interpreted these magmatic rocks to have intruded syn-tectonically during D_2-M_2, hence, they combined the data for these two samples to provide an estimate of 2487 ± 6 Ma for the age of the Grace Lake Granodiorite and the D_2 event.

[1]Following the recommendations of Ricci *et al.* (1993) the Chelnok 'supracrustals' have been renamed the Chelnok Paragneiss.

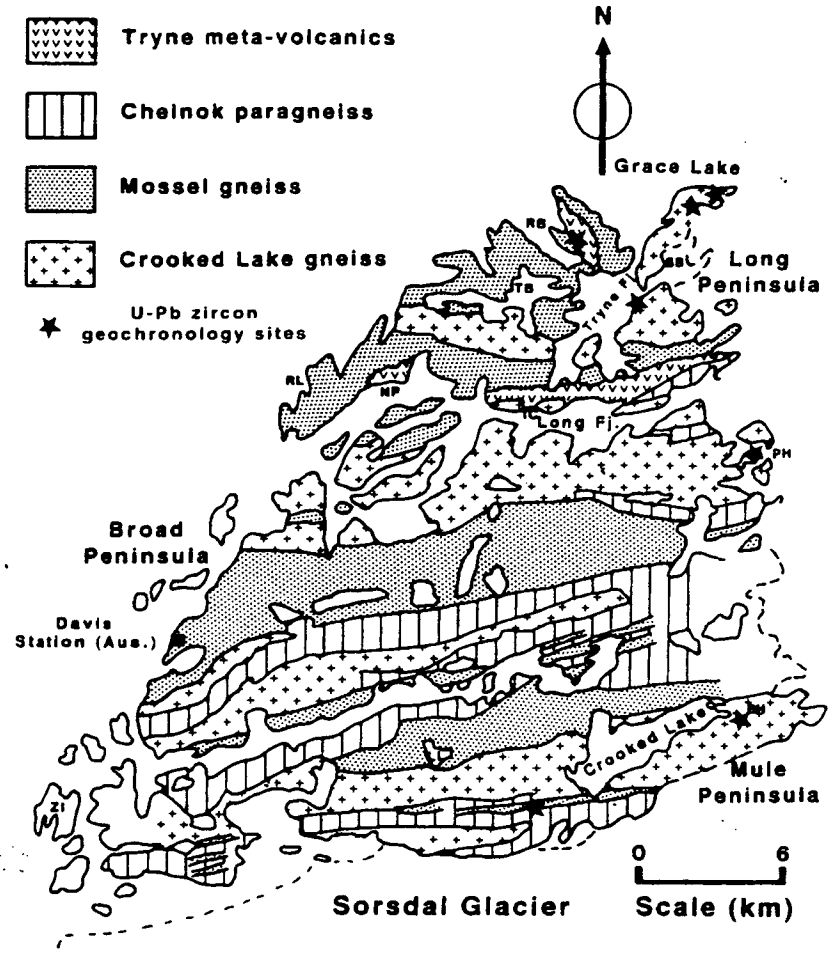

Figure 8.1 Geological map of the Vestfold Hills according to Collerson *et al.* (1983). Their map has been reproduced here with little modification to allow comparisons with new field observations made during the course of this study (described in the next chapter).

8.3 Previous accounts of lithologies and structures

Largely following the chronological scheme originally set out by Oliver *et al.* (1982), but incorporating revisions by Collerson *et al.* (1983) and the U-Pb zircon dating of Black *et al.* (1991a), all the gneissic units in the Vestfold Hills can be described relative to a simple deformational framework whereby gneisses formed either pre-D_1 (> *ca.* 2500 Ma), or post-D_1 to pre-/syn-D_2 (> *ca.* 2480 Ma). The various gneisses are described below within this context.

8.3.1 Pre-D_1 gneiss suites

Tryne Metavolcanics (pre- ca. 2526 ±6 Ma)

Described as a variable sequence of metavolcanic rocks by Collerson *et al.* (1983), the Tryne unit is reported to be the oldest recognized suite in the Vestfold Hills, comprising ultrabasic, basic, intermediate and acidic lithologies. These are commonly layered on a decimetre- to metre-scale and are often associated with an interbedded (by implication) metasedimentary component. Layering is typically transposed (S_1 or composite $S_{1/2}$), but where relatively undeformed these predominantly two-pyroxene mafic gneisses contain xenolithic ultramafic nodules which include lherzolite, harzburgite and hornblendite. The 'metavolcanics' are cut by 'differentiated units' of medium- to coarse-grained pyroxenite, hornblendite, gabbro and leucogabbro which sometimes preserve igneous modal layering (Collerson *et al.*, 1983, p.77).

Chelnok Paragneiss (pre- ca. 2526 ±6 Ma)

The Chelnok Paragneiss as defined by Collerson *et al.* (1983) essentially correlates with the Layered Paragneiss of Oliver *et al.* (1982) and consists mainly of garnetiferous pelite and semipelite, with less abundant psammite, quartzite, calc-silicates and banded iron formation. Collerson *et al.* (1983) noted that some outcrop areas contain a minor mafic granulite component but were unable to resolve if there is a genetic relationship to the Tryne Metavolcanics, or whether the Chelnok Paragneiss represents a separate sedimentary-volcanic sequence. Contacts with later, more abundant, felsic orthogneisses (Mossel Gneiss and CLG) were regarded by these authors to be tectonic in origin.

Taynaya Paragneiss (pre-2501 ±4 Ma)

In the region around Taynaya Bay a recently recognized paragneiss suite, termed the Taynaya Paragneiss by Harley (1993), crops out as a discontinuous layer or boudin train. These gneisses consist of highly-magnesian, silica-undersaturated, sapphirine-bearing lithologies and are distinguished from the Chelnok Paragneiss (Fe-rich) on the basis of their unusual chemistry. In terms of relative age, they are clearly older than the host orthogneiss (Mossel Gneiss), but their temporal relationship to the other pre-D_1 gneissic components, the Tryne Metavolcanics and Chelnok Paragneiss, is not known.

Mossel Gneiss (2526 ±6 to 2501 ±4 Ma)

The Mossel Gneiss is depicted by Collerson *et al.* (1983; see Figure 8.1) to be the most abundant lithology in the Vestfold Hills. This unit broadly correlates with the 'Layered

Orthogneiss' of Oliver *et al.* (1982) and is described as dominantly comprising quartzo-feldspathic orthogneisses, containing boudinaged layers of metapyroxenite, gabbro and leucogabbro. The Mossel Gneiss are locally dissected by pegmatitic veins of blue quartz, sometimes containing plagioclase and orthopyroxene. Two broad varieties of Mossel Gneiss can be recognized: those that are compositionally layered on a millimetre- to centimetre-scale or those occurring as relatively homogeneous, finely foliated and lineated, tonalite to trondhjemite sheets.

8.3.2 D_1 deformation and metamorphism (*ca.* 2501 Ma)

The lithological association described above was pervasively deformed in a high-grade deformational event (D_1-M_1) at about 2500 Ma (Black *et al.*, 1991a) that produced a strong gneissic foliation associated with tight to isoclinal folding responsible for inter-layering these rocks at outcrop scale. However, it is important to note that this deformation was first described by Oliver *et al.* (1982) as being composite in nature and therefore the oldest lithologies (pre-Mossel Gneiss) might retain the effects of an earlier tectonic history (see later discussion). Metamorphic conditions for the M_1 event are poorly constrained at present. Collerson & Sheraton (1986) estimated metamorphic conditions for this event to be 1000-1100 °C and 8-10 kbar based primarily on the composition of coexisting pyroxenes in mafic granulites (Tryne Metavolcanics). However, these conditions are probably a significant overestimate of the metamorphic grade, with more recent work on the sapphirine granulites (Taynaya Paragneiss) and calc-silicates (Chelnok Paragneiss) constraining M_1 conditions to *ca.* 830-880 °C and 3.5-8.5 kbar (Harley, 1993; Harley, Snape & Fitzsimons, 1995).

8.3.3 Post-D_1 to pre-/syn-D_2 gneiss suites

Crooked Lake Gneiss (2501 ±4 to 2484 ±6)

The compositionally varied CLG is considered by Collerson *et al.* (1983) to have intruded synchronously during folding associated with the D_2-M_2 high-grade event. These orthogneisses are medium- to coarse-grained, and rang from gabbroic and dioritic to tonalitic, granodioritic and granitic in composition. They commonly contain abundant xenoliths of both accidental and cognate origin. Contacts with the other units are typically sub-concordant and in contrast to the older suites, the CLG only has a relatively simple fabric.

Grace Lake Granodiorite (2489 ±8 to 2481 ±14 Ma)

The youngest gneissic unit recognised so far in the Vestfold Hills is the Grace Lake Granodiorite which, according to Black *et al.* (1991a, 1991b), occurs as irregular sheets and pods in the north of the region, where it post-dates all the previously defined units and was possibly emplaced syn-kinematically with D_2. Although of limited extent, this characteristically white migmatitic gneiss can be readily identified in the field occurring either with 'a homogeneous granitic-pegmatitic fabric or displaying a weak biotite foliation', and accidental or cognate xenoliths are common (Black *et al.*, 1991a, p.288).

8.3.4 D_2 deformation and metamorphism (*ca.* 2487 ± 6 Ma see later discussion).

The D_2-M_2 high-grade event produced a broadly E-W trending fabric in the terrane and all the units described above were folded at this time. The event is described as being dominated by tight and isoclinal macroscopic fold structures with axes that plunge at moderate angles to the NNE (Oliver *et al.*, 1982; Collerson *et al.*, 1983; Collerson & Sheraton, 1986). Both Oliver *et al.* (1982) and Collerson *et al.* (1983) note that fabric development is quite variable, sometimes comprising a strong L-tectonite component defined by elongate mosaics of pyroxene, feldspar or occasionally quartz, but that more typically L-S- or S-fabrics dominate. Metamorphic conditions for this event have been estimated by Collerson & Sheraton (1986) to be 750-850 °C and 6-8 kbar based on a variety of thermobarometers.

8.3.5 Post-D_2 geological evolution

Subsequent to D_2 deformation at about 2480 Ma (age interpreted from Black *et al.*, 1991a) the gneiss complex was deformed into outcrop- to regional-scale open warps (F_3). The regional warping occurred late in the high-grade evolution of the terrane. It re-oriented F_2 structures, the main foliation (S_2), and all older structures from roughly N-S in the Rybnaya Bay to Grace Lake area, to ENE-WSW in the south and central regions. At outcrop-scale F_3 locally re-oriented all older high-grade structures from generally steeply dipping to more flat-lying orientations. Intrusion of a suite of undeformed mafic dykes at 2477 ± 5 Ma (Black *et al.*, 1991a) provides a minimum age for both D_2 and D_3, and this is the oldest undeformed mafic dyke suite in the Vestfold Hills.

The geological history after the high-grade deformational and metamorphic events outlined above has been examined in detail by a number of recent studies. Passchier *et al.* (1991) and Dirks *et al.* (1994) have defined a relatively clear Proterozoic event sequence for the Vestfold Hills, consisting of localized mylonite, ultramylonite and pseudotachylite

development punctuated by multiple dyke emplacement (see Lanyon *et al.*, 1993, and references therein). These features, however, are not considered in detail in this study.

8.4 Geochemical characteristics of the Vestfold Hills orthogneisses: an appraisal of previous results

8.4.1 General outline of previous results.

The most comprehensive account of the geochemical nature of the Vestfold Hills gneisses is by Sheraton & Collerson (1984). Their data acquisition largely reflects fieldwork by Collerson and co-workers and closely adheres to the lithochronological scheme proposed by Collerson *et al.* (1983). A summary of 90 major and trace-element geochemical analyses are presented in Sheraton & Collerson (1984) with a discussion of the possible magmatic, sedimentary and metamorphic processes thought likely to have contributed to, or subsequently modified, the gneiss protoliths. Of the 90 analyses, 39 samples are from the compositionally varied CLG, 36 are dominantly tonalitic Mossel Gneiss, with somewhat fewer analyses representing the Tryne Metavolcanics (15) and Chelnok Paragneiss (8). The salient geochemical features of the orthogneisses are described briefly here, but the Chelnok Paragneiss will not be considered further. The following account is essentially a critique of the paper by Sheraton & Collerson (1984; unless otherwise referenced) in the light of recent work.

8.4.2 Principal geochemical characteristics of the main orthogneiss units

Tryne Metavolcanics

The Tryne Metavolcanics is the oldest unit recognized by Collerson *et al.* (1983), dominantly comprising mafic granulite with minor quartz diorite and tonalitic orthogneisses that exhibit a range of SiO_2 from 46.9 to 63.5 wt%. The mafic granulites are comparable to olivine tholeiites in composition with, for example, moderately incompatible elements (Nb, La, Ce, Y, P, Zr, T & Y) and ratios such as Ce/Y being of typical tholeiite affinity. Some, however, are slightly nepheline normative, a feature that may be attributable to the varied nature of the rocks grouped within this 'suite'. Similarly, analyses of two chemically distinct mafic granulites within the Tryne Metavolcanics which have higher concentrations of most incompatible elements, particularly Ba, La and Ce, are thought by Sheraton & Collerson (1984) to reflect derivation from a distinct, probably enriched, mantle source. The mafic 'metavolcanics' also show a wide scatter of LILE (Rb, Ba, Th & K) which is attributed to the effects of high-grade metamorphism.

Mossel Gneiss

The Mossel Gneiss predominantly comprises tonalites with lesser quartz diorite, trondhjemite, granodiorite and granite. Most Mossel Gneiss and the felsic CLG varieties have been termed 'depleted' on the basis of low abundance of Y (hence HREE) allowing for variation in SiO_2. Geochemically, these are thought to be comparable to depleted Napier Complex granites (see Figure 8.2), although the Mossel Gneiss has higher TiO_2, P_2O_5, Y, Zr, Nb, La, Ce, Ga/Al, but lower Sr, Ti/Y, Ce/Y and CaO.

Crooked Lake Gneiss (CLG)

The geochemical database for the Crooked Lake suites comprises major- and trace-element analyses for 39 samples largely reflecting compositional variability and relative abundances in the southern Vestfold Hills. The CLG has a wide compositional range comprising several different suites which Sheraton and Collerson (1984) have grouped on geochemical grounds (Figure 8.3). The first group comprises one gabbro analysis, with more analyses representing the tonalites and diorites. Two other relatively K-rich groups are formally defined and are sub-divided into a *Monzodiorite Suite* (potassic quartz diorite-quartz monzodiorite-granite) and a *Monzonite Suite* (monzodiorite-monzonite-quartz monzonite-granite).

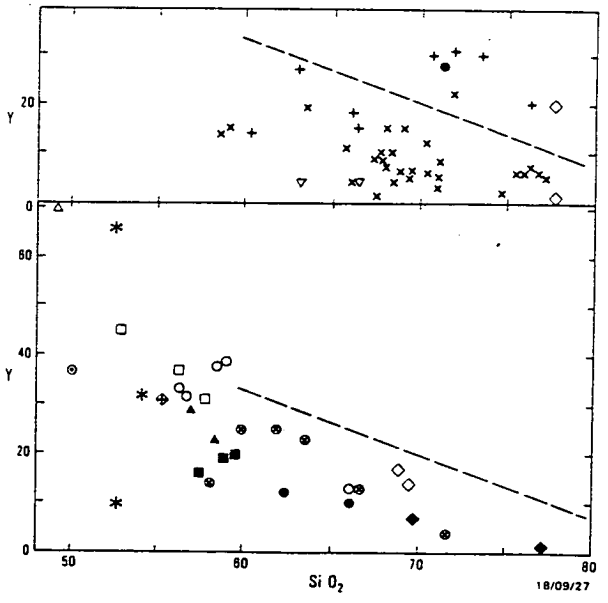

Figure 8.2 Plots of Y *vs.* SiO_2 from Sheraton & Collerson (1983; figure 7) for the Mossel Gneiss, and Chelnok Paragneiss (upper plot) and CLG (lower plot). Dashed line indicates approximate boundary between fields of depleted (low-Y) and undepleted orthogneisses of the Napier Complex. Figures are shown here without revision.

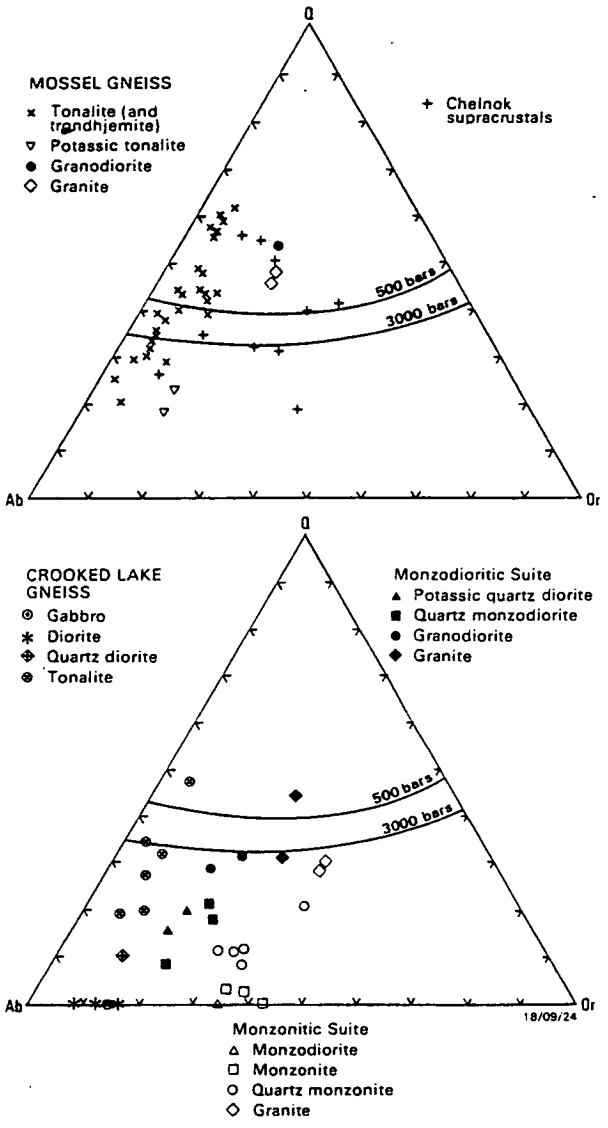

Figure 8.3 Geochemical groupings of the Mossel Gneiss and CLG according to Sheraton & Collerson (1983; figure 4) based on normative *Q-Ab-Or* diagrams. Quartz feldspar field boundaries and positions of quaternary isobaric minima at 500 and 3000 bars (after Tuttle & Bowen, 1958) are indicated. Figures are shown here without revision.

8.4.3 Geochemical constraints on igneous petrogenesis

Sheraton and Collerson (1984) consider the origin of the Vestfold Hills orthogneisses via two main genetic models: partial melting of a variety of possible source materials, and crystal fractionation. They approach petrogenetic modelling by reference to a small number of diagnostic bivariate trace-element diagrams and by application of mixture-modelling calculations to what they consider to be cogenetic suites. A brief précis of their conclusions are presented here, followed in the next section by an outline of some of the problems associated with the approach.

Origin of the tonalites

Sheraton and Collerson (1984) argued that the Tryne Metavolcanic, Mossel Gneiss and CLG tonalites are all broadly similar. Therefore they considered the origin of these different suites in the general context of tonalite generation. Largely based on high Ce/Y and low Y (and hence HREE) concentrations (Figure 8.1), the tonalites are considered to have formed by partial melting of mafic rocks (amphibolite or eclogite), leaving residual garnet, hornblende, or both. There is a 'good' correlation between TiO_2 and Y which is taken to imply hornblende-dominated control. Sheraton and Collerson (1984, p.58) stated that because 'hornblende has a relatively large, and similar, mineral-melt distribution coefficient for Ti and Y, a melt in equilibrium with an amphibole-rich source residue (but no other major Ti or Y-bearing phase) should have Ti/Y not very different from that of the source'. They acknowledge that the importance of crystal fractionation cannot easily be estimated because the composition and nature of the fractionating assemblage cannot be determined from these metamorphic rocks. Nonetheless, they note that simple mixing calculations (least squares) are most consistent with 50-60% fractionation of roughly equal proportions of hornblende and plagioclase (with minor apatite and zircon), but that progressive partial melting was the major factor responsible for the variability within Vestfold Hills tonalites.

For their modelling, Sheraton & Collerson (1984) assume a Tryne 'Metavolcanic' tholeiite starting composition, and by applying a variety of equilibrium batch-melting calculations find the best agreement for a high proportion of residual hornblende (>50 %), with subsidiary clinopyroxene ± olivine probable and residual garnet (up to 20 %) and apatite (up to 0.3 %) possible.

Origin of the monzodioritic and monzonitic CLG suites

Although more enriched in incompatible elements than the tonalites, Sheraton & Collerson (1984) noted that these 'suites' have a number of important similarities in chemical composition. In particular there are high Sr concentrations, and high Ti/Y, Ce/Y and ***mg***. These features, combined with isotopic data (Collerson *et al.*, 1983, described in the next section), led the authors to deduce an origin for these gneisses involving melting of a mafic source similar to that of the tonalites (Hbl + Cpx ± Ol). Differences are attributed to 'more enriched source materials, lower percentage melting, more extensive crystal fractionation, or combinations of these' (Sheraton & Collerson, 1983, p.59).

Origin of the gabbroic and dioritic CLG

As Sheraton and Collerson (1984) acknowledged, there is a paucity of chemical data for the mafic CLG which makes interpretation of their genetic relationships difficult. However, they noted that gabbro #5371 is difficult to reconcile with hornblende-rich cumulate origin and is inconsistent with the gabbro being parental to the tonalites. Instead they attributed this gabbro to a possibly unrelated magma type emplaced at about the same time as the other CLG.

8.4.5 Overall petrogenetic or tectonomagmatic environment

Sheraton and Collerson (1984) argued that the most probable source for the Mossel and Crooked Lake magmas would be through partial melting of subducted, hydrated, oceanic crust. Intracrustal melting for *most* magma types is not implicated, although they noted that textural evidence implies derivation of Mossel tonalite by partial melting of mafic Tryne Metavolcanics (see also Collerson & Sheraton, 1986).

8.4.6 A critique of the Sheraton and Collerson (1984) approach

The Sheraton and Collerson (1984) study is perhaps best viewed in the context of the first regional geochemical examination of the Vestfold Hills terrane. The very nature of the regional-scale sampling strategy means that many of the rocks that are grouped together into suites are probably not directly related in terms of age or genesis. This problem is confirmed by new field work presented in the next chapter.

As a consequence, modelling between 'suites' that comprise a variety of rock types is only likely to constrain magma petrogenesis in the broadest terms (*cf.* Hanson, 1989). Nevertheless, Sheraton and Collerson (1984) have established a tectonomagmatic model that is testable and that provides a geochemical framework for more detailed study. However, a number of specific criticisms are worth noting in this section; these can be grouped into *classification problems* and *petrogenetic problems*, although all the criticisms essentially stem from an inadequate field-based framework centred on regional mapping in the southern high-strain region.

Further general problems of classifying or grouping orthogneiss lithologies on petrographic or geochemical grounds have been outlined in Chapter 1. For the Vestfold Hills, where suites have been grouped according to their chemistry, the main problem concerns element mobility. For example, the primary classification of the compositionally varied CLG is based on apparent groupings on a normative *Q-Ab-Or* diagram (Figure 8.3), but in different

sections of their account, Sheraton and Collerson (1984) argued that LILE (including K) appear to have been mobile. The potential for so called 'potassium-metasomatism' would suggest that classifications that rely heavily on the alkalis (*e.g. Ab-An-Or*; O'Conner, 1965; AFM, Irvine & Baragar, 1971; TAS, Le Maitre *et al.*, 1989) should be treated with caution.

Similar problems affect some of the interpretations that Sheraton and Collerson (1984) place on protolith petrogenesis. Although they note that LILE were mobile in many rocks, they were unable to establish if LILE metasomatism affected all rocks or whether the process was selective. Unfortunately the LILE are used in an inconsistent manner with respect to possible models for protolith petrogenesis; sometimes they are discounted (*e.g.* Ba behaviour in spidergram figure 3, p.54), whereas other times they are utilized (*e.g.* Ba/Sr, p.59).

More specific problems concern the 'mixture-modelling approach'. Although this technique is commonly used by some petrologists, I doubt the validity of the approach in anything but the very simplest of petrogenetic systems. Perhaps this is something of a personal prejudice, but the uncertainties regarding distribution coefficients, a lack of independent constraint on the fractionating assemblage and the unlikelihood of having a constant assemblage for an extended range of fractionated products, poor knowledge of element mobility during metamorphism, and even more fundamental assumptions regarding the nature of chemical differentiation in intrusive complexes, all mean that such numerical treatment of geochemical data provides apparently quantified petrogenetic models that are not justified by the inherent uncertainties (*cf.* Hanson, 1989; Roberts & Clemens, 1995).

The problems noted above raise a number of important questions regarding existing models for the origin and evolution of the Vestfold Hills gneiss complex. These are outlined towards the end of this chapter in Section 8.6, which defines a series of geochemical objectives within the overall goals of the project.

8.5 Isotope studies and geochronology

8.5.1 Conventional isotopic data (Sr and Nd isotopes)

Pre-D_1 gneiss suites

Isotopic data for the Tryne Metavolcanics and Chelnok Paragneiss are of a preliminary nature. Collerson *et al.* (1983) presented a poorly defined Sm-Nd isochron (MSWD=64)

with an apparent age of 2923 ± 570 Ma and individual model ages, based on chondrite normalized compositions (Nd_{CHUR}), that range from 2165 to 2659 Ma.

From field evidence, Collerson *et al.* (1983) and Collerson & Sheraton (1986) argued that the Mossel Gneiss may be genetically related to the Tryne Metavolcanics, and by assuming local isotopic resetting at *ca.* 2500 Ma, they attempted to combine isotopic results for both lithologies. This procedure creates regression ages of 2810 ± 271 Ma with an initial $^{143}Nd/^{144}Nd$ ratio (I_{Nd}) of 0.50832 ± 21 (by the method of McIntyre *et al.*, 1966), or 2859^{+335}_{-256} (by the Cameron *et al.*, 1981, free-line method) which, the authors argued, are in excellent agreement with a Rb-Sr isochron age of 2774^{+353}_{-278} Ma (I_{Sr}=0.7021^{-15}_{+12}). The best estimate provided by Collerson *et al.* (1983) for the crystallization age of the Mossel Gneiss igneous precursor is 3062 ± 212 Ma based on combined regional Rb-Sr analyses, and they also cited a poorly-defined Sm-Nd whole-rock isochron age of 2488 ± 600 Ma.

Post-D_1 to pre-/syn-D_2 gneiss suites

The isotopic results described by Collerson *et al.* (1983) for the CLG are poorly constrained, with Nd_{CHUR} model ages that vary between 2462 and 2511 Ma, and Rb-Sr age estimates that range between 2454 ± 117 Ma (I_{Sr} = 0.7021 ± 5) and an apparently precise age of 2416 ± 21 Ma (I_{Sr} = 0.7022 ± 3). These results for the CLG and the Rb-Sr age of 2456 ± 163 Ma for the Mossel Gneiss are interpreted by Collerson *et al.* (1983) to date the D_2-M_2 event and the intrusion of CLG magmas (at about 2400-2500 Ma).

8.5.2 U-Pb zircon geochronology

The significance of early isotopic results, especially the 2800-3000 Ma ages attributed to D_1-M_1 by Collerson *et al.* (1983), has been reassessed in the light of a recent U-Pb zircon study by Black *et al.* (1991a). Black *et al.* (1991a) demonstrated that the age of the Mossel Gneiss varies from 2526 ± 6 to 2501 ± 4 Ma , and that crystallization ages for the CLG range from 2501 ± 4 Ma through 2493 ± 5 to 2484 ± 6 Ma, with a late 'syn-tectonic' granodiorite yielding a combined age of 2487 ± 6 Ma.

Implications for conventional isotope systems

In order to compare their dated rocks with those in the existing classification of Collerson *et al.* (1983), Black *et al.* (1991a) presented several Sr-isotope analyses. Initial Sr ratios (recalculated for U-Pb zircon age) and Nd_{CHUR} model ages for Mossel Gneiss (I_{Sr} = 0.7015, Nd_{CHUR} = 2.49 Ga) and CLG (Nd_{CHUR} = 2.38 Ga) lithologies are broadly in agreement with

values obtained by Collerson *et al.* (1983), however, values for CLG sample VH27[2] (I_{Sr} = 0.7016) and Grace Lake Granodiorite sample VH19 (I_{Sr} = 0.7036) are more variable than previous estimates. Of particular interest, the youngest sample of Grace Lake Granodiorite (2481 ± 14 Ma) has a Nd CHUR model age of 2.82 Ga which coincides with the oldest age obtained for xenocrystic zircons in the same rock, with this sample and Mossel Gneiss sample VH21 containing inherited zircon populations that range in age from ~2600 to 2800 Ma. The existence of older crustal protolith in the Vestfold Hills with a minimum age of 2800 Ma is also in agreement with 'ages' obtained by Collerson *et al.* (1983) for their D_1-M_1 event.

Based on variations in crystallization age, geochemistry and initial Sr-isotope ratios for different components of the Mossel Gneiss and CLG, Black *et al.* (1991) concluded that there must have been at least three of four parent magmas involved in the production of felsic crust at this time. However, the spatial and temporal distribution, geochemical relationships, and petrogenetic processes involved in the production of these suites are largely unknown. Moreover, it is obvious that the existing geochemical account and the range of crystallization ages for these suites clearly raises questions as to the degree to which gneiss units are tectonically repeated.

8.6 Summary, research rationale, objectives and methodology

8.6.1 Problems or inconsistencies with previous accounts of the geological evolution

Largely stemming from the revised chronostratigraphy presented in Black *et al.* (1991a), it is apparent that there are a number of problems or inconsistencies in the accounts of the geology of the Vestfold Hills. Many of these problems (outlined below) arise from previous fieldwork that, largely through logistic constraints, concentrated in the southern high-strain region of the terrain.

General problems of mapping in this high-grade terrane

Defining gneiss suites according to composition is suitable for some units, such as the Chelnok and Taynaya Paragneisses, but problems arise where related rocks differ markedly in composition (*e.g.* the compositionally varied CLG) or, conversely, where similar lithologies are potentially unrelated (*e.g.* felsic Mossel Gneiss and CLG of tonalitic to

[2] VH samples referred to in this section are not from this study.

granitic composition). These problems can be resolved according to relative age if there are well defined time-markers, for instance, Mossel Gneiss and CLG suites should be distinguishable on the basis that the latter is discordant to an early foliation, S_1, and retains the effects of only the late deformation, D_2. This general observation holds in low-strain areas but, perhaps more commonly, S_1 and S_2 are virtually coplanar and early structures are typically highly transposed by later ones.

Gneissic transposition renders regional mapping problematical and is perhaps partly responsible for a series of revisions of the summary geological map (1:250 000 scale) for the Vestfold Hills (*e.g.* Oliver *et al.*, 1982; Collerson *et al.*, 1983; Black *et al.*, 1991a). Figure 8.1 is a copy of the map presented by Collerson *et al.* (1983) which has been reproduced subsequently in a number of studies (*e.g.* Sheraton & Collerson, 1984; Collerson & Sheraton, 1986; Passchier *et al.*, 1991). It is included here without revision to facilitate discussion and comparison with more detailed mapping (1:14 000) described in the next chapter. This study accepts many aspects of the existing scheme but highlights areas where revisions or further distinctions should be made.

In order to clearly identify problems with the geological scheme outlined above, it is useful at this stage to outline a series of questions. Then, in the following chapter, the results of fieldwork and detailed mapping are presented. By initially mapping in low-strain areas, concentrating on the CLG, the simplest gneiss unit of widespread extent, new field observations help to unravel the geological complexities in this high-grade terrane.

Currently unanswered questions

1. What was the precise timing of magmatism, metamorphism and deformation?

As noted above, the zircon U-Pb study of Black *et al.* (1991a) was able to constrain the time of D_1-M_1 & D_2-M_2 by dating of pre-deformational and post-deformational intrusive suites. This resulted in an apparently tight age bracket for D_1-M_1 at about 2501 Ma, and a minimum age for D_2 and D_3 at 2477 ± 5 Ma.

The precise timing of D_1 remains open, however, since the Mossel Gneiss and CLG overlap in age at 2501 Ma. Either the event is within the uncertainty of the SHRIMP technique or the 2501 Ma Mossel gneiss is actually a felsic gneiss of the CLG (see *general problems* above). Similar ambiguity concerns the timing of D_2, both in relative and absolute terms. Oliver *et al.* (1982) and Collerson *et al.* (1983) argued that CLG magmatism occurred synchronously with D_2 deformation, whereas Black *et al.* (1991a) found that the CLG has a range of ages

from 2501 ± 4 Ma in the south, through 2493 ± 5 Ma in the central region, to 2484 ± 6 Ma in the north. Black *et al.* (1991a) further advocated that the syn-tectonic component is restricted to a minor gneissic unit, the Grace Lake granodiorite, from which they estimate the time of the D_2 event to be 2487 ± 6 Ma. However, as this age is older than the youngest CLG (within error), either the pre-deformational relationship of some CLG magmas to the D_2 event is incorrect, or the pooled age for the two granodiorites does not define D_2.

2. How much tectonic repetition is there in the gneiss complex and was there a temporal evolution in CLG magmatism?

Although there has been general agreement that there are three main gneiss suites that were tectonically repeated by F_2 folds (*e.g.* Oliver *et al.*, 1982; Collerson *et al.*, 1983; Parker, 1983; Collerson & Sheraton, 1986), there is not a detailed model that adequately defines the character and scale of folding. Moreover, Sheraton & Collerson (1984) noted that the CLG is geochemically diverse and, although they were unable to distinguish any systematic spatial distribution within their sub-suites, Black *et al.* (1991a) identified what could be a progressive south to north younging in the CLG magmatism. These observations bring into question the extent to which gneiss units were tectonically repeated by F_2 and also indicates that temporal and spatial variations were likely within the Crooked Lake magmatic episode.

3. What is the status and regional distribution of gneiss lithologies?

Various authors disagree as to the status and regional extent of all the main gneiss lithologies, especially in the northern Vestfold Hills. For example, Black *et al.* (1991a) were unable to identify the Tryne Metavolcanics at the type area and instead considered the Tryne area to be dominantly comprised of Chelnok Paragneiss (*cf.* Collerson *et al.* 1983, figure 1, *vs.* Black *et al.* 1991a, figure 1). Similarly, Black *et al.* (1991a) argued that most of the orthogneiss in the Grace Lake area is Mossel Gneiss which conflicts with the map of Collerson *et al.* (1983; *cf.* maps above) where it is depicted as CLG.

4. Is it possible to identify the geochemically-defined CLG groups of Sheraton & Collerson (1984) based on field criteria?

The geochemical study of Sheraton & Collerson (1984) and the U-Pb zircon study of Black *et al.* (1991a) have established that there are compositionally and temporally distinct gneiss units grouped within the CLG. However, from their studies it is not currently known if all or indeed any of the suites are genetically related and the spatial distribution of protolith types remains unresolved.

5. Were all the *ca.* 2500 Ma orthogneiss suites produced by a common tectonomagmatic process?

Sheraton & Collerson (1984) proposed that the majority of the Vestfold Hills orthogneisses probably formed by partial melting of subducted hydrated oceanic crust. However, they acknowledge that this petrogenetic model is tentative and based on a regional study and limited dataset. It is apparent from the geochemical and conventional isotopic outline presented in the previous two sections (Section 8.4 & 8.5) that much remains to be done in the Vestfold Hills. One of the main aims of this study is to test and refine the existing petrogenetic model through an integrated and detailed petrographic, geochemical and isotopic analysis.

6. Was there a significant metamorphic or tectonic history prior to the *ca.* 2500 Ma events?

As originally defined by Oliver *et al.* (1982), D_1 is a term used to denote a *composite* deformation that possibly comprised more than one tectonic episode, a subtle point apparently overlooked in later studies (*e.g.* Sheraton & Collerson, 1984; Black *et al.* 1991a; Harley, 1993). In support of older crustal material, Black *et al.* (1991a) found inherited zircons in some orthogneisses that are at least as old as 2700-2800 Ma. Further evidence based on a *ca.* 2.8 Ga Nd_{CHUR} model age from one of the rocks with inherited zircons would tend to confirm that there is crust of such antiquity either within or beneath the Vestfold Hills. However the majority of Sr- and Nd-isotopic data are more difficult to interpret. Most orthogneisses studied by Collerson *et al.* (1983) and Black *et al.* (1991a) have *ca.* 2500 Ma model ages but regionally defined 'isochrons' of *ca.* 3000 Ma led Collerson *et al.* (1983) to advocate an older crustal history for the terrane. One of the objectives of this study is to re-examine Sr and Nd isotopes from the Vestfold Hills in order to resolve this apparent discrepancy, and to assess whether isotopically evolved (older) crust was involved in *ca.* 2500 Ma protolith petrogenesis.

If there was a significant Archaean crustal history prior to 2500 Ma, then this has important implications for the terrane in general and, more specifically, it also creates potential links between the Vestfold Hills and others areas in the East Antarctic Shield. In particular, 2800 Ma ages are emerging as regionally important as it is now recognised that there were major events in the adjacent Rauer Group (Kinny *et al.*, 1993; see Chapter 6) and elsewhere in East Antarctica at this time (Harley & Black, 1997).

8.6.2 Objectives and methodology

The objectives in the Vestfold Hills are very similar to those described for the Rauer Group in Section 2.7.3, and can be considered in terms of specific and wider goals. The questions posed above essentially define many of the specific objectives, and as with the Rauer Group, the wider objectives are essentially aimed towards:

- understanding the petrogenetic history of individual orthogneiss suites;
- relating magmatism to a tectonomagmatic framework for the Vestfold Hills in the context of the East Prydz Bay region;
- comparing Archaean gneiss suites in the Vestfold Hills with those in the adjacent reworked Rauer Group mobile belt and with other Archaean terranes in the EAS in order to assess the nature and timing of terrane amalgamation.

The methodology adopted to accomplish these objectives and to answer the questions posed above, can be broken down into four phases: *fieldwork, petrography and mineral chemistry, geochemical and isotopic analysis,* and *data integration.* This is the same methodology that adopted for the Rauer Group, but there are differences in emphasis in this terrane (outlined below).

Fieldwork (Chapter 9)

In practical terms, work in the Vestfold Hills focused on low-strain areas where intrusive phases can be related to a structural and magmatic chronology of events. Detailed field observations of relict igneous features can then be directed towards defining which lithologies are most likely to be directly petrogenetically related. From this basis, the objective is to establish the spatial distribution of different suites and to assess regional correlations.

Petrography and mineral chemistry

Because the orthogneisses in the Vestfold Hills proved to be more compositionally diverse than those in the adjacent Archaean Rauer Group, less emphasis was placed on detailed petrography and mineral chemistry. Nevertheless, a preliminary account of relict igneous phases and textures and subsequent overprinting relationships is integrated with field relations and the general geochemical account that is presented in Chapter 11.

Geochemical and isotopic analysis

A combined geochemical and isotopic study is the most commonly adopted approach to understanding protolith petrogenesis in high-grade terranes (*e.g.* Questions 4 & 5 above). Although representative samples from all the main orthogneiss suits present in the Vestfold Hills were collected (*ca.* 350 samples) only a general account of selected suites is presented in this study. Rather than randomly select orthogneisses from throughout the terrane, I decided to concentrate on one previously unstudied CLG suite from the central northern Vestfold Hills (termed the Lake Africa Suite). However, a general overview of the large regional dataset is also included in Chapter 11, which includes Sr- and Nd- isotope analysis. This conventional radiogenic-isotope approach which was primarily undertaken to understand protolith petrogenesis, rather than to provide chronological constraints. Isotopic dating using the SHRIMP U-Pb technique is considered separately in Chapter 10, and this precise age data is used to interpret the Sr- and Nd-isotope results.

Data integration

Much of the data from the first three phases is brought together in the conclusions section of Chapter 11 in the context of protolith petrogenesis. The final chapter in Part 3 (Chapter 12) evaluates previous accounts of the geology and geochemistry of the Vestfold Hills terrane and summarizes the main conclusions from Part 3.

Finally, the Vestfold Hills is considered in a wider context in **Part 4: Discussion and conclusions**. In this chapter (Chapter 13), conclusions from the Vestfold Hills and Rauer Group are integrated into an Archaean geological framework for the East Prydz Bay region. The final section in this chapter outlines the wider implications from this study, what further steps (detailed modelling) can be undertaken with the existing dataset and what further research is required in the area.

Chapter 9

Field relations and preliminary petrographic observations from the gneiss complex

9.1 Introduction

This chapter presents a summary of field observations made during the course of mapping. Initial work focused on the relatively unstudied northern low strain area between Long Peninsula and Grace Lake (Figure 9.1*[1]), and was then extended into the higher-strain southern region of Broad Peninsula (see Figure 9.2 for localities). Similarly, detailed mapping was also carried out in sub-areas around Crooked Lake-Boulder Hill, Lebed Lake, Zolotov Island and SW Broad Peninsula.

Intrusive relations that occur mostly in regions of relatively low finite strain allow a reconstruction of the magmatic history of the terrane, which in turn places constraint on the nature and timing of metamorphism and deformation. Of prime importance is the Crooked Lake Gneiss (CLG). This gneiss suite is of regional extent and originally comprised a number of compositionally varied magmatic centres that intruded in the interval between the first two major deformations (D_1 & D_2). New field observations presented here closely examine the CLG in order to define the temporal evolution of magmatism with respect to the deformational history.

The structure of this chapter largely reflects the importance of the CLG in defining the geological history of the region, hence well-preserved features of this suite from the northern low-strain region are described first. Rather than describe a region-by-region account of the mapping, only a summary of the most important observations is described here. One of the key observations made during the course of mapping is that strain distribution is heterogeneous throughout the Vestfold Hills. The field descriptions presented here account for this variability and provide a comprehensive geological framework within which to interpret (or re-interpret) geochemical and isotopic data. From this basis it is then possible to more fully understand the tectonomagmatic processes involved in the *ca.* 2500 Ma accretion event (discussed in Chapters 11-13).

[1] Figure 9.1* is a colour geological map, Figure 9.15* is a structural summary and Figure 9.27* is a schematic rock-relations diagram; all are enclosed in the pocket at the rear of the thesis.

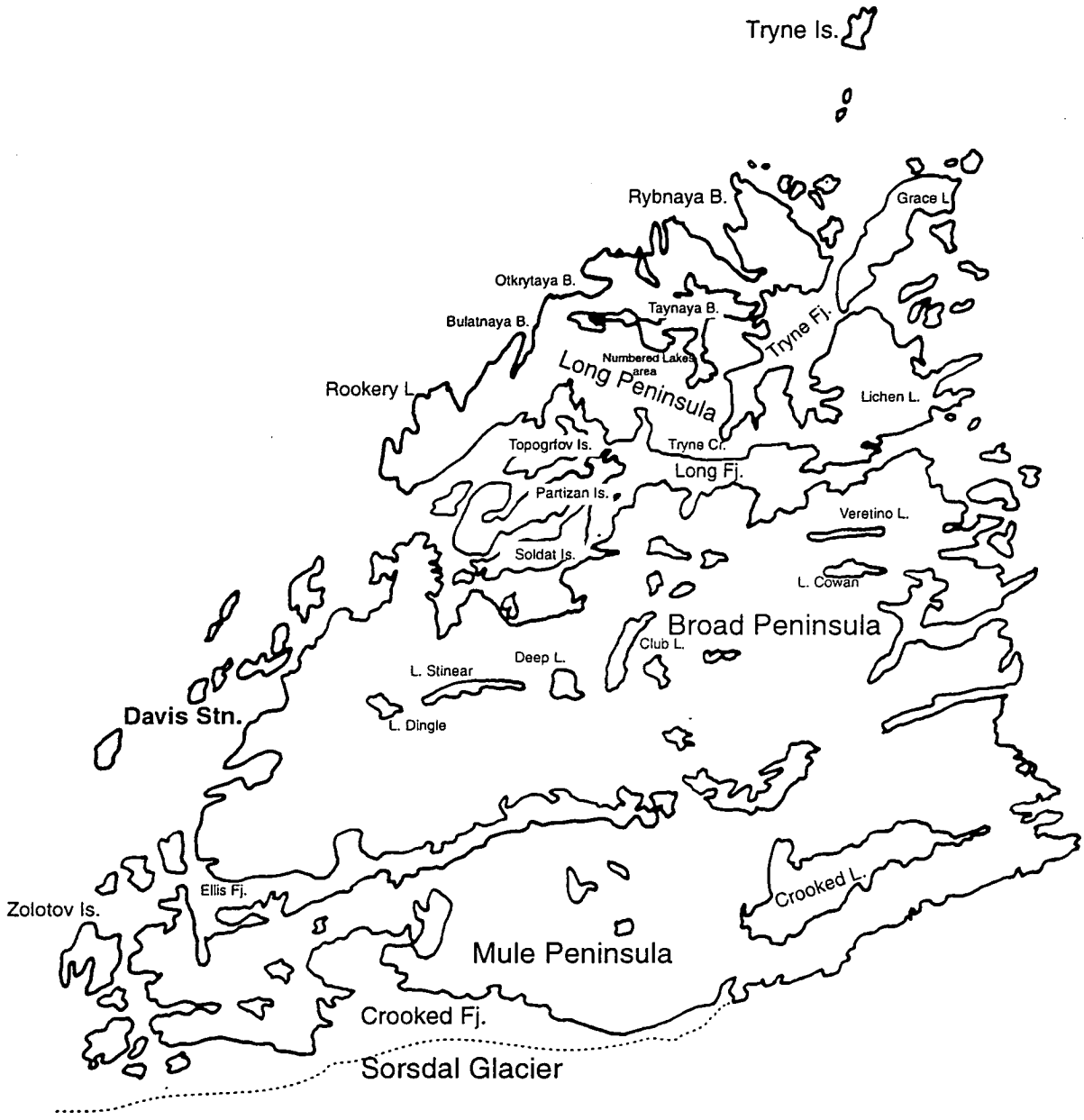

Figure 9.2 Summary of place names referred to in the text.

9.2 Magmatic constraints on geological evolution: the CLG

The key to answering some of the questions outlined in the previous chapter (Section 8.6) can be found in igneous relationships that are preserved in areas of low strain. The best preserved and structurally simplest of the low-strain areas are dominated by CLG and detailed mapping of this lithology reveals a more complex intrusive history than has

previously been recognised. It is these relationships that provide an insight into the geological evolution of the terrane.

9.2.1 Preserved intrusive features in the CLG

Field evidence indicates that the Crooked Lake protolith intruded in a wide variety of forms, ranging from small mafic dykes (Figure 9.3) to irregularly shaped, km-scale, composite plutons (see Figure 9.1*). The best preserved igneous features occur in relatively competent plutons in areas of low late (D_2) strain, where igneous features, such as xenolithic wall zones (Figure 9.4), primary igneous layering (Figure 9.5), and intrusive relationships (Figure 9.6), are preserved. Despite deformation during the D_2 event, individual plutons are of mappable extent forming stock-like bodies that range in size from about 0.5 to >1 km diameter (see Figure 9.1*). Relationships within individual plutons preserve clear compositional gradients from ultramafic cumulates to more differentiated intermediate varieties, with gradational transitions occurring on metre to 10-m scales. It is clear, therefore, that these composite bodies are relict magmatic (intrusive) centres.

Contacts with the older gneisses vary between clean intrusive discordances with S_1 gneissic layering (Figure 9.6), to heterogeneous veining, brecciation or bulk assimilation and rafting of older gneissic lithologies. Some xenolithic wall zones comprise 3 or 4 xenolith types (Figure 9.4), including ultramafic cumulates, fine-grained layered pyroxene granulites (Figure 9.7), felsic gneiss, and more rarely calc-silicate paragneiss. At the margin of some of these xenolithic wall zones the host gneisses are net-veined, although they commonly retain their original orientation and gneissic layering. Where the proportion of melt (Crooked Lake protolith) to assimilant is greater, large detached blocks of country rock occur are preserved as rafted xenolithic fragments or pendants (typically 10s metres scale). Further from these contacts, xenoliths typically become less numerous, smaller, and commonly show evidence of digestion or melting, producing ghosted or autolithic xenolith forms (Figure 9.8). These intrusive contacts and xenolithic relationships preserved in the CLG help define the structural evolution in this region (*e.g.* Figures 9.6 & 9.7).

9.2.2 An outline of the variety and regional distribution of CLG magma types

This section provides an overview of the variability and regional distribution of the CLG as depicted on Figure 9.1*.

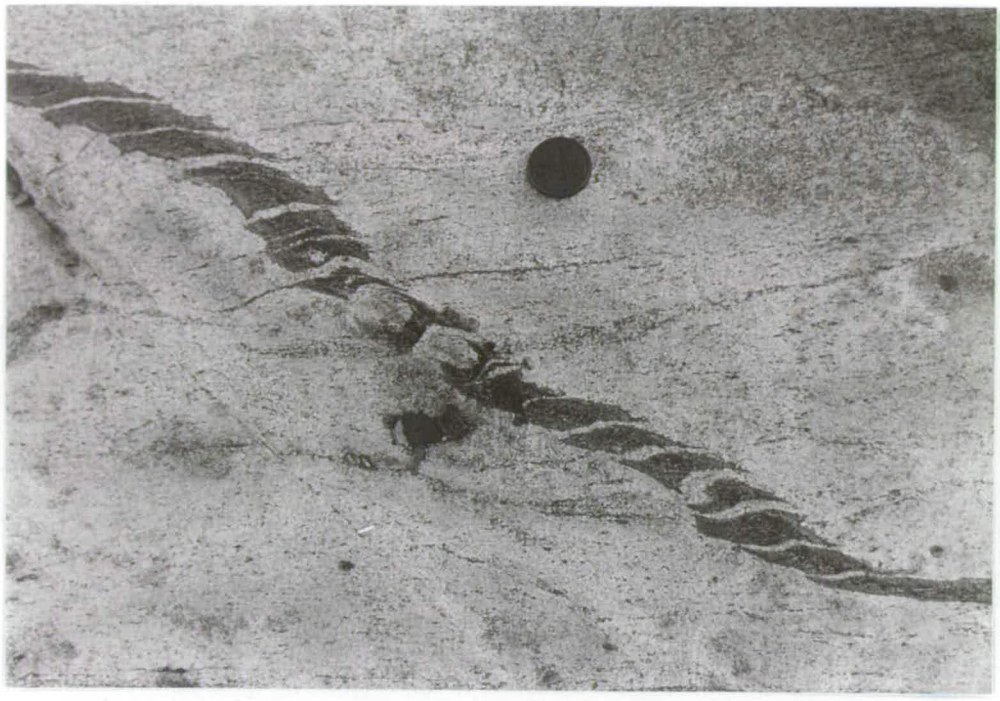

Figure 9.3 Intrusive CLG mafic dyke cuts across an early foliation and schlieren in Mossel Gneiss but has then been strongly deformed and boudinaged. There is an internal foliation in the dyke (S_2) that is parallel to the surrounding composite foliation ($S_{1/2}$; locality: NW Taynaya Bay area; lens cap for scale is 50 mm in diameter).

Figure 9.4 An example of a xenolithic wall zone. This area locally contains up to 70 % xenoliths of at least 4 distinctly different populations including the Taynaya EMG. Note felsic net-veining in the felsic - intermediate gneiss in the centre (locality: central southern Long Peninsula on the coast of Long Fjord; notebook for scale is 10 x 20 cm).

Figure 9.5 Centimetre-scale rhythmic graded layers in gabbroic CLG. The pen points in the upward direction (lower colour index) of graded layers (locality: Long Peninsula on the coast of Long Fjord WSW of Rookery Lake; pen for scale is 15 cm long).

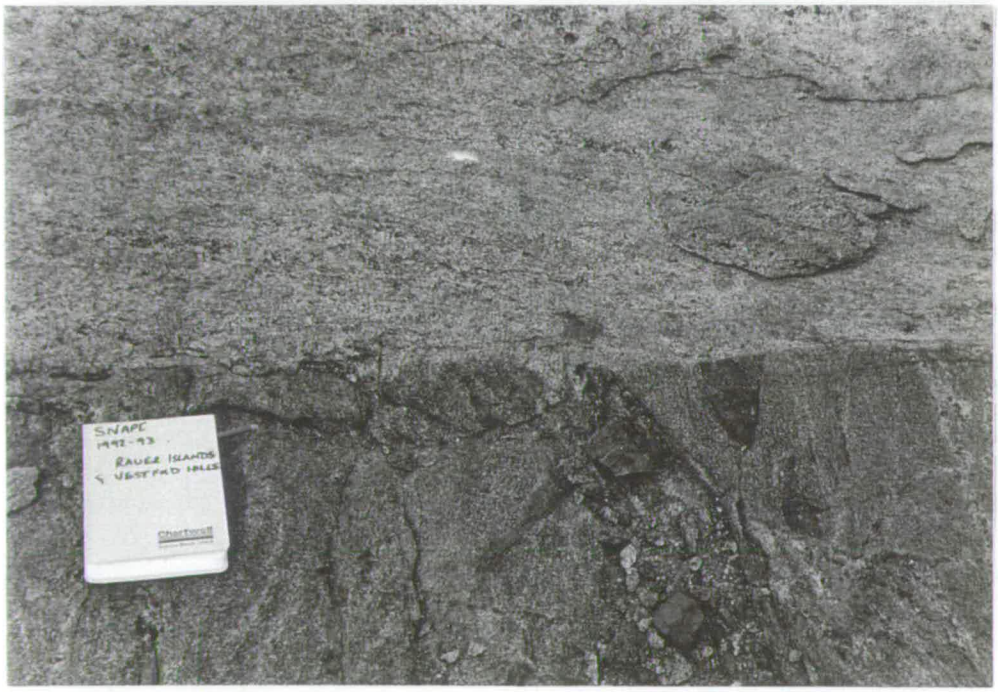

Figure 9.6 Discordance between EMG and intrusive intermediate CLG. Note that the intrusive contact truncates elongate xenoliths and an early layering/foliation, but that the later gneiss also has a foliation that trends from top left to centre right (locality: S Long Peninsula; notebook for scale is 10 cm wide).

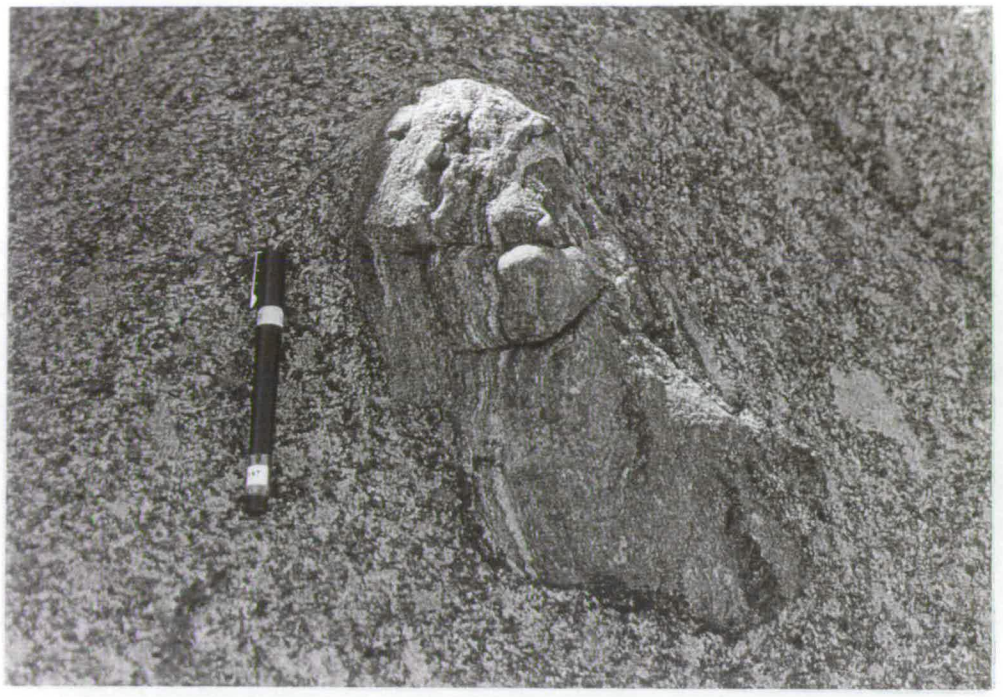

Figure 9.7 Xenolithic relations in the CLG. Strong layering in the EMG xenolith reveals an earlier deformational history, the host here has a largely igneous texture although there is a weak tectonic fabric just visible as it is wrapped around the top of the xenolith (Long Peninsula on the coast of Long Fjord WSW of Rookery Lake; pen for scale is 15 cm long).

Figure 9.8 Partly digested or autolithic Mossel Gneiss xenolith in intermediate CLG (locality: Long Peninsula on the coast of Long Fjord WSW of Rookery Lake; pen for scale is 15 cm long).

Intermediate CLG

The most abundant CLG lithology in the northern Vestfold Hills is coarse-grained and of intermediate but variable composition, comprising hornblende- and quartz-bearing monzonites, monzodiorites and diorites. These are readily distinguished from the Mossel Gneiss because the CLG are generally only weakly foliated, contain less quartz, and have a higher colour index (in the sense of Thorpe & Brown, 1985). Gradational contacts to more felsic and mafic varieties occur locally. Although mapped as one lithology (Figure 9.1*) it is apparent that this gneiss suite encompasses more than one intrusion and is not a single highly attenuated differentiated pluton that has been tectonically repeated. For example, intermediate CLG in the Rybnaya Bay and NE Grace Lake areas are characterised by a nodular highly xenolithic lithology of broadly dioritic composition (Figure 9.9); whereas intermediate CLG in the central Taynaya Bay region is typically monzonitic in composition. Although the gneisses in the Taynaya Bay region are locally xenolithic, this is not a distinctive feature as with the CLG further north. Locally, both of the dioritic and monzonitic rock types become more quartz rich. Where such areas become extensive, such as Soldat Island, they have been mapped as a separate felsic suite comprising quartz monzonites (mostly), quartz diorites and tonalites. However, it is worth emphasising that it is sometimes difficult to distinguish between such felsic CLG and Mossel Gneiss. Where both gneiss types are intimately interleaved at outcrop and regional scales, such as near the Numbered Lakes area (see Figures 9.1* & 9.2), they have been grouped as 'Composite Felsic Orthogneiss'.

Similar gradational contacts and mapping difficulties led to a simplified grouping around Broad Peninsula, where the CLG is distinguished as being a dominantly feldspar-phyric intermediate to felsic type (monzonite dominates) with abundant large mesoperthite phenocrysts. Approximately 70 % of the CLG in this region is of this rock type, with most of the remaining CLG comprising equigranular intermediate to felsic compositions as described above. These two regionally important CLG types are locally gradational. Based on cross-cutting criteria and the limited geochronology that is available, it is likely that these different suites represent more than two spatially and temporally distinct magma batches. Although it is not always easy to distinguish between the porphyritic and equigranular variations at 14 000 (airphoto) scale by outcrop mapping, the overall distinction is important because the porphyritic variety (as described from Platcha Hut by Black *et al.*, 1991a), is different in age to other intermediate gneisses. Furthermore, this textural type is very rare north of Tryne Crossing or further south (a poorly defined boundary with equigranular intermediate CLG runs roughly east-west where the text is placed on Figure 9.1*).

Ultramafic-mafic-intermediate CLG associations

Although not as extensive as the intermediate to felsic CLG, the most distinctive feature of the CLG in the northern region is the presence of well-preserved ultramafic-mafic-intermediate associations. As with the majority of intermediate compositions described above, grouping suites into 'Ultramafic to Melagabbroic' and 'Gabbroic to Monzodioritic' CLG is lithological rather than strictly cogenetic. Some of the rock types shown on Figure 9.1*, such as the 'Hornblende-Phyric Suite' near Lake Abraxas and the folded complex east of Tryne Fjord, are clearly differentiated plutons that are partly dismembered and tectonically repeated by F_2. However, considerable regional variation occurs between these groups. Some units, such as those near Taynaya Bay [GR 900 003] are characterised by a primary spotted cumulate texture with abundant hornblende and biotite (Figure 9.10). Others, such as the ultramafic-melagabbro association that occurs towards the west of the Numbered Lakes area [GR 875 015], are coarse-grained equigranular clinopyroxene-orthopyroxene ± plagioclase rocks. This suite is also possibly directly related to the Hornblende-Phyric Suite described above, which more typically occurs as a distinctive spotted green rock (Figure 9.11). The best example of the Hornblende-Phyric Suite occurs at Norite Point (described below, see Figure 9.18) and comprises clinopyroxene with lesser orthopyroxene and plagioclase all overprinted by poikiloblastic hornblende. The significance of these textures is considered further below.

Felsic CLG

As with the mafic lithologies described above, there are also important regional variations within the differentiated CLG protolith types. The homogeneous and migmatitic granodiorites (Grace Lake Granodiorite unit) shown on Figure 9.1*, for example, are two distinctive rock types that are well represented in the Tryne Fjord area but are uncommon further south.

A relatively undeformed example of the homogeneous granodiorite occurs on the central eastern side of Tryne Fjord and has been dated at 2489 ± 8 Ma by Black *et al.* (1991a). However, this granodiorite differs in form and texture from the Grace Lake Granodiorite at the type location 5 km to the NNE, which tends to be more podiform in geometry and is perhaps better described as a heterogeneous migmatitic white gneiss containing abundant mafic schlieren and schollen. The granodiorite at the type locality (Grace Lake Granodiorite *s.s.*) has been dated at 2481 ± 14 Ma (Black *et al.*, 1991a) and occurs as discontinuous sheets from Grace Lake, through Snezhnyy Bay, into the Taynaya Bay region (see Figure

9.1*). Since local intrusive discordances of homogeneous granodiorite commonly occur within individual Grace Lake-type bodies, it is likely that some components of the Grace Lake Granodiorite represent mobilisate associated with D_2-M_2 (Figure 9.12). These observations suggest that not all the units described by Black *et al.* (1991a; 1991b) as 'Grace Lake Granodiorite' are genetically related to the migmatitic granodiorite at the type locality. Instead there are a number of spatially and temporally separate granitic and granodioritic intrusions. The distribution of these different granitic (*s.l.*) rock types is distinguished in Figure 9.1*, and the homogeneous granodiorite, migmatitic 'Grace Lake' Granodiorite and the late syn-deformational granites (monzogranites and syenogranites) are separated.

Intermediate dykes[2]

The 'Intermediate CLG dykes' are an additional group of intrusions that are possibly unrelated to the more typically coarse-grained CLG. These occur throughout the northern region (Figure 9.1*) and are distinctive intrusions that were emplaced before, during and after D_2/D_3 deformation. Mineralogically they comprise plagioclase - clinopyroxene ± orthopyroxene ± hornblende ± quartz, and because they are typically medium-grained and granular, they are sometimes difficult to distinguish from strongly transposed EMG (*cf.* Section 9.4.1).

9.2.3 Relative chronology of Crooked Lake magmatism

Within individual km-scale plutons (present size after deformation), magmas differentiated to produce pyroxenite cumulates (websterites), oikocrystic and spotted gabbros (Figure 9.10 & 9.11) and more fractionated feldspar-dominated varieties with minor quartz (monzodiorites). Generally, it is these more felsic rock types that retain primary textural and geochemical evidence for assimilation of the surrounding gneisses, as described above in Section 9.2.1.

Closely following mafic plutonism, more voluminous intermediate to felsic magmas were emplaced. These are dominantly diorites, monzonites through to quartz-bearing monzonites, with lesser amounts of tonalite and homogeneous granodiorite. The distinctive migmatitic

---

[2] The term dyke is used fairly specifically in this study and is restricted to medium-grained planar intrusions that are discordant to either earlier structures or rock types. Dyke in this sense usually refers to intermediate to mafic compositions. Although felsic dykes do occur occasionally, they more commonly form networks (*e.g.* Figure 9.4) or irregular bodies. They are distinguished by the terms network, pod, sheet and vein. Having made this distinction, it should be noted that some of the CLG units described as 'plutons' were possibly dyke- or sill-like in geometry.

Figure 9.9 Dioritic CLG with abundant nodular xenoliths of Taynaya EMG (locality: Rybnaya Bay area; notebook for scale is 10 x 20 cm).

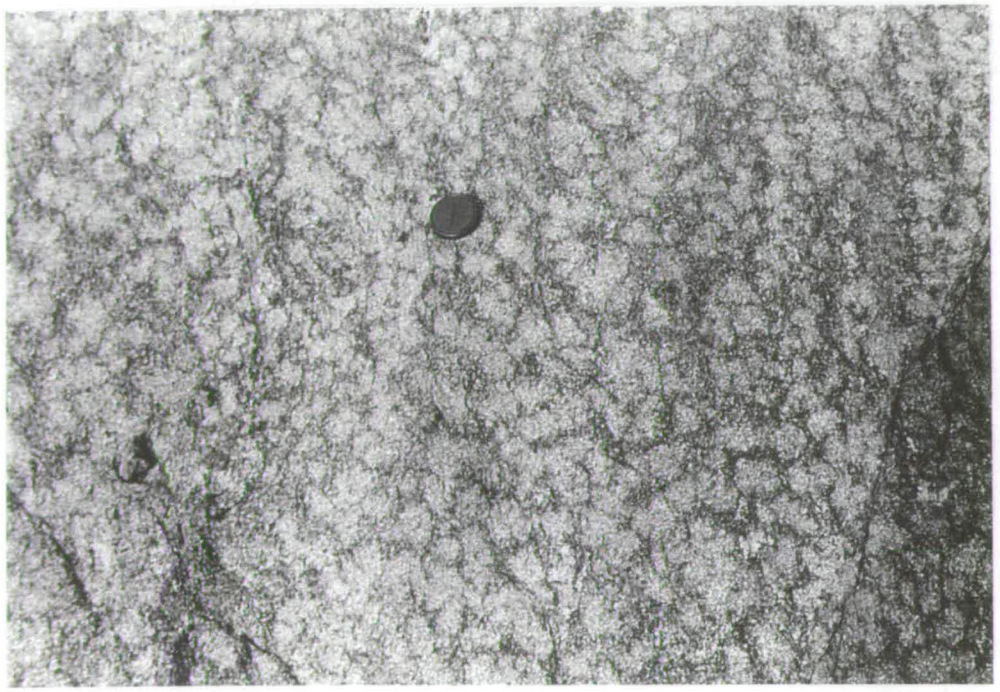

Figure 9.10 Spotted cumulate CLG gabbro (locality: W Taynaya Bay; lens cap for scale is 50 mm in diameter).

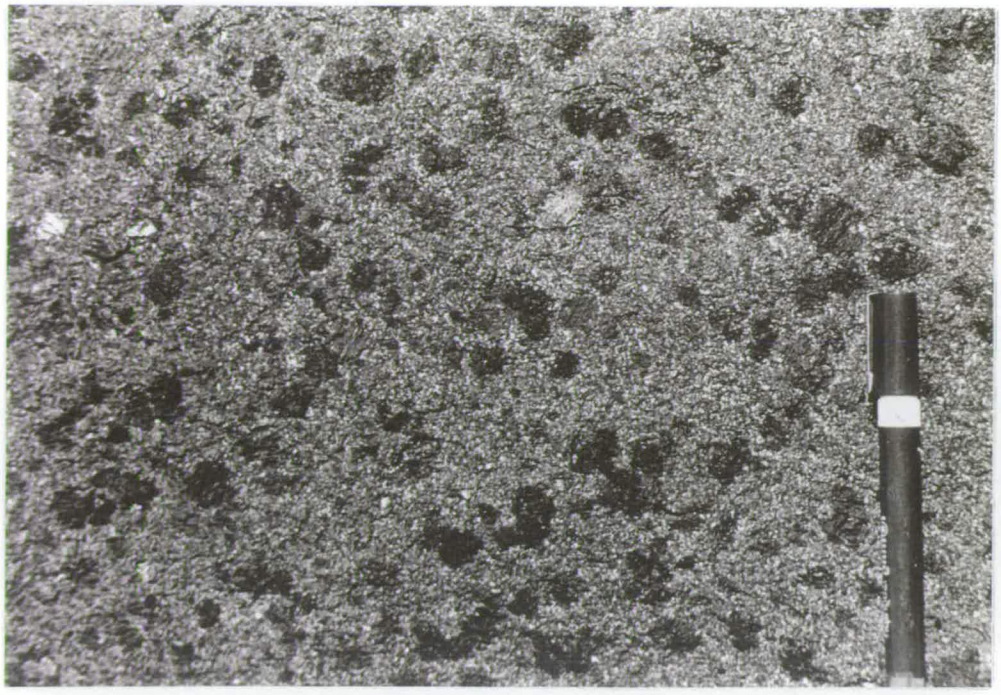

Figure 9.11 Hornblende-Phyric Suite CLG melagabbro. Note that prominent Hornblende poikiloblasts occur in a medium-grained clinopyroxene - plagioclase - orthopyroxene (minor) groundmass (locality: Hornblende-Phyric Suite in central Long Peninsula; pen for scale is 1 cm thick.

Figure 9.12 Migmatitic Grace Lake Granodiorite gneiss. Note that finely layered mafic xenoliths and schlieren are enclosed in a foliated granodioritic gneiss. Within this package late granitic to granodioritic mobilisate cross-cuts fabric elements (S_2) and occurs as melt patches and veins (locality: Grace Lake area near the type locality of the Grace Lake Granodiorite; pen for scale is 15 cm long).

Grace Lake Granodiorite was also emplaced in the northern region relatively late in this magmatic episode.

The final phase of Crooked Lake magmatism is typified by syn-tectonic intrusion of granitic (*s.s.*) sheets and pods. These usually occur as homogeneous podiform to sheet-like bodies which are broadly elongate parallel to S_2. Where they occur in older CLG, they are often slightly discordant to S_2, but share a weak biotite fabric of the same orientation. In some units, granitic melts are preserved as axial planar (S_2) leucosomes. Such leucosomes are parallel to S_2 on the limbs of folds but are typically folded by parasitic asymmetric folds (F_2) except where they cut across hinges in local zones of extension (see Figures 10.2 & 10.3a & b).

In addition to the coarse-grained CLG described above, an extensive 'suite' of generally finer-grained pre-, syn- and post-deformational diorite to quartz-diorite dykes intruded. Pre-deformational dykes are distinguished on the basis that they are strongly deformed by D_2; they are typically strongly attenuated and folded by regional (F_{2r}) and minor (F_{2m}) folds and sometimes have a strong S_2 fabric. By contrast, syn-deformational dykes clearly intruded after all the main Crooked Lake magmatic phases and also cross-cut the late fabric (S_2) in the Grace Lake Granodiorite (Figure 9.12). However, such dykes are locally intruded by late granites and axial-planar leucosomes, and felsic mobilisate associated with the migmatitic granodiorite described above. Post-deformational intermediate dykes are relatively rare, but are distinguished because they cross-cut D_2 and D_3 structural elements and also truncate the earliest high-grade ductile shear zones (possibly related to D_3). One of these dykes from the Grace Lake area (Figure 9.1*) has been dated by Black *et al.* (1991a) at 2477 ± 5 Ma.

9.2.4 Relationship of Crooked Lake intrusives to the D_2-M_2 event

The Crooked Lake magmatic episode, as defined here, encompasses all the intrusive phases that occurred after D_1-M_1 (*e.g.* Figure 9.6) but that have been affected by D_2-M_2. None of the rock types described above (Sections 9.2.2. & 9.2.3) experienced the D_1-M_1 event. Expressed differently, despite the mineralogical and geochemical similarity between Mossel Gneiss and some CLG (Sheraton & Collerson, 1984; see Chapters 8 & 11), the D_1 event (2496.3 ± 0.7 Ma; Chapter 10) appears to represent a break in magma genesis.

Originally it was thought that the Crooked Lake protolith intruded syn-tectonically throughout the D_2 event (*e.g.* Oliver *et al.*, 1982; Collerson *et al.*, 1983; Sheraton &

Collerson, 1984), whereas Black *et al.* (1991a) restricted the syn-tectonic component to the Grace Lake Granodiorite. However, relationships in the northern region indicate that only minor intrusions were emplaced syn-kinematically during D_2. Components of the Grace Lake Granodiorite, as defined in the type area are possible examples, but more typically syn-tectonic intrusions are restricted to granite sheets and pods, laterally continuous intermediate dykes, and granitic leucosomes of apparently local derivation. Axial-planar leucosome within one of these intermediate dykes has been investigated by SHRIMP U-Pb zircon analysis (Chapter 10) and directly constrains the age of D_2-M_2 to 2475.3 ± 0.7 Ma. These results and field observations indicate that the 2487 ± 6 Ma estimate for the age of D_2-M_2 is too old, and that most CLG magmatism predates D_2. Note also that this younger age is close to and within error of the 2481 ± 14 Ma age obtained for the Grace Lake granodiorite at the type locality and that this interpretation is also consistent with the age of the post deformational quartz diorite dykes, one of which has been dated at 2477 ± 5 Ma (Black *et al.*, 1991a). This dyke and the syn-tectonic leucosome provide minimum age constraints for the main fabric-producing late deformation (D_2) and the regional warping event (D_3) which must have closely followed D_2. Alternatively the open warping is merely a late phase of the main (D_2) fabric-producing event (discussed further in Chapters 12 & 13).

9.3 Status and regional distribution of gneiss lithologies: constraints on the amount of tectonic repetition

Detailed documentation of intra-suite relations within the CLG not only characterises the geometry, composition and temporal distribution of intrusions associated with the Crooked Lake magmatic episode, but it can also be used to constrain the regional distribution and status of the older lithologies in the Vestfold Hills. This in turn provides the basis from which to constrain the amount and scale of tectonic repetition in the terrane.

9.3.1 Lithological constraints on the amount of tectonic repetition

For the northern region, encompassing Long Peninsula and northern Broad Peninsula, the distribution of CLG is more abundant than recognised by either Collerson *et al.* (1983) or Black *et al.* (1991a). The Rybnaya Bay area provides one example where observations made in this study differ from those of previous studies. In this area CLG is the dominant gneiss type, whereas Collerson *et al.* (1983) depict much of the area as an extension of the Tryne Metavolcanics (see Figure 8.1). Much of the area is now mapped as medium-grained CLG diorite (age 2484 ± 6 Ma; Black *et al.*, 1991a). Admittedly it is difficult to distinguish between this diorite and the early pre-D_1 mafic components in the area (part of the Tryne

'Metavolcanics', see discussion below) because the two rock types have a similar mineralogy and texture and the boundary between them is irregular and strongly deformed. Boundary mapping is further complicated because the CLG diorite contains abundant xenoliths, locally up to 40 %, of the older more mafic suite (*cf.* Figure 9.9). Nevertheless, there are intrusive relationships and gradational contacts between the diorite suite and compositionally varied gabbros, leucogabbros and granites (*s.l.*) that are characteristic of CLG elsewhere. In addition, geochemical similarities (Chapter 11) and extrapolation from the diorite at the zircon dating locality (Black *et al.*, 1991a, figure 1) further supports a CLG rather than Tryne Metavolcanic affinity for the gneisses in this region.

There are further discrepancies between this study and earlier accounts of the geology of the northern region. In the area to the east of Tryne Fjord, Collerson *et al.* (1983) described CLG whilst Black *et al.* (1991a) argued that it is dominantly Mossel Gneiss intruded by minor Grace Lake Granodiorite. Neither view is entirely correct: Mossel Gneiss enclosing a boudin train of the Taynaya Paragneiss occurs near the fjord, whereas the discontinuous outcrops near the ice sheet comprise xenolithic dioritic CLG. As Black *et al.* (1991a) described for the type area, the Grace Lake Granodiorite occurs throughout the region as a distinctive white migmatitic gneiss with abundant mafic schlieren and schollen. This rock type can be mapped as a sizeable although discontinuous 'train' between Grace Lake and Taynaya Bay, with further outcrops in the central islands area and also 25 km to the north on the remote Murphy Rocks. However, as noted above in Section 9.2.2, it is distinct from the 2489 ± 8 Ma granodiorite on the eastern margin of Tryne Fjord (Black *et al.*, 1991a) and both of these are different to the 'Grace Lake Granodiorite' pods mapped further south near Platcha Hut (Black *et al.*, 1991b), which are better described as homogeneous coarse-grained (syn-tectonic) granites.

In summary, there is considerable local and regional variation within the CLG in the northern region. In contrast to earlier published accounts, the CLG occurs in three main areas separated by older gneiss lithologies (mostly Mossel Gneiss). These areas are: (i) northern Broad Peninsula (ii) central Long Peninsula from Rookery Lake, through southern Taynaya Bay, to eastern Tryne Fjord, and (iii) Rybnaya Bay. Between these areas there are important regional differences in CLG protolith type. Rybnaya Bay mostly comprises xenolithic diorites; the central Long Peninsula area contains more potassic suites, mostly monzonites, monzogabbros and gabbros; whilst northern Broad Peninsula has abundant alkali feldspar-phyric monzonites. As a first order observation, such compositional variation indicates that the CLG was not one suite tectonically repeated, but rather comprised a number of separate intrusions. Moreover, it *is* possible to identify individual suites or units

that were transposed and boudinaged on a local scale by F_2 folds (see Figures 9.1* and 9.6*) and in these areas the detailed map pattern of CLG does not reveal significant regional tectonic repetition. When combined with structural observations (Figure 9.6*), these folded units define mappable F_2 structures in some low-strain areas in the northern region.

9.3.2 Structural constraints on the amount of tectonic repetition

The distribution of gneiss units on existing published maps shows that major units trend essentially E-W and implies that they are tectonically repeated N-S about >km-scale folds. This is the case in general terms but synform-antiform pairs in the northern region (shown on Figure 9.15*) indicate that the scale of folding is much smaller (*ca.* ≤ 500 m-scale wavelengths). The macroscopic folds shown in Figure 9.15* have been mapped largely on the basis of regional asymmetric fold vergence (*e.g.* Figures 9.13 & 9.14), but also where transposed and dismembered lithologies can be traced around fold closures. Other well-defined examples of F_2 folding can be seen in the northern Vestfold Hills. Perhaps the best example occurs to the east of Tryne Fjord where a pre-D_1 mafic unit (fine- to medium-grained granulite) can be traced in detail around a west-facing fold closure. Although there is extensive local transposition, this fold can be clearly distinguished by aerial reconnaissance.

The conclusion from these observations of F_2 geometries on Long Peninsula is that the km-wide E-W trending units depicted by Oliver *et al.* (1982) and Collerson *et al.* (1983) were not repeated by F_2 structures. Moreover, whilst fold wavelengths in low-strain areas are in the order of 500 m, wavelengths decrease towards the south side of Long Peninsula. F_2 structures are difficult to map in this region of generally higher strain as folds are often highly attenuated with a strong foliation and transposed gneissic layering (*cf.* Figure 9.16).

9.3.3 Extrapolation into the southern region

A number of subareas south of Long Fjord have been mapped in detail (this study and Parker *et al.*, 1983) but in general the original maps published by Oliver *et al.* (1982) and Collerson *et al.* (1983) are accurate and at a reasonable scale to portray the overall geology. Intrasuite variations within the CLG comparable with those seen in the north can be recognised in the field, although it is difficult to reconstruct a relative magmatic chronology since there is an intense S_2 fabric, and initially discordant relationships are now virtually parallel (Figure 9.14 & 9.16). The area to the ENE of Crooked Lake (type locality of the CLG), for example, comprises a variety of CLG types that range in composition from melagabbros and gabbros through to monzodiorites and diorites, but the high degree of

Figure 9.13 Metre-scale asymmetric fold vergence in felsic sheets. Parasitic fold axes plunge steeply indicating that this fold has an overall s-geometry. The host lithology is intermediate CLG (locality: south side of Face Lake [GR 875 007]; notebook for scale is 10 x 20 cm and is indicated by arrow).

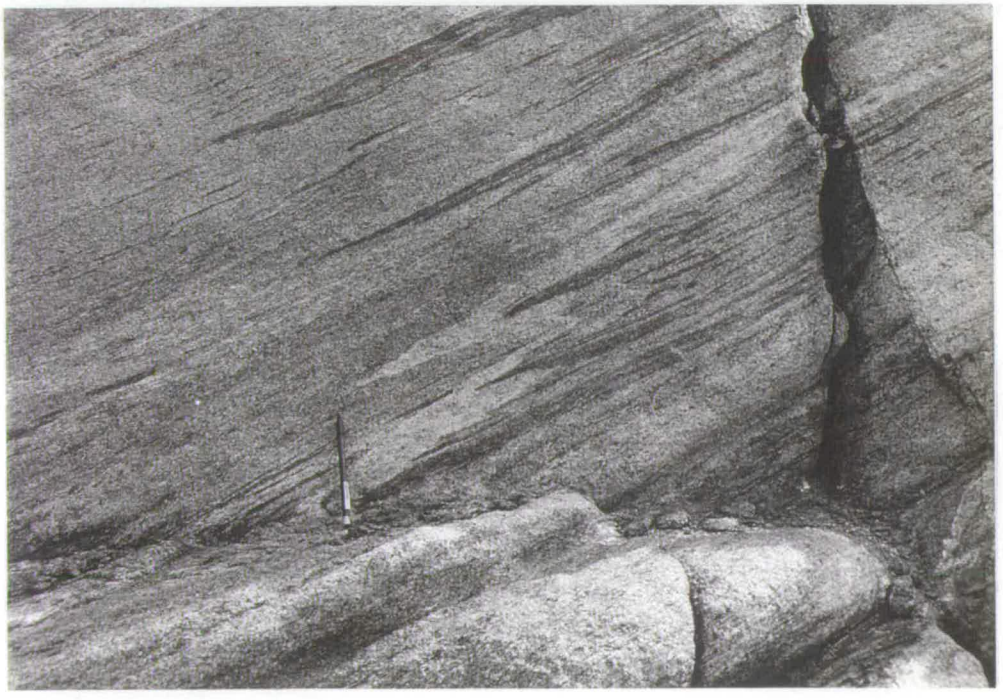

Figure 9.14 Decimetre-scale asymmetric folds defined by felsic CLG vein. Note that the vein cross-cuts the S_1 foliation and small-scale folds in layered Mossel Gneiss. Mafic streaks in the Mossel Gneiss are strongly transposed F_1 folds defined by EMG which are cross-cut by felsic layers that have a sub-concordant S_2 fabric and virtually co-planar geometries (locality: NE Rybnaya Bay area; pen for scale is 15 cm long).

Figure 9.16 An example of a strongly foliated orthogneiss in the southern high-strain (D_2) region. The main lithology types are intermediate and felsic CLG with minor EMG (left of pen). Such strong interlayering of gneiss units is a common feature in the southern region (locality ~0.5 km NE of Boulder Hill, SW Vestfold Hills; Pen for scale is 15 cm long).

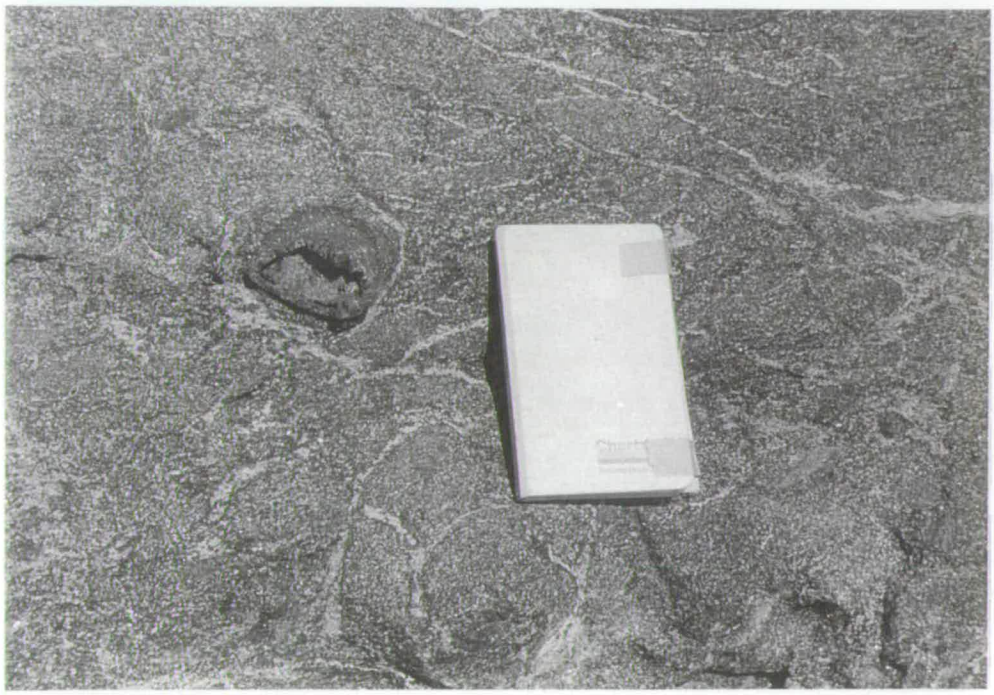

Figure 9.17 Typical example of Taynaya EMG. Medium-grained, granular, Cpx - Opx - Plag dominates with a proud-weathering cognate ultramafic xenolith (Cr-Cpx - Opx ± Ol ± Phlogopite). This EMG is clearly net-veined by felsic Mossel Gneiss (locality: E-side of Taynaya Bay; notebook for scale is 10 x 20 cm).

transposition associated with the late deformation (*e.g.* Figure 9.16) has rendered these gneisses difficult to map at 1:14 000 (air photo) scale. Such relatively high strain (D_2) is common throughout the southern region with a transition occurring across the south side of Long Peninsula into a zone of relatively lower strain.

This N-S strain gradient has had a number of important influences on the interpretations of the geology in the southern Long Peninsula region. In this area, Collerson *et al.* (1983) described the oldest sequence found in the terrane, the Tryne Metavolcanics, which they defined as an ultramafic to acidic volcanic succession that occurs predominantly in a ½ to ¾ km wide band near Long Fjord (see Figure 8.1). Although there is a significant mafic component here, approximately 30 %, there is no *prima facie* evidence (*e.g.* pillow lavas, interbedded pyroclastics or sediments) for a volcanic succession in this region. There are minor mafic components within the Chelnok Paragneiss that may be of volcanic derivation. In detail, the region around Tryne Crossing is a zone of strain intensification, resulting in a fine intercalation of early (pre-D_1) mafic gneiss and metasediments, with more abundant younger orthogneisses. This interpretation is similar to Black *et al.* (1991a), but whilst these workers note the presence of an early mafic gneiss, they considered it of insignificant distribution to present on a map and instead grouped it with the Chelnok Paragneiss (Black *et al.*, 1991a, figure 1). This grouping assumes that all the early mafic components are volcanics and ignores that 60-70 % of the outcrop depicted as paragneiss is felsic orthogneiss. The paragneiss is only a minor constituent of this area. Unfortunately, primary geological relationships between the Chelnok Paragneiss and the early mafic gneiss have been obscured by the overall high state of strain. Nevertheless, the strain intensification that occurs near Long Fjord is not an abrupt change, but rather a general trend where strongly deformed rocks often enclose relatively low-strain domains. These domains are important because they elucidate the relationships between the oldest gneisses, the Chelnok Paragneiss and the Tryne Metavolcanics, and the younger Mossel and Crooked Lake orthogneisses.

9.4 Geological evidence from low-strain windows

9.4.1 The status of the Tryne Metavolcanics

Further evidence against the ultramafic, gabbroic, intermediate and felsic rocks in the southern Long Peninsula region being part of a volcanic succession can be seen at the most westerly extension of the 'metavolcanics' as depicted by Collerson *et al.* (1983; see Figure 8.1). At this small promontory, here called 'Norite Point' (Figure 9.18), a variety of gneiss lithologies were tectonically juxtaposed. However, as the promontory coincides with an F_2

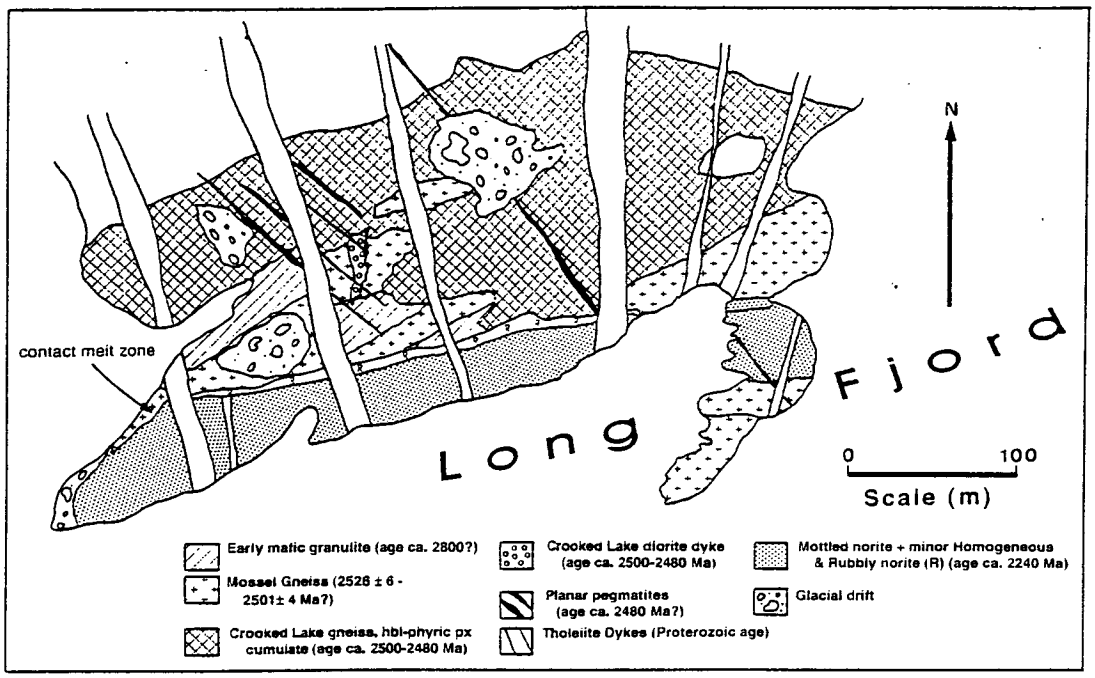

Figure 9.18 Lithological map of Norite Point. This small peninsula was previously mapped as Tryne Metavolcanics (Collerson *et al.*, 1983) but actually comprises a number of compositionally different rock types of markedly different age (locality: on the northern coast of Long Fjord).

closure defined by a massive weakly-deformed CLG gabbro which has largely escaped the effects of high strain, the geological relationships between lithologies are preserved. In this area there is only about 10 % early mafic granulite (*i.e.* pre-D_1 mafic granulite of age >2500 Ma), with the ultramafic, gabbroic and felsic rock types being temporally and genetically very different lithologies. The ultramafics are weakly foliated hornblende-phyric Crooked Lake pyroxene cumulates (age *ca.* 2490 Ma), the gabbro is of noritic composition and is a southerly extension of the *ca.* 2240 Ma (post-deformational) Norite 'ring' dyke that cuts across the gneiss complex (Seitz, 1991; Lanyon *et al.*, 1993), and the felsic gneiss is of Mossel affinity (age *ca.* 2526 ± 6 Ma to 2501 ± 4 Ma).

The complexity of the relationships preserved in the Norite Point low-strain area shows that lithologies previously mapped as Tryne Metavolcanics are in fact a tectonic admixture of rock types of markedly different composition and age. These findings might explain the erroneous interpretation of the Rb-Sr and Sm-Nd whole-rock isochrons for rocks in the southern Long Peninsula region. As Black *et al.* (1991a) demonstrated, Collerson *et al.* (1983) combined unrelated samples together in order to provide a sufficient spread of points

to define an isochron (see Section 8.5). In conclusion, I suggest that the term 'Tryne Metavolcanics' be abandoned.

Arguably the best description of the geology in the Tryne Crossing region is that originally proposed by Oliver *et al.* (1982). Their map (figure 1) depicts a south to north transition from acid to intermediate orthogneiss, layered grey gneiss, layered paragneiss, and acid to intermediate orthogneiss. In order to reconcile differences in the interpretation of the geology of the Long Peninsula region, a new scheme is proposed here. By extrapolation from detailed observations in areas of low late strain, such as Norite Point, pre-D_1 lithologies have been divided into three broad types (excluding the Taynaya Paragneiss):

- (i) layers of mostly (>50%) fine-grained two-pyroxene + plagioclase granulite, here termed 'Early Mafic Gneiss' (EMG)

- (ii) layers of mostly felsic gneiss that are correlated with the Mossel Gneiss

- (iii) Chelnok Paragneiss, which comprises garnetiferous semi-pelites, psammites, quartzites with minor interbedded calc-silicates, and metaironstones. Metabasite within areas dominated by the Chelnok Paragneiss is less than 10 % and occurs as concordant layers within the gneiss: they may have been interbedded lavas or alternatively they are transposed originally discordant mafic dykes.

Taken regionally, the fine-grained mafic layers have a variety of compositions but are all grouped as EMG in this scheme. Only one sub-type is particularly distinctive and of mappable extent. This suite, termed here the Taynaya EMG, occurs predominantly in the Taynaya Bay and Rybnaya Bay areas (see previous discussion of this region). It is characterised by the presence of abundant ovoid to rounded ultramafic nodules and is typically net-veined or agmatised by later orthogneiss suites (Figure 9.17; *cf.* Collerson *et al.*, 1983, fig. 2; Collerson & Sheraton, 1986; Harley, 1993). The EMG further south and east is typically xenolith-absent and homogeneous in texture but more diverse in composition.

Mapping in the region mapped as Tryne Metavolcanics at the type area (Collerson *et al.*, 1983), shows EMG and felsic Mossel Gneiss are interlayered on a metre-scale, largely reflecting D_1. Although the distinction between these two units is somewhat arbitrary (> or < 50 % fine-grained mafic component), individual mafic- or felsic-dominated packages can be mapped along strike for up to 3-4 km (largely reflecting D_2 deformation). The distribution of the main gneiss suites in this region is presented in Figure 9.1*.

To summarize: in this study there are four main departures from published accounts of the Tryne Metavolcanics. These are:

- The EMG, as defined here, corresponds to one component of the Tryne Metavolcanics (Collerson *et al.*, 1983). Field relations also indicate that there is more than one distinct protolith type (*e.g.* the distinctive Taynaya EMG), as first suggested on geochemical grounds by Sheraton & Collerson (1984).

- The mafic component associated with the Chelnok Paragneiss is of relatively minor extent; it might be of volcanic origin, but could equally represent deformed intrusive mafic dykes.

- Much of the Tryne Metavolcanics mapped in the Rybnaya Bay area are fine- to medium-grained dioritic CLG. Nevertheless, one component previously grouped with the metavolcanics, the Taynaya EMG, does crop out in this region. Although of relatively minor extent overall, xenoliths of this suite in host CLG are locally very abundant (up to 40 %).

- The overall succession in the Tryne-crossing area can be explained by tectonic intercalation of a variety of temporally and genetically different rock types in an area of relatively high strain. Nevertheless, it is possible to unravel the geological relations in this area because strain distribution is heterogeneous and intrusive contacts and cross-cutting relationships are preserved in low-strain windows, such as Norite Point.

9.4.2 The relationship between the Mossel Gneiss and the EMG

Although the formal status of the Tryne Metavolcanics has been redefined into a non-genetic grouping ('EMG'), many of the observations made by Collerson *et al.* (1983) regarding the character of the pre-D_1 gneisses are still relevant. Of particular importance is the contention that the Mossel Gneiss is derived by partial melting of the mafic components of the Metavolcanics/EMG (see also Sheraton & Collerson, 1984; Collerson & Sheraton, 1986). As Collerson *et al.* (1983, p.77) noted 'it appears that part of the felsic component of the Mossel Gneiss formed by melting and deformation of metabasite Tryne Metavolcanic protoliths. During the initial stages of this process, mafic granulites partially melted to produce trondhjemitic and tonalitic compositions which net-veined the parent lithology, resulting in the formation of agmatite structures (figure 2b). As the amount of felsic melt increased, discordant veins and sheets were formed, commonly with inclusions of "restite", either as diffuse patches or sharply bounded blocks (figure 2c)'. This description provides a good summary of the melting relations observed in the Taynaya EMG during the course of this study. In the Taynaya Bay region (type locality), this suite is texturally and compositionally similar to figure 2b of Collerson *et al.* (1983) and a similar plate is included here as Figure 9.17. Clearly, the leucosome material shown in the figures and described by Collerson *et al.* (1983) would be a potential way of dating the D_1-M_1 event. For this reason

EMG material throughout the region was carefully examined with respect to their melting relationships. A previously unreported occurrence of Taynaya EMG in the Bulatnaya Bay area is well-preserved in a low-strain area within a fold (F_2) hinge region. Spectacular melting relations observed in this area are briefly described in a regional context here because leucosomes from this area have been studied by SHRIMP U-Pb dating to constrain the age of the D_1-M_1 melting event. Further details of the field relations specific to the dated sample are described in Chapter 10.

Taynaya EMG at Bulatnaya Bay

Field relations in the Bulatnaya Bay region are complex because all the principal orthogneiss units occur in close proximity as tectonically interleaved and transposed gneisses. Nevertheless, a dismembered and refolded boudin train of Taynaya EMG occurs throughout an area of about 1 km^2 and provide the best preserved examples of *in situ* melting relationships in the Vestfold Hills. Apparently unmelted EMG occurs in many 1-10 m boudins, where granulite assemblages of clinopyroxene, orthopyroxene and plagioclase dominate. One example near a large NE-SW trending dyke [GR 835 015] is compositionally graded from ultramafic compositions on the margins to a mafic centre (Figure 9.19). It is not clear whether this unusual feature was originally a differentiated sill (*cf.* Walker, 1932) or was produced by isoclinal folding, as it is truncated at either end. If it is an isoclinal fold, it must be a pre-D_1 structure because both the Mossel Gneiss and nearby intermediate CLG cross-cut the boudin train and the layering. Similarly, a strongly folded CLG dyke cross-cuts earlier (F_1) fold axes defined by the boudin train.

The CLG also cross-cut several different compositions or textural varieties of Mossel Gneiss. The Mossel Gneiss in the low-strain areas varies from homogeneous, with a weak foliation, to moderately foliated with mafic schlieren and schollen. In some areas there are particularly well preserved melting relations with respect to the EMG. There is a wide range of leucosome morphologies, from apparently isolated patch leucosomes, to interconnected networks, veins and sheets (Figures 10.3c, 9.20 & 9.21). In some areas, felsic leucosome dominates and rafted remnants and partly-digested autoliths (restite) are entrained in Mossel protolith.

As with many migmatites it is difficult to assess in the field the relative roles of *in situ* melting versus 'injected component'. Given the extensive distribution of Mossel Gneiss in the Vestfold Hills, the relative paucity of EMG, and the generally similar trace-element characteristics of the Mossel, EMG and Crooked Lake Gneisses, it is likely that late-stage

Figure 9.19 Taynaya EMG at Bulatnaya Bay. Note that this mafic layer is compositionally zoned from ultramafic at the margins to mafic in the centre. Note also the cognate xenoliths (indicated by arrow; locality: Bulatnaya Bay Complex, W Long Peninsula; notebook for scale is 10 x 20 cm).

Figure 9.20 Melting relations in Taynaya EMG showing patch and vein leucosome (locality: Bulatnaya Bay Complex, W Long Peninsula; pen for scale is 15 cm long).

Figure 9.21 Melting relations in Taynaya EMG showing patch and vein leucosomes grading into more extensive sheets (locality: Bulatnaya Bay Complex, W Long Peninsula; pen for scale, top centre, is 1 cm wide).

Figure 9.22 Relatively flat-lying, metre-scale, disharmonic folds in Chelnok Paragneiss. Folds of this type are termed 'F_1', although they fold primary compositional layering (bedding) and a pre-existing foliation. These folds are typically strongly overprinted by an associated axial-planar fabric ('S_1') (locality: near the coast of Long Fjord, NE Broad Peninsula; lens cap for scale is 50 mm in diameter).

Mossel magmatism was the cause of melting rather than the felsic gneisses being the product of incipient melting as a consequence of high-temperature metamorphism. Nevertheless, the isolated patch leucosomes described above (see Figure10.3c) are the best candidates thus far discovered for *in situ* melting of EMG during D_1-M_1. Unfortunately, although these leucosomes are clearly affected by F_1, primary textural relations that confirm the 'syn-tectonic' timing of melt generation are *not* preserved in these polydeformed gneisses. These features and interpretations are discussed further in Chapter 10 in the context of isotope geochronology and the timing of crustal accretion and deformation in the Vestfold Hills.

9.4.3 The Chelnok Paragneiss: Evidence for a tectonothermal history prior to the *ca.* 2500 Ma events?

In a similar way that relationships are preserved in the Norite Point low-strain window, pre-D_1-M_1 geological information can be found in the Chelnok Paragneiss where packages of paragneiss have escaped pervasive D_2 deformation. Where paragneiss units and younger, (typically granitic) orthogneisses are juxtaposed, there is a significant rheological contrast. In some areas of southern Long Peninsula and NE Broad Peninsula this led to strain partitioning, producing large-scale boudinage features separated by high-strain zones (Figures 9.1* & 9.15*). In these *ca.* 1 to <500 m-wide low-strain domains, a variably transposed set of centimetre- to metre-scale early folds have been favourably preserved (Figure 9.22 & 9.23). These structures fold a compositional layering (bedding) and an early foliation, have a new flat-lying axial-planar fabric and fold axes that commonly plunge at a shallow angle. The orientation of such F_1 structures can be distinguished from post-D_2 open warping (F_3) on the basis of intrusive contacts. Where CLG granites intruded through low-strain domains, they cross-cut early structural features, but have a moderate S_2 foliation with a steeply-dipping orientation. Since S_2 in the granites immediately adjacent to the paragneisses parallels the regional trend and the high-strain zones, it is possible to distinguish between relict pre-D_2 flat-lying structures and those produced by post-D_2 open warping.

In the light of the aforementioned field observations it is now possible to place microtextural and petrological information from the paragneisses into a relative chronology. Preliminary studies of some lithologies from the low-strain domains reveals assemblages and relationships not previously recognised in the terrane, especially for calc-silicate and metaironstone compositions.

Figure 9.23 Small fold (F_1) in calc-silicate layer from the Chelnok Paragneiss. Calc-silicate layer and early foliation (pre-S_1) have been folded and a new fabric developed axial planar to this fold (S_1). This S_1 fabric is orientated 38° to 350° and the fold axis plunges at about 40° to 020°.

Petrography and mineral chemistry of meta-ironstone VH543

Figure 9.24 is a thin section photomicrograph from a metaironstone layer within the Chelnok Paragneiss. This section is taken from a small (cm-scale) fold closure with a flat-lying axial plane. Layering is defined by alternating quartz- and pyroxene-rich horizons that are interpreted to be relict primary compositional features (bedding). The pyroxene-rich layers comprise exsolved sub-calcic clinopyroxene and pigeonite. Individual layers are locally homogeneous in terms of bulk X_{Mg}[3], but there is considerable variation between layers. For example, orthopyroxenes in some layers have a consistent X_{Mg} of 0.12, whilst adjacent layers have higher X_{Mg} values of 0.25. Such extremely Fe-rich compositions and distinct compositional variation between layers indicates that these pyroxenes are not detrital or relict igneous grains but are metamorphic in origin. Moreover, since exsolution lamellae are folded (Figure 9.24) and overprinted by neoblast clinopyroxene or sub-calcic clinopyroxene (these commonly form axial-planar arrays), it is apparent that these grains

[3] $X_{Mg} = Mg^{2+}/Mg^{2+} + Fe^{2+}$

formed and exsolved (cooled) prior to the first phase of folding. These mineralogical and microtextural features indicate that granulite facies sub-calcic clinopyroxene and pigeonite formed and subsequently cooled prior to the D_1-M_1 event. However, the age and significance of this 'event' is unknown at present (discussed further below), and thermobarometric study of these samples is beyond the scope of the present work.

In summary, there is a distinct early phase of folding that does not have the same orientation as the F_2 structures, that is, they were not co-linear fold generations of the same 'event'. Instead, F_1 folds *and an early fabric* have usually been transposed into parallelism with S_2.

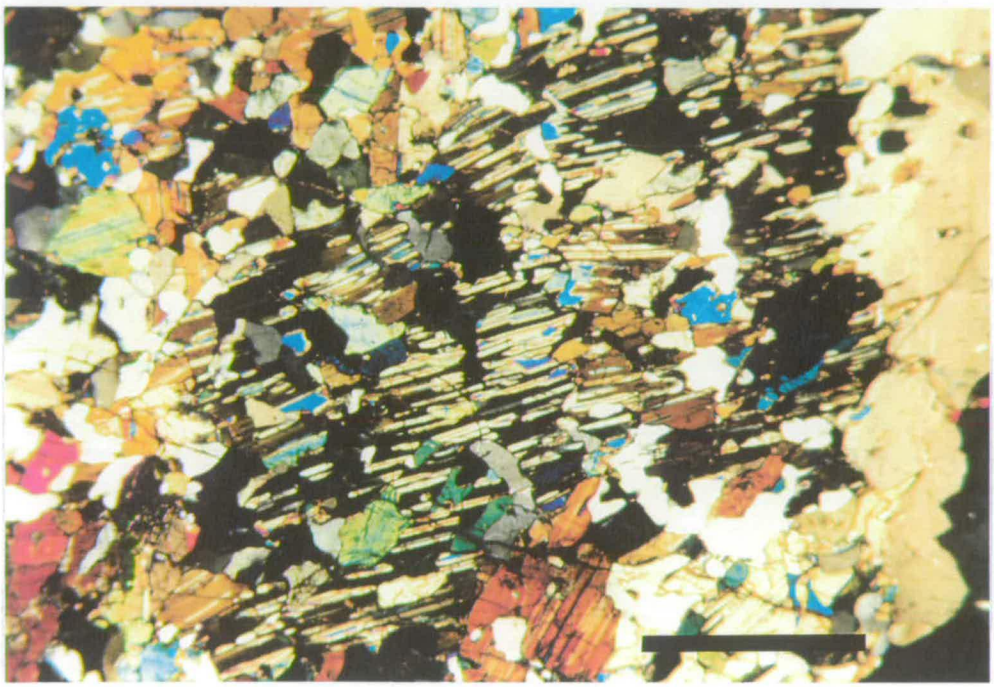

Figure 9.24 Photomicrograph (crossed polars) from a polished section of a metaironstone layer within the Chelnok Paragneiss. Millimetre- to cm-scale layering is defined by alternating quartz-rich and pyroxene-rich horizons. This Section, taken near the closure of a decimetre-scale fold, is of a pyroxene-rich layer. An axial-planar fabric is present in the adjacent quartz-rich layers (not shown here) and is defined by elongate to lobate exsolved sub-calcic clinopyroxenes. Neoblast clinopyroxene (Cpx2) with the same orientation can be seen to overprint *deformed* clinopyroxene (Cpx1) lamellae in host orthopyroxene (Opx), formed by exsolution from original pigeonite. This implies that metamorphic sub-calcic clinopyroxene (in adjacent more Fe-rich layers) and pigeonite *formed and exsolved* prior to folding and new pyroxene growth. More typically, the new fabric is parallel to, and indistinguishable from, compositional layering and the first foliation. The orientation of these structures is essentially flat-lying (*cf.* Figure 9.13) and although not evident at the microscale in this sample, the regional 'S_2' orientation, defined by a fabric in intrusive CLG, is steeply-dipping (locality: near the coast of Long Fjord, NE Broad Peninsula; scale bar is about 2 mm).

These observations have potentially important implications for reconstructing the Archaean metamorphic *P-T-t* path, and also indicate the need for geochronology focusing on these rock types.

9.5 Further observations regarding the metamorphic history

9.5.1 An outline of the problems

An outline of the metamorphic conditions during the principal high-grade events is reviewed in the previous chapter (Section 8.3). It is apparent from revised field relations (this chapter), geochronology (Black *et al.*, 1991a; this study, Chapter 10) and more recent metamorphic studies (*e.g.* Harley, 1993; Harley, Snape & Fitzsimons, 1995), that there are problems with early accounts of the metamorphic history of the terrane. Although Collerson and co-workers (*e.g.* Collerson *et al.*, 1983b); Collerson & Sheraton, 1986) describe a variety of granulite assemblages from the Vestfold Hills, there are no thorough accounts of mineral chemistry of textural context for their work. In particular, thin sections examined in a regional context in this study indicate that initial ultra-high temperature (UHT) estimates of 1000-1100 °C at 8-10 kbar were probably derived from co-existing igneous mesoperthite-antiperthite and clinopyroxene-orthopyroxene pairs. This possibly explains why Harley (1993) and Harley, Snape & Fitzsimons (1995) found no evidence for such extreme metamorphic conditions, and instead constrained D_1-M_1 to 830-880 °C and 3.5-8.5 kbar from the sapphirine-bearing Taynaya Paragneisses, and less than ~840 °C from the calc-silicate Chelnok Paragneisss.

Clearly there is a need for an extensive metamorphic study in the Vestfold Hills. Although this is beyond the scope of this thesis, a number of important observations and potentially useful rock types have been sampled during the course of fieldwork. Also, since some of these observations have implications for the geochemical and isotopic evolution of the terrane, a number of potentially important problems are highlighted.

9.5.2 Currently unanswered questions regarding the metamorphic evolution of the Vestfold Hills

To illustrate some of the important aspects of the metamorphic history that are currently unknown, a series of questions are posed below and are then critically assessed on the basis of field observations and preliminary petrography.

1. Do early fabrics and exsolved sub-calcic pyroxenes indicate a discrete pre-D_1-M_1 'event' of regional significance in the Vestfold Hills?

An alternative explanation might be that these high-grade assemblages formed as a consequence of local transient geothermal effects associated with Mossel Gneiss magmatism (*cf.* Lister & Baldwin, 1993). A more comprehensive study (beyond the scope of this thesis) is required to confirm the importance of these observations, and structurally-oriented samples of metaironstones and calc-silicates (*e.g.* Figures 9.22, 9.23 & 9.24) have been collected from the Long Fjord region for more detailed metamorphic work at a later date (discussed further in Chapter 13).

2. What were the P-T conditions of the principal high-grade events and were there regional variations in metamorphic grade?

P-T estimates and regional variations in metamorphic grade are particularly difficult to establish in the Vestfold Hills because the Fe-rich Chelnok Paragneisses are dominantly semi-pelitic, rather than pelitic, and as such are of limited thermobarometric use. Similarly, although the EMG and CLG mafic granulites are variable in bulk composition, garnet-bearing assemblages (hence reliable thermobarometers, see Section 4.2.5) are rare. A potentially useful suite of calc-silicate paragneisses were sampled from throughout the Vestfold Hills during the course of fieldwork, but they have not been studied in detail during the course of this thesis. However, preliminary work on these rock types (Harley, Snape & Fitzsimons, 1995) further supports the view that peak metamorphic conditions (D_1-M_1) did not exceed 840 °C, and also indicates locally high water activities on the basis of garnet (grossular-andradite) + clinopyroxene + scapolite + zoisite assemblages. Nevertheless, pressure estimates for this event are still poorly constrained at present and both pressure and temperature conditions for D_2-M_2 have yet to be quantified.

P-T estimates made by Collerson and co-workers for D_2-M_2 are derived from assemblages from the Chelnok Paragneisses and are *inferred* to reflect this younger event because appreciably higher temperatures were obtained from co-existing pyroxenes. Since application of two-pyroxene thermometry to metamorphic conditions is suspect (see reviews by Essene, 1987 & Harley, 1989), and because it is possible that these are igneous grains, there is no reason to assume that the Chelnok Paragneiss assemblages reflect equilibration during D_2-M_2. Given the recent temperature estimates of *ca.* 840 °C from the calc-silicates, and 830-880 °C from the Taynaya Paragneiss, it is possible that the *P-T* estimates of Collerson & Sheraton (1986) for the Chelnok Paragneisses (700-900 °C & 5-8.5 kbar) also reflect D_1-M_1 and do not record D_2-M_2 conditions.

Unfortunately, almost[4] all the CLG orthogneisses lack garnet and do not have assemblages suitable for quantitative thermobarometry. However, qualitative mineralogical and textural observations from the CLG imply that D_2-M_2 occurred at upper amphibolite-facies conditions. In particular, mafic granulites such as the Hornblende-Phyric Suite (Figure 9.1*) are characterised by the late development of hornblende ± biotite assemblages. Only a limited number of samples from the CLG suites have been studied petrographically, but textural evidence from mafic CLG from the northern region indicates that poikiloblastic hornblende is a replacement product after clinopyroxene, orthopyroxene and plagioclase, indicating the very generalised reaction:

$$Hbl + Qtz = Opx + Cpx + Plag + H_2O \qquad [9.1]$$

proceeding from right to left (see Spear, 1993).

Field and microtextural observations indicate that hornblende developed before and/or synchronously with D_2-M_2. In some lithologies, hornblende poikiloblasts are progressively deformed into S_2 high-strain fabrics (Figure 9.25). Elsewhere, such as in the Tryne region (see Figure 9.1*), steeply-plunging overprinting L_2 mineral-elongation lineations defined by hornblende occur in mafic granulites (EMG). In some areas, such as Norite Point, retrograde amphibolite layers developed in otherwise (igneous) pyroxene-dominated melagabbros. In such areas, hornblende occurs as disseminated very coarse poikiloblasts in otherwise massive largely undeformed melagabbros. Hornblende also occurs locally concentrated into planar or weakly-deformed localized zones that were presumably fluid conduits. Such late-stage hornblende development is a common feature of the CLG gneisses. However, it is not clear if this is a consequence of late-stage growth during the magmatic stage or if hornblende growth is linked to unrelated fluid infiltration possibly associated with the syntectonic granites and pegmatites. It is also unclear whether CLG protoliths were emplaced at lower- or mid-crustal depths. It is traditionally assumed that D_2 coincided with the 'recorded' peak of metamorphism, presumably as a consequence of favourable kinetics associated with deformation/ recrystallization. It is possible that CLG were intruded in the lower crust but that the D_2-M_2 'event' occurred at lower pressures and temperatures but with higher fluid activity (relating to the syn-tectonic granite magmatism).

---

[4] There is one exception. In the central Taynaya Bay area a deformed CLG dyke cross-cuts a phlogopite- and sapphirine-bearing Taynaya Paragneiss boudin and locally has garnet-bearing assemblages as a consequence of metasomatic alteration to high alumina and Fe-rich bulk compositions. However, this single example has not yet been studied in detail.

3. What was the metamorphic history after the high-grade events and what are the implications for the geochemical and isotope chemistry of CLG protolith?

A surprisingly comprehensive metamorphic history is known for the Vestfold Hills after the *ca.* 2500 Ma events. This history has been pieced together from studies of localized Proterozoic structures (dykes, brittle faults, mylonites, ultramylonites and pseudotachylites) and xenoliths within the Proterozoic dykes (Figure 9.26; Passchier *et al.*, 1991; Seitz, 1991; Dirks *et al.*, 1994; Harley & Christy, 1995). The dykes have proved particularly important as time markers, and a number of different suits have been precisely dated by SHRIMP U-Pb zircon geochronology revealing that at least 9 generations of mafic dyke intruded between 2477 ± 5 Ma and 1241 ± 5 Ma (Black *et al.*, 1991a; 1991b; Lanyon *et al.*, 1993).

Although the dykes, the xenoliths enclosed within them, and localized deformation structures, reveal that the Vestfold Hills terrane enjoyed a complex metamorphic history, there is little evidence of this in the high-grade gneisses. Most gneisses retain either partially recrystallized igneous phases and textures or their upper amphibolite to granulite high-grade assemblages that formed during the *ca.* 2500 Ma events. The only exception occurs in the SW corner of the terrane, where an upper amphibolite to lower granulite-facies garnet overprint (age younger than 1241 ± 5 Ma) has affected the dykes and adjacent gneisses.

Fieldwork was undertaken in the SW as a comparison with the northern low-strain area to establish whether distinctive CLG suites recognised in the north are present in the region, and to sample paragneisses from within the garnet zone for U-Pb monazite dating (work in progress with PD Kinny & SL Harley). Petrographic observations for selected gneisses from Zolotov Island indicates that garnet development occurred locally throughout the gneisses and mafic dykes. In both these lithologies, garnet growth was strongly controlled by fluid access and is related to mylonite development. Similarly, early-formed (*ca.* 2500 Ma) orthopyroxene and garnet in leucosomes within Chelnok Paragneisses reacted to form plagioclase - quartz - orthoclase (minor) symplectites.

The reason for the (geographically) limited but pervasive effects of this event as opposed to the other events shown on Figure 9.26 clearly relates to fluids, and the garnet zone is attributed to fluid infiltration, probably during either the 1000 Ma or 500 Ma events that are documented from adjacent regions (*e.g.* see Chapter 2). These observations are important in the context of this study for a number of reasons:

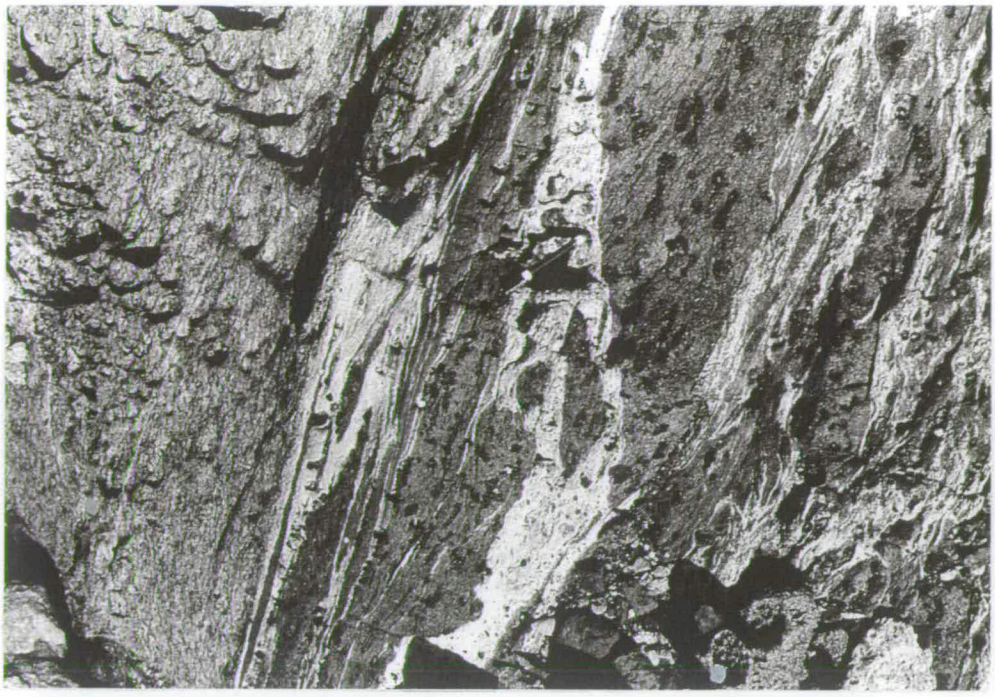

Figure 9.25 Deformed Hornblende-Phyric Suite. Note that hornblende poikiloblasts are locally transposed into the high-strain fabric which corresponds to S_2 in the region (locality: central Long Peninsula; pen for scale is 15 cm long).

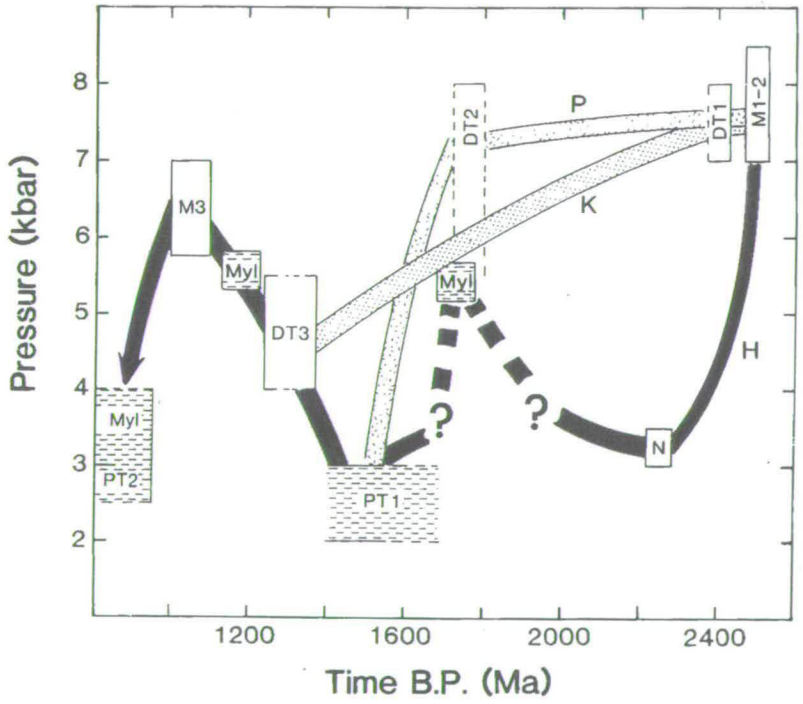

Figure 9.26 Pressure-time evolution for the Vestfold Hills. The solid line (H) is the preferred P-t path and is after Harley, Snape and Black (1995). Paths P and K refer to Passchier *et al.* (1991) and Kuehner & Green (1991) respectively. Question marks on the solid path reflect uncertainties in the pressures of mylonite deformations. M3 refers to the garnet overprint in the SW Vestfold Hills. DT1-3 are the main dyking events (after Harley, Snape & Black, 1995; see also other references therein).

- The style of this overprint is reminiscent of the 500 Ma event in the adjacent Rauer Group and may therefore provide the first direct link between the two terranes.

- The limited extent of reworking implies that most high-grade gneisses were neither significantly recrystallized after the D_2/D_3 episode (*ca.* 2475.3 ± 0.7 Ma; see Chapter 10) nor affected by fluid infiltration at 500 Ma (*cf.* descriptions in Part 2 & consequences described in Chapter 11).

- Reaction textures between garnet and orthopyroxene were clearly produced by superimposing two unrelated metamorphic events, and could otherwise be interpreted as isothermal decompression textures (*e.g.* Collerson & Sheraton, 1986; *cf.* Harley, 1989; Hand *et al.*, 1994).

9.6 Discussion and conclusions

Regional mapping and detailed observations of intrusive contacts between CLG suites and older gneiss lithologies have resolved a number of inconsistencies or unanswered questions identified in previous geological accounts of the Vestfold Hills. The conclusions from the fieldwork aspect of this study have been summarized on a schematic rock-relations diagram (Figure 9.27*) and can be considered further by reference to the six broad questions posed in Chapter 8 (Section 8.6.1).

1. The timing of magmatism, metamorphism and deformation

The Crooked Lake magmatic episode, as defined here, lasted throughout the D_1-M_1 to D_2-M_2 interval. Most CLG suites did not intrude syn-tectonically with D_2 as previously supposed (*e.g.* Oliver *et al.*, 1982; Collerson *et al.*, 1983), although minor granite (*s.s.*) sheets and pods, intermediate dykes and locally-derived leucosome did crystallize during this event. These observations are used to provide a geological framework to guide sample selection for further zircon geochronology (described in the next chapter). It is also apparent from these field observations that a previous estimate of 2487 ± 6 Ma for the age of D_2, based on pooled data from two granodiorites (2481 ± 14 Ma & 2489 ± 8 Ma; Black *et al.*, 1991a), is too old. The older of these granodiorites is a homogeneous CLG suite and is distinct from the younger, heterogeneous, migmatitic granodiorite at Grace Lake. The term Grace Lake granodiorite is retained but is restricted to the migmatitic variety as seen at the type area.

With respect to the precise timing of D_1-M_1, field observations indicate that migmatites in Taynaya EMG may have developed at the peak of thermal metamorphism. In particular,

patch leucosomes described above and shown in Figures 10.3c are the best candidates for *in situ* melting during this early event.

2. Temporal evolution in CLG magmatism: Constraints on the amount of tectonic repetition

CLG protoliths intruded as a number of temporally and spatially distinct magmatic centres or dykes of diverse composition. Within the CLG there was a temporal evolution of magmatism and, in general, mafic suites preceded more voluminous intermediate to felsic compositions. One further sample of CLG was selected for U-Pb zircon dating from the central Long Peninsula region to determine if there is a south to north progression in age. However, given the regional distribution and observed intrusive sequence of Crooked Lake protolith types, it is unlikely that there was a simple south to north progression. When combined with detailed structural mapping, the distribution of CLG suites on regional and local scales has constrained the amount of tectonic repetition by F_2 to be local (< 500 m scale) rather than regional (> km scale).

3. The status and regional distribution of gneiss lithologies

The amount of CLG in the northern region is considerably greater than previously recognised, with the areas around Rybnaya Bay, east of Tryne Fjord, and much of central western Long Peninsula, now identified as being mostly CLG. These areas were previously mapped as either Mossel Gneiss or Tryne Metavolcanics and recognition that there is appreciable CLG in these areas further elucidates geological relationships with the older gneiss lithologies. By extrapolation from the low-strain northern region, or from low-strain windows within the otherwise high-strain southern region, it is apparent that much of the area mapped as Tryne Metavolcanics is a tectonic admixture of lithologies. From observations at the type area, the status of the Tryne Metavolcanics as a volcanic-sedimentary succession is disputed and I propose that the term 'Tryne Metavolcanics' be abandoned.

4. Recognition in the field of previously-defined geochemical suites

Field observations indicate that the three geochemical groupings of Sheraton & Collerson (1984) are lithological rather than genetic, and that many rock types cannot be strictly related because they differ in age. For example, the granodiorites and granites of the monzodiorite suite (see Figure 8.3), and the granites in the monzonitic suite, generally intruded later than the other rock types in the respective suites. Conversely, gabbroic

compositions in the 'miscellaneous' suite are most probably related to various monzogabbros, monzodiorites and monzonites, although the exact genetic relationship within or between suites is difficult to define on the basis of field relations alone (discussed further in Chapters 11 & 12).

5. Are all the ca. 2500 Ma orthogneisses related by a common tectonomagmatic process?

In common with previous geochemical studies in the terrane (*e.g.* Sheraton & Collerson, 1984) some intra-suite compositional variations are thought to be linked by crystal fractionation on geochemical grounds, but additionally it is now possible to define comagmatic suites in the field (*e.g.* the LAS and RLS suites described in Chapter 11). It is likely that all the CLG suites are related by a common tectonomagmatic process to some extent, but modelling between suites that are derived from a variety of source components is only likely to constrain magma petrogenesis in the broadest terms (*cf.* Hanson, 1989). Some of these problems can be overcome by directing geochemical modelling to clearly comagmatic suites, whereby relict igneous phases and textures, combined with field observations that constrain the amount of magma-host rock interaction (see descriptions of the CLG above), can be used to independently constrain magma petrogenesis. Such an approach has been adopted in this study and an integrated interpretation based on field relations, petrographic observations, and geochemical and isotopic data, is described in Chapter 11.

6. Evidence for a metamorphic and tectonic history prior to the ca. 2500 Ma events

Geological relations that are preserved in low-strain domains indicate that the Chelnok Paragneiss retains small-scale flat-lying folds (F_1) that were variably transposed into parallelism with generally steeply-dipping D_2 structures. F_1 structures fold a compositional layering and a metamorphic fabric and have a new axial-planar foliation that is often flat-lying. These early structures are intruded by CLG granites that have a steeply-dipping S_2 foliation which indicates that the flat-lying orientation was not produced by regional warping (F_3). Microtextural observations in key lithologies within the Chelnok Paragneiss indicate that high-temperature (granulite facies) mineral assemblages formed and exsolved (cooled) prior to F_1 folding. However, in order to assess the regional significance of these observations a detailed metamorphic and geochronological study is required.

9.7 Strategy for detailed analytical work from a revised geological framework

This chapter has outlined a revised geological framework for the Vestfold Hills that is used in later sections to refine models for the magmatic, metamorphic and tectonic evolution of this high-grade terrane. Field observations described here highlight how little is known of the high-grade history, and illustrate that many aspects require further investigation. Unfortunately, a detailed kinematic account of the tectonic development of the complex is beyond the scope of this thesis. Nevertheless, some conjectural ideas are outlined in the final chapter in the context of *terrane amalgamation in Prydz Bay* (Section 13.2). For reasons outlined in Chapters 1 and 8, detailed follow-up work during the course of this thesis has focused on understanding the geochemical and isotopic evolution of the CLG. Because the CLG are the least deformed and most diverse of the Vestfold Hills orthogneisses, they are potentially the most useful protoliths to understand the petrogenetic processes involved in crust formation. Hence, various aspects of the geochemical and isotopic evolution of the CLG are described in the next two chapters.

Chapter 10

Refinement of the timing of magmatism, metamorphism and deformation from U-Pb zircon dating

10.1 Introduction

Although the zircon dating of Black *et al.* (1991a) broadly constrains the temporal evolution of the Vestfold Hills gneiss complex, it is apparent from the field studies described in the previous chapter that the observed relationships between magmatism and deformation are not fully consistent with the available age data. As a result, the time scale and spatial relations of magmatic and high-grade deformational events in the Vestfold Hills remain to be clarified. This chapter builds on the field observations as described in the previous chapter and reports new U-Pb zircon dating that precisely constrains the protolith ages of key orthogneiss lithologies. This enables a better definition of the ages of the principal high-grade deformation events.

10.2 Rationale for further geochronology

Detailed field studies in low-strain domains in the northern Vestfold Hills has led to a revised and more comprehensive geological event sequence than has been previously recognised for the early evolution of the terrane (see previous chapter). Key samples from within this sequence have been selected for U-Pb zircon dating in order to address problems identified during the fieldwork. In brief, these problems concern the precise timing of magmatism and deformation, the extent and scale of tectonic repetition, and the contention that there was a temporal evolution in CLG magmatism. The data presented here also have a bearing on the unresolved question of whether there was a significant metamorphic or tectonic history prior to the *ca.* 2500 Ma events.

10.2.1 Problems related to the timing of magmatism, metamorphism and deformation

What was the precise timing of D_1?

Since the Mossel and Crooked Lake gneiss suites overlap in age at 2501 Ma (Black *et al.*, 1991a) and because lithologies directly associated with the D_1 event have not been dated directly, the precise timing of D_1 remains uncertain (described in Section 8.7.1).

What was the precise timing of D_2?

Oliver *et al.* (1982) and Collerson *et al.* (1983) argued that the CLG was intruded synchronously with D_2, whereas Black *et al.* (1991a) restricted the syn-tectonic component to the minor Grace Lake granodiorite in the north. Their estimate for the mean age of D_2 (2487 ± 6 Ma) is within error of the youngest deformed CLG, dated at 2484 ± 6 Ma. Clearly it is important to identify which CLG components, if any, were intruded syn-tectonically.

Was there a temporal evolution in CLG magmatism?

Black *et al.* (1991a) defined a range of ages for the CLG, from 2501 ± 4 Ma in the south, through 2493 ± 5 Ma in the central region, to 2484 ± 6 Ma in the north. Such a distribution of ages implies that was a temporal evolution in CLG magmatism, although Black *et al.* (1991a) were unable to confirm if there is a systematic south to north progression, or more local variability.

How much tectonic repetition is there in the gneiss complex?

In their geochemical study of the Vestfold Hills, Sheraton & Collerson (1984) identified a number of chemically distinct CLG suites, but were unable to relate these suites to a spatial or temporal variation in CLG magmatism. However, if the CLG suites in the north have a different age and composition to those in the central and southern regions, then it is likely that CLG gneiss suites were not tectonically repeated from south to north as previously supposed (*e.g.* Oliver *et al.*, 1982; Collerson *et al.*, 1983). It is important, therefore, to establish the age of individual CLG plutons.

10.3 Sample selection for refined geochronology

From a detailed examination of the spatial and temporal evolution of CLG (see previous chapter) it is apparent that most protoliths were emplaced in the D_1-M_1 to D_2-M_2 interval

and were not intruded syn-tectonically as previously reported (*e.g.* Collerson *et al.*, 1983). In order to further test the hypothesis that CLG magmatism progressed from south to north, a sample was chosen from the central northern Vestfold Hills (sample **VH407**) that clearly intruded before D_2.

Additionally, important lithological differences exist between the three Grace Lake Granodiorite localities described by Black *et al.* (1991a; 1991b), of which two were sampled and combined to provide an estimate for the age of D_2. Only felsic mobilisate components of the migmatitic variety are now considered to be syntectonic (see Section 9.2.4). The presence of such locally derived melts in this gneiss is consistent with observations from elsewhere in the terrane that minor granite sheets and pods, intermediate dykes, and locally derived leucosome crystallized during D_2. In order to directly constrain the age of this event, the most convincing 'syn-tectonic' component of the CLG was selected (sample **VH179**).

Although the pre-D_1 Tryne Metavolcanics (Collerson *et al.*, 1983) have been disputed as a simple genetically related succession at the type locality (Section 9.4.1), early mafic gneisses (EMG; these were previously grouped with the Tryne Metavolcanics) that contain refolded D_1 folds do occur in the complex. One group of EMG, characterized by ovoid ultramafic xenoliths (Taynaya EMG), preserves migmatitic features considered to reflect melting during D_1-M_1. Collerson *et al.* (1983) suggested that at least some of the Mossel Gneiss was derived from melting of this rock type, an interpretation apparently supported on geochemical grounds (Sheraton & Collerson, 1984). A sample of leucosome from Taynaya EMG (sample **VH514c**) was selected in order to directly constrain the age of D_1-M_1 and evaluate the role of EMG in the formation of the Mossel Gneiss.

10.3.1 Detailed field relations of samples (see Figure 10.1 for sample locations)

Syn-D_2 leucosome (sample VH179; GR845018; 68°28'S 78°11'30"E)

The dominant gneiss lithology in the region (see Figure 10.1) is felsic CLG that is cut by a number of intrusive dioritic CLG dykes. Both host CLG and the dykes were deformed by D_2 and are usually co-planar with the regional S_2 foliation and gneissic layering. Sample VH179 is of an axial-planar felsic leucosome enclosed within one of these deformed CLG dykes (Figure 10.2). This sample of leucosome, however, was taken from within a metre-scale asymmetric parasitic fold hinge. The leucosome veins on the limbs of the fold parallel S_2 (Figure 10.3a) but in the hinge region they coalesce into discordant boudinaged patches that are perpendicular to the fold hinge (Figure 10.3b). Since the leucosome is both folded by F_2 and also cuts across the fold hinge in local regions of extension, it is likely that the

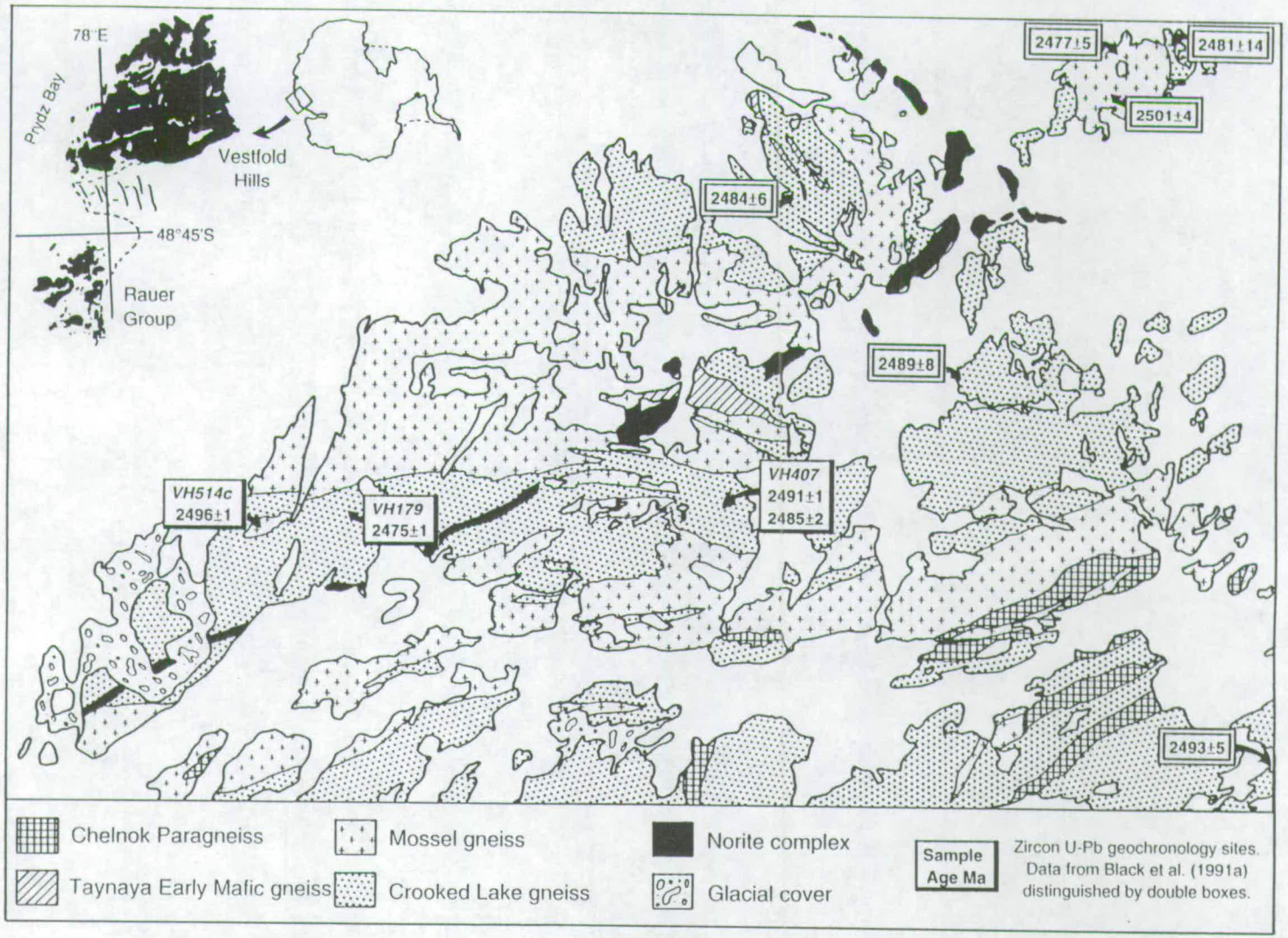

Figure 10.1 Outline geological map of the northern Vestfold Hills showing the distribution of the main lithologies and the location of zircon U-Pb geochronology sites from this study and Black *et al.* (1991a). Ages are rounded to the nearest m.y. See text for precise positions of these samples.

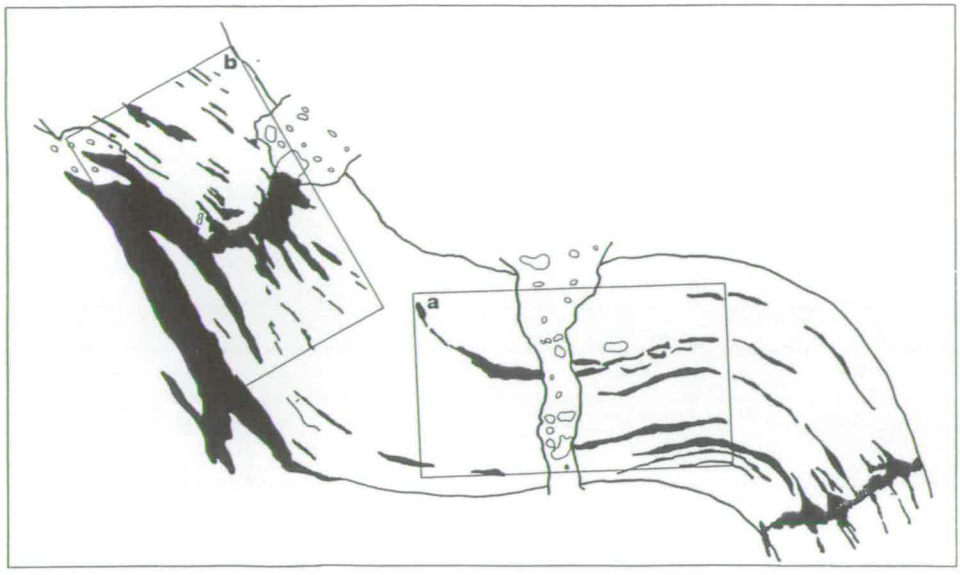

Figure 10.2 Sketch showing the field relations of syn-D_2 leucosome (solid black ornament) in a deformed intermediate (dioritic) CLG dyke (no shading). Note that leucosomes are folded about the F_2 parasitic fold; they are parallel on the limbs but are locally discordant where regions of the fold underwent extension. Insets a and b refer to areas shown in Figures 10.3a and 10.3b. Rubble/dirt denoted by 'bouldery' ornament; length of dyke exposed is approximately 3 metres.

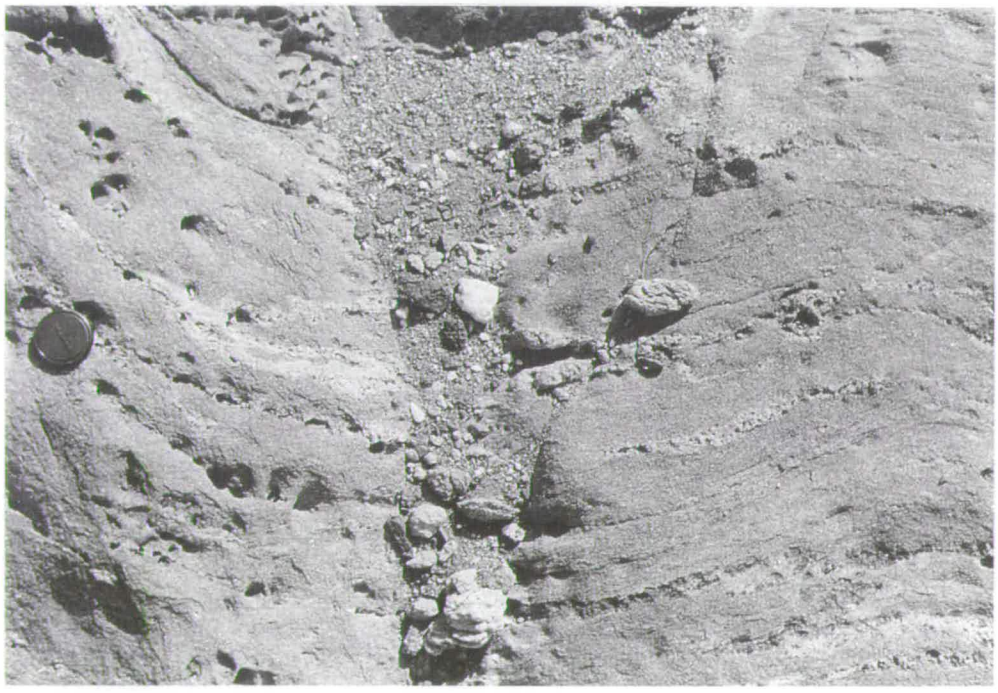

Figure 10.3a. see overleaf for figure caption

(b)

(c)

Figure 10.3 (a) D_2 leucosome on the limb of the fold shown in Figure 10.2. Note that the orientation parallels S_2 (small black lens cap for scale is 50 mm in diameter); (b) D_2 leucosome near the uppermost fold hinge shown a Figure 10.2. Note that the leucosomes coalesce and cross-cut the dyke (small black lens cap for scale is 50 mm in diameter); (c) D_1 patch leucosome with host Taynaya EMG (details described in main body of text).

melt crystallized at the same time as the deformation. Hence, dating VH179 directly constrains the age of D_2-M_2.

Lake Africa suite CLG (sample VH407; GR897015; 68°28'S 78°19'30"E)

This monzodioritic gneiss is from a CLG suite which is informally called the Lake Africa Suite (LAS) here. The LAS is a differentiated pluton with compositions that range from ultramafic oikocrystic cumulates to leucocratic monzodiorites. The more felsic varieties have features characteristic of AFC processes, such as partly digested xenoliths and elevated $\delta^{18}O$ values (~1.2 ‰ higher than the cumulates; Section 11.5). Hence, VH407 might be expected to have multiple zircon populations. One population would be likely to reflect the crystallization age of the pluton, any other(s) would be inherited from the contaminant (*e.g.* earlier CLG or Mossel Gneiss).

D_1-M_1 leucosome (sample VH514c; Grid Reference 823013; 68°28'S 78°09'E)

Sample VH514c was collected from leucosome patches in the Taynaya EMG near Bulatnaya Bay. This locality was chosen because it is a low-strain area where field relations confirm that this EMG suite, and associated leucosomes and felsic gneiss (Mossel Gneiss), were folded (F_1) and boudinaged prior to refolding by F_2 (folded CLG dykes clearly cut across F_1 fold closures in the EMG and felsic gneiss). Also, the melting relationships preserved at this location are the best candidates so far observed for direct *in situ* melting of EMG to produce Mossel Gneiss. Nevertheless, VH514c is an end member of a range of partial melt morphologies. There is a gradation from apparently isolated cm- to dm-scale felsic melt patches (this sample, Figure 10.3c), to inter-connected patches and veins, to larger areas of leucosome where undigested EMG blocks become progressively detached and xenolithic, and finally to felsic areas where xenoliths are common and schlieren and schollen textures dominate in unequivocal Mossel Gneiss.

It should be noted that the samples also have catalogue numbers in the AGSO system. These are: VH514c - 95286606; VH407 - 95286605; and VH179 - 95286604.

10.4 U-Pb isotope geochronology

The analysis of zircons by SHRIMP was performed by Lance Black at the Australian National University (ANU). Details of the analytical procedures provided here and outlined in the Appendix (1) and were largely written by Lance. He also undertook the statistical

treatment of the raw data at ANU using their software. However, the geological interpretations of this data are my own.

10.4.1 Analytical and data treatment procedures

Zircons were separated by standard heavy liquid and magnetic procedures before mounting in epoxy resin discs with fragments of SL13 standard zircon. Discs were polished and Au-coated prior to ion microprobe analysis on SHRIMP II at ANU, Canberra.

For the typically concordant zircon analyses obtained in this study, ^{206}Pb, ^{207}Pb and ^{208}Pb generally had correlated non-linear trends, which reflect real variation in target composition during analysis. Cubic spline interpolation was used to approximate these clearly non-linear trends. This interpolation involves the construction of a continuous cubic polynomial curve through each four consecutive data points, and the joining of these curves for the entire data set to form a cubic spline curve. The procedure, which is similar to using a French curve, is part of the KaleidaGraph® data analysis/graphics application package. For each analysis a set of 7 ratios was obtained by referencing the interpolated value of the numerator isotope (^{204}Pb, ^{206}Pb or ^{208}Pb) to the measurement time of each of the measured ^{206}Pb values. The means and standard errors of the Pb isotope ratios in table 1 are derived from each set of 7 individual ratios. This procedure dramatically lowers the unrealistically high uncertainties that would have been derived from a single linear regression through all data points of any particular isotopic species.

The data are presented on conventional $^{207}Pb/^{235}U$-$^{206}Pb/^{238}U$ concordia diagrams (Figures 10.4a, c, e). Additionally, in an effort to resolve the subtle complexities of some data sets, the analyses have also been plotted on probability distribution diagrams (Figures 10.4b, d, f). These differ from histograms in giving individual weighting to each analysis, which is represented by a single, solid bell-shaped curve of equal area. More precise analyses are more highly kurtose than those that are not, and therefore dominate in the definition of populations. The form of the final curve for a sample is obtained by summing all the components of individual analyses at any particular value of the abscissa (*e.g.* $^{207}Pb/^{206}Pb$ age). Because of the nature of this construction, the ordinate has no absolute significance but does serve to illustrate the relative frequencies of the various age components. The nature of the overall probability distribution trend for each sample is used to help evaluate whether there appears to be distinct age populations in the data (these will be significant only if these data are concordant), in which case these ages are taken as being geologically significant. The precision of all ages reported in the text and shown on the diagrams is given

at the 95 % (2 σ) confidence level, and the error polyhedra presented on all concordia diagrams (Figures 10.4a, c, e) are also for 2 σ confidence limits.

10.4.2 Isotopic results

The isotopic data for zircons from the 3 samples studied here are presented in Table 10.1. Conventional $^{207}Pb/^{235}U$-$^{206}Pb/^{238}U$ concordia diagrams are shown in Figure 10.4. A probability distribution diagram for the $^{207}Pb/^{206}Pb$ zircon ages for each sample is also shown; the population characteristics are discussed below.

Leucosome in Taynaya EMG (VH514c)

Zircons in this sample are of igneous origin. They are elongated, subhedral, relatively large grains that commonly contain small rounded to angular high-U cores that sometimes preserve oscillatory zoning. Surrounding mantles, which are volumetrically dominant, have rounded terminations; they are also rhythmically zoned. Many grains also have thin low-U rims that are too narrow to analyse. These rims are attributed to a post-crystallisation tectonothermal event (see discussion section & Black *et al.*, 1991b); the cores are considered to have been inherited from the mafic gneiss and the mantles formed during the crystallisation of the leucosome.

39 spot analyses were made on zircons from this sample; 31 were from the oscillatory zoned mantle and they define a $^{207}Pb/^{206}Pb$ age of 2495.1 ± 1.2 Ma. Of the 8 analyses not included in this age estimate, two were from the inherited oscillatory zoned cores and gave much older ages (~2935 & 2691 Ma). A third analysis from an annealed part of one of these cores has a younger age of ~2572 Ma, which is attributed to Pb loss associated with the annealing processes. The other 5 analyses not included in the 2495.1 ± 1.2 Ma estimate have ages between ~2510 and 2500 Ma and were from rounded cores or inadvertent partial analyses of such cores. Of the remaining 31 analyses, a further refinement to the data can be made by omitting the 6 youngest data points. This treatment of the data is justified on statistical and geological grounds, as it reduces the chi-square value from 3.2 to unity and because these samples are thought to have suffered a degree of Pb loss, probably associated with later tectonothermal events that affected the terrane. Evidence for such Pb loss is supported by other isotopic studies in the terrane (Black *et al.*, 1991a; 1991b) and by the thin low-U metamorphic overgrowths. Although only slightly different from the age estimate derived from 31 analyses, the reduced dataset yields a preferred age of 2496.3 ± 0.7 Ma, which is taken as the crystallisation age of the leucosome.

58.1	304	213	0.701	104712	0.0170	0.476±.012			
59.1	178	490	2.755	346021	0.0050	0.479±.012	10.82±.28	0.16406±.00026	2498±3
60.1	176	327	1.858	20000000	0.0000	0.474±.012	10.70±.28	0.16385±.00038	2496±4
61.1	178	418	2.342	139470	0.0130	0.465±.012	10.45±.27	0.16282±.00026	2485±3
62.1	252	319	1.265	1000000	0.0001	0.474±.012	10.63±.27	0.16270±.00020	2484±2
63.1	326	251	0.770	1000000	0.0000	0.476±.012	10.69±.27	0.16285±.00019	2486±2
64.1	287	676	2.358	1000000	0.0001	0.462±.012	10.42±.27	0.16346±.00021	2492±2
65.1	200	520	2.595	125313	0.0140	0.480±.012	10.78±.27	0.16285±.00023	2485±2
66.1	358	255	0.713	355872	0.0050	0.479±.012	10.76±.27	0.16277±.00017	2485±2
67.1	173	454	2.620	800000	0.0020	0.464±.016	10.45±.35	0.16324±.00024	2490±2
68.1	319	892	2.799	746269	0.0020	0.465±.015	10.46±.35	0.16309±.00017	2488±2
69.1	153	455	2.967	1000000	0.0001	0.477±.016	10.74±.36	0.16344±.00026	2492±3
70.1	153	404	2.638	2439024	0.0010	0.476±.016	10.70±.36	0.16291±.00027	2486±3
71.1	923	1198	1.297	313480	0.0050	0.472±.016	10.66±.36	0.16387±.00023	2496±2
72.1	446	370	0.828	261097	0.0050	0.475±.016	10.70±.37	0.16329±.00017	2490±2
73.1	237	631	2.665	3225806	0.0000	0.478±.016	10.75±.37	0.16322±.00022	2489±2
74.1	325	171	0.527	191571	0.0070	0.473±.016	10.66±.36	0.16357±.00020	2493±2
75.1	174	479	2.752	1000000	0.0001	0.470±.016	10.59±.36	0.16355±.00026	2493±3
76.1	361	235	0.653	4000000	0.0000	0.470±.016	10.55±.35	0.16270±.00019	2484±2

Leucosome in Crooked Lake gneiss (VH179)

101.1	45	52	1.154	43234	0.0410	0.470±.012	10.50±.28	0.16223±.00051	2479±5
102.1	219	403	1.843	303030	0.0060	0.473±.012	10.56±.27	0.16185±.00023	2475±2
103.1	500	1158	2.314	1724138	0.0010	0.470±.012	10.47±.27	0.16138±.00025	2470±3
104.1	919	765	0.832	305810	0.0060	0.470±.012	10.50±.27	0.16202±.00011	2477±1
105.1	722	863	1.195	552486	0.0030	0.462±.012	10.30±.26	0.16159±.00012	2472±1
106.1	302	681	2.257	763359	0.0020	0.473±.015	10.53±.34	0.16143±.00073	2471±8
107.1	856	855	1.000	1282051	0.0010	0.471±.012	10.52±.27	0.16203±.00011	2477±1
108.1	905	808	0.893	512821	0.0030	0.474±.012	10.58±.27	0.16188±.00010	2475±1
109.1	771	1208	1.568	456621	0.0040	0.467±.012	10.44±.26	0.16197±.00012	2476±1
110.1	513	893	1.739	279330	0.0060	0.470±.012	10.48±.27	0.16182±.00026	2475±3
111.1	59	66	1.128	24931	0.0720	0.469±.012	10.45±.28	0.16170±.00045	2474±5
112.1	535	886	1.655	1000000	0.0001	0.471±.012	10.51±.27	0.16192±.00014	2476±1
113.1	923	342	0.371	2564103	0.0010	0.476±.012	10.63±.27	0.16192±.00020	2476±2
115.1	1731	909	0.525	2380952	0.0010	0.473±.012	10.58±.27	0.16223±.00008	2479±1
115.2	42	47	1.108	37078	0.0480	0.470±.012	10.44±.28	0.16131±.00084	2469±9
116.1	317	587	1.849	1063830	0.0020	0.475±.012	10.60±.27	0.16169±.00019	2473±2
117.1	324	747	2.305	259067	0.0070	0.484±.012	10.81±.28	0.16192±.00018	2476±2
118.1	608	729	1.198	2857143	0.0000	0.455±.015	10.14±.34	0.16173±.00013	2474±1
119.1	247	533	2.160	1000000	0.0001	0.458±.015	10.25±.34	0.16228±.00022	2480±2
120.1	295	422	1.433	401606	0.0040	0.464±.016	10.36±.35	0.16177±.00021	2474±2
121.1	391	685	1.753	189036	0.0070	0.470±.016	10.48±.35	0.16191±.00016	2476±2
122.1	576	716	1.243	263158	0.0050	0.469±.016	10.47±.35	0.16192±.00021	2476±2
123.1	314	705	2.242	1587302	0.0010	0.471±.016	10.53±.35	0.16203±.00019	2477±2
124.1	224	416	1.857	165563	0.0090	0.470±.016	10.52±.36	0.16227±.00022	2480±2
125.1	511	752	1.472	336700	0.0040	0.469±.016	10.48±.35	0.16187±.00014	2475±2
126.1	1707	812	0.476	462963	0.0030	0.472±.016	10.59±.35	0.16272±.00022	2484±2
127.1	515	804	1.559	1000000	0.0001	0.472±.016	10.50±.35	0.16150±.00016	2471±2
128.1	299	664	2.216	1960784	0.0010	0.465±.016	10.38±.36	0.16172±.00039	2474±4
129.1	354	623	1.762	200000	0.0070	0.467±.016	10.42±.35	0.16180±.00027	2474±3

f_{206} is the proportion, expressed as a percentage, of common ^{206}Pb to total ^{206}Pb. The reported ages are derived from $^{207}Pb/^{206}Pb$ ratios derived from the ^{204}Pb correction technique (Compston et al., 1984).

59.1	178	490	2.755	346021	0.0050	0.479±.012	10.82±.28	0.16406±.00026	2498±3
60.1	176	327	1.858	20000000	0.0000	0.474±.012	10.70±.28	0.16385±.00038	2496±4
61.1	178	418	2.342	139470	0.0130	0.465±.012	10.45±.27	0.16282±.00026	2485±3
62.1	252	319	1.265	1000000	0.0001	0.474±.012	10.63±.27	0.16270±.00020	2484±2
63.1	326	251	0.770	1000000	0.0000	0.476±.012	10.69±.27	0.16285±.00019	2486±2
64.1	287	676	2.358	1000000	0.0001	0.462±.012	10.42±.27	0.16346±.00021	2492±2
65.1	200	520	2.595	125313	0.0140	0.480±.012	10.78±.27	0.16285±.00023	2485±2
66.1	358	255	0.713	355872	0.0050	0.479±.012	10.76±.27	0.16277±.00017	2485±2
67.1	173	454	2.620	800000	0.0020	0.464±.016	10.45±.35	0.16324±.00024	2490±2
68.1	319	892	2.799	746269	0.0020	0.465±.015	10.46±.35	0.16309±.00017	2488±2
69.1	153	455	2.967	1000000	0.0001	0.477±.016	10.74±.36	0.16344±.00026	2492±3
70.1	153	404	2.638	2439024	0.0010	0.476±.016	10.70±.36	0.16291±.00027	2486±3
71.1	923	1198	1.297	313480	0.0050	0.472±.016	10.66±.36	0.16387±.00023	2496±2
72.1	446	370	0.828	261097	0.0050	0.475±.016	10.70±.37	0.16329±.00017	2490±2
73.1	237	631	2.665	3225806	0.0000	0.478±.016	10.75±.37	0.16322±.00022	2489±2
74.1	325	171	0.527	191571	0.0070	0.473±.016	10.66±.36	0.16357±.00020	2493±2
75.1	174	479	2.752	1000000	0.0001	0.470±.016	10.59±.36	0.16355±.00026	2493±3
76.1	361	235	0.653	4000000	0.0000	0.470±.016	10.55±.35	0.16270±.00019	2484±2

Leucosome in Crooked Lake gneiss (VH179)

101.1	45	52	1.154	43234	0.0410	0.470±.012	10.50±.28	0.16223±.00051	2479±5
102.1	219	403	1.843	303030	0.0060	0.473±.012	10.56±.27	0.16185±.00023	2475±2
103.1	500	1158	2.314	1724138	0.0010	0.470±.012	10.47±.27	0.16138±.00025	2470±3
104.1	919	765	0.832	305810	0.0060	0.470±.012	10.50±.27	0.16202±.00011	2477±1
105.1	722	863	1.195	552486	0.0030	0.462±.012	10.30±.26	0.16159±.00012	2472±1
106.1	302	681	2.257	763359	0.0020	0.473±.015	10.53±.34	0.16143±.00073	2471±8
107.1	856	855	1.000	1282051	0.0010	0.471±.012	10.52±.27	0.16203±.00011	2477±1
108.1	905	808	0.893	512821	0.0030	0.474±.012	10.58±.27	0.16188±.00010	2475±1
109.1	771	1208	1.568	456621	0.0040	0.467±.012	10.44±.26	0.16197±.00012	2476±1
110.1	513	893	1.739	279330	0.0060	0.470±.012	10.48±.27	0.16182±.00026	2475±3
111.1	59	66	1.128	24931	0.0720	0.469±.012	10.45±.28	0.16170±.00045	2474±5
112.1	535	886	1.655	1000000	0.0001	0.471±.012	10.51±.27	0.16192±.00014	2476±1
113.1	923	342	0.371	2564103	0.0010	0.476±.012	10.63±.27	0.16192±.00020	2476±2
115.1	1731	909	0.525	2380952	0.0010	0.473±.012	10.58±.27	0.16223±.00008	2479±1
115.2	42	47	1.108	37078	0.0480	0.470±.012	10.44±.28	0.16131±.00084	2469±9
116.1	317	587	1.849	1063830	0.0020	0.475±.012	10.60±.27	0.16169±.00019	2473±2
117.1	324	747	2.305	259067	0.0070	0.484±.012	10.81±.28	0.16192±.00018	2476±2
118.1	608	729	1.198	2857143	0.0000	0.455±.015	10.14±.34	0.16173±.00013	2474±1
119.1	247	533	2.160	1000000	0.0001	0.458±.015	10.25±.34	0.16228±.00022	2480±2
120.1	295	422	1.433	401606	0.0040	0.464±.016	10.36±.35	0.16177±.00021	2474±2
121.1	391	685	1.753	189036	0.0070	0.470±.016	10.48±.35	0.16191±.00016	2476±2
122.1	576	716	1.243	263158	0.0050	0.469±.016	10.47±.35	0.16192±.00021	2476±2
123.1	314	705	2.242	1587302	0.0010	0.471±.016	10.53±.35	0.16203±.00019	2477±2
124.1	224	416	1.857	165563	0.0090	0.470±.016	10.52±.36	0.16227±.00022	2480±2
125.1	511	752	1.472	336700	0.0040	0.469±.016	10.48±.35	0.16187±.00014	2475±2
126.1	1707	812	0.476	462963	0.0030	0.472±.016	10.59±.35	0.16272±.00022	2484±2
127.1	515	804	1.559	1000000	0.0001	0.472±.016	10.50±.35	0.16150±.00016	2471±2
128.1	299	664	2.216	1960784	0.0010	0.465±.016	10.38±.36	0.16172±.00039	2474±4
129.1	354	623	1.762	200000	0.0070	0.467±.016	10.42±.35	0.16180±.00027	2474±3

f_{206} is the proportion, expressed as a percentage, of common ^{206}Pb to total ^{206}Pb. The reported ages are derived from $^{207}Pb/^{206}Pb$ ratios derived from the ^{204}Pb correction technique (Compston et al., 1984).

Table 10.1 U-Th-Pb isotopic composition of zircon from the Vestfold Hills

Grain area	U ppm	Th ppm	Th/U	$^{206}Pb/^{204}Pb$	f_{206}	$^{206}Pb/^{238}U$ ±1 σ error	$^{207}Pb/^{235}U$ ±1 σ error	$^{207}Pb/^{206}Pb$ ±1 σ error	Age (Ma) ±1 σ error
					Leucosome in Taynaya mafic gneiss (VH514c)				
1.1	716	314	0.439	228833	0.0080	0.573±.014	16.89±.43	0.21384±.00033	2935±2
2.1	427	388	0.908	1000000	0.0001	0.471±.012	10.65±.27	0.16388±.00016	2496±2
3.1	445	661	1.486	1136364	0.0020	0.478±.012	10.82±.27	0.16402±.00015	2498±2
4.1	491	539	1.098	1000000	0.0001	0.480±.012	10.87±.28	0.16408±.00015	2498±2
5.1	602	367	0.610	1000000	0.0001	0.473±.012	10.69±.27	0.16384±.00013	2496±1
6.1	496	272	0.548	666667	0.0030	0.476±.012	10.78±.28	0.16427±.00014	2500±1
7.1	880	520	0.591	1282051	0.0010	0.465±.012	10.48±.27	0.16345±.00011	2492±1
8.1	353	277	0.784	1063830	0.0020	0.479±.012	10.81±.28	0.16380±.00030	2495±3
9.1	312	415	1.329	183824	0.0100	0.465±.012	10.43±.26	0.16264±.00018	2483±2
9.2	350	409	1.169	261780	0.0050	0.476±.016	10.66±.36	0.16227±.00019	2480±2
10.1	570	451	0.792	5555556	0.0000	0.474±.012	10.69±.27	0.16370±.00013	2494±1
11.1	1209	395	0.327	502513	0.0040	0.524±.013	13.30±.34	0.18418±.00021	2691±2
11.2	541	22	0.041	1000000	0.0001	0.498±.013	11.77±.30	0.17151±.00022	2572±2
11.3	267	163	0.609	70323	0.0200	0.482±.016	10.82±.36	0.16283±.00031	2485±3
12.1	449	317	0.707	203666	0.0090	0.478±012	10.80±.27	0.16394±.00015	2497±2
13.1	379	492	1.296	100000	0.0180	0.479±.012	10.78±.27	0.16306±.00017	2488±2
14.1	366	293	0.801	2272727	0.0010	0.478±.012	10.79±.27	0.16386±.00016	2496±2
15.1	346	274	0.790	322581	0.0060	0.470±.012	10.58±.27	0.16337±.00019	2491±2
16.1	627	391	0.624	320513	0.0060	0.475±.012	10.73±.28	0.16367±.00013	2494±1
17.1	400	455	1.138	432900	0.0040	0.478±.012	10.80±.27	0.16383±.00016	2496±2
18.1	236	155	0.658	1000000	0.0001	0.479±.012	10.85±.28	0.16414±.00021	2499±2
19.1	493	330	0.669	1694915	0.0010	0.477±.012	10.79±.27	0.16406±.00015	2498±2
20.1	418	323	0.773	143678	0.0120	0.476±.012	10.74±.28	0.16371±.00016	2494±2
21.1	304	241	0.793	452489	0.0040	0.484±.013	10.99±.30	0.16460±.00029	2504±3
22.1	317	240	0.757	67204	0.0270	0.477±.012	10.79±.28	0.16407±.00018	2498±2
23.1	357	245	0.686	366300	0.0050	0.472±.012	10.66±.27	0.16392±.00018	2496±2
24.1	472	508	1.076	740741	0.0020	0.481±.012	10.88±.28	0.16417±.00024	2499±2
25.1	361	232	0.643	25349	0.0700	0.475±.012	10.69±.27	0.16323±.00018	2489±2
26.1	238	174	0.732	1000000	0.0001	0.466±.016	10.55±.35	0.16421±.00020	2500±2
27.1	344	183	0.531	543478	0.0030	0.461±.015	10.41±.35	0.16374±.00017	2495±2
28.1	325	154	0.474	200803	0.0070	0.475±.016	10.76±.36	0.16419±.00017	2499±2
29.1	233	166	0.713	101937	0.0140	0.471±.016	10.63±.36	0.16355±.00021	2493±2
30.1	345	396	1.149	140647	0.0100	0.473±.016	10.68±.37	0.16387±.00018	2496±2
31.1	266	189	0.707	164204	0.0090	0.484±.016	10.92±.37	0.16364±.00029	2494±3
32.1	192	149	0.776	1000000	0.0001	0.469±.016	10.68±.36	0.16522±.00024	2510±2
33.1	327	295	0.901	102775	0.0140	0.473±.016	10.69±.36	0.16405±.00019	2498±2
34.1	333	303	0.910	230415	0.0060	0.476±.016	10.68±.36	0.16285±.00031	2485±3

Figure 10.4. (a) Conventional $^{207}Pb/^{235}U$ - $^{206}Pb/^{238}U$ concordia diagram for zircons from VH514c (D_1-M_1 leucosome). Three older analyses are not represented. (b) Probability distribution diagram for $^{207}Pb/^{206}Pb$ zircon ages (excluding three older analyses) from VH514c (D_1-M_1 leucosome). On this diagram each analysis contributes an equal bell-shaped area whose kurtosis is governed by precision; more precise ages, resulting from analyses with higher U contents (at any fixed age), produce more pronounced peaks, and therfore have more influence on pooled ages. The distribution of the 36 analyses is represented by the sum of the shaded and unshaded areas. The shaded area represents the 25 analyses that form a normal distribution. (c) Conventional $^{207}Pb/^{235}U$-$^{206}Pb/^{238}U$ concordia diagram for zircons from VH407 (LAS CLG). The tightly packed analyses do not conform to a simple population as shown on figure 4d. (d) Probability distribution diagram for $^{207}Pb/^{206}Pb$ zircon ages from VH407 (LAS CLG). The two depicted populations, which yield ages of 2491.0 ± 1.1 Ma and 2485.0 ± 1.6 Ma, are not obvious from morphological criteria, but are supported by the statistical treatment and geological evidence for assimilation (see text). (e) Conventional $^{207}Pb/^{235}U$-$^{206}Pb/^{238}U$ concordia diagram for zircons from VH179 (D_2-M_2 leucosome). All but the two oldest analyses are within error of each other. (f) Probability distribution diagram for $^{207}Pb/^{206}Pb$ zircon ages from VH179 (D_2-M_2 leucosome). All but two of the ages are normally distributed.

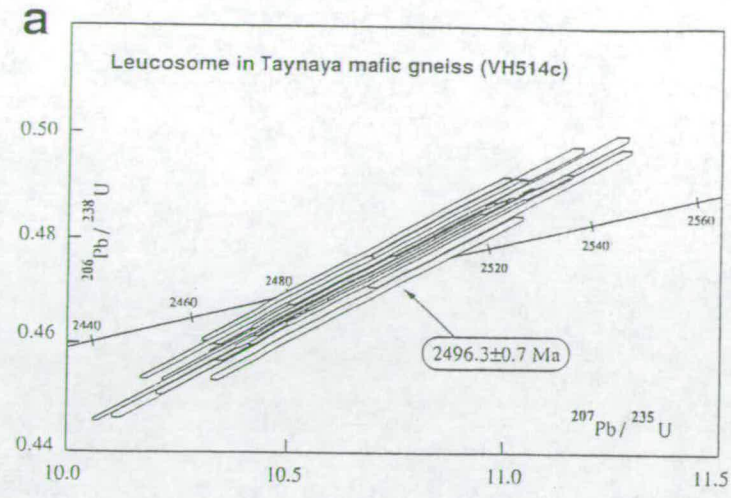
a
Leucosome in Taynaya mafic gneiss (VH514c)
0.50
0.48
0.46
0.44
206Pb / 238U
2440
2460
2480
2520
2540
2560
2496.3±0.7 Ma
207Pb / 235U
10.0
10.5
11.0
11.5

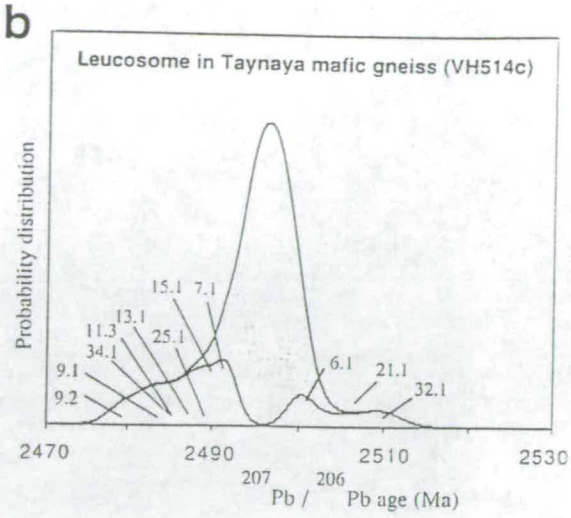
b
Leucosome in Taynaya mafic gneiss (VH514c)
Probability distribution
15.1
7.1
13.1
11.3
25.1
34.1
9.1
9.2
6.1
21.1
32.1
2470
2490
2510
2530
207 Pb / 206 Pb age (Ma)

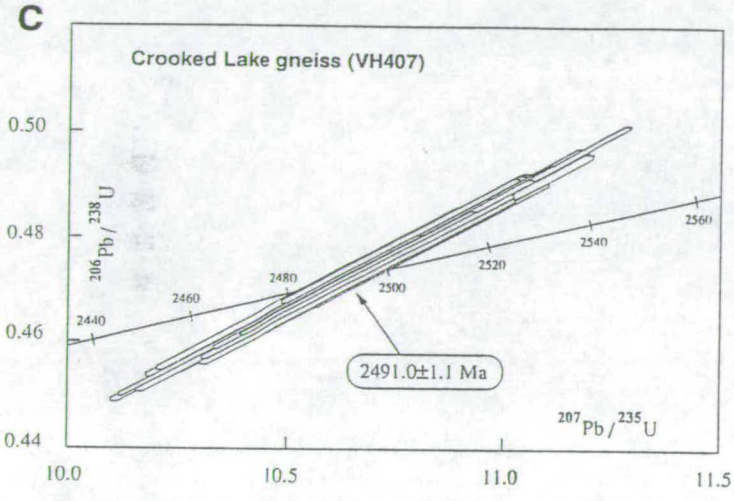
c
Crooked Lake gneiss (VH407)
0.50
0.48
0.46
0.44
206Pb / 238U
2440
2460
2480
2500
2520
2540
2560
2491.0±1.1 Ma
207Pb / 235U
10.0
10.5
11.0
11.5

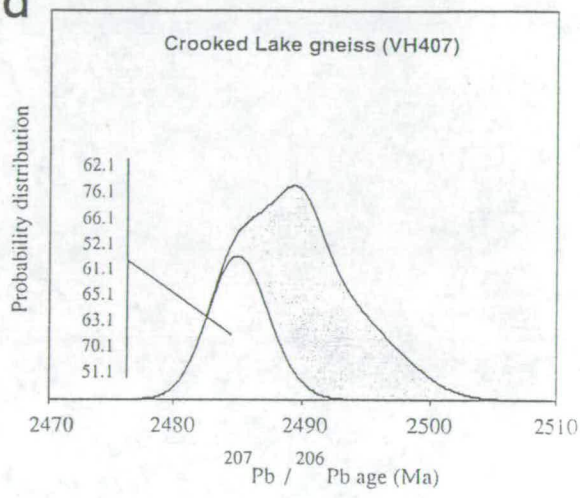
d
Crooked Lake gneiss (VH407)
Probability distribution
62.1
76.1
66.1
52.1
61.1
65.1
63.1
70.1
51.1
2470
2480
2490
2500
2510
207 Pb / 206 Pb age (Ma)

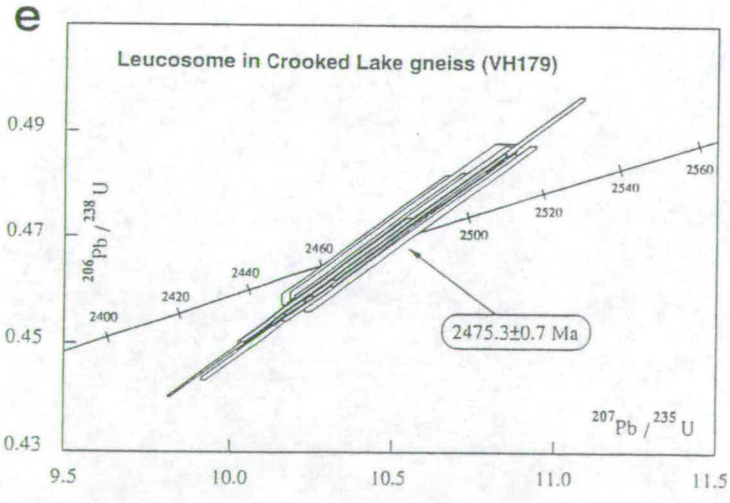
e
Leucosome in Crooked Lake gneiss (VH179)
0.49
0.47
0.45
0.43
206Pb / 238U
2400
2420
2440
2460
2500
2520
2540
2560
2475.3±0.7 Ma
207Pb / 235U
9.5
10.0
10.5
11.0
11.5

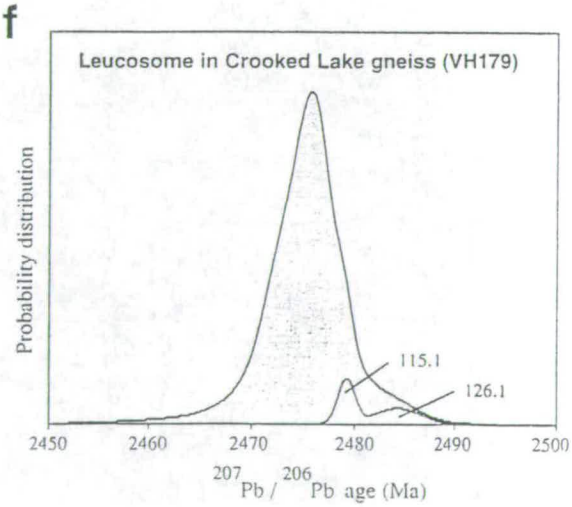
f
Leucosome in Crooked Lake gneiss (VH179)
Probability distribution
115.1
126.1
2450
2460
2470
2480
2490
2500
207 Pb / 206 Pb age (Ma)

Lake Africa suite CLG (VH407)

Most of the zircons in this sample are relatively equant multifaceted grains. Zoning, if present, is only poorly developed which probably reflects the low-U contents of these grains. Cracks are relatively common, inclusions are relatively rare, and some grains are deeply embayed. In common with VH514c, many grains have an irregular very thin low-U rim, a feature that is consistent with metamorphic zircon growth during a subsequent tectonothermal event, as are the numerous facets.

The 26 analyses of zircons from this sample define a reasonably tight population with an age estimate of 2488.9 ± 1.4 Ma and a chi-square of 2.9. However, this age can be refined by progressively omitting samples until a statistically simple grouping, with a chi-square that is indistinguishable from unity, is obtained. Exclusion of the 9 youngest analyses produces such a grouping, with the remaining 17 data points defining a slightly older age (2491 ± 1.1 Ma; Figure 10.4c) than that derived from the full dataset. In contrast to VH514c, however, the omitted data are not simply skewed to younger values (*cf.* Figures 10.4d & f), but instead define a separate symmetrical distribution that defines an independent age of 2485 ± 1.6 Ma. Although there are no immediately obvious chemical or morphological criteria that distinguish the two groupings, it is possible on geological grounds (discussed further below) that these data populations reflect two distinct episodes of zircon growth. The oldest age of 2491 ± 1.1 Ma is thought to represent the age of an inherited CLG zircon population and the 2485 ± 1.6 Ma age is thought to be the true crystallisation age of the Lake Africa Suite pluton.

Leucosome in deformed CLG dioritic dyke (VH179)

Although the zircons separated in this sample are mostly broken fragments, euhedral faces and complex facets are sometimes preserved. Trails of fine inclusions are common in many grains, and some also have rhythmic zoning. In addition, 4 grains have rounded cores, 2 of which were analysed.

All 27 zircon analyses (excluding those of the cores) yield an age of 2475.3 ± 0.7 Ma from a single population of $^{207}Pb/^{206}Pb$ ages that are within analytical error of each other. This age is taken to be the crystallisation age of the leucosome and on the basis of field criteria (outlined in Section 10.3.1 above) is also interpreted to be the precise age of the D_2-M_2 event. The 2 rounded cores (which have high U; Table 10.1) yield significantly older ages than that of the leucosome; one has an age of 2484 ± 5 Ma and the other an age of 2479 ± 3

Ma. It is possible that the younger of the two grains was inherited from the deformed intermediate dyke, and the older core from the host CLG.

10.5 Discussion: interpretation of zircon geochronology

10.5.1 The age of D_1-M_1 and the origin of the Mossel Gneiss

Sample VH514c, the leucosome in the Taynaya EMG, has a preferred crystallization age of 2496.3 ± 0.7 Ma. This age is marginally younger than the previous estimate of 2501 Ma for the age of D_1-M_1 (Black *et al.*, 1991). Field relations imply that the leucosome formed by partial melting of the Taynaya EMG, hence it is most likely that the age directly dates the D_1-M_1 event. Although partial melting of the EMG occurred during this event, at least some of the Mossel gneiss is older and was probably not derived directly from EMG during D_1-M_1. However, these data cannot be used to constrain the age of these source components. First, there appear to be only two old grains in this rock. Both have similar U, Th and Th/U to the other zircons, and therefore probably also crystallised from a relatively felsic rock, making it very likely that they are xenocrystic components within the EMG. Second, the range of ages obtained for the same phase of one of these old grains indicates that isotopic resetting has occurred. Therefore the inherited ages provide neither unequivocal older nor younger limits for the age of the EMG.

10.5.2 The age of the LAS (CLG) pluton: constraints on AFC and tectonic repetition

Sample VH407 has the most complex distribution of zircon ages with two statistically distinct gaussian age populations of 2485 ± 1.6 and 2491 ± 1.1 Ma. However, VH407 was specifically selected for dating from a large number of CLG samples primarily because it was from a large differentiated pluton that has assimilation - fractional crystallisation (AFC) characteristics (see Section 9.2 & Chapter 11). This sample was collected from adjacent to a zone that has abundant partly digested xenoliths and on the basis of these features and geochemical and stable isotope data is thought most likely to have assimilated surrounding crust, including marginally older CLG. Partly digested xenoliths (*e.g.* Figure 9.8) of these CLG suites are difficult to distinguish from EMG and Mossel Gneiss. These lines of evidence provide the best explanation for the bimodal distribution of zircons in the Lake Africa suite CLG. The alternative interpretation for the younger zircon sub-population being reset by a later tectonothermal event is difficult to reconcile with the observation that it is defined by a non-skewed age distribution (Figure 10.4d).

The 2485 ± 1.6 and 2491 ± 1.1 Ma crystallization ages of the LAS further support the contention that there was a temporal evolution within CLG magmatism. Despite a certain amount of overlap for SHRIMP analyses from the CLG (this study & Black *et al.*, 1991a; see Figure 13.1), it is apparent that CLG suites (including the Grace Lake Granodiorite) intruded throughout the D_1-M_1 to D_2-M_2 interval. Although the youngest CLG suites occur in the north, there is insufficient evidence to confirm a south to north progression on isotopic grounds. Moreover, relatively young CLG magma types (syn-D_2), such as intermediate dykes and granite sheets, cross-cut older CLG suites in all regions. A further conclusion from the distribution of CLG zircon data, is that suites are sufficiently different in age on a km scale to preclude simple tectonic repetition by F_2 regional folding (*cf.* McLeod *et al.*, 1966; Oliver *et al.*, 1982; Collerson *et al.*, 1983).

10.5.3 The age of D_2-M_2 and the relationship of CLG lithologies to deformation

Sample VH179, the leucosome in a dioritic CLG dyke, has a crystallization age of 2475.3 ± 0.7 Ma which is interpreted to be the age of D_2-M_2. This age indicates that the previous estimate for this event (Black *et al.*, 1991a) was too old by 11 m.y., and that only minor components of the Grace Lake granodiorite are syn-tectonic. This age is also significantly younger than any of the main CLG plutons, which were intruded in the time interval between D_1 and D_2, and confirms that only minor components intruded syn-tectonically.

10.6 Summary and conclusions

New SHRIMP U-Pb zircon dating of syn-metamorphic leucosomes directly constrains the age of the two principal high-grade deformation events in the Vestfold Hills to 2496.3 ± 0.7 Ma (D_1-M_1) and 2475.3 ± 0.7 Ma (D_2-M_2). A third sample, from a deformed Crooked Lake gneiss pluton, has two statistically defined zircon age populations. The youngest of these ages (2485.0 ± 1.6 Ma) is interpreted to be the crystallization age of the pluton, whilst the older age (2491.0 ± 1.6 Ma) is considered to reflect inheritance of marginally older assimilated CLG protoliths. The revised timing of high-grade events and additional age information for the CLG presented here allows a reassessment of the geological evolution of the Vestfold Hills terrane. Most importantly, the implications for structural, petrogenetic and conventional isotopic studies (discussed in Chapters 9 - 12) are that CLG lithologies were not tectonically repeated on a km-scale from south to north as originally proposed (*e.g.* Oliver *et al.* 1982; Collerson *et al.*, 1983). The wider implications of the refined geochronological scheme are discussed further in the next two chapters and in the conclusions (Chapter 13) in Part 4.

Chapter 11

Geochemical and isotopic evolution of the Vestfold Hills orthogneisses

11.1 Introduction

11.1.1 Sample selection for geochemical and isotopic analysis

This chapter presents geochemical and conventional stable- and radiogenic-isotope data for the principal orthogneiss units in the Vestfold Hills. Only limited new data are presented for the EMG and Mossel suites because these pre-D_1 orthogneisses are commonly strongly deformed, which has resulted in distinct gneiss components being finely interlayered at handspecimen scale. Moreover, it is also difficult to define cogenetic suites or associations in the field for these units and there is often textural evidence for partial melting during or before D_1-M_1.

Sheraton & Collerson (1984) established that the Mossel Gneiss is dominantly tonalitic in composition and is similar in geochemical character (*e.g.* Y 'depletion', see Section 8.4) to the CLG. Hence, it is likely that petrogenetic deductions derived from detailed observations within the CLG will also be broadly applicable to the Mossel Gneiss. Nevertheless, six additional analyses of the Mossel Gneiss are included in Appendix 2 and are briefly described in this chapter.

New field observations described in Chapter 9 established that rocks previously grouped with the Tryne Metavolcanics include younger Mossel and CLG lithologies that were tectonically interleaved at outcrop scale. This implies that the geochemical account of Sheraton & Collerson (1984) for even the mafic components of the Tryne unit (*i.e.* EMG, see Chapter 9) should be treated with caution. Nevertheless, a limited new dataset for some pre-D_1 mafic components is included in Appendix 2. This work is restricted to the distinctive Taynaya EMG (see Section 9.4.1) and geochemical data for this suite are described in this chapter as part of a regional account of the orthogneiss lithologies. Emphasis is therefore placed on the lithologically diverse CLG. This is partly to define or confirm the status of field-defined suites or associations, but also because the CLG has the best potential for understanding crust-forming processes in the terrane.

11.1.2 Approach and technical difficulties

The approach adopted in this study is largely geochemical and isotopic, and relatively little emphasis is placed on petrography/mineral chemistry (discussed in Chapters 1 & 8). The bulk of this chapter describes the general geochemical characteristics of the CLG, but focuses on one sub-suite, the Lake Africa Suite (LAS), in detail. This suite was chosen because it is compositionally diverse and has clear textural evidence for assimilation in the most differentiated units. Field observations (Chapter 9) and U-Pb zircon geochronology (Black *et al.*, 1991a; this study, Chapter 10) have established that assimilation was likely to have been an important process that influenced the chemical evolution of many CLG suites. Therefore, to examine the possible consequences of this process further, a combined geochemical and isotopic study has been undertaken on 9 samples from the LAS. Individual representatives from other CLG sub-suites and the pre-D_1 gneiss units were also examined in this detailed manner. Unfortunately, analytical problems associated with ICP-MS determination of REE (see Appendix 1), and ID-MS determination of Sm, have severely limited the breadth of coverage and more importantly the time available to investigate comparative and more quantitative (modelling) aspects of the results.

11.2 Geochemical characteristics of the main orthogneiss lithologies

11.2.1 Overview of the principal orthogneiss lithologies

Field observations and macroscopic characteristics that are used to distinguish or classify the principal gneiss lithologies are described in Chapter 9 and are illustrated in several figures. In this section a limited number of Mossel Gneiss (n=6) and EMG (n=11) samples are considered along side a much larger CLG dataset (n=161) that comprises 14 sub-suites that have been distinguished petrographically, spatially or temporally.

The Taynaya EMG (mostly from Bulatnaya Bay)

The Taynaya EMG in the Bulatnaya Bay area are not strongly deformed, have a range of compositions, and there are clear textural gradations between EMG that have migmatite features and those that appear to have had no (or only minor) partial-melt removal. The rocks described here are *not* directly associated with the migmatites (see Sections 9.4 & 10.3.1) and probably represent pristine palaeosome (protolith).

Mossel Gneiss

The Mossel Gneisses described here are taken from throughout the northern region and are relatively homogeneous samples that do not have strongly attenuated leucosomes or xenolithic/layering features that often typify this gneiss unit (*cf.* Figure 9.5d). They are compared with the CLG geochemically, partly to define the principal geochemical characteristics of the gneiss, but also to illustrate that it is difficult to distinguish the Mossel Gneiss from evolved CLG on geochemical grounds alone.

Crooked Lake Gneiss (CLG)

The CLG is lithologically diverse. It ranges in composition from ultramafic to granitic with potassic compositions (monzodiorites and monzonites) being most abundant. A number of suites have been distinguished and are defined and described in more detail in the following sections. Abbreviations used here are included on the 'abbreviations and symbols' card in the pocket at the rear of this thesis.

11.2.2 Principal geochemical characteristics

Major elements

Compositionally, all (except one[1]) of the orthogneisses define a broad calc-alkaline trend on an AFM diagram (Figure 11.1). Most of the Mossel Gneisses are indistinguishable from the CLG, however, the Taynaya EMG are distinct and are displaced towards the alkali apex on Figure 11.1.

The general similarity between CLG and Mossel Gneiss, and the distinct chemistry of the Taynaya EMG, is further highlighted by the relationships between major and trace elements with respect to ***mg*** or SiO_2 (Figures 11.2 & 11.3 respectively). In general, there is a very poor correlation between most elements and ***mg***. Compositions for ultramafic CLG and Taynaya EMG are highly magnesian (***mg*** ~ 80). Most Taynaya EMG vary from about ***mg*** 83 to 70, whereas the CLG varies from about ***mg*** 85 to 5. Most Mossel Gneisses vary between about ***mg*** 50 and 30 and are similar to the felsic CLG. Major-element variations with ***mg*** for all suites are dominated by poorly-defined trends of increasing SiO_2 and K_2O, decreasing

[1]One Mossel Gneiss sample (VH 542) has anomalously high $Fe_2O_{3(t)}$ and distinctive chemistry. This sample is a garnet-bearing granite from adjacent to the Chelnok Paragneiss and it is likely to have been derived directly by partial melting of this unit. This sample is not considered in detail in this study.

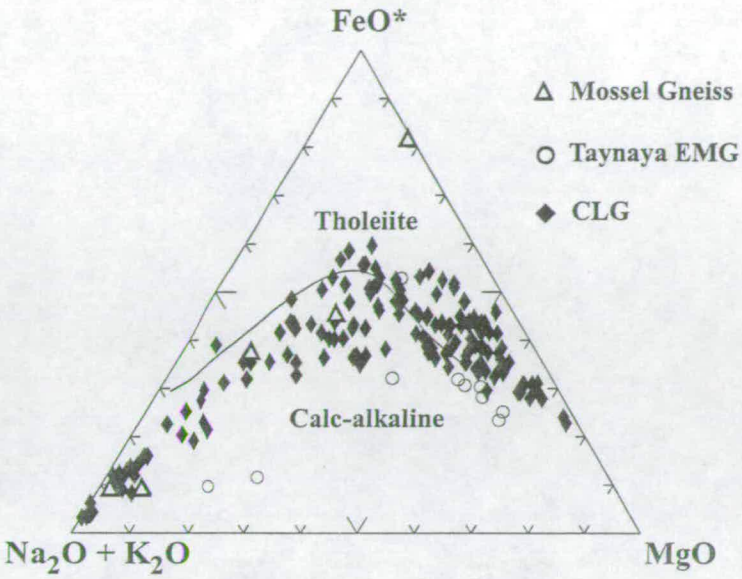

Figure 11.1 Igneous AFM diagram with tholeiitic and calc-alkaline trends defined after Irvine & Baragar (1971). Filled diamonds = CLG; open triangles = Mossel Gneisses; open circles = Taynaya EMG.

CaO and MnO, and broad inflections of Al_2O_3, Na_2O, TiO_2 and P_2O_5. Most of these trends are more clearly illustrated using SiO_2 as abscissa (Figure 11.3).

Normative mineralogy

The wide range of bulk compositions for the Taynaya EMG, CLG and Mossel Gneiss is reflected in normative mineralogies. The Taynaya EMG can be distinguished from the other suites by having higher normative *Ol* relative to SiO_2 or ***mg***, whilst the Mossel Gneisses are indistinguishable from felsic CLG. The Mossel Gneisses, and many of the CLG, are *Q*-normative, although some of the most basic CLG are weakly *Ne*-normative. Unlike the study of Sheraton & Collerson (1984), this dataset does not appear to have three natural groupings on a *Q-Ab-Or* diagram (*cf.* Section 8.4 & Figure 8.3). However, the syn-tectonic granites loosely cluster between the 0.5 to 3 kbar *Q-Ab-Or* isobaric minima (Figure 11.4). Most of the remaining *Q*-normative compositions straddle the monzodiorites, gabbros, diorites, quartz diorites and tonalites of Sheraton & Collerson (1984).

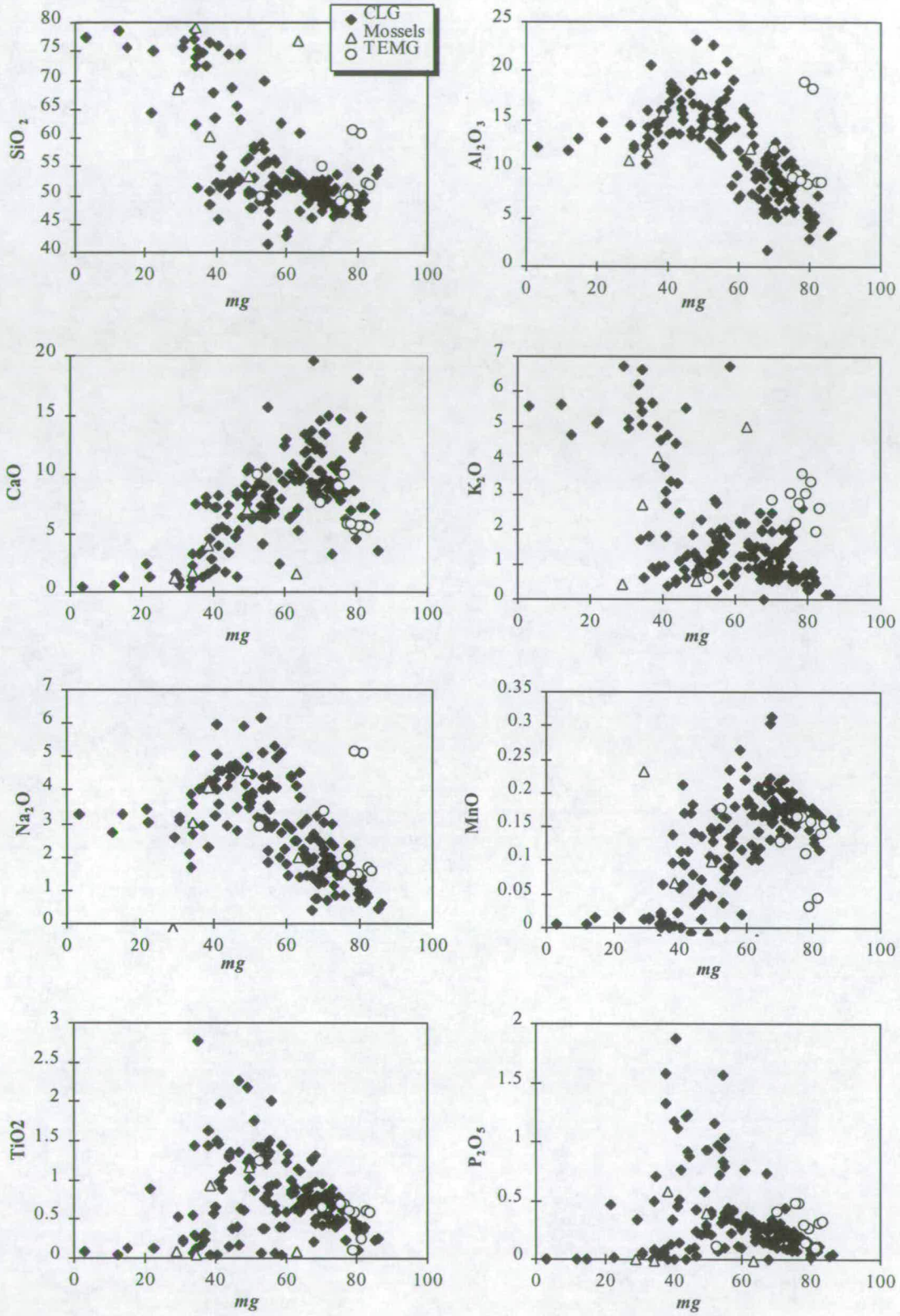

Figure 11.2 Major-element variations *vs.* ***mg*** for the Vestfold Hills orthogneiss units.

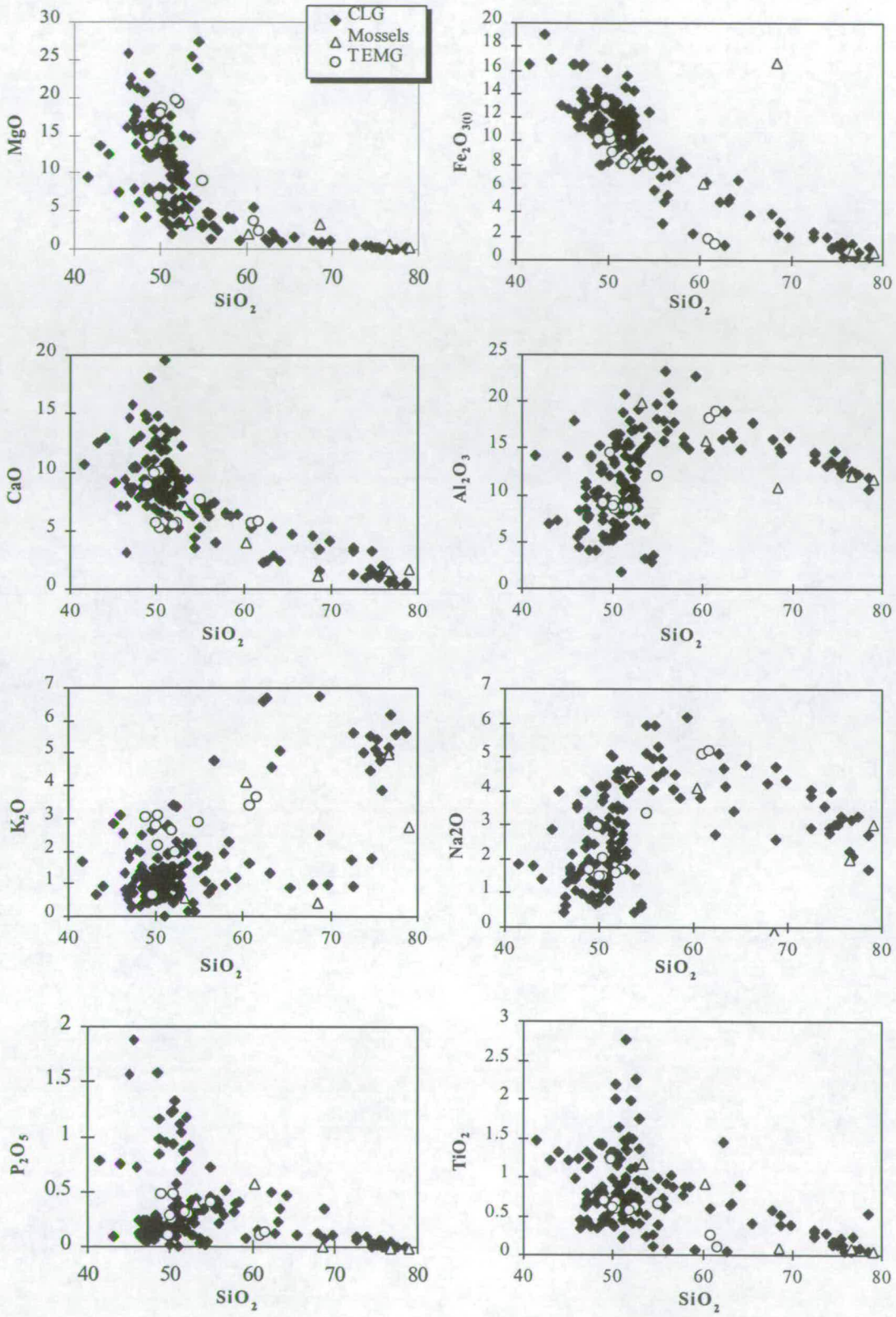

Figure 11.3 Major-element variations *vs.* SiO_2 for the Vestfold Hills orthogneiss units.

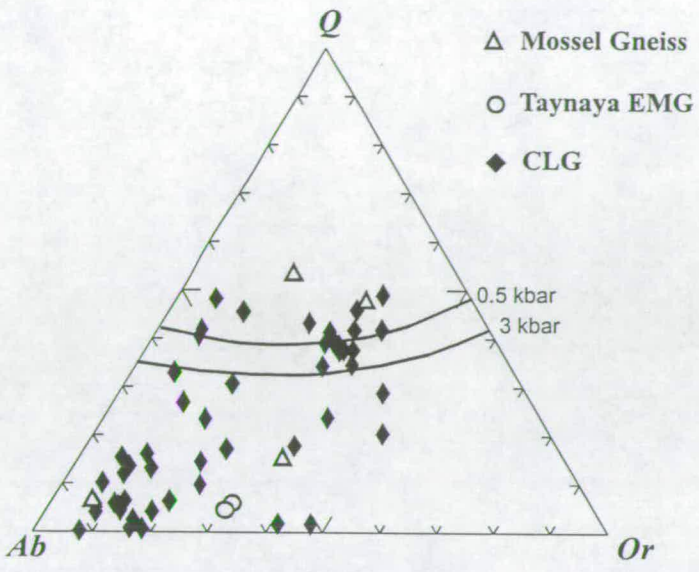

Figure 11.4 Normative *Q-Ab-Or* diagram for *Q*-normative orthogneisses. Quartz-feldspar field boundaries and positions of the quaternary isobaric minima at 0.5 and 3 kbar are indicated (after Tuttle & Bowen, 1958, *in* Sheraton & Collerson, 1984).

Trace elements

Trace elements that have a strong affinity for ferromagnesian phases (Ol-Opx-Cpx), such as the compatible elements (CE) Ni and Cr, are well correlated with ***mg***, and these elements decease sharply with decreasing ***mg***-number (or increasing SiO_2) within suites. Sc also decreases sharply but is less well correlated. Those elements that commonly behave incompatibly in basaltic/andesitic magmas (IE), by contrast, are not well correlated with either ***mg***, SiO_2, or even other IE such as Zr (Figure 11.5).

The Taynaya EMG form a distinctive high-***mg*** group characterized by high Rb, Ni, La, Ce, Nd and Y (discussed further below). Two samples also have very high Nb. As with other geochemical relations (described above), the CLG and Mossel Gneisses are indistinguishable. For the main CLG dataset there are general trends of increasing Pb (with SiO_2 or decreasing ***mg***), a reasonably strong inflection for Sr, and possible inflections for Zr, Rb, and LREE. Other IE are highly variable.

Preliminary conclusions and implications

The Taynaya EMG forms a distinct compositional group that is not thought to be *directly* related to the CLG or Mossel Gneisses. It is not possible to distinguish between the CLG and Mossel Gneisses on major- and trace-element grounds alone.

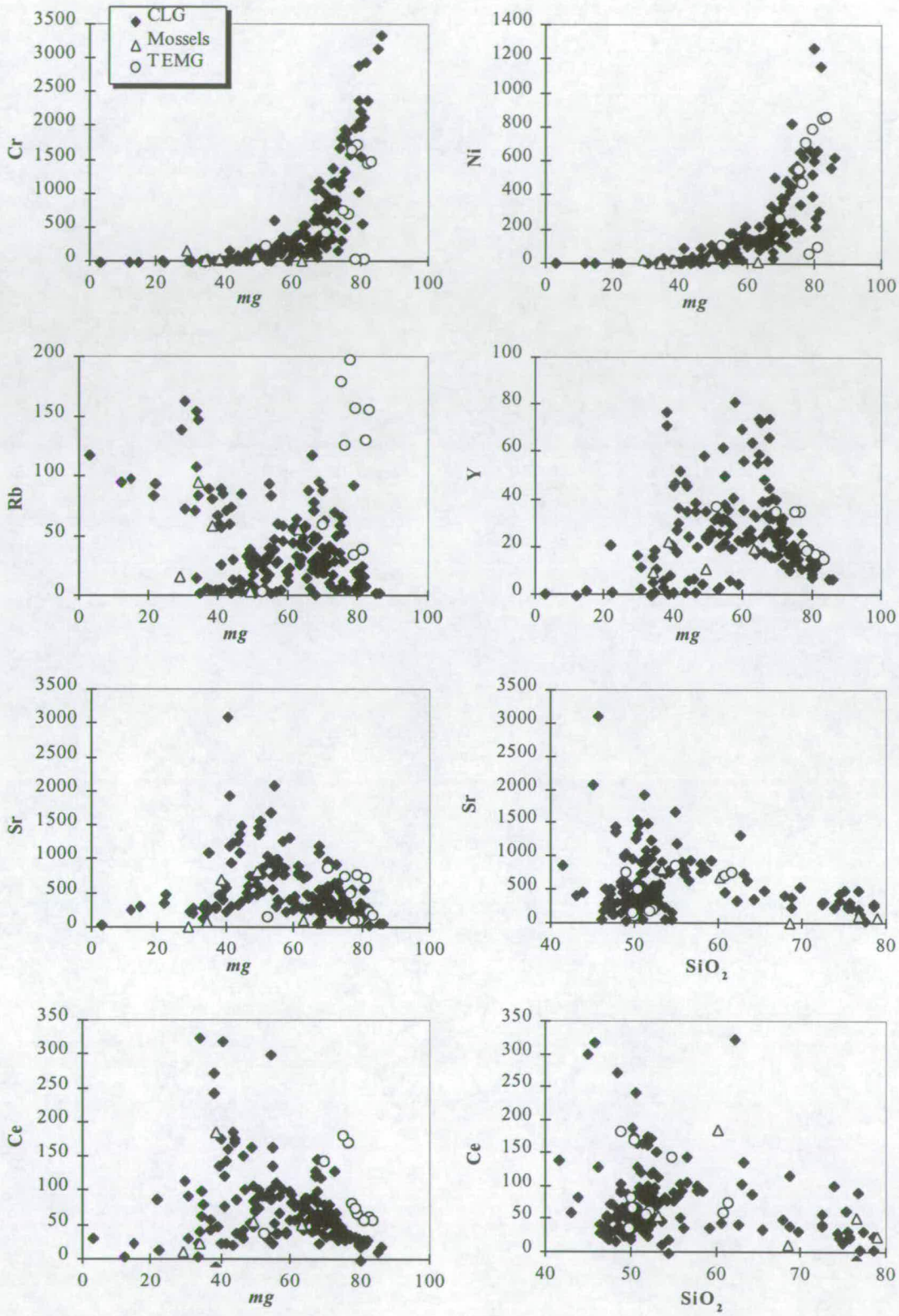

Figure 11.5 Selected trace elements plotted against ***mg***, SiO_2 and incompatible elements (continued over page).

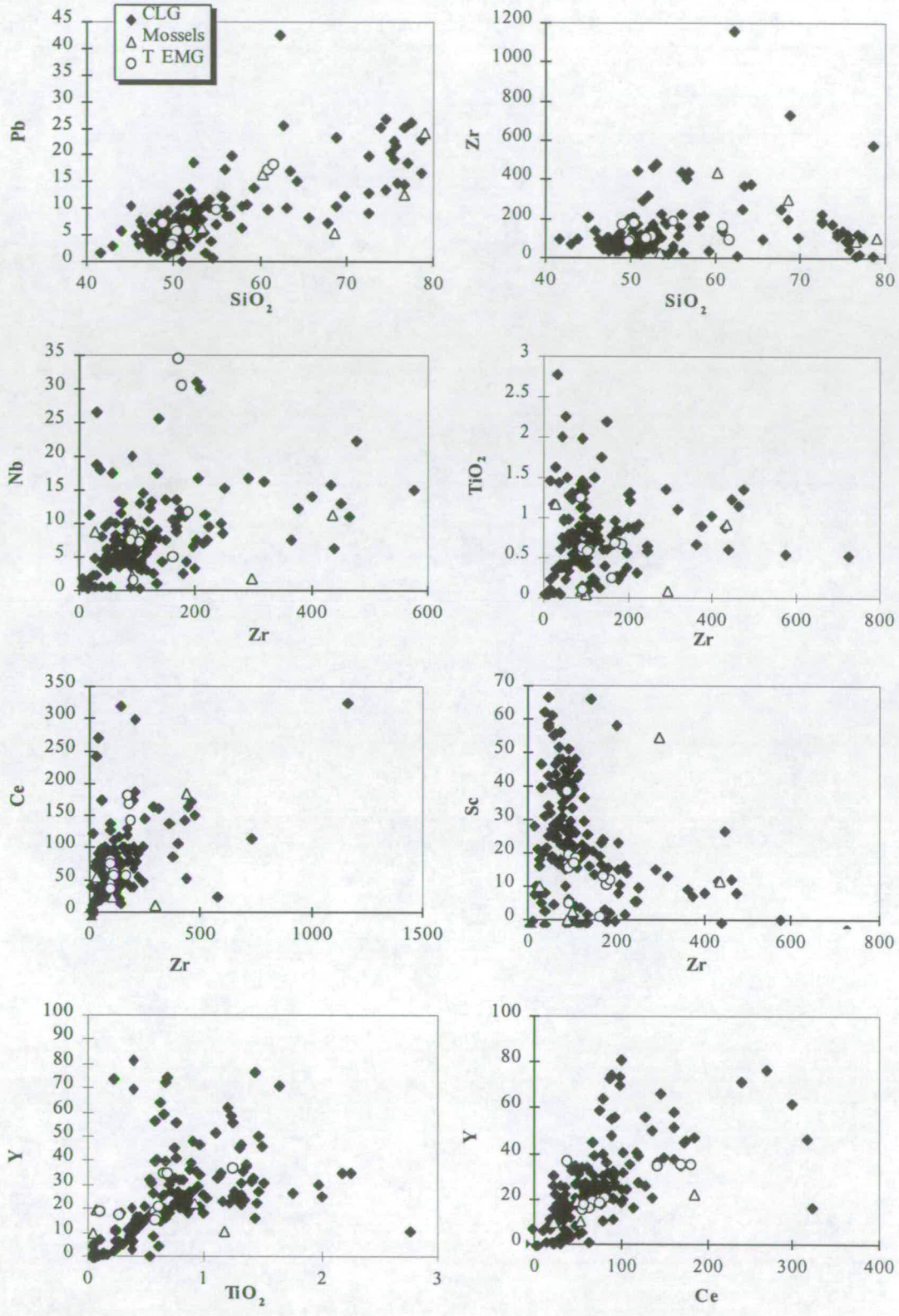

Figure 11.5 cont. Selected trace elements plotted against ***mg***, SiO_2 and incompatible elements.

It is likely that IE variability within the CLG, and differences with the Taynaya EMG, reflects three main processes:

- ***Variations in the conditions of partial melting*** (*e.g.* extent of partial melting, source composition, and proportion of assimilated components).

- ***Variations in crystal fractionation history*** (*e.g.* temporal and compositional changes in the fractionating assemblage and hence *D*-values).

- ***Trace-element mobility*** as a consequence of metamorphism (especially LILE).

The following sections examine these processes further by first examining the CLG in more detail. However, there are two immediate implications for previous work and tectonomagmatic models for the evolution of the CLG (reviewed in Chapter 8). Firstly, petrogenetic modelling using least-squares techniques (*e.g.* Sheraton & Collerson, 1983) is likely to be influenced by variable fractionating assemblages (changing *D*-values). This is apparent from many of the major- and trace-element diagrams presented in Figures 11.2, 11.3 & 11.5. Secondly, previous modelling and isotope studies are likely to be biased by combining unrelated suites and/or including suites that were strongly influenced by assimilation (discussed further in Chapters 12 & 13).

11.3 The Crooked Lake Gneiss in detail

11.3.1 Geochemical character of field-defined suites

A number of CLG sub-suites (below) have been distinguished based on a variety of field, petrographic, temporal and spatial criteria (see Chapter 9). The criteria used to define each suite are described first, and then a brief comparative summary of the geochemistry is provided.

Many of the groups distinguished here overlap in composition to some extent (Figure 11.6) and it is likely that most are broadly related by common petrogenetic processes, such as derivation from similar source (mantle) reservoirs, interaction with the same crust, and comparable fractionation histories. However, there are differences between many groups, and variables such as extent of partial melting, the nature of fractionating assemblages, degree of assimilation or even extent of metasomatism are all potentially different in detail. For some suites, it is possible to qualitatively distinguish 'distinctive' chemical characteristics. Quantitative discriminant-function analysis or analysis of variance

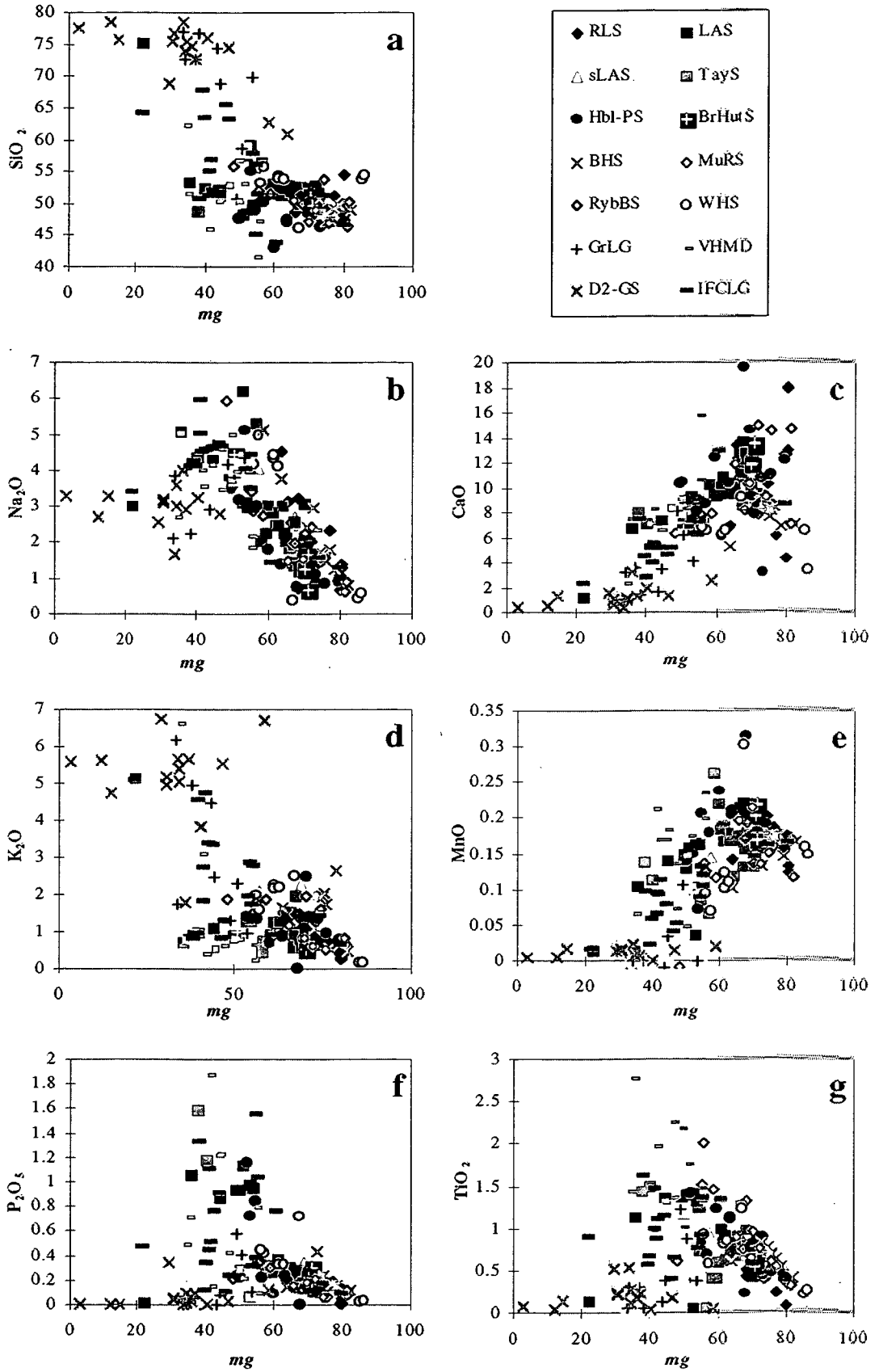

Figure 11.6 Selected major- and trace-element plots *vs. mg* for all CLG suites.

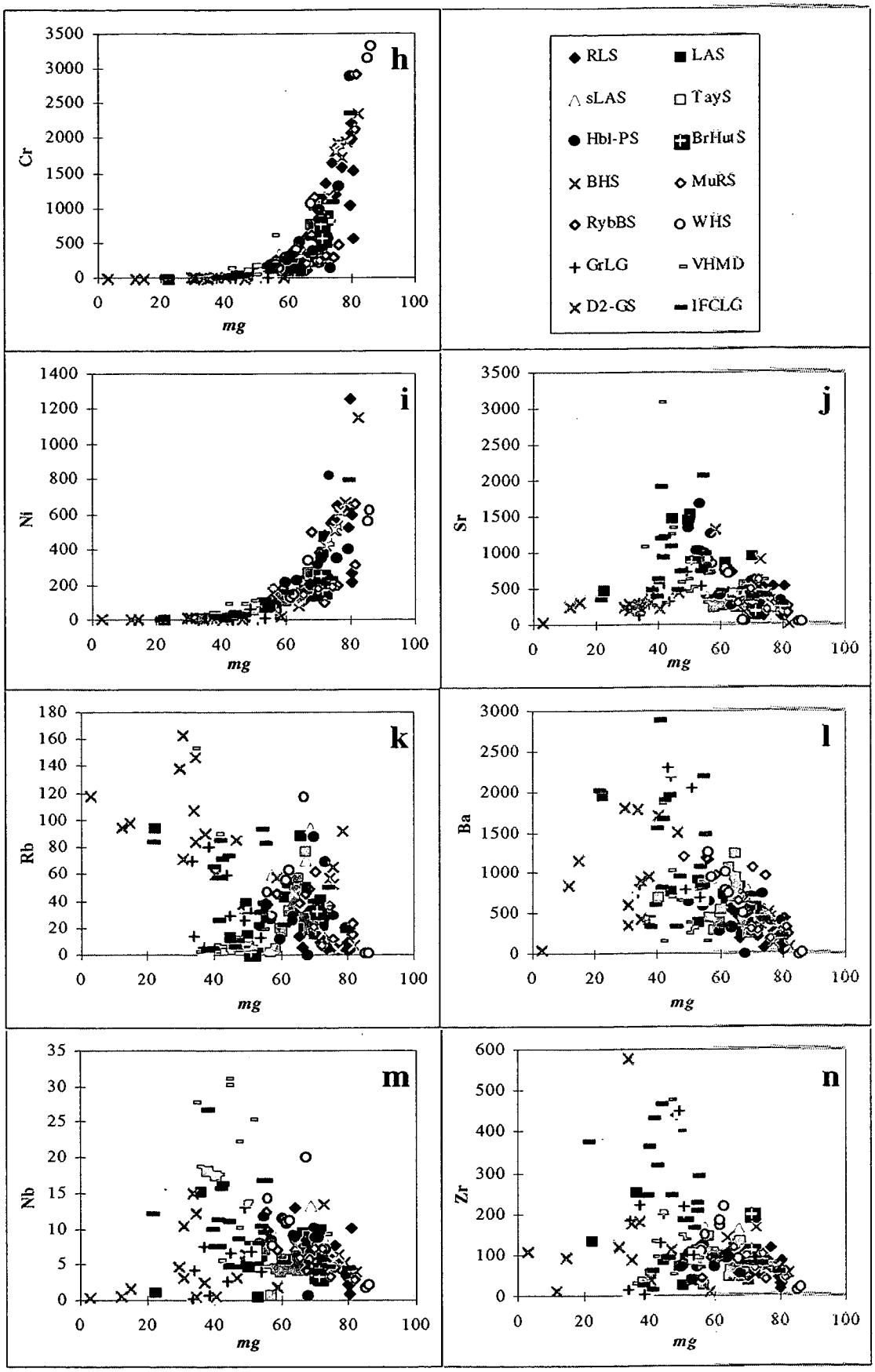

Figure 11.6 cont. Selected major- and trace-element plots *vs. mg* for all CLG suites.

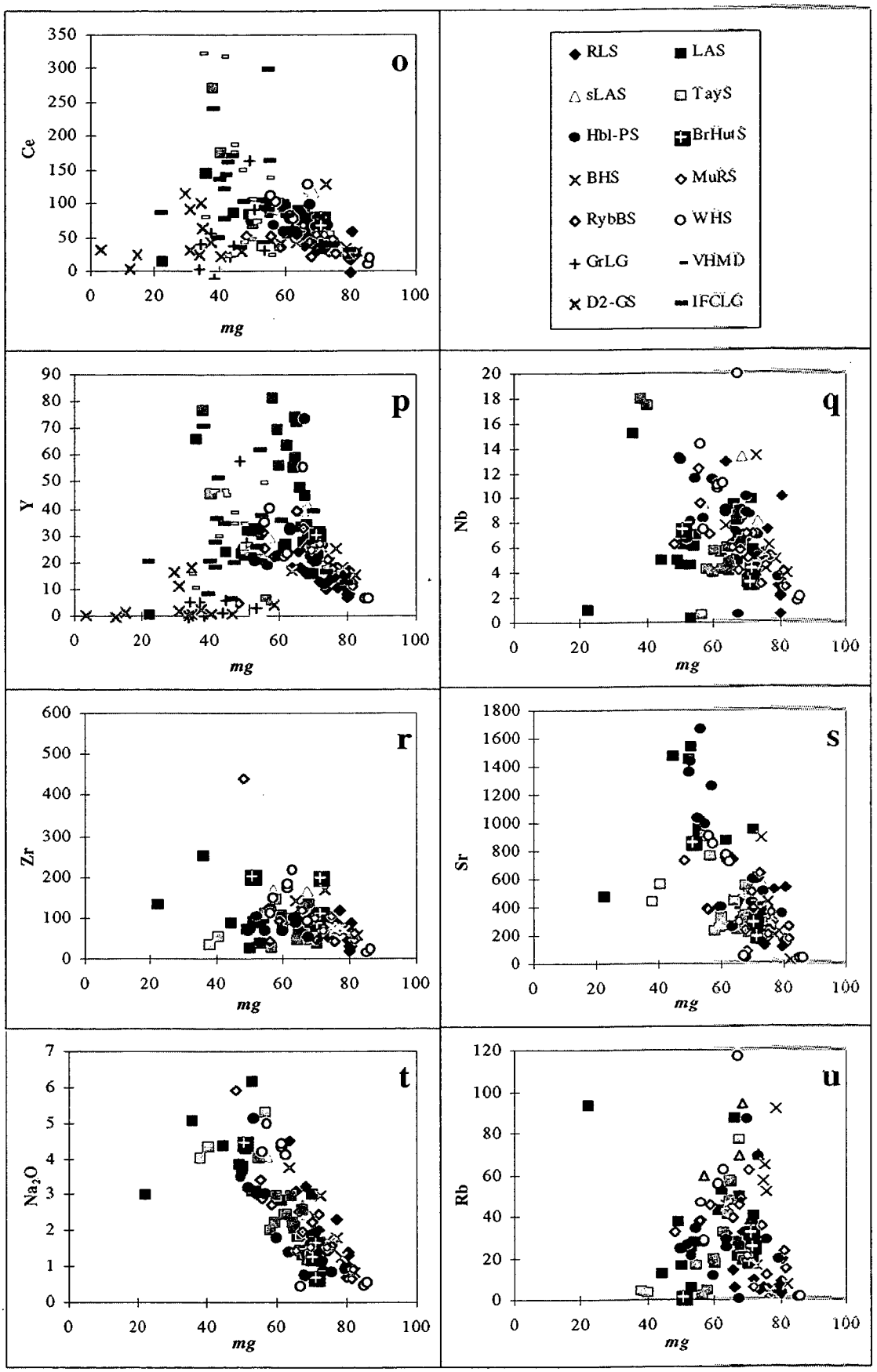

Figure 11.6 cont. Selected major- and trace-element plots *vs. mg* for all CLG suites.

has not been attempted here, mainly because the procedure is strongly influenced by small and/or non-normal datasets, but also because complex mathematical transformations of the type described by Rollinson (1993, and references therein) are required to avoid spurious correlations relating to the constant-sum problem (discussed further in Chapter 13).

1. RLS. The Rookery Lake Suite (UM-M-I association)

This suite occurs in a limited area on the south coast of Long Peninsula 3.5 km WNW from Rookery Lake. The RLS occurs in a low-strain area associated with a steeply-plunging, parasitic, F_2, asymmetric z-fold that is oriented E-W. The suite has been extensively sampled because it is lithologically diverse over a limited area, variations are gradational, and delicate igneous features are well-preserved (see Figure 9.3c). It is likely that the RLS also occurs further south on Topografov Island. Further to the north it becomes strongly transposed into a <1 m wide dyke-like layer, although compositional variations within the layer are still present along strike and presumably reflect the primary variability seen in the low-strain area.

Geochemically, this group has high ***mg***-numbers (mostly between 75 and 80) and relatively low Sr compared with other UM-M-I suites on southern Long Peninsula, such as the LAS or the Hbl-PS (described below).

2. LAS. The Lake Africa Suite (UM-M-I association)

This suite corresponds to the large ultramafic-mafic complex that occurs between Lake Africa and Tryne Fjord (shown on Figure 9.1*). Members within this suite are restricted to those that appear to be related by igneous gradations, and CLG intrusions that are obviously younger have been excluded from this suite. Two evolved samples are included in this suite. They are relatively felsic varieties that are endemic to certain areas of the complex and are interpreted to be back-veined late-stage differentiates. However, it is possible that these two rocks are not strictly co-magmatic with the rest of the suite; they are included in this description and Figure 11.6, but have not been included in the more detailed descriptions outlined in later sections.

Relative to the other UM-M-I associations, the LAS has a trend of increasing $(Ce/Y)_N$ with decreasing ***mg***, although the two distinctive highly evolved rocks mentioned above have very high $(Ce/Y)_N$. Other elements, such as P, are highly variable. This suite is distinct from the RLS by having higher Sr and lower $(Ce/Y)_N$.

3. sLAS. Southern Lake Africa Suite (M-I association)

In the field this suite appears to be similar in composition to the LAS although, based on field and structural criteria, it is not possible to establish whether these two suites are strictly related. Also, the outer zone of this complex has distinctive Fe-rich blebs and small ghosted xenoliths that are not characteristics of the LAS. Hence the sLAS is treated as a separate sub-group.

Geochemically, the sLAS are similar to other M-I associations in the region. Only 4 samples were analysed for major and trace elements, and it is difficult to establish whether these are similar to the LAS or not. Most bivariate plots have overlapping geochemical characteristics, although the suite does appear to have higher $(Ce/Y)_N$ than most of the LAS, possibly reflecting a greater degree of assimilation in this pluton.

4. TayS. Taynaya Suite (UM-M-I association)

This suite occurs on the east side of Taynaya Bay and extends eastwards along the coast of Tryne Fjord. This UM-M-I association is typified by cumulo-phyric textures (*e.g.* Figure 9.4d). Although not all members of this suite have such textures, there are gradational contacts and relationships that imply that many of the rocks in this region are probably co-magmatic.

The majority of the TayS have ***mg***-numbers between 68.6-54.7, but two samples have ***mg***-numbers of about 40. Not outwith the range of other CLG, although most of the TayS are chemically distinct by having high Y and relatively low $(Ce/Y)_N$. The 2 low-***mg*** samples are characterised by high Ce, $(Ce/Y)_N$ and also have high Nb and Rb.

5. Hbl-PS. Hornblende-phyric suite (UM-M-I association)

Although it is recognized that the poikiloblastic hornblende that characterizes this suite is of metamorphic or possibly late-magmatic origin, this group is distinguished as a distinct gneiss suite. It occurs between Norite Point and the 'ring' structure in the central Long Peninsula region (Figure 9.1*). Typically, this suite is an ultramafic to melagabbroic association dominated by websterites and hornblende pyroxenites. It is not possible to determine from field criteria whether the majority of the intermediate CLG in the centre of the 'ring' are comagmatic, therefore they are not included in this suite.

The Hbl-PS has no obvious distinguishing geochemical features relative to other UM-M-I CLG suites. Sample VH467 has been included in the VHMD set because it is fine-to

medium-grained and locally cross-cuts the Hbl-PS. However, the dyke appears to be a part of this complex and is interpreted on field criteria to be directly related to this suite. Geochemically, this dyke is very similar to the Hbl-PS and it does not have the distinctive characteristics described for some of the other VHMD (suite 12 below)

6. BrHutS. Brooks Hut suite (UM-M-I association)

This characteristic association occurs in the Brooks Hut area (GR 850 940) as a large boudinaged layer that is of mappable extent for several km. Although of generally higher strain than either the TayS or LAS, cumulo-phyric textures are locally preserved and are a prominent feature of this suite.

The BrHutS has no obvious distinguishing geochemical features relative to other UM-M-I CLG suites.

7. BHS. Boulder Hill Suite (M-I association)

This suite occurs in the Boulder Hill area in the southern Vestfold Hills near to the type locality of the Crooked Lake Gneiss. As described in Chapter 9, it is often difficult to distinguish or establish comagmatic associations in this relatively high-strain area, and the BHS is a tentative grouping of moderately to strongly foliated mafic-intermediate gneisses.

The BHS has no obvious distinguishing geochemical features relative to many other UM-M-I CLG suites, although many rocks within the suite have relatively high A/CNK, which possibly reflects the greater abundance of *metamorphic* biotite and amphibole in this region.

8. MuRS. Murphy Rocks Suite (UM-M-I association)

This suite of CLG occurs in the remote Murphy Rocks area to the extreme north of the Vestfold Hills (~25 km north of Long Peninsula). Only two gneiss lithologies occur on these islands, this UM-M-I CLG association and minor migmatitic Grace Lake Granodiorite (*s.s.*).

The MuRS has no obvious distinguishing geochemical features relative to many of the other UM-M-I CLG suites.

9. RybBS. Rybnaya Bay Suite (UM-M)

This suite occurs on the NE coast of Rybnaya Bay and comprises websterites, melagabbros and gabbros, that are similar in appearance to the hornblende-absent members of the Hbl-PS

described above. It is possible that the two suites are related and they may be tectonically repeated equivalents, however, it is not possible to establish this link for certain and the two suites are treated as separate for now.

The RybBS has no obvious distinguishing geochemical traits relative to many other UM-M-I CLG suites.

10. WHS. Watts Hut Suite (M-I association).

This distinctive M-I CLG association occurs near Watts Hut in the southern Vestfold Hills (GR 885 870). As with the BHS described above, this region is strongly deformed and it is difficult to establish genetic links with the intermediate to felsic compositions.

The WHS has no obvious distinguishing geochemical features relative to other UM-M-I CLG suites, although in common with the BHS from the southern region, many rocks have relatively high A/CNK relative to ***mg***.

11. GrLG. Grace Lake granodioritic gneiss (F migmatite)

This suite is restricted to the heterogeneous granodioritic migmatite as defined at the type area (near Grace Lake, GR 958 083), and includes examples from NW Long Peninsula, W Tryne Fjord, Taynaya Bay and Topografov and Partizan Islands. Some of the chemical analyses catalogued in Appendix 2 and shown in the plots (*e.g.* Figure 11.6) include mafic schlieren that are probably xenolithic in origin.

This suite is characterised by high SiO_2. Compared with the late granites (D2-GS below), this suite has relatively high CaO and low K_2O, although there is much overlap, and both suites are weakly peraluminous I-type 'granites' with A/CNK between 1.0 and 1.1 (Chappell & White, 1974; White & Chappell, 1977).

12. VHMD. Vestfold Hills mafic dykes (M-I in composition)

These dykes are distinct from the post-deformational tholeiites described by Sheraton & Collerson (1986), Seitz (1991) and Lanyon *et al.* (1993). Most of the samples included in this suite intruded pre-D_2/D_3, although based on textural and morphological criteria some were emplaced synchronously with D_2 (and hence S_2). This group also includes rare post-deformational intermediate dykes (hornblende-bearing diorites and quartz-bearing diorites) such as the one dated in the Grace Lake area by Black *et al.* (1991a) at 2477 ± 5 Ma.

Although spatially and temporally distinct, these dykes are grouped together because they are all broadly intermediate in composition and have similar dyke-like morphologies.

Geochemically, the VHMD are amongst the most diverse of the suites described here. About half the dykes are indistinguishable on geochemical grounds from coarse-grained intermediate CLG, and it appears that some are apophyses from the main intrusions. The syn-tectonic and post-deformational dykes are clearly not related in this way, but at least some of these dykes are similar in chemistry to intermediate CLG (*e.g.* Post-D_2 dyke VH20). Five of the dykes, however, have distinctly high Nb, Nb/Nb*, and TiO_2, but low K_2O and $(Ce/Y)_N$, the latter implying flat REE patterns. These geochemical features are more akin to Fe-tholeiites typical of the younger Proterozoic dykes (Seitz, 1991; discussed further below and in Chapter 13).

13. D2-GS. Syn-deformational (D_2) granite suite (F in composition)

This group is texturally and compositionally variable but samples have been grouped together based on mode of occurrence, namely syn-tectonic emplacement during D_2.

Following the nomenclature of Chappell & White (1974) and White & Chappell (1977), the granites are weakly peraluminous I-types, with A/CNK generally between 1.0 and 1.1 (discussed further below). Even sample VH299, which is a large intrusive sheet hosted in Chelnok Paragneiss, is not strongly peraluminous (*i.e.* not S-type).

Perhaps not surprisingly, the D2-GS have higher SiO_2 than the other suites, although they overlap to some extent with the GrLG (12 above). The D2-GS suite also has higher K_2O reflecting the abundance of potassium feldspar in these monzogranites and syenogranites (not distinguished in Figure 9.2*). CaO is very low, as are oxides such as P_2O_5, Na_2O, TiO_2 and MnO. Many of these oxides are also low in ultramafic compositions, but are higher in intermediate or more evolved compositions, and inflections on many bivariate diagrams (*e.g.* P_2O_5 *vs.* ***mg***) are consistent in a broad sense with a change in fractionating assemblage. For example, a general trend within the granites towards decreasing P_2O_5 and Zr with either decreasing ***mg*** or increasing SiO_2 implies apatite and zircon fractionation respectively, and low TiO_2 and MnO implies ilmenite ± magnetite control.

14. IFCLG. Intermediate to felsic CLG

The IFCLG are an assorted group of intermediate to felsic CLG from throughout the northern region. These rocks are not thought to be strictly related to each other, but they

include representatives from most of the main intermediate and felsic lithologies within the broad CLG grouping.

The IFCLG have transitional major-element chemistry between the UM-M-I suites, and the felsic Grace Lake Granodioritic gneiss (GrLG) and syn-deformational granites (D2-GS). Accordingly, most samples have intermediate to low ***mg***-numbers and moderate to high SiO_2. Trace-element abundances and ratios, however, are highly variable and many samples have very high Zr, Ce, P_2O_5, Rb and Ba, but low TiO_2 and MnO.

11.3.3 Summary and discussion

Within the general Crooked Lake Gneiss classification, 14 sub-suites have been distinguished based primarily on field criteria. Many of these suites overlap on geochemical variation diagrams and, therefore, it is likely that most are related by common geochemical processes. Only a few of the suites are sufficiently distinctive in terms of geochemistry, and in particular IE abundances and concentrations, to support the separate field-defined status of these suites.

The suites that appear distinct in some way are:

- ***Suite 4.*** The TaySS with high Y, low TiO_2 and K_2O.
- ***Suite 11.*** The GrLG. Although similar to the D2-GS in many respects, the GrLG has lower K_2O and higher CaO, reflecting granodioritic rather than granitic (*s.s.*) compositions.
- ***Suite 12.*** The VHMD. A compositionally varied group. Approximately half the dykes are tholeiites or transitional tholeiites in composition, and have low $(Ce/Y)_N$ (discussed further below).
- ***Suite 13.*** The D2-GS. Characterised by very high $(Ce/Y)_N$ and low TiO_2, MnO and P_2O_5.
- ***Suite 14.*** IFCLG. Transitional with the UM-M-I associations (suites 1-10) and the D2-GS granites. Many samples also have high $(Ce/Y)_N$.

Most UM-M-I associations are sufficiently similar to be unable to either establish or refute direct genetic links. In relation to question 2 posed in Chapter 8, it is not possible to establish the extent to which these CLG suites have been tectonically repeated on geochemical grounds alone, although a number of groups are chemically distinct to some extent.

The mafic suites in detail

Most mafic suites (1-10 above) are sufficiently similar to consider the behaviour of groups of elements in a general context of fractional-crystallization or partial-melting histories. Within-group variations are primarily attributed to crystal fractionation and/or assimilation processes. Between suite variations could also reflect different partial-melting parameters.

Major elements

SiO_2 is variable and not well-correlated with ***mg*** or other elements for these mafic rocks. K_2O is also variable, but has a broad positive trend with decreasing ***mg***. Other oxides, such as TiO_2, P_2O_5 and Na_2O, increase with decreasing ***mg***, whilst CaO and MnO are poorly correlated but tend to decrease overall (see Figures 11.2, 11.3, 11.5 & 11.6).

Trace elements

For the trace elements, those elements that are strongly compatible with ferromagnesian phases (*e.g.* Ni, Sc, Cr) are well correlated with ***mg*** and decrease sharply across the compositional range ***mg*** 85 to 55. Elements that appear to have behaved incompatibly across this range include Sr, Ce, Nd, La and Y. Zr is highly variable. Rb possibly has a sharp inflection; this might reflect biotite fractionation, but more likely it reflects late-stage growth of biotite through late-magmatic or metamorphic fluid-infiltration, presumably relating to syn-D_2 granite intrusion. Hence, little emphasis is placed on Rb or other potentially mobile LILE in the following discussion, although mobility is discussed further in connection with Rb-Sr isotopes (Section 11.6).

Two suites, the LAS and Hbl-PS, have high Sr. For the LAS this is not surprising because the suite has abundant plagioclase. The reason for the high Sr in the dominantly ultramafic to melagabbroic Hbl-PS is less obvious. The dominant mineralogy of these rocks is clinopyroxene and hornblende, and Sr would not normally be expected to be strongly compatible in either of these minerals.

Trace-element ratios

Despite the enormous variability of many trace elements within individual suites, a number of trace-element ratios are fairly constant throughout the compositional range ***mg*** 85 to 55. For example, petrogenetically diagnostic ratios such as Zr/Nb and $(Ce/Y)_N$ are broadly consistent for most suites between ***mg*** 85 and 55, and range between 5-20 and 3-10 respectively. More evolved compositions (***mg*** <55) are presumably either strongly affected

by assimilation, have significantly different melting histories, or more likely, have trace-element ratios that were modified by changing fractionating assemblages that had relatively high *D*-values for some elements (most likely through accessory phases joining the early-formed assemblage, discussed further below).

11.3.4 Preliminary constraints on fractional crystallization from major- and trace-element bivariate diagrams

Trends of increasing Al_2O_3 and decreasing CaO with decreasing ***mg*** strongly imply that clinopyroxene was the dominant fractionating phase in the ultramafic, mafic and intermediate CLG suites. This is further indicated by high but steeply decreasing Cr and Ni trends with falling ***mg***.

Although plagioclase is abundant in relatively low-***mg*** compositions, trends of increasing Na_2O, Al_2O_3, and Sr throughout the range ***mg*** 85 - 40, imply that early plagioclase fractionation was not significant.

As described for mafic granulites in the Rauer Group (Chapters 5-7), it is very difficult to distinguish between the effects of orthopyroxene and olivine fractionation/accumulation, except where well-defined geochemical controls are apparent (*e.g.* Cox *et al.*, 1979). The presence of primary orthopyroxene and clinopyroxene 'accumulations' in some ultramafic lithologies suggests that pyroxenes were probably important fractionating phases. Olivine is absent in all the Vestfold Hills orthogneiss lithologies except in cognate(?) ultramafic xenoliths in the Taynaya EMG (Harley, pers. comm.). The Taynaya EMG also has higher normative *Ol* which implies that olivine may have been present in this suite. By contrast, *Ol* is generally low in the majority of CLG lithologies.

The proposition that much intrasuite variation within the CLG is predominantly controlled by amphibole and plagioclase, as advocated by Sheraton & Collerson (1984), is not supported by observations here. Petrographic observations indicate that hornblende poikiloblasts developed locally, but that they formed later than orthopyroxene, clinopyroxene, plagioclase, and minor and accessory phases. It is not clear whether these formed at a late magmatic stage or are associated with amphibolite-grade metamorphism associated with D_2. Bivariate geochemical diagrams further indicate that a hornblende - plagioclase combination was not the principal differentiating assemblage. For example, high ***mg*** (or high MgO, low SiO_2) rocks have relatively low Y, Nb and Ti; elements that might normally be expected to be compatible or only weakly incompatible in hornblende (*cf.*

Rollinson, 1993, table 4.1). However, entry of hornblende into the fractionating assemblage at an intermediate stage is possible, since moderately low-***mg*** compositions have highly variable Y (*e.g.* TayS).

As described above for individual CLG suites, it is likely that crystal fractionation of a variety of minor and accessory phases was important for some elements. For example, TiO_2 appears to decrease with falling ***mg*** in some suites (*e.g.* TayS), which is consistent with Fe-Ti oxide fractionation. In more general terms, the trend towards alkali enrichment (calc-alkaline) is consistent with the early onset of magnetite and/or ilmenite fractionation (*cf.* Wilson, 1993 and references therein). An inflection (?) for Zr implies that zircon fractionation might also have occurred at a relatively early stage (***mg*** $\approx$ 60; Figure 11.6r).

11.4 REE and Spidergrams

11.4.1 REE Results

REE patterns for most of the Vestfold Hills orthogneisses are very similar to each other. REE were determined by ICP-AES for 9 samples from the LAS to assess intrasuite variation. Although there is variation in $(Ce/Yb)_N$, from 5.2 to 13.4, all patterns for the LAS have slightly concave MREE-HREE, and slightly convex LREE-HREE (Figure 11.7a). REE patterns for the Taynaya EMG, Mossel Gneiss (Figure 11.7b), and Syn-D_2 leucosome (Figure 11.7c) are indistinguishable from the LAS. Two intermediate mafic dykes (VHMD), one pre-D_2 and the other post-D_2, also have similar REE patterns to the LAS (Figure 11.7d). However, the syn-deformational intermediate dyke from central Taynaya Bay (VH33) has a flat REE pattern and major- and trace-element chemistry more typical of tholeiite or transitional tholeiite compositions. Samples representing the GrLG (VH35) and D_2-Granite (VH299) also have distinctive REE profiles, characterised by highly fractionated REE patterns with $(Ce/Yb)_N$ of ~ 25 and 41 respectively. The GrLG and D2-GS are also depleted in the MREE relative to HREE (Figure 11.7c) and have pronounced positive Eu anomalies.

11.4.2 Spidergrams

PM- and MORB-normalized incompatible-element diagrams (*e.g.* Figure 11.8) for *most* of the Vestfold Hills orthogneisses are characterized by enriched and fractionated patterns with high LILE/HREE, LREE/HREE and pronounced negative HFSE anomalies. Figures 11.8 a & b illustrate some of the similarities between selected suites from the CLG (RLS & LAS)

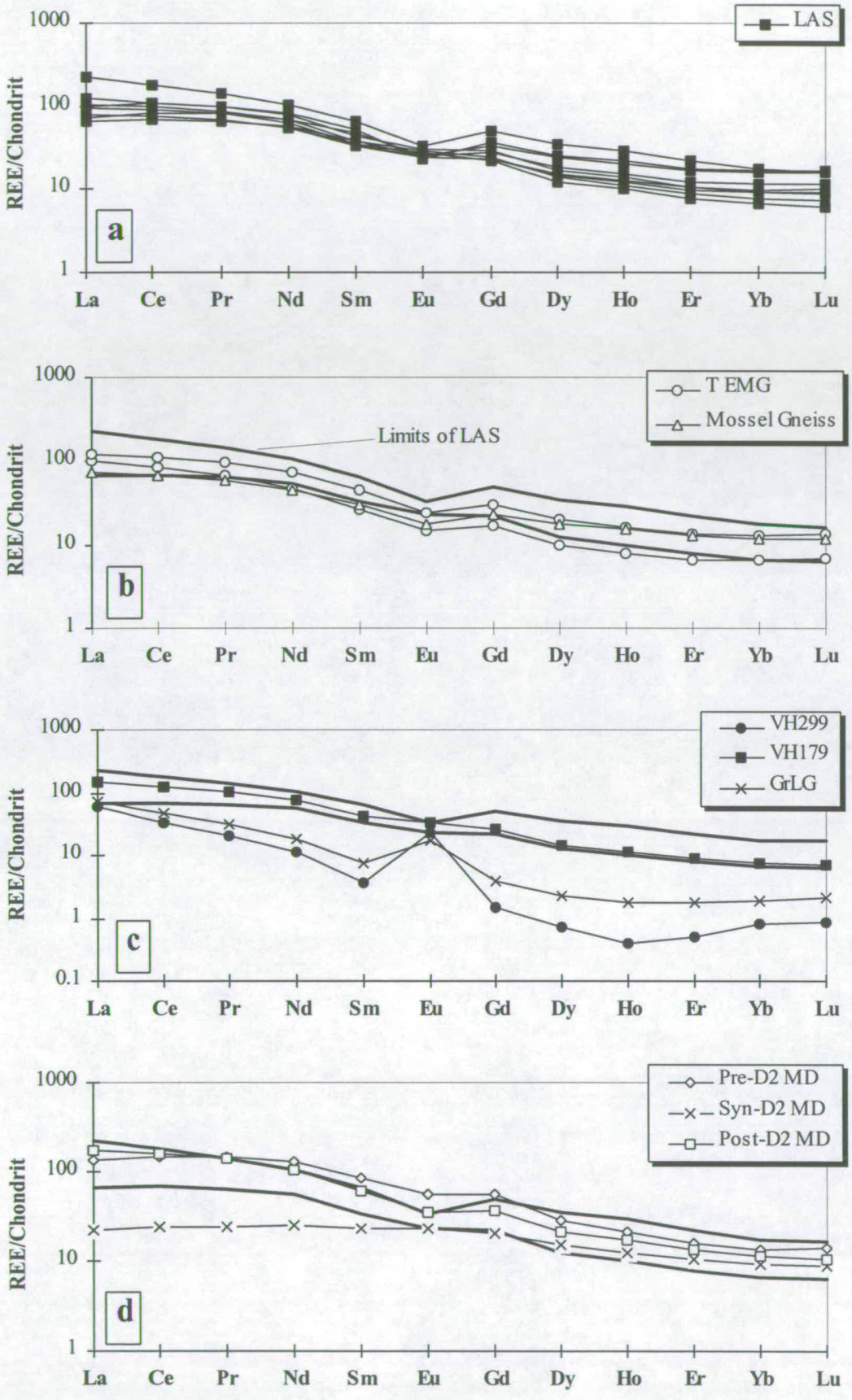

Figure 11.7 Chondrite-normalized REE data for selected Vestfold Hills orthogneisses.

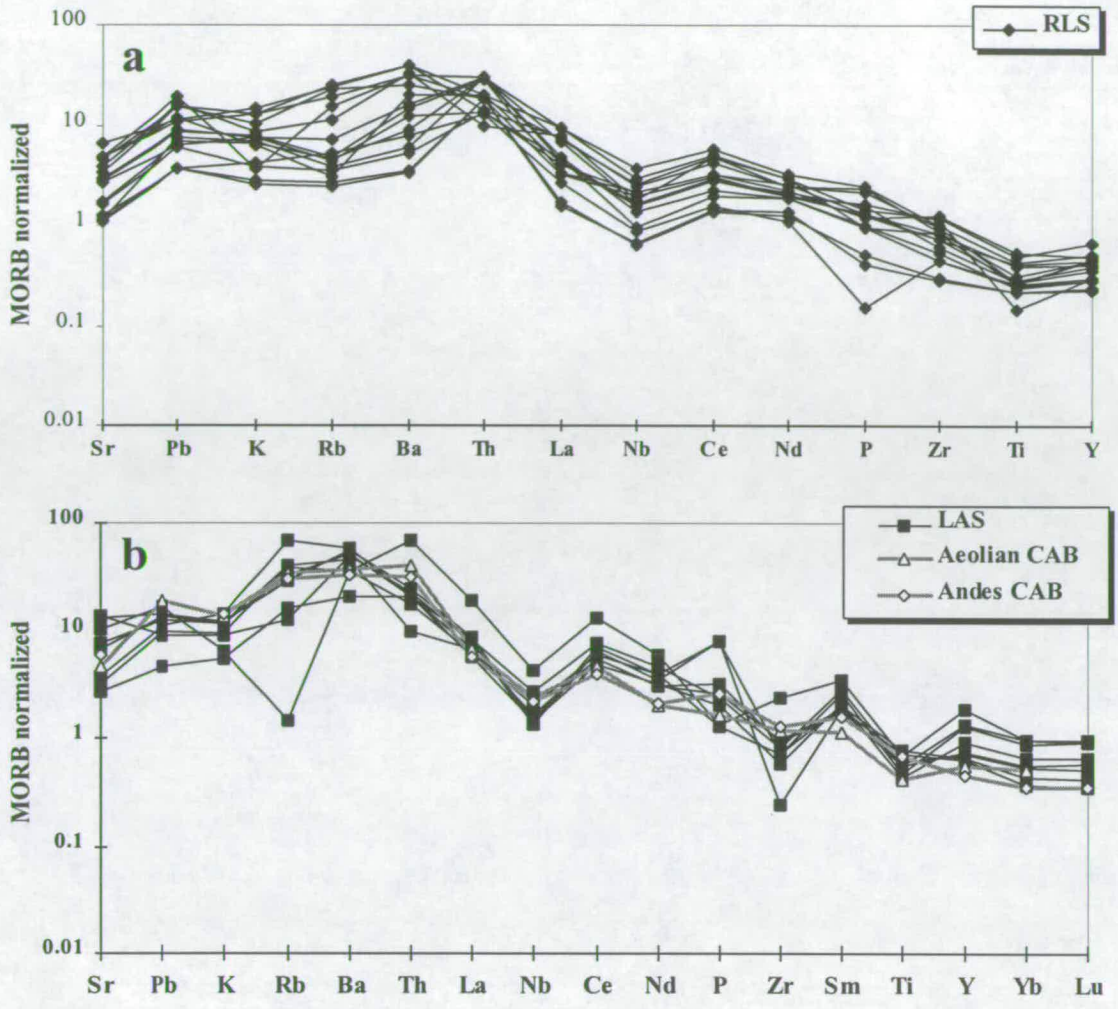

Figure 11.8 Modified MORB-normalized spidergrams for the Rookery Lake Suite and Lake Africa Suite CLG. Note that the two plots comprise different elements, because full REE analyses for the RLS (a) are not currently available. In (b), two Phanerozoic continental-arc basalts (CAB) are shown for comparison (Aeolian CAB from Francalanci *et al.*, 1993; Andes CAB from Hickey *et al.*, 1986).

and two representative continental volcanic-arc basalts (CAB). Note that in Figure 11.8b the overall patterns are similar, although the LAS has higher MREE and Y, which has resulted in more pronounced negative Ti and Zr anomalies than in the two continental volcanic-arc basalt examples chosen.

11.4.3 Trace-element discrimination diagrams (TEDDs)

A number of the TEDDs outlined in Section 1.4.2 may be applicable to some of the Vestfold Hills orthogneisses. Five are for basalts and one is for granites, and a selection of plots are presented in Figures 11.9a-d. Most of the mafic to ultramafic compositions are well represented by the RLS and LAS, and these two suites plot on most of the TEDDs in the

fields that correspond to continental-arc calc-alkali basalts. The only TEDD suitable for more evolved compositions (granites) is the Nb-Y diagram of Pearce *et al.* (1984). The Grace Lake Granodiorite, syn-deformational granites, and assorted intermediate to felsic CLG all broadly correspond to *volcanic-arc granites* or *syn-collisional granites* (see Figure 11.9d).

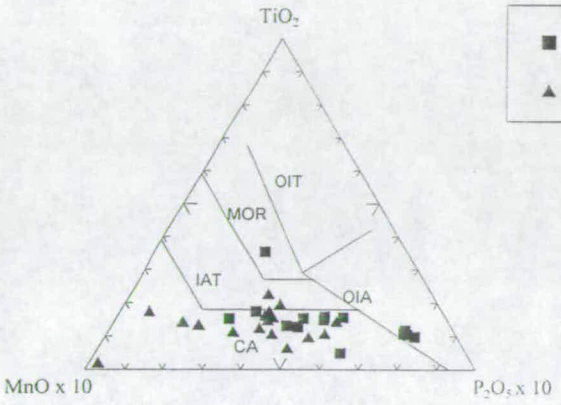

Figure 11.9a TiO_2-MnO-P_2O_5 TEDD

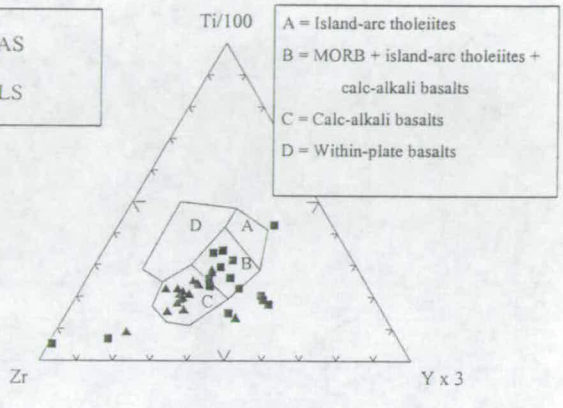

Figure 11.9b Ti-Zr-Y TEDD

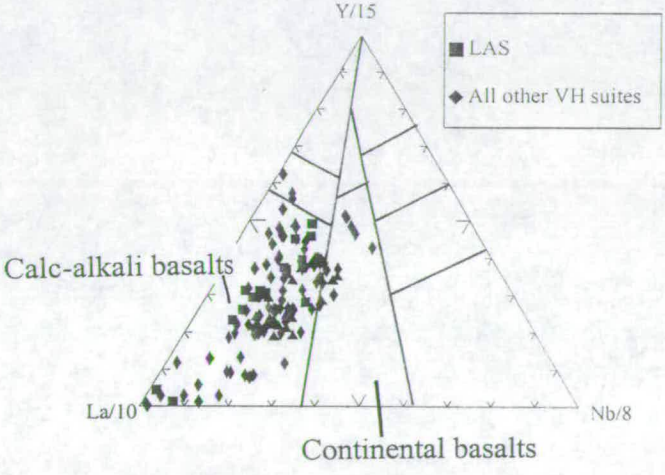

Figure 11.9c La-Y-Nb TEDD.

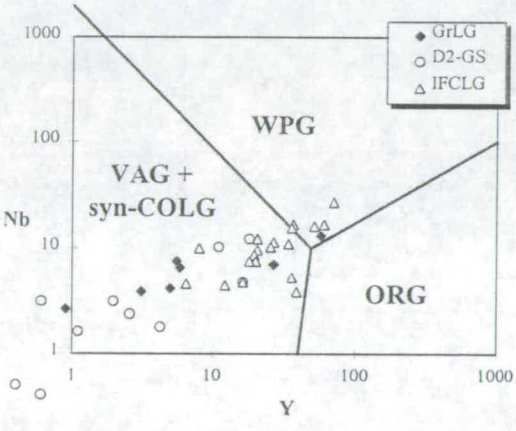

Figure 11.9d Nb-Y TEDD.

Figure 11.9 Selected TEDDs illustrating that the CLG is geochemically similar to modern calc-alkaline volcanic arcs. (a) is after Mullen (1983), and illustrates that the RLS and LAS suites plot in the *island-arc calc-alkaline basalt* field. (b) is after Pearce & Cann (1973); most RLS and LAS plot in the calc-alkali basalt field. (c) is after Cabanis & Lecolle (1989); most Vestfold Hills orthogneisses of all compositions plot in the *calc-alkali basalts* field. (d) is after Pearce *et al.* (1984); the three suites studied here (GrLG, D2-GS, IFCLG) mostly plot in the *volcanic-arc granites + syn-collisional* field.

11.4.4 Discussion and interpretation of REE and spidergrams

Variability within the LAS

Within suite REE variations for the LAS are relatively limited throughout the compositional range analysed here (***mg*** 49.5-67.6). High ***mg*** compositions have the lowest $(Ce/Yb)_N$ (5.8 and 13.4). Assuming that enrichment of a trace element relative to the original liquid is largely governed by fractional crystallization (Equation 5.1) dominated by clinopyroxene (D_{Ce} & D_{Yb} approach $K_{dCpx/Ce}$ & $K_{dCpx/Yb}$), modest amounts of fractional crystallisation (F = 0.2) from a low abundance starting composition (*e.g.* VH403) can produce a range of $(Ce/Yb)_N$ similar to the LAS (6.4-13.1). Values less than 6.4 can be produced by assuming a combined cumulate and trapped liquid origin. For instantaneous crystal removal, the equation for the concentration of a trace element in the crystals relative to the original liquid during fractional crystallization is given by (from Rollinson, 1993):

$$C_{crystal}=C_{initial\ liquid} \cdot DF^{(D-1)}$$

where $C_{crystal}$ = concentration of the element in the crystal; $C_{initial\ liquid}$ = concentration in the original liquid; D = bulk distribution coefficient, F = fraction of liquid remaining. Assuming that some degree of equilibration between crystal and remaining liquid occurred, and that the dominant proportion of Ce and Yb will reside in the trapped-liquid component, values of $(Ce/Yb)_N$ of ~ 5.8 can be modelled fairly easily.

In conclusion, much of the observed major and trace-element variability within the LAS can be explained by fractional crystallization/accumulation processes. The effects of assimilation, although evident in the field, are not obviously manifest in the trace-element variations described in this section.

General variability in the Vestfold Hills orthogneisses

The overall similarity between CLG and Mossel Gneiss, especially in trace-element and REE plots, strongly implies that these two suites were derived from similar source regions in terms of bulk chemistry, residual phases, and/or melt extraction process. Although the Taynaya EMG have distinctive chemistry, similarities in REE patterns and spidergrams implies that they may also be genetically related in some way (discussed further below).

The chemical variability observed for the VHMD, such as Nb and TiO_2 (see Section 11.3), is reflected in the REE profile of VH33, which has a flat patterns more typical of tholeiite

magmas. This probably indicates that some of the dykes were derived from a source that was 'distinct' from the main orthogneiss suites, because variations in extent of partial melting or crystal fractionation cannot account for these major differences (*cf.* Sheraton *et al.*, 1992).

The Grace Lake Granodiorite and granite samples described here are also distinct from the CLG. Their overall profiles could be attributed to extensive residual garnet in the source, disequilibrium partial melting with residual accessory phases, or extensive accessory phase fractional crystallization (in trace-element terms). Other possibilities or variables include second-stage melting of an already fractionated and evolved product, as indicated on textural grounds (*e.g.* Figure 9.5b). Clearly, a detailed understanding of the evolution of these gneisses is not straightforward.

General observations and working hypotheses from REE and spidergrams

Fractionated REE patterns and distinctive spidergrams with high LILE and LREE relative to HREE and HFSE, are characteristic of calc-alkaline continental-arc rocks. Such a general setting is also indicated by a variety of TEDDs. However, more detailed consideration of the origin and evolution of the Vestfold Hills orthogneisses is reserved until after presentation of isotope data in the next sections. All the geochemical observation described above are discussed further in Section 11.8 (below).

11.5 Oxygen isotopes

Oxygen-isotope ratios have been determined for 9 samples from the LAS. This suite was chosen because it has clear textural evidence for AFC, a feature typical of CLG from the northern region. The LAS is also a good candidate for detailed isotopic study because it was possible to independently constrain the crystallization age by U-Pb zircon dating (Chapter 10), thereby providing a robust framework from which to consider combined oxygen and time-integrated radiogenic-isotope (source) signatures.

Oxygen-isotope results are presented in Table 11.1, and analytical techniques and errors are described in Appendix 1.

Table 11.1 Oxygen-isotope ratios for the LAS.

No.	Suite	Description	mg	$\delta^{18}O_{(1)}$	$\delta^{18}O_{(2)}$	$\delta^{18}O_{(av)}$	
VH130	LAS	Spotted gabbro	66.2	6.37	6.15	6.3	
VH131	LAS	Intermediate gabbro	62.3	6.33	6.03	6.2	
VH136	LAS	Intermediate gabbro	61.4	7.16	7.18	7.2	
VH137	LAS	Leucogabbro	49.5	7.06	7.21	7.1	
VH403	LAS	Spotted melagabbro	67.6	6.54		6.5	
VH404	LAS	Spotted melagabbro	67.0	6.17		6.2	
VH405	LAS	Leucogabbro	50.0	6.75	7.24	7.0	
VH406	LAS	Leucogabbro nr pluton margin	51.2	6.71	6.88	6.8	
VH407	LAS	Leucogabbro nr pluton margin	36.0	6.69	6.48	6.6	
						6.7	± 0.41

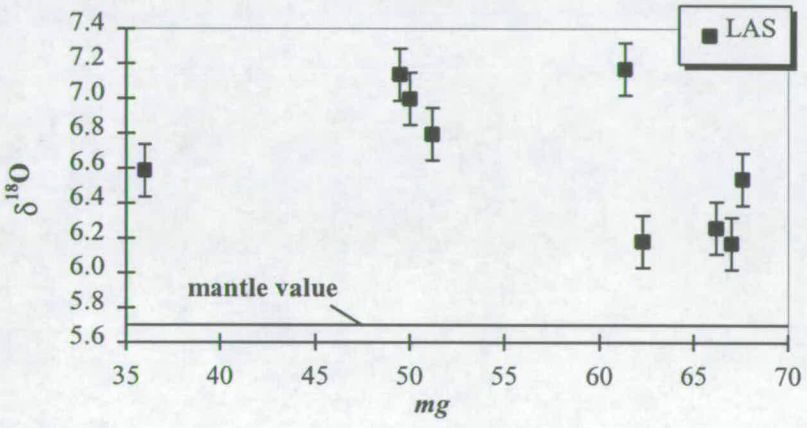

Figure 11.10 Oxygen-isotope ratios for the LAS. Mantle value is shown for comparison.

11.5.1 Results

The LAS (as described in Sections 11.3.1) samples that have been studied isotopically range in composition from ultramafic to leucocratic quartz-bearing monzonite/monzodiorite, and have ***mg*** numbers that vary from 67.6 to 36.0. Across this compositional range, $\delta^{18}O$ values are moderately restricted and lie between 6.1 and 7.2 ‰. There is not a strong correlation between $\delta^{18}O$ and ***mg*** (Figure 11.10), although generally the evolved low-***mg*** compositions have high $\delta^{18}O$ values. There is also a crude correlation between proximity to xenoliths and elevated $\delta^{18}O$.

11.5.2 Discussion and interpretation

Principal observations and similarities with the SLC (Rauer Group)

Oxygen isotope compositions for the LAS are *relatively* close to estimated values of the mantle (~5.7 ‰; Taylor 1980) and in this respect are *broadly* similar to the SLC (Section 6.2.2). As with the SLC, the LAS does not have extreme values or a wide range of $\delta^{18}O$, hence it is unlikely that there was extensive hydrothermal activity typical of most high-level intrusions (*e.g.* Taylor & Forrester, 1977; 1979; and references in Section 6.2.2). However, when compared in detail with the SLC, the LAS has generally higher average $\delta^{18}O$ (Table 11.2), higher $\delta^{18}O$ for a given ***mg***-number, and has a larger compositional range. There are two main processes that may explain why $\delta^{18}O$ are slightly elevated in the LAS. The first involves melting of a source region that has elevated $\delta^{18}O$, the most likely reservoir for this model being hydrothermally altered MORB (subducted slab?), which commonly has $\delta^{18}O$ between 7 and 10 ‰ (*e.g.* Taylor & Sheppard, 1986, figure 12). The second process involves assimilation of felsic crust. Given that there is only a total range of 1.1 ‰, it is unlikely that assimilation involved significant amounts of metasedimentary wallrock, which might be expected to have appreciably higher $\delta^{18}O$ values (*e.g.* Taylor & Sheppard, 1986, figure 12; Rollinson, 1993, figure 7.6). However, from the restricted dataset presented here, it is not possible to distinguish between these two elevated oxygen-isotope reservoirs based on oxygen-isotope analysis alone. It is primarily for this reason that Sr-isotope ratios were also determined on these samples (below).

Table 11.2 Comparison of oxygen-isotope composition between the SLC and LAS.

Suite	$\delta^{18}O$ range (‰)	median, average & st. dev. (‰)
SLC	5.8 - 6.3	6.2, 6.1 ± 0.3
LAS	6.1 - 7.2	6.6, 6.7 ± 0.4

11.6 Rb-Sr isotopes

Sr-isotope ratios have been successfully determined for 9 CLG from the LAS, and a number of additional analyses from representative gneiss suites comprising: two deformed mafic dykes (VHMD), one Grace Lake Granodiorite (GrLG), one late granite suite (D2-GS), two Taynaya EMG and 1 Mossel Gneiss. Additional Sr-isotope data are also documented by Collerson *et al.* (1983) and Black *et al.* (1991a), although it is not always possible to place their samples in the geological framework presented here (see Chapter 9). Analytical results

and calculated parameters are presented in Table 11.3, analytical techniques and errors are described in Appendix 1.

11.6.1 Results

The LAS generally has very low Rb/Sr and a restricted range of $^{87}Rb/^{86}Sr$ between 0.004 and 0.589. $^{87}Sr/^{86}Sr$ are well correlated with $^{87}Rb/^{86}Sr$ (Figure 11.11a) and range from 0.702503 ± 27 to 0.721028 ± 25. These data define an errorchron for the suite that corresponds to an age of 2204 ± 150 Ma with an MSWD of ~21 (Figure 11.11a). These 'ages' (and associated errors) change little if CLG sample VH 179 (D2-GS), or Taynaya EMG sample VH262, are added to the population (Figure 11.11b), but there is a marked change if the mafic dykes (VH 20 & VH 33) are included (2324 ± 310 Ma, MSWD = 138). ε_{Sr}, calculated for the LAS at 2485 Ma (from U-Pb zircon dating, see Chapter 10), inevitably has a strong negative correlation with $^{87}Rb/^{86}Sr$, and is also reasonably well correlated with other indices of differentiation, such as 1/Sr, ***mg***, and SiO_2.

11.6.2 Discussion and interpretation

The high MSWD of ~21 for the isochron diagram shown in Figure 11.11a indicates that there is significantly more scatter than can be explained by analytical error alone. There are three possible interpretations for such data:

- The errorchron age is significant and corresponds to a poorly defined whole-rock closure age for the LAS.
- The data define a mixing array as a consequence of assimilation. Calculated ε_{Sr} may potentially elucidate the process and extent of assimilation if this is the case.
- The errorchron reflects disturbance during metamorphism. The age and calculated ε_{Sr} may or may not be meaningful in this case.

Arguments against whole-rock closure ages

The LAS samples studied here were selected from a region at least 300 x 200 m and isotopic communication across such distances is not likely to be possible in the absence of a major tectonothermal or, perhaps more importantly, fluid-infiltration event. The *ca.* 2200 Ma age roughly corresponds to the age of the intrusive norite complex (2240 Ma; Lanyon *et al.*, 1993). However, at this time the present Vestfold Hills exposure level is known to have been at shallow depths in the crust (Harley, 1993b; Seitz, 1994), and although of undoubted

high temperature, the thermal affects of the norite intrusion are not thought to be greater than metre-scales based on field and petrographic evidence (SL Harley, pers. comm., 1997).

Arguments against assimilation

A number of features of the Sr-isotope data are impossible to reconcile with an assimilation model. In a general context, mantle-derived melts that assimilate continental crust can result in both positive (most usual) or negative ε_{Sr}, depending upon whether the $^{87}Sr/^{86}Sr$ in the source (mantle or depleted mantle) and assimilant (crust) evolved with higher or lower production of ^{87}Sr than Bulk Earth until the assimilation event (*i.e.* Rb/Sr > or < ~0.03). Although very high Rb/Sr are possible through normal crustal fractionation processes, mantle evolution is more restricted (not less than BABI at 4.6 Ga; see Faure, 1986) and this provides a lower limit from which to consider Sr-isotope mixing via crust-mantle interaction. However, as Figures 11.12a & b illustrate, ε_{Sr} in some LAS samples are too low to be accounted for by derivation from a DM source or even by assimilation of a long-term depleted (*i.e.* very low Rb/Sr) lower-crustal reservoir (*cf.* the Lewisian; Dicken, 1981). Nevertheless, it is worth considering the isotopic evolution of the LAS further, through both assimilation and metamorphic disturbance models, in an effort to understand the origin of the ε_{Sr} array.

In the Vestfold Hills there are three groups of potential assimilants:

- ***The Mossel Gneiss, which is characterised by very low Rb/Sr.*** For example, VH26 of Black *et al.* (1991a) has $^{87}Rb/^{86}Sr$ of 0.0393 and ε_{Sr} at 2485 Ma of ~ -2. Such a value is within the upper and lower limits of the LAS data and would have little effect on the isotopic evolution of the CLG through assimilation.

- ***Unexposed ca. 2800 Ma crust***, as identified from inherited zircons (Black *et al.* 1991a; this study, Chapter 10). The Sr-isotope character of this crust could be ultradepleted, but given that there is only 300 m.y. to evolve significantly depleted Sr-isotope compositions relative to BSE estimates, the minimum $^{87}Sr/^{86}Sr$ that could be expected at 2500 Ma would have an ε_{Sr} value of no less than -9, even choosing highly favourable model parameters[1] (*viz.* DM established through progressive crust extraction from 4.55 Ga; derivation from DM at 2.8 with Rb/Sr subsequently depleted in Rb leaving a crustal reservoir with $^{87}Rb/^{86}Sr$ of 0.005).

- ***The EMG, which has relatively high Rb/Sr,*** with a representative sample (VH262; Table 11.3) having $^{87}Rb/^{86}Sr$ of 1.7966 and ε_{Sr} at 2485 Ma of -19.5. Such a strongly negative ε_{Sr} value might at

[1] A more realistic estimate of the lowest reservoir value (ε_{Sr}) that could expected for a DM source would probably only be a few epsilon units less than bulk earth at this time.

first appear to be a source of negative ε_{Sr} for the LAS, but the problem remains that it is not possible to evolve such low $^{87}Sr/^{86}Sr$ compositions prior to the crustal assimilation (as above).

In summary, ε_{Sr} values of less than -9 cannot be explained through primary igneous processes (*i.e.* derivation through mantle or crustal melting, including assimilation).

Constraints on the nature and timing of Rb-Sr open-system behaviour

Further indirect evidence against assimilation and in favour of isotopic disturbance can be seen by reconsidering the components in Figure 11.11b. In the figure, there is a strong negative relationship between ε_{Sr} and Rb/Sr. In the analytical sense, ε_{Sr} can be thought of as a time-integrated but directly determined isotopic composition (initial $^{87}Sr/^{86}Sr$ expressed in user-friendly numbers) that *should* be independent of the amount of Rb, Sr, and the effects of bulk composition (also *probably* constant sum problems, but *cf.* Butler, 1982 *vs.* Dodson, 1982). However, Rb/Sr is a bivariate ratio in a multivariate system and, as such, correlations with ε_{Sr} could effectively be controlled by Rb and/or Sr and/or other possible external influences (see also Section 6.5.4).

Geochemical observations described in the previous sections indicate that Sr is highest in low-***mg***, high Al_2O_3 bulk compositions that correspond to samples with abundant plagioclase rather than pyroxenes or hornblende. However, there is no obvious correlation between Rb and bulk composition (*e.g.* Sr, ***mg***, SiO_2, MgO or Zr). During normal fractional crystallization processes, Rb/Sr should increase in progressively more evolved compositions because D_{Sr} is generally >> D_{Rb} except possibly where biotite forms early. Although this general relationship might be complicated by cumulate processes, a general increase in Rb should still occur in low-***mg*** compositions. The relationships shown in Figures 11.6j, k, s, & u, however, imply that Sr was largely immobile, presumably buffered by plagioclase, but that Rb was highly mobile. Such relationships are, perhaps, considered to be 'normal' in high-grade metamorphism (*e.g.* Tarney & Windley, 1977; Rollinson & Windley, 1980), although this proposition can be examined more closely by reconsidering the relationship between Rb, Sr and ε_{Sr}.

In a simple assimilation model, variations in initial $^{87}Sr/^{86}Sr$ are controlled directly by Sr-mixing irrespective of Rb concentrations. Although the exact relationships between ε_{Sr} and Sr will depend on assimilant - melt ratio and D_{Sr} (see DePaolo, 1981), the shift in ε_{Sr} due to assimilation will be proportional to the amount of assimilated Sr. Therefore it is possible that there will be a relationship between Sr and ε_{Sr} in an assimilation-dominated model. Conversely, if the most likely model of metasomatism is considered in detail, Rb is much

Table 11.3 Sr-isotope ratios and calculated parameters for Vestfold Hills orthogneisses.

Sample	Suite	Sr (ppm)	Rb (ppm)	Rb/Sr	$^{87}Rb/^{86}Sr$	$^{87}Sr/^{86}Sr$	(2σ)	$^{87}Sr/^{86}Sr_i$	$\varepsilon_{Sr(zir)}$	T_{BSE} (Ga.)
VH130	LAS	433.0	88.0	0.2033	0.5890	.721028	25	.699874	-25.27	2.25
VH131	LAS	772.2	53.3	0.0690	0.1997	.708682	23	.701510	-1.95	2.41
VH136	LAS	893.6	43.2	0.0484	0.1400	.706610	28	.701582	-0.93	2.40
VH137	LAS	1477.2	37.9	0.0257	0.0742	.704569	25	.701902	3.64	0.85
VH403	LAS	368.7	49.6	0.1344	0.3892	.715170	26	.701191	-6.50	2.38
VH404	LAS	312.9	20.8	0.0666	0.1928	.708696	18	.701773	1.79	2.56
VH405	LAS	1569.6	16.4	0.0105	0.0303	.703097	22	.702010	5.17	2.03
VH406	LAS	1096.5	23.8	0.0217	0.0627	.704115	15	.701864	3.10	1.82
VH407	LAS	1190.9	1.8	0.0015	0.0043	.702503	.27	.702350	10.01	1.89
VH20	VHMD	600.1	12.4	0.0207	0.0598	.705180	17	.703032	19.74	-1.35
VH33	VHMD	305.2	5.5	0.0179	0.0519	.703650	23	.701786	1.98	2.20
VH262	TEMG	215.4	130.4	0.6056	1.7616	.763553	20	.700281	-19.46	2.43
VH179	LGS	1036.8	6.8	0.0065	0.0189	.702868	24	.702188	7.71	1.93

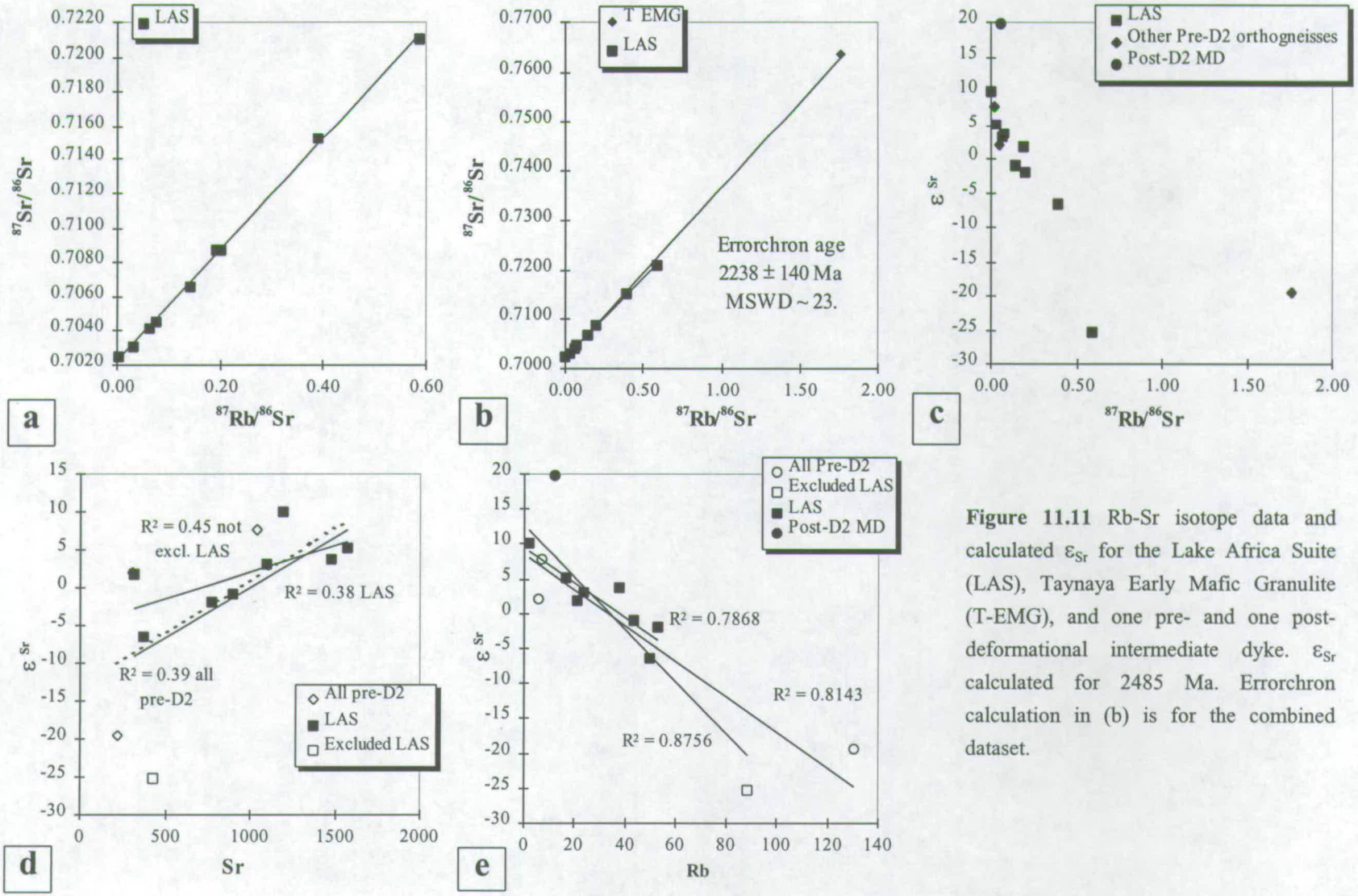

Figure 11.11 Rb-Sr isotope data and calculated ε_{Sr} for the Lake Africa Suite (LAS), Taynaya Early Mafic Granulite (T-EMG), and one pre- and one post-deformational intermediate dyke. ε_{Sr} calculated for 2485 Ma. Errorchron calculation in (b) is for the combined dataset.

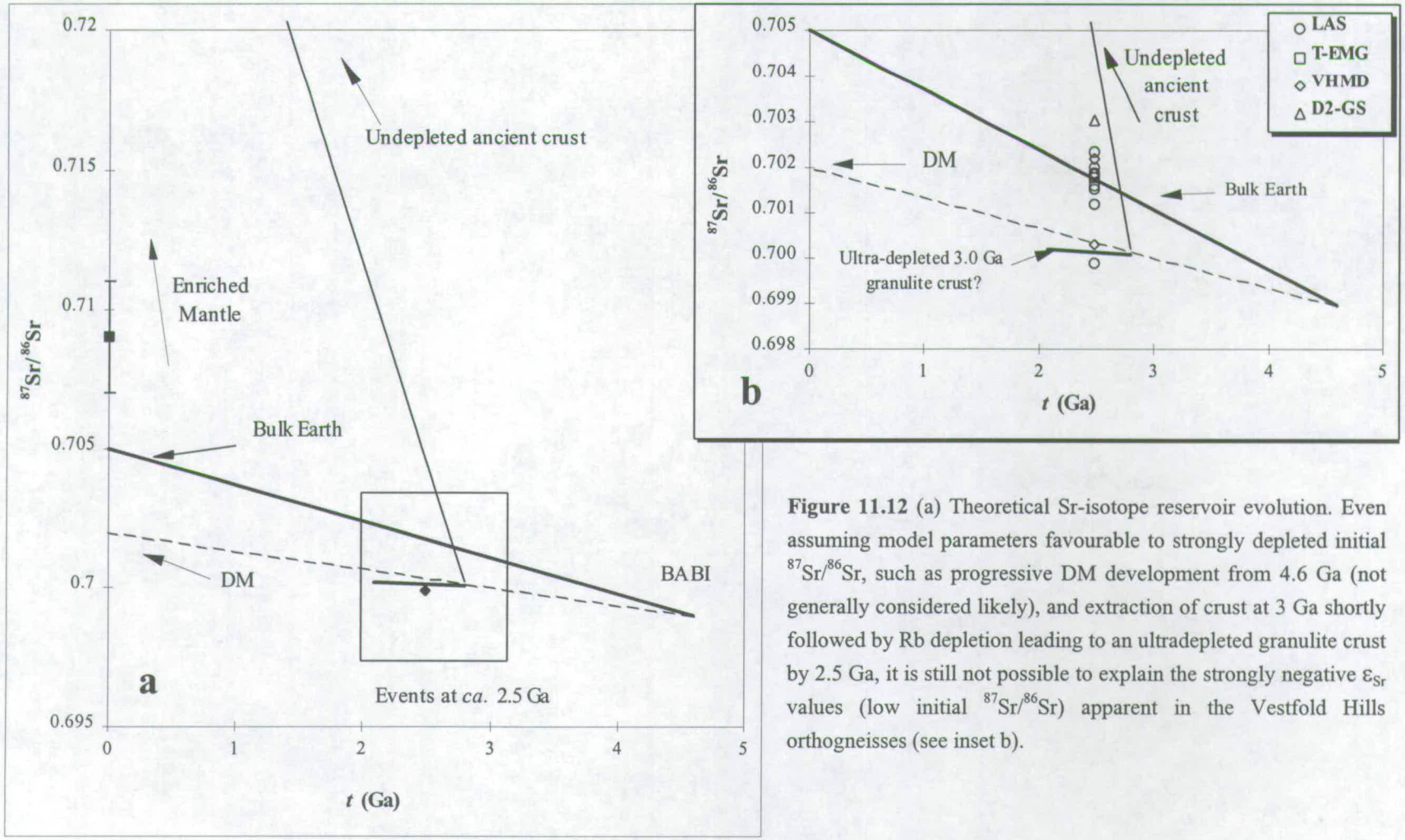

Figure 11.12 (a) Theoretical Sr-isotope reservoir evolution. Even assuming model parameters favourable to strongly depleted initial $^{87}Sr/^{86}Sr$, such as progressive DM development from 4.6 Ga (not generally considered likely), and extraction of crust at 3 Ga shortly followed by Rb depletion leading to an ultradepleted granulite crust by 2.5 Ga, it is still not possible to explain the strongly negative ε_{Sr} values (low initial $^{87}Sr/^{86}Sr$) apparent in the Vestfold Hills orthogneisses (see inset b).

more likely to be mobile than Sr. This is particularly so for the Vestfold Hills orthogneisses which have biotite (the principle Rb host) as a late retrograde phase (see Chapter 9) and have abundant, presumably relatively stable, plagioclase. In this scenario, the amount of change in Rb, either by enrichment or depletion, will be the key feature that determines the apparent shift in ε_{Sr} (background similar to discussion in Section 6.5.4)

Figures 11.11b-e illustrate the relationships between Rb, Sr and ε_{Sr} for the LAS and the other Vestfold Hills orthogneisses studied here. Note that in Figures 11.11d & e and Table 11.4 that there are poor correlations between Sr and ε_{Sr} for the LAS, and even when the anomalously low sample is excluded, the correlation is little improved. However, there is a very strong correlation between ε_{Sr} and Rb for all the LAS rocks. Moreover, the correlation is improved when the strongly negative ε_{Sr} sample is included in the dataset implying that Rb enrichment in this sample may be responsible for the strongly negative ε_{Sr} values. Figures 11.11d & e also illustrate the results for an expanded dataset that includes all the pre-D_2 orthogneisses and the post-D_2 (2477 ± 5 Ma; Black *et al.*, 1991a) mafic dyke (VH20, re-sampled in this study). Note that there is an excellent correlation between ε_{Sr} and Rb, although there is also a less well-defined correlation for Sr. Note also that the post-deformational mafic dyke appears distinct on both Figures 11.11c & e, despite having a similar age and composition. It is possible that this is the only sample with a true igneous ε_{Sr} value, and would be compatible with derivation from a mantle or DM source and assimilation of evolved 'normal' crust with high time-integrated $^{87}Sr/^{86}Sr$ (high Rb/Sr environment).

Although observations of the relationships between Rb, Sr and ε_{Sr} presented above are not incontrovertible evidence that Rb metasomatism was the main or sole cause of the ε_{Sr} array, comparison with the Kalka intrusion (regarded by many as the type example of large-scale crustal assimilation of a mantle-derived plutonic suite), illustrates that Rb and ε_{Sr} do not necessarily have to correlate (Table 11.4). The arguments presented here imply that the 2204 ± 150 Ma age is spurious and does not directly constrain either the age of the protolith or the age of metamorphism. However, the strong correlation between $^{87}Rb/^{86}Sr$ and $^{87}Sr/^{86}Sr$ implies that metamorphism probably occurred soon after protolith formation. By analogy with the Rauer Group, if metamorphic redistribution took place a long time after protolith formation, at 500 Ma for instance, there would be a much greater potential for a large scatter on an isochron diagram if redistribution of Rb was the main cause of perturbation. This is partly because it is highly unlikely that $^{87}Sr/^{86}Sr$ would be mobile at

length-scales of 100s of metres, and hence the possibility of a young whole-rock isochron is not great where only relatively small time-integrated fluid fluxes are involved.

Given the now well-established chronology in the Vestfold Hills, the most likely time of disturbance to the system would have been during D_2-M_2 (2475.3 ± 0.7 Ma). This would also coincide with biotite development in the orthogneisses (parallel to S_2), since this is likely to be the main Rb host. However, as described above, this only leaves ~10 m.y. for $^{87}Sr/^{86}Sr$ to evolve along a low Rb/Sr trajectory prior to disturbance. Although secondary fractionation of Rb/Sr exerts a powerful 'lever' effect (*cf.* Figure 6.8) on apparent ε_{Sr} values, 10 m.y. is still insufficient time to account for ε_{Sr} less than about -10. This implies that Rb-Sr systems for samples VH130 and VH262 could not have been entirely closed from 2475 Ma to the present day, because the time interval between crystallization and disturbance needs to be of the order 100 - 1000 m.y. (*cf.* Sections 6.4 & 6.5, details not included here).

The most likely cause of the anomalously low initial ε_{Sr} in samples VH130 and VH262 relates to $^{87}Sr/^{86}Sr$ diffusion exchange via a mechanism similar to that described for Sm-Nd isotopes in the Rauer Group. This model requires that high Rb samples evolve to very high $^{87}Sr/^{86}Sr$ with time, but that a small amount of diffusion/advection exchange with a low $^{87}Sr/^{86}Sr$ reservoir occurred a long time after the thermal peak of metamorphism *and* the main fluid infiltration event. However, distinguishing between or quantifying the relative effects of diffusion-controlled isotopic exchange *versus* secondary Rb/Sr fractionation is not possible from the current dataset. Moreover, returning to the previous discussion regarding correlations between Rb, Sr and ε_{Sr}, the strong correlations between Rb and ε_{Sr} would still be valid whichever mechanism was dominant.

Only two conclusions can be drawn with confidence. The first is that ε_{Sr} values do not reflect those of the protolith. The second is that metamorphic redistribution of Rb at 2475 Ma cannot be the sole disturbance mechanism responsible for the observed data. Hence, the 'errorchron ages' are probably just an artefact of mixing and diffusion processes and are not of direct chronological significance. However, the retention of a relatively strong correlation between $^{87}Rb/^{86}Sr$ and $^{87}Sr/^{86}Sr$, and a strong correlation between ε_{Sr} and Rb, implies that secondary fractionation of Rb/Sr shortly after crystallization was the *main* cause of disturbance to Rb-Sr whole-rock isotope systems. If the timing of Rb mobility was at 500 Ma, for example, the potential to produce a very wide range of ε_{Sr} would be much greater (*cf.* Figures 6.3 & 6.18). However, the influence of an event a long time after crystallization (500 or 1000 Ma) is required to explain the observed data, and small amounts of fluid must have been present to enhance diffusion distances beyond the inter-mineral scale.

Table 11.4 Table of correlations between ε_{Sr}, Sr and Rb for the Vestfold hills orthogneisses and the Kalka Intrusion, Giles Complex, Australia (Kalka data are after Gray *et al.*, 1981). Values of r and r^2 are two-sided product-moment correlation coefficients, the rank correlation is also provided for comparison and is included to illustrate the strong link between Rb and ε_{Sr} regardless of the non-normal data distribution and strong bias inherent from including the two lowest ε_{Sr} samples.

	r^2		r		Rank correlation	
	Sr	Rb	Sr	Rb	Sr	Rb
ε_{Sr}			0.62	0.94	0.77	-0.92
LAS	0.38	0.88	DF=7	DF=7	n=9	n=9
			< 95% CL	>>99% CL	<98% CL	>99% CL
ε_{Sr}			0.67	0.89	0.79	-0.88
LAS	0.45	0.79	DF=6	DF=6	n=9	n=8
(ex. outlier)			>95% CL	>99% CL	<98% CL	>98% CL
ε_{Sr}			0.62	0.90	0.71	-0.86
All pre-D2 VH	0.39	0.79	DF=10	DF=10	n=12	n=12
gneisses			>95% CL	>>99% CL	>98% CL	>>99% CL
ε_{Sr}			0.92	0.002	-0.85	-0.19
Kalka (Gray *et* *al.*, 1981)	0.85	0.0005	DF=9	DF=9	n=11	n=11
			>>99% CL	<<95% CL	>99% CL	<<80% CL

11.6.3 Summary of conclusions

Sr-isotope ratios for the LAS do *not* reflect the crystallization history of the complex and cannot be combined with other isotope systems to constrain AFC processes. The main mechanism of open-system disturbance to the Sr-isotope system is attributed to Rb mobility shortly after crystallization, probably during the D_2-M_2 event. However, $^{87}Sr/^{86}Sr$ diffusion at whole-rock scales is also required a long time after these events (at least 10^7 - 10^8 y.) to explain initial Sr ratios that are near to BABI estimates at 4.6 Ga. The Christmas tree relationship of Rb *vs.* ***mg*** shown in Figure 6.6 is a function of preferential Rb loss in whole-rock systems that do not contain appreciable biotite or hornblende, possibly coupled with Rb gain in those that do. These results demonstrate that Rb, and probably other LILE, should not be relied upon to establish petrogenetic models for protolith formation in this terrane.

11.7 Sm-Nd isotopes

As described for oxygen- and Sr-isotopes in the previous sections, Nd-isotope ratios have mainly been determined for the LAS. A limited number of representatives from the other

Table 11.5 Nd-isotope data and calculated parameters for the LAS.

Sample No.	Suite	$^{143}Nd/^{144}Nd(m)$	(2σ)	$^{147}Sm/^{144}Nd$	(2σ)	$^{143}Nd/^{144}Nd$ (i)	$\varepsilon_{Nd(zir)}$	(2σ)	T_{CHUR} (Ga)	2σ (Ga)	T_{DM} (Ga)	2σ (Ga)
VH130	LAS	0.511609	7	0.1319	0.0005	0.509448	0.64	0.03	2.41	<0.01	2.79	<0.01
VH131	LAS	0.511536	7	0.1277	0.0001	0.509444	0.57	0.11	2.42	0.01	2.78	0.01
VH136	LAS	0.511444	7	0.1347	0.0025	0.509236	-3.51	0.66	2.92	0.01	3.20	0.08
VH137	LAS	0.511285	11	0.1158	0.0002	0.509388	-0.54	0.16	2.54	0.02	2.83	0.01
VH403	LAS	0.511717	5	0.1440	0.0036	0.509357	-1.14	1.04	2.65	0.02	3.04	0.14
VH404	LAS	0.511713	7	0.1436	0.0000	0.509361	-1.07	0.14	2.64	0.02	3.03	0.02
VH405	LAS	0.511259	7	0.1167	0.0001	0.509347	-1.33	0.10	2.61	0.01	2.90	0.01
VH406	LAS	0.511294	5	0.1191	0.0002	0.509343	-1.41	0.02	2.62	<0.01	2.91	<0.01
VH407	LAS	0.511340	7	0.1224	0.0000	0.509334	-1.60	0.13	2.65	0.01	2.95	0.01

suites were also analysed, but the results are poor (see discussion in Appendix 1). The results (and calculated parameters) that have relatively low errors are presented in Table 11.5, and analytical procedures are included in Appendix 1.

11.7.1 Results

The LAS has a moderately restricted range of $^{147}Sm/^{144}Nd$ from 0.1158 to 0.1440 with measured $^{143}Nd/^{144}Nd$ that vary from 0.511259 to 0.511717. On a Sm-Nd isochron diagram there is a positive correlation between $^{147}Sm/^{144}Nd$ and $^{143}Nd/^{144}Nd$, but the data[2] yield a poorly defined Model 1[3] solution corresponding to 2694 ± 740 Ma (ε_{Nd} = 1.1; MSWD = 157). Nevertheless, because the crystallization age of the complex is known to be 2485 ± 1.6 Ma (Chapter 10), the data can be considered by reference to model-reservoir parameters and, as Figure 11.13 illustrates, most of the samples are not far removed from CHUR. Compared with the SLC and TTLC orthogneiss suites in the Rauer Group, the LAS has a much more restricted range of initial isotopic compositions (discussed further in Chapter 13), and most samples have ε_{Nd} between 0.6 ± 0.3 and -1.6 ± 0.1.

11.7.2 Discussion and interpretation

Although errors on $^{147}Sm/^{144}Nd$ (and hence ε_{Nd}) for two samples are unacceptably high, variations between the remaining samples are considered to be of geological significance.

As described at some length in Chapter 6, there are two main models that can account for deviations from an ideal isochron relationship in such rocks, involving either assimilation of older crust (Hypothesis A) or metamorphic disturbance (Hypothesis B). As with the SLC in the Rauer Group, each of these models will be considered in detail.

Hypothesis A (AFC)

The simplest interpretation for the spread in ε_{Nd} for the LAS is through derivation from a slightly depleted mantle source, with selective or progressive assimilation involving older, isotopically evolved crust. Following procedures outlined in Chapter 6 (Equations 6.1 & 6.2), various bulk mixing calculations have been performed on a variety of end-member compositions, and are very briefly summarized in Table 11.6. By rearranging Equation 6.2, the simple two-component mixing model becomes:

---

[2] The two samples with relatively large errors on $^{147}Sm/^{144}Nd$ are excluded from the calculation.

[3] Regression techniques are outlined in Appendix 1.

$$X_a = \frac{C_{Nd(m)} \cdot (\varepsilon_{Nd(m)} - \varepsilon_{Nd(hyb)})}{\varepsilon_{Nd(hyb)} \cdot (C_{Nd(a)} - C_{Nd(m)}) - (C_{Nd(a)} \cdot \varepsilon_{Nd(a)} - C_{Nd(m)} \cdot \varepsilon_{Nd(m)})} \quad [11.2]$$

which can be used to estimate the amount of contamination required to produce the observed variations in the LAS.

Limits for primary mantle melts probably range between CHUR & DM, although the crust probably had a wider range of compositions. In an effort to constrain the nature of potential assimilants further, a number of different isotopic compositions are documented in Table 11.6. Although it is difficult to relate individual samples reported by Collerson *et al.* (1983) to the geological framework outlined here (for reasons outlined in Chapter 9), the most isotopically evolved crust is likely to be similar to Grace Lake Granodiorite (GrLG) VH35 (this study) and *VH19* of Black *et al.* (1991a). These samples are thought to be representative of the Grace Lake Granodiorite, which has a 2.8 Ga Nd_{CHUR} model age, inherited *ca.* 2.8 Ga zircons, and has highly fractionated REE profiles (*i.e.* low $^{147}Sm/^{144}Nd$ and steep $^{143}Nd/^{144}Nd$ evolution trajectory relative to CHUR). Assuming that such crust was initially derived from CHUR at 2.8 Ga, the minimum ε_{Nd} value at 2485 Ma that can reasonably be expected for this currently unexposed isotopically evolved crust is ~ -4.6.

All the data points on Figure 11.13c are isotopic compositions representative of crust that could have interacted with the LAS. Inherited zircons that are marginally older than the

Table 11.6 Theoretical mixing of mantle-derived magmas with a variety of possible crust components. The results indicate that fairly large amounts of crustal contamination (20-30%) are required to account for the observed spread in values between 0.6 and -1.6. The most likely mantle composition would have been an undepleted source with ε_{Nd} similar to CHUR, since a DM source would require unfeasibly large amounts of contamination to account for low ε_{Nd} samples.

	Mantle- derived composition		**Crust at 2485 Ma**		**Hybrid *X***	**Mix (%)**
Model	ε_{Nd}	Nd ppm	ε_{Nd}	Nd ppm	ε_{Nd}	
DM + 2.8 Ga	+4	40	-4.6	34	-1.6	46
Crust	+4	40-60	-4.6	34	0	13-19
Near CHUR	0	40	+2	40	+0.6	30
Near CHUR	0	40	-2	40	-1.6	80
Near CHUR	0	40	+4	40	+0.6	15
Near CHUR	0	40	-4	40	-1.6	40
Near CHUR	0	40	+5	40	0.6	23
Near CHUR	-0.5	40	-4.6	40	-1.6	30

LAS crystallization age have been recognized within the overall zircon population (statistically defined), indicating the presence of auto-assimilated CLG. Also, ghosted xenoliths from within the complex are recognizable as both felsic and mafic pre-D_1 orthogneisses (Mossel Gneiss and Taynaya EMG). Given the textural evidence for assimilation and the wide range of isotopic compositions present in the terrane at 2485 Ma, relatively large amounts of assimilation (20 -30 %) are required to explain the ε_{Nd} values within the LAS (see Table 11.6 for summary; calculations and graphs not shown for brevity). Derivation from a DM source can be excluded because the amount of crustal assimilation required to shift the isotopic composition of the complex to the observed values would need to be impossibly large.

Hypothesis B (open-system exchange during metamorphism)

Although there is only a small range of ε_{Nd} for the LAS samples, comprising ~2 epsilon units, it is relatively unlikely that secondary disturbance to the Sm-Nd system was the cause of this variation. A number of lines of evidence suggest that ε_{Nd} values are probably not far removed from protolith compositions, the most important being the limited time available to evolve apparent ε_{Nd} between protolith formation and metamorphism. Assuming derivation from a CHUR source (average LAS ≅ CHUR), and because the time interval between protolith formation and the last metamorphic episode are known to be only 10 m.y., secondary fractionation of $^{147}Sm/^{144}Nd$ ($\Delta^{147}Sm/^{144}Nd$) would need to be very large to account for a deviation of even 1 epsilon unit. For example, $^{147}Sm/^{144}Nd$ of 0.1400 altered by 20 % would only have a shift $\Delta\varepsilon_{Nd}$ of 0.04 (notation as described in Chapter 6). Similar severe time constraints would limit the extent to which different bulk compositions could evolve to reservoirs of significantly different isotopic potential (see Chapter 6 for background).

However, there are two possible scenarios that may potentially have led to the observed variability in ε_{Nd} for the LAS via open-system exchange during metamorphism. The first scenario involves direct isotopic exchange with adjacent gneisses during the D_2-M_2 event ($\Delta\varepsilon_{Nd(tmet)}$ as described in Section 6.5.4). Although this is the only mechanism that can account for the observed SLC data, this is less likely to have been important for the LAS for a number of reasons:

- The length-scales between different units is greater for the LAS, with proximity to pre-D_1 gneiss units being a minimum of 5-25 metres. Therefore transport distances would need to be proportionally much more.

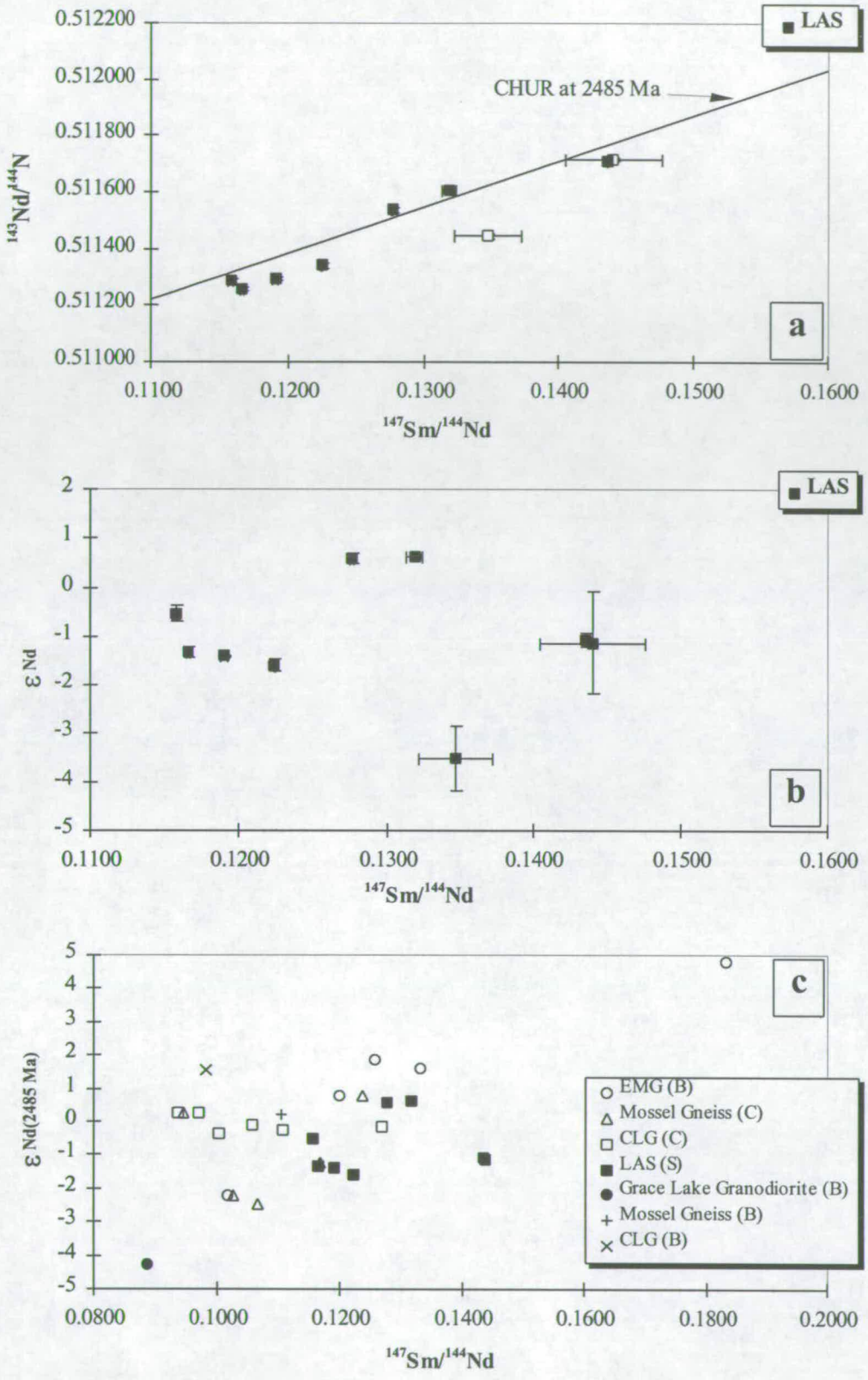

Figure 11.13 (a) Sm-Nd isochron diagram for the Lake Africa Suite (LAS). (b) LAS data expressed in epsilon notation, calculated assuming a crystallization age of 2485 Ma. (c) all available Sm-Nd isotope data for the Vestfold Hills. Suffix (B) is from Black et al., 1991a; (C) is from Collerson et al., 1983; (S) is from this study.

- Nd abundances are much greater in the LAS than either the SLC or TTLC, and much of the Nd is likely to be contained in apatite, zircon or other accessory phases with very low diffusivities and dissolution rates for Nd.

- There are only small differences in Nd-isotopic compositions between the different gneiss units at 2485 Ma, much less so than the SLC at 500 Ma.

The second scenario, however, circumvents these problems by proposing perturbation a long time after protolith formation. As described above for Rb-Sr isotopes, a *small* amount of Rb mobility or isotopic exchange at least 10^7 or 10^8 years after protolith formations is required to explain the observed Sr-isotope data. Although reasons 1 and 2 (above) still hold, with sufficient time, adjacent gneiss units would evolve to distinct Nd-isotope compositions. Nevertheless, a pervasive metamorphic event at this time would seem unlikely on geological grounds, because the last obvious recrystallization clearly occurred pre- or syn-D_2 at 2475 Ma (see Chapters 9 & 10).

On balance, small isotopic shifts from an initially Chondrite-like source through assimilation of older gneiss units is the most likely process to have modified the isotopic composition of the LAS. However, it is very difficult to specifically test for closed-system isotopic evolution, and a small amount of isotopic disturbance at a much later time cannot be ruled out.

11.7.4 Summary of conclusions

The LAS has ε_{Nd} values that are near to CHUR and are interpreted to be of primary protolith origin. Small intrasuite variations within the LAS are best explained by relatively high amounts of assimilation (20 - 30 %, in accordance with field relations) of marginally older crust that has both positive and negative ε_{Nd} values at 2485 Ma. However, ε_{Nd} values for the LAS as a whole are probably not much different to those of the protolith and hence the mantle source region. Nevertheless, there is no constraint on the amount of metamorphic perturbation that might have affected these rocks. Metamorphism is unlikely to have significantly altered the average ε_{Nd} value of the LAS, although it may explain the internal variations within the suite.

The implications for combined isotopic and/or trace-element petrogenetic modelling are assessed in the next section.

11.8 Summary, discussion and conclusions

11.8.1 Summary of geochemical and isotopic results

The three principal orthogneiss suites in the Vestfold Hills are broadly calc-alkaline in composition. This is exemplified by a trend towards alkali enrichment on an AFM diagram, and by trace and rare-earth elements that have enriched and fractionated LILE and LREE relative to MORB. The only exceptions appear to be a minor suite of mafic to intermediate dykes that are tholeiitic in composition (major and trace-element chemistry).

Whole-rock geochemistry for a large CLG dataset has been compared with a smaller number of representatives of the Taynaya EMG and Mossel Gneisses. A comparison of major and trace elements has established that the felsic CLG and the Mossel Gneiss are virtually indistinguishable on geochemical grounds, but that the mafic Taynaya EMG is distinctive and has higher LILE, Ni and normative *Ol*. However, REE and spidergram patterns for the three main orthogneiss units are very similar. REE patterns for all the main suites are particularly distinctive, and are characterised by moderate to high LREE/HREE, with slightly convex upward LREE but slightly concave upward MREE-HREE. MORB-normalized spidergrams for all units are characterised by highly enriched but variable LILE, and pronounced negative HFSE anomalies relative to LILE (*e.g.* PM-normalised, not shown) or REE (*e.g.* MORB-normalized, see Figure 11.8).

The results from O and Nd isotopes are most consistent with derivation from an undepleted mantle or mafic lower crustal source, but with minor variations attributed to contamination by older felsic and mafic lithologies. The results from Sr-isotope studies, however, indicate major secondary perturbation to the Rb-Sr system by metamorphic processes. Moreover, because minor *tertiary* disturbance must also have occurred a long time after crystallization (*ca.* 10^7 - 10^8 y.), there is a possibility that Nd-isotope signatures were also slightly affected. Nevertheless, although a similar disturbance model cannot be excluded entirely for Nd isotopes, it is unlikely that apparent ε_{Nd} for the LAS (~-0.6 ± 1) is much different from that of the protolith.

In an attempt to define the petrogenetic evolution of the Vestfold Hills orthogneisses, a number of problems or difficulties have been encountered in this study and identified in previous accounts. Whilst not embarking on a detailed or quantified exercise to explain the many and varied geochemical subtleties of the suites studied here, it may be constructive to review what aspects and approaches cannot be used sensibly in this terrane, before suggesting how advances may be made.

11.8.2 Problems that concern a geochemical classification scheme for the CLG

Sheraton & Collerson (1984) established a three-fold division of the CLG based on apparent groupings on a *Q-Ab-Or* diagram. They proposed dividing the gneisses into a 'Miscellaneous Suite', comprising gabbros, diorites and tonalites; and two potassic groups comprising a 'Monzonitic Suite' and a 'Monzodioritic Suite'. The first criticism of this approach is that the scheme relies heavily on isochemical metamorphism of the alkalis (*Ab-Or*), which even according to Sheraton & Collerson (1984) were possibly amongst the most mobile elements during metamorphism. Large-scale potassium metasomatism is not envisaged and the rocks studied here probably are broadly calc-alkaline in composition, with measured alkalis more-or-less corresponding to those of the protolith. However, small changes to either Na or K might be expected to have a profound affect on a classification scheme based almost entirely on normative *Ab* and *Or*. It is for this reason that further alkali-element-based geochemical classifications (see Section 8.4.6), such as the subdivision of the subalkalic igneous rocks using the K_2O *vs.* SiO_2 scheme of Le Maitre *et al.* (1989), have not been applied in this study.

Other 'classification problems' concern the use of strongly compatible elements to propose that individual rocks are either related or unrelated in some way, when the discriminant elements (*e.g.* Sr in a websterite) are potentially influenced by crystal fractionation/ accumulation processes. A further problem that is apparent from this study is the erroneous use of calculated initial Sr-isotope ratios to infer distinct crustal reservoirs for some orthogneisses (*e.g.* Collerson *et al.*, 1983; Black *et al.*, 1991a). These two aspects are discussed further in the next two sections in the context of protolith petrogenesis.

11.3.3 Problems with modelling protolith petrogenesis in detail: this study and previous attempts

A number of important limitations restrict the application of forward or inverse modelling techniques to unravelling the origin of the Vestfold Hills orthogneisses in detail. Equilibrium or fractional trace-element forward modelling requires identification of primary magma composition, whereas inverse modelling requires either a very simple dataset or independent knowledge of fractionating assemblages, mineral-melt K_d values, and assimilant composition(s). Basically, none of these variables or conditions are accurately known for any of the Vestfold Hills protoliths and attempting to constrain them is not a trivial task.

Unlike the tholeiitic SLC, where most elements appear to be related by a relatively simple crystal-fractionation/accumulation mechanism, the CLG suites have complex and sometimes

irregular geochemical signatures. Many of these patterns are thought to reflect changes in fractionating assemblage, as elements that initially behaved incompatibly became relatively compatible as magmatic centres evolved. Although no attempt has been made in this study to quantify fractionating assemblages in terms of modal percentages, the following phases are implicated for at least some bulk compositions: Cpx, Opx, Plag, Ilm/Mt, alkali feldspar (mesoperthite), apatite and zircon; other possibilities such as olivine, hornblende, biotite and accessory phases cannot be excluded on the basis of the available geochemical (or petrographic) data.

Attempts made in this study to constrain AFC processes or the isotopic composition of the source region are severely hampered by metamorphic perturbation to the Sr-isotope system. Previous studies in the terrane concluded that metasomatism was limited to selective mobility of LILE (*e.g.* Collerson *et al.*, 1983; Sheraton & Collerson, 1984; Sheraton & Black, 1988). As noted by Sheraton & Collerson (1984), '*some*' LILE appear to have been mobile in '*some*' of the rocks. However, some of the scatter on the bivariate trace-element diagrams presented here may also reflect open-system behaviour for elements other than LILE, but it is extremely difficult to establish the extent to which individual elements, or sets of elements, were mobile during metamorphism (*e.g.* Kim & Jacobi, 1996) even when specifically sampling to constrain metasomatism directly (*e.g.* Rockow *et al.*, 1997; also discussed critically in Section 13.4.1).

The petrogenetic conclusions reached by Sheraton & Collerson (1984) were largely deduced from a regionally collected dataset primarily using least-squares modelling techniques. However, the data presented in Chapter 11 indicate that no single set of fractional crystallization or partial-melting variables could even come close to explaining the geochemical relations of some of the suites sampled here. Therefore, it is likely that previous modelling attempts based on least-squares techniques are not likely to be unique or even particularly precise or informative solutions. In my view, and based on the data and discussion presented above, attempts at quantifying assemblages or degrees of fractionation (*e.g.* Sheraton & Collerson, 1984, p.60) probably conveys a false sense of confidence in how much can reasonably be deduced of the chemical evolution of the Vestfold Hills orthogneisses.

To conclude, the observed geochemical relationships within and between suites are not sufficiently simple to allow inverse or forward modelling *in detail*. However, a number of generalizations may provide an indication of the large-scale processes involved in magma genesis.

11.8.4 Steps towards an integrated petrogenetic and tectonomagmatic model for the Vestfold Hills orthogneisses

A critique of which previous and present observations are of petrogenetic use

Although a number of general and specific problems have been have been shown to be inherent in previous geochemical studies in the Vestfold Hills, some of the broad petrogenetic conclusions made in these reconnaissance studies (*e.g.* Sheraton & Collerson, 1984) are probably valid. To clearly establish which observations or conclusions warrant further consideration, but without undertaking a laborious discussion of every statement made in previous studies, observations have been grouped into three categories (below). The first two categories illustrate some of the conclusions that are deemed to be unjustifiable on the basis of this study. The third category comprises positive observations from this and previous studies that can be built upon.

- ***(i) Observations that may be adversely influenced by metamorphic processes.*** Although mobility is likely to be highly bulk-composition dependent and controlled by the stability/instability of phases during recystallization, it appears to be restricted to LILE depletion and enrichment in some but not all rocks. A major weakness of previous studies in the terrane *and of this study* (*e.g.* Collerson *et al.*, 1983; Sheraton & Collerson, 1984; Black *et al.*, 1991a; discussed in Chapter 13), is that there is no consistent assessment of which elements were mobile in which rocks. Examples or inconsistencies identified in previous studies (*e.g.* Collerson *et al.*, 1983; Sheraton & Collerson, 1984; Collerson & Sheraton, 1986) include:

  - explaining Ba/Sr in terms of crystal fractionation,
  - interpretations involving Sr isotopes,
  - attributing variable LILE enrichment directly to mantle metasomatism.

- ***(ii) Observations that may be influenced by crystal fractionation/accumulation processes.*** Examples include some trends on bivariate diagrams and ratios between compatible and incompatible elements. For reasons discussed in Section 11.8.2 (above), the variability and unknown parameters that were involved in crystal fractionation means that detailed modelling for individual suites is beyond the scope of this study. However, typical observations that fall into this category include:

  - attributing low Sr abundances in gabbro #5371, and highly variable trace-element characteristics in the strongly fractionated granites, to different source components,
  - interpreting trends or ratios involving normative *Di* to partial-melting behaviour.

- ***(iii) Broad observations that are consistent for a wide range of bulk compositions and for the majority of suites.*** These generalisations are most robust geochemical criteria with which to interpret large-scale petrogenetic processes. Observations made by Sheraton & Collerson (1984) that fall into this category include:

- low Y, Ti, P_2O_5, Zr, Nb abundances,
- high abundances of LREE and high Ce/Y,
- a strong covariance between Ti and Y,
- similar spidergram patterns for a wide variety of rock types.

To these observations a number of positive conclusions from this study that are thought to be of petrogenetic relevance can be added to the list:

- REE patterns are very consistent for the majority of suites (excluding the highly fractionated late granites and the rare tholeiite dykes),
- high LREE/HREE,
- many compositions have low HFSE relative to LREE (or LILE, although such relationships should be treated with caution in detail),
- pronounced negative Nb anomalies relative to La and Ce ($Nb/Nb^* \sim 0.4$),
- initial Nd-isotopic ratios consistent with mantle derivation at *ca.* 2.5 Ga,
- dykes (*i.e.* liquids) that have very similar major- and trace-element characteristics to the cumulates.

From their observations now placed in the third category above, Sheraton & Collerson (1984) concluded that the main orthogneisses in the Vestfold Hills (CLG and Mossel Gneiss), were derived from a mafic source that had major residual amphibole, and possibly garnet, with the most likely scenario involving partial melting of subducted, hydrated, ocean crust. Since their paper was published, a great deal of work has been conducted on the processes involved in subduction zone magmatism, and it is now recognised that the geochemical features originally recognised by Sheraton & Collerson (1984) and many of the observations highlighted in this study could have been produced through a variety of mechanisms.

By comparison with Phanerozoic analogues, a number of possible 'source reservoirs' are possible, the most likely of which are:

- Melting mafic rocks in the lower crust (amphibolite or garnet granulite), direct melting of subducted or underplated hydrated slab.
- Melting of fluid-enriched mantle wedge in an island-arc setting (ocean-ocean collision).
- Melting of subcontinental lithosphere in an active continental margin (ocean-continent collision).

Each of these potential 'source reservoirs' is worth considering further as a possible origin of the Vestfold Hills orthogneisses.

Steps towards understanding petrogenesis and constructing a tectonomagmatic model

The role of intracrustal melting

Derivation of most of the Vestfold Hills orthogneisses by partial melting of felsic crust, or crust with significant residual plagioclase, is unlikely. Eu anomalies are small for all compositions and are positive for the granites. Sr abundances are generally high, as are compatible elements such as Cr, Ni, and Sc; elements that are not normally found in abundance in felsic crust.

The only exception to this general observation is the Grace Lake Granodiorite, which probably did form by intracrustal melting of a heterogeneous felsic and mafic source. Extreme fractionation of LREE/HREE and a relative depletion in MREE in the Grace Lake Granodiorite suggests garnet and/or accessory phase control (*cf.* Watt & Harley, 1993; Nabalek & Glascock, 1995; Bea, 1996). A mixed source is further indicated by partly-digested mafic and felsic xenoliths (restite), although textural evidence (*e.g.* Figure 9.12) illustrates that much of the Grace Lake Granodiorite may be itself be the residual product after partial-melt removal (a restite with restites...). Nevertheless, the presence of inherited zircons with a mixed age population also implies interaction/derivation from a heterogeneous source. Although a large number of potential source compositions and possible melting histories could theoretically explain the geochemistry of the Grace Lake Granodiorite, melting of metasedimentary source rocks such as the Chelnok Paragneiss is not implicated. Amongst other reasons, this is because A/CNK ratios are only weakly peraluminous (*e.g.* Miller, 1985) and metasedimentary restites are not present (*e.g.* Chappell & White, 1974). For comparison, one granite sampled from adjacent to the Chelnok Paragneiss (VH542) has very distinctive chemistry compared with all other Vestfold Hills orthogneisses. It has an A/CNK of >5.0, contains entrained garnet + biotite restites, and is of obvious metasedimentary derivation.

In a very general sense, the chemical and isotopic heterogeneity displayed in the Grace Lake Granodiorite contrasts with relative chemical and isotopic homogeneity of the CLG. Sheraton & Collerson (1984) established that Mossel Gneiss and CLG tonalite could, theoretically, be derived by partial melting of a tholeiitic source leaving residual hornblende ± garnet. However, relatively high CE abundances of many of the CLG *and associated comagmatic dykes* (*i.e.* not just a cumulate artefact; sample VH467 has 181 ppm Ni, 605 ppm Cr and 39.6 ppm Sc) that are as high or higher than typical abundances in MORB, suggest that an ultramafic source is much more likely. The production of voluminous mafic, intermediate, and felsic magmas of *relative* geochemical homogeneity (*i.e.* consistent patterns on spidergrams and coherent REE patterns) would require a large homogeneous

ultramafic reservoir. Clearly the most obvious location for such a reservoir would be in the mantle rather than in the crust.

Mantle melting: constraints on source and process

The most common scenario for modern calc-alkaline magmatism is through subduction-zone processes (*e.g.* Wilson, 1989). Models for arc genesis have received a great deal attention in the last decade and many of the geochemical features similar to those outlined above (Category (iii) above) for the Vestfold Hills orthogneisses have been attributed to multicomponent derivation in a volcanic-arc setting. In particular, elevated LILE and LREE, high LREE/HREE, and low HFSE and HREE relative to N-MORB (*e.g.* Figure 11.9) have been attributed to processes that include:

- ***Small degree slab-derived melts interacting with mantle wedge material.*** Direct addition of small-degree melt fractions derived from the slab, mixing with larger degree melts from the mantle wedge (*e.g.* Yogodzinski, 1994).

- ***Fluid-induced wedge melting.*** Mantle melting triggered by influx of fluid from the slab (*e.g.* Wilson, 1989; Hawkesworth *et al.*, 1991; Stolper & Newman, 1994). This may involve either oceanic (depleted) lithosphere (*e.g.* White & Patchett, 1984) or subcontinental lithosphere (*e.g.* Pearce, 1983).

- ***Multisource interactions.*** Complex and highly variable trace-element and isotope signatures have been attributed to multisource components involving sediment, slab and mantle wedge (*e.g.* Ellam & Hawkesworth, 1989; Francalanci *et al.*, 1993; Hoogewerff *et al.*, 1997)

- ***Direct slab melting.*** Many earlier studies attributed volcanic-arc signatures to direct melting of the slab (*e.g.* Fitton, 1971; and Sheraton & Collerson, 1984, for the Vestfold Hills). Although complex fluid-flux melting of the mantle wedge is currently in vogue, and thermal considerations suggest that most modern slab material will not melt in subduction zones (*e.g.* Peacock *et al.*, 1994), the possibility of direct slab melting cannot be ignored for Archaean rocks (*e.g.* Drummond & Defant, 1990; McCulloch, 1993).

Many of the 'finer details' of the processes of arc magmatism outlined above have been concluded on the basis of combined isotope and trace-element studies. For reasons described in Sections 11.5 - 11.7, such an approach is not possible for the Vestfold Hills orthogneisses. Nevertheless, some additional contraints are possible.

Fluid-enhanced enrichment rather than direct slab melting

Although it is difficult to establish whether a small-degree melt fraction interacted with subcontinental lithosphere or depleted mantle-wedge material, a number of observations

imply that direct slab or mantle melting was *not* the sole origin of the Vestfold Hills orthogneisses.

The first observation is made by analogy with modern well-studied continental arcs, where combined trace-element and isotopic data indicate that calc-alkaline volcanism is the product of multisource - multiprocess components (*e.g.* Francalanci *et al.*, 1993).

The second observation concerns MORB-normalized IE patterns for the Vestfold Hills orthogneisses. Many of the features observed for the LAS and RLS suites cannot be explained by direct slab melting or even by direct melting of an ultramafic mantle source. For example, whilst the REE profiles can be readily reproduced by modest amounts of partial melting leaving residual garnet, amphibole and clinopyroxene (results not shown for brevity), it is difficult to explain the strong depletion in Zr relative to Sm. If partial melting was the cause of the negative Zr anomaly relative to the REE, there would have to be a residual phase strongly enriched in Zr relative to Sm, whereas most mantle or ultramafic phases have similar K_d values for these elements. Two other possibilities, invoking fractionation/accumulation processes or assimilation, can be considered and dismissed following similar arguments to those discussed in a previous section for the TTLC. In the case of accumulation models, it is probable that Zr/Sm was influenced by zircon fractionation. However, in the case of the LAS, which includes compositions that range from websterite to intermediate monzodiorite, all samples have a negative Zr anomaly. Moreover, it cannot be that Zr behaved much more incompatibly than Sm and was efficiently expelled from the system because, as noted above, K_d values for Sm and Zr are not vastly different in most phases, even in intermediate compositions (*e.g.* Rollinson, 1993, table 4.1). Also, a relatively high concentration of Zr in many samples, coupled with the presence of zircons, strongly suggests that Zr behaviour was approximately compatible. Induced anomalies by assimilation can also be discounted for a number of reasons. One reason is that although the most likely contaminants also have negative Zr anomalies, they generally have lower or only similar absolute concentrations of incompatible elements. Therefore, the effects of bulk mixing are not significant (see earlier comments in Section 5.4.4) and an impossibly large amount of contamination would be required to account for the observed data if the Zr anomaly was not inherited from the source.

In conclusion, a process other than partial melting of a simple MORB-source or depleted MORB-source is required to explain the HFSE and HREE depletion relative to LREE and LILE (see also Pearce, 1983, and references in Hawkesworth *et al.*, 1993). Clearly, there is a strong appeal to subduction-zone processes, since it is in this environment that pronounced negative HFSE anomalies are most commonly produced.

Continental-arc rather than island-arc derivation

Island-arc and continental-arc volcanics have a number of important geochemical similarities but also have distinctive differences. For the trace elements, the main similarities are high LREE and LILE relative to HREE and HFSE, whereas the main differences concern the degree of enrichment in all incompatible elements relative to MORB or other arc-related basalts (*e.g.* Figure 11.8b). Although it is difficult to compare incompatible-element *abundances* between plutonics and volcanics, the same generalisations hold true, that is, subduction-related plutonic centres associated with continental crust generally have higher incompatible-element abundances. Also related to this observation, calc-alkaline plutonism tends to predominate in continental settings (Wilson, 1989), although tholeiitic and potassic magmas occur in both oceanic- or continental-arc settings. From these general considerations alone, the mid- to lower-crustal section of a continental arc (*e.g.* some parts of the Aeolian arc) or an Andean-type active continental margin would provide a suitable, general, modern analogue for the Vestfold Hills at *ca.* 2500 Ma. Such an origin is further suggested by a number of the TEDDs described in Section 11.4.3.

Six of the TEDDs described in Table 1.1 are potentially relevant to the Vestfold Hills orthogneisses; five are for basalts, and one is for granites. The following TEDDs were described in Section 11.4.3 and most of the results are fairly self-explanatory:

Table 11.7 Summary of the results for TEDDs discussed in Section 8.4.3.

TEDD	Tectonomagmatic setting
TiO_2-MnO*10-P_2O_5*10	Most samples plot in the *continental-arc basalts* field
Ti/100-Zr-Y*3	Most samples plot in the *calc-alkali basalts* field.
Ti/100-Zr-Sr/2 (?)	Most samples plot in the field of *calc-alkali basalts*, with high Sr samples (plagioclase cumulates) plotting towards the Sr apex.
La/10-Y/5-Nb/8	All rocks correspond to *calc-alkali basalts*.
Zr/4-2Nb-Y	Most samples plot in the fields of *volcanic-arc basalts*.
Nb-Y	TEDD for granites (Pearce *et al.*, 1984), only the D2-GS, IFCLG and GrLG were plotted, all correspond to the volcanic arc-granites + *syn-collisional granites*.

Most TEDDs support what is readily apparent from the MORB-normalised spidergram, that LREE are enriched relative to HREE (+Y) and HFSE, especially Nb. One further important and encouraging conclusion is that IE variations support the contention based on the major-element alkali-based classification scheme (*e.g.* AFM diagram of Irvine & Baragar, 1971) that the suites *are* broadly calc-alkaline in composition.

Further evidence in favour of a continental- rather than island-arc setting is implied by the presence of inherited zircons in gneisses. The inherited zircon range in age up to about 2800 Ma (Black *et al.*, 1991a; this study, Chapter 10) and are found in a variety of gneiss types (*e.g.* CLG diorites, Mossel Gneiss and also the Grace Lake Granodiorite). This age implies that juvenile magmas that were derived at *ca.* 2500 Ma have interacted with crust that is at least 300 m.y. older. By analogy with most modern active oceanic island arcs, magmas are generally not associated with felsic crust that is 300 m.y. older than the age of the arc. Whereas active continental margins or continental arcs are characterised by young arc rocks that interact with ancient crust (*e.g.* Thorpe *et al.*, 1982).

Conclusions and a testable tectonomagmatic model for the Vestfold Hills orthogneisses

In conclusion, derivation of the Vestfold Hills orthogneisses by direct melting of an eclogitic source of tholeiitic composition as originally proposed by Sheraton & Collerson (1984) is *not* supported by this study. Although it has not been possible to develop a refined or quantified petrogenetic model, general geochemical considerations imply that much of the *ca.* 2500 Ma orthogneisses are the plutonic remnants of a calc-alkaline continental arc. Largely by analogy with much better studied unmetamorphosed modern equivalents, the preferential transfer of relatively soluble LREE and LILE by a slab-derived fluid is implicated to explain the incompatible trace-element patterns that have been observed for the majority of the Vestfold Hills orthogneisses. However, no attempts have been made in this study to quantify the origin of the observed geochemical patterns by reference to possible geochemical contributions from slab, wedge, enriched lithosphere and crust, primarily because the rock types that are available do not easily lend themselves to such treatment.

Crystal fractionation and accumulation has obviously had a large affect on the bulk composition of the gneiss protolith. As with possible partial-melting histories described above, the details of this crystal fractionation process are not constrained quantitatively in this study, although it is obvious that no single fractionating/accumulating assemblage can explain the observed geochemical variability even within individual suites.

There is potential to pursue a better understanding of the petrogenesis of individual CLG orthogneiss suites, but a great deal of detailed study will be required to achieve worthwhile results that are based on more than speculation. A number of suggestions as to how these results may be achieved is presented in *suggestions for further research* in Chapter 13.

Chapter 12

Summary, discussion, and implications for the geological evolution of the Vestfold Hills

12.1 Introduction

This chapter is a brief summary of the new observations and different interpretations made during the course of this study regarding the geological and geochemical evolution of the Vestfold Hills. Although some of this chapter is a repetition of the main conclusions presented in Chapters 8-11, discussion in this chapter is developed within the context of previous work and the conclusions are ultimately integrated into a general tectonomagmatic model. The structure of this chapter broadly follows the layout of Chapter 8 - *Geological outline of the Vestfold Hills*, and references to subsequent detailed accounts and arguments presented in this study are provided after the heading of each section.

12.2 Summary and discussion of lithological and structural revisions

12.2.1 Pre-D_1 gneiss suites

Tryne Metavolcanics (Section 9.4.1)

The Tryne Metavolcanics of Collerson *et al.* (1983) has been abandoned as a formal unit. It is apparent from field observations that post-D_1 (CLG) and even post-D_2 (Norite 'ring' dyke) lithologies were included in the original 'metavolcanic' package. Pre-D_1 suites that were previously grouped as metavolcanics have been subdivided into a three-fold non-genetic scheme comprising: Chelnok Paragneiss, Mossel Gneiss, and Early Mafic Gneiss (EMG).

Chelnok Paragneiss (Section 9.4.3)

The Chelnok Paragneiss is usually tectonically imbricated with other Pre-D_1 gneiss units. It was not possible to establish in this study whether minor EMG components in the Chelnok Paragneiss are of extrusive volcanic origin, or comprise younger intrusives that were subsequently transposed into parallelism with the metasedimentary rocks.

Taynaya Paragneiss (Figure 9.1)*

The only new observations of the Taynaya Paragneiss concern the spatial distribution of this distinctive gneiss unit in the northern Vestfold Hills, and the unit has been mapped along strike for several km around the open regional fold in the northern Tryne Fjord area (see Figure 9.1*). Despite extensive regional mapping, this unit does not occur in the central or southern Vestfold Hills, and consequently its relationship to the Chelnok Paragneiss and EMG is not known.

Mossel Gneiss (Section 9.4.2)

The Mossel Gneiss is less widespread in the northern Vestfold Hills than previously supposed, and much of the previous reconnaissance mapping of this unit is actually CLG. This study only makes minor revisions to previous accounts of the Mossel Gneiss, and confirms that at least minor components were derived through partial melting of EMG as originally proposed by Collerson *et al.* (1983). However, the precise nature of migmatisation and the relative input of injection, as distinct from *in situ*, melting, is still not known.

12.2.2 D_1-M_1 (Section 9.4)

The first regionally recognized deformation (D_1) produced a strong gneissic foliation and tight to isoclinal folding that was responsible for inter-layering pre-D_1 lithologies at outcrop scale. Recognition that there are local low-strain domains within the regional D_2 fabric indicates that F_1 and F_2 were not coaxial. Detailed observations of small-scale F_1 folds that are preserved in low-strain areas indicate that flat-lying folds in metaironstone layers fold compositional layering (transposed bedding) that is now defined by exsolved metamorphic sub-calcic pyroxenes. These folds have a flat-lying axial planar fabric (S_1) that cross-cuts pyroxene exsolution lamellae in fold hinge regions, which indicates that a high-temperature metamorphic mineral assemblage and layering had already developed prior to D_1-M_1. These conclusions support early observations made by Oliver *et al.* (1982) that D_1 is possibly a composite deformation comprising more than one tectonic episode. Nevertheless, the main regional early deformation episode, which presumably corresponds to the peak of metamorphism, is still described as D_1-M_1 in this study.

No direct constraints are placed on the metamorphic conditions of D_1 from this study, although samples of Chelnok Paragneiss that are of potential thermobarometric importance, comprising calc-silicate, metaironstone and Grt-Opx semipelitic bulk compositions, have been collected from throughout the Vestfold Hills for future study.

12.2.3 Post-D_1 to pre/syn-D_2 gneiss suites

Crooked Lake Gneiss (Section 9.2)

Detailed observations of the field relations and spatial distribution of CLG in the northern region has enabled a more comprehensive assessment of the geological evolution of the Vestfold Hills than has previously been recognized. A formal, albeit broad, definition of the Crooked Lake Gneiss is used in this study, and refers to all the orthogneiss units that intruded between D_1 and D_2. In contrast to the early reconnaissance studies in the terrane (*e.g.* McLeod *et al.*, 1966; Oliver *et al.*, 1982; Collerson *et al.*, 1983; Parker *et al.*, 1983), the CLG is recognised as a lithologically diverse group of spatially and temporally distinct plutons. CLG magmatism is now known to have lasted for approximately 20 m.y., with intrusions occurring as a number of small composite plutons, dykes and sills. Compositions include pyroxenite - hornblende pyroxenite - melagabbro - gabbro - monzogabbro/ monzodiorite - monzonite - tonalite and granodiorite. A number of additional suites, including the homogeneous Grace Lake Granodiorite variants (Black *et al.*, 1991a); pre-, and syn-deformational intermediate dykes; and a suite of syn-deformational (D_2) monzogranites and syenogranites are also included within this overall grouping. There are exceptions to the CLG 'post-D_1 to pre-D_2' definition of the CLG as described above; the rare post-deformational intermediate dykes are loosely included in scheme because they are chemically similar to the CLG; conversely, field observations and distinctive geochemical features support the separate status of the Grace Lake Granodiorite Gneiss as proposed by Black *et al.* (1991a), although the term should be restricted to the *migmatitic* variety as seen at the type area. Although the Grace Lake Granodiorite and some pre-D_2 intermediate dykes have distinctive chemistry and were probably derived from a different source, they are nonetheless discussed with the CLG.

In a further departure from previous accounts of the geology of the terrane, the results of this study indicate that most CLG did not intrude syn-tectonically with D_2. Oliver *et al.* (1982) and Collerson *et al.* (1983) originally considered the CLG to be of syn-D_2 origin, whilst Black *et al.* (1991a) restricted the syn-deformational component to the Grace Lake Granodiorite. Field observations (Section 9.2.4) and SHRIMP U-Pb zircon geochronology (Chapter 10) indicate that neither view is entirely correct, and syn-deformational components are restricted to minor late granites (*s.s.*) and remobilised components in the Grace Lake Granodiorite unit.

12.2.4 D_2-M_2 (Section 9.3)

Scale and character of F_2

Regional mapping of the spatial distribution of CLG, combined with detailed structural observations, has constrained the scale of F_2 to be of less than *ca.* 500 m wavelengths in the low-strain northern area. This view is different to the structural scheme originally proposed for the Vestfold Hills (*e.g.* McLeod *et al.*, 1966; Oliver *et al.*, 1982; Collerson *et al.*, 1983; Parker *et al.*, 1983) and implies that km-scale macroscopic units (*e.g.* Snape & Harley, 1996, figure 2) were not tectonically repeated by F_2 regional folds. This conclusion is supported to some extent by geochemical studies (Section 11.3.3) and U-Pb zircon dating (Black *et al.*, 1991a; this study, Chapter 10).

In all regions, D_2 fabric elements are the dominant, tectonic, outcrop-scale structures. Foliations are defined by aligned biotite or, more commonly, by ferromagnesian and quartzofeldspathic aggregates. In the northern region, lineations are only poorly developed and, using the terminology of Oliver *et al.* (1982), S-tectonites dominate. However, where L_2 are developed, they are parallel to local F_2 axes and are defined by hornblende mineral-elongation lineations, elongate aggregates of ferromagnesian minerals, and occasionally elongate quartz stringers. The numerous xenoliths in the CLG orthogneisses also commonly parallel S_2 (oblate spheroid geometries) or, more rarely, L_2 elongation directions (prolate spheroid geometries).

Timing of late open folding (D_3)

All of the aforementioned D_2 fabric elements were reoriented by F_3 open-warping. The relative timing of this regional folding event is placed after fabric development associated with F_2, hence F_3 post-dates axial-planar leucosome associated with F_2 (dated at 2475.3 ± 0.7 Ma; Section 10.4), but predate intrusion of the oldest post-deformational intermediate dykes suite (2477 ± 5 Ma; Black *et al.*, 1991a). Clearly, the technical development of the U-Pb zircon dating technique is not yet able to distinguish between the timing of these two high-grade events. Nevertheless, both deformation phases are distinct, of regional extent, and occurred at about 2475 Ma.

Effects and origin of late open folding (D_3)

Although the gneiss units in the Vestfold Hills are commonly described as being oriented roughly E-W, but reoriented N-S by open warping in the northern region (*e.g.* Oliver *et al.*, 1982; Collerson *et al.*, 1983; Parker *et al.*, 1983), observations from the Tryne Islands (see

Oliver *et al.*, 1982; figure 1) and the remote Murphy Rocks area 35 km north of the main outcrop (this study), implies that this description may not be strictly correct. Since all the currently exposed outcrops in the north, from northern Long Peninsula to Murphy Rocks, are oriented roughly N-S, a better description might be: 'the Vestfold Hills gneisses are oriented N-S and were reoriented E-W by F_3 open warping'. This might seem a pedantic point except that the E-W orientation is parallel to the Sϕrsdal Glacial which marks the boundary between the relatively stable Archaean Vestfold Hills craton to the north, and the Proterozoic-Palaeozoic mobile belt to the south. Although a detailed kinematic study of the D_3 open folding and associated high-grade shear zones has not been undertaken here, it is possible that this similarity in orientation is not a coincidence. A number of other seemingly isolated observations may help further explain the regional structural development:

- Rare high-grade shear zones that developed at about the same time as F_3 regional and local folds, strike ENE-WSW and have dextral top-to-the-NW thrust geometries (from the Long Fjord area).

- S_2 fabric development is strongest in the southern region proximal to the Sorsdal Glacier.

- The outcrops in the Murphy Rocks area have a similar strain state to the northern Vestfold Hills, whereas there is a distinct tightening of F_2 structures across southern Long Peninsula towards the south. In this transitional area, numerous low-strain windows are preserved that retain relict igneous features and early fold (F_1) geometries. Such low-strain windows were not found in the southern region in this study, and the region from central Broad Peninsula to the Sϕrsdal Glacier is dominated by relatively high-strain fabrics characterised by a very strong biotite and amphibole foliation.

Although there is no conclusive evidence from this study, it is likely that F_2 folds and the corresponding S_2 foliation were tightened and accentuated in the southern region by D_3. Therefore it is possible that the N-S strain gradient relates more to the development of D_3 than D_2. One possible explanation is that localised NW-SE compression and shearing was associated with a terrane-scale transpressional structure initiated at *ca.* 2475 Ma. In such a model, the regional open warp and N-S strain gradient would correspond to a large-scale drag fold with an overall geometry implying dextral transpression with a top-to-the-NW thrust component (Figure 12.1). This would explain the overall map pattern for the Vestfold Hills (F_{3r}; see Figure 9.1*), minor high-grade shear zones with transcurrent thrust geometries, and the generally shallow-plunging orientation of the regional open warp (F_{3r}) and minor open warps (F_{3m}). Further speculation may account for the D_2-D_3 episode as a related development of one collisional phase, beginning with E-W compression which subsequently developed into dextral transpression along the southern margin of the present Vestfold Hills.

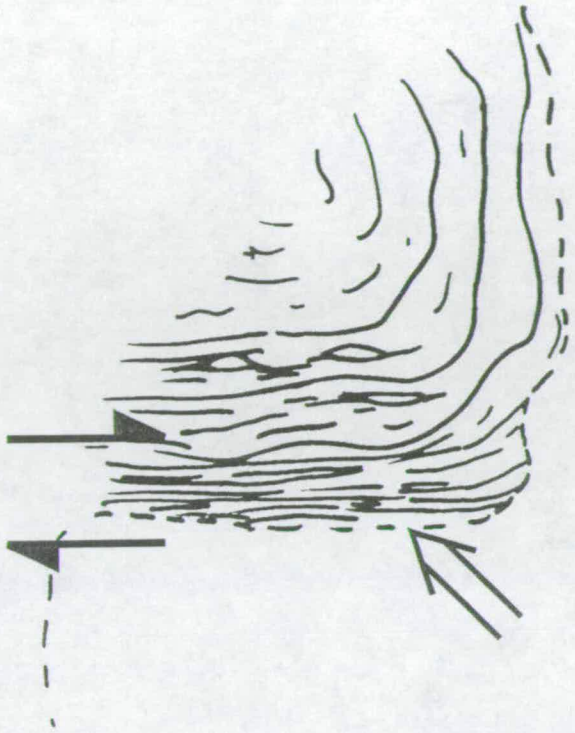

Figure 12.1 Highly schematic kinematic model for D_3 evolution of the Vestfold Hills. Open arrows indicate the thrust component as deduced from top-to-the-NW shearzones and the regional F_3 geometry. The speculative model presented here implies initiation of a major long-lived transpressional boundary at 2475 Ma.

Such oblique collision is typical of more recent collisional settings (*e.g.* Avé Lallemant, 1997) and would require only a 30 degree displacement in the orientation of the local principal stress orientation.

In conclusion, although much work needs to be done to unravel the kinematics involved in the D_3 event in the Vestfold Hills, it seems most likely that gneisses in the south were re-oriented into an E-W orientation very shortly after D_2, and that the structural trend parallels a major tectonic lineament (see also Dirks *et al.*, 1994) that was initiated at about 2475 Ma.

12.3 Summary and discussion of the geochemical evolution of the Vestfold Hills orthogneisses

12.3.1 Summary of the geochemistry of the principal orthogneisses (Sections 11.3 & 11.8.2)

The main revisions or criticisms of previous geochemical studies in the Vestfold Hills concern the division of sub-suites within the overall CLG grouping, and approaches towards sample selection and geochemical modelling that have been adopted to constrain protolith petrogenesis.

General observations and problems with geochemistry-based classifications

It is apparent from this study that the origin and evolution of the CLG is complex and involved a number of discrete intrusions that all probably had either distinct or at least subtly different petrogenetic histories. Rather than classify or distinguish CLG suites based on geochemical criteria, a number of subdivisions have been proposed based on lithological association and detailed field observations.

Examples of some specific problems include the geochemical classification scheme proposed by Sheraton & Collerson (1984) for the CLG, as outlined in Section 8.4. For instance, granites (*s.s.*) that are included in both the 'Monzodioritic Suite' and 'Monzonitic Suite' (see Figure 8.3) cannot be *strictly* related to the intermediate compositions in the 'suites' because the granites are younger by several million years. However, two compositionally distinct granite types have been identified in this study, and the syn-deformational pink syenogranites and white monzogranites of the D2-GS probably correspond to the granites in the Monzonite and Monzodioritic Suites respectively.

There are also other problems with the Sheraton & Collerson (1984) scheme. For example, gabbros and previously undocumented ultramafic CLG lithologies are gradational with, and probably directly related to, some of the intermediate compositions of broadly monzodioritic to quartz monzodioritic composition (*cf.* Figure 8.3). By contrast, other suites such as the monzonite at Platcha Hut (Black *et al.*, 1991a), do not appear to be directly related to ultramafic-mafic associations. Although such monzonites would be grouped with the 'Monzonite Suite' on geochemical grounds (Sheraton & Collerson, 1984), the monzonite at Platcha Hut is distinct in age from other members of the 'Monzonite Suite', such as the monzodiorites at the type area of the CLG (Collerson *et al.*, 1983; Black *et al.*, 1991a). Similarly, the alkali-feldspar phyric monzonite at Platcha Hut is texturally distinct

from the equigranular monzonites in the central northern region. Furthermore, as Sheraton & Collerson (1984, p. 56) noted, samples such as #5192 are monzodioritic on the basis of petrography, but are similar to the Monzonitic Suite in terms of chemical composition.

A further potential problem with the three-fold classification scheme proposed by Sheraton & Collerson (1984) for the CLG concerns the choice of discriminatory elements. The normative *Q-Ab-Or* diagram relies heavily on the major elements Na_2O and K_2O, which are potentially amongst the most mobile major elements during high-grade metamorphism. Nevertheless, because many intermediate to felsic compositions contain appreciable primary alkali feldspar, large amounts of K mobility are not expected or observed, although in detail this cannot be assumed.

In conclusion, whilst the geochemical grouping of Sheraton & Collerson (1984) represents the distribution of some of the different rock types in the Vestfold Hills, the groups cannot be considered as strictly cogenetic. It is also difficult to see how the scheme could be used further to explore the genesis of the CLG or even to group rocks spatially. Therefore, it is preferable that the geochemically defined 'Monzonitic' and 'Monzodioritic' suites be abandoned in favour of the field-defined associations described in this study and outlined in Figure 9.1*.

Petrogenetic models (Section 11.8.4)

A re-evaluation of previously published accounts of the petrogenetic evolution of the terrane has established that detailed modelling within or between suites by methods such as inverse or forward-modelling least-squares techniques are not straightforward and are of probable limited worth. Largely using least-squares techniques, Sheraton & Collerson (1984, p. 51) deduced an origin of the Mossel Gneiss and CLG through 'melting of a mafic source (? subducted hydrated oceanic crust) leaving major residual hornblende (± garnet)'. However, whilst geochemical observations made during the course of this study support the general contention that subducted oceanic crust was probably *involved* in magma genesis, it is unlikely that *direct* slab melting was the sole source of the Vestfold Hills orthogneisses.

Geochemical results and observations made during this study indicate that all the main orthogneiss suites are broadly calc-alkaline in character, and that most have similar REE and spidergram patterns. REE patterns for all the main suites are particularly distinctive, and are characterised by moderate to high LREE/HREE, with slightly convex upward LREE but slightly concave upward MREE-HREE. Incompatible-element patterns for all units are

characterised by highly enriched but variable LILE, and pronounced negative HFSE anomalies relative to LILE or REE. These common geochemical characteristics are taken in conjunction with geological observations to imply derivation in a continental-arc setting where subducted oceanic crust was involved in calc-alkaline magma genesis, but where the bulk of melting originated in the mantle above a subduction zone.

12.4 Summary and discussion of isotope studies and geochronology

12.4.1 A critique of previous Sr and Nd isotopes from the results of this study (Sections 11.6 & 11.7)

Initial attempts by Collerson *et al.* (1983) to determine the ages of the principal gneiss units in the Vestfold Hills using Sr and Nd isotopes have been shown by Black *et al.* (1991a) and this study (Chapters 10 & 11) to be in significantly in error. For example, Collerson *et al.* (1983) estimated the age of the Mossel Gneiss to be about 3200-2800 Ma based on Rb-Sr and Sm-Nd isochrons. This was apparently supported by similar ages from Sm-Nd isochrons (2923 ± 570 Ma) for combined Tryne Metavolcanics and Chelnok Paragneisses, which were interpreted by Collerson *et al.* (1983) as further confirmation that pre-D_1 gneisses and the first major tectono-thermal event formed between about 2800 - 3000 Ma. However, field observations (Chapter 8) and U-Pb zircon dating (Black *et al.*, 1991a) have established that these results are spurious and the product of combining unrelated samples.

Attempts by Collerson *et al.* (1983) to constrain the protolith age of the CLG and the timing of D_2-M_2 provided better estimates from what is now known through U-Pb zircon dating (Black *et al.*, 1991a; this study, Chapter 10). For example, Collerson *et al.* (1983) described Nd_{CHUR} model ages for the CLG of between 2462 and 2511, and calculated a 2411 ± 211 Sm-Nd isochron age from regionally-collected CLG. Collerson *et al.* (1983) also estimated the age of D_2-M_2 to be 2456 ± 163 Ma, apparently from a partially reset Rb-Sr isochron 'subset' within an overall 3200 Ma 'isochron' relationship (!). Nevertheless, on the basis of all the available data, and possibly in the belief that the CLG was emplaced syn-tectonically with D_2, they concluded that both CLG protolith formation and D_2-M_2 occurred at *ca.* 2400-2500 Ma.

In addition to their chronological data, both Collerson *et al.* (1983) and Black *et al.* (1991a) compared Rb and Sr chemistry between the CLG and Mossel Gneiss. Collerson *et al.* (1983) observed that the Mossel Gneiss has significantly lower concentrations of Rb and Sr than the CLG, and that the Mossel Gneiss also has lower Rb/Sr, even though the CLG has more

basic compositions. Collerson *et al.* (1983) also noted that a mean Rb/Sr of 0.0153 for the Mossel Gneiss is a very depleted ratio, even when compared with the strongly LILE depleted Lewisian Complex. Black *et al.* (1991a) presented Sr-isotope data for 3 of their dated samples, and also noted that their Mossel Gneiss sample ($VH26_{Black}$) has appreciably lower Rb/Sr (0.0393) than either the CLG (0.1442) or the Grace Lake Granodiorite (0.2216). Their interpretation of the chronological information presented in Collerson *et al.* (1983) is also worthy of further discussion in the light of results presented in this study (Chapters 10 & 11).

Briefly, Black *et al.* (1991a) noted that although the Rb-Sr age of 2416 ± 21 Ma produced by Collerson *et al.* (1983) is apparently precise, it is not consistent with the U-Pb zircon data. They attribute the isochron age to being an artefact of combining unrelated samples to produce a meaningless alignment of analyses. Moreover, the isochron is essentially a two point line comprised of 5 samples with $^{87}Rb/^{86}Sr$ between 0.1 - 0.19, combined with 2 values near to 2.0 (see Collerson *et al.*, 1983, figure 3c). The 5 low Rb/Sr samples are monzonitic in composition, whilst the 2 high Rb/Sr samples are granitic (D2-GS of this study). Black *et al.* (1991a) proposed that the granites may not be comagmatic and suggested that these two samples were either preferentially affected by post-crystallization processes, or that they were derived from a distinct source.

Black *et al.* (1991a) made a number of further interpretations from the recalculated initial Sr data presented in Collerson *et al.* (1983). They (Black *et al.* 1991a, p. 307) suggested that low initial $^{87}Sr/^{86}Sr$ ratios in the Mossel Gneiss 'imply that any incompatible element-enriched metasomatic fluid involved in magma generation could not have been significantly enriched in ^{87}Sr, and source enrichment could not have occurred long before the melting event'.

However, results from this study indicate that the original dating based on Sm-Nd and Rb-Sr isotopes (Collerson *et al.* 1983), and subsequent re-interpretations of the Sr-isotope data (Black *et al.*, 1991a), are all spurious. The reconnaissance Sr and Nd isotope study undertaken by Collerson *et al.* (1983), and interpretations based on Sr isotopes, can now be re-evaluated on the basis of precise U-Pb zircon geochronology and the revised geological and geochemical framework presented in this study (and Black *et al.*, 1991a). From this study, it is apparent that three main factors that have adversely influenced previous interpretations:

- ***Combining unrelated samples.*** Samples were combined together for the purposes of geochemical modelling (Sheraton & Collerson, 1984) and isochron construction (Collerson *et al.*, 1983) that were either not strictly comagmatic or are completely unrelated in space and time. The worst cases involve samples from the Tryne Metavolcanic area, where samples have been re-interpreted in this study to come from rock types that have distinctly different isotopic histories and possibly differ in age by as much as 500 Ma (see Section 9.4.1 & Figure 9.8).

- ***Metamorphic disturbance to Rb-Sr isotope system.*** The use of Rb-Sr isotopes to constrain protolith ages, and inferences about crust-formation processes or mantle reservoir characteristics based on LILE or Sr-isotopic compositions, are likely to be seriously in error. Results presented in this study indicate that closed-system Sr-isotope evolution cannot be assumed for *any* of the Vestfold Hills orthogneisses. In a further deviation from both previous isotopic studies in the terrane (*i.e.* Collerson *et al.*, 1983; Black *et al.*, 1991a), Rb/Sr for the CLG are now known to significantly overlap those reported for the Mossel Gneiss. Some of the relatively evolved (*e.g.* low ***mg***) samples studied here have lower Rb/Sr than most of the Mossel Gneisses reported by Collerson *et al.* (1983). This implies that Rb/Sr is not a good discriminant to evaluate Mossel Gneiss versus CLG parentage (*cf.* Black *et al.*, 1991a). The results of this study indicate that Rb/Sr and ε_{Sr} values reflect the degree of retrogression associated with the D_2-M_2 event, and bulk compositional and petrological controls on the behaviour of Rb during metamorphism.

- ***Assimilation of isotopically distinct crust.*** In contrast to the behaviour of Sr isotopes during D_2-M_2, measured $^{147}Sm/^{144}Nd$, $^{143}Nd/^{144}Nd$, and calculated initial $^{143}Nd/^{144}Nd$, are thought to broadly reflect the isotopic composition of the CLG protolith (similar to CHUR, $\varepsilon_{Nd} = \sim 0.6 \pm 1$ epsilon unit). This condition probably does not hold for the Pre-D_1 lithologies, which commonly have textural evidence for partial-melting during D_1-M_1. Moreover, whilst the CLG is thought to largely reflect juvenile crustal additions, small variations in ε_{Nd} are present that reflect assimilation of crustal components that had appreciably different isotopic compositions at *ca.* 2485 Ma.

In conclusion, Sr and Nd isotopes in the Vestfold Hills cannot be used to provide meaningful chronological information. Furthermore, the use of combined radiogenic isotopes to constrain protolith-forming processes is not possible because Sr-isotopes do not faithfully record protolith isotopic compositions. Combined O and Nd isotopes are also of little petrogenetic value because there is only a very small spread in isotopic composition in these systems. However, both O- and Nd-isotope ratios are consistent with the LAS, and presumably much of the CLG, being juvenile crustal additions that were derived from an undepleted mantle source. Although there is abundant textural evidence in the CLG for assimilation, O- and Nd-isotopic compositions and a broad similarity between trace-element signatures of the CLG and other gneiss suites, implies that assimilated crust was not significantly different in composition to primary CLG magmas. These observations support the contention that immobile trace-element patterns reflect source characteristics and were not inherited by assimilating distinctive felsic continental crust.

12.4.2 Further constraints on the age of orthogneisses and high-grade deformation events from U-Pb zircon geochronology (Chapter 10)

It became apparent during the course of fieldwork that additional U-Pb zircon dating was required in the Vestfold Hills to establish the age distribution of CLG orthogneisses further, and to precisely constrain the timing of D_1-M_1 and D_2-M_2. Results from 3 key samples support a number of revisions to accounts of the geological history of the Vestfold Hills made on the basis of field observations. Briefly, these revisions are:

- ***There was a temporal variability in CLG magmatism.*** Rather than one large plutonic suite or association that was subsequently tectonically repeated by D_2 folding, a number of spatially and temporally distinct intrusions are recognised. This is supported by a variety of crystallization ages and intrusive morphologies that range from km-scale plutons that were emplaced at 2501 ± 5 Ma in the south, to small-scale but widespread intrusions of syn-tectonic granite sheets at 2475.3 ± 0.7 Ma.

- ***The age of D_1-M_1 is constrained to be 2496.3 ± 0.7 Ma*** from partial-melt morphologies associated with Taynaya EMG. The age of this event was originally constrained to be *ca.* 2501 Ma from CLG and Mossel Gneiss that overlap in age at 2501 Ma.

- ***The age of D_2-M_2 is constrained to be 2475.3 ± 0.7 Ma*** from axial planar leucosomes associated with F_2 development. The age of this event was previously reported to be 2487 ± 6 Ma from combined Grace Lake Granodiorite samples in the northern Vestfold Hills.

These results have a number of implications for the geological evolution of the Vestfold Hills. A further distinct age for the LAS pluton supports field observations and geochemical evidence that F_2 folding did not tectonically repeat the CLG at regional scales greater than a few kilometres. The much more precisely determined age for D_2-M_2 (2475.3 ± 0.7 Ma) and the crystallization age for the post D_2/D_3 intermediate dyke dated by Black *et al.* (1991a) indicates that D_2 and D_3 must have occurred in rapid succession. However, a number of aspects of the geochronological history have not yet been resolved. The ages of the Chelnok and Taynaya Paragneisses, and the EMG are not yet known, and the age of the metamorphic overprint in the SW corner of the terrane remains to be determined.

12.5 A summary of the origin and evolution of the Vestfold Hills gneiss complex

The initially proposed research programme in the Vestfold Hills was described in Chapter 8 according to *specific objectives* and *wider objectives*. The two main *wider objectives* mainly concern terrane-scale comparisons and attempts to relate magmatism in the Vestfold Hills to a tectonomagmatic framework in order to contribute to an understanding of the nature and timing of terrane amalgamation in the East Antarctic Shield. These objectives are considered further in the next chapter (Chapter 13, Part 4) in conjunction with the Rauer Group Archaean domain and on the basis of the results of the *specific objectives* in the Vestfold Hills.

The main *specific objectives* in the Vestfold Hills were proposed in Chapter 8 according to a number of *currently unanswered questions*. These questions were addressed in Chapters 9 to 11, and a brief summary of the answers is presented below.

12.5.1 Previously unanswered questions and further constraints from this study

1. What was the precise timing of magmatism, metamorphism and deformation.

- D_1 occurred at 2496.3 ± 0.7 Ma.
- D_2 occurred at 2475.3 ± 0.7 Ma.
- The felsic Mossel Gneiss ranges in age from 2526 ± 6 Ma until D_1-M_1.
- The oldest CLG has been dated at 2501 ± 5 Ma. A number of younger intrusions were emplaced throughout the Vestfold Hills until D_2-M_2. Minor post-deformational dykes (*ca.* 2477 ± 5 Ma) also have geochemical signatures that place them with the CLG magmatic episode.

2. How much tectonic repetition is there in the gneiss complex and was there a temporal evolution in CLG magmatism

- Tectonic repetition is constrained to be local at scales of no more than 1-2 km, rather than regional at scales of 10-20 km as previously supposed (*e.g.* Collerson *et al.*, 1983).
- F_2 folds have wavelengths of about 500 m or less and are not greater than km scales as previously inferred (*e.g.* Collerson *et al.*, 1983).

- There was a temporal evolution in CLG magmatism but it was probably not a straightforward south to north progression as tentatively proposed by Black *et al.* (1991a)

- D_1-M_1 punctuated magmatic activity in the Vestfold Hills with subsequent CLG activity initially dominated by mafic and intermediate plutonism before reverting back towards more felsic compositions culminating in syn-deformational granite magmatism during D_2-M_2. The CLG granites, granodiorites and tonalites are not observed to be cross-cut by the mafic to intermediate compositions, whereas the felsic compositions commonly cross-cut the more massive mafic intrusions.

3. What is the status and regional distribution of gneiss lithologies?

- The Tryne Metavolcanics unit of Collerson *et al.* (1983) has been abandoned, and an additional non-genetic unit is proposed in this study to account for some of the Early Mafic Gneiss (EMG) components in the Tryne Crossing area.

- The Mossel Gneiss is found to be of lesser extent in the northern region than previously supposed; and the dominant lithology in the north is the CLG.

- The term 'Grace Lake Granodiorite' is retained but is restricted the migmatitic variety as seen at the type area; homogeneous granodiorites previously grouped with this unit are considered to be distinct CLG intrusions.

4. Is it possible to identify the geochemically-defined CLG groups of Sheraton & Collerson (1984) based on field criteria?

- Most of the *members* of the 'Monzonite' and 'Monzodiorite' suites are identifiable in the field, but geological observations and geochemical and isotopic results suggests that the *suites* are not strictly comagmatic associations.

- Geochemically-defined suites have been abandoned in this study in favour of field-defined suites or lithological associations.

5. Were all the ca. 2500 Ma orthogneiss suites produced by a common tectonomagmatic process?

- In detail there is a great deal of geochemical diversity within the orthogneiss suites which is attributed to variations in the extent of partial melting and nature of fractional crystallization/accumulation processes.

- Nevertheless, there are sufficient geochemical commonalities to indicate that *most* of the Taynaya EMG, Mossel Gneiss and CLG were ultimately derived in a continental arc setting.

- Direct partial melting of subducted hydrated oceanic crust (MORB) as previously proposed is *not* considered to be the main source of gneiss protolith, although slab-derived components, possibly transported by fluids released from the slab, are implicated.

6. Was there a significant metamorphic or tectonic history prior to the ca. 2500 Ma events?

- There is tentative evidence for a tectonothermal history prior to D_1-M_1 although the status of the 'event' has not yet been resolved.

- The *ca.* 2800-3000 Ma crust originally reported by Collerson *et al.* (1983) has not been found *in situ*, and such ages are now known to be spurious. It seems likely that most of the Vestfold Hills orthogneisses intruded at about 2500 Ma, as noted by Black *et al.* (1991a).

- However, the Chelnok Paragneiss and EMG have yet to be dated, and protolith of *ca.* 2800 Ma age is known to have been beneath the Vestfold Hills at 2500 Ma on the basis of inherited zircons (Black *et al.*, 1991a; this study, Chapter 10).

12.5.2 Summary of the geological evolution of the Vestfold Hills

An summary of the Archaean - early Proterozoic geological evolution of the Vestfold Hills has been compiled on a schematic figure (Figure 9.27*), which is included in the pocket at the back of the thesis. The *wider implications* and *suggestions for further research* in the Vestfold Hills is discussed in the next chapter (Chapter 13).

Chapter 13

Discussion, conclusions and wider context

13.1 Introduction: discussion, conclusions and wider context

A summary of the main results and conclusions for the Vestfold Hills and Rauer Group Archaean terranes is presented in Chapters 7 & 12. In this chapter I discuss the data further in the context of *terrane accretion in East Prydz Bay* and *Archaean magmatism and the growth of continental crust*, and also highlight some of the *implications for geochemical and isotopic studies in high-grade terranes*. The following part of this chapter is *an appraisal of the scientific approach adopted in this study*, and the concluding section provides an outline of *suggestions for further research* in the region.

13.2 Magmatism, crustal accretion and terrane assembly in East Prydz Bay

13.2.1 Refined Archaean geological histories in East Prydz Bay

Archaean geological histories for the Vestfold Hills and Rauer Group have been established from detailed field observations combined with analysis of geochemical and isotopic data. The results are summarized in Table 13.1. Both terranes have protracted geological event sequences, and as with most ancient high-grade terranes, our knowledge of the earliest geological history is largely fragmentary. The jigsaw pieces in Table 13.1 cannot be accurately placed in the event sequences, but are placed nearest to their probable age.

13.2.2 Magmatism in the Rauer Group

The early geological and geochemical development of the Rauer Group Archaean domain was dominated by felsic magmatism of tonalite-trondhjemite-granite (TTG) affinity. These gneisses are potentially as old as 3470 Ma based on the presence of inherited zircons in younger gneiss suites (Section 6.3). From a limited geochemical dataset (Harley *et al.*, 1992), and largely by analogy with more extensively studied TTG suites (*e.g.* Martin, 1986, 1987, 1994; McCulloch, 1993), these rocks are thought to have been produced by partial melting of hornblende eclogite or garnet amphibolite at P >16 kbar, possibly corresponding to ancient subducted oceanic crust (*e.g.* Martin, 1994).

RAUER GROUP				VESTFOLD HILLS	
Age & evidence	**This study + compilation**		**Sims *et al.* (1994)**	**This study + compilation**	**Age & evidence**
3470-3269 (direct zircon dating of protoliths) >2844 (Inherited zircons in SLC)	TTLC / Mather Paragneiss	Composite Layered Orthogneiss (CLO) Magmatism			
2844 (direct zircon dating of protoliths)		SLC Magmatism			
2844 (post-dates SLC) to *ca.* **2800** (pre-dates TG sheets)	UHT Metamorphism	Early Deformation (D1) Mafic Dyke Intrusion (MD1) Deformation (D2) Mafic Dyke Intrusion (MD2) Regional Deformation (D3)		Unexposed crust / Taynaya Paragneiss / Chelnok Paragneiss / EMG	*ca.* **2800** (inherited zircons)
2800 (direct zircon dating of protoliths)		Felsic Magmatism (TG)			
2800 (post-dates TG) to 1000 (pre-1000 Ma structures and felsic intrusions)		Deformation (D4)	D1?	Felsic Magmatism (Mossel Gneiss)	**2526-2501** (direct zircon dating of protoliths)
				Regional Deformation (D1-M1)	**2496** (direct zircon dating of leucosomes)
				Mafic-Intermediate-Felsic Magmatism (CLG)	**2496-2475** (direct zircon dating of protoliths)
		Partial melting of TG (TrG)	D2?	Second Regional Deformation D2-M2	**2475** (direct zircon dating of leucosomes)
		Regional deformation (D5)		Regional Warping (D3) Pegmatites Shear Zones First Post-D3 Mafic Dyke Intrusion	*ca.* **2475** (constrained by direct zircon dating of **2477** ± 5 Ma post-D3 dyke)
			Dyke 1 Dyke 2	High-Mg dykes (?) Fe-rich Tholeiite Dykes (?)	Interval 2477-2240
			Dyke 3 Fe-rich D3 mylonite	High-Mg Norite Complex Group 1? Fe-rich Tholeiite Dykes (Low-Ti and Plag megacrystic subgroups?)	**2240** (direct zircon dating of late-stage melts)
			D4 Pegmatite 4 Dyke 4 high-Mg	Group 2 Fe-rich Tholeiite Dykes	**1754** (direct zircon dating of late-stage melts)
	Filla Paragneiss	Mafic dykes (MD3)	Dyke 5 Fe-rich Dyke 6 high-Mg D5 Dyke 7 Dyke 8 Dyke 9	Mylonites Pseudotachylite Mylonite Lamprophyre Dykes	Interval 1754-1380
				Group 3 Fe-rich Tholeiite Dykes	**1380** (direct zircon dating of late-stage melts)
			Dyke 10 Dyke 11	Lamprophyre Dykes Mylonites	Interval 1380-1241
				Group 4 Fe-rich Tholeiite Dykes	**1241** (direct zircon dating of late-stage melts)
		Regional deformation (D6)	Regional deformation (D6)		*ca.***1000 ?** (single zircon rim)
ca. **1000** (correlation with orthogneiss protolith dated by U-Pb zircons)		Mafic dyke suites (MD4)	Dyke 12		
		Felsic Magmatism and partial melting	Dyke 13 Fe-rich Dyke 14 high-Mg		
		Regional deformation (D7)	Regional Deformation (D7) Pegmatite 2	Garnet overprint SW Vestfold Hills	
510 metamorphic zircons **500** igneous zircons in sheared pegmatite		Rehydration and regional deformation (D8)	Pegmatite 4 D9 D10 D11 Dyke 15 Lamprophyre		*ca.* **500** (unpublished Rb-Sr mineral isochron)

Table 13.1 A summary of the geological histories for the Rauer Group and Vestfold Hills. Data compiled from this study, Collerson et al. (1983); Harley et al. (1987); Seitz (1991); Kinny et al. (1993); Lanyon et al. (1993); Dirks et al. (1993, 1994).

Mafic magmatism also played an important part in the evolution of the terrane. Two relict mafic magmatic centres are recognized in the Archaean domain (SLC and TTLC) that are unrelated to each other spatially, genetically and probably temporally. Cross-cutting relations confirm that the TTLC is at least 2800 m.y. old (Chapter 3), and whilst the complex has not yet been dated directly, it is possibly the oldest of the two suites. Incompatible-element patterns for the TTLC and the oldest TTG are sufficiently similar to speculate that there may be a genetic link, which implies that the TTLC may have formed in the interval 3270-3470 Ma (Section 6.3). Most importantly, a *tentative* petrogenetic model has been proposed in this study that accounts for pronounced negative HFSE anomalies (HFSE/HFSE*) in the TTLC by a mechanism that is similar to those thought to have resulted in modern boninite magmas. Although a direct comparison between the TTLC and boninites cannot be made, because the TTLC is a layered cumulate intrusion, crystal accumulations or cumulate processes cannot readily account for the trace-element characteristics of the complex. Moreover, the distinctive geochemical patterns cannot be explained by bulk assimilation of felsic crust or crustal metasomatism, hence, a primary source with negative HFSE anomalies is envisaged (Chapters 5 & 7). The most likely scenario for such a source is above a subduction zone where depleted mantle has been subsequently enriched in relatively soluble elements that were ultimately derived from subducted oceanic crust. *If* this model is correct, the origin of the TTLC is markedly different to that proposed for the SLC.

The SLC is known to have intruded into Composite Layered Orthogneiss (mostly TTG compositions) at about 2840 Ma. Petrological evidence implies that the complex may have intruded and crystallized at deep to mid-crustal levels (Chapter 4). The incompatible-element geochemical patterns of this complex are best explained by an origin related to rifting in a tectonomagmatic setting analogous to the early Tertiary East Greenland margin. Minor similarities between the SLC and arc-like rocks can be explained by modest amounts of bulk crustal contamination, although for the most part, the complex is similar to differentiated Fe-tholeiite intrusions in East Greenland (Chapter 7).

The final phase of magmatism in the Rauer Group was dominated by small-scale felsic and mafic intrusions (sheets and dykes). The felsic sheets are predominantly of tonalitic composition (*ca.* 2800 Ma TG) and probably formed by migmatisation of Composite Layered Orthogneiss material from within the Archaean domain. Intrusion of tholeiitic mafic dykes that have enriched to transitional chemistry may have promoted such partial melting in the interval 2840-2800 Ma, although there is no direct evidence for such a link. It is also possible that the dykes are related to the same rifting event that has been proposed

for the origin of the SLC, although tholeiitic compositions that are more N-MORB-like may reflect a rift-to-drift transition at about this time (Chapter 7).

13.2.3 Magmatism in the Vestfold Hills

The main phase of magmatic activity in the Vestfold Hills occurred during a short 50 m.y. time period that spans the Archaean-Proterozoic boundary. The timing and petrogenetic origin of the Vestfold Hills orthogneisses are distinctly different from those in the adjacent Rauer Group, and are broadly calc-alkaline in character (Chapter 11). Most orthogneisses in the Vestfold Hills also have incompatible-element patterns that are similar to modern day calc-alkaline magmas that are associated with continental volcanic-arc settings. By analogy with better preserved and more thoroughly studied modern analogues, magma genesis is largely attributed to melting that originated in metasomatically enriched mantle above a subduction zone, probably in a continental setting (Chapters 11 & 12).

During the final stages of calc-alkaline magmatism, minor tholeiitic mafic dykes were also emplaced. It is likely that these were related to Proterozoic mafic dyke swarms that intermittently intruded into the Vestfold Hills crust for a period spanning almost 1.5 b.y. A *speculative* model is presented below that proposes a causative link between the Proterozoic dyking events, their distinctive but highly varied chemistry, and events at 2500 Ma.

However, it should be emphasised that many aspects of the tectonomagmatic models described in this and the previous sections are tentative and require a great deal of further study (discussed further below).

13.2.4 Timing of terrane assembly in East Prydz Bay

Geochronological evidence against direct Archaean links

Although early models assumed that the Archaean rocks in the Rauer Group correlate directly with those in the Vestfold Hills (*e.g.* Sheraton & Collerson, 1983; Sheraton *et al.*, 1984), observations made during the course of this study highlight the considerable differences between the two terranes. Detailed mapping of intrusive relations in the Vestfold Hills and Rauer Group (*e.g.* Chapters 3 & 9), combined with metamorphic (*e.g.* Harley Snape & Black, 1995), geochemical (*e.g.* Chapter 5, 7 & 11), and isotopic studies (*e.g.* Chapters 6, 10 & 11), does not support models that advocate Proterozoic reworking of Vestfold Hills-type Archaean crust in the Rauer Group, or a shared geological history from the end-Archaean (*cf.* Sims *et al.*, 1994). Event sequences that have been established for the

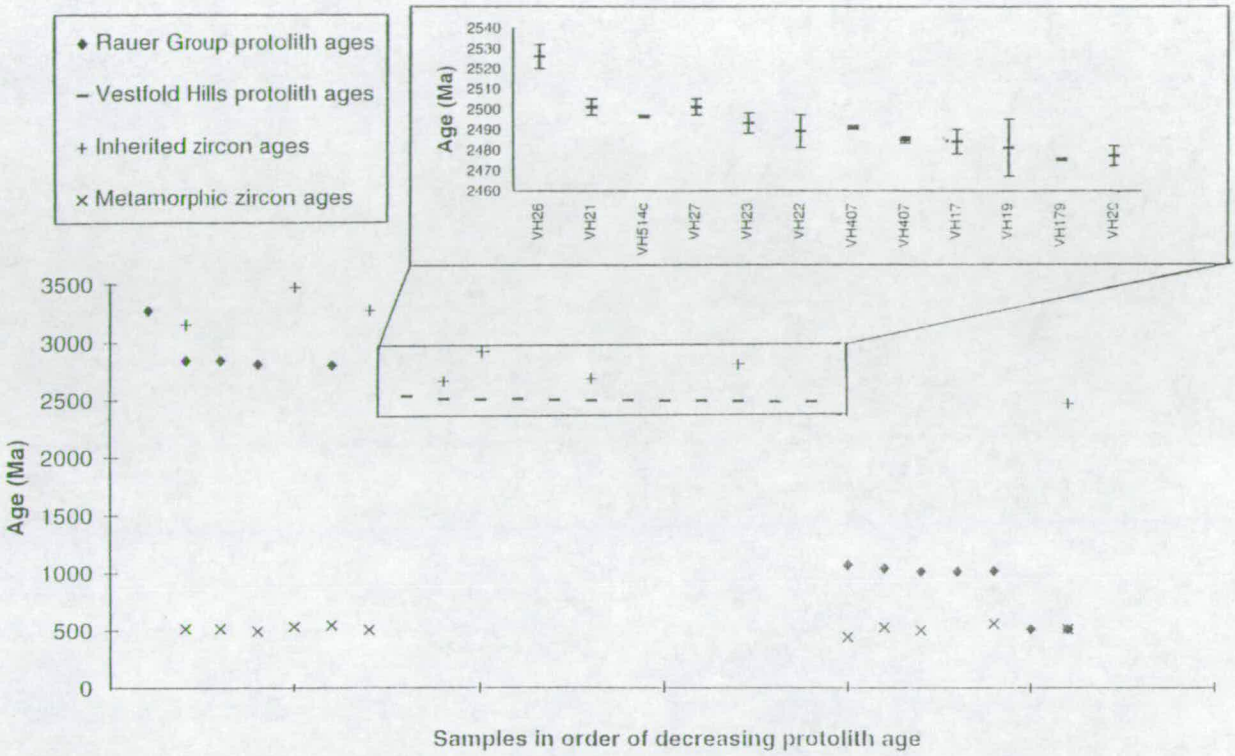

Figure 13.1 Distribution of zircon data for Archaean gneisses in East Prydz Bay (compiled from Black *et al.*, 1991a; Kinny *et al.*, 1993; this study, Chapter 10).

Vestfold Hills and Rauer Group (summarized in Table 13.1) clearly illustrate the differences between the two adjacent regions. This is also highlighted by a detailed comparison of all the U-Pb zircon data for East Prydz Bay, which shows that the distribution of zircon ages for the two regions, given their close proximity, is remarkably different (Figure 13.1).

Despite the detailed geological histories established for the Vestfold Hills and Rauer Group during the course of this study, terrane and event correlations within the East Prydz Bay region are still not completely resolved. It is apparent from Figure 13.1 that the Vestfold Hills crust accreted, and was metamorphosed and deformed, in a narrow 50 m.y. time window spanning the Archaean-Proterozoic boundary (Black *et al.*, 1991a; this study, Chapter 10). In contrast, the Rauer Group had a much more dynamic geological history, with crust-forming episodes at ~3270, ~2800, ~1000 and ~500 Ma (Kinny *et al.*, 1993; this study, Chapter 6). Although there are pre- *ca.* 2500 Ma zircons in some Vestfold Hills lithologies, their significance remains unclear. Inherited zircon components in VH541c (see

Chapter 10), and the samples studies by Black *et al.* (1991a, 1991b), indicate that older crustal components were assimilated by end-Archaean mantle-derived orthogneiss protoliths (see Chapters 11 & 12). Although no simple age population has yet been obtained for these older source components, at least some have minimum ages of 2800-2900 Ma. Whether this corresponds to events of similar age elsewhere, particularly the adjacent Rauer Group, remains speculative at present.

In addition to the contrasting protolith ages in the two terranes, there are further important geological differences. For example, it is clear from field relations that there are no vestiges of the Rauer Group Archaean domain in the Vestfold Hills. Similarly, the Rauer Group does not contain Vestfold Hills-type crust, whereas Vestfold Hills-type crust occurs for 50 km northwards along the Prydz Bay coast (from the southern Vestfold Hills to Murphy Rocks). Moreover, *all* lithologies in the Rauer Group were affected by events at *ca.* 1000 and 500 Ma, features that are not immediately apparent in the zircon data from the Vestfold Hills (see Figure 13.1), although other mineral chronometers in the Vestfold Hills terrane do record an event at 500 Ma (unpublished AGSO data, LP Black, pers. comm., 1996; discussed further below).

Notwithstanding the deficiencies noted above, the speculative tectonic model presented in Chapter 12 for the Vestfold Hills advocates that a major tectonic lineament between the 'Rauer Group' and the Vestfold Hills was established by 2475 Ma. Such a model would be consistent with the two terranes having a shared Proterozoic history, as proposed largely on the basis of one-to-one mafic dyke correlations between dykes that are deformed and metamorphosed in the Rauer Group but that are essentially pristine in the Vestfold Hills (*e.g.* Collerson & Sheraton, 1986b; Dirks *et al.*, 1993b; Sims *et al.*, 1994). However, such correlations are not straightforward because dykes cannot be directly traced from the Vestfold Hills into the Rauer Group as the Sørsdal Glacier obscures all bedrock exposure for an across-strike distance of about 15 km.

Problems with one-to-one dyke correlations between the Rauer Group and Vestfold Hills

Although the proposition that mafic dyke generations in the Rauer Group match one-to-one with those in the Vestfold Hills is a logical and attractive model (*e.g.* Collerson & Sheraton, 1986b; Sims *et al.*, 1994), there is currently no petrological, geochemical or isotopic evidence to support a direct correlation between *any* dykes. Unfortunately, none of the tholeiites in either terrane are sufficiently distinctive or well-characterized to allow an

unequivocal link to be established with any confidence. Nevertheless, Sims *et al.* (1994) argued that their geochemical data from the Rauer Group does match well with those described from the Vestfold Hills. However, there are problems associated with their model. For example, although they attributed the absence of Vestfold Hills-like lamprophyres in the Rauer Group to preferential loss of LILE during high-grade metamorphism, leaving what are now essentially tholeiite compositions for these 'missing' dykes, their geochemical arguments remain unconvincing (*e.g.* 'correlations' between #Mg and Cr + Ni; see Sims *et al.*, 1994, figure 7). Further problems with the one-to-one dyke correlation model are also apparent from field observations made during the course of this study. Specific problems include:

- Mafic dykes (MD1 and MD2) that are contained within the SLC cannot correlate with the Proterozoic dykes in the Vestfold Hills because they predate the *ca.* 2800 intrusive tonalite.

- The last 3 mafic dyke generations reported in the Rauer Group cross-cut Proterozoic gneisses dated at 1040-1000 Ma and therefore cannot correlate with any of the dykes that have been dated in the Vestfold Hills (the youngest is 1240 Ma; Lanyon *et al.*, 1993).

- Deformed intermediate mafic dykes of calc-alkaline character and that are of *ca.* 2500 Ma age in the Vestfold Hills have not been found in the Rauer Group. Similarly, the extensive *ca.* 2240 Ma Norite Complex (Seitz, 1991; Lanyon *et al.*, 1993) appears to be confined to the Vestfold Hills.

In conclusion, whilst there are Fe- and Mg-tholeiites in both the Rauer Group and the Vestfold Hills (and most other Archaean cratons, *e.g.* Hall & Hughes, 1993), there are dykes in the Rauer Group that *do not* correlate with those in the Vestfold Hills, and vice versa. Hence, the presence of mafic dykes in both terranes cannot be cited as evidence that the terranes were juxtaposed throughout the Proterozoic.

Problems with structural correlations

The concentration of reworked Archaean material in the eastern Rauer Group (*e.g.* Kinny *et al.*, 1993), led Dirks *et al.* (1993b) to correlate the apparent N-S age boundary with the orientation of Proterozoic compressional and extensional structures observed in the Vestfold Hills. However, as Figure 2.1 illustrates, Archaean and Proterozoic crust in the Rauer Group is intimately interleaved and the protolith age-boundary is difficult to define because it reflects the *ca.* 1000 Ma ductile deformation event.

Vestfold Hills - Rauer Group terrane juxtaposition at ca. 1000 or 500 Ma?

Metamorphic and structural reworking in the SW Vestfold Hills has previously been correlated with *ca.* 1050 - 1000 Ma events in the adjacent Rauer Group (Black *et al.*, 1991b; Passchier *et al.*, 1991), and may have been associated with burial or loading of the Vestfold Hills to 6-7 kbar, possibly by overthrusting from the south (*e.g.* Sheraton *et al.*, 1983; Passchier *et al.*, 1991). The development of garnet-bearing amphibolite-facies assemblages in partially hydrated mafic dykes in the SW Vestfold Hills (*e.g.* Sheraton & Collerson, 1983; see also Chapters 8 & 9) was related to fluid access along shear zones (this study). Although this overprint has been ascribed an age of 1050-1000 Ma, it has not yet been dated directly. Moreover, a *ca.* 500 Ma Rb-Sr mineral isochron (unpublished AGSO data; LP Black pers. comm., 1996), implies a Pan-African age. To conclude therefore, the timing of terrane amalgamation between the Vestfold Hills and Rauer Group remains open.

Correlations in the East Antarctic Shield or elsewhere?

Detailed event sequences have now been established for the Rauer Group and Vestfold Hills that provide a framework for interpreting metamorphic textures and thermobarometry, and geochemical and isotopic studies. This integrated approach offers the best possibility for comparisons between distant regions. However, similar or directly comparable accounts with the same chronology of magmatic events have not been described from elsewhere in Antarctica, or in continents that were juxtaposed in Gondwana reconstructions (*e.g.* Dalziel, 1991; 1992; *cf.* also Yoshida & Santosh, 1995, and references therein; Harley pers. comm., 1997).

Nevertheless, it is apparent that evidence for a number of major events of regional and global extent are preserved in the Vestfold Hills and Rauer Group terranes. The Grenvillian and Pan-African events as seen in the Rauer Group are perhaps the most immediately recognizable episodes in the region, although as noted by Rogers *et al.* (1995) and Davidson (1995), these events are recorded in North America, India, Australia, and throughout the East Antarctic Shield. Unlike some other areas in the East Antarctic Shield, such as the Bunger Hills - Windmill Islands areas (*e.g.* Sheraton *et al.*, 1993), direct correlations to adjacent continents are not straightforward. For the Vestfold Hills, the most promising area for a direct Gondwana correlation would be the Singhbhum Craton of India (*cf.* Collerson & Sheraton, 1986b; Tani & Yoshida, 1995), although this area is known to be a granite-greenstone terrane, and whether any *ca.* 2500 Ma crust is present, remains to be seen.

Somewhat surprisingly, the nearest parallel geological history to either the Rauer Group or the Vestfold Hills is the Napier Complex of Enderby Land. Although a detailed geochemical comparison of protolith types between these areas is not currently possible, a tantalising geochronological history is emerging from the Napier Complex. Harley & Black (1997) have established protolith-formation ages of 3840-3770, 2980 and 2840-2820 Ma for the Napier Complex, with the 2840-2820 Ma age corresponding to the well-known ultra-high temperature metamorphic event in the area (*e.g.* Harley & Hensen, 1990). This was followed by lower-temperature granulite and upper amphibolite-facies metamorphism and deformation at 2480-2450 Ma. The similarity in the ages and events with those now recorded in the Rauer Group and Vestfold Hills is uncanny, although perhaps somewhat paradoxical, given that the Rauer Group and Vestfold Hills appear to have such different histories in detail!

13.3 Wider implications

13.3.1 Archaean magmatism and the growth of continental crust

Secular evolution of magmatism: the Archaean-Proterozoic boundary, komatiites, norites and boninites

It is commonly perceived that there has been a secular change in the general composition of mafic and felsic magmatism on Earth, and although the Archaean-Proterozoic boundary is not thought to be marked by a common contemporaneous event, it is considered to reflect fundamental changes in magmatic regime at about 2500 Ma (Hall & Hughes, 1993). Windley (1993, p.9) suggested that there were 'no significant orogens from 2.5 to 2.1 Ga (a supercontinent?)'. It is interesting to speculate that such a hiatus of orogenic activity may be considered less likely if the Vestfold Hills marks the tip or remains of a major 2.5 Ga accretionary orogen that extends under the ice cap or into currently unexplored territory in India for several thousand kilometres (*cf.* Collerson & Sheraton, 1986a). In this respect there may be some support for the contention made by Kröner (1991) that this event-gap is an artefact due to insufficient data or poor preservation. Regardless of such speculative models, there clearly are differences in the distribution of magmatic rocks in the modern and ancient rock record.

Perhaps the most striking difference is the prevalence of TTG suites in the Archaean, where their mode of origin is often linked to differences in the thermal regime of subduction zones (*e.g.* Martin, 1986, 1994; Windley, 1993, 1995). However, there were also important changes in the abundance and compositions of mafic magma types with time. In particular,

there may have been a gradual transition from komatiites, through siliceous high-Mg norites, to boninites; a trend that Hall & Hughes (1987; 1993) argued reflects a decrease in the Earth's heat production. Although few would dispute the link between the observation that most komatiites are of Archaean age and that there was higher heat production in the Archaean (*e.g.* Bickle, 1986), the nature of the transition in mafic magmatism is the subject of considerable debate (*e.g.* Windley, 1995).

Hall & Hughes (1993) advocated that norite magmatism helps define a petrogenetic break between the Archaean and the Proterozoic; other authors question if there is any real justification for a boundary at all (see references in Windley, 1995). Nonetheless, one of the key questions in Precambrian geology concerns the extent to which norites and boninites are related to komatiites by variations in the degree of partial melting, crystal fractionation, crystal accumulation or crustal contamination. Although Hall & Hughes (1987; 1993) confidently stated that 'there would seem to be no justification whatever' for the hypothesis that siliceous high-Mg basalts (norites) can be derived from komatiites by contamination, others would disagree (*e.g.* Sun *et al.,* 1989; Seitz & Keays, 1997). This debate (*e.g.* Hall & Hughes, 1990; 1993; Seitz & Keays, 1997) is potentially relevant to the origin of the siliceous high-Mg TTLC in the Rauer Group, and may also have an indirect bearing on the origin of the Norite Complex in the Vestfold Hills and the evolution of the Vestfold Hills during the Proterozoic.

At present, the origin of siliceous high-Mg basalts is attributed to two broad models: either they were highly contaminated komatiite-derived melts, or they were produced through an origin that was related in some way to boninites. To further explore this discussion, and because recent and potentially relevant work on the Norite Complex in the Vestfold Hills has concluded in favour of a komatiite link (Seitz & Keays, 1997), it is worth considering the origin of the Norite Complex further.

Seitz & Keays (1997) noted that the Vestfold Hills Norite Complex has Pd values that are similar to many siliceous high-Mg basalts (~16 ppb), but that such values are appreciably higher than those found in komatiites. Seitz & Keays (1997, p.722) stated that 'if siliceous high-Mg basalts are contaminated komatiites, as suggested by Sun *et al.* (1989), an explanation needs to be found for the higher Pd contents of siliceous high-Mg basalts relative to the komatiites'. They attributed this important discrepancy to AFC processes (14% A and 35% FC): 'given that komatiitic magmas contain approximately 10 ppb Pd, 35 % fractional crystallization would increase the Pd content of the residual melt to 13.5 ppb, assuming that no Pd was lost to the fractionating crystals. As the assimilated crust would

also have contained some Pd (perhaps 0.5 ppb), it is clear that the Pd contents of the siliceous high-Mg basalts could have been produced by AFC acting on komatiitic magmas'. However, there are a number of important problems with this model. The first concerns the nature of the assimilant, as it is apparent from Sheraton & Collerson (1984) and this study that assimilation of average or almost any Vestfold Hills crust would not produce the high Rb/Ba reported by Seitz & Keays (1997) for the Norite Complex (see their figure 4). The second problem concerns Ir and Pd abundances as calculated for the assimilation model. Seitz & Keays (1997) incorrectly assumed that assimilation of crust would *increase* Pd, when in fact, it would *decrease* (largely by dilution) if 14 % felsic crust was added to a komatiitic melt. The discrepancy from this model leaves ~ 40% excess Pd in the Norite that cannot be explained by AFC alone. The mass balance for Ir is even worse. Assuming an 'average' komatiite composition of ~1.2 ppb (Seitz & Keays, 1997, table 7), and virtually no Ir in the crust (~ 0.1 - 0.01 ppb), a minimum of ~ 40 % crustal contamination would be required to produce Ir values of about 0.34 ppb, the value suggested by Seitz & Keays (1997) as an 'average' for the Norite Complex and other siliceous high-Mg basalts. If there was 40 % crustal contamination, Pd concentrations would be even lower (~7 ppb) and the complex would have abundant felsic xenoliths (which it does not).

If Seitz & Keays (1997) are mistaken in their final conclusions regarding the origin of the Norite Complex, then the most likely alternative model is similar to that advocated by Hall & Hughes (1993 p.631) to account for the geochemistry of Proterozoic norites. They suggest that 'it was the sub-continental lithospheric mantle, previously depleted from the production of immense volumes of Archaean mafic komatiitic - tholeiitic suites, that was contaminated and replenished by hydrous partial melts from subducted crust .... and (which) then partially melted to give rise to noritic intrusions. In this respect, there is an analogy between the formation of these magnesian, siliceous, LILE- and LREE-rich mafic magmas, and those which formed boninite suites more recently (Crawford, 1989)'.

This petrogenetic model is loosely related to that envisaged for the TTLC (Chapter 7), and is essentially the same as that advocated by Collerson & Sheraton (1986) to explain the origin of the Proterozoic Fe- and Mg-tholeiite dykes in the Vestfold Hills. Collerson & Sheraton (1986) attributed intersuite geochemical variations in these dykes to a heterogeneous, metasomatised, sub-continental lithospheric mantle. Since the most likely mechanism for the generation of such a mantle reservoir is by subduction (*e.g.* Pearce, 1983), it is possible that there was a causative link between events at 2.5 Ga, and the tholeiitic dyke magmatism that continued sporadically for the following 1.5 b.y (*cf.* Hoek &

Seitz, 1995). The key question that remains is, why was there such a protracted event sequence in the Vestfold Hills between 2.5 Ga until at least 1. Ga?

A tentative model for the Proterozoic evolution of the Vestfold Hills

The Vestfold Hills is probably *the* most intensively studied dyke terrane in the world (*e.g.* Harding & McLeod, 1967; Sheraton & Black, 1981; Collerson & Sheraton, 1986b; Sheraton *et al.*, 1987; Kuehner, 1987, 1992; Black *et al.*, 1991b; Passchier *et al.*, 1990, 1991; Kuehner & Green, 1991; Seitz, 1991, 1993, 1994; Lanyon *et al.*, 1993; Hoek, 1991, 1995; Dirks *et al.*, 1994; Harley & Christy, 1995; Hoek & Seitz, 1995; Seitz & Keays, 1997), and a relatively clear Proterozoic event sequence has been defined that consists of localized mylonite, ultramylonite and pseudotachylite development punctuated by multiple dyke emplacement. The most important omission from most of these studies, however, is a unifying tectonomagmatic model that can account for the juxtaposition of compressional and extension structures, and explain why there was repeated dyke emplacement and reactivation of the terrane for 1.5 b.y. (the only exception being Hoek & Seitz, 1995).

It is possible that the answer lies in events that were initiated at 2.5 Ga. The down-going slab associated with the proposed 2.5 Ga continental volcanic arc could have produced a suitable, enriched, sub-continental lithospheric mantle source for the dykes (including the Norite Complex; *cf.* Collerson & Sheraton, 1986b). Similarly, the mechanism for repeatedly tapping this source, as expressed in the many different dyke suites, may also have been related to events initiated at this time. One of the conclusions from this study is that the southern margin of the Vestfold Hills represents a major tectonic boundary that was possibly initiated at 2475 Ma. Dirks *et al.* (1994) observed that localized mylonites, ultramylonites and pseudotachylites are more pervasively developed in the southern Vestfold Hills, and that structures developed and were reactivated at sporadic times throughout the period 2474 to *ca.* 1000 Ma or younger. I would suggest that all these observations can be explained by long-lived but sporadic movement on an major terrane boundary that resulted in regions or periods of transpression and transtension. Such boundaries are well-established from more recent plate reconstructions (Harland *et al.*, 1989; Twiss & Moores, 1992;), and are an integral part of the theory of suspect terranes (Howell, 1989). Such a scenario would explain the close spatial and temporal link between compressive and extensional structures (*e.g.* Passchier *et al.*, 1990, 1991; Dirks *et al.*, 1994) with the dykes emplaced passively in regions of extension. It would also explain the apparently discordance in the event sequences between the Vestfold Hills and allochthonous Rauer Group, and would also provide a simple tectonic model for the *P, T, t* path that has

been deduced for the Vestfold Hills during the Proterozoic (see Figure 9.27). In simplistic terms, periods of transpression would have distributed a shear component on either side of the terrane boundary (*cf.* Twiss & Moores, 1992), resulting in a close and sometimes progressive rotation of extensional structures (dykes) roughly oriented at >45° to the strike-slip boundary (*cf.* Dirks *et al.* 1994). During periods or regions of extensive transtension, crustal thinning, basin formation and more extensive dyke emplacement may have been possible. This would have been followed by sedimentation, burial, and ultimately crustal thickening, which may explain why the Vestfold Hills crust experienced repeated shallow- and deep-level metamorphic episodes (see Figure 9.27). In some respects this model is similar to that advocated by Hoek & Seitz (1995), the main difference being the underlying mechanism. They argued in favour of mantle melting episodes controlling dyke emplacement, whereas I would speculate that magma generation occurred passively in response to tectonism. This type of situation has been demonstrated in many small basins associated with the opening of the NE Atlantic.

Clearly, this model is a speculative interpretation of the available geological and geochemical data. As with many terrane-scale problems in East Antarctica, it is very difficult to guess the picture when there is only one small piece of the jigsaw left uncovered by ice.

Problems of dealing with Precambrian high-grade terranes

It is generally accepted that applying empirical discriminatory geochemical parameters derived from modern suites to increasingly ancient terranes is of dubious value (Pearce *et al.*, 1984; Hall & Hughes, 1993). Finding a viable alternative to such a uniformitarian approach, however, is not a trivial task. Moreover, the problems are not simply philosophical ones that concern the possibility that different processes may have operated in the Archaean, since *all* the direct evidence of the Earth's early history is contained in high-grade terranes that have experienced several metamorphic and deformation events (Nutman *et al.*, 1993).

The role of deformation has obviously had a major affect on the ease with which interpretations can be made in high-grade terranes. In some areas, progressive transposition has been documented which indicates that large tracts of 'layered gneisses' actually comprise protoliths that are markedly different in age and origin (*cf.* Fiskenaesset Complex, Ashwal & Myers, 1994; this study, Chapter 9). Similarly, many (if not most) recent studies of protolith-forming processes in Precambrian high-grade terranes have assumed that

metamorphism occurred largely isochemically, and that many isotopic parameters, especially Nd-isotope ratios, retain a record of their protolith-forming processes. However, one of the most important conclusions from this study is that geochemical and isotopic parameters can be *selectively* disturbed during metamorphism with little obvious change to bulk compositions, mineralogy or texture (discussed further below). It is apparent from the geochemical and isotopic evidence presented here, that much work remains to be done to understand the causes and possible consequences of metasomatism and isotopic perturbation during metamorphism. In particular, the perception that Nd isotopes are something of a panacea for all Archaean high-grade terrane problems needs to be critically re-assessed.

13.3.2 Constraints on the behaviour of trace elements and radiogenic isotopes during metamorphism

The importance of fluids and time

In a general context, isochemical metamorphism is an essential pre-requisite if the magmatic processes that were involved in protolith formation in the East Antarctic Shield, or elsewhere, are to be understood. This is often *assumed* for a wide range of elements in metamorphic rocks that experienced diverse *P, T, t,* and fluid-infiltration histories, but a number of secondary processes are capable of significantly altering the chemical composition of igneous rocks during metamorphism (summarized in Figure 13.2). These processes operate on a variety of scales that range from inter-mineral chemical exchange to regional-scale metasomatism (see Oliver, 1996). In practice many of these processes can be readily identified or accounted for; For instance, the influence of tectonic mixing and partial melting can often be discerned from field relations, and any chemical changes attributed to solid diffusion are likely to be restricted to mineral- or handspecimen-scales for most elements. By far the most important processes involved in open-system chemical and isotopic behaviour concern the role and timing of fluid infiltration. This is because fluids are capable of dissolving, transporting, and exchanging elements by advection, and to a lesser extent diffusion, on scales up to 10s of kilometres. Where such fluid infiltration occurs a long time after protolith formation, there is also an enhanced possibility that long-lived radiogenic isotopes will be affected.

This study has shown that geochemical and isotopic parameters can be selectively disturbed with little obvious change to bulk composition, mineralogy or texture. For the Archaean high-grade gneisses of the Prydz Bay region, anhydrous granulites that retain abundant mineralogical and textural evidence of their igneous parentage dominate. Following the approach adopted by previous studies in the region (*e.g.* Sheraton & Collerson, 1984;

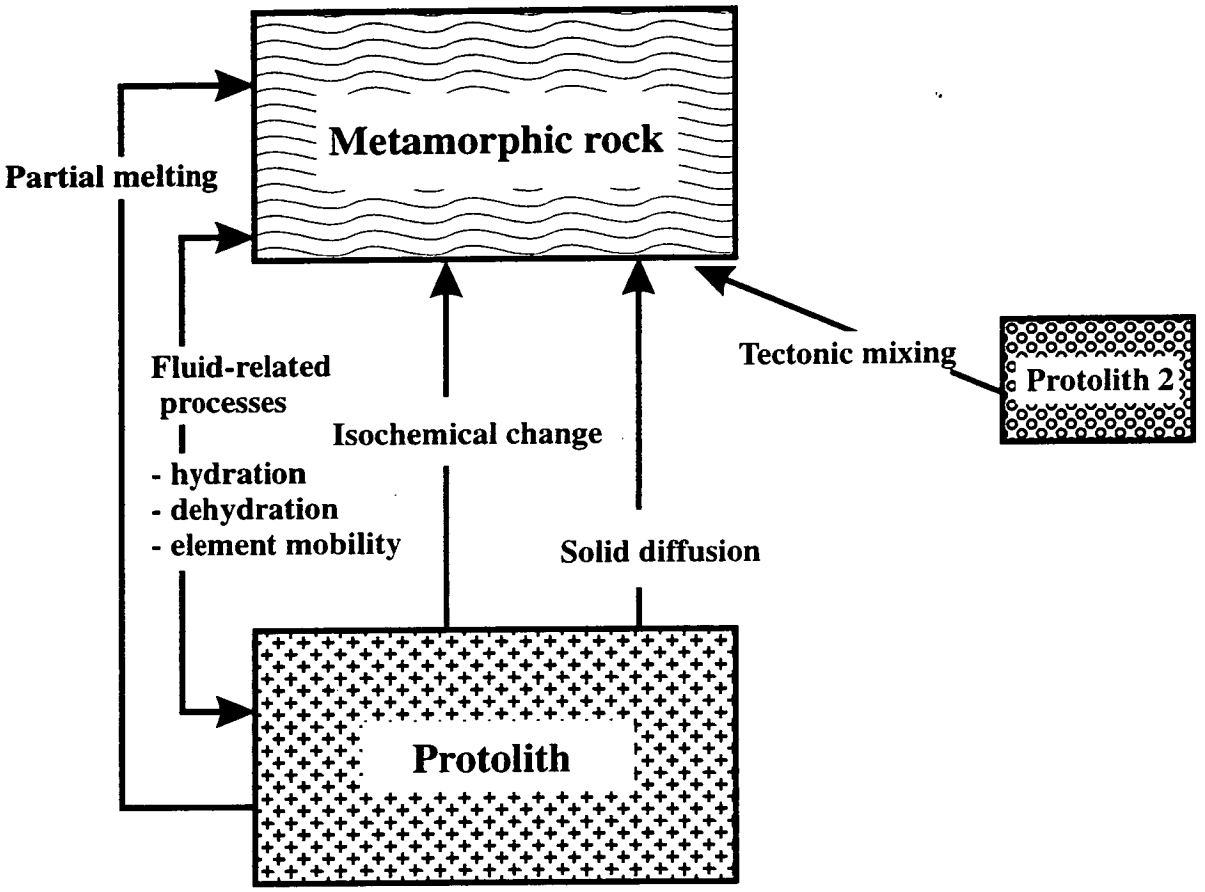

Figure 13.2 Flow diagram showing the principal processes which control the chemical composition of metamorphic rocks (after Rollinson, 1993).

Sheraton *et al.*, 1984), and in common with *most* geochemical studies in high-grade terranes (*e.g.* Gray *et al.*, 1981; Sheraton *et al.*, 1983; 1984; 1993; Jahn & Zhang, 1984; Jahn *et al.*1984; Windrim & McCulloch, 1986; Bickle *et al.*, 1993; Davis *et al.*, 1994; Janser, 1994; Kerr & Fryer, 1994; Luais & Hawkesworth, 1994; Kim & Jacobi, 1996; Sandeman *et al.*, 1997), samples were collected primarily to elucidate protolith origin, and few samples were selected to specifically constrain the extent of metasomatism or isotopic exchange. Indeed, rocks that have obvious high-strain fabrics, hydrous retrograde assemblages, or that occur adjacent to fluid conduits (late shear zones and pegmatites), were specifically not included in the geochemical dataset examined in the study. This strategy is critically reviewed further below (Section 13.4).

Nevertheless, despite this sampling strategy, it is apparent from the geochemical and isotopic data presented in this study that the extent of open-system chemical and especially isotopic exchange is much greater than previously reported for both the Rauer Group and the Vestfold Hills. Whilst it has not been possible to constrain the extent and breadth of chemical mobility in either of these terranes, it is apparent that certain elements and radiogenic isotopes were pervasively disturbed in the Rauer Group and, to a lesser extent, the Vestfold Hills (see Chapters 4-11). However, there are important differences in the way these two terranes responded to, or were affected by, Proterozoic and/or early Palaeozoic tectonothermal events. These differences reflect a variety of factors that include fluid-infiltration histories, the bulk composition of individual gneiss units, and petrological characteristics (*e.g.* trace-element residences).

Controls on fluid-rock interaction: trace-element residence in metamorphic rocks

During infiltration, fluid and host rock compositions exchange according to a complex interaction between fluid flux and external and internal buffering mechanisms (*cf.* Rice & Ferry, 1982; Spear, 1993). Although the influence of mineral chemistry and assemblage stability/instability as an internal buffering mechanism have been studied in detail for major elements and the major constituents of most fluids (*e.g.* H_2O, CO_2), comparatively little is known about the trace-element contents of individual mineral species or fluids (exceptions include Grauch, 1989; Pan & Fleet, 1996). Similarly, few workers have considered the distribution (residence) of trace elements in whole-rock systems, or how the behaviour of individual mineral species can influence trace-element and radiogenic-isotope behaviour during metamorphism.

Observations made in this study illustrate aspects of open-system processes that are apparently not appreciated by many geochemists that currently study high-grade terranes. One important conclusion is that the extent of trace-element and isotope mobility is strongly dependent upon whole-rock bulk composition. In the Rauer Group, for instance, low IE-abundance compositions (*e.g.* the TTLC) appear to be prone to *relatively* large amounts of chemical and isotopic open-system exchange, so-much-so that Nd isotopes appear to be reset at outcrop scales. By comparison, compositions that have intermediate compositions (*e.g.* the SLC) preserve evidence for more restricted amounts of open-system exchange, and initial Nd-isotope ratios reflect disequilibrium resetting as a consequence of isotopic exchange with adjacent whole-rock isotopic systems (reservoirs) that have distinct isotopic compositions. Although a number of external variables (*e.g.* fluid pathways and fluxes) are

also important, there are two main reasons why *adjacent* suites may respond differently to the same metamorphic fluid event.

The first reason concerns the effects of bulk mixing during fluid-enhanced chemical exchange (both concentration and isotopic profiles). Where fluids interact with rocks that have low trace-element concentrations, the potential for large gains by bulk mixing is proportionally much greater than for rocks that already have high trace-element concentrations. For example, trace-element concentrations may be up to several orders of magnitude lower in komatiites than in many granites, and this is one of the reasons that komatiites are notoriously prone to both crustal contamination *and* greenschist-facies alteration. It is also the reason why many komatiites have whole-rock Sm/Nd 'isochrons' that are older or younger than the crystallization ages (*e.g.* Tourpin *et al.*, 1991; Gruau *et al.*, 1992; Vrevsky *et al.*, 1996).

The second reason concerns direct petrological controls on fluid-enhanced exchange. Where trace elements reside in major phases that recrystallize or readily exchange with fluids, such as feldspars and pyroxenes, there will be a much greater potential for chemical loss or gain during fluid infiltration than if the trace elements mainly reside in relatively 'inert' accessory phases. However, even where a significant proportion of the total trace-element and REE budget is contained in accessory phases, CL and BEI reveal that many 'inert' accessory phases have exchanged chemically and isotopically with fluids during retrogression (*e.g.* Friend & Kinny, 1995; Hanchar & Millar, 1993; this study, Chapters 4 & 6).

Realization that adjacent layers or bulk compositions may respond differently during retrograde fluid infiltration has important implications for Nd-isotope arrays that systematically correlate with petrological or chemical variables such as differentiation indices (*e.g.* mineralogy, $^{147}Sm/^{144}Nd$, bulk composition, SiO_2, ***mg***). This observation has implications for AFC models that are based on combined radiogenic isotopes and trace elements (see also Roberts & Clemens, 1995). It is also particularly relevant to the study of Archaean high-grade terranes, which commonly experience polyphase histories and where there is a often a long time period between protolith formation and younger fluid infiltration (reworking) events.

Nd-isotope mobility and implications for models of Archaean crust-mantle evolution

Although resetting of Nd isotopes at intermineral scales during high-grade metamorphism is well documented (*e.g.* Futa, 1981; McCulloch & Black, 1984), *most* isotope geochemists assume that the scale of Nd-isotopic perturbation is less than the typical size of a large sample (~5-20 kg of a coarse-grained rock). However, it is apparent from this study that significant perturbation can occur, without significant metasomatic alteration, due to direct $^{143}Nd/^{144}Nd$ fluid-rock exchange. The mechanism or process is envisaged to be akin to that advocated for oxygen-isotope exchange and 'front' propagation (*e.g.* Bickle & Baker, 1990; Bickle & Chapman, 1990).

Hence, the model-age approach to Nd-isotope studies and the more general application of Nd isotopes to petrogenetic studies of high-grade (reworked) Precambrian rocks has been rarely tested to ensure that there has not been Nd-isotope perturbation (exceptions include Black & co-workers and Gruau & co-workers). Nevertheless, a number of criteria are commonly cited as evidence that there has not been metamorphic disturbance. For example, Cohen *et al.* (1991) for the Lewisian, and Bowring and co-workers (*e.g.* Bowring & Housh, 1995; Bowring *et al.*, 1995) for the Slave Province of Canada, argued that because juxtaposed mafic and felsic layers have distinct isotopic characteristics (*i.e.* ε_{Nd} values), then adjacent layers did not isotopically exchange. They therefore assume that Nd-isotope movement was restricted to less than handspecimen scales. However, this need not be the case since individual layers have appreciably different assemblages that are capable of internally buffering the fluid-rock system during fluid infiltration (both areas comprise variably rehydrated granulites).

Another often-cited discriminant that apparently mitigates against Nd-isotope mobilization, are coherent trace-element patterns (*e.g.* Collerson *et al.*, 1991; Bennett *et al.*, 1993). Using such criteria for discerning open-system behaviour in the Nd-isotope system is tenuous for a number of reasons:

- The REE, especially Sm/Nd, tend to have a systematic interdependence for both primary and secondary processes.
- Even small changes to $^{147}Sm/^{144}Nd$ a considerable time after protolith formation may have a profound affect on calculated ε_{Nd}.

- It is very difficult to discern direct $^{143}Nd/^{144}Nd$ exchange because the resulting arrays are very similar to those produced by AFC processes (perhaps this is one reason why AFC models derived on the basis of combined Nd-isotopes and trace elements often do not agree with calculations based in bivariate trace-element or combined major- and trace-element relationships; see Roberts & Clemens, 1995). The possibility for overlooking Nd-isotope mobility is further enhanced because samples are rarely taken within the context of a well-defined field-based framework or where independent constraints on the amount of fluid-rock interaction or fluid pathway are known.

The wider implications for petrogenetic studies based on Nd isotopes in high-grade terranes are important, but are particularly profound when formulating models for Precambrian crustal growth. Crustal growth models that are based directly on calculated Nd-isotope parameters from polymetamorphic high-grade terranes (*e.g.* Bowring *et al.*, 1989; 1995; Bowring & Housh, 1995), or even low-grade terranes that experienced extensive fluid infiltration a long time after protolith formation (*e.g.* Arndt, 1986; Arndt & Jenner, 1986; Gruau *et al.*, 1992), should be viewed cautiously. Similarly, it is doubtful whether interpretations based on Nd- or combined-isotope studies that appeal to heterogeneous, 'extreme', or 'unusual' processes of accretion-differentiation (*e.g.* Whitehouse, 1989; Collerson *et al.*, 1991; Bennett *et al.*, 1993; Bowring and co-workers) are valid. A detailed examination of many such studies indicates that heterogeneous ε_{Nd} values have been derived from gneisses with variable bulk compositions but that have hydrous metamorphic mineral assemblages. In some cases, variably retrogressed mafic gneiss enclaves have been studied that have apparently similar or well-correlated REE patterns, but that are enclosed in a much larger volume of dominantly felsic crust. From the observations made during the course of this study, such ε_{Nd} values should not form the basis for models of extreme mantle differentiation in the Archaean (*e.g.* Collerson *et al.*, 1991; Bennett *et al.*, 1993), especially for the so-called 'spike' of high positive ε_{Nd} values in *ca.* 4.0 - 3.6 Ga gneisses as described by Vervoot *et al.* (1996). Moreover, circumstantial evidence against open-system isotopic behaviour based on apparent inter-element correlations or a lack of spatial homogenisation, are insufficient criteria on which to base such models. Even apparently well-correlated isochrons are no guarantee that measured isotope ratios equate to those of the protolith, as Perrera (unpublished PhD thesis, University of Edinburgh) found for the re-worked granulites of Sri Lanka, when he derived an ε_{Nd} value of +28 from a *ca.* 3000 Ma isochron with a MSWD of <1.

In conclusion, when Nd isotopes are to be used to formulate petrogenetic models of Precambrian crustal growth, the models should be rigorously tested to confirm that the Nd-isotope system has indeed remained closed since protolith formation. This is particularly

relevant to rocks of Archaean age, since all such early crust has been reworked by at least one metamorphic event, and because models for Precambrian evolution tend to be more speculative than those for more recent times.

13.4 An appraisal of the scientific approach adopted in this study and suggestions for further research

13.4.1 An appraisal of the rationale and scientific approach adopted in this study

The underlying rationale for this project was to concentrate on establishing well-constrained geological frameworks from which to understand protolith petrogenesis in the Archaean orthogneiss suites. Largely through the work of Sheraton and co-workers (*e.g.* Sheraton *et al.*, 1983, 1984; Sheraton & Collerson, 1984; Sheraton & Black, 1987), a number of broad petrogenetic models were already established to account for the origin of the most abundant felsic lithologies prior to this study. However, a number of problems were identified with these reconnaissance geochemical surveys, which mostly stemmed from an inadequate field-based framework from which to interpret their data. In particular, geochemical modelling did not appear particularly well constrained and it was apparent that many geochemically-defined suites contained members that could not be strictly related because they were markedly different in age (*e.g.* Black *et al.*, 1991a; Kinny *et al.*, 1993). On balance, therefore, the overall approach was designed to more fully document the geology and geochemistry of Archaean protoliths. Ultimately it was hoped that this approach would also further elucidate protolith-forming processes in the Archaean of East Prydz Bay, which would thereby provide the most powerful means by which to consider terrane correlations in the region and other pre-Gondwana areas. Unfortunately, it was not until the radiogenic isotope work was completed that it was realised that the degree of open-system behaviour associated with the various metamorphic events was much greater than previously recognized. One of the contributing factors that led to this discovery stems from detailed examination of previously unrecognised ultramafic - mafic suites that have demonstrable comagmatic relations.

The decision to study mafic cumulates in preference to the more extensive felsic orthogneisses is a departure from previous studies in East Prydz Bay. The main advantages afforded by such an approach are:

- ***Mafic suites tend to be of lower strain than felsic rocks.*** This is crucial because the strain state often determines how easy it is to define cogenetic suites, but also because there are well-established links between metasomatism and deformation (*e.g.* Condie & Sinha, 1996).

- ***The ability to define cogenetic suites in the field*** means that it is often possible to elucidate petrogenetic processes because there is an *a priori* reason to assume that geochemical or isotopic compositions were related by a single igneous differentiation event. By contrast, felsic-dominated orthogneiss regions typically consist of 'layered grey gneisses' that are often not *strictly* related. Such gneisses often comprise tectonic intercalations or chemical segregations of variable age and origin.

- ***Mafic bulk compositions generally melt at higher temperatures*** than felsic rocks and are therefore less prone to migmatisation.

The main disadvantage concerns the difficulties of petrogenetic modelling because metamorphosed mafic cumulates are not ideally suited to whole-rock geochemical studies. Nevertheless, a pragmatic approach has been followed in this study because although 'analysing metamorphosed Archaean mafic rocks is clearly problematical' (Hall & Hughes, 1993 p.627), the advantages appeared to outweigh the disadvantages at the outset.

On balance, the problems inherent when dealing with metamorphosed cumulates *have* been offset by the geological, geochemical and isotopic information gained from the ultramafic - mafic - intermediate centres considered in this study. The theoretical or empirical basis for interpreting whole-rock geochemistry of layered cumulates is still a long way behind our understanding of basalt petrogenesis, primarily because cumulates are conceptually much more difficult to deal with. Nevertheless, in many high-grade terranes, detailed examination of intrusive mafic complexes may offer significant insight into early crustal growth. As emphasised in this study, relatively massive mafic plutonic centres commonly form the locus of low-strain domains in complex polyphase terranes (*cf.* Ashwal & Myers, 1994). Such strain partitioning often preserves a detailed record of primary features and may also allow a detailed and protracted post-crystallization geological history to be deduced in terranes that are otherwise pervasively overprinted by successive events.

13.4.2 Suggestions for further regional study

There is a great deal that remains to be studied in the East Prydz Bay region, and it would be impossible to outline all the possible avenues here. Nevertheless, a number of *suggestions for further research* arise directly from this study. The most pressing areas where further

work is needed are outlined below and are loosely grouped into *magmatism*, *metamorphism*, *deformation*, *geochronology*, and *geochemical and isotopic processes*.

Magmatism

Further geochemical and isotopic data are required to substantiate the petrogenetic models proposed in this study. However, it is likely that for the Archaean Rauer Group domain, the greatest advances toward understanding protolith origin will be made by first focusing on the extent and consequences of open-system behaviour during metamorphism (discussed below).

Nevertheless, a study of platinum-group elements and application of Re-Os isotopes to the TTLC and possibly the SLC may yield further insight into the origin of these layered complexes. The Re-Os system would be particularly suited to the TTLC because the suite is inferred to the product of a large degree partial melt, therefore Re and Os abundances should be high enough to measure relatively easily. Furthermore, because Re and Os would have much higher abundances in the layered complexes than in the crust, the effects of crustal contamination or metasomatism are usually easy to determine (more easily than Nd or Sr isotopes; Rob Ellam, pers. comm., 1997).

Metamorphism

Although considerable metamorphic work has been undertaken in the Rauer Group, very little reliable thermobarometry has been undertaken in the Vestfold Hills. Well-defined suites of metasedimentary rocks belonging to the Chelnok and Taynaya Paragneiss units have been sampled with a view to petrological and thermobarometric analysis. An extensive suite of calc-silicates and impure marbles that were primarily collected from the northern region, with less numerous samples from the central and southern regions, are likely to prove the most useful basis from which to deduce the *P, T,* fluid history in the Vestfold Hills. A representative suite of Grt-Opx- and Grt-Cpx-bearing Fe-rich mafic rocks and semipelites has also been collected from adjacent to the calc-silicates. In addition, there are a number of samples of pyroxenite and metaironstone lithologies that may yield detailed thermal histories from exsolved and co-existing pyroxenes. Finally, there is a diverse spectrum of feldspar textures and intergrowths that may potentially be used to elucidate igneous and metamorphic thermal and fluid histories.

All samples currently reside in the collection at Edinburgh.

Deformation

Although it is likely that there will always be room for further structural work and alternative interpretations in the Rauer Group, a detailed understanding of the structural evolution of the Vestfold Hills is a more pressing and achievable goal. The main aspect of the structural evolution in the Vestfold Hills that requires further study concerns the kinematic development of the early high-grade structures. Although the structural scheme presented in this study is more comprehensive than in previous accounts, a number of hypotheses have been proposed that need to be tested by detailed kinematic analysis. In particular, although S-fabrics dominate in the northern Vestfold Hills, it is important to establish the regional pattern of lineations in order to fully understand the nature and orientation of regional and minor F_3 open warping. This would require detailed, oriented, petrographic analysis. In the southern region, similar detailed kinematic analysis is required to unravel the relative importance of S_2 and $S_{3?}$ fabric elements and to confirm or refute the general distribution and orientation of the late thrust geometries.

Geochronology

In order to elucidate the behaviour of radiogenic isotopes during metamorphism (discussed further below), and to better constrain event sequences and regional correlations, further SHRIMP U-Pb zircon and monazite dating is required. The following is a brief list of key samples that could be dated using material collected during the course of this study.

<u>In the Rauer Group</u>

- Leucogabbroic TTLC to date the age of the complex (see Chapters 3 & 5).
- Cross-cutting felsic melt trellis structures and axial-planar veins in the TTLC to determine a minimum age for the complex and the age of early folding in the Rauer Group (see Chapter 3).
- Direct dating of the cross-cutting tonalite in the SLC. This important time marker requires further detailed study (see Chapters 3 & 6).
- Detailed analysis of the TTG in the Rauer Group to establish crystallization ages and the ages of remelting events (see Chapters 2, 3 & 6).

In the Vestfold Hills

- Zircons from the Taynaya and Chelnok Paragneiss units are currently being examined by PD Kinny to establish provenance ages for these metasedimentary rocks. In addition, zircons and monazites from the same samples are being examined to confirm the age of peak metamorphism (from leucosomes) and to establish the age of the garnet overprint in the SW Vestfold Hills.

- Direct dating of the Taynaya EMG at Bulatnaya Bay would be useful, but it is likely that baddeleyite separation would be required to date these mafic rocks.

- Dating further examples of layered Mossel Gneisses may push back the age of the oldest felsic orthogneisses.

- There is considerable scope to determine more crystallization ages from the various CLG plutons, but it is doubtful that such work would significantly change the existing scheme (Chapter 10). Nevertheless, greater constraint on the age of the unexposed crust from inherited zircon populations would be useful.

Geochemical and isotopic processes

Although further use could be made of the existing dataset, for example, detailed modelling or comparison with experimentally derived phase relations, by far the most pressing need is for a greater understanding of the causes and consequences of open-system behaviour as a consequence of metasomatism. This is not a topic that can be dealt with as an adjunct to a regional geological and geochemical study such as this, but is the most logical extension of this study.

Petrological controls on metasomatism and isotopic perturbation

It is likely that the most useful direction of further research in the East Prydz Bay region, based on observations made during the course of this study, concerns the geochemical and isotopic response to metamorphism. In particular, the long time that elapsed between protolith formation and fluid infiltration ($>10^9$ yrs), combined with the comprehensive geological and chronological frameworks that now exist for the Vestfold Hills and Rauer Group, would prove an ideal location to study the underlying mechanisms that govern trace-element and radiogenic-isotope mobility.

13.5 Concluding statement

Although some authors (*e.g.* Hamilton, 1995; Park, 1995) believe that uniformitarian plate-tectonic models have been applied uncritically to the early Precambrian, others have argued that plate-tectonic processes initiated shortly after core-mantle differentiation and were certainly operating by about 4.0-3.6 Ga (*e.g.* Kröner, 1991; Windley, 1993, 1995; Burke, 1995). If there is a consensus, it appears to be that plate-tectonics did operate in the early stages of Earth evolution, but that details, such as rates of movement, temperatures, and crustal thickness, were probably different than today. However, arguably the most important point regarding the operation of plate tectonics in the Archaean was made by Kevin Burke at the recent Precambrian meeting in Montreal, and this is that uniformitarian plate-tectonic theory is the only truly *testable* model for Earth evolution. Therefore, 'there is a burden on those who reject a plate tectonic model for the ancient world to produce evidence from the rocks that a radically different process was operating' (Burke, 1995).

I would further add from the conclusions of this study, that the genesis of most Archaean orthogneisses in the East Prydz Bay region can probably be explained by processes analogous to those operating today. More importantly, however, I would suggest that unusual or radical models for the evolution of the early Earth, such as early Archaean ultradepleted mantle reservoirs (*e.g.* Collerson *et al.*, 1991; Bennett *et al.*, 1993; Bowring and co-workers), should be rigorously examined by considering more obvious and testable alternatives, namely, that many high-grade protoliths have *not* remained closed chemical and isotopic systems since initial formation.

References

Ague J.J. 1991. Evidence for major mass transfer and volume strain during regional metamorphism of pelites. *Geology*, **19**, 855-858.

Aitchison J. 1986. *The Statistical Analysis of Compositional Data.* Methuen, New York. 625 pp.

Allègre C.J. & Minster J.F. 1978. Quantitative models of trace element behaviour in magmatic processes. *Earth and Planetary Science Letters,* **38**, 1-25.

Allègre C.J., Treuil M., Minster J.F., Minster B. & Albarede F. 1977. Systematic use of trace elements in igneous processes. Part I: Fractional crystallisation processes in volcanic suites. *Contributions to Mineralogy and Petrology*, **60**, 57-75.

Anders E. & Grevesse N. 1989. Abundance of the elements: Meteoric and solar. *Geochimica et Cosmochimica Acta*, **53**, 197-214.

Anderson D.J. & Lindsley D.L. 1988. Internally consistent solution models for Fe-Mg-Mn-Ti oxides: Fe-Ti oxides. *American Mineralogist*, **73**, 714-785.

Anovitz L.M. & Essene E.J. 1987. Compatibility of geobarometers in the system CaO-FeO-Al_2O_3-SiO_2-TiO_2 (CFAST): Implications for garnet mixing models. *Journal of Geology,* **95**, 633-645.

Arnason J.G., Bird D.K., Bernstein S., Rose N.M. & Manning C.E. 1997. Petrology and geochemistry of the Kruuse Fjord Gabbroic Complex, East Greenland. *Geological Magazine*, **134**, 67-89.

Arndt N.T. 1983. Element mobility during komatiite alteration. *Eos,* **64**, 331.

Arndt N.T. 1986. Komatiites: A dirty window to the Archaean mantle. *Terra Cognita*, **6**, 59-66.

Arndt N.T. & Jenner G.A. 1986. Crustally contaminated komatiites and basalts from Kambalda, western Australia. *Chemical Geology,* **56**, 229-255.

Ashwal L.D. & Myers J.S. 1994. Archaean anorthosites. In: Condie K.C. (ed) *Archaean crustal evolution; Developments in Precambrian Geology 11.* Elsevier. 315-356.

Avé Lallemant H.G. 1997. Transpression, displacement partitioning, and exhumation in the eastern Caribbean/South American plate boundary zone. *Tectonics*, **16**, 272-289.

Ayres M. & Harris N. 1997. REE and Nd-isotope fractionation during crustal anatexis: constraints from Himalayan leucogranites. *Chemical Geology*, **139**, 249-269.

Barnes S.J. 1986. The effect of trapped liquid crystallization on cumulus mineral compositions in layered intrusions. *Contributions to Mineralogy and Petrology,* **93**, 524-531.

Barnicoat A.C. & Cartwright I. 1995. Focused fluid-flow during subduction - oxygen isotope data from high-pressure ophiolites of the western Alps. *Earth and Planetary Science Letters*, **132**, 53-61.

Barnicoat A.C. & Cartwright I. 1997. The gabbro-eclogite transformation: an oxygen isotope and petrographic study of west Alpine ophiolites. *Journal of Metamorphic Geology*, **15**, 93-104.

Bea F. 1996. Residence of REE, Y, Th and U in granites and crustal protoliths; implications for the chemistry of crustal melts. *Journal of Petrology*, **37**, 521-552.

Bebout G.E. & Barton M.D. 1989. Fluid flow and metasomatism in a subduction zone hydrothermal system: Catalina Schist terrane, California. *Geology,* **17**, 976-980.

Bebout G.E. & Barton M.D. 1993. Metasomatism during subduction: products and possible paths in the Catalina Schist, California. *Chemical Geology,* **108**, 61-92.

Bennett V.C., Nutman A.P. & McCulloch M.T. 1993. Nd isotopic evidence for transient highly depleted mantle reservoirs in the early history of the Earth. *Earth and Planetary Science Letters,* **119**, 299-317.

Bhattacharya A., Krishnakumar K.R., Raith M. & Sen S.K. 1991. An improved set of a-X parameters for Fe-Mg-Ca garnets and refinements of the orthopyroxene-garnet thermometer and the orthopyroxene-garnet-plagioclase-quartz barometer. *Journal of Petrology,* **32**, 629-656.

Bickle M.J. 1986. Implications of melting for stabilisation of the lithosphere and heat loss in the Archaean. *Earth and Planetary Science Letters*, **80**, 314-324.

Bickle M.J. & Baker J. 1990. Advective-diffusive transport of isotopic fronts: an example from Naxos, Greece. *Earth and Planetary Science Letters,* **97**, 78-93.

Bickle M.J & Chapman H.J. 1990. Strontium and oxygen isotope decoupling in the Hercynian Trois Seigneurs Massif, Pyrenees: Evidence for fluid circulation in a brittle regime. *Contributions to Mineralogy and Petrology*, **104**, 332-347.

Bickle M. J. & McKenzie D. 1987. The transport of heat and matter by fluids during metamorphism. *Contributions to Mineralogy and Petrology,* **95**, 384-392.

Bickle M.J., Bettanay L.F., Chapman H.J., Groves D.I., McNaughton N.J., Campbell I.H. & de Laeter J.R. 1989. The age and origin of younger granite plutons of the Shaw Batholith in the Archaean Pilbara block, western Australia. *Contributions to Mineralogy and Petrology,* **101**, 361-376.

Bickle M.J., Bettanay L.F., Chapman H.J., Groves D.I., McNaughton N.J., Campbell I.H. & de Laeter J.R. 1993. Origin of the 3500-3300 Ma calc-alkaline rocks in the Pilbara Archaean: isotopic and geochemical constraints from the Shaw Batholith. *Precambrian Research*, **60**, 117-149.

Black L.P. 1988. Isotopic resetting of U-Pb zircon and Rb-Sr and Sm-Nd whole-rock systems in Enderby Land, Antarctica: Implications for the interpretation of isotopic data from polymetamorphic and multiply deformed terraines. *Precambrian Research,* **38**, 355-365.

Black L.P., Harley S.L., Sun S.S. & McCulloch M.T. 1987. The Rayner Complex of East Antarctica: complex isotopic systematics within a Proterozoic mobile belt. *Journal of Metamorphic Geology,* **5**, 1-26.

Black L.P. & James P.R. 1983. Geological history of the Archaean Napier Complex in Enderby Land. In: Oliver R.L., James P.R. & Jago J.B. (eds), *Antarctic Earth Science.* Australian Academy of Science, Canberra. 11-15.

Black L.P., Kinny P.D. & Sheraton J.W. 1991a. The difficulties of dating mafic dykes: an Antarctic example. *Contributions to Mineralogy and Petrology,* **109**, 183-194.

Black L.P., Kinny P.D., Sheraton J.W. & Delor C.P. 1991b. Rapid production and evolution of late Archaean felsic crust in the Vestfold Block of East Antarctica. *Precambrian Research*, **50**, 283-310.

Black L.P. & McCulloch M.T. 1987. Evidence for isotopic equilibration of Sm-Nd whole-rock systems in early Archaean crust of Enderby Land, Antarctica. *Earth and Planetary Science Letters,* **82**, 15-24.

Black L.P., Sheraton J.W. & James P.R. 1986a. Late Archaean granites of the Napier Complex, Enderby Land, Antarctica: A comparison of Rb-Sr, Sm-Nd and U-Pb systematics in a complex terrain. *Precambrian Research,* **32**, 343-368.

Black L.P., Williams I.S. & Compston W. 1986b. Four zircon ages from one rock: the history of a 3930 Ma-old granulite from Mount Sones, Antarctica. *Contributions to Mineralogy and Petrology,* **94**, 427-437.

Bohlen S.R., Wall V.J. & Boettcher A.L. 1983. Experimental investigations and geologic applications of equilibria in the system FeO-TiO_2-Al_2O_3-SiO_2-H_2O. *American Mineralogist*, **68**, 1049-1058.

Borg S.G. & DePaolo D.J. 1994. Laurentia, Australia and Antarctica as a late Proterozoic supercontinent: constraints from isotopic mapping. *Geology*, **22**, 307-310.

Bowen N.L. 1928. *The Evolution of the Igneous Rocks.* Princeton University Press (reprinted in 1956 by Dover Publ. NY). 334 pp.

Bowring S.A. & Housh T.B. 1995. The Earth's early evolution. *Science,* **269**, 1535-1540.

Bowring S.A., Coleman D.S. & Housh T.B. 1995. The 4.0 Ga Acasta gneisses: constraints on the growth and recycling of continental crust. *Abstract, International conference on tectonics and metallogeny of early/mid Precambrian orogenic belts, Montreal. Canada.* p 275.

Bowring S.A., King J.E., Housh T.B., Isachsen C.E. & Podosek F.A. 1989. Neodymium and lead isotope evidence for enriched early Archaean crust in North America. *Nature*, **340**, 222-225.

Bowring S.A., Williams I.S. & Compston W. 1989. 3.96 Ga gneisses from the Slave Province, NWT Canada. *Geology*, **17**, 971-975.

Brown G.M. 1968. *Layered Igneous Rocks.* Oliver & Boyd, Edinburgh.

Brown W.L. & Parsons I. 1994. Feldspar in igneous rocks. In: Parsons I. (ed) *Feldspars and their reactions*, Kluwer Academic. 449-499.

Buddington A.F. & Lindsley D.M. 1964. Iron-titanium oxide minerals and synthesised equivalents. *Journal of Petrology*, **5**, 310-357.

Buick I.S. & Holland T.J.B. 1991. The nature and distribution of fluids during amphibolite facies metamorphism, Naxos (Greece). *Journal of Metamorphic Geology,* **9**, 301-314.

Burke K. 1995. Did plate tectonics operate in the Archaean? *Abstract, International conference on tectonics and metallogeny of early/mid Precambrian orogenic belts, Montreal. Canada.* p 277.

Burton K.W. & O'Nions R.K. 1991. High-resolution garnet chronometry and the rates of metamorphic processes. *Earth and Planetary Science Letters*, **107**, 649-671.

Burton K.W., Cohen A.S., O'Nions R.K. & O'Hara M.J. 1994. Archaean crustal development in the Lewisian complex of northwest Scotland. *Nature*, **370**, 552-555.

Butler J.C. 1982. Artificial isochrons. *Lithos*, **15**, 207-214.

Butler J.C. & Woronow A. 1986. Discrimination among tectonic settings using trace element abundance of basalts. *Journal of Geophysical Research,* **91**, B10289-B10300.

Cabinis B. & Lecolle M. 1989. Le diagramme La/10-Y/15-Nb/8: un outil pour la discrimination des séries volcaniques et la mise en evidence des processus de mélange et/ou de contamination croûtale. *CR Acad, Sci. Ser. II,* **309**, 2023-2029.

Carswell D.A. & Harley S.L. 1989. Mineral thermometry and barometry. In: Carswell D.A. (ed), *Eclogite Facies Rocks.* Blackie & Sons, Glasgow. 83-110.

Cartwright I., Buick I.S. & Harley S.L. 1997. Timing and mechanisms of carbon isotope exchange in granulite-facies calc-silicate boudins, Rauer Group, East Antarctica. *American Mineralogist,* **82**, 392-404.

Chappell B.W. & White A.J.R. 1974. Two contrasting granite types. *Pacific Geology,* **8**, 173-174.

Chen C.-H., Shieh Y.N., Lee T., Chen C.-H. & Mertzman S.A. 1990. Nd-Sr-O isotopic evidence for source contamination and an unusual mantle component under Luzon arc. *Geochimica et Cosmochimica Acta,* **54**, 2473-2483.

Chivas A.R., Andrew A.S., Sinha A.K. & O'Neil J.R. 1982. Geochemistry of a Pliocene-Pleistocene oceanic-arc plutonic complex, Guadalcanal. *Nature,* **300**, 139-143.

Clarke G.L. 1988. Structural constraints on the Proterozoic reworking of Archaean crust in the Rayner Complex, MacRobertson & Kemp Land Coast, East Antarctica. *Precambrian Research,* **40/41**, 137-156.

Cliff R.A. 1985. Isotopic dating in metamorphic belts. *Journal of the Geological Society, London,* **142**, 97-110.

Cohen A.S., O'Nions R.K. & O'Hara M.J. 1991. Chronology and mechanism of depletion in Lewisian granulites. *Contributions to Mineralogy and Petrology,* **106**, 142-153.

Collerson K.D. & Sheraton J.W. 1986a. Age and geochemical characteristics of a mafic dyke swarm in the Archaean Vestfold Block, Antarctica: Inferences about Proterozoic dyke emplacement in Gondwana. *Journal of Petrology,* **27**, 853-886.

Collerson K.D. & Sheraton J.W. 1986b. Bedrock geology and crustal evolution of the Vestfold Hills. In: Pickard J. (ed.) *Antarctic Oasis.* Academic Press, Sydney. 21-62.

Collerson K.D., Campbell L.M., Weaver B.L. & Palacz Z.A. 1991. Evidence for extreme mantle fractionation in early Archaean ultramafic rocks from northern Labrador. *Nature,* **349**, 209-214.

Collerson K.D., Reid E., Millar D. & McCulloch M.T. 1983. Lithological and Sr-Nd isotopic relationships in the Vestfold Block: Implications for Archaean and Proterozoic crustal evolution in the East Antarctic Shield. In: Oliver R.L., James P.R. & Jago J.B. (eds.) *Antarctic Earth Science.* Australian Academy of Science, Canberra. 77-84.

Compston W., Williams I.S. & Clement S.W.J. 1982. U-Pb ages with single zircons using sensitive high mass-resolution microprobe. *30th Annual Conference of Mass Spectrometry,* 585-593

Compston W., Williams I.S. & Meyer C. 1984. U-Pb geochronology of zircons from lunar breccia 73217 using a sensitive high-resolution ion-microprobe. *Proceedings of the 14th Lunar Science Conference, Journal of Geophysical Research,* **89**, B525-B534.

Condie K.C. & Sinha A.K. 1996. Rare earth and other trace element mobility during mylonitisation: A comparison of the Brevard and Hope Valley shear zones in the Appalachian Mountains, USA. *Journal of Metamorphic Geology,* **14**, 213-226.

Cox K.G. 1980. A model for flood basalt volcanism. *Journal of Petrology,* **21**, 629-650.

Cox K.G., Bell, J.D. & Pankhurst R.J. 1979. *The Interpretation of Igneous Rocks.* George, Allen & Unwin, London. 450 pp.

Crawford A.J., Falloon T.J. & Green D.G. 1989. Classification, petrogenesis and tectonic setting of boninites. In: Crawford A.J. (ed) *Boninites and Related Rocks.* Unwin-Hymen Press, London. 1-49.

Cross W., Iddings J.P., Pirsson L.V. & Washington H.S. 1903. *Quantitative Classification of Igneous Rocks.* University of Chicago Press.

Cumming G.L. & Richards J.R. 1975. Ore lead isotope ratios in a continuously changing Earth. *Earth and Planetary Science Letters,* **28**, 155-171.

Dalziel I.W.D. 1991. Pacific margins of Laurentia and East Antarctica-Australia as a conjugate rift pair: Evidence and implications for an Eocambrian supercontinent. *Geology,* **19**, 598-601.

Dalziel I.W.D. 1992. Antarctica; a tale of two supercontinents? *Annual review of Earth and Planetary Science Letters,* **20**, 501-526.

Darwin C.R. 1844. *Geological observations on the volcanic islands visited during the voyages of H.M.S. Beagle, with brief notices on the geology of Australia and the Cape of Good Hope, being the second part of the voyage of the Beagle.* Smith, Elder & Co., London.

Davidson A. 1995. A review of the Grenville orogen in its North American type area. *AGSO Journal of Australian Geology and Geophysics*, **16**, 3-24.

Davidson J.P. & Harmon R.S. 1989. Oxygen isotope constraints on the petrogenesis of volcanic arc magmas from Martinique, Lesser Antilles. *Earth and Planetary Science Letters*, **95**, 255-270.

Davies W.J., Fryer B.J. & King J.E. 1994. Geochemistry and evolution of late Archaean plutonism and its significance to the tectonic development of the Slave craton. *Precambrian Research*, **67**, 207-241.

Defant M.J. & Drummond M.S. 1990. Derivation of some modern arc magmas by melting of young subducted lithosphere. *Nature*, **347**, 662-665.

DePaolo D.J. 1981. Trace element and isotopic effects of combined wallrock assimilation and fractional crystallisation. *Earth and Planetary Science Letters,* **53**, 189-202.

DePaolo D.J. 1988. *Neodymium Isotope Geochemistry: An Introduction.* Springer Verlag, New York.

DePaolo D.J. & Wasserburg G.J. 1979. Petrogenetic mixing models and Nd-Sr isotopic patterns. *Geochimica et Cosmochimica Acta*, **43**, 615-627.

Dicken A.P. 1981. Isotope geochemistry of Tertiary igneous rocks from the Isle of Skye, NW Scotland. *Journal of Petrology*, **22**, 155-189.

Dirks P.H.G.M. & Wilson C.J.L. 1995. Crustal evolution of the East Antarctic mobile belt in Prydz Bay: continental collision at 500 Ma? *Precambrian Research,* **75**, 189-208.

Dirks P.H.G.M., Carson C.J. & Wilson C.J.L. 1993. The deformational history of the Larsemann Hills, Prydz Bay - the importance of the Pan-African (500 Ma) in East Antarctica. *Antarctic Science*, **5**, 179-192.

Dirks P.H.G.M., Hoek, J.D., Wilson C.J.L. & Sims J.R. 1994. The Proterozoic deformation of the Vestfold Hills basement complex, East Antarctica: Implications for the tectonic evolution of adjacent granulite belts. *Precambrian Research,* **65**, 277-295.

Dodson M.H. 1982. On 'spurious' correlations in Rb-Sr isochron diagrams. *Lithos*. **15**, 215-219.

Drummond M.S. & Defant M.J. 1990. A model for trondhjemite-tonalite-dacite genesis and crustal growth via slab melting: Archaean to modern comparisons. *Journal of Geophysical Research*, **95**, 21503-21521.

Drummond M.S., Ragland P.C. & Wesolowski D. 1986. An example of trondhjemite genesis by means of alkali metasomatism: Rockford Granite, Alabama Appalachians. *Contributions to Mineralogy and Petrology*, **93**, 98-113.

Ellam R.M. & Hawkesworth C.J. 1988. Elemental and isotopic variations in subduction related basalts: evidence for a three component model. *Contributions to Mineralogy and Petrology*, **98**, 72-80.

Ellis D.J. 1980. Osumilite-sapphrine-quartz granulites from Enderby Land, Antarctica: P-T conditions of metamorphism, implications for garnet-cordierite equilibria and evolution of the deep crust. *Contributions to Mineralogy and Petrology*, **74**, 201-210.

Ellis D.J. 1983. The Napier and Rayner Complexes of Enderby Land, Antarctica: contrasting styles of metamorphism and tectonism. In: Oliver R.L., James P.R. & Jago J.B. (eds.) *Antarctic Earth Science*. Australian Academy of Science, Canberra. 20-24.

Elthon D. 1983 Isomolar and isostructural pseudo-liquidus phase-diagrams for oceanic basalts. *American Mineralogist*, **68**, 506-511.

Essene E.J. 1989. The current status of thermobarometry in metamorphic rocks. In: Daly J.S., Cliff R.A. & Yardley B.W.D. (eds.) *Evolution of Metamorphic Belts*. Special Publication of the Geological Society, London, **43**, 1-44.

Falloon T.J. & Green D.H. 1988. Anhydrous partial melting of peridotite from 8 to 35 kbar and the petrogenesis of MORB. *Journal of Petrology, Special Lithosphere Issue*, 379-414.

Faure G. 1986. *Principals of Isotope Geology*. 2nd edition, Wiley, New York. 589pp.

Ferry J.M. 1983. Regional metamorphism of the U.S.A; a case study of the role of fluid in metamorphic petrogenesis. *Journal of the Geological Society, London*, **140**, 551-576.

Ferry J.M. 1986. Reaction progress: A monitor of fluid-rock interaction during metamorphic and hydrothermal events. In: Walther J.V. & Wood B.J. (eds) *Fluid-rock Interactions During Metamorphism*. Springer, New York. 60-88.

Ferry J.M. & Dipple G.M. 1991. Fluid flow, mineral reactions, and metasomatism. *Geology*, **19**, 211-214.

Fitton J.G. 1971. The generation of magmas in island arcs. *Earth and Planetary Science Letters*, **11**, 63-67.

Fitton J.G., Saunders A.D., Larsen L.M., Hardarson B.S. & Norry M.J. *in press*. Volcanic rocks from the southeast Greenland margin at 63°N: Composition, petrogenesis and mantle sources.

Fitzsimons I.C.W. & Harley S.L. 1994. The influence of retrograde cation exchange on granulite P-T estimates and a convergence technique for the recovery of peak metamorphic conditions. *Journal of Petrology*, **35**, 543-576.

Fletcher I.R. & Rosman K.J.R. 1982. Precise determination of initial ε_{Nd} from Sm-Nd isochron data. *Geochimica et Cosmochimica Acta*, **46**, 1983-1987.

Floyd P.A. & Winchester J.A. 1975. Magma-type and tectonic setting discrimination using immobile elements. *Earth and Planetary Science Letters,* **27**, 211-218.

Foley S.F. & Wheller G.E. 1990. Parallels in the origin of the geochemical signatures of island arc volcanics and continental potassic igneous rocks: The role of residual titanites. *Chemical Geology,* **85**, 1-18.

Forester R.W. & Taylor, Jr H.R. 1977. $^{18}O/^{16}O$, D/H and $^{13}C/^{12}C$ studies of the Tertiary igneous complex of Skye, Scotland. *American Journal of Science,* **277**, 136-177.

Fourcade S., Maury R.C., Defant M.J. & McDermott F. 1994. Mantle metasomatic enrichment versus arc crust contamination in the Phillipines: Oxygen isotope study of Batan ultramafic nodules and northern Luzon arc lavas. *Chemical Geology*, **114**, 199-215.

Fowler M.B., Friend C.R.L. & Whitehouse M.J. 1995. Crust formation in the Lewisian. *Nature*, **375**, p 366.

Francalanci L., Taylor S.R., McCulloch M.T. & Woodhead J.D. 1993. Geochemical and isotopic variations in the calc-alkaline rocks of Aeolian arc, southern Tyrrhenain Sea, Italy: constraints on magma genesis. *Contributions to Mineralogy and Petrology,* **113**, 300-313.

Friend C.R.L. & Kinny P.D. 1995. New evidence for protolith ages of Lewisian granulite, northwest Scotland. *Geology*, **23**, 1027-1030.

Friend, P.F., Harland, W.B., Rogers, D.A., Snape, I. & Thornley, R.S.W. 1997. Late Silurian and Early Devonian stratigraphy and probable strike-slip tectonics in northwestern Spitsbergen. *Geological Magazine*, **134**, 459-479.

Fuhrman M.L. & Lindsley D.H. 1988. Ternary-feldspar modelling and thermometry. *American Mineralogist*, **73**, 201-215.

Futa K. 1981. Sm-Nd systematics of a tonalitic augen gneiss and its constituent minerals from northern Michigan. *Geochimica et Cosmochimica Acta*, **45**, 1245-1249.

Galan G., Pin C. & Duthou J-L. 1996. Sr-Nd isotopic record of multi-stage interactions between mantle-derived magmas and crustal components in a collision context - The ultramafic-granitoid association from Vivero, Hercynian belt, NW Spain. *Chemical Geology*, **131**, 67-91.

Gammons C.H., Wood S.A. & Williams-Jones A.E. 1996. The aqueous geochemistry of the rare earth elements and yttrium: VI. Stability of neodymium chloride complexes from 25 to 300°C. *Geochimica et Cosmochimica Acta*, **60**, 4615-4630.

Goldstein S.I. 1988. Decoupled evolution of Nd and Sr isotopes in the continental crust. *Nature,* **336**, 733-738.

Goldstein S.L., O'Nions R.K. & Hamilton P.J. 1984. A Sm-Nd study of atmospheric dusts and particulates from major river systems. *Earth and Planetary Science Letters*, **70**, 221-236.

Graham C.M. & Powell R. 1984. A garnet-hornblende geothermometer and application to the Pelona Schist, southern California. *Journal of Metamorphic Geology,* **2**, 13-32.

Gray C.M., Cliff R.A. & Goode A.D.T. 1981. Neodymium-strontium isotopic evidence for extreme contamination in a layered basic intrusion. *Earth and Planetary Science Letters,* **56**, 189-198.

Gray D.R., Gregory R.T. & Durney D.W. 1991. Rock-buffered fluid-rock interaction in deformed quartz-rich turbidite sequences, eastern Australia. *Journal of Geophysical Research,* **96**, 19681-19704.

Green T.H., Sie S.H., Ryan C.G. & Cousins D.R. 1989. Proton microprobe-determined partitioning of Nb, Ta, Zr, Sr and Y between garnet, clinopyroxene and basaltic magma at high pressure and temperature. *Chemical Geology,* **74**, 201-216.

Greenwood R.C., Fallick A.E. & Donaldson C.H. 1992. Oxygen isotope evidence for major fluid flow along the contact zone of the Rum ultrabasic intrusion. *Geological Magazine,* **129**, 243-246.

Grove T.J., Gerlach D.C. & Sando T.W. 1982. Origin of late calc-alkaline series lavas at Medicine Lake Volcano by fractionation, assimilation and mixing. *Contributions to Mineralogy and Petrology,* **80**, 160-182.

Gruach R.I. 1989. Rare-earth elements in metamorphic rocks. In: Lipin B.R. & McKay G.A. (eds), *Geochemistry and Mineralogy of Rare Earth Elements, Reviews in Mineralogy,* **21**. 147-161.

Gruau G., Rosing M., Bridgwater D. & Gill R.C.O. 1996. Resetting of Sm-Nd systematics during metamorphism of >3.7-Ga rocks: implications for isotopic models of early Earth differentiation. *Chemical Geology,* **133**, 225-240.

Gruau G., Tourpin S., Fourcade S. & Blais S. 1992. Loss of isotopic (Nd, O) and chemical (REE) memory during metamorphism of komatiites: New evidence from eastern Finland, *Contributions to Mineralogy and Petrology,* **117**, 66-82.

Hall R.P. & Hughes D.J. 1987. Noritic dykes of southern West Greenland: Early Proterozoic boninitic magmatism. *Contributions to Mineralogy and Petrology,* **97**, 169-182.

Hall R.P. & Hughes D.J. 1990. Noritic magmatism. In: Hall R.P. & Hughes D.J. (eds) *Early Precambrian basic magmatism.* Blackie. 83-110.

Hall R.P. & Hughes D.J. 1993. Early Precambrian crustal development: Changing styles of mafic magmatism. *Journal of the Geological Society, London,* **150**, 625-635.

Hamlyn P.R. & Keays R.R. 1986. Sulfur saturation and 2nd stage melts - application to the Bushveld platinum metal deposits. *Economic Geology,* **81**, 1431-1445.

Hanchar J.M. & Miller C.F. 1993. Zircon zonation patterns as revealed by cathodoluminescence and backscattered electron images: Implications for interpretation of complex crustal histories. *Chemical Geology,* **110**, 1-13.

Hand M., Scrimgeour I., Powell R., Stuwe K. & Wilson C.J.L. 1994. Metapelitic granulites from Jetty Peninsula, East Antarctica - formation during a single event or by polymetamorphism. *Journal of Metamorphic Geology,* **12**, 557-573.

Hanson G.N. 1989. An approach to trace element modelling using a simple igneous system as an example. In: Lipin B.R. & McKay G.A. (eds) *Geochemistry and Mineralogy of Rare Earth Elements, Reviews in Mineralogy,* **21**, 79-97.

Hanson. G.N. 1980. Rare-earth elements in petrogenetic studies of igneous systems. *Annual Review of Earth and Planetary Science Letters,* **8**, 371-406.

Harding R.R. & McLeod I. 1967. Age of dolerite dykes in the Vestfold Hills, Antarctica. *Nature,* **215**, 149-150.

Harland, W.B., Scott, R.A., Auckland, K.A. & Snape, I. 1992. The Ny Friesland Orogen, Spitsbergen. *Geological Magazine.* **129**, 679-708.

Harley S.L. 1983. Regional geobarometry-geothermometry and metamorphic evolution of Enderby Land, Antarctica. In: Oliver R.L., James P.R. & Jago J.B. (eds), *Antarctic Earth Science.* Australian Academy of Science, Canberra. 25-30.

Harley S.L. 1984a. An experimental study of the partitioning of Fe and Mg between garnet and orthopyroxene. *Contributions to Mineralogy and Petrology,* **86**, 359-373.

Harley S.L. 1984b. The solubility of alumina in orthopyroxene coexisting with garnet in FeO-MgO-Al_2O_3-SiO_2 and CaO-FeO-MgO-Al_2O_3-SiO_2. *Journal of Petrology,* **25**, 665-696.

Harley S.L. 1985. Garnet-orthopyroxene bearing granulites from Enderby Land, Antarctica: Metamorphic pressure-temperature-time evolution of the Archaean Napier Complex. *Journal of Petrology*, **26**, 819-856.

Harley S.L. 1987. Precambrian geological relationships in high-grade gneisses of the Rauer Islands, East Antarctica. *Australian Journal of Earth Science,* **34**, 175-207.

Harley S.L. 1988. Proterozoic granulites from the Rauer Group, East Antarctica. I. Decompressional pressure-temperature paths deduced from mafic and felsic gneisses. *Journal of Petrology,* **29**, 1059-1095.

Harley S.L. 1989. The origins of granulites: A metamorphic perspective. *Geological Magazine*, **126**, 215-247.

Harley S.L. 1991. Metamorphic evolution of granulites from the Rauer Group, East Antarctica: Evidence for decompression following Proterozoic collision. In: Thomson M.R.A., Crame J.A. & Thomson J.W. (eds.) *Geological Evolution of Antarctica.* Cambridge University Press. 99-105.

Harley S.L. 1992. Proterozoic granulite terranes. In: Condie K. (ed.) *Proterozoic Crustal Evolution.* Elsevier, Amsterdam. 301-359.

Harley S.L. 1993. Sapphirine granulites from the Vestfold Hills, East Antarctica: Geochemical and metamorphic evolution. *Antarctic Science,* **5**, 389-402.

Harley S.L. & Black L.P. 1987. The Archaean geological evolution of Enderby Land, Antarctica. In: Park R.G. & Tarney J. (eds.) *Evolution of the Lewisian and Comparable High-Grade Terranes.* Special Publication of the Geological Society, London, **27**, 285-296.

Harley S.L. & Black L.P. 1997. A revised Archaean chronology for the Napier Complex, Enderby Land, from SHRIMP ion microprobe studies. *Antarctic Science,* **9**, 74-91.

Harley S.L. & Buick I.S. 1992. Wollastonite-scapolite assemblages as indicators of granulite pressure-temperature-fluid histories: The Rauer Group, East Antarctica. *Journal of Petrology*, **33**, 693-728.

Harley S.L. & Carswell D.A. 1995. Ultradeep crustal metamorphism: A prospective view. *Journal of Geophysical Research*, **100**, 8367-8380.

Harley S.L. & Christy A.G. 1995. Titanium-bearing sapphrine in a partially melted aluminous granulite xenolith, Vestfold Hills, Antarctica: Geological and mineralogical implications. *European Journal of Mineralogy*, **7**, 637-653.

Harley S.L. & Fitzsimons I.C.W. 1991. Pressure-temperature evolution of metapelitic granulites in a polymetamorphic terrane: The Rauer Group, East Antarctica. *Journal of Metamorphic Geology,* **9**, 231-243.

Harley S.L. & Fitzsimons I.C.W. 1995. High grade metamorphism and deformation in the Prydz Bay region, East Antarctica: Terranes, events and regional correlations. *Journal of the Geological Society, India,* **34**, 73-100.

Harley S.L. & Green D.H. 1982. Garnet-orthopyroxene barometry for granulites and peridotites. *Nature,* **300**, 697-701.

Harley S.L. & Hensen B.J. 1990. Archaean and Proterozoic high-grade terranes of East Antarctica (40-800°): A case study of diversity in granulite facies metamorphism. In: Ashworth J.R. & Brown M. (eds). *High-temperature Metamorphism and Crustal Anatexis.* London, Unwin Hyman. 320-370.

Harley S.L., Fitzsimons I.C.W. & Buick I.S. 1994. Reactions and textures in wollanstonite-scapolite granulites and their significance for pressure-temperature-fluid histories of high-grade terranes. *Precambrian Research,* **66**, 309-323.

Harley S.L., Fitzsimons I.C.W., Buick I.S. & Watt G. 1992. The significance of reworking, fluids and partial melting in granulite metamorphism, East Prydz Bay, Antarctica. In: Yoshida Y., Kaminuma K. & Shiraishi K. (eds), *Recent Progress in Antarctic Earth Science.* Terrapub, Tokyo. 119-127.

Harley S.L., Snape I. & Black L.P. 1997. Age and history of early events in a layered meta-igneous complex, Rauer Group, East Antarctica: evidence for a distinct Archaean terrane. *Precambrian Research,* **in press.**

Harley S.L., Snape I. & Fitzsimons I.C.W. 1995. Regional correlations and terrane assembly in East Prydz Bay: Evidence from the Rauer Group and Vestfold Hills. *Terra Antartica,* **1**, 49-60.

Hashiguchi H., Yamada R. & Inoue T. 1983. Practical application of low Na_2O anomalies in footwall acid lava for delimiting promising areas around the Kosaka and Fukazawa Kuroko deposits, Akita Prefectural, Japan. In: Ohmoto H & Skinner B.J. (eds), *The Kuroko Massive Sulfide Deposits, Economic Geology, Monograph* 5, 387-394.

Hawkesworth C.J. & Norry M.J. 1983. *Continental Basalts and Mantle Xenoliths.* Shiva Publishing Ltd. 272 pp.

Hawkesworth C.J., Gallagher K., Hergt J.M. & McDermott F. 1993a. Trace element fractionation processes in the generation of island arc basalts. *Philosophical Transactions of the Royal Society of London,* **A342**, 179-191.

Hawkesworth C.J., Gallagher K., Hergt J.M. & McDermott F. 1993b. Mantle and slab contributions in arc magmas. *Annual Review of Earth and Planetary Science Letters,* **21**, 175-204.

Hawkesworth C.J., Hergt J.M., Ellam R.M. & McDermott F. 1991. Element fluxes associated with subduction related magmatism. *Special Publications of the Royal Society of London,* **A335**, 393-405.

Heinrich C.A., Bain J.H.C., Fardy J.J. & Waring C.L. 1993. Bromine/chlorine geochemistry of hydrothermal brines associated with Proterozoic metasediment-hosted copper mineralization at Mount Isa, northern Australia. *Geochimica et Cosmochimica Acta,* **57**, 2991-3000.

Helgeson H.C. 1979. Mass transfer among minerals and hydrothermal solutions. In: Barnes H.L. (ed) *Geochemistry of Hydrothermal Ore Deposits.* John Wiley, New York. 568-610.

Hensen B.J. & Zhou B. 1995. A Pan-African granulite facies metamorphic episode in Prydz Bay, Antarctica: Evidence from Sm-Nd garnet dating. *Australian Journal of Earth Science,* **42**, 245-258.

Hickey R.L. & Frey F.A. 1982. Geochemical characteristics of boninite series volcanics: Implications for their source. *Geochimica et Cosmochimica Acta,* **46**, 2099-2115.

Hinton R.W. & Upton B.G.J. 1991. The chemistry of zircon: Variations within and between large crystals from syenite and alkali basalt xenoliths. *Geochimica et Cosmochimica Acta,* **53**, 197-214.

Hoek J.D. 1991. A classification of dyke-fracture geometry with examples from Precambrian dyke swarms in the Vestfold Hills, Antarctica. *Geologische Rundschau,* **80/2**, 233-248.

Hoek J.D. 1995. Dyke propagation and arrest in Proterozoic tholeiitic dyke swarms, Vestfold Hills, East Antarctica. In: Baer G. & Heimann A. (Eds) *Physics and Chemistry of Dykes*. Balkema, Rotterdam, 79-94.

Hoek J.D. & Seitz H.M. 1995. Continental mafic dyke swarms as tectonic indicators: An example from the Vestfold Hills, East Antarctica. *Precambrian Research,* **75**, 121-140.

Hoek J.D., Dirks P.G.H.M. & Passchier C.W. 1992. A late-Proterozoic extensional-compressional tectonic cycle in East Antarctica. In: Yoshida Y., Kaminuma K. & Shiraishi K. (eds). *Recent Progress in Antarctic Earth Science.* Terrapub, Tokyo. 137-143.

Hofmann A.W. 1988. Chemical differentiation of the Earth: The relationship between mantle, continental crust, and oceanic crust. *Earth and Planetary Science Letters,* **90**, 297-314.

Holland T.J.B. & Powell R. 1990. An enlarged and updated internally consistent thermodynamic dataset with uncertainties and correlations: The system K_2O-Na_2O-CaO-MgO-MnO-FeO-Fe_2O_2-Al_2O_3-TiO_2-SiO_2-C-H_2-O_2. *Journal of Metamorphic Geology,* **8**, 89-124.

Holness M.B. & Graham C.M. 1991. Equilibrium dihedral angles in the system H_2O-CO_2-NaCl-calcite, and implications for fluid flow during metamorphism. *Contributions to Mineralogy and Petrology,* **108**, 368-383.

Hoogewerff J.A., van Bergen M.J., Vroon P.Z., Hertogen J., Wordel R., Sneyers A., Nasution A., Varekamp J.C., Moens H.L.E. & Mouchel D. 1997. U-series, Sr-Nd-Pb isotope and trace element systematics across an active island arc-continent collision zone: Implications for element transfer at the slab-wedge interface. *Geochimica et Cosmochimica Acta,* **61**, 1057-1072.

Howell D.G. 1989. *Tectonics of Suspect Terranes: Mountain Building and Continental Growth.* Chapman & Hall, London, 232 pp.

Humphries S.E. 1984. The mobility of the rare earth elements in the crust. In: Henderson P. (ed), *Rare Earth Element Geochemistry.* Elsevier, Amsterdam. 315-341.

Hunter R.H. & Sparks R.S.J. 1987. The differentiation of the Skaergaard intrusion. *Contributions to Mineralogy and Petrology,* **95**, 451-461.

Huppert H.E. & Sparks R.S.J. 1988. The generation of graphic magmas by intrusion of basalt into continental crustal material. *Geochimica et Cosmochimica Acta,* **29**, 599-624.

Huppert H.E., Sparks R.S.J., Turner J.S. & Arndt N.T. 1984. Emplacement and cooling of komatiite lavas. *Nature*, **309**, 19-22.

Irvine T.N. 1975. Crystallisation sequences in the Muskox intrusion and other layered intrusions, II. Origin of chromitite layers and similar deposits of other magmatic ores. *Geochimica et Cosmochimica Acta,* **42**, 991-1020.

Irvine T.N. 1980. Magmatic infiltration metosomatism, double-diffusive fractional crystallisation, and adcumulus growths in the Muskox Intrusion and other layered intrusions. In: Hargreaves R.B. (ed). *Physics of Magmatic Processes.* Princeton University Press. 325-383.

Irvine T.N. 1987. Processes involved in the formation and development in layered igneous rocks. Appendix II. In: Parsons I. (ed) *Origins of igneous layering.* NATO ASI Series C196, D Riedel Publishing Company, 649-656.

Irvine T.N. & Baragar W.R.A. 1971. A guide to the chemical classification of the common volcanic rocks. *Canadian Journal of Earth Science,* **8**, 523-548.

Irving A.J. & Frey F.A. 1978. Distribution of trace elements between garnet megacrysts and host volcanic liquids of kimberlitic to rhyolitic composition. *Geochimica et Cosmochimica Acta,* **42**, 771-787.

Irving A.J. & Frey F.A. 1984. Trace element abundances in megacrysts and their host basalts: Constraints on partition coefficients and megacryst genesis. *Geochimica et Cosmochimica Acta,* **48**, 1201-1221.

Jacobsen S.B. & Wasserberg G.J. 1980. Sm-Nd isotopic evolution of chondrites. *Earth and Planetary Science Letters*, **50**, 139-155.

Jahn B. & Zhang Z. 1984. Archaean granulite gneisses from eastern Hebei Province, China: Rare earth geochemistry and tectonic implications. *Contributions to Mineralogy and Petrology*, **85**, 224-243.

Jahn B., Vidal P. & Kröner A. 1984. Mulit-chronometric ages and origin of Archaean tonalitic gneisses in Finnish Lapland: A case for long crustal residence time. *Contributions to Mineralogy and Petrology*, **86**, 398-408.

James D.E. 1981. The combined use of oxygen and radiogenic isotopes as indicators of crustal contamination. *Annual Review of Earth and Planetary Science Letters* **9**, 311-344.

James P.R. & Black L.P. 1981. A review of the structural evolution and geochronology of the Archaean Napier Complex of Enderby Land, Australian Antarctic Territory. In: Glover J.E. & Groves D.I. (eds) *Archaean Geology: Second International Symposium, Perth, 1980.* Special Publication of the Geological Society of Australia. 7, 71-83.

James P.R. & Tingey R.J. 1983. The Precambrian geological evolution of the East Antarctic metamorphic shield - a review. In: Oliver R.L., James P.R. & Jago J.B. (eds) *Antarctic Earth Science.* Australian Academy of Science, Canberra. 5-10.

Janser B.W. 1994. The Star Lake Pluton, La Ronge Domain, northern Saskatchewan: Petrogenesis of a Proterozoic island-arc pluton. *Precambrian Research*, **70**, 145-164.

Jochum K.P., Seufert H.M. & Thirlwall M.F. 1990. High-sensitivity Nb analysis by spark source mass spectrometry (SSMS) and calibration of XRF Nb and Zr. *Chemical Geology,* **81**, 1-16.

Johannes W., Holtz F. & Moller F.H. 1995. REE distribution in some layered migmatites: Constraints on their petrogenesis. *Lithos*, **35**, 139-152.

Kay M. A. 1977. The origin of antiperthites in anorthosites. *American Mineralogist,* **62**, 905-912.

Kelemen P.B., Johnson K.T.M., Kinzler R.J. & Irving A.J. 1990a. High-field-strength element depletions in arc basalts due to mantle-magma interaction. *Nature*, **345**, 521-524.

Kelemen P.B., Joyce D.B., Webster J.D. & Holloway J.R. 1990b. Reaction between ultramafic rock and fractionating basaltic magma II. Experimental investigation of reaction between olivine tholeiite and harzburgite at 1150-1050°C and 5kb. *Journal of Petrology*, **31**, 99-134.

Kelemen P.B., Shimizu N. & Dunn T. 1993. Relative depletion in niobium in some arc magmas and the continental crust: Partitioning of K, Nb, La and Ce during melt/rock reaction in the upper mantle. *Earth and Planetary Science Letters*, **120**, 111-134.

Kerr R.A. 1985. Plate tectonics goes back 2 billion years. *Science,* **230**, 1364-1367.

Kerr A. & Fryer B.J. 1994. The importance of late- and post-orogenic growth in the early Proterozoic: Evidence from Sm-Nd isotopic studies of igneous rocks in the Makkovik Province, Canada. *Earth and Planetary Science Letters*, **125**, 71-88.

Kim J. & Jacobi R.D. 1996. Geochemistry and tectonic implications of Hawley Formation meta-igneous units: northwestern Massachusetts. *American Journal of Science*, **296**, 1126-1174.

Kinny P.D., Black L.P. & Sheraton J.W. 1993. Zircon ages and the distribution of Archaean and Proterozoic rocks in the Rauer Islands. *Antarctic Science,* **5**, 192-206.

Kröner A. 1984. Evolution, growth and stabilization of the Precambrian lithosphere. *Physical and Chemical Earth*, **15**, 69-106.

Kröner A. 1985a. Evolution of the Archaean continental crust. *Annual Review of Earth and Planetary Science Letters*, **13**, 49-74.

Kröner A. 1985b. Ophiolites and the evolution of tectonic boundaries in the Late Proterozoic Arabian-Nubian shield of northeast Africa and Arabia. *Precambrian Research*, **27**, 277-300.

Kröner A. 1991. Tectonic evolution in the Archaean and Proterozoic. *Tectonophysics*, **187**, 393-410.

Kuehner S.M. 1989. Petrology and geochemistry of Early Proterozoic high-Mg dykes from the Vestfold Hills, Antarctica. In: Crawford A.J. (ed) *Boninites and Related Rocks.* Unwin-Hymen Press, London. 208-231.

Kuehner S.M. & Green D.H. 1991. Uplift history of the East Antarctic Shield: constraints imposed by high-pressure experimental studies of Proterozoic mafic dykes. In: Thomson M.R.A., Crame J.A. & Thomson J.W. (eds). *Geological Evolution of Antarctica.* Cambridge University Press. 1-6.

Langmuir C.H. 1989. Geochemical consequence of in-situ crystallisation. *Nature,* **340**, 199-205.

Lanyon R., Black L.P. & Seitz H.M. 1993. U-Pb zircon dating of mafic dykes and its application to the Proterozoic geological history of the Vestfold Hills, East Antarctica. *Contributions to Mineralogy and Petrology,* **115**, 184-203.

Larsen L.M. & Nielsen T.F.D. 1991. Importance of iron-rich tholeiitic magmas at divergent plate margins: A reappraisal. *Geology,* **19**, 269-272.

Larsen R.B., Brooks C.K. & Bird D.K. 1992. Methane-bearing, aqueous saline solutions in the Skaergaard Intrusion, East Greenland. *Contributions to Mineralogy and Petrology,* **112**, 428-437.

Lasaga A.C. 1989. Fluid flow and chemical reaction kinetics in metamorphic systems - a new simple model. *Earth and Planetary Science Letters,* **94**, 417-424.

Lasaga A.C. & Rye D.M. 1993. Fluid flow and chemical reaction kinetics in metamorphic systems. *American Journal of Science.* **293**, 361-404.

Le Maitre R.W., Bateman P., Dudek A., Keller J., Lameyre Le Bas M.J., Sabine P.A., Schmid R., Sorensen A., Wooley A.R. & Zanettin B. 1989. *A Classification of Igneous Rocks and Glossary of Terms.* Blackwell, Oxford. 193 pp.

Le Roex A.P., Watkins R.T. & Reid A.M.. 1996. Geochemical evolution of the Okenyenya sub-volcanic ring complex, northwestern Namibia. *Geological Magazine,* **133,** 645-670.

Lee H.Y. & Ganguly J. 1988. Equilibrium compositions of coexisting garnet and orthopyroxene: Experimental determinations in the system FeO-MgO-Al_2O_2-SiO_2, and applications. *Journal of Petrology,* **29**, 93-114.

Lindsley D.H. 1983. Pyroxene thermometry. *American Mineralogist,* **68**, 477-493.

Lindsley D.H. & Anderson D.J. 1983. A two-pyroxene thermometer. *Proceedings of the Lunar and Planetary Science Conference,* **13**, A887-A906.

Lister G.S. & Baldwin S.L. 1993. Plutonism and the origin of metamorphic core complexes. *Geology,* **21**, 607-610.

Longstaffe F.J. & Schwarcz H.P. 1977. $^{18}O/^{16}O$ of Archaean clastic metasedimentary rocks: a petrogenetic indicator for Archaean gneisses? *Geochimica et Cosmochimica Acta,* **41**, 1303-1312.

Luais B. & Hawkesworth C.J. 1994. The generation of continental crust: An integrated study of crust-forming processes in the Archaean of Zimbabwe. *Journal of Petrology,* **35**, 43-93.

Marquer D. & Burkhard M. 1992. Fluid circulation, progressive deformation and mass transfer processes in the upper crust: The example of basement-cover relationships in the External Crystalline Massifs, Switzerland. *Journal of Structural Geology,* **14**, 1047-1057.

Marshall L.A. & Sparks R.S.J. 1984. Origin of some mixed-magma and net-veined ring intrusions. *Journal of the Geological Society, London,* **141**, 171-182.

Martin D. 1989. A stirring tale of crystal and currents. *New Scientist,* **25**, 53-59.

Martin H. 1986. Effect of steeper Archaean geothermal gradient on geochemistry of subduction-zone magmas. *Geology,* **14**, 753-756.

Martin H. 1987. Petrogenesis of Archaean trondhjemites, tonalites and granodiorites from eastern Finland: Major and trace element geochemistry. *Journal of Petrology,* **28**, 921-953.

Martin H. 1994. Archaean grey gneisses and the genesis of continental crust. In: Condie K.C. (ed) *Archaean Crustal Evolution. Developments in Precambrian Geology 11.* Elsevier 205-260.

Martin D. & Nokes R. 1988. Crystal settling in a vigorously convecting magma chamber. *Nature*, **332**, 534-536.

Matsuhisha Y. 1979. Oxygen isotope composition of volcanic rocks from the East Japan island arcs and their bearing on petrogenesis. *Journal of Volcanology and Geothermal Research*, **5**, 271-296.

McBirney A.R. 1975. Differentiation of the Skaergaard intrusion. *Nature*, **253**, 691-694.

McBirney A.R. 1980. Mixing and unmixing of magmas. *Journal of Volcanology and Geothermal Research*, **7**, 357-371.

McBirney A.R. 1984. *Igneous Petrology*. Freeman, Cooper & Co., San Francisco, USA. 504 pp.

McBirney A.R. 1987. Constitutional zone refining of layered intrusions. In: Parsons I. (ed) *Origins of Igneous Layering*. D. Reidel Publishing Co., 437-452.

McBirney A.R. 1989. The Skaergaard Layered Series: I. Structure and average compositions. *Journal of Petrology*, **30**, 363-397.

McBirney A.R. & Noyes R.M. 1979. Crystallization and layering of the Skaergaard intrusion. *Journal of Petrology*, **20**, 487-554.

McCulloch M.T. 1993. The role of subducted slabs in an evolving earth. *Earth and Planetary Science Letters*, **115**, 89-100.

McCulloch M.T. & Black L.P. 1984. Sm-Nd isotopic systematics of Enderby Land granulites and evidence for the redistribution of Sm and Nd during metamorphism. *Earth and Planetary Science Letters*. **71.** 46-58.

McCulloch M.T. & Gamble J.A. 1991. Geochemical and geodynamical constraints on subduction zone magmatism. *Earth and Planetary Science Letters*, **102**, 358-374.

McDonough W.F. & Sun S.S. 1995. The Composition of the Earth. *Chemical Geology*, **120**, 223-253.

McKenzie D. & O'Nions R.K. 1991. Partial melt distributions from inversion of rare earth element concentrations. *Journal of Petrology*, **32**, 1020-1091.

McLeod I.R., Trail D.S., Cook P.J. & Wallis G.R. 1966. *Geological work in Antarctica, January to March, 1965. Bureau of Mineral Resources. Australia, Record 1966/9.*

McNaughton N.J. & Wilson A.F. 1983. The geochemical and oxygen isotope affinities of Proterozoic mafic granulites from the Einasleigh Metamorphics, northern Queensland. *Precambrian Research*, **21**, 21-37.

Meissner R. 1986. *The Continental Crust, A Geophysical Approach*. Academic Press, 426 pp.

Meschede M. 1986. A method of discriminating between different types of mid-ocean ridge basalts and continental tholeiites with a Nb-Zr-Y diagram. *Chemical Geology*, **56**, 207-218.

Miller C.F. 1985. Are strongly peraluminous magmas derived from pelitic sedimentary sources? *Journal of Geology*, **93**, 673-689.

Moores E.M. 1991. Southwest US-East Antarctica (SWEAT) connection: A hypothesis. *Geology*, **19**, 425-428.

Morimoto N. 1988. Nomenclature of pyroxenes. *Mineralogical Magazine*, **52**, 535-550.

Morse S.A. 1980. *Basalts and Phase Diagrams*. Springer, New York, Berlin, Heidelberg.

Muir R.J., Fitches W.R. & Maltman A.J. 1994. The Rhinns Complex: Proterozoic basement on Islay and Colonsay, Inner Hebrides, Scotland, and in Inishstrahull, NW Ireland. *Transactions of the Royal Society of Edinburgh*, **85**, 77-90.

Mullen E.D. 1983. $MnO/TiO_2P_2O_5$: A minor element discriminant for basaltic rocks of oceanic environments and its implications for petrogenesis. *Earth and Planetary Science Letters*, **62**, 53-62.

Munksgaard N.C, Thost D.E. & Hensen B.J. 1992. Geochemistry of Proterozoic granulites from the Northern Prince-Charles Mountains, East Antarctica. *Antarctic Science*, **4**, 59-69.

Murton B.J., Peete D.W., Arculus R.J., Pearce J.A. & Van der Laan S.R. 1992. Trace element geochemistry of volcanic rocks from site 786: The Izu-Bonin forearc. *Proceedings of the Ocean Drilling Program-Scientific Results*, **125**, 211-235.

Nabelek P.I. & Glascock M.D. 1995. REE-depleted leucogranites, Black Hills, south Dakota - a consequence of disequilibrium melting of monazite-bearing schists. *Journal of Petrology*, **36**, 1055-1071.

Nakamura N. 1974. Determination of REE, Ba, Fe, Na, and K in carbonaceous and ordinary chondrites. *Geochimica et Cosmochimica Acta*, **38**, 757-773.

Naslund H.R. 1990. The differentiation of the Skaergaard Intrusion. A discussion of Hunter & Sparks (in *Contributions to Mineralogy and Petrology*, **95**, 451-461). *Contributions to Mineralogy and Petrology*, **104**, 235-247.

Neilson RL. 1988. A model for the simulation of combined major and trace element liquid lines of descent. *Geochimica et Cosmochimica Acta*, **52**, 27-38.

Newton R.C. & Perkins D. 1982. Thermodynamic calibration of geobarometers based on the assemblages garnet-plagioclase-orthopyroxene (clinopyroxene)-quartz. *American Mineralogist*, **67**, 203-222.

Norrish K. & Hutton J.T. 1969. An accurate X-ray spectrographic method for the analysis of a wide range of geological samples. *Geochimica et Cosmochimica Acta*, **33**, 431-453.

Norton D. & Taylor Jr H.P. 1979. Quantitative simulation of the hydrothermal systems of crystallizing magmas on the basis of transport theory and oxygen isotope data: An analysis of the Skaergaard intrusion. *Journal of Petrology*, **20**, 421-486.

Norton D. 1988. Metasomatism and permeability. *American Journal of Science*, **288**, 604-618.

Noyes R.M. 1979. Crystallisation and layering of the Skaergaard intrusion. *Journal of Petrology*, **20**, 487-554.

Nutman A.P., Friend C.R.L., Baadsgaard H. & McGregor V.R. 1989a. Evolution and assembly of Archaean gneiss terranes in the Godthåbsfjord region, southern west Greenland: Structural, metamorphic and isotopic evidence. *Tectonics*, **8**, 573-589.

Nutman A.P., Rivers T., Longstaffe F. & Park J.F.W. 1989b. The Ataneq Fault and mid-Proterozoic retrograde metamorphism of early Archaean tonalites of the Isukasia area, southern West Greenland: Reactions, fluid compositions and implications for regional studies. In: Bridgwater D. (ed), *Fluid Movements - Element Transport and the Composition of the Deep Crust*. Kluwer Academic Publishing. 151-170.

Nutman A.P., Friend C.R.L., Kinny P.D. & McGregor V.R. 1993. Anatomy of an early Archaean gneiss complex: 3900 to 3600 Ma crustal evolution in southern West Greenland. *Geology*, **21**, 415-418.

O'Conner J.T. 1965. A classification for quartz-rich igneous rock based on feldspar ratios. *US Geological Survey Prof. Paper* **525B**, B79-B84.

O'Hara M.J. 1968. The bearing of phase equilibria studies on the origin and evolution of basic and ultrabasic rocks. *Earth Science Reviews*, **4**, 69-133.

O'Hara M.J. & Mathews R.E. 1981. Geochemical evolution in an advancing, periodically replenished, periodically tapped, continuously fractionated magma chamber. *Journal of the Geological Society, London,* **138**, 237-277.

Oliver N.H.S. 1996. Review and classification of structural controls on fluid flow during regional metamorphism. *Journal of Metamorphic Geology,* **14**. 477-492.

Oliver R.L., James P.R. & Jago J.B. 1983. *Antarctic Earth Science - Proceedings of the Fourth International Symposium on Antarctic Earth Sciences, Adelaide, South Australia.* Australian Academy of Science, Canberra.

Oliver R.L., James P.R., Collerson K.D. & Ryan A.B. 1982. Precambrian geologic relationships in the Vestfold Hills, Antarctica. In: Craddock C. (ed), *Antarctic Geoscience.* Madison, University of Wisconsin Press. 435-444.

Olsen B.A., McSween, Jr. H.Y. & Sando T.W. 1983. Petrogenesis of the Concord gabbro-syenite complex, North Carolina. *American Mineralogist*, **68**, 315-333.

Pan Y. & Fleet M.E. 1996. Rare earth element mobility during prograde granulite facies metamorphism: Significance of fluorine. *Contributions to Mineralogy and Petrology*, **123**, 251-262.

Park G. 1995. Plate tectonics in the early Precambrian: Another look at an old problem. *Abstract, International conference on tectonics and metallogeny of early/mid Precambrian orogenic belts, Montreal. Canada.* p 32.

Parker A.J., James P.R., Oliver R.L. & Mielnik V. 1983. Structure, fabric development and metamorphism of Archaean gneisses of the Vestfold Hills, East Antarctica. In: Oliver R.L., James P.R. & Jago J.B. (eds) *Antarctic Earth Science.* Australian Academy of Science, Canberra. 77-84.

Passchier C.W., Bekendam R.F., Hoek J.D., Dirks P.G.H.M. & De Boorder H. 1991. Proterozoic geological evolution of the northern Vestfold Hills, Antarctica. *Geological Magazine,* **128**, 307-318.

Passchier C.W., Hoek J.D., Bekendam R.F. & De Boorder H. 1990. Ductile reactivation of Proterozoic brittle fault rocks; An example from the Vestfold Hills, East Antarctica. *Precambrian Research,* **47**, 3-16.

Paster T.P., Schauwecker D.S. & Haskin L.A. 1974. The behaviour of some trace elements during solidification of the Skaergaard layered series. *Geochimica et Cosmochimica Acta,* **38**, 1549-1577.

Patchett P.J. 1989. Radiogenic isotope geochemistry of rare earth elements. In: Lipin B.R. & McKay G.A. (eds), *Geochemistry and mineralogy of rare earth elements. Reviews in Mineralogy*, **21**. 25-41.

Patchett P.J. 1992. Isotopic studies of Proterozoic crustal growth and evolution. In: Condie K.C. (ed) *Proterozoic Crustal Evolution; Developments in Precambrian Geology*, **10**, 481-508.

Peacock S.M., Rushmer T. & Thompson A.B. 1994. Partial melting of subducting oceanic crust. *Earth and Planetary Science Letters*, **121**, 227-244.

Pearce J.A. 1983. Role of the sub-continental lithosphere in magma genesis at active continental margins. In: Hawkesworth C.J. & Norry M.J. (eds), *Continental Basalts and Mantle Xenoliths*. Nantwich, Shiva. 230-249.

Pearce J.A. & Cann J.R. 1973. Tectonic setting of basic volcanic rocks determined using trace element analyses. *Earth and Planetary Science Letters*, **19**, 290-300.

Pearce J.A. & Gale G.H. 1977. Identification of ore-deposition environment from trace element geochemistry of associated igneous host rock. *The Geological Society of London, Special Publications*, **7**, 14-24.

Pearce J.A. & Norry M.J. 1979. Petrogenetic implications of Ti, Zr, Y and Nb variations in volcanic rocks. *Contributions to Mineralogy and Petrology*, **69**, 33-47.

Pearce J.A. & Parkinson I.J. 1993. Trace element models for mantle melting: application to volcanic arc petrogenesis. In: Prichard H.M., Alabaster T., Harris N.B.W. & Neary C.R. (eds), *Magmatic Processes and Plate Tectonics, The Geological Society of London, Special Publications*, **76**, 373-403.

Pearce J.A., Harris N.B.W. & Tindle A.G. 1984. Trace element discrimination diagrams for the tectonic interpretation of granitic rocks. *Journal of Petrology*, **25**, 956-983.

Perkins D. & Newton R.C. 1981. Charnockite geobarometers based on coexisting garnet-pyroxene-plagioclase-quartz. *Nature*, **292**, 144-146.

Petersen J.S. 1987. Solidification contraction: Another approach to cumulus processes and the origin of igneous layering. In: Parsons I. (ed) *Origins of Igneous Layering*, D. Reidel Publishing Co., 505-526.

Philippot P. & Selverstone J. 1991. Trace-element-rich brines in eclogitic veins: implications for fluid composition and transport during subduction. *Contributions to Mineralogy and Petrology*, **106**, 417-430.

Pickard J. 1986. *The Antarctic Oasis: Terrestrial Environments and History of the Vestfold Hills*. Sydney, Academic Press, 465 pp.

Powell R. 1984. Inversion of the assimilation and fractional crystallisation (AFC) equations; characterisation of contaminants from isotope and trace element relationships in volcanic suites. *Journal of the Geological Society, London*, **141**, 447-452.

Powell R. & Holland T.J.B. 1988. An internally consistent dataset with uncertainties and correlations: 3. Applications to geobarometry, worked examples and a computer program. *Journal of Metamorphic Geology*, **6**, 173-204.

Presnall D.C., Dixon J.R., O'Donnell T.H. & Dixon S.A. 1979. Generation of mid-ocean ridge tholeiites. *Journal of Petrology*, **20**, 3-35.

Redman B.A. & Keays R.R. 1985. Archaean basic volcanism in the Eastern Goldfields Province, Yilgarn block, western-Australia. *Precambrian Research*, **30**, 113-152.

Ren L., Zhao Y., & Chen T., 1992. Re-examination of the metamorphic evolution of the Larsemann Hills, eastern Antarctica. In: Yoshida Y., Kaminuma K. & Shiraishi K. (eds). *Recent Progress in Antarctic Earth Science*. Terrapub, Tokyo. 145-153.

Ricci C.A., Herve F., Krynauw J.R. & LeMasurier W.E. 1993. Naming of igneous and metamorphic rock units in Antarctica: recommendation by the SCAR Working Group on Geology. *Antarctic Science,* **5**, 103-105.

Rice J.M. & Ferry J.M. 1982. Buffering, infiltration and the control of intensive variables during metamorphism. In: Ferry J.M. (ed) *Characterization of Metamorphism Through Mineral Equilibria,Reviews in Mineralogy*, **10**, 263-326.

Roberts M.P. & Clemens J.D. 1995. Feasibility of AFC models for the petrogenesis of calc-alkaline magma series. *Contributions to Mineralogy and Petrology*, **121**, 139-147.

Robinson P. 1980. The composition space of terrestrial pyroxenes - internal and external limits. In: Prewitt C.T. (ed) *Pyroxenes, Reviews in Mineralogy*, **7**, 419-494.

Rockow K.M., Haskin L.A., Jolliff B.L. & Fountain D.M. 1997. Constraints on element mobility associated with the conversion of granulite to eclogite along fractures in an anorthositic complex on Holsnøy, Norway. *Journal of Metamorphic Geology*, **15**, 409-418.

Rogers J.J.W., Miller J.S. & Clements A.S. 1995. A Pan-African zone linking East and West Gondwana. In: Yoshida M. & Santosh M. (eds) *India and Antarctica During the Precambrian*, Geological Society of India, memoir 34, 11-24.

Rollinson H.R. 1987. Early basic magmatism in the evolution of Archaean high-grade gneiss terrains: an example from the Lewisian of NW Scotland. *Mineralogical Magazine*, **51**, 345-355.

Rollinson H.R. 1993. *Using Geochemical Data: Evaluation, Presentation, Interpretation.* Longman Scientific and Technical, 352 pp.

Rollinson H.R. 1996. Tonalite-trondhjemite-granodiorite magmatism and the genesis of Lewisian crust during the Archaean. In: Brewer T.S. (ed) *Precambrian Crustal Evolution in the North Atlantic region, Geological Society Special Publications*, **112**, 25-42.

Rollinson H.R. & Windley B.F. 1980a. Selective elemental depletion during metamorphism of Archaean granulites, Scourie, NW Scotland. *Contributions to Mineralogy and Petrology,* **72**, 257-263.

Rollinson H.R. & Windley B.F. 1980b. An Archaean granulite-grade tonalite-trondhjemite-granite suite from Scourie, NW Scotland: geochemistry and origin. *Contributions to Mineralogy and Petrology,* **72**, 265-281.

Rosing M.T. 1990. The theoretical effect of metasomatism on Sm-Nd isotopic systems. *Geochimica et Cosmochimica Acta,* **54**, 1337-1341.

Rudnick R.L., McLennan S.M. & Taylor S.R. 1985. Large ion lithophile elements in rocks from high pressure granulite facies terranes. *Geochimica et Cosmochimica Acta*, **49**, 1645-1655.

Sandeman H.A., Clark A.H., Styles M.T., Scott D.J., Malpas J.G. & Farrar E. 1997. Geochemistry and U-Pb and ^{40}Ar-^{39}Ar geochronology of the Man of War Gneiss, Lizard Complex, SW England: pre-Hercynian arc-type crust with a Sudeten-Iberian connection. *Journal of the Geological Society, London*, **154**, 403-417.

Sandiford M. 1985. The metamorphic evolution of granulites at Fyfe Hills - implications for Archaean crustal thickness in Enderby Land, Antarctica. *Journal of Metamorphic Geology*, **3**, 155-178.

Saunders A.D. & Tarney J. 1984. Geochemical characteristics of basaltic volcanism within back-arc basins. In: Kokelaar B.P. & Howells M.F. (eds), *Marginal Basin Geology, The Geological Society of London, Special Publications*, **16**, 59-76.

Sawyer E.W. 1991. Disequilibrium melting and the rate of melt-residuum separation during migmatisation of mafic rocks from the Grenville Front, Quebec. *Journal of Petrology*, **32**, 701-738.

Seitz H.M. 1991. *Geochemistry and Petrogenesis of High-Mg Tholeiites and Lamprophyres in the Vestfold Hills, Antarctica.* PhD thesis (unpublished), Univ. Tasmania.

Seitz H.M. 1994. Estimation of emplacement pressure for 2350 Ma high-Mg tholeiite dykes, Vestfold Hills, Antarctica. *European Journal of Mineralogy*, **6**, 195-208.

Seitz H.M. & Keays R.R. 1997. Platinum Group element segregation and mineralization in a Noritic Ring Complex formed from Proterozoic siliceous high magnesium basalt magmas in the Vestfold Hills, Antarctica. *Journal of Petrology*, **38**, 703-725.

Selverstone J., Franz G., Thomas S. & Getty S.R. 1992. Fluid variability in 2 GPa eclogites as an indicator of fluid behaviour during subduction. *Contributions to Mineralogy and Petrology*, **112**, 341-357.

Selverstone J., Morteani G. & Staude J.-M. 1991. Fluid channelling during ductile shearing: transformation of granodiorite into aluminous schist in the Tauern Window, Eastern Alps. *Journal of Metamorphic Geology*, **9**, 419-431.

Sheraton J.W. & Black L.P. 1981. Geochemistry and geochronology of Proterozoic tholeiite dykes of East Antarctica: evidence for mantle metasomatism. *Contributions to Mineralogy and Petrology*, **78**, 305-317.

Sheraton J.W. & Black L.P. 1987. Geochemistry and geochronology of Proterozoic tholeiite dykes of East Antarctica - evidence for mantle metasomatism. *Contributions to Mineralogy and Petrology*, **78**, 305-317.

Sheraton J.W. & Black L.P. 1988. Chemical evolution of granitic rocks in the East Antarctic Shield, with particular reference to post-orogenic granites. *Lithos*, **21**, 37-52.

Sheraton J.W. & Collerson K.D. 1983. Archaean and Proterozoic geological relationships in the Vestfold Hills - Prydz Bay area, Antarctica. *BMR Journal of Australian Geology Geophysics*, **8**, 119-128.

Sheraton J.W. & Collerson K.D. 1984. Geochemical evolution of Archaean granulite-facies gneisses in the Vestfold Block and comparisons with other Archaean gneiss complexes in the East Antarctic Shield. *Contributions to Mineralogy and Petrology*, **87**, 51-64.

Sheraton J.W., Black L.P. & McCulloch M.T. 1984. Regional geochemical and isotopic characteristics of high-grade metamorphics of the Prydz Bay area: the extent of Proterozoic reworking of Archaean continental crust in East Antarctica. *Precambrian Research*, **26**, 169-198.

Sheraton J.W., Black L.P. & Tindle A.G. 1992. Petrogenesis of plutonic rocks in a Proterozoic granulite-facies terrane - the Bunger Hills, East Antarctica. *Chemical Geology*, **97**, 163-198.

Sheraton J.W., Black L.P., McCulloch M.T. & Oliver R.L. 1990. Age and origin of a compositionally varied mafic dyke swarm in the Bunger Hills, East Antarctica. *Chemical Geology*, **85**, 215-246.

Sheraton J.W., Ellis D.J. & Kuehner S.M. 1985. Rare-earth element geochemistry of Archaean orthogneisses and evolution of the East Antarctic Shield. *BMR Journal of Australian Geology and Geophysics*, **9**, 207-218.

Sheraton J.W., England R.N. & Ellis D.J. 1982. Metasomatic zoning in sapphirine-bearing granulites from Antarctica. *BMR Journal of Australian Geology & Geophysics*, **7**, 269-273.

Sheraton J.W., Offe L.A., Tingey R.J. & Ellis D.J. 1980. Enderby Land, Antarctica - an unusual Precambrian high-grade metamorphic terrain. *Journal of the Geological Society of Australia*, **27**, 1-18.

Sheraton J.W., Tingey R.J., Black L.P. & Oliver R.L. 1993. Geology of the Bunger Hills area, Antarctica: Implications for Gondwana correlations. *Antarctic Science*, **5**, 85-102.

Sheraton J.W., Tingey R.J., Black L.P., Offe L.A. & Ellis D.J. 1987. Geology of Enderby Land and western Kemp Land, Antarctica. *Australian Bureau of Mineral Resources, Bulletin*, **223**, 51 pp.

Shibata K., Yanai K. & Shiraishi K. 1986. Rb-Sr whole rock ages of metamorphic rocks from eastern Queen Maud Land, East Antarctica. *Memoirs of the Japanese National Institute for Polar Research, Special Issue*, **43**, 133-148.

Sims J.R., Dirks P.H.G.M., Carson C. & Wilson C.J.L. 1994. The structural evolution of the Rauer Group, East Antarctica: mafic dykes as passive markers in a composite Proterozoic terrain. *Antarctic Science*, **6**, 379-394.

Skelton A.D.L., 1992. *Petrological, Geochemical and Field Studies of Fluid Infiltration During Regional Metamorphism of the Dalradian of the SW Scottish Highlands.* Ph.D. thesis (unpublished), University of Edinburgh.

Skelton A.D.L., Graham C.M. & Bickle M.J. 1995. Lithological and structural controls on regional 3-D fluid flow patterns during greenschist facies metamorphism of the Dalradian of the SW Scottish Highlands. *Journal of Petrology*, **36**, 563-586.

Snape I. & Harley S.L. 1996. Magmatic history and the high-grade geological evolution of the Vestfold Hills, East Antarctica. *Terra Antartica*, **3**, 23-38.

Solomon G.C. & Taylor H.P. 1991. Oxygen isotope studies of Jurassic fossil hydrothermal systems, Mojave Desert, South-eastern California. In: Taylor H.P., O'Neil J.R (Jr) & Kaplan I.R. (eds). *Stable Isotope Geochemistry, Special Publication of the Geochemical Society. No.* **3**, 467-485.

Sparks R.S.J., Huppert H.E., Kerr D.P., MacKenzie D.P. & Tait S.R. 1985. Postcumulus processes in layered intrusions. *Geological Magazine*, **5**, 555-568.

Sparks R.S.J., Huppert H.E., Koyaguchi T. & Hallworth M.A. 1993. Origin of modal and rhythmic igneous layering by sedimentation in a convecting magma chamber. *Nature*, **361**, 246-249.

Spear F.S., 1993. *Metamorphic Phase Equilibria and Pressure-Temperature-Time Paths.* Mineralogical Society of America Monograph, Washington D.C. 799 pp.

St-Onge M.R. & Lucas S.B. 1995. Large-scale fluid infiltration, metasomatism and re-equilibration of Archaean basement granulites during Paleoproterozoic thrust belt construction, Ungava Orogen, Canada. *Journal of Metamorphic Geology*, **13**, 509-535.

Stahle H.J., Raith M., Hoernes S. & Delfs A. 1987. Element mobility during incipient granulite formation at Kabbadurga, Southern India. *Journal of Petrology*, **28**, 803-834.

Steiger R.H. & Jäger E. 1977. Subcommission on Geochronology: Convention on the use of decay constants in geo- and cosmochronology. *Earth and Planetary Science Letters*, **36**, 359-362.

Stern R.A. & Hanson G.N. 1991 Archaean high-Mg granodiorite: a derivative of light rare earth element- enriched monzodiorite of mantle origin. *Journal of Petrology*, **32**, 201-238.

Stewart B.W. & DePaolo D.J. 1987. Nd and Sr isotopic evidence for open system behaviour in the Skaergård intrusion. *Geological Society of America Abstracts*, **18**, p 764.

Stewart B.W. & DePaolo D.J. 1990. Isotopic studies of processes in mafic magma chambers: II The Skaergaard Intrusion, East Greenland. *Contributions to Mineralogy and Petrology*, **104**, 125-141.

Stolper E. & Newman S. 1994. The role of water in the petrogenesis of Mariana trough magmas. *Earth and Planetary Science Letters*, **121**, 293-325.

Stolz A.J., Varne R., Davies G.R., Wheller G.E. & Foden J.D. 1990. Magma source components in an arc-continent collision zone: the Flores-Lembata sector, Sunda arc, Indonesia. *Contributions to Mineralogy and Petrology*, **105**, 585-601.

Streckeison A. 1976. To each plutonic rock it's proper name. *Earth Science Review*, **12**, 1-33.

Sun S.S. & Hanson G.N. 1975. Origin of Ross Island basanitoids and limitations upon the heterogeneity of mantle sources for alkali basalts and nephelinites. *Contributions to Mineralogy and Petrology*, **52**, 77-106.

Sun S.S. & McDonough W.F. 1989. Chemical and isotopic systematics of oceanic basalts: implications for mantle composition and processes. In: Saunders A.D. & Norry M.J. (eds), *Magmatism in Ocean Basins. The Geological Society of London, Special Publication*, **42**. 313-345.

Sun S.S., Nesbitt R.W. & McCulloch M.T. 1989. Geochemistry and petrogenesis of Archaean and early Proterozoic siliceous high magnesian basalts. In: Crawford A.J. (ed) *Boninites and Related Rocks*. Unwin Hyman, London. 148-173.

Sutton J. & Watson J. 1951. The pre-Torridonian metamorphic history of the Loch Torridon and Scourie areas in the NW Highlands, and its bearing on the chronological classification of the Lewisian. *Journal of the Geological Society, London*, **106**, 241-307.

Tarney J. & Weaver B.L. 1987. Geochemistry of the Scourian complex: petrogenesis and tectonic models. In: Park R.G. & Tarney J. (eds). *Evolution of the Lewisian and Comparable High-Grade Terrain's. Special Publication of the Geological Society, London*, **27**. 45-56.

Tarney J. & Windley B.F. 1977. Chemistry, thermal gradients and evolution of the lower continental crust. *Journal of the Geological Society of London*, **134**, 153-172.

Taylor H.P. Jr. 1971. Oxygen isotope evidence for large-scale interaction between meteoric groundwaters and Tertiary granodiorite intrusions, western Cascade Range, Oregon. *Journal of Geophysical Research*, **76**, 7855-7874.

Taylor H.P. Jr. 1980. The effects of assimilation of country rocks by magmas on $^{18}O/^{16}O$ and $^{87}Sr/^{86}Sr$ systematics in igneous rocks. *Earth and Planetary Science Letters*, **47**, 243-254.

Taylor H.P. Jr. & Forester R.W. 1971. Low-^{18}O igneous rocks from the intrusive complexes of Skye, Mull, & Ardnamurchan, western Scotland. *Journal of Petrology,* **12**, 465-497.

Taylor H.P. Jr. & Forester R.W. 1979. An oxygen and hydrogen isotope study of the Skaergaard intrusion and its country rocks: a description of a 55 My old fossil hydrothermal system. *Journal of Petrology*, **20**, 355-419.

Taylor S.R. & McLennan S.M. 1985. *The Continental Crust: Its Composition and Evolution.* Blackwell, Oxford. 312 pp.

Taylor H.P. Jr. & Sheppard S.M.F. 1986. Igneous rocks: I. Processes of isotopic fractionation and isotope systematics. In: Valley J.W., Taylor Jr H.P. & O'Neil J.R. (eds). *Stable Isotopes in High Temperature Geological Processes. Reviews in Mineralogy*, **16**, 227-272.

Thompson R.N. 1984. Dispatches from the basalt front. 1. Experiments. *Proceedings of the Geologists Association*, **95**, 249-262.

Thompson M.R.A., Crame J.A. & Thompson J.W. 1991. *Geological Evolution of Antarctica - Proceedings of the Fifth International Symposium on Antarctic Earth Sciences*, Cambridge University Press. 24-28.

Thompson R.N. 1987. Phase equilibria constraints on the genesis and magmatic evolution of oceanic basalts. *Earth Science Review,* **24**, 161-210.

Thompson R.N., Morrison M.A., Dickin A.P. & Hendry G.L. 1983. Continental flood basalts... Arachnids rule OK In: Hawkesworth C.J. & Norry M.J. (eds). *Continental Basalts and Mantle Xenoliths.* Shiva, Nantwich. 158-185.

Thorpe R.S. & Brown G.C. 1985. *The Field Description of Igneous Rocks.* Geological Society of London Handbook Series, 4. Open University Press. 162 pp.

Thorpe R.S., Francis P.W., Hamill M. & Baker M.C.W. 1982. The Andes. In: Thorpe R.S. (ed) *Andesites: Orogenic Andesites and Related Rocks.* Chichester, Wiley, 187-205.

Tikoff B. & Teyssier C. 1992. Crustal-scale, en-echelon "P-shear" tensional bridges: A possible solution to the batholith room problem. *Geology*, **20**, 927-930.

Tilley C.E. 1962. Origin of basalt magmas: An experimental study of natural and synthetic rock systems. *Journal of Petrology*, **3**, 342-352.

Tingey R.J. 1981. *Geological investigations in Antarctica 1968-69: the Prydz Bay - Amery Ice Shelf Prince Charles Mountains area.* Bureau of Mineral Resources, Canberra, Record 1981/34: 1-72 (unpublished).

Tingey R.J. 1982. The geologic evolution of the Prince Charles Mountains - an Antarctic Archaean cratonic block. In: Craddock C. (ed) *Antarctic Geoscience.* University of Wisconsin Press, 455-464.

Tingey R.J. 1991. The regional geology of Archaean and Proterozoic rocks in Antarctica. In: Tingey R.J. (ed). *The Geology of Antarctica.* Clarendon Press, Oxford. 1-73.

Tuttle O.F. & Bowen N.L. 1958. The origin of granite in the light of experimental studies in the system $NaAlSi_3O_8$-$KAlSi_3O_8$-SiO_2-H_2O. *Memoirs of the Geological Society of America*, No. 74. 153 pp.

Twiss R.J. & Moores E.M. 1992. *Structural Geology.* WH Freeman & Co. 532 pp.

Valley J.W. & O'Neil J.R. 1984. Fluid heterogeneity during granulite facies metamorphism in the Adirondacks - stable isotope evidence. *Contributions to Mineralogy and Petrology*, **85**, 158-173.

Van Breeman O. & Dallmeyer R.D. 1984. The scale of Sr isotopic diffusion during post-metamorphic cooling of gneisses in the Inner Piedmont of Georgia, southern Appalachians. *Earth and Planetary Science Letters*, **68**, 141-150.

Van Calsteren P.W.C. 1978. Geochemistry of the polymetamorphic mafic-ultramafic complex at Cabo Ortegal (NW Spain). *Lithos*, **11**, 61-72.

Vervoort J.D., Patchett P.J., Gehrels G.E. & Nutman A.P. 1996. Constraints on early Earth differentiation from hafnium and neodymium isotopes. *Nature,* **379**, 624-627.

Wager L.R. & Brown G.M. 1968. *Layered Igneous Rocks*. Oliver & Boyd. 588 pp.

Walsh J.N. & Clarke E. 1982. The role of fractional crystallization in the formation of granitic and intermediate rocks of the Beinn Chaisgidle Centre, Mull, Scotland. *Mineralogical Magazine*, **45**, 247-255.

Walther J.V. 1994. Fluid-rock reactions during metamorphism at mid-crustal conditions. *Journal of Geology,* **102**, 559-570.

Walther J.V. & Orville P.M. 1982. Volatile production and transport in regional metamorphism. *Contributions to Mineralogy and Petrology,* **79**, 252-257.

Watt G. R. & Harley S.L. 1993. Accessory phase controls on the geochemistry of crustal melts and restites produced during water-undersaturated partial melting. *Contributions to Mineralogy and Petrology,* **114**, 550-556.

Weaver B.L. & Tarney J. 1980. Rare-earth element geochemistry of Lewisian granulite-facies gneisses, northwest Scotland: implications for the petrogenesis of the Archaean lower continental crust. *Earth and Planetary Science Letters*, **51**, 279-296.

Weaver B.L. & Tarney J. 1981a. Chemical changes during dyke metamorphism in high-grade basement terrains. *Nature*, **289**, 47-49.

Weaver B.L. & Tarney J. 1981b. Lewisian gneiss geochemistry and Archaean crustal development models. *Earth and Planetary Science Letters*, **55**, 171-180.

Weaver B.L. & Tarney J. 1983. Elemental depletion in Archaean granulite-facies rocks. In: Atherton M.P. & Gribble C.D. (eds). *Migmatites, Melting and Metamorphism*. Shiva Publishing Ltd., Nantwich, UK. 250-263.

Weaver B.L. & Tarney J. 1984. Empirical approach to estimating the composition of the continental crust. *Nature,* **310**, 575-577.

Weaver B.L., Tarney J. & Windley B. 1981. Geochemistry and petrogenesis of the Fiskenaesset anorthosite complex southern West Greenland: nature of the parent magma. *Geochimica et Cosmochimica Acta,* **45**, 711-725.

Weibe R.A. 1993. The Pleasant Bay layered gabbro-diorite, coastal Maine: Ponding and crystallization of basaltic injections into a silicic magma chamber. *Journal of Petrology,* **34**, 461-489.

Weibe R.A. & Wild T. 1983. Fractional crystallization and magma mixing in the Tigalak layered intrusion, the Nain anorthosite complex, Labrador. *Contributions to Mineralogy and Petrology*, **84**, 1047-1056.

Weinstein S.A., Yuen D.A. & Olsen P.L. 1988. Evolution of crystal-settling in magma-chamber convection. *Earth and Planetary Science Letters*, **87**, 237-248.

Wells P.R.A. 1980. Thermal models for the magmatic accretion and subsequent metamorphism of continental crust. *Earth and Planetary Science Letters*, **46**, 252-265.

White A.J.R. & Chappell B.W. 1977. Ultrametamorphism and granitoid genesis. *Tectonophysics*, **43**, 7-22.

White W.M. & Patchett J. 1984. Hf-Nd-Sr isotopes and incompatible element abundances in island arcs: implications for mantle origins and crust-mantle evolution. *Earth and Planetary Science Letters*, **67**, 167-185.

Whitehouse M.J. 1989. Sm-Nd evidence for diachronous crustal accretion in the Lewisian complex of northwest Scotland. *Tectonophysics*, **161**, 245-256.

Williams I.S., Compston W., Black L.P., Ireland T.R. & Foster J.J. 1984. Unsupported radiogenic Pb in zircon: a cause of anomalously high Pb-Pb, U-Pb and Th-Pb ages. *Contributions to Mineralogy and Petrology*, **88**, 322-327.

Wilson J.R., Menuge J.F., Pederson S. & Engell-Sorensen O. 1987. The southern part of the Fongen-Hyllingen layered mafic complex, Norway. Emplacement and crystallisation of compositionally stratified magma. In: Parsons I. (ed) *Origins of Igneous Layering* Riedel, 145-184.

Wilson M. 1989. *Igneous Petrogenesis*. Unwin Hyman, London. 466 pp.

Wilson M. 1993. Magmatic differentiation. *Journal of the Geological Society, London*, **150**, 611-624.

Winchester J.A. & Floyd P.A. 1977. Geochemical discrimination of different magma series and their differentiation products using immobile elements. *Chemical Geology*, **20**, 325-343.

Winchester J.A. & Max M.D. 1984. Element mobility associated with syn-metamorphic shear zones near Scotchport, NW Mayo, Ireland. *Journal of Metamorphic Geology*, **2**, 1-11.

Windley B.F. 1981a. Phanerozoic granulites. *Journal of the Geological Society, London*, **138**, 745-751.

Windley B.F. 1981b. Precambrian rocks in the light of the plate-tectonic concept. In: Kroner A. (ed) *Precambrian Plate Tectonics*. Elsevier, Amsterdam, 1-20.

Windley B.F. 1993. Uniformitarianism today: plate tectonics is the key to the past. *Journal of the Geological Society, London*, **150**, 7-19.

Windley B.F. 1995. *The Evolving Continents*, 3rd edition, Wilely, 526 pp.

Windrim D.P. & McCulloch M.T. 1986. Nd and Sr isotopic sytematics of central Australian granulites chronology of crustal development and constraints of the evolution of the lower continental crust.. *Contributions to Mineralogy and Petrology*, **94**, 289-303.

Wood B.J. & Walther J.V. 1986. Fluid flow during metamorphism and its implications for fluid-rock ratios. In: Walther J.V. & Wood B.J. (eds) *Fluid-Rock Interactions during Metamorphism, Reviews in Mineralogy*, **5**,. Springer-Verlag, New York. 89-108.

Wood D.A., Joron J.L., Treuil M., Norry M. & Tarney J. 1979. Elemental and Sr isotope variations in basic lavas from Iceland and the surrounding ocean floor. *Contributions to Mineralogy and Petrology*, **70**, 319-339.

Wood S.A. 1990a. The aqueous geochemistry of the rare earth elements and yttrium. 1. Review of available low-temperature data for inorganic complexes and the inorganic REE speciation of natural waters. *Chemical Geology*, **82**, 159-186.

Wood S.A. 1990b. The aqueous geochemistry of the rare earth elements and yttrium. 2. Theoretical predictions of speciation in hydrothermal solutions to 350°C at saturation water vapour pressure. *Chemical Geology*, **82**, 99-125.

Woodhead J.D., Harmon R.S. & Fraser D.G. 1987. O, S, Sr and Pb isotope variations in volcanic rocks from the Northern Mariana islands: implications for crustal recycling in intra-oceanic arcs. *Earth and Planetary Science Letters*, **83**, 39-52.

Yasutaka T. & Yoshida M. 1995. The displacement direction of the Arena Gneiss in central Sri Lanka: Implications for structural correlations in the East Gondwanaland. In: Yoshida M. & Santosh M. (eds) *India and Antarctica During the Precambrian*, Geological Society of India, memoir 34. 221-239.

Yoder H.S. & Tilley C.E. 1962. Origin of basalt magmas: an experimental study of natural and synthetic rock systems. *Journal of Petrology*, **3**, 342-532.

Yoder H.S. (ed) 1979. *The Evolution of Igneous Rocks: Fiftieth Anniversary Perspectives.* Princeton University Press. 588 pp.

Yogodzinski G.M., Volynets O.N., Koloskov A.V., Seliverstov N.I. & Matvenkov V.V. 1994. Magnesian andesites and the subduction component in a strongly calc-alkaline series at Piip Valcano, Far Western Aleutians. *Journal of Petrology*, **35**, 163-204.

York D. 1967. The best isochron. *Earth and Planetary Science Letters*, **2**, 479-482.

York D. 1969. Least squares fitting of a straight line with correlated errors. *Earth and Planetary Science Letters*, **5**, 320-334.

Yoshida M. & Santosh M. *India and Antarctica During the Precambrian*, Geological Society of India, memoir 34. 412 pp.

Zhao Y., Liu X., Song B., Zhang Z., Li J., Yao Y. & Wang Y. 1995. Constraints on the stratigraphic age of metasedimentary rocks from the Larsemann Hills, East Antarctica: possible implications for Neoproterozic tectonics. *Precambrian Research*, **75**, 175-188.

Zhao Y., Song B., Wang Y., Ren L., Li J. & Chen T. 1992. Geochronology of the late granite in the Larsemann Hills, East Antarctica. In: Yoshida Y., Kaminuma K. & Shiraishi K. (eds). *Recent Progress in Antarctic Earth Science.* Terrapub, Tokyo. 155-161.

Appendix 1

Analytical techniques and errors

A1.1 Oxygen-isotope analysis

A1.1.1 Sample preparation

Samples were prepared for whole-rock analysis by crushing into a coarse gravel using a jaw-crusher. An aliquot of this material was then totally reduced to a relatively fine fraction (~200 UK mesh size) by grinding in a tungsten tema at 15 second intervals to avoid preferential mineral loss as fines. To get close to a uniform 200 mesh size, samples were initially dry sieved, then wet sieved in distilled water and acetone to remove fines, with the final fraction for analysis collected between 75 μm and 63 μm (~190-250 mesh size). Samples were then reacted with warm dilute HCl overnight to remove all secondary calcite and dolomite. The remaining acid was removed by washing several times in distilled water and then finally in acetone. As a final check to ascertain that the aliquot for oxygen-isotope analysis was compositionally the same as the initial whole-rock composition (less volatiles and secondary carbonate), a treated 200-mesh-size powder was analysed by XRF. There were no appreciable differences.

A1.1.2 Oxygen extraction and isotopic analysis

Whole-rock oxygen-isotope ratios were determined largely following the method described by Clayton & Mayeda (1965). Prior to oxygen extraction by fluorination, samples of about 10 mg were first degassed at 200 °C for 1 hour to drive off H_2O, and were then briefly pre-fluorinated. Oxygen was then separated from the whole-rock powders by fluorination using ClF_3, which was reacted at 650 °C for 12 hours. A control subset was reacted for 72 hours with no discernible difference, and all samples are thought to have reacted completely in 12 hours. The extracted O_2 was then converted to CO_2 by heating with a carbon rod prior to isotopic analysis using a VG® SIRA 10 mass spectrometer.

All oxygen-isotope ratios are compared relative to the V-SMOW standard and are expressed in parts per mil (‰) where:

$$\delta^{18}O\ (‰) = \frac{^{18}O/^{16}O_{Sample} - {}^{18}O/^{16}O_{Standard}}{^{18}O/^{16}O_{Standard}} \times 1000$$

A1.1.3 Accuracy and precision

Whole-rock standards are not commonly used for oxygen-isotope analysis of silicates, instead pure quartz standards (NBS and SURRC in-house standards) were run alongside the whole-rock samples. Accuracy relative to these standards was better than 0.5 ‰. Most analyses were run several times (up to 5 analyses) yields and results being consistent throughout. Precision on duplicates was 0.14 ± 0.09 ‰ for 11 samples. Overall error estimates for the samples presented in Tables 6.1 and 11.1 are therefore near to the commonly quoted error of ~ 0.2 ‰.

A1.2 Radiogenic-isotope analysis

All radiogenic-isotope analyses were undertaken at SURRC under the supervision of Graeme Rogers and Rob Ellam, and the day-to-day management of Anne and Vinny. $^{143}Nd/^{144}Nd$, $^{147}Sm/^{144}Nd$ and $^{87}Sr/^{86}Sr$ were all analysed as detailed below. $^{87}Rb/^{86}Sr$ were analysed by XRF at Edinburgh by using an analytical programme designed to optimise precision for Rb and Sr, incorporating multiple sample analysis and multi-standard calibration. Selected samples were cross-checked by isotope dilution (ID) and were found to be in excellent agreement.

A1.2.1 Sr- and Nd-isotope chemistry

Sample dissolution

Samples were dissolved in PFA teflon screw-top beakers (Savillex) using 10 mls 40 % HF and 1 ml 14M HNO_3 and were placed on a hotplate overnight. The beakers were removed, cooled, and then the solution was dried down under lamps. The residue was then dissolved in 3 mls 14M HNO_3 overnight on a hotplate, and dried down as before. The residue was dissolved in 8 mls 6M HCl overnight on a hotplate. After cooling, from those samples which were to be analysed for Sm-Nd isotopes, a weighed aliquot of about 1/3 the volume of the solution was taken, to which was added weighed quantities of ^{145}Nd and ^{149}Sm spikes for isotope dilution determination of Sm and Nd concentrations. The remaining 2/3 aliquot was used for the determination of the isotopic composition of both Sr and Nd. ^{87}Rb and ^{84}Sr spikes were also added to this solution for the determination of Rb and Sr concentrations by

isotopic dilution analysis. In the case of those samples which were to be analysed only for Rb-Sr isotopes the ^{87}Rb and ^{84}Sr spikes were added to the whole solution. All solutions were dried down and the final residues each taken up in 2 mls 2.5M HCl.

Column chemistry

Sr and the REE were separated using standard cation exchange chromatography techniques. The sample was transferred to a centrifuge tube and any residue was centrifuged off. The solution was then loaded onto a pre-conditioned cation exchange column containing 10 mls Bio-Rad AG50W x 8, 200-400 mesh resin. The sample was washed in with 2*1 ml 2.5M HCl. For samples where Rb and Sr were to be collected, 29 mls 2.5M HCl were eluted, followed by collection of Rb in 7 mls 2.5M HCl; this was then evaporated to dryness. 10 mls 2.5M HCl was then eluted. The Sr fraction was collected with a further 10 mls 2.5M HCl, and evaporated to dryness. Sr blanks were less than 1 ng. For Sm and Nd spiked samples, the Sr fraction did not need to be collected, and so 56 mls 2.5M HCl were eluted.

The REE were separated by further eluting 20 mls 2.5M HCl and 10 mls 3M HNO_3. The next 26 mls 3M HNO_3 were collected, and evaporated to dryness. Sm and Nd were isolated from Ba and the other REE using 3 columns.

Column 2 (Sm and Nd separation): The residue from column 1 was dissolved in 1 ml of "orange cocktail". The cocktail consists of 75 % CH_3OH - 25 % orange cocktail mix: The mix is made up of 1336 mls H_2O - 406 mls CH_3COOH - 256 mls 5M HNO_3. The sample was loaded onto a column containing 8 mls of Bio-Rad AG1 x 8, 200-400 mesh anion exchange resin which had been pre-conditioned with 5 mls "orange cocktail". This column was encased in a water jacket through which water was kept at 25 °C by a thermostatically-controlled water bath. The sample was washed in with 2*1 ml "orange cocktail", and eluted with 10 mls "orange cocktail". For spiked samples, the next 17 mls "orange cocktail" were collected which contained the Sm fraction; this was then evaporated to dryness. A further 12 mls "orange cocktail" were then eluted. For unspiked samples, 29 mls "orange cocktail" were eluted. The next 29 mls "orange cocktail" containing the Nd fraction were then collected, and the solution evaporated to dryness.

Column 3 (Ba clean-up): The residue from column 2 was dissolved in 1 ml of 3M HNO_3 and loaded into a Sr-Spec column to remove any remaining Ba. The sample was eluted with a further 6 mls of 3M HNO_3, this was then evaporated to dryness.

Sm and Nd blanks were less than 0.2 ng.

A1.2.2 Rb-Sr and Sm-Nd Mass spectrometry

Rb

Rb samples were run on single collector VG MM30 thermal ionisation mass spectrometer. Rb samples were dissolved in a few μl of RO H_2O in a glass spitzer, loaded onto a Ta side filament of an outgassed triple Ta filament assembly, and carefully dried down so as to avoid the sample bubbling up on the filament. Beams were managed to give a peak intensity of about 5 pA ^{87}Rb. Peak intensities were corrected for zero and dynamic memory.

Sr

Sr samples were run on a VG Sector 54-30 thermal ionisation mass spectrometer with 8 Faraday collectors. Sr samples were dissolved in 1μl 1M H_3PO_4 and were loaded onto a single outgassed Ta filament. A small current is passed through the filament to dry the sample which is then increased slowly until the H_3PO_4 fumes off and the filament glows dull red. $^{87}Sr/^{86}Sr$ ratios were acquired in multi-dynamic mode (to avoid inter-collector gain calibration uncertainties) using a 3 collector peak jumping routine. Sr concentrations were determined using a static configuration for the measurement of ^{84}Sr. The data were collected in 15 blocks of 10 cycles/block, giving 150 ratios in total. Each cycle comprised 3 sequences; after each sequence the magnet was switched to place a different isotope into any given collector. The integration time for each sequence within a cycle was 5 seconds with a 2 second wait time between each sequence to allow the magnet to settle. Sr beams were managed to give an intensity of 10 pA ^{88}Sr. ^{87}Sr peak intensities were corrected for any Rb interference (if necessary). The $^{87}Sr/^{86}Sr$ ratio was corrected for mass fractionation using $^{86}Sr/^{88}Sr = 0.1194$. Repeat analysis of NBS 987 Sr standard gave $^{87}Sr/^{86}Sr = 0.710246 \pm 12$ (2σ).

Nd

Nd analyses were performed on a VG Sector 54-30 thermal ionisation mass spectrometer. Nd samples were dissolved in water and loaded on the Ta side filaments of an outgassed triple filament assembly with a Re centre filament. The sample was dried very carefully at 0.5 A. For Nd isotopic composition runs, beams were managed to give a ^{144}Nd intensity of 10 pA with a centre filament current of 4 A. Data were acquired in multi-dynamic mode using a 5 collector peak jumping routine. The data were collected in 12 blocks of 10 cycles/block, giving 120 ratios in total, with each cycle comprising 4 sequences. The

integration time for each sequence within a cycle was again 5 seconds. $^{143}Nd/^{144}Nd$ ratios were corrected for mass fractionation using $^{146}Nd/^{144}Nd = 0.7219$. Peak intensities were corrected for background and the ^{144}Nd peak was corrected for Sm interference. During the course of this study, the JM Nd standard gave $^{143}Nd/^{144}Nd = 0.511500 \pm 10$ (2σ.).

Sm

Sm analysis was also performed on the Sector 54-30 instrument. Loading techniques were the same as those for Nd. Sm beams were managed to give a ^{149}Sm beam intensity of 0.5pA. The analyses were performed in static mode, with 3 blocks of 10 cycles being collected. The integration time for each cycle was 5 seconds. Peak intensities are corrected for background. Measured Sm/Nd ratios are considered to be better than 0.15 % (2σ).

A1.2.3 Isotope dilution calculations

Rb, Sr, Sm and Nd concentrations were analysed by isotope dilution at SURRC using ^{87}Rb, ^{84}Sr, ^{149}Sm, ^{145}Nd spikes. Concentrations are calculated from the measured ratio of the mixture of spike and sample of the spike isotope relative to another isotope of known natural abundance (*i.e.* $^{87}Rb/^{85}Rb$, $^{84}Sr/^{88}Sr$, $^{145}Nd/^{143}Nd$, $^{149}Sm/^{147}Sm$). The procedure is illustrated for $^{87}Rb/^{86}Sr$ in detail in Faure (1986). For Sr, Sm and Nd, a correction is made for mass fractionation following the method described by Krough & Hurley (1968). At SURRC, the above ratios are compatible with $^{88}Sr/^{86}Sr = 8.37521$, $^{146}Nd/^{143}Nd = 1.41$ and $^{152}Sm/^{147}Sm = 1.76$.

A1.2.4 Calculation of errors

Analytical errors for individual elements were calculated by *isotope dilutions spreadsheet version 2.01* at SURRC. In the spreadsheet, elemental concentrations are expressed as ppm ($\mu g.g^{-1}$) and abundances of ^{87}Rb, ^{86}Sr, ^{147}Sm and ^{144}Nd are expressed in moles/g. Importantly, the spreadsheet calculates an error magnification factor (EMF), which is a measure of how optimal the spike to sample ratio was. For ideal ratios, this value should be close to unity, as the EMF is multiplied with the mass spectrometer error which ultimately yields the calculated analytical error.

An important and very time-consuming aspect of this study was spent working through systematic laboratory error in the ID technique. All the first batch samples were underspiked for Sm, which resulted in non-normal exponential error to be induced in the Sm determination. This is because there is a small, largely unavoidable, error in the

determination of the ^{149}Sm spike as used at SURRC. At favourable sample to spike ratios, the amount of error introduced is very small, much less than can be measured; but at very high sample/spike (*i.e.* under spiking), the errors increase exponentially. Whilst approximately the same spike was added to all samples, those with Sm concentrations > ~5 ppm were prone to over estimating $^{147}Sm/^{144}Nd$ (hence lower ε_{Nd}). All samples that were identified to be affected in this way were reanalysed at more appropriate sample to spike ratios, once the ID spreadsheet 2.01 was developed in 1995. Errors quoted in the tables in the text are thought to be normally distributed realistic estimates. Analyses with unacceptably large errors have been omitted from this study.

All errors are quoted as 2σ absolute values. Errors for $^{147}Sm/^{144}Nd$ have been calculated according to Tebbutt (1994, see Section A1.7 below). Errors for ε_{Nd} and ε_{Sr} are calculated for the age of crystallization as determined by U-Pb zircon analysis, where errors for ε_{Nd}, for example, are determined by combining maximum $^{147}Sm/^{144}Nd$ and minimum $^{143}Nd/^{144}Nd$.

A note on ε_{Sr} errors

Since there is a large difference between Sr and Rb abundances in many of these samples, it is worth noting that the percentage errors for $^{87}Rb/^{86}Sr$ will be largest for low Rb samples (< ~3 ppm level), where Rb determination approaches detection limits of the XRF technique. However, since low Rb samples have very low Rb/Sr in the orthogneisses analysed in this study, the errors involved in the back calculation procedure for these samples are minimal. Moreover, the most strongly affected samples lie near to Bulk Earth (see Chapter 11), and are not the extreme values discussed in Chapters 6 and 11.

A1.2.4 Fitting Rb-Sr and Sm-Nd isochrons (with calculated errors).

The following section has been summarized from the isotope plotting program ISOPLOT (version 2.90 written by KR Ludwig, Berkeley Isotope Geochronology Centre).

Model 1 solutions

Model 1 solutions are based on York's original algorithm, which assumes that the only cause for scatter from a straight line are the assigned errors. The points are therefore weighted proportional to the inverse-square of these errors. A test of the Model-1 assumption is provided by the probability of fit value: If more than 15-20 %, the Model-1 assumptions are

probably (but not certainly) justified. If less than 20% or so, another model may be more appropriate.

If the Model 1 solution is assumed the actual errors are calculated from the observed scatter thus invoking the use of the Student's-*t* multiplier to convert from estimated errors to 95%-confidence errors, this also specifies that the true errors and error-correlations of the data points are for some reason directly proportional to the ones assigned to them. Generally, Model-1 solutions are attempted first and such values are quoted throughout unless otherwise stated.

Model 3 solutions

Model-3 solutions are noted where 'isochrons' are even remotely sensible (*i.e.* for Rb/Sr in Chapter 11). In this model, scatter is assumed to be the result of the assigned X-Y errors plus a normally-distributed variation (of unknown magnitude) in the Y-values. This model (similar to the McIntyre *et al.*, 1966, Model 3) may be realistic in the case of Rb-Sr and other isochron data for rocks whose initial ratios were variable.

A note on isochron errors (MSWDs)

All errors are quoted as the mean weight of standard deviates (MSWD), which in it's simplest form is as a crude measure of how well the calculated isochron can account for the observed spread of data within the calculated errors for the x, y co-ordinates. It might seem obvious to state that even a poorly defined array of x, y co-ordinates will have a very low MSWD if the errors are large or if all the points are clustered (*i.e.* insufficient spread of denominator ratio). All MSWDs have been calculated using absolute values for errors on x and y.

A1.3 XRF Analysis

The following account is partly from Fitton *et al.* (in press). All samples described or presented in this study were analysed at Edinburgh under the guidance and supervision of Godfrey Fitton and Dodie James.

A1.3.1 Sample preparation

Generally, the samples analysed during this study weighed between 5 and 20 kg, depending on grainsize (with larger samples for the coarse-grained rocks). Samples were cut into small

pieces with a diamond-tipped saw and any obvious veins removed. Saw marks were ground away on a diamond wheel, and the fragments were rinsed in clean water and dried before being ground to a fine powder in a tungsten-carbide Tema barrel. The powders were analysed in Edinburgh by X-ray fluorescence (XRF) spectrometry.

Major-element concentrations were determined after fusion with a lithium borate flux containing La_2O_3 as a heavy absorber, by a method similar to that developed by Norrish and Hutton (1969). Rock powder was dried at 110°C for at least 1 hour, and a nominal but precisely-weighed 1-g aliquot ignited at 1100°C to determine loss on ignition (LOI). The residue was then mixed with Johnson Matthey Spectroflux 105 in a sample:flux ratio of 1:5, based on the unignited sample mass, and fused in a muffle furnace in a Pt5%Au crucible. After the initial fusion, the crucible was reweighed and any flux weight loss was made up with extra flux. After a second fusion over a Meker burner, the molten mixture was swirled several times to ensure homogeneity, cast onto a graphite mold, and flattened with an aluminium plunger into a thin disk. The mold and plunger were maintained at a temperature of 220° C on a hotplate.

Trace-element concentrations were determined on pressed-powder samples. Six grams of rock powder were mixed thoroughly with four drops of a 2% aqueous solution of polyvinyl alcohol. The mixture was formed into a 38-mm disc on a 40-mm diameter polished tungsten carbide disc, backed and surrounded by boric acid, and compressed in a hydraulic press at 0.6 tons/cm^2.

A1.3.1 XRF analysis and operating conditions

The fused and pressed samples were analysed using a Philips PW 1480 automatic X-ray fluorescence spectrometer with a Rh-anode X-ray tube. Because many analyses had extremely low concentrations of incompatible trace elements, the analytical conditions and calibrations for these elements were optimized for low concentrations where appropriate. Background positions were placed as close as possible to peaks and long count times were used at both peak and background positions. Where background count rates were measured on either side of the peak, as in most trace-element determinations, the count time was divided equally between the two positions.

Corrections for matrix effects on the intensities of major-element lines were made using theoretical alpha coefficients calculated on-line using the Philips software. The coefficients were calculated to allow for the amount of extra flux replacing volatile components in the

sample so that analytical totals should be 100% less the measured LOI. Intensities of the longer wavelength trace-element lines (La, Ce, Nd, Cu, Ni, Co, Cr, V, Ba, and Sc) were corrected for matrix effects using alpha coefficients based on major-element concentrations measured at the same time on the powder samples. Matrix corrections were applied to the intensities of the other trace-element lines by using the count rate from the RhKα Compton scatter line as an internal standard (Reynolds, 1963). Line-overlap corrections were applied using synthetic standards.

The spectrometer was calibrated with USGS and CRPG standards, using the values given by Jochum *et al.* (1990) for Nb and Zr, and Govindaraju (1994) for the other elements. Excellent calibration lines were obtained using these standards. Trace-element analytical precision was estimated by analysing several standards repeatedly during the analysis of the samples documented in Appendix 2. The results are given in Table A1.1 below. Some elements (especially Nb) were determined at least three times on the low-abundance samples, and the results averaged. The averages are believed to be precise to ±0.1 ppm for Nb. For the TTLC, all samples were analysed for Nb in this way in 1994, and were then reanalysed again in 1996. Variability between the two runs were all <0.5 ppm, and the relative positions of all samples with respect to each other were the same. That indicated that the signal to noise ratio is significantly above background. Accuracy is more difficult to quantify but may be assessed by comparing average standard concentrations reported in Table 1.1 with those given by Govindaraju (1994). Major-element precision is governed more by reproducibility in making the fused beads than by counting statistics. Calibration lines are excellent for all major elements so accuracy and precision are closely similar. Typical major-element precision estimates are given in Table 1.2.

A1.4 REE analysis by ICP-MS and ICP-AES

Approximately 5 months of this study was spent at SURRC on technique development to obtain acceptable REE analyses from the ICP-MS, and to establish whether $^{147}Sm/^{144}Nd$ could be measured using this more cost-effective technique (relative to ID-MS). In brief, a series of elution experiments were run to remove the effects of matrix interference, and a number of different cation exchange techniques were attempted. Unfortunatley, the problem concerns the operation of the ICP-MS. To date, no whole-rock samples have been successfully analysed by the SURRC ICP-MS, and many of my samples and experiments are still 'pending'.

As an alternative, all my REE were analysed at Royal Holloway by Nick Walsh using ICP-AES. Standard cation exchange techniques as described in Section A1.2.1 were employed to separate REE from the major cations. The REE fraction was then measured on a Phillips PV8210 1.5-m ICP-AES. The results are excellent. A blank and inhouse standard were run with every six samples, and every tenth analysis a sythetic standard containing all the REE and Y was run to check for instrument drift. As an illustration of the accuracy of the technique, Sm and Nd data from the ICP-AES were compared with the ID-MS data. All the analyses were within 10% (2σ) for Sm and well within 10% (2σ) for Nd (full details available on request). These results indicate that the REE presented in this study are better than the ± 10 % that Nick Walsh recommends for the errors from his lab.

A1.5 U-Pb and REE analysis by ion probe

A1.5.1 Zircon preparation and analysis by SHRIMP

Zircons were separated by standard heavy liquid and magnetic procedures before mounting in epoxy resin discs with fragments of SL13 standard zircon. Discs were polished and Au-coated prior to ion microprobe analysis on SHRIMP II at the Australian National University, Canberra. U-Pb analyses were performed following the techniques of Compston *et al.* (1984), Williams *et al.* (1984) and Black *et al.* (1991a). Pb/U and Pb/Pb isotopic ratios were measured at a mass resolution of 6500. Fractionation between U and Pb was monitored by reference to a $^{206}Pb/^{238}U$ ratio of 0.0928 for interspersed analyses of the SL13 standard zircon based on a power law ($^{206}Pb+/^{238}U+ = a(^{238}UO+/^{238}U+)2$) relationship. The precision of the Pb/U ratios of the unknowns is controlled largely by the precision of $^{206}Pb/^{238}U$ for the standard (1.5%). $^{232}Th/^{238}U$ is derived from measured $^{232}ThO+/^{238}U+$ by the linear relationship: $^{232}Th/^{238}U = (0.03446\ (^{238}UO+/^{238}U+) + 0.8680)^{232}ThO+/^{238}U+$. Radiogenic Pb corrections were derived following the subtraction of contemporaneous common Pb (Cumming & Richards, 1975).

A1.5.2 Data treatment procedures and SIMS analysis of RI15 zircons

Specific details of data treatment and procedures are documented in the main body of the text (Chapters 6 & 11). Analyses of samples SH45 and RI43 were carried out over a 2 day session. Sample RI15 was analysed in two later sessions in order to clarify apparent age / chemistry relations within complex zircons. All the Vestfold Hills samples (VH179, VH407, VH514c) were analysed in a continuous three-day session.

Table A1.1 Typical XRF results of international standards analysed during the course of this study. These three standards were analysed three times each before and after every batch of samples to monitor spectrometer performance.

XRF	BCR-1			BIR-1			BHVO-1		
	Mean	1 σ	n	Mean	1 σ	n	Mean	1 σ	n
Nb	13.3	0.1	3	0.6	0.2	3	20.1	0.1	3
Zr	190.8	0.4	3	13.4	0.3	3	177.7	0.4	3
Y	37.2	0.2	3	16.4	0.6	3	28.1	0.4	3
Sr	333.7	0.4	3	110.6	0.4	3	403.0	0.9	3
Rb	48.1	0.6	3	0.2	0.3	3	9.6	0.3	3
Th	6.1	0.4	15				1.4	0.5	15
Pb	14.0	0.4	15				2.5	0.5	15
La	24.9	0.7	15	0.9	1.1	15	14.7	2.1	3
Ce	53.7	1.3	15	1.0	1.8	15	39.2	0.6	3
Nd	28.6	1.0	15	2.0	1.0	15	26.4	0.8	3
Zn	126.3	0.5	3	69.6	0.2	3	105.1	0.6	3
Cu	26.6	0.5	3	118.0	0.5	3	132.2	3.0	3
Ni	14.2	0.2	3	152.8	1.0	3	114.3	1.2	3
Co	37.7		1	52.9		1	43.3		1
Cr	28.0	1.0	3	375.0	2.0	3	287.7	0.5	3
V	390.2	1.4	3	313.7	2.8	3	308.1	1.5	3
Ba	682.3	6.1	3	17.3	2.0	3	133.6	3.1	3
Sc	31.7	0.9	3	39.5	0.3	3	29.8	0.4	3
Ga	21.9		1	16.0		1	21.3		1

Table A1.2 XRF major and trace trace-element precision.

Element	Precision (2 σ)	Element	Precision (2 σ)
Fe	0.03 wt.%	Th	0.4
Mn	0.007	Pb	0.4
Ti	0.006	La	1.0
Ca	0.03	Ce	1.5
K	0.005	Nd	1.0
P	0.003	Zn	0.5
Si	0.10	Cu	0.5
Al	0.05	Ni	1.0
Mg	0.05	Co	1.0
Na	0.05	Cr	1.0
Nb	0.1 ppm	V	2.0
Zr	0.4	Ba	5.0
Y	0.4	Sc	0.5
Sr	0.5	Ga	0.4
Rb	0.3		

SIMS analysis at Edinburgh

SIMS trace element (REE , Y. U, Th, Hf) analyses of one chemically heterogeneous zircon from RI15 was carried out on a Cameca-ims4f ion microprobe at Edinburgh. A primary beam of O- ions was produced a 8 nA current and 14.5 kV and focused onto a 25 micron spot. Secondary ions accelerated through 4.5 kV were measured at a high energy offset of 120 V. Isotope ratios for trace elements were measured referenced against 30Si and recalculated to ppm. contents by calibration against standard zircon SL1 and NBS 610 glass, following the procedures described by Hinton and Upton (1991).

A1.6 Electron probe micro-analysis (EPMA)

A1.6.1 Instrument and operating procedures

Major-element concentrations of phases were obtained by wavelength dispersive EPMA using a Cameca Camebax Microbeam microprobe at Edinburgh. Analyses were usually performed at an accelerating voltage of 20 kV and a beam current of 20 nA, yielding a spot analysis of about 5 X. Feldspars, and amphiboles were analysed by rastoring the electron beam at 20 k rastor to avoid devolatilizing alkalis. Alternatively, for the fine-grained exsolution lamellae, precision was sacrificed by a factor of about two for spatial resolution, and operating conditions of 15 kV and 10 nA with a spot analysis of about 2 μm were adopted. Absolute abundances for each element were determined by comparison of X-ray count data with the standard for that element. Correction for matrix-interference effects was made by on-line PAP correction. Counting times at peak and background spectrometer positions were 30 and 15 seconds respectively.

A1.6.2 Normalization procedures

Analyses are reported as weight percentage oxide and as cations per formula unit (pfu). Cations pfu have been calculated assuming pyroxenes = 6, feldspars = 8, garnet = 12 and amphibole = 23 oxygens. All end-member compositions are determined following Deer *et al.* (1992). When variations were used, details are included in the main body of the text.

A1.6.3 Modal analysis

Detailed analysis of ternary feldspar exsolution microtextures were undertaken using the image processing on the Cameca. Details are given in the main body of the text.

A1.7 Error propagation (after Tebbutt, 1994)

Addition, subtraction, multiplication and division

The error, ± y, for a function of the sort Y=A+B+C, where errors on A, B and C are a, b and c respectively is:

$$y = \sqrt{a^2 + b^2 + c^2}$$

Where the function is of the sort Y=A/B.C the error is:

$$\frac{y}{Y} = \sqrt{\frac{a^2}{A} \quad \frac{b^2}{B} \quad \frac{c^2}{C}}$$

A1.8 Techniques references

Black L.P., Kinny P.D. & Sheraton J.W. 1991a. The difficulties of dating mafic dykes: an Antarctic example. *Contributions to Mineralogy and Petrology,* **109**, 183-194.

Compston W., Williams I.S. & Meyer C. 1984. U-Pb geochronology of zircons from lunar breccia 73217 using a sensitive high-resolution ion-microprobe. *Proceedings of the 14th Lunar Science Conference, Journal of Geophysical Research,* **89**, B525-B534.

Cumming G.L. & Richards J.R. 1975. Ore lead isotope ratios in a continuously changing Earth. *Earth and Planetary Science Letters,* **28**, 155-171.

Deer W.A, Howie R.A. & Zussman J. 1992. An introduction to the rock-forming minerals. (2nd ed), Longman, Harlow, 696 pp.

Faure G. Priciples of Isotope Geology (2nd ed.). John Wiley & Sons, Chichester, 589 pp.

Fitton J.G., A.D. Saunders, L.M. Larsen, B.S. Hardarson & Norry M.J.*In press*. Volcanic rocks from the southeast Greenland margin at 63°N: composition, petrogenesis and mantle sources. *Proceedings of the Ocean Drilling Programme, Scientific Results,* 152: College Station, TX (Ocean Drilling Program).

Govindaraju K. 1994. 1994 compilation of working values and sample description for 383 geostandards, *Geostandards Newsletter* 18:1–158.

Hinton R.W. & Upton B.G.J. 1991. The chemistry of zircon: Variations within and between large crystals from syenite and alkali basalt xenoliths. *Geochimica et Cosmochimica Acta,* **53**, 197-214.

Jochum, K.P., Seufert, H.M. & Thirlwall, M.F., 1990. High-sensitivity Nb analysis by spark-source mass spectrometry (SSMS) and calibration of XRF Nb and Zr, *Chemical Geology,* 81:1–16.

Krough T.E.,& Hurley P.M. 1968. Strontium isotope variation and whole-rock isochron studies, Grenville Province, Ontario. *Journal of Geophysical Research,* 73, 7107-7125.

McIntyre G.A., Brooks C., Compston W. & Turek A. 1966. A statistical assessment of Rb-Sr isochrons. *Journal of Geophysical Research,* 71, 5459-5468.

Norrish, K., and Hutton, J.T., 1969. An accurate X-ray spectrographic method for the analysis of a wide range of geological samples, *Geochimica et Cosmochimica Acta,* 33:431-453.

Reynolds, R.C. 1963. Matrix corrections in trace element analysis by X-ray fluorescence: estimation of the mass absorption coefficient by Compton scattering. *Americal mineralogist,* 48:1133-1143.

Tebbutt P. 1994. *Basic Mathematics for Chemists.* John Wiley & Sons, Chichester, 244 pp.

Williams I.S., Compston W., Black L.P., Ireland T.R. & Foster J.J. 1984. Unsupported radiogenic Pb in zircon: a cause of anomalously high Pb-Pb, U-Pb and Th-Pb ages. *Contributions to Mineralogy and Petrology,* **88**, 322-327.

Appendix 2

XRF data

Sample	RI3	RI4	RI5	RI10	RI11	RI14	RI15	RI18	RI19
Suite	OIK MD	E MD	E MD	SLC MT	SLC MT	E MD	SLC	SLC	SLC MT
GR	188 612	188 613	189 613	189 613	189 613	189 613	189 613	189 614	189 613
Major elements (wt%)									
SiO_2	45.77	49.82	48.32	51.06	46.91	49.54	39.68	50.58	47.20
Al_2O_3	12.68	13.55	12.71	17.07	14.39	15.06	15.33	3.26	14.57
Fe_2O_3	16.69	14.47	17.56	12.09	18.75	14.33	27.25	12.51	18.94
MgO	6.11	6.57	5.94	6.00	5.42	7.07	3.74	19.87	3.54
CaO	10.20	10.04	9.94	7.19	7.19	10.46	6.28	11.73	6.51
Na_2O	3.12	3.25	2.57	3.97	3.40	2.40	2.22	0.74	3.69
K_2O	0.64	1.00	0.35	1.05	0.93	0.44	0.38	0.15	1.59
TiO_2	3.09	1.41	2.78	1.07	3.01	1.04	2.43	0.30	3.53
MnO	0.21	0.19	0.27	0.15	0.19	0.20	0.75	0.16	0.18
P_2O_5	1.15	0.13	0.30	0.07	0.12	0.17	0.78	0.02	0.25
LOI%	0.45	-0.09	0.00	0.20	-0.28	-0.18	0.14	0.60	-0.18
Total	100.12	100.33	100.72	99.92	100.03	100.51	98.97	99.92	99.82
mg	43.4	48.8	41.5	51.0	37.7	50.8	22.3	76.9	28.2
Trace elements (ppm)									
La	28.6	6.5	9.2	2.8	23.5	9.7	52.5	-2.2	22.1
Ce	75.0	6.0	27.2	15.2	14.0	25.0	120.1	4.8	47.9
Nd	48.0	5.9	19.0	7.1	10.2	11.7	66.0	6.6	26.4
Nb	26.3	5.8	12.9	4.9	7.8	7.7	22.3	1.8	16.6
Zr	751.5	81.8	195.3	63.8	106.1	129.3	9002.0	20.6	207.4
Y	92.9	26.6	53.1	13.4	23.2	30.7	354.4	11.9	36.9
Sr	276.8	229.8	190.9	562.9	413.3	122.3	127.0	30.3	399.9
Rb	3.4	7.8	3.5	22.5	10.9	4.1	5.3	1.5	46.8
Th	5.4	4.1	4.4	3.6	5.5	3.1	15.9	1.9	9.2
Pb	6.8	8.6	4.6	9.3	6.0	16.7	5.5	-0.1	14.2
Zn	134.0	110.1	144.9	85.4	130.5	121.7	123.0	76.4	146.7
Cu	149.8	14.5	88.3	85.6	209.7	134.6	1190.0	5.4	358.0
Ni	96.8	85.2	46.1	177.6	196.6	167.5	158.0	256.5	106.1
Cr	163.3	196.6	139.2	86.4	67.8	166.8	15.1	2062.0	24.3
V	297.5	348.6	389.6	202.7	589.8	197.3	219.6	130.5	446.5
Ba	93.5	20.7	74.5	252.4	163.2	119.8	41.0	18.7	274.0
Sc	42.0	46.3	50.4	19.0	29.4	36.7	41.9	47.4	31.8
CIPW									
Q	0.00	0.00	1.61	0.00	0.00	0.00	0.00	0.00	0.00
Or	3.94	6.02	2.13	6.24	5.70	2.63	2.44	0.89	9.83
Ab	29.18	29.69	23.95	35.99	31.67	21.92	21.86	6.64	34.71
An	19.49	19.77	22.97	25.92	22.06	29.54	28.62	5.13	19.39
C	0.00	0.00	0.00	0.00	0.00	0.00	2.05	0.00	0.00
Di	20.31	24.06	20.96	7.71	11.31	17.74	0.00	42.32	10.21
Hy	7.84	3.24	19.06	9.56	9.55	20.29	15.54	29.20	7.95
Ol	7.25	11.88	0.00	10.21	10.19	3.36	19.52	13.47	6.71
Mt	5.00	3.09	4.65	2.72	4.90	2.70	4.50	1.88	5.51
Ilm	4.49	1.99	4.02	1.51	4.36	1.47	3.71	0.42	5.16
Ap	2.51	0.27	0.65	0.15	0.26	0.35	1.78	4.60	0.54

Sample	RI20	RI22	RI23	RI24	RI25	RI26	RI27	RI28	RI30
Suite	E MD	SLC MT	SLC MT	SLC MT	SLC MT	SLC MT	SLC MT	SLC MT	SLC MT
GR	189 613	188 612	188 612	188 612	188 612	188 612	188 612	188 612	188 612
Major elements (wt%)									
SiO_2	50.16	52.51	48.82	48.97	47.37	48.80	45.16	53.66	47.81
Al_2O_3	14.06	20.31	11.29	12.56	13.39	9.13	9.21	20.10	14.17
Fe_2O_3	14.84	9.28	18.76	17.70	16.77	19.70	20.49	8.25	18.27
MgO	5.79	2.61	10.72	9.26	9.47	13.21	14.33	2.72	5.88
CaO	10.04	7.56	5.17	5.94	6.76	4.77	6.26	7.48	7.38
Na_2O	3.24	5.03	2.56	2.76	2.70	1.82	1.16	5.10	3.10
K_2O	0.46	1.17	0.83	0.76	0.99	0.81	1.29	0.95	0.81
TiO_2	1.43	1.29	1.49	1.65	1.66	1.50	1.44	0.96	2.39
MnO	0.21	0.10	0.23	0.22	0.21	0.25	0.33	0.10	0.21
P_2O_5	0.16	0.17	0.18	0.15	0.19	0.16	0.15	0.17	0.12
LOI%	0.08	0.42	0.12	0.16	0.42	0.06	0.13	0.41	0.13
Total	100.48	100.44	99.94	100.12	99.93	100.23	99.95	99.90	100.27
mg	45.0	37.1	54.5	52.3	54.2	58.4	59.5	40.9	40.3
Trace elements (ppm)									
La	4.1	20.5	12.3	10.0	15.0	17.1	7.7	19.3	16.2
Ce	19.4	32.0	31.8	25.6	25.4	37.3	14.7	32.3	31.0
Nd	13.3	17.1	19.4	16.6	18.3	17.6	8.7	21.9	21.6
Nb	7.1	9.5	10.5	7.8	9.7	9.4	8.3	9.0	13.3
Zr	108.3	121.3	142.7	105.9	142.7	126.3	106.8	129.7	154.3
Y	36.1	22.6	25.2	23.3	28.6	25.9	24.3	23.1	34.3
Sr	136.2	665.2	332.1	360.3	410.6	236.8	47.5	619.9	417.9
Rb	2.6	9.8	19.4	8.5	24.0	23.3	99.5	6.8	8.0
Th	3.2	0.9	6.0	5.4	5.2	7.6	10.7	1.9	4.6
Pb	8.2	10.4	12.5	12.2	9.1	9.6	1.0	13.4	7.4
Zn	127.9	70.0	155.6	141.4	129.6	147.5	181.9	64.6	139.0
Cu	150.1	58.1	119.3	117.6	137.2	86.2	50.5	66.4	185.8
Ni	94.1	53.2	291.8	249.3	257.4	385.8	418.4	58.6	148.8
Cr	131.5	17.5	146.6	145.9	137.2	188.5	206.4	13.5	61.7
V	287.3	150.9	291.0	321.8	301.6	355.0	403.8	110.1	370.3
Ba	67.9	284.0	143.1	163.1	190.3	186.6	999.1	242.4	152.6
Sc	36.2	14.7	35.6	35.1	35.4	47.6	52.8	14.3	36.4
CIPW									
Q	0.00	0.00	0.00	0.00	0.00	0.00	0.00	0.00	0.00
Or	2.75	6.90	5.01	4.63	6.01	4.93	7.87	5.60	4.98
Ab	29.76	45.21	23.58	25.45	24.88	16.77	10.72	45.92	28.88
An	23.00	29.43	17.32	20.16	22.06	14.72	16.58	29.24	23.20
C	0.00	0.00	0.00	0.00	0.00	0.00	0.00	0.00	0.00
Di	21.51	5.63	6.24	7.31	8.89	6.78	11.54	5.47	11.22
Hy	13.47	1.45	30.86	28.07	15.31	42.30	21.52	7.98	16.84
Ol	3.99	6.30	11.27	8.33	16.69	8.78	26.23	1.49	6.95
Mt	3.13	2.92	3.21	3.38	3.39	3.22	3.17	2.58	4.22
Ilm	2.04	1.80	2.13	2.36	2.37	2.15	2.07	1.35	3.45
Ap	0.35	0.35	0.38	0.31	0.40	0.35	0.31	0.36	0.25

Sample	RI31	RI32	RI33	RI34	RI35	RI36	RI37	RI38	RI39
Suite	SLC MT	SLC MT	SLC MT	SLC MT	SLC	SLC	SLC	UMD	E MD
GR	188 612	188 612	188 612	188 612	188 612	188 612	188 612	188 612	188 612
Major elements (wt%)									
SiO_2	48.15	49.83	49.45	46.84	43.08	49.75	46.94	48.03	50.79
Al_2O_3	13.90	15.23	12.76	13.22	7.99	12.35	10.75	6.28	13.55
Fe_2O_3	17.25	15.29	15.95	17.85	21.39	12.67	15.24	14.76	13.84
MgO	8.81	6.86	9.77	9.06	17.87	9.48	11.51	19.67	6.35
CaO	6.75	6.60	6.94	6.58	5.90	10.84	9.74	6.36	10.39
Na_2O	2.95	3.30	2.87	2.92	1.31	2.59	2.12	0.78	3.06
K_2O	0.92	0.96	0.99	1.21	0.37	0.58	0.67	1.18	0.45
TiO_2	1.76	1.65	1.16	1.85	0.68	1.09	1.44	1.04	1.35
MnO	0.21	0.18	0.22	0.23	0.23	0.18	0.20	0.20	0.20
P_2O_5	0.17	0.17	0.09	0.20	0.07	0.08	0.14	0.12	0.12
LOI%	0.03	0.09	0.02	0.30	1.04	0.40	0.80	0.52	-0.14
Total	100.89	100.16	100.19	99.99	99.92	100.00	99.54	98.94	99.97
mg	51.7	48.5	56.2	51.6	63.7	61.1	61.3	73.6	49.0
Trace elements (ppm)									
La	13.7	15.6	9.5	8.8	14.0	9.1	10.6	9.8	3.3
Ce	32.3	30.5	19.9	30.4	13.5	17.6	27.3	15.9	6.9
Nd	20.0	15.3	10.9	14.6	3.3	11.1	17.9	8.5	9.3
Nb	9.6	9.9	5.6	13.0	2.1	3.8	6.3	5.4	5.3
Zr	129.7	136.4	73.8	147.1	52.2	89.6	112.8	82.8	82.5
Y	27.6	27.9	19.4	30.5	12.2	24.5	27.4	13.5	26.2
Sr	378.2	423.8	375.4	334.2	294.9	314.3	264.5	78.9	142.3
Rb	20.5	15.3	9.9	38.5	8.3	11.7	20.2	58.2	6.1
Th	5.7	5.5	4.5	6.3	7.8	3.8	5.4	6.2	3.4
Pb	8.3	6.8	8.9	8.2	11.9	10.8	9.6	0.4	2.7
Zn	131.2	114.1	111.8	138.7	140.1	80.3	103.9	96.7	101.6
Cu	120.9	104.9	52.5	155.7	212.8	533.4	129.8	156.9	237.9
Ni	241.8	186.5	277.5	258.9	1279.0	536.7	552.4	1175.0	75.0
Cr	114.8	85.8	133.1	118.0	326.5	512.8	1254.0	2525.7	183.5
V	321.2	266.1	367.3	304.8	195.3	383.1	390.3	177.3	322.3
Ba	204.4	154.0	78.0	236.2	297.6	160.9	131.0	216.4	33.7
Sc	35.9	28.4	43.7	40.9	28.3	55.7	50.4	28.2	43.5
CIPW									
Q	0.00	0.00	0.00	0.00	0.00	0.00	0.00	0.00	0.00
Or	5.50	5.78	5.90	7.33	2.25	3.47	4.06	7.04	2.72
Ab	26.88	30.26	26.14	26.87	12.06	23.60	19.57	7.08	28.10
An	22.30	24.42	19.30	19.87	15.20	20.67	18.35	10.28	22.41
C	0.00	0.00	0.00	0.00	0.00	0.00	0.00	0.00	0.00
Di	8.42	6.29	12.04	9.81	11.48	26.70	24.33	16.70	23.60
Hy	14.98	21.16	17.02	7.57	11.86	11.21	9.80	35.40	17.24
Ol	15.61	6.02	14.95	21.88	43.70	9.89	18.36	19.10	0.70
Mt	3.46	3.36	2.82	3.59	2.33	2.74	3.16	2.69	3.04
Ilm	2.49	2.34	1.64	2.65	0.97	1.53	2.07	1.47	1.92
Ap	0.37	0.37	0.19	0.42	0.15	0.18	0.30	0.25	0.26

Sample	RI40	RI43	RI44	RI45	RI46	RI47	RI49	RI50	RI51
Suite	SLC	SLC MT	MD	TTLC	TTLC	TTLC	TTLC	TTLC	TTLC
GR	189 614	188 612	188 612	101 538	101 538	101 538	101 538	101 538	101 538
Major elements (wt%)									
SiO_2	48.42	47.99	47.80	53.04	52.50	53.76	50.71	53.54	52.11
Al_2O_3	6.92	15.36	14.92	3.74	16.87	3.71	14.09	3.26	5.65
Fe_2O_3	15.58	16.93	14.75	7.79	5.74	8.85	13.31	7.39	9.35
MgO	12.39	4.70	7.34	20.88	8.98	20.30	7.60	18.28	17.02
CaO	13.76	7.18	10.81	13.07	12.36	11.98	11.26	15.94	14.83
Na_2O	1.41	3.52	2.50	0.64	2.80	0.78	1.99	0.87	0.73
K_2O	0.38	1.17	0.46	0.093	0.401	0.122	0.174	0.165	0.093
TiO_2	0.75	2.78	1.07	0.201	0.194	0.271	1.035	0.240	0.261
MnO	0.26	0.17	0.20	0.158	0.100	0.184	0.204	0.165	0.180
P_2O_5	0.07	0.11	0.18	0.013	0.019	0.019	0.076	0.014	0.022
LOI%	0.24	-0.31	0.34	0.44	0.30	0.12	-0.25	0.18	0.25
Total	100.15	99.60	100.37	100.07	100.26	100.10	100.20	100.04	100.50
mg	62.5	36.8	51.1	84.9	76.6	82.8	54.5	83.8	79.2
Trace elements (ppm)									
La	2.5	8.4	14.0	10.9	4.5	9	1.4	4	4.8
Ce	9.9	28.1	26.4	32.6	16.2	26.8	11.4	15.2	16.3
Nd	6.8	9.0	15.2	13.4	7.1	11.2	6.9	7.1	8.7
Nb	2.7	8.0	6.4	0.9	2.4	1.0	3.9	1.1	1.3
Zr	48.3	108.9	129.5	20.4	34.1	37.6	59.3	31.4	32
Y	18.3	22.2	32.2	13.4	12.9	22.7	22.5	17.3	17.7
Sr	135.0	444.6	126.7	13.4	125.9	27.4	108.7	22.5	27.1
Rb	2.3	27.6	1.9	4.6	7.9	2.9	2.2	3.8	3.5
Th	4.2	8.0	3.3	-0.5	-1.8	-0.3	1.8	0	0.7
Pb	3.3	6.5	4.3	4.9	1.5	2.5	3.2	0.2	2.1
Zn	131.6	116.2	115.8	86	32	64	88	40	63
Cu	46.8	289.8	155.1	33	93	38	141	85	285
Ni	304.8	180.0	180.3	453	160	497	107	493	393
Cr	1124.0	58.0	170.4	2593	74	2537	188	1421	381
V	235.6	616.1	217.0	146	104	145	328	165	190
Ba	38.7	197.9	77.5	17	83	57	38	41	32
Sc	34.9	28.9	40.2	49	24	40	47	56	60
CIPW									
Q	0.00	0.00	0.00	0.00	0.00	0.24	2.51	7.95	0.00
Or	2.28	7.18	2.79	0.59	2.36	0.59	1.19	1.19	0.59
Ab	12.95	32.76	22.96	5.44	23.67	6.62	16.94	7.44	6.20
An	11.70	23.48	28.77	7.79	32.61	7.14	28.85	3.73	12.85
C	0.00	0.00	0.00	0.00	0.00	0.00	0.00	0.00	0.00
Di	46.14	10.16	19.93	45.10	21.30	41.65	20.87	60.47	49.14
Hy	7.24	10.74	8.33	33.05	15.57	40.52	23.91	24.18	24.35
Ol	16.08	6.80	12.57	5.14	1.61	0.00	0.00	0.00	3.63
Mt	2.40	4.64	2.75	2.48	2.46	2.62	3.65	2.49	2.62
Ilm	1.06	4.02	1.52	0.38	0.38	0.57	1.91	0.38	0.57
Ap	0.15	0.24	0.37	2.33	4.63	0.05	0.19	2.34	4.65

Sample	RI52	RI53	RI54	RI55	R156	RI58	RI59	RI60	RI61
Suite	TTLC	TTLC	TTLC	TTLC	TTLC	TTLC	TTLC	TTLC	TTLC
GR	101 538	101 538	101 538	101 538	101 538	101 538	101 538	101 538	125 542
Major elements (wt%)									
SiO_2	53.22	52.81	52.09	52.38	51.34	54.95	53.06	54.41	51.35
Al_2O_3	7.18	16.00	4.94	16.47	21.07	3.02	4.54	3.59	20.75
Fe_2O_3	7.81	5.63	9.70	5.25	4.62	8.90	6.89	9.02	4.58
MgO	15.46	10.36	18.27	10.11	6.76	24.45	18.37	26.24	6.90
CaO	14.56	12.85	13.34	13.07	12.26	7.31	15.41	5.84	11.49
Na_2O	0.89	1.98	0.71	1.87	2.43	0.69	0.93	0.48	2.64
K_2O	0.086	0.230	0.079	0.225	0.326	0.270	0.058	0.054	0.842
TiO_2	0.258	0.194	0.267	0.149	0.158	0.187	0.216	0.144	0.163
MnO	0.158	0.099	0.187	0.098	0.076	0.189	0.158	0.179	0.082
P_2O_5	0.017	0.012	0.019	0.004	0.012	0.013	0.025	0.009	0.013
LOI%	0.47	0.05	0.06	0.21	0.61	0.16	0.24	-0.05	0.92
Total	100.11	100.22	99.66	99.84	99.66	100.14	99.90	99.92	99.73
mg	80.6	79.4	79.8	80.1	75.4	85.2	84.8	85.9	76.0
Trace elements (ppm)									
La	3.6	1.8	6.2	3.9	4.6	7.6	7.7	2.6	3
Ce	14.6	9.8	24.3	11.4	15	19.3	32.4	16	9.3
Nd	7.3	4.2	10.9	3.9	4.2	6.4	10.1	4.7	3.1
Nb	1.0	0.7	1.1	0.9	2.0	1.0	0.8	0.5	2.1
Zr	31.9	23.3	33.6	17	23.9	27.7	25	15	26.4
Y	16.6	8.9	18.2	8.3	7.7	12.9	11.3	6.5	8.7
Sr	34.3	119	24.1	116.7	157	18.3	22.1	16.7	189.8
Rb	1.8	1.9	1.4	2.9	3.2	7.7	1.4	0.8	20.5
Th	-0.8	-2.4	0.8	-1.3	-2.4	-0.6	-1.1	-0.6	-1.8
Pb	1.7	1.4	2.6	0.9	3	0.8	0.4	1.6	8
Zn	42	32	70	31	30	65	81	95	26
Cu	375	248	278	108	199	32	27	12	186
Ni	349	184	383	166	154	573	488	539	169
Cr	368	151	364	175	69	2326	3359	2589	69
V	177	107	184	95	74	100	149	97	68
Ba	20	62	19	53	121	59	19	23	125
Sc	56	24	56	29	17	35	47	31	12
CIPW									
Q	1.97	1.97	0.00	2.11	0.86	0.82	0.00	0.00	0.00
Or	0.60	1.18	0.60	1.21	1.80	1.80	0.60	0.60	4.80
Ab	7.62	16.74	6.10	16.16	20.84	5.92	7.96	4.10	22.70
An	14.98	34.16	10.32	35.41	46.11	4.26	9.28	8.54	43.79
C	0.00	0.00	0.00	0.00	0.00	0.00	0.00	0.00	0.00
Di	47.85	24.08	43.89	24.11	11.24	24.45	52.03	16.96	9.22
Hy	23.72	19.01	33.62	18.45	16.25	59.85	24.80	64.25	14.82
Ol	0.00	0.00	2.21	0.00	0.00	0.00	2.40	3.01	1.75
Mt	2.64	2.46	2.65	2.37	2.50	2.50	2.49	2.34	2.50
Ilm	0.58	0.38	0.58	0.19	0.38	0.39	0.38	0.19	0.39
Ap	4.69	0.00	4.70	0.00	2.35	2.35	7.03	2.34	2.35

Sample	RI62	RI63	RI64	RI65	RI66	RI67	RI68	RI70	RI72
Suite	TTLC	TTLC	TTLC	TTLC	TTLC	TTLC	TTLC	TTLC	TTLC
GR	125 542	125 542	134 543	134 543	134 543	134 543	134 543	134 543	134 543
Major elements (wt%)									
SiO_2	51.53	53.78	48.29	48.09	52.82	53.46	54.88	53.53	53.56
Al_2O_3	15.73	3.94	4.60	4.95	2.36	4.04	4.83	4.97	5.34
Fe_2O_3	6.03	8.83	18.23	13.23	18.89	7.03	8.12	8.06	11.03
MgO	9.65	20.29	16.64	13.77	25.68	20.04	25.07	16.78	20.94
CaO	12.53	11.47	9.92	16.56	0.79	14.05	6.19	14.66	8.27
Na_2O	2.79	0.83	0.63	0.87	0.04	0.77	0.60	1.28	0.65
K_2O	0.449	0.188	0.310	0.314	0.068	0.078	0.112	0.226	0.068
TiO_2	0.188	0.263	1.126	1.290	0.487	0.205	0.148	0.309	0.241
MnO	0.117	0.174	0.256	0.203	0.336	0.157	0.167	0.154	0.201
P_2O_5	0.007	0.030	0.066	0.042	-0.009	0.011	0.002	0.033	0.014
LOI%	1.12	-0.06	-0.46	0.55	-1.11	0.30	0.09	0.15	-0.11
Total	100.14	99.74	99.61	99.87	100.35	100.14	100.21	100.15	100.20
mg	77.0	82.8	65.7	68.6	74.0	85.7	86.6	81.4	79.9
Trace elements (ppm)									
La	9.7	6.9	5.5	23.6	-2.7	7.1	5.5	6	0.9
Ce	21.3	17.8	23.5	70.3	1.8	21.2	13.6	18.5	7.8
Nd	7.7	8	16.1	33.3	0.1	6.1	6.3	9.1	5.1
Nb	1.3	1.9	5.4	5.3	18.7	0.7	0.4	2.0	1.9
Zr	22	37	73.9	80.9	39.4	24.2	16.9	47.4	22.3
Y	10.6	18.9	22	38.8	7.3	14.1	8.6	20.1	12.3
Sr	121.4	28.3	98.4	59	2.5	25.5	33.8	39.2	32
Rb	6.1	9.6	4.1	4.5	4.9	2.5	1.3	7.8	1.2
Th	-0.7	0.1	3.1	2	3.2	-0.5	-1.3	-0.2	0.8
Pb	2.3	0.9	0.4	2.3	1.9	2.8	0.6	1.8	1.8
Zn	41	55	114	90	244	56	48	45	65
Cu	52	92	77	444	23	46	52	84	618
Ni	189	535	1017	1163	984	402	520	342	483
Cr	159	2372	3240	1293	2112	2388	2220	1533	251
V	109	143	290	373	105	141	93	178	151
Ba	80	46	89	65	34	29	33	73	20
Sc	28	41	43	58	22	48	30	51	44
CIPW									
Q	0.00	0.78	0.00	0.00	0.00	0.00	0.86	0.00	1.36
Or	2.36	1.20	1.79	1.80	0.59	0.60	0.59	1.18	0.60
Ab	23.59	7.11	5.39	7.46	0.34	6.60	5.11	10.79	5.54
An	29.93	6.68	10.05	8.97	4.95	7.26	10.73	7.28	10.51
C	0.00	0.00	0.00	0.00	0.01	0.00	0.00	0.00	0.00
Di	27.43	38.38	32.17	61.22	0.00	49.79	15.20	52.92	23.47
Hy	4.84	42.57	31.38	0.93	89.11	29.04	64.98	22.01	55.63
Ol	9.00	0.00	13.12	12.92	1.19	3.81	0.00	2.58	0.00
Mt	2.46	2.64	3.81	4.11	2.89	2.50	2.34	2.60	2.48
Ilm	0.38	0.58	2.11	2.50	0.95	0.38	0.19	0.57	0.38
Ap	0.00	7.03	0.16	9.39	0.00	2.35	0.00	0.07	2.33

Sample	RI73	RI74	RI75	RI76	RI77	RI80	RI81	RI83	RI84
Suite	TTLC	TTLC	TTLC	TTLC	TTLC	TTLC	TTLC	TTLC	TTLC
GR	134 543	134 543	134 543	134 543	134 543	134 543	134 543	125 542	125 542
Major elements (wt%)									
SiO_2	53.06	53.08	52.63	52.55	52.76	53.67	52.87	54.18	49.28
Al_2O_3	5.85	7.12	15.65	13.34	15.59	5.67	15.42	4.94	13.49
Fe_2O_3	9.88	8.20	6.02	6.31	6.21	9.54	5.73	7.13	15.88
MgO	18.97	15.44	10.43	11.43	10.27	18.43	10.67	21.30	6.32
CaO	11.17	14.85	12.59	13.93	12.39	11.29	12.54	10.75	10.70
Na_2O	0.70	0.97	1.99	1.90	2.06	0.70	2.14	0.97	2.50
K_2O	0.074	0.086	0.264	0.211	0.253	0.098	0.332	0.147	0.267
TiO_2	0.261	0.276	0.195	0.235	0.205	0.259	0.192	0.193	1.673
MnO	0.178	0.159	0.108	0.115	0.111	0.176	0.098	0.158	0.221
P_2O_5	0.017	0.022	0.016	0.017	0.018	0.016	0.008	0.011	0.156
LOI%	0.01	0.04	0.22	0.17	0.15	0.21	0.01	0.27	-0.42
Total	100.17	100.24	100.11	100.21	100.02	100.06	100.01	100.05	100.07
mg	80.1	79.8	78.4	79.2	77.6	80.2	79.6	86.2	45.5
Trace elements (ppm)									
La	2.2	4.3	3.6	4.1	4.2	2.3	3.3	5.1	1.3
Ce	14.2	12.2	13.5	15.4	13.6	19.6	11.4	13.3	14.7
Nd	5.7	6.1	4.8	5	4.3	9.6	4	5.7	11.1
Nb	0.6	0.7	0.5	0.7	0.5	0.6	1.0	0.8	3.3
Zr	28.4	33.5	26.3	29.7	31.8	33.4	26.8	24.5	86.7
Y	16.1	18.1	10.6	13.2	12	15.2	8.3	11.4	39.3
Sr	39.5	50.3	114.8	101.9	115.8	25.1	115.6	35.9	107.5
Rb	1	0.7	1.7	1.3	1.5	1.1	2.6	3.5	4.4
Th	-0.5	-1.2	-2.2	-1.6	-1.8	0.2	-1.9	-0.6	2.5
Pb	1.4	1.4	1.2	2.4	2.1	0.6	1.6	-0.3	1.5
Zn	59	43	33	35	35	57	31	41	106
Cu	533	358	123	257	178	316	161	40	85
Ni	437	358	185	247	181	432	197	525	83
Cr	290	348	151	220	144	305	137	2912	158
V	165	189	110	132	111	161	99	116	309
Ba	28	28	60	68	64	27	74	50	47
Sc	49	54	26	36	25	52	28	38	44
CIPW									
Q	0.26	1.57	1.62	1.59	2.37	2.76	0.00	0.00	0.43
Or	0.59	0.60	1.77	1.19	1.79	0.59	1.77	0.60	1.80
Ab	5.95	8.30	16.81	16.24	17.56	5.95	18.05	8.30	21.46
An	13.00	14.61	33.78	26.62	33.78	13.00	30.34	9.09	23.70
C	0.00	0.00	0.00	0.00	0.00	0.00	0.00	0.00	0.00
Di	33.24	48.10	24.22	34.45	20.72	33.28	26.94	36.32	25.38
Hy	43.71	23.57	18.92	16.99	20.87	41.17	20.00	41.87	18.89
Ol	0.00	0.00	0.00	0.00	0.00	0.00	5.97	0.92	0.00
Mt	2.62	2.64	2.46	2.49	2.48	2.62	2.46	2.49	4.71
Ilm	0.57	0.58	0.38	0.38	0.38	0.57	0.38	0.38	3.27
Ap	4.66	0.05	4.62	4.68	0.05	4.66	0.00	0.02	0.38

Sample	RI108	SH11	SH14	SH49	SH52A	SH63	SH64	SH65	SH66
Suite	SLC	SLC	SLC	SLC MT	E MD	PT MD	PT MD	E MD	PT MD
GR	125 542	101 538	125 542	125 542	125 542	18# 61#	18# 61#	18# 61#	18# 61#
Major elements (wt%)									
SiO_2	50.33	51.05	47.58	46.68	47.67	47.57	47.73	49.29	47.68
Al_2O_3	2.94	20.71	12.32	13.37	13.80	14.67	14.75	13.22	14.73
Fe_2O_3	17.67	7.36	20.70	20.09	16.28	12.93	12.86	15.45	12.99
MgO	22.78	4.56	4.39	5.57	7.51	7.80	7.73	7.66	7.81
CaO	3.77	9.16	8.73	6.90	10.90	11.06	11.02	9.16	11.09
Na_2O	0.17	4.30	3.14	3.25	2.67	3.15	3.07	3.01	2.99
K_2O	0.66	1.05	0.47	0.99	0.46	0.49	0.58	0.86	0.42
TiO_2	0.36	0.55	2.25	3.26	1.00	1.29	1.28	1.07	1.27
MnO	0.26	0.10	0.17	0.21	0.18	0.21	0.20	0.20	0.21
P_2O_5	0.02	0.16	0.45	0.19	0.08	0.09	0.09	0.16	0.09
LOI%		0.98	-0.18	-0.32	0.10	0.80	1.02	0.07	0.74
Total	98.97	99.97	100.02	100.19	100.65	100.05	100.32	100.15	100.02
mg	77.0	56.5	30.8	36.8	49.2	55.8	55.8	51.0	55.8
Trace elements (ppm)									
La	1.5	6.0	30.3	11.9	0.4	2.1	-1.5	11.7	-2.2
Ce	5.9	10.3	67.3	36.4	5.4	8.5	4.4	28.7	4.4
Nd	4.5	5.8	37.8	16.2	6.2	6.7	3.1	18.8	6.2
Nb	2.1	1.5	16.1	11.3	2.2	3.1	3.4	5.4	3.4
Zr	28.8	35.0	246.3	148.7	48.5	78.5	80.5	102.2	78.3
Y	8.9	8.3	59.8	30.4	23.7	28.2	28.1	25.5	28.5
Sr	13.6	395.2	256.3	363.8	154.8	139.7	163.2	350.7	142.3
Rb	38.5	12.5	0.8	12.9	1.7	5.6	7.5	7.3	6.7
Th	7.3	2.0	5.1	7.0	3.8	2.7	3.2	3.7	3.6
Pb	2.1	20.8	1.6	9.6	2.6	3.5	5.9	6.8	2.5
Zn	140.6	64.3	126.2	146.6	137.1	93.5	95.0	144.8	93.5
Cu	791.0	54.4	27.3	244.6	98.5	194.0	158.2	9.7	146.7
Ni	2247.6	118.6	14.3	190.4	123.4	118.5	112.3	304.1	114.1
Cr	2628.4	242.3	55.3	89.5	215.9	291.0	293.5	185.0	292.9
V	151.4	118.1	865.6	582.7	326.6	294.0	290.5	279.4	299.0
Ba	106.0	212.9	86.7	185.8	28.0	20.2	34.8	93.1	17.4
Sc	18.6	7.6	38.3	34.3	55.3	53.0	47.8	29.2	50.0
CIPW									
Q		0.00	0.00	0.00	0.00	0.00	0.00	0.00	0.00
Or		6.21	2.93	6.10	2.74	2.94	3.46	5.21	2.51
Ab		36.53	29.71	30.41	24.47	25.13	25.35	27.59	26.33
An		34.13	19.11	19.77	24.83	24.90	25.23	20.43	26.05
C		0.00	0.00	0.00	0.00	0.00	0.00	0.00	0.00
Di		8.26	18.75	11.69	23.87	24.32	23.88	19.90	23.55
Hy		0.00	16.80	12.97	1.55	0.00	0.00	8.26	0.00
Ol		10.38	4.29	8.73	18.27	15.51	15.47	14.00	15.97
Mt		2.14	4.13	5.19	2.67	2.97	2.96	2.74	2.95
Ilm		0.76	3.30	4.73	1.42	1.83	1.82	1.52	1.81
Ap		0.33	0.99	0.41	0.17	0.19	0.19	0.35	0.20

Sample	SH69	SH70	SH71	SH72	SH73	SH74	SH76	SH77	SH79
Suite	E MD	E MD	PT MD	MD	MD	PT MD	PT MD	L MD	SLC
GR	18# 61#	18# 61#	18# 61#	18# 61#	18# 61#	18# 61#	18# 61#	18# 61#	18# 61#
Major elements (wt%)									
SiO_2	49.43	47.74	47.46	48.95	47.87	48.79	49.73	47.63	28.45
Al_2O_3	14.38	13.34	14.69	15.08	13.66	13.40	13.28	13.45	4.59
Fe_2O_3	11.39	13.43	12.84	12.01	14.89	14.86	14.02	15.50	48.74
MgO	8.75	10.35	7.73	8.51	7.55	6.48	5.87	6.74	7.58
CaO	12.51	10.19	11.10	11.39	10.80	10.52	9.73	10.37	4.27
Na_2O	2.07	2.37	2.97	2.52	2.93	2.82	3.58	2.90	0.75
K_2O	0.35	0.80	0.63	0.42	0.79	0.42	1.06	0.91	0.35
TiO_2	0.74	0.97	1.27	0.82	1.16	2.17	2.09	2.22	6.37
MnO	0.18	0.18	0.20	0.17	0.20	0.23	0.22	0.25	0.44
P_2O_5	0.06	0.13	0.10	0.07	0.09	0.21	0.21	0.22	0.73
LOI%	0.48	0.84	1.28	0.22	0.20	0.28	0.40	0.36	-0.39
Total	100.34	100.34	100.27	100.80	101.27	100.78	100.18	100.54	101.88
mg	61.7	61.8	55.8	59.8	51.5	47.8	46.8	47.7	24.6
Trace elements (ppm)									
La	10.7	-2.2	-1.5	6.4	3.2	10.3	17.9	9.8	14.7
Ce	15.6	4.4	11.6	17.3	7.8	27.4	33.3	31.4	66.1
Nd	9.9	5.0	6.2	11.4	6.3	16.3	23.6	17.9	37.8
Nb	3.5	2.1	3.5	6.4	3.1	11.1	12.1	12.1	25.2
Zr	53.2	51.3	77.4	93.1	60.1	153.6	162.9	146.9	225.3
Y	25.9	16.5	27.8	26.0	21.8	45.5	46.8	50.8	46.9
Sr	115.1	205.1	147.7	117.2	217.0	179.8	258.4	164.9	65.9
Rb	0.9	14.8	6.0	0.4	5.2	1.8	5.9	13.7	7.1
Th	1.6	3.2	3.5	2.1	4.3	3.4	4.3	4.5	24.4
Pb	1.7	6.0	8.2	3.6	6.7	5.6	13.9	8.9	2.8
Zn	83.6	97.8	98.6	91.6	151.9	116.2	126.5	138.1	392.0
Cu	122.6	143.6	160.9	51.2	5.7	98.6	78.4	15.3	319.4
Ni	162.9	429.2	115.2	141.9	120.8	45.2	37.7	44.6	205.4
Cr	195.3	963.3	297.7	175.5	202.9	165.6	127.5	170.0	236.9
V	267.4	280.0	293.9	257.8	289.1	343.0	336.7	365.9	979.8
Ba	57.3	99.4	41.0	55.3	34.5	64.8	117.1	129.8	-27.0
Sc	50.1	31.7	52.2	44.9	53.7	52.5	49.6	59.7	31.9
CIPW									
Q	0.00	0.00	0.00	0.00	0.00	0.00	0.00	0.00	0.00
Or	2.09	4.81	3.82	2.49	4.76	2.58	6.42	5.51	2.39
Ab	18.82	21.57	24.47	22.85	24.27	26.11	32.95	26.74	5.59
An	29.29	23.71	25.44	28.90	22.24	23.36	17.46	21.57	9.31
C	0.00	0.00	0.00	0.00	0.00	0.00	0.00	0.00	0.00
Di	26.55	21.33	24.13	22.17	25.48	23.24	24.49	23.84	7.65
Hy	13.54	4.40	0.00	8.01	0.00	16.13	3.34	2.97	0.00
Ol	6.16	19.90	15.47	11.81	17.02	1.04	8.05	11.74	52.41
Mt	2.37	2.62	2.96	2.45	2.84	3.96	3.85	3.99	9.44
Ilm	1.05	1.37	1.81	1.16	1.65	3.12	2.99	3.17	10.18
Ap	0.12	0.28	0.22	0.15	0.19	0.45	0.45	0.47	1.74

Sample	VH6	VH9	VH10	VH11	VH12	VH14	VH15	VH20	VH21
Suite	VHMD	VHMD	VHMD	VHMD	MoG	VHMD	D2-GS	VHMD	GrLG
GR	910 078	962 084	948 073	910 060	882 052	908 061	915 071	900 036	962 084
Major elements (wt%)									
SiO_2	53.03	56.59	50.16	50.45	53.34	41.51	75.85	52.99	68.68
Al_2O_3	14.69	19.71	16.24	16.41	19.77	14.17	13.62	19.08	15.03
Fe_2O_3	11.36	5.42	13.42	13.61	8.24	16.46	0.31	7.63	2.3
MgO	5.59	2.52	4.96	5.09	3.83	9.5	0.1	3.16	0.88
CaO	8.25	7.4	6.6	6.56	7.04	10.62	2	8.16	3.45
Na_2O	3.94	4.96	4.11	4.13	4.59	1.85	3.23	4.57	4.71
K_2O	0.801	0.837	0.552	0.493	0.535	1.689	3.838	1.252	2.496
TiO_2	1.752	1.02	1.31	1.297	1.165	1.463	0.041	1.357	0.375
MnO	0.174	0.048	0.17	0.182	0.099	0.199	0.001	0.072	0.034
P_2O_5	0.213	0.282	1.214	1.226	0.39	0.784	-0.004	0.422	0.078
LOI%	0.16	1.63	0.48	0.51	0.57	1.48	0.29	0.78	0.68
Total	99.96	100.42	99.22	99.96	99.57	99.73	99.28	99.47	98.71
mg	50.8	49.4	43.7	43.9	49.4	54.8	40.3	46.5	44.5
Trace elements (ppm)									
La	33.4	40.5	75.2	68.7	23.1	46.4	19.2	58.9	25.5
Ce	72.8	105.9	185.9	174	53.7	136.7	21.5	150.2	37.8
Nd	35	50.7	100.8	93.8	24.7	89.8	0	75.1	7.9
Nb	25.4	13.9	30.1	31	8.8	9.4	0.5	22.2	6.6
Zr	137	400.6	207.8	203.1	27.9	92.5	39.2	476.2	198.3
Y	26.2	24.1	46.8	45.2	10.3	49.8	0.4	38.4	5.8
Sr	525.9	619.7	1259.3	1347.1	805.4	855.2	223.7	589.3	373.5
Rb	6.3	10.5	3.2	1.6	3	31.8	58.8	12.5	29.6
Th	-0.1	0.9	2.9	3	-0.5	6.3	0.3	-0.1	-1.1
Pb	7.9	8.6	6.7	8.4	6.2	1.6	14.8	9.3	10.3
Zn	131.4	62.6	156	141.8	95.3	137.2	4.4	93.8	31.2
Cu	27.7	21.5	97.1	125.4	11.1	117	-1.3	44.4	7.5
Ni	65.3	34.4	41.1	39.2	35.7	69.2	3.7	38.5	5.9
Cr	169.2	41.3	38.3	40.5	81.3	145.6	-7.9	65.2	2.5
V	154	84.2	160.4	167.3	109.3	369	0.4	104.2	21.5
Ba	302.6	385.7	1018.3	694.1	292.3	834.8	1696.3	652.7	2184.6
Sc	25.6	8	10.4	7.8	10.2	47.4	-1.3	8	-0.7
CIPW									
Q	2.16	6.57	7.06	0.09	2.67	0.00	38.28	1.21	24.63
Or	4.78	5.02	3.34	2.96	3.21	10.30	22.88	7.53	15.05
Ab	33.68	42.61	35.61	35.53	39.46	4.90	27.58	39.37	40.67
An	20.24	29.49	24.81	24.94	32.27	26.19	10.01	28.36	12.76
C	0.00	0.00	0.00	9.26	0.00	0.00	0.52	0.00	0.00
Di	16.03	4.68	0.49	0.00	0.51	18.77	0.00	8.11	3.26
Hy	14.49	5.29	26.08	26.87	14.80	0.00	0.25	7.58	0.72
Ol	0.00	0.00	0.00	0.00	0.00	24.57	0.00	0.00	0.00
Mt	4.76	3.71	4.17	4.12	3.93	4.43	0.00	4.22	0.26
Ilm	3.36	1.97	2.55	2.50	2.25	2.87	2.36	2.62	0.73
Ap	0.50	0.66	2.88	2.89	0.92	1.87	0.00	1.00	0.18

Sample	VH22	VH24	VH27	VH28	VH29	VH30	VH31	VH32B	VH33
Suite	VHMD	VHMD	GrLG	GrLG	TayS	TayS	TayS	TayS	VHMD
GR	900 036		915 071	915 070					892 035
Major elements (wt%)									
SiO_2	62.26	51.41	76.98	76.65	52.05	52.21	52.57	48.54	51.96
Al_2O_3	16.02	20.66	12.34	12.61	9.62	10.68	11.84	15.16	13.82
Fe_2O_3	4.92	8.09	0.33	0.37	12.1	11.84	11.74	14.01	14.57
MgO	1.22	2.08	0.08	0.11	10.59	9.47	8.47	4.09	4.94
CaO	2.32	7.48	0.99	1.48	9.65	9.37	9.31	7.99	8.22
Na_2O	2.7	5.02	2.09	2.26	2.25	2.47	2.99	4.01	3.55
K_2O	6.608	0.626	6.19	4.97	1.516	1.262	0.915	0.837	0.401
TiO_2	1.439	2.772	0.057	0.05	0.663	0.629	0.588	1.428	1.975
MnO	0.018	0.065	0.005	0.003	0.166	0.167	0.182	0.137	0.169
P_2O_5	0.49	0.71	-0.006	-0.005	0.297	0.313	0.275	1.582	0.141
LOI%	0.48	0.56	0.29	0.91	0.91	1.43	1.15	0.57	0.44
Total	98.48	99.47	99.35	99.41	99.81	99.84	100.03	98.35	100.19
mg	34.2	35.0	33.7	38.4	64.7	62.6	60.2	38.0	41.5
Trace elements (ppm)									
La	137.5	34	5.6	8.2	36.5	43.7	36.7	124.5	3.1
Ce	322.9	78.9	3.3	-11.8	74.5	78.7	93.1	270.8	22.6
Nd	131.8	34.8	-0.8	-14.6	54.6	64.8	61.6	142.5	17.6
Nb	27.7	18.7	0.3	0.6	4.9	4.3	5.8	18	5.4
Zr	1159.6	30.5	13.7	5.4	81.2	97.6	77.5	34.9	93.8
Y	15.9	10.3	-0.5	-0.2	58.8	63.9	56.2	76.7	30
Sr	318.7	1088.6	121.5	471.1	251.2	264.4	333.4	449	298.9
Rb	153.1	2	69.8	80.5	47.4	32.4	17.6	4.4	5.6
Th	135.3	0	0.1	1	2.3	4.2	4.4	7	2.5
Pb	42.5	6.6	18.7	14.6	5.6	6.7	7.8	8.8	2.8
Zn		68.8	4.4	6	154.3	176.7	157.4	173.8	146
Cu		22.6	0.8	4.4	50.6	58.6	65.5	109.5	56
Ni		29.5	2.3	2.9	144.9	120.6	103.4	14.8	92.7
Cr		14.5	-5.7	-6	198.4	128.8	90.7	-8.9	137.5
V		158.8	8.5	-3	195.2	157.4	140.1	337.2	155.6
Ba		416.7	755.9	6210	1238.9	1072.3	545.8	411.7	157.6
Sc		5.2	-3.4	-2.2	40.5	41.1	41.7	19.8	22.7
CIPW									
Q	16.21	2.83	39.21	41.72	0.00	3.16	0.00	0.00	3.71
Or	39.93	3.75	36.88	29.78	9.15	7.65	5.52	5.12	2.40
Ab	23.36	43.11	17.83	19.39	19.45	21.45	25.84	35.10	30.46
An	8.50	32.47	4.95	7.45	11.92	14.71	16.53	21.61	20.88
C	1.41	0.00	0.41	0.83	0.00	0.00	0.00	0.00	0.00
Di	0.00	0.38	0.00	0.00	28.37	25.12	23.50	7.27	16.17
Hy	3.11	5.08	0.20	0.28	22.22	25.90	23.12	16.32	17.14
Ol	0.00	0.00	0.00	0.00	3.70	0.00	0.60	3.59	0.00
Mt	1.67	3.30	0.00	0.00	3.20	3.17	3.09	4.39	5.11
Ilm	2.79	5.34	2.34	2.27	1.29	1.23	1.14	2.81	3.80
Ap	1.16	1.67	0.00	0.00	0.70	0.74	0.65	3.79	0.33

Sample	VH36	VH37	VH38A	VH38B	VH39A	VH39B	VH46	VH48	VH55
Suite	GrLG	D2-GS	TayS	TayS	TayS	TayS	GrLG	GrLG	ICLG
GR	892 035	893 035							
Major elements (wt%)									
SiO_2	74.72	68.77	56.21	52.15	51.73	51.71	58.54	50.8	55.99
Al_2O_3	14.69	14.46	20.85	16.84	9.01	9.27	14.92	16.44	16.79
Fe_2O_3	1.11	3.21	4.93	11.12	12.56	12.29	7.88	10.54	8.1
MgO	0.3	0.64	3.07	3.58	11.11	10.97	3.88	4.84	4.66
CaO	3.28	1.53	7.21	7.15	10.03	9.83	6.21	8.14	6.18
Na_2O	4	2.57	5.3	4.34	2.04	2.1	3.8	4.17	4.44
K_2O	1.799	6.726	0.732	0.938	1.466	1.423	2.294	1.319	1.726
TiO_2	0.177	0.52	0.057	1.498	0.695	0.667	0.874	1.23	0.909
MnO	0.007	0.013	0.065	0.114	0.173	0.17	0.1	0.107	0.103
P_2O_5	0.027	0.344	0.333	1.17	0.27	0.252	0.411	0.575	0.388
LOI%	0.32	0.58	0.95	0.76	0.83	0.84			0.29
Total	100.43	99.36	99.71	99.66	99.91	99.52	98.9	98.17	99.58
mg	36.2	29.5	56.6	40.3	65.0	65.2	50.8	49.0	54.7
Trace elements (ppm)									
La		51.7	28.2	86.3	38.6	32.7	54.1	71.5	41.3
Ce		114.2	37	174.4	89.5	87	92	162.5	91.6
Nd		51.7	18.8	98.1	74.5	61.1	47	91.3	43.2
Nb		4.7	0.6	17.5	4.2	4.5	6.9	12.9	9.5
Zr		727.3	25.8	55	52.5	60.4	216	449.4	224.3
Y		16.4	5.8	45.7	74.1	72.5	27.3	58	20.5
Sr		233.7	767.4	562.2	247.7	250.6	771.4	728.8	800.8
Rb		137.9	2.4	4.1	57.4	56.6	31.7	26.1	38.8
Th		5.4	0	3.4	3.3	3.1	0.4	2.7	1.3
Pb		23.3	8.4	11.2	6.2	6.4	10.6	10	11.9
Zn		40.5	71.4	120.4	114.7	119.7	85.1	118.1	92.3
Cu		8.5	6.8	76.3	83	82.8	20.4	16.8	38.9
Ni		8.2	29.7	8.2	149.8	148.7	46.9	60.1	84.4
Cr		4.2	124.9	-11.8	210.4	204.4	96.3	126.1	168
V		20	33.5	214.2	194.9	189.3	116.1	154.2	127.8
Ba		1800.1	449.9	698.5	941.4	829.7	2045.5	791.9	827.2
Sc		-2.9	7.5	17.8	40.4	43.7	14.8	26.6	14.2
CIPW									
Q	37.11	25.15	2.13	2.95	0.00	0.00	9.63	0.00	3.31
Or	10.61	40.29	4.40	5.65	8.84	8.61	13.78	8.00	10.33
Ab	33.79	22.04	45.57	37.44	17.61	18.19	32.69	36.24	38.06
An	16.07	5.42	31.44	24.16	11.32	11.94	17.16	22.85	21.06
C	0.26	1.01	0.00	0.00	0.00	0.00	0.00	0.00	0.00
Di	0.00	0.00	2.19	3.48	30.51	29.42	9.31	12.09	6.03
Hy	0.75	1.62	11.09	16.22	22.01	22.82	11.27	6.16	15.02
Ol	0.00	0.00	0.00	0.00	4.49	3.90	0.00	6.83	0.00
Mt	0.00	2.01	2.29	4.43	3.25	3.22	3.50	4.06	3.54
Ilm	1.06	1.00	0.11	2.90	1.35	1.30	1.69	2.40	1.75
Ap	6.25	0.81	0.78	2.76	0.64	0.60	0.97	1.37	0.91

Sample	VH57	VH58	VH62	VH64	VH66	VH67	VH69	VH71	VH80
Suite	BHS	BHS	BHS	BHS	BHS	BHS	BHS	BHS	MoG
GR	89# 14#	89# 14#	89# 14#	89# 14#	89# 14#	89# 14#	89# 14#	89# 14#	
Major elements (wt%)									
SiO_2	47.05	50.79	47.05	48.03	60.79	49.69	49.19	48.91	60.3
Al_2O_3	10.9	11.97	9.8	10.28	14.71	9.45	9.11	7.26	15.81
Fe_2O_3	11.25	9.21	11.3	10.99	6.56	10.13	11.13	10.51	6.46
MgO	15.94	11.71	16.88	16.17	5.53	17.87	17.77	23.25	1.92
CaO	8.23	9.41	8.31	7.8	5.25	6.95	8.5	7.14	3.96
Na_2O	1.72	2.97	1.54	1.59	3.78	1.27	1.81	0.81	4.06
K_2O	1.951	1.106	1.756	2.054	1.643	2.635	0.57	0.475	4.134
TiO_2	0.788	0.814	0.693	0.704	0.602	0.552	0.658	0.411	0.921
MnO	0.167	0.133	0.175	0.176	0.102	0.146	0.174	0.166	0.067
P_2O_5	0.238	0.439	0.198	0.203	0.15	0.156	0.167	0.113	0.577
LOI%	1.35	1.45	1.86	1.7	0.49	0.96	0.7	0.85	0.69
Total	99.58	100	99.56	99.7	99.61	99.81	99.78	99.9	98.9
mg	74.8	72.7	75.8	75.5	63.9	78.7	77.0	82.3	38.4
Trace elements (ppm)									
La	10.2	48.2	8.7	11.7	25.3	8.9	13.5	8.6	92.4
Ce	33.5	129	28.4	30.1	42.6	32.4	30.4	27	185.1
Nd	17.4	66.7	14.7	15.6	16.5	14.8	18.7	11.9	65.5
Nb	4.7	13.5	4.4	5.5	7.8	5.2	6.3	4	11.3
Zr	75.8	168.7	67.3	72.3	139.7	67.1	78.3	58.1	435
Y	19.8	25.7	17.9	18.2	17.2	18.2	25.4	15	22.2
Sr	440.4	903.7	337	295.6	456.4	231.2	216.2	32.6	678
Rb	57.1	16.8	52	65.1	45.1	92	3.7	7.3	57.1
Th	4.2	1.3	3.4	4.1	1.9	7.5	1	2.5	2.2
Pb	4.9	5.3	4.8	3.6	9.6	4.6	0.8	4.9	16.3
Zn	96.2	99.8	93.9	95.5	76.1	80.2	89.6	80	84.5
Cu	13.3	51.3	22.8	15.2	6.5	8.2	46.6	87.8	25.9
Ni	506.4	419.5	538	510.3	83.5	666.5	616.7	1153	15.9
Cr	1803.2	1156.2	1930.4	1812.1	350.8	1949.3	1712.7	2353.5	25.4
V	205.2	139.2	202	199.9	128.7	173.3	204.8	143.5	70.5
Ba	476.4	359.3	457.8	522.8	684.5	310.2	127.2	95.1	2013.9
Sc	33.6	24.2	29.4	30.2	16.2	25.1	34.8	24.3	11.6
CIPW									
Q	0.00	0.00	0.00	0.00	12.88	0.00	0.00	0.00	10.57
Or	11.85	6.68	10.72	12.50	9.84	15.88	3.43	2.86	24.98
Ab	14.95	25.68	13.46	13.85	32.42	10.96	15.60	6.98	35.13
An	16.71	16.42	15.13	15.29	18.57	12.55	15.33	15.05	12.99
C	0.00	0.00	0.00	0.00	0.00	0.00	0.00	0.00	0.00
Di	18.91	22.65	20.88	18.53	5.49	17.19	21.16	16.11	2.65
Hy	1.83	9.80	5.28	8.95	16.22	15.12	19.78	33.50	6.94
Ol	30.25	12.73	29.40	25.73	0.00	23.83	19.85	21.62	0.00
Mt	3.41	3.43	3.29	3.29	3.09	3.03	3.19	2.82	3.59
Ilm	1.54	1.58	1.36	1.38	1.16	1.07	1.27	0.80	1.79
Ap	0.57	1.04	0.47	0.48	0.35	0.37	0.39	0.27	1.37

Sample	VH91	VH94	VH126	VH128	VH129	VH130	VH131	VH132	VH133
Suite	D2-GS	RLS	LAS	LAS	LAS	LAS	D2-GS	LAS	D2-GS
GR									
Major elements (wt%)									
SiO_2	62.69	51.06	52.23	51.7	48.72	50.83	51.21	59.22	75.41
Al_2O_3	19.06	11.31	7.23	15.64	12.3	7.95	10.33	22.62	13.03
Fe_2O_3	1.27	10.88	11.79	11.78	14.05	12.61	12.18	2.23	1.03
MgO	0.86	11.22	14.64	4.5	7.55	11.77	9.6	1.2	0.26
CaO	2.46	8.81	8.47	7.35	9.29	11.97	10.8	6.41	1.12
Na_2O	5.12	3.22	1.78	4.37	3.13	1.83	2.47	6.18	3
K_2O	6.716	1.395	0.93	1.106	1.148	1.525	1.232	1.145	5.407
TiO_2	0.041	0.441	0.51	1.351	1.408	0.903	0.914	0.055	0.121
MnO	0.019	0.183	0.186	0.14	0.164	0.214	0.179	0.036	0.006
P_2O_5	0.114	0.251	0.101	0.87	0.964	0.282	0.308	0.07	0.012
LOI%	0.72	0.83	0.63	0.68	0.63	0.54	0.69	0.79	0.52
Total	99.07	99.6	99.93	99.49	99.65	100.42	99.91	99.96	99.92
mg	58.7	68.4	71.9	44.5	52.9	66.2	62.3	53.0	34.6
Trace elements (ppm)									
La	28.6	28.2	17.7	46.1	42.3	41.9	23.7	33.2	48.3
Ce	39.9	56.4	51.5	85.7	90.6	87.8	58.7	37	62.2
Nd	6.6	27.1	39.2	48.1	50	59.6	35.4	11.3	17.6
Nb	1.8	9.1	5.9	5	4.7	9.5	5.7	0.4	0.4
Zr	6.9	100.9	91.3	86.9	87.2	86.4	100.1	37.2	89.1
Y	4.3	15.7	31.8	23.9	32.7	48	26.9	2.4	0.6
Sr	1307.5	528.7	291.1	1480.4	1011.2	424.8	758.7	934.8	215.9
Rb	57.3	24.8	40.7	12.8	25.6	87.8	53.2	5.9	83.2
Th	1	3.5	4.6	4	4	4	1.9	-1.4	20.4
Pb	25.5	7.4	4.8	10.5	7.2	5.4	6.8	13.9	22.8
Zn	18.3	99.7	127.3	117.1	128.5	124	105.4	33.1	8.5
Cu	69.4	13.7	24.7	52.4	101.3	97.7	98	3	1.7
Ni	14.9	210.9	474.6	27.7	94.4	166.4	132	4	2.1
Cr	1.4	767.6	891.4	28.9	140.3	286.7	197.1	-5.4	-16.5
V	3.6	109	137	202.8	264.9	189.4	207.7	13.5	11.7
Ba	3341.6	432.3	366.3	771.3	911.9	822.6	642.2	382.5	890.6
Sc	-2.6	26.8	26.2	15.2	26.3	35.9	33.4	2.5	-1.5
CIPW									
Q	1.49	0.00	0.00	0.00	0.00	0.00	0.00	3.76	34.70
Or	40.34	8.42	5.73	6.68	6.98	9.12	7.41	6.83	32.13
Ab	44.04	27.84	14.46	37.77	26.88	15.66	21.27	52.77	25.52
An	9.34	12.55	9.81	20.22	16.70	9.08	13.70	30.88	5.51
C	0.00	0.00	0.00	0.00	0.00	0.00	0.00	0.00	0.24
Di	0.99	24.58	27.04	9.26	19.59	39.71	31.48	0.58	0.00
Hy	1.72	2.82	37.10	16.24	10.85	10.35	14.34	2.75	0.65
Ol	0.00	19.46	1.54	0.94	9.60	10.17	5.74	0.00	0.00
Mt	0.00	2.88	3.02	4.22	4.33	3.52	3.56	1.93	0.00
Ilm	0.48	0.86	1.05	2.62	2.76	1.73	1.77	0.11	1.12
Ap	0.27	0.59	0.25	2.06	2.31	0.66	0.73	0.16	2.80

Sample	VH134	VH136	VH137	VH140	VH163	VH164	VH165	VH166	VH167
Suite	LAS	LAS	LAS	LAS	RLS	RLS	RLS	RLS	RLS
GR									
Major elements (wt%)									
SiO_2	75.05	51.38	50.55	49.73	52.02	48.28	54.43	47.22	47.23
Al_2O_3	13.07	11.11	15.01	12.06	9.6	4.14	2.81	7.8	7.69
Fe_2O_3	1.31	12.19	12.64	13.69	9.93	10.66	12.5	12.43	13.24
MgO	0.18	9.24	5.91	7.64	9.05	20.78	23.95	17.58	18.01
CaO	1.22	10.03	8.06	9.06	13.43	13.09	4.44	10.29	8.5
Na_2O	3.01	2.83	3.84	3.11	3.12	0.99	0.68	1.46	1.49
K_2O	5.131	1.244	1.265	1.111	0.928	0.302	0.398	0.698	0.711
TiO_2	0.126	0.998	1.272	1.321	0.796	0.351	0.097	0.452	0.373
MnO	0.013	0.167	0.149	0.162	0.168	0.175	0.6	0.185	0.201
P_2O_5	0.01	0.371	0.93	0.942	0.167	0.061	0.015	0.144	0.117
LOI%	0.46	0.39	0.32	0.96	0.81	0.87	0.04	1.14	1.53
Total	99.58	99.95	99.95	99.79	100.02	99.7	99.96	99.4	100.03
mg	22.4	61.4	49.5	53.9	65.6	80.3	80.1	74.8	73.9
Trace elements (ppm)									
La	17.4	23.3	38.4	37.6	30.8	6.8	3.8	26.7	18.6
Ce	13.3	55.9	83.2	87.6	58	16.3	-2.4	35.6	27.2
Nd	-2.9	32.2	44.4	52.3	32.6	14.1	5.6	23	20.5
Nb	1	5.8	5	6.2	6.4	2.2	0.8	5.7	4.7
Zr	135.2	96.5	73.5	98.3	127.1	30.7	18.1	75.4	55.2
Y	0.4	25.5	23.6	30.6	23.8	8.4	6.9	13.7	10.2
Sr	474	878.2	1452.8	955.6	441.9	139.2	163.4	191.3	130.1
Rb	93.6	43.2	37.9	27.9	14.3	3.4	9.2	5.9	4.9
Th	-0.3	4	4.6	5.2	1.9	3.4	3.2	5.8	5.7
Pb	20.5	6.1	7	6.5	8	1.8	3.9	3.4	3.7
Zn	17.6	101.4	115.8	120.5	79.6	77.1	271.7	98	118.8
Cu	2.8	107.8	76.1	119.5	57.7	8.6	6.6	8.9	8.6
Ni	2.5	123.2	43.9	97.7	108.7	600.3	1259.9	572	554.9
Cr	-13.2	208.9	53.5	145.4	118.8	2070.5	2216.6	1192.8	1655.2
V	19.4	222.3	245	261.1	231	133.5	42.8	128.6	104.8
Ba	1955.2	727.6	764.1	685.9	457.9	49.5	203	124	84.4
Sc	1.4	25.7	18.1	22.1	29.4	46.4	10	27.4	26.8
CIPW									
Q	35.35	0.00	0.00	0.00	0.00	0.00	0.00	0.00	0.00
Or	30.58	7.46	7.58	6.72	5.57	1.82	2.38	4.24	4.37
Ab	25.69	24.29	32.94	26.93	24.85	8.55	5.82	12.71	12.43
An	6.04	14.14	20.26	16.03	9.60	6.09	3.48	13.03	12.97
C	0.37	0.00	0.00	0.00	0.00	0.00	0.00	0.00	0.00
Di	0.00	27.50	11.61	19.37	45.95	47.63	14.95	30.90	24.42
Hy	0.45	13.18	11.58	16.36	0.00	5.08	70.14	6.85	14.22
Ol	0.00	6.97	7.32	5.62	7.66	27.26	0.67	28.13	27.72
Mt	0.00	3.67	4.07	4.18	3.38	2.74	2.34	2.91	2.82
Ilm	0.58	1.92	2.45	2.57	1.54	0.68	0.19	0.88	0.76
Ap	2.34	0.87	2.18	2.23	0.39	0.14	3.52	0.34	0.28

Sample	VH168	VH169	VH170	VH171	VH172	VH173	VH174	VH175	VH176
Suite	RLS	RLS	RLS	RLS	RLS	RLS	RLS	RLS	RLS
GR									
Major elements (wt%)									
SiO_2	48.9	51.3	50.02	48.74	51.12	50.01	49.17	47.44	47.05
Al_2O_3	8.62	9.41	5.09	9.56	11.52	10.19	5.17	4.14	8.54
Fe_2O_3	13.43	10.86	10.05	13.07	10.59	11.24	7.98	11.2	12.09
MgO	16.49	17.47	18.87	12.26	10.95	12	15.58	21.32	18.44
CaO	7.84	6.25	12.64	10.73	9.18	9.6	17.99	12.62	8.64
Na_2O	2.01	2.34	1.24	2.54	3.23	3.03	1.38	1.06	1.76
K_2O	0.81	0.657	0.451	0.821	1.373	1.08	0.403	0.279	0.79
TiO_2	0.442	0.241	0.4	0.865	0.513	0.459	0.415	0.361	0.632
MnO	0.203	0.181	0.176	0.164	0.166	0.183	0.133	0.177	0.187
P_2O_5	0.184	0.195	0.018	0.139	0.277	0.219	0.114	0.047	0.154
LOI%	0.61	0.99	0.67	0.79	0.85	1.4	1.17	1	0.89
Total	99.54	99.89	99.63	99.68	99.77	100.11	99.51	99.64	99.17
mg	72.0	77.1	79.7	66.3	68.4	80.5	80.4	80.0	76.2
Trace elements (ppm)									
La	17.1	16	10.3	13	29.2	36.5	18.1	6.1	15.6
Ce	33.4	34.2	18.7	38.4	50.8	59.2	23.3	16.9	38.2
Nd	24.2	21.7	12.5	25.4	27.8	33.4	20.9	15.2	28.7
Nb	5.6	5.4	3	7.5	8.4	10.2	3.4	2.3	7.6
Zr	63.8	119.1	46.4	127.6	93.1	87.2	47.2	30.2	87.8
Y	13	10.6	10.7	17.9	16.3	17	10.6	8.3	14.9
Sr	326	534.3	122.8	320.2	546.2	548.5	181.5	129	297.3
Rb	9.5	4	6.9	6.1	32.1	19.6	4.6	3.2	5.6
Th	5.7	3.8	2.4	5.4	2.6	5.8	2.5	3.5	2.5
Pb	4.3	5.8	1.8	4.2	5.3	9.4	2.9	1.8	3
Zn	117.1	95.3	68.9	98	89.4	98.7	41.4	76.9	98.8
Cu	9	4.8	8.9	9.6	8.9	7.7	9.7	7	7.8
Ni	478.3	623.7	522.1	250	195.9	214.7	270	645.5	648.2
Cr	1357.1	1571	1029.1	605.3	652.7	555.1	1528.2	1994.5	1896.8
V	103.7	85.7	149.4	242.1	116.9	125.6	142.3	127.7	147.1
Ba	218.8	276.6	108.6	199.6	537.1	439.2	73.6	45.9	169.4
Sc	24.2	19.5	42.8	36.7	26	26.5	66.3	39.6	27.7
CIPW									
Q	0.00	0.00	0.00	0.00	0.00	0.00	0.00	0.00	0.00
Or	4.90	3.96	2.72	4.96	8.27	2.40	2.44	1.69	4.80
Ab	17.39	20.21	10.69	21.97	27.87	5.05	4.74	9.18	15.31
An	12.38	13.50	7.12	12.53	13.14	7.23	6.88	5.85	13.43
C	0.00	0.00	0.00	0.00	0.00	0.00	0.00	0.00	0.00
Di	21.08	13.47	45.12	33.12	25.39	66.02	66.43	46.16	23.67
Hy	16.26	28.94	11.99	0.31	2.32	0.00	0.00	1.49	6.87
Ol	23.81	16.41	18.74	21.58	18.39	12.01	11.69	32.06	31.14
Mt	2.88	2.58	2.81	3.51	2.98	2.85	2.84	2.76	3.18
Ilm	0.86	0.47	0.77	1.68	0.99	0.83	0.81	0.70	1.23
Ap	0.44	0.46	4.25	0.33	0.65	0.27	0.27	0.11	0.37

Sample	VH181	VH183	VH195	VH196	VH197	VH198	VH199	VH201	VH204
Suite	VHMD	EMG	Hbl-PS	sLAS	sLAS	sLAS	sLAS	VHMD	D2-GS
GR									
Major elements (wt%)									
SiO_2	45.74	50.27	50.83	52.58	52.39	48.47	52.68	48.55	75.73
Al_2O_3	17.83	8.51	5.71	10.3	10.55	10.31	14.19	10.4	13.04
Fe_2O_3	12.78	10.2	12.21	10.79	10.32	11.15	10.51	11.06	1.22
MgO	4.19	18.72	15.91	10.68	10.87	14.47	6.68	14.39	0.1
CaO	7.14	5.31	10.68	8.91	8.65	8.57	7.03	8.85	1.29
Na_2O	4.01	1.49	1.14	2.7	2.46	1.89	4.06	2.32	3.26
K_2O	3.097	3.089	1.373	1.995	2.268	2.002	2.085	1.502	4.748
TiO_2	0.972	0.589	0.897	0.671	0.765	0.643	0.948	0.693	0.136
MnO	0.213	0.158	0.155	0.188	0.181	0.177	0.145	0.174	0.015
P_2O_5	1.875	0.263	0.09	0.275	0.339	0.245	0.425	0.251	0.004
LOI%	0.72	0.36	0.85	1.01	0.81	1.63	0.85	1.14	0.32
Total	98.57	98.96	99.85	100.1	99.6	99.59	99.6	99.33	99.86
mg	40.7		73.2	67.5	68.8	73.3	57.1	73.2	14.7
Trace elements (ppm)									
La	129	38.4	21.2	51.7	70.1	34.9	48.2	20.3	21.4
Ce	317.7	66.9	67.3	120.4	117.7	49.7	91.2	55.8	23.1
Nd	163.2	29.4	49	62.2	57	31.1	46.3	28.2	5.1
Nb	17.6	8.8	7	8.8	13.3	8.2	9.5	9.2	1.6
Zr	134.9	91.9	95.3	166.2	127.5	80.8	167.7	83.6	92.3
Y	46.5	18.9	26.5	39.3	40.7	17.2	29.2	18.3	1.1
Sr	3087.9	103.9	189.4	422.3	520.6	558.3	775.7	631.5	307.4
Rb	89	156.3	68.7	69.8	94.4	69.6	59.3	37.3	97.2
Th	7.5	9.6	5.4	11.8	31.1	5.2	3.1	4.5	5.8
Pb	4.8	6.3	3.9	9.5	10.6	7.1	7.2	3.4	21.6
Zn	146.6	145.2	97.9	113	104.3	104.5	100.8	92.7	16.4
Cu	29.7	6.5	21.5	63.6	60.4	34.6	59.7	23.3	1.1
Ni	8.5	790.8	238.2	260.2	303.2	450.9	132.2	425.3	2.2
Cr	-14.4	1702.8	561.9	740.2	799.2	891.4	335.3	816.8	-14.7
V	19.6	138.1	164.5	148.9	131.4	151.5	171	154.9	18.6
Ba	1852.6	357	476.5	703.2	789.2	561.4	930.3	482.6	1136.9
Sc	-1.1	15.7	37.7	22.9	19.3	21.9	16.7	26.5	0
CIPW									
Q	0.00	0.00	0.00	0.00	0.00	0.00	0.00	0.00	35.83
Or	18.90	18.67	8.28	12.00	13.68	12.18	12.58	9.12	28.18
Ab	22.59	12.89	9.84	23.26	21.24	15.52	35.08	20.18	27.70
An	22.21	7.58	6.54	10.28	11.27	14.67	14.64	13.90	6.43
C	0.00	0.00	0.00	0.00	0.00	0.00	0.00	0.00	0.19
Di	1.44	14.01	37.59	26.54	24.34	22.10	14.76	23.67	0.00
Hy	0.00	16.29	23.38	13.91	16.55	6.60	7.05	2.53	0.25
Ol	18.01	25.70	8.87	8.86	7.28	23.81	9.43	25.38	0.00
Mt	3.70	3.10	3.55	3.20	3.35	3.23	3.62	3.27	0.00
Ilm	1.91	1.14	1.74	1.30	1.48	1.30	1.84	1.35	0.76
Ap	4.49	0.62	0.21	0.65	0.80	0.59	1.01	0.60	0.00

Sample	VH218	VH219	VH220	VH239	VH240	VH244	VH257	VH258	VH259
Suite	ICLG	RLS	RLS	Hbl-PS	Hbl-PS	Hbl-PS	EMG	EMG	EMG
GR									
Major elements (wt%)									
SiO_2	63.13	53.01	49.51	49.01	49.74	43.04	50.37	54.94	48.94
Al_2O_3	16.65	13.53	9.73	7.8	13.81	6.92	9.44	12.14	9.21
Fe_2O_3	4.93	9.83	11.8	10.97	12.92	19.03	9.09	7.99	10.26
MgO	2.09	8.28	12.73	12.1	8.15	13.56	14.19	8.9	14.9
CaO	5.2	7.03	10.28	14.53	8.63	12.45	10.01	7.64	9
Na_2O	4.67	4.51	2.42	1.63	3.14	1.8	2.05	3.36	1.72
K_2O	1.307	1.53	1.113	0.832	1.303	0.678	2.192	2.882	3.05
TiO_2	0.642	0.69	0.673	0.792	0.665	1.22	0.691	0.657	0.692
MnO	0.052	0.142	0.176	0.174	0.178	0.238	0.164	0.128	0.165
P_2O_5	0.231	0.283	0.153	0.163	0.218	0.096	0.479	0.404	0.483
LOI%	0.63	0.66	0.82	1.39	0.91	0.75	0.91	0.69	0.95
Total	99.53	99.5	99.41	99.39	99.86	99.78	99.59	99.73	99.37
mg	47.1	63.8	69.3	69.8	56.8	59.9	76.6	70.0	75.3
Trace elements (ppm)									
La	51	35.9	12.3	29.9	31.8	20.2	71.6	66.6	80.4
Ce	101.9	68.6	36.7	65.4	66.6	57.8	169.8	142.8	181
Nd	39.4	35.3	22.1	40.7	36.1	37.1	81.9	65.3	81.2
Nb	8.5	13	6.7	10.1	8.3	11.4	30.4	11.8	34.4
Zr	245.9	104.7	75.4	80.4	123.2	70.6	177.5	186.8	171.2
Y	19.8	18.4	15.8	22.5	18.8	22.3	35	34.5	35
Sr	740.2	750	382.8	438.4	1250.2	401.8	497.8	851.7	746.2
Rb	10.2	31.5	29.3	19	27	11.5	125.1	58.8	179
Th	-0.6	3.8	3.4	6.1	8.1	8.9	18.5	3.3	25.9
Pb	10	5.6	7.5	5.3	7.6	2.9	5.7	9.8	7.1
Zn	68.7	86.2	87	86.6	101.5	117	106.8	76.4	132.2
Cu	8.8	7.6	11.5	84.7	97.1	241.9	8.3	7.7	9
Ni	28.3	144	235.5	131.7	84.3	214.3	469.8	268.1	550.5
Cr	34.1	397.9	562.2	206.5	89.2	254.1	706.7	427.1	747.3
V	61.9	115.5	165	240.8	253.9	438	114.5	97.4	121.9
Ba	957.2	546.8	339.8	330.5	638.5	271.7	703	1179.5	991
Sc	5.5	21.3	31	44.9	22.5	40.2	10.5	11.9	13.2
CIPW									
Q	17.54	0.00	0.00	0.00	0.00	0.00	0.00	0.00	0.00
Or	7.83	9.22	6.74	5.06	8.08	4.11	13.22	17.30	18.47
Ab	40.07	38.91	20.98	14.20	25.94	1.85	17.70	28.88	13.51
An	20.90	12.40	12.70	11.85	20.84	9.04	10.29	9.68	8.61
C	0.00	0.00	0.00	0.00	0.00	0.00	0.00	0.00	0.00
Di	2.99	17.21	31.04	49.25	17.43	43.92	29.63	20.92	27.08
Hy	5.74	1.75	4.11	1.72	9.82	0.00	4.74	13.26	0.00
Ol	0.00	15.26	19.54	12.56	12.79	26.96	18.70	4.57	25.83
Mt	3.15	3.24	3.23	3.42	3.24	4.05	3.24	3.18	3.26
Ilm	1.24	1.34	1.31	1.55	1.33	2.38	1.34	1.27	1.35
Ap	0.54	0.67	0.36	0.39	0.53	0.23	1.13	0.95	1.15

Sample	VH261	VH262	VH265	VH266.1	VH266.2	VH285	VH286	VH287	VH289A
Suite	EMG	EMG	EMG	EMG	EMG	Hbl-PS	Hbl-PS	Hbl-PS	D2-GS
GR									
Major elements (wt%)									
SiO_2	50.02	52.31	51.83	60.84	61.57	49.31	46.43	48.28	73.88
Al_2O_3	8.78	8.61	8.62	18.22	18.9	5.55	8.37	9.72	13.19
Fe_2O_3	10.81	8.55	8.14	1.77	1.33	10.04	16.47	12.9	1.91
MgO	18.01	19.2	19.63	3.63	2.34	18.61	21.66	15.15	0.48
CaO	5.72	5.7	5.49	5.64	5.83	12.2	3.17	7.91	0.99
Na_2O	1.51	1.71	1.59	5.09	5.18	0.91	0.86	1.72	3.57
K_2O	2.781	1.967	2.641	3.409	3.642	0.764	1.33	1.392	5.04
TiO_2	0.619	0.607	0.582	0.258	0.107	0.456	0.445	0.815	0.274
MnO	0.111	0.14	0.155	0.044	0.032	0.155	0.191	0.181	0.022
P_2O_5	0.291	0.305	0.319	0.098	0.142	0.129	0.241	0.181	0.088
LOI%	0.43	0.64		0.76	0.57	1.27	0.94	1.21	0.42
Total	99.53	99.64	99.64	99.76	99.64	99.39	100.11	99.46	99.86
mg	77.7	82.5	83.5	81.1	78.7	79.5	73.4	71.1	34.5
Trace elements (ppm)									
La	38.1	37.5	27.2	28.7	39.1	14.7	24.5	22.7	64.5
Ce	80.6	62.5	55.9	57.8	74	22.2	41.4	54.5	99.7
Nd	32.8	26.1	25	23.3	26.2	21.9	25	31.7	37
Nb	8.6	7.7	7.2	5	1.6	3.6	5.3	8.7	12
Zr	94.3	108.6	104.9	161.4	93.3	68	83.6	96.3	174.5
Y	20.5	16.5	15.2	17.3	18.6	15.1	11.5	20.2	18.3
Sr	104.3	210.5	173.5	704.3	757	353.8	512.4	596.6	221.2
Rb	196.7	130	155.2	37.9	33.2	19.5	27.8	34.8	146.4
Th	14	6.9	9.4	-0.5	-0.3	3.1	7.6	4	36.1
Pb	4	5.3	6	17.2	18.2	4.2	6.5	2.7	25.3
Zn	105.1	109.4	113	26.8	16.7	76.8	140.9	103.1	24.1
Cu	7	4.6	3.1	2.9	3	44.4	29	56	2.4
Ni	711.5	848.4	862.1	101.1	55.7	397.1	818.5	352.2	6.4
Cr	1643.8	1441.7	1461.6	23.2	15	2885.1	138.9	432.3	-12.8
V	151.6	116.8	114.1	33.2	17.8	146	55.4	158.6	23.4
Ba	447.6	530.9	377.5	761.8	1225.1	404.5	744	532.6	423.3
Sc	19.6	18.3	16.9	1.2	5.1	47.8	9.8	29.4	3.1
CIPW									
Q	0.00	0.00	0.00	3.27	4.21	0.00	0.00	0.00	31.41
Or	16.81	11.81	15.86	20.35	21.72	4.64	8.04	8.46	29.96
Ab	13.07	14.70	13.67	43.51	44.23	7.91	7.45	14.98	30.38
An	9.17	10.17	8.72	16.97	17.72	9.05	14.48	15.12	4.36
C	0.00	0.00	0.00	0.00	0.00	0.00	0.34	0.00	0.27
Di	14.28	13.09	13.31	7.75	7.24	41.63	0.00	19.34	0.00
Hy	17.77	31.91	24.69	5.54	2.52	15.75	33.33	16.30	1.20
Ol	23.87	13.35	18.79	0.00	0.00	16.92	32.03	20.34	0.00
Mt	3.14	3.10	3.07	0.00	0.00	2.91	2.89	3.45	0.00
Ilm	1.20	1.17	1.12	0.12	0.46	0.89	0.86	1.59	0.31
Ap	0.69	0.72	0.75	0.23	0.33	0.31	0.57	0.43	0.21

Sample	VH289B	VH290A	VH290B	VH294	VH299	VH310	VH311	VH312	VH318
Suite	D2-GS	D2-GS	D2-GS	D2-GS	D2-GS	BrHutS	BrHutS	BrHutS	BrHutS
GR									
Major elements (wt%)									
SiO_2	76.72	77.47	78.55	75.51	74.47	51.44	51.1	57.98	49.71
Al_2O_3	12.02	12.29	11.82	12.39	13.5	6.82	5.65	16.14	5.14
Fe_2O_3	1.42	0.65	0.31	1.47	0.96	11.05	13.28	8.2	13.4
MgO	0.3	0.01	0.02	0.31	0.4	13.09	15.03	4.05	15.69
CaO	0.6	0.38	0.56	1.02	1.32	13.34	11.86	6.53	13.59
Na_2O	3.17	3.26	2.71	3.09	2.78	1.67	1.26	4.45	0.69
K_2O	5.175	5.585	5.609	4.952	5.526	0.876	0.538	0.984	0.754
TiO_2	0.238	0.084	0.04	0.213	0.167	0.699	0.578	0.87	0.555
MnO	0.013	0.004	0.004	0.015	0.013	0.17	0.204	0.102	0.219
P_2O_5	0.041	0.001	-0.003	0.055	0.032	0.309	0.222	0.386	0.19
LOI%	0.27	0.16	0.2	0.3		0.46	0.35	0.87	0.29
Total	99.97	99.89	99.82	99.47	99.16	99.92	100.07	100.56	100.23
mg	30.7	3.1	11.9	30.7	46.6	71.3	70.4	50.9	71.1
Trace elements (ppm)									
La	60.5	23.3	14.8	19.6	26.9	37.1	24	61.9	30.4
Ce	90.3	29.4	2.1	30.6	28.8	79.2	48.2	100.2	68.2
Nd	28.1	9.9	1.6	8.7	10.2	52.1	43.2	54.8	50.2
Nb	10.3	0.3	0.4	3.1	3.1	4.4	3.5	7.5	3.3
Zr	119.2	105.1	11.2	117.1	109.4	110.2	88.4	203	199.9
Y	11.1	-0.1	-0.7	2	0.6	29.8	26.3	24.5	30.5
Sr	195.7	22.9	240.1	277.5	428.9	397.5	304.8	872.1	201.1
Rb	162.3	117.6	94	71.4	84.4	25.6	19	1.8	32.7
Th	43	28.3	-2.3	1.3	-0.5	4.1	5.1	1.2	5.1
Pb	25.3	26.1	16.8	19.1	26.6	4	4.7	6.3	3.3
Zn	17.4	5.6	2.7	17.2	11.2	88.8	106.3	92.5	123.2
Cu	1.4	0.1	0	1.9	1.6	51.4	109.4	10.8	140.5
Ni	4.7	2.2	1.3	4.6	3.3	169.7	246.3	43.4	251.1
Cr	-16.8	-17.1	-15.4	-0.6	-12.1	888.2	769	115.6	561.8
V	15.1	9.3	7.3	15.8	14.2	181.6	187.2	118.9	197.6
Ba	341	32.9	837.6	604.8	1484.8	520.4	327.4	802.2	467.1
Sc	3.7	1.1	-0.6	-1.6	4.2	42.5	43.3	14.9	58.1
CIPW									
Q	36.96	36.36	40.19	36.44	34.07	0.00	0.00	8.42	0.00
Or	30.67	33.06	33.23	29.55	32.91	5.25	3.22	5.87	4.51
Ab	26.90	27.63	22.99	26.40	23.70	14.34	10.81	37.99	5.91
An	2.72	1.89	2.79	4.75	6.39	8.65	8.29	21.35	8.81
C	0.21	0.19	0.27	0.23	0.63	0.00	0.00	0.00	0.00
Di	0.00	0.00	0.00	0.00	0.00	45.33	40.26	7.17	46.89
Hy	0.75	2.49	4.99	0.78	1.00	15.16	26.83	13.16	18.11
Ol	0.00	0.00	0.00	0.00	0.00	5.96	5.90	0.00	11.25
Mt	0.00	0.00	0.00	0.00	0.00	3.23	3.06	3.47	3.02
Ilm	0.58	1.77	2.33	0.43	1.33	1.35	1.11	1.67	1.07
Ap	9.53	0.00	0.00	0.13	7.47	0.73	0.52	0.90	0.45

Sample	VH321A	VH321B	VH322A	VH322B	VH326	VH330	VH331	VH332	VH333
Suite	Hbl-PS	Hbl-PS	Hbl-PS	Hbl-PS	Hbl-PS	ICLG	ICLG	ICLG	ICLG
GR									
Major elements (wt%)									
SiO_2	47.22	47.37	49.04	51.02	48.49	51.46	56.77	52.02	63.38
Al_2O_3	7.47	7.44	5.63	1.73	10.48	15.01	17.69	17.99	16.05
Fe_2O_3	16.34	16.52	12.18	13.1	11.63	9.99	7.15	9.65	5.21
MgO	13.69	13.76	18.26	13.2	13.01	5.85	2.43	3.37	1.64
CaO	10.32	10.29	11.09	19.56	9.31	7.2	4	5.5	2.79
Na_2O	1.39	1.41	0.84	0.76	1.86	3.52	4.55	4.57	4.12
K_2O	0.89	0.922	0.975	0.012	2.495	2.781	4.76	3.391	4.584
TiO_2	1.115	1.131	0.479	0.221	0.769	1.359	0.882	1.103	0.663
MnO	0.209	0.204	0.177	0.313	0.174	0.12	0.093	0.114	0.059
P_2O_5	0.203	0.235	0.169	-0.005	0.28	1.034	0.507	0.766	0.344
LOI%	0.82	0.73	1.1	0.41	0.87	1.11	0.55	0.8	0.65
Total	99.67	100.01	99.94	100.32	99.37	99.43	99.38	99.27	99.49
mg	63.7	63.6	75.9	67.9	70.1	55.1	41.6	42.3	39.8
Trace elements (ppm)									
La	25.1	21.8	19.8	28.8	36	81.9	66.8	74.1	81.7
Ce	51.2	47.6	31.4	98.1	63.3	162.5	142.7	161.2	136.5
Nd	39.4	40.8	21.3	86.3	33.1	78.4	71.5	93.8	58.1
Nb	8.8	9.1	5.1	0.6	8.8	16.8	15.7	16.3	7.5
Zr	87.9	99.9	71.2	53	109	290.7	433.5	317.6	364.7
Y	32.4	33	13.8	73.6	25.2	37.4	36	51.7	20.4
Sr	259.3	253	258.9	40.7	601.4	988	942.8	1223.6	622.8
Rb	25	28.6	28.5	0.2	86.9	82.5	84.8	71.1	65.5
Th	7.8	6.9	4.8	3	5.4	2.5	1.9	3.1	0.1
Pb	5.1	5.2	4.8	0.1	4.8	11.1	19.7	13.6	17.1
Zn	123.6	123.3	82.9	121.7	96.9	110.5	90.4	115.9	69.7
Cu	162.5	160.4	49	115.4	47.6	49.2	28	35.8	19.3
Ni	220	219.1	345.2	195.3	311.6	101.2	20.6	21.6	10.4
Cr	509.6	525.9	1320.2	382.6	966.1	172.7	21.1	13.3	-2.1
V	311.8	318.1	142.3	246.8	185.7	134.4	94	136.4	61.3
Ba	312.5	323.1	401.1	1.6	541.3	1467.8	1669.4	1901.2	1541.1
Sc	44.3	46	41.1	60.8	26	14.8	11.6	12.9	8.9
CIPW									
Q	0.00	0.00	0.00	0.00	0.00	0.00	0.00	0.00	13.59
Or	5.40	5.57	5.89	7.18	15.11	16.84	28.60	20.50	27.49
Ab	12.07	12.19	7.27	6.51	15.65	30.52	39.15	37.16	35.38
An	11.81	11.49	8.91	1.29	13.20	17.36	14.02	18.98	11.77
C	0.00	0.00	0.00	0.00	0.00	0.00	0.00	0.00	6.30
Di	31.96	31.76	37.01	78.65	25.96	9.98	2.29	3.14	0.00
Hy	14.19	13.96	18.32	4.19	0.00	11.48	9.00	0.00	6.44
Ol	18.02	18.39	18.35	6.34	24.29	4.49	0.53	11.10	0.00
Mt	3.89	3.90	2.93	2.53	3.37	4.25	3.51	3.86	3.18
Ilm	2.17	2.19	0.93	0.42	1.50	2.64	1.70	2.14	1.28
Ap	0.48	0.56	0.40	0.00	0.66	2.45	1.19	1.82	0.81

Sample	VH400	VH401	VH402	VH403	VH404	VH405	VH406	VH407	VH409
Suite	TayS	TayS	TayS	LAS	LAS	LAS	LAS	LAS	TayS
GR									
Major elements (wt%)									
SiO_2	52.12	52.68	52.87	50.83	50.89	50.47	48.08	53.31	52.56
Al_2O_3	8.27	12.33	9.33	6.44	5.91	15.49	12.91	16.27	10.7
Fe_2O_3	15.56	10.14	14.22	12.45	13.35	12.32	13.89	11.19	10.75
MgO	10.29	8.7	10.04	12.38	12.92	5.88	6.95	3	10.72
CaO	10.14	9.38	9.38	13.7	12.82	8.06	8.92	6.77	8.52
Na_2O	2	2.99	2.24	1.33	1.43	3.82	4.27	5.09	2.56
K_2O	0.432	1.252	0.745	1.011	0.576	0.945	1.025	0.694	1.943
TiO_2	0.396	0.755	0.4	0.752	0.692	1.157	1.399	1.13	0.718
MnO	0.263	0.118	0.22	0.205	0.221	0.128	0.157	0.103	0.155
P_2O_5	0.311	0.299	0.26	0.15	0.237	0.934	1.126	1.054	0.273
LOI%							0.61	0.42	
Total	99.79	98.65	99.71	99.24	99.04	99.21	99.337	99.031	98.89
mg	58.1	64.3	59.7		67.0	50.0	51.2	36.0	67.6
Trace elements (ppm)									
La	35.1	36	36.1	22.2	21.1	30.3	43	81.3	33.9
Ce	100.6	88.3	98.3	67.1	54.6	69.9	83.9	145.3	80.2
Nd	80.6	56.7	69.3	45.6	39.1	40	52.5	71.4	38.4
Nb	4.3	6.1	4	7.1	5	4.7	6.3	15.2	9
Zr	144.7	46.4	108.6	75.2	61.6	25.5	90.4	250.8	134.2
Y	81.2	55.3	69.5	45	33.6	22.6	31.9	66.3	27.2
Sr	232	441.4	250.6	361.5	306.5	1543.8	1078	1170.9	552.6
Rb	4.6	41.1	19.7	49.5	20.9	16.5	23.8	1.9	76.9
Th	5.3	4.2	4.6	3.3	4	4.3	2.6	13.3	3.5
Pb	5.8	8.8	4.5	4.8	2.3	4.4	5.7	8.3	6.4
Zn	227.3	92.4	206.1	110.9	117.9	111	121.1	120.4	100.8
Cu	75.7	79	72.5	36.5	139.3	82.5	118.5	50.2	70
Ni	139.6	109.5	130.3	130	264.2	42.5	72.9	25.4	263.9
Cr	181.1	93.8	170.2	272.1	221.4	62.7	114	54.3	677.4
V	138.1	170.9	143.5	183.6	178.5	239.1	279.6	142.3	152.9
Ba	285.1	702.4	387.4	499.9	283.8	693.7	758.7	482.7	668.9
Sc	65.8	33.8	47.9	56	46.6	16.1	23.7	9.3	20.9
CIPW									
Q	0.93	0.00	1.06	0.00	0.00	0.00			0.00
Or	2.59	7.56	4.47	6.08	3.48	5.69			11.71
Ab	17.20	25.86	19.25	11.46	12.36	32.90			22.09
An	12.51	16.89	13.41	8.77	8.18	22.73			12.21
C	0.00	0.00	0.00	0.00	0.00	0.00			0.00
Di	30.03	23.17	26.32	48.00	44.67	9.67			23.45
Hy	32.45	20.25	31.31	15.26	22.80	15.67			19.26
Ol	0.00	0.76	0.00	5.30	3.38	4.98			5.96
Mt	2.79	3.34	2.80	3.32	3.25	3.92			3.28
Ilm	0.76	1.47	0.77	1.45	1.34	2.24			1.39
Ap	0.73	0.71	0.61	0.35	0.56	2.20			0.65

Sample	VH410	VH411	VH412	VH413	VH414	VH415	VH416	VH418	VH419
Suite	TayS	TayS	TayS	ICLG	TayS	VHMD	VHMD	LAS?	LAS?
GR									
Major elements (wt%)									
SiO_2	55.65	49.67	50.35	50.7	50	52.53	50.27	50.39	51.99
Al_2O_3	15.81	8.95	6.14	15.95	7.03	13.96	13.33	9.2	12.76
Fe_2O_3	8.35	12.73	13.61	12.6	13.2	12.7	13.17	11.32	8.67
MgO	4.8	12.43	14.21	3.68	13.58	5.29	6.1	13.61	9.79
CaO	6.79	11.06	12.11	7.52	12.74	8.46	9.01	9.56	10.2
Na_2O	4.04	1.87	1.18	4.12	1.35	3.47	3.7	1.97	3.04
K_2O	1.058	0.931	0.555	0.836	0.762	0.61	0.721	1.245	0.913
TiO_2	0.726	1.265	0.793	1.633	0.969	2.257	2.185	0.752	0.427
MnO	0.084	0.13	0.185	0.097	0.158	0.135	0.146	0.16	0.131
P_2O_5	0.348	0.144	0.133	1.328	0.156	0.237	0.301	0.271	0.16
LOI%									
Total	97.67	99.19	99.26	98.46	99.95	99.65	98.93	98.48	98.07
mg	54.7	67.2	68.6	38.0	68.3	46.6	49.3	71.6	70.3
Trace elements (ppm)									
La	40.7	18.8	20.8	98.3	20.5	13.9	13.9	25.5	11.7
Ce	85.4	48.6	64.6	240.6	60.4	41.1	46.6	61.5	32
Nd	42.6	30.2	38.5	135.1	36.5	29.3	33.9	32.6	19.2
Nb	7	8.2	6.5	26.6	6.3	10.2	13.5	10	3.7
Zr	111.4	61.5	59.4	28.3	47.4	52.6	148.7	62.1	39.6
Y	21	27.2	31.8	71	33.8	34.6	34.4	22.3	16
Sr	895.5	331.2	225.7	467.7	248.2	474.1	462.1	609.9	959.8
Rb	16.4	27.9	19	3.9	25.4	3.1	3.4	36.6	23.2
Th	1.4	4.9	3.9	8.8	3.7	3.5	3.9	5.5	3.8
Pb	12.2	4.1	2.8	12.5	3.9	5.3	4.5	3.3	5.4
Zn	109.3	82.4	92	149.1	95.6	141	148.5	99.1	74.9
Cu	34.8	117.5	123.5	87.6	144	45.1	66.1	12.5	98.7
Ni	63	172.2	212.5	15	210.1	85.6	107.7	382	171.3
Cr	166.2	769.4	1032.4	1.3	1034.9	123.9	175.4	1139.2	282
V	137.6	322.6	301	275.8	287.8	150.6	150.9	156.3	136.8
Ba	845.8	401.4	252.6	337	377.4	326	258.4	574.6	401.6
Sc	17.3	55.6	55.2	17.9	57.7	18.8	20.5	24.9	31.2
CIPW									
Q	6.33	0.00	0.00	2.25	0.00	5.25	0.00	0.00	0.00
Or	6.44	5.60	3.34	5.07	4.55	3.65	4.35	7.54	5.54
Ab	35.23	16.12	10.18	35.75	11.55	29.73	31.95	17.09	26.41
An	22.55	13.52	10.01	23.14	11.00	20.98	18.00	12.90	18.97
C	0.00	0.00	0.00	0.00	0.00	0.00	0.00	0.00	0.00
Di	8.00	33.32	40.63	5.18	41.84	16.26	20.86	27.21	25.64
Hy	15.88	15.53	25.46	17.63	16.43	13.71	13.42	18.65	12.46
Ol	0.00	9.03	5.15	0.00	8.77	0.00	1.02	11.17	6.90
Mt	3.33	4.08	3.39	4.66	3.62	5.52	5.45	3.35	2.87
Ilm	1.42	2.45	1.53	3.18	1.86	4.34	4.24	1.46	0.83
Ap	0.83	0.34	0.31	3.16	0.37	0.56	0.71	0.64	0.38

Sample	VH420	VH421	VH422	VH423	VH423A	VH424	VH426	VH427	VH428
Suite	D2-GS	ICLG	RybBS	RybBS	RybBS	RybBS	RybBS	RybBS	$GrLG_b$
GR									
Major elements (wt%)									
SiO_2	72.56	67.87	50.1	46.35	50.44	48.85	47.22	53.68	72.52
Al_2O_3	13.74	15.93	5.3	4.51	6.95	8.92	7.64	7	14.32
Fe_2O_3	1.91	3.89	8.22	12.43	13.53	9.75	14.09	10.23	2.31
MgO	0.54	1.2	17.46	25.87	12.32	12.06	15.57	14.36	0.57
CaO	1.32	4.48	14.74	7.16	11.84	14.92	10.29	9.35	3.24
Na_2O	2.91	4.25	0.9	0.64	1.46	2.43	1.53	1.55	3.86
K_2O	5.637	0.947	0.638	0.823	1.175	0.588	0.828	1.607	1.749
TiO_2	0.236	0.577	0.367	0.333	0.891	0.77	0.649	0.503	0.298
MnO	-0.026	0.022	0.117	0.17	0.196	0.135	0.214	0.151	-0.001
P_2O_5	0.086	0.122	0.076	0.119	0.16	0.213	0.184	0.068	0.067
LOI%									
Total	98.92	99.29	97.92	98.4	98.97	98.64	98.23	98.51	98.93
mg	37.2	39.3	81.7	81.4	65.6	72.2	69.8	74.6	34.1
Trace elements (ppm)									
La	25.2	28.4	9.4	9.6	24.3	18.1	18	17.1	26.9
Ce	41.3	47.9	22.9	27.9	68.2	54.5	54.6	46.6	38.8
Nd	14.6	14.1	15.8	17.3	47.2	37.7	36.4	25.1	8.6
Nb	2.4	10	2.9	4.2	6	7.2	7.2	3.2	4.2
Zr	179.6	245.3	46	60.2	117.2	67.9	98.7	103.9	184.7
Y	2.6	8.1	12.5	11.2	39.1	26.8	24.8	20.8	5
Sr	296.3	396.5	268	174.2	295.8	640.7	506.6	214.7	307.3
Rb	88.9	4.6	15.4	23.5	38.9	6.4	21.1	35.8	14.3
Th	2.5	-1.4	1.6	5.5	3.8	5.2	5.9	3	-1.1
Pb	19.9	7.2	3.2	7.7	2.3	8.5	3.8	5.3	12.8
Zn	20.3	48.7	57.9	116.6	112.1	57.2	114.3	65.3	31.6
Cu	7.5	5.7	34.6	27.3	119.7	36.7	68.4	39	3.7
Ni	5.3	7.7	309.7	663	146.9	94.5	178.5	184.7	5.5
Cr	2.9	10.7	2921.8	2121.8	214.3	323.2	253.2	295.9	0
V	27	49.1	157.1	94.1	239.3	240.9	179.6	143	44.6
Ba	957.3	596.6	248.2	324.4	648.5	284.3	305.1	968.7	846
Sc	-0.4	5.6	58.5	27.1	43.4	51.4	40	38.9	2.2
CIPW									
Q	31.00	28.57	0.00	0.00	0.00	0.00	0.00	0.41	36.17
Or	33.68	5.65	3.88	5.00	7.10	3.55	5.04	9.72	10.45
Ab	24.89	36.29	7.83	5.56	12.63	13.27	13.34	13.43	33.03
An	6.05	21.62	8.78	7.19	9.14	11.95	11.89	7.57	15.81
C	0.66	0.06	0.00	0.00	0.00	0.00	0.00	0.00	0.35
Di	0.00	0.00	52.26	22.69	40.34	49.82	31.88	31.59	0.00
Hy	1.36	3.39	10.76	16.57	19.01	0.00	8.25	33.16	1.44
Ol	0.00	0.00	12.82	39.33	6.13	11.86	24.68	0.00	0.00
Mt	0.00	3.04	2.78	2.73	3.54	3.36	3.21	2.97	0.63
Ilm	0.33	1.11	0.72	0.65	1.73	1.49	1.27	0.98	0.57
Ap	0.20	0.29	0.18	0.28	0.38	0.50	0.44	0.16	0.16

Sample	VH440	VH442	VH454	VH455	VH456	VH457	VH458	VH459	VH460
Suite	EMG	ICLG	MuRS	MuRS	GrLG	MuRS	MuRS	MuRS	MuRS
GR									
Major elements (wt%)									
SiO_2	49.78	52.84	51.9	51.4	69.8	55.91	51.17	51.39	49.94
Al_2O_3	14.61	8.7	15.18	11.4	16.12	23.16	11.12	14.27	5.5
Fe_2O_3	13.12	9.88	10.95	10.81	1.92	3.01	11.6	11.57	16.04
MgO	6.91	11.01	6.52	12.22	1.06	1.34	11.46	7.88	16.44
CaO	9.93	12.19	7.86	8	4.15	6.3	9.27	7.93	8.13
Na_2O	2.95	2.09	3.43	2.23	4.35	5.91	1.99	2.73	0.73
K_2O	0.636	1.311	1.536	1.948	0.974	1.849	1.472	1.884	1.464
TiO_2	1.241	0.581	1.508	0.961	0.385	0.611	0.747	1.446	1.317
MnO	0.177	0.145	0.135	0.135	0	-0.01	0.169	0.115	0.191
P_2O_5	0.106	0.104	0.337	0.269	0.103	0.216	0.167	0.304	0.129
LOI%									
Total	99.45	98.86	99.35	99.37	98.86	98.3	99.17	99.51	99.89
mg	52.5	70.0	55.5	70.3	53.6	48.3	67.4	58.8	68.2
Trace elements (ppm)									
La	16.5	29	25.8	16.1	17.6	26.4	18.5	15.1	9.4
Ce	36.9	79	50.8	31.4	29.7	52.1	42.9	36	22.1
Nd	21.3	52.2	25.4	14	8.3	15.3	21.1	15.8	12.9
Nb	7.5	3.9	12.3	5.2	3.9	6.3	4.1	7	5.8
Zr	88.5	77.4	122.3	46.7	99.7	439	51.8	93	96
Y	36.7	39.4	30.9	20.6	3.1	4.4	32.7	22.4	25.7
Sr	148.1	378.2	383.9	388.9	533.8	734.2	230.1	405.5	93.4
Rb	2.9	39.5	37.8	61.6	12.4	32.1	45.5	45.5	48.4
Th	3.8	1.8	3.7	3.6	-0.4	0.3	3.8	3.8	6.7
Pb	3.3	5.1	11	8	12.4	17.4	5.1	10.6	4.9
Zn	110.8	105.2	103.5	88.7	21.4	42.6	114.1	97.9	123.4
Cu	64.3	105.6	31.5	82	9.3	8.7	58.3	57.8	43
Ni	112.1	213	112.6	381.7	6.8	13.9	203.2	174.5	499.1
Cr	218.3	831.6	234	871.7	3.2	12.2	599.2	301.5	1162.5
V	289.6	200.5	252.5	233.9	33.2	51	206.5	268.3	372.2
Ba	188.4	707.5	1181.1	1056	692.6	1199.1	694.5	963.5	482.4
Sc	38.4	47.9	18.8	24.8	-0.6	-0.9	32.1	18.7	39.9
CIPW									
Q	0.00	0.00	0.00	0.00	30.94	0.00	0.00	0.00	0.00
Or	3.82	7.90	9.21	11.68	5.82	11.13	8.86	11.29	8.78
Ab	25.36	18.03	29.45	19.15	37.23	50.92	17.14	23.42	6.27
An	25.14	10.69	21.80	15.57	20.15	30.39	17.37	21.41	7.52
C	0.00	0.00	0.00	0.00	0.62	0.51	0.00	0.00	0.00
Di	19.85	40.42	12.58	18.38	0.00	0.00	22.87	13.32	26.26
Hy	13.75	16.68	18.67	20.03	2.67	1.92	22.57	21.51	37.33
Ol	5.39	1.83	0.16	9.07	0.00	1.03	6.04	1.24	6.87
Mt	4.04	3.08	4.43	3.62	0.00	0.85	3.32	4.33	4.14
Ilm	2.39	1.13	2.91	1.85	6.73	1.18	1.44	2.78	2.54
Ap	0.25	0.25	0.79	0.63	0.24	0.51	0.39	0.71	0.30

Sample	VH461	VH462	VH463	VH464	VH466A	VH466B	VH467	VH468	VH469
Suite	MuRS	Hbl-PS	Hbl-PS	ICLG	Hbl-PS	Hbl-PS	VHMD	Hbl-PS?	ICLG
GR									
Major elements (wt%)									
SiO_2	50.36	47.74	47.7	64.23	48.89	48.86	47.18	54.98	55.04
Al_2O_3	13.52	14.07	14.25	14.82	12.78	13.12	11.41	19.72	18.16
Fe_2O_3	12.86	12.83	12.94	6.67	14.41	13.87	13.63	5.88	8.38
MgO	7.78	6.06	6.23	0.88	7.48	7.97	7.95	3.2	2.79
CaO	7.69	10.29	10.51	2.35	8.88	8.16	15.69	7.37	5.3
Na_2O	2.88	3.5	3.61	3.42	3.2	3.01	2.16	5.1	5.95
K_2O	1.782	1.17	1.139	5.09	1.059	1.341	0.229	1.399	1.825
TiO_2	2.004	1.265	1.249	0.893	1.406	0.822	1.319	0.377	0.988
MnO	0.125	0.14	0.14	0.016	0.148	0.206	0.235	0.072	0.095
P_2O_5	0.36	0.231	0.222	0.471	1.156	0.837	0.092	0.725	0.447
LOI%									
Total	99.36	97.3	98	98.85	99.41	98.19	99.9	98.82	98.98
mg	55.9	49.8	50.2	21.7	52.1	54.6	55.0	53.3	41.1
Trace elements (ppm)									
La	16.7	30.2	27.2	40.3	39.5	46.9	7.9	40.7	35.5
Ce	36.4	71.5	71.5	85.8	92	101.8	23.3	90	76.6
Nd	17.4	39.4	39	44.5	53	53.5	13.6	39.4	33.1
Nb	9.6	13.2	13.1	12.2	6.7	11.6	4.7	8	7.5
Zr	43.1	68.8	73.2	375.8	101.5	70	68.5	39.4	59.4
Y	25.3	25	24.8	20.6	31	31.9	21.7	20.2	18
Sr	373.1	1354.6	1432.2	344.7	1028	994	304.1	1670.5	1193.5
Rb	37.7	23.9	23.8	83.3	26.3	33.6	1.3	21.5	25.7
Th	2.6	5.8	7.1	1.6	5.4	8.7	4.5	3.4	0.3
Pb	8.3	4.8	7.2	15	5.7	6	5.3	7	6.8
Zn	112.5	96.9	92.4	66.9	128.4	118.5	99	49.6	83.2
Cu	22.2	111.1	111.4	31.1	117.7	82.9	13.4	59.3	48.8
Ni	174.3	50.9	48.8	4	75.7	90.5	181.3	42.9	15.7
Cr	254.4	44.4	44	1.1	118.4	174.2	605.1	18	14.8
V	339.2	353.2	367.6	39.1	289.1	209.9	302.4	73.3	182.2
Ba	1170.6	639.7	633.9	2010.5	784.4	579.7	146.7	730.5	813.3
Sc	21.4	23.5	22.6	7.2	22.4	16.4	39.6	8	4.7
CIPW									
Q	0.00	0.00	0.00	18.47	0.00	0.00	0.00	0.45	0.00
Or	10.70	7.18	6.94	30.57	6.37	8.17	1.37	8.40	10.96
Ab	24.76	24.89	23.14	29.41	27.56	26.25	12.78	43.85	51.17
An	19.00	19.97	19.92	8.72	17.69	18.89	21.01	27.22	17.74
C	0.00	0.00	0.00	0.55	0.00	0.00	0.00	0.00	0.00
Di	14.06	25.89	26.60	0.00	15.97	14.13	46.74	4.16	4.96
Hy	19.21	0.00	0.00	5.93	13.80	12.62	0.00	10.72	1.88
Ol	2.40	11.68	11.78	0.00	8.89	12.87	8.12	0.00	6.66
Mt	5.16	4.16	4.11	3.53	4.29	3.47	4.14	2.77	3.67
Ilm	3.87	2.50	2.45	1.72	2.72	1.61	2.54	0.73	1.91
Ap	0.85	0.56	0.53	1.11	2.73	2.00	0.22	1.71	1.05

Sample	VH494	VH496	VH499	VH500	VH501	VH511	VH527	VH532	VH534
Suite	$GrLG_h$	GrLG	D2-GS	MoG	MoG	ICLG	WHS	WHS	WHS
GR									
Major elements (wt%)									
SiO_2	74.48	72.53	78.54	79.04	76.67	52.5	53.71	54.53	46.18
Al_2O_3	13.64	14.47	10.61	11.75	12.06	16.96	3.18	3.63	5.47
Fe_2O_3	1.17	2.38	1.07	0.68	0.82	9.41	9.13	9.2	16.48
MgO	0.43	0.67	0.26	0.17	0.67	3.53	25.33	27.44	16.04
CaO	1.71	3.56	0.41	1.65	1.49	5.18	6.57	3.52	9.35
Na_2O	2.91	4.05	1.68	3.03	1.97	4.61	0.46	0.58	0.42
K_2O	4.489	0.928	5.669	2.714	4.982	3.365	0.161	0.156	2.517
TiO_2	0.138	0.313	0.539	0.051	0.079	1.137	0.232	0.262	1.239
MnO	-0.008	0.001	-0.017	-0.028	-0.017	0.079	0.16	0.15	0.303
P_2O_5	0.006	0.059	-0.002	-0.008	-0.009	0.912	0.024	0.039	0.729
LOI%									
Total	98.97	98.97	98.76	99.05	98.71	97.68	98.96	99.5	98.73
mg	43.5	37.1	33.7	34.4	63.1	44.0	85.3	86.2	67.1
Trace elements (ppm)									
La	16.4	30.1	12.8	11.4	27.6	79.8	4.1	4.5	44.3
Ce	20.3	55.6	22.4	22.2	50	170.2	10.3	17.8	128
Nd	0	18.8	1.6	7	12.5	79.9	8.2	10.9	83.5
Nb	2.6	7.5	15	8.7	2.3	10.9	1.8	2.2	20
Zr	129.7	221.6	575.9	102.1	89.8	465.1	16.8	23.3	91.8
Y	0.9	5.5	0.1	9.4	19.1	34.6	6.2	6.3	55.7
Sr	329.8	280.1	272.9	82.7	91.3	1077.9	45.9	47.5	58.2
Rb	58.9	6.2	107.4	94	55.1	73.2	1.3	1.3	116.8
Th	2.1	2.3	1.6	18.5	5	3.3	2	1.7	9
Pb	13.6	9	23	24.1	12.7	18.7	1.7	0.6	3.2
Zn	15.1	31	12.3	14.1	5.4	121.2	82.1	82.6	179.2
Cu	6.8	4.6	5.6	9.8	15.6	45.6	9.5	9.3	21.8
Ni	2.5	6.8	7.5	4	8.7	35.2	558.4	626	336.9
Cr	-2.1	-0.4	8.6	-1.3	-6.1	70.2	3128.1	3327.5	1054.3
V	11.1	21.7	19.2	8.5	8.6	130.8	105	89.9	328
Ba	2302.6	365.1	1777.8	1279.2	679.2	1958.4	3.8	28.7	499.1
Sc	-1.1	1.4	-0.1	2.3	0.1	11.9	28	20.8	50.9
CIPW									
Q	36.42	37.37	46.33	47.63	42.45	0.00	0.00	0.00	0.00
Or	26.79	5.55	33.88	16.17	29.79	20.50	0.97	0.93	15.28
Ab	24.87	34.65	14.38	25.85	16.87	40.21	3.96	4.97	3.65
An	8.57	17.47	2.06	8.25	7.48	16.13	6.25	6.93	5.76
C	0.89	0.48	0.98	0.84	0.73	0.00	0.00	0.00	0.00
Di	0.00	0.00	0.00	0.00	0.00	3.47	21.19	8.30	29.91
Hy	1.08	1.69	0.65	0.43	1.69	1.67	63.21	74.71	13.92
Ol	0.00	0.00	0.00	0.00	0.00	9.67	1.35	0.98	23.25
Mt	0.00	0.75	0.00	0.00	0.00	3.94	2.56	2.59	4.08
Ilm	0.90	0.60	1.86	1.67	1.46	2.23	0.45	0.50	2.42
Ap	0.00	0.14	0.00	0.00	0.00	2.18	0.06	9.15	1.73

Sample	VH535	VH536	VH537	VH539	VH540	VH542
Suite	WHS	WHS	WHS	WHS	WHS	GrtGr
GR						
Major elements (wt%)						
SiO_2	54.25	54.09	53.66	55.78	53.36	68.5
Al_2O_3	15.89	16.1	15.31	17.98	17.26	10.88
Fe_2O_3	8.46	8.21	8.52	7.02	8.56	16.68
MgO	6.45	6.26	6.84	4.48	5.19	3.26
CaO	6.21	6.36	6.61	6.59	6.86	1.07
Na_2O	4.35	4.42	4.12	4.97	4.19	-0.15
K_2O	2.248	2.186	2.208	1.588	1.99	0.415
TiO_2	0.858	0.823	0.855	0.601	0.932	0.081
MnO	0.124	0.102	0.111	0.07	0.094	0.231
P_2O_5	0.35	0.335	0.331	0.415	0.441	0.005
LOI%						
Total	99.18	98.89	98.56	99.49	98.88	100.97
mg	61.5	61.5	62.7	57.2	56.0	29.1
Trace elements (ppm)						
La	35.6	35.8	34.9	41.1	47.2	4.3
Ce	77.2	81.5	77.3	102.4	111.3	10.1
Nd	37.9	37.3	37.1	54.9	55.9	5.8
Nb	10.8	11.1	11.2	7.6	14.4	1.7
Zr	171.9	182.7	218.7	150.7	111.4	296.9
Y	23.2	22.1	23.5	40.4	35.2	168.4
Sr	754.7	783.3	717.9	853.4	909.4	8
Rb	54.8	55.9	62.9	28.5	46.5	15.8
Th	3.1	4.9	4.4	2	3.1	8.6
Pb	11.7	10.2	10.4	10.1	8	5.4
Zn	102.7	96.4	101.6	87	107	31.3
Cu	45.5	16.9	59.5	47.2	24.2	9.3
Ni	136.4	125.2	141	57.9	77.2	20.9
Cr	360.7	359.7	409.9	139.5	211.3	137.7
V	147.6	145.1	150.6	104.9	157.6	65
Ba	1008.6	802.3	752.2	941.6	1250.9	63.7
Sc	14.1	15.4	16.1	13.6	15.6	54.6
CIPW						
Q	0.00	0.00	0.00	0.36	0.00	49.05
Or	13.48	13.14	13.32	9.48	11.97	2.46
Ab	37.34	38.05	35.59	42.48	36.08	0.00
An	17.44	17.94	17.11	22.29	22.81	5.33
C	0.00	0.00	0.00	0.00	0.00	8.52
Di	9.27	9.62	11.41	6.48	7.21	0.00
Hy	10.44	8.86	10.31	13.72	12.79	32.18
Ol	6.09	6.59	6.33	0.00	2.71	0.00
Mt	3.47	3.43	3.49	3.08	3.59	2.30
Ilm	1.65	1.59	1.66	1.15	1.80	0.15
Ap	0.82	0.79	0.78	0.97	1.04	0.00

Appendix 3

REE data

Sample	RI10	RI11	RI19	RI22	RI23	RI30	RI33	RI35	RI108	RI4	RI5
Suite	SLC MT	SLC MT	SLC MT	SLC MT	SLC MT	SLC MT	SLC MT	SLC MT	SLC MT	SLC MD	SLC MD
REE (ppm)											
La	8.7	12.4	25.7	18.9	16.2	14.9	9.3	11.5	2.9	6.3	12.8
Ce	19.9	29.4	58.6	43.3	39.3	39.6	23.0	19.4	8.1	17.0	34.8
Pr	2.2	3.6	7.0	5.2	4.7	5.0	2.7	1.9	0.9	2.2	4.6
Nd	9.9	15.5	28.9	21.0	19.8	22.5	12.2	8.3	4.4	12.0	22.9
Sm	2.2	3.5	6.3	4.4	4.2	5.2	2.7	1.8	1.1	3.0	5.9
Eu	1.4	1.6	2.4	2.0	1.4	1.9	1.2	0.8	0.4	1.3	2.1
Gd	2.5	4.1	6.9	4.7	4.6	5.9	3.3	2.2	1.3	3.9	7.7
Dy	2.6	4.3	6.8	4.3	4.6	6.0	3.6	2.3	1.4	4.6	8.6
Ho	0.5	0.8	1.3	0.8	0.9	1.2	0.7	0.4	0.3	0.9	1.8
Er	1.3	2.1	3.1	1.9	2.2	3.0	1.9	1.1	0.8	2.5	4.6
Yb	1.3	2.0	3.0	1.7	2.2	2.8	1.8	1.0	0.8	2.5	4.5
Lu	0.2	0.3	0.5	0.3	0.4	0.4	0.3	0.2	0.1	0.4	0.7
Chondrite normalized (Nakamura, 1974)											
La	26.4	37.7	78.1	57.4	49.2	45.3	28.3	35.0	8.8	19.1	38.9
Ce	23.0	34.0	67.7	50.0	45.5	45.8	26.5	22.5	9.4	19.7	40.2
Pr	18.3	29.5	57.0	42.6	38.5	41.2	22.4	15.8	7.3	17.7	38.0
Nd	15.7	24.6	45.9	33.3	31.4	35.7	19.4	13.2	7.0	19.0	36.3
Sm	10.6	17.2	31.1	21.8	20.5	25.5	13.3	9.0	5.2	14.8	29.1
Eu	18.2	20.8	31.2	26.0	18.6	25.2	15.5	9.7	4.5	16.2	27.4
Gd	9.0	15.0	25.0	16.9	16.6	21.4	12.1	7.9	4.7	14.2	27.9
Dy	7.6	12.4	19.8	12.5	13.3	17.5	10.4	6.6	4.2	13.3	25.1
Ho	6.4	10.6	16.8	10.3	11.4	15.0	9.0	5.4	3.5	11.8	22.7
Er	5.8	9.4	14.0	8.5	10.0	13.1	8.3	4.8	3.5	11.3	20.3
Yb	6.0	9.1	13.5	7.9	10.1	12.7	8.4	4.7	3.6	11.5	20.5
Lu	5.9	9.1	13.3	7.7	10.6	12.7	8.6	4.4	3.8	11.8	21.2
$(Ce/Yb)_N$	3.8	3.7	5.0	6.3	4.5	3.6	3.2	4.8	2.6	1.7	2.0
Eu/Eu*	1.9	1.3	1.1	1.4	1.0	1.1	1.2	1.2	0.9	1.1	1.0

Sample	RI113	SH70	RI47	RI56	RI59	RI63	VH130	VH131	VH136	VH137	VH403
Suite	SLC MD	SLC MD	TT LC	TT LC	TT LC	TT LC	LAS	LAS	LAS	LAS	LAS
La	10.9	6.0	10.1	6.4	11.1	6.8	32.7	26.2	25.9	34.3	24.0
Ce	27.7	15.4	26.5	13.0	29.4	17.2	93.5	66.1	65.2	84.2	71.7
Pr	3.4	1.9	2.9	1.3	3.0	2.0	12.2	8.3	8.2	10.3	9.8
Nd	16.3	9.4	12.4	5.1	10.3	8.8	51.1	34.9	35.0	43.5	44.0
Sm	4.1	2.2	2.6	1.0	1.5	1.9	10.7	6.9	6.8	7.6	9.6
Eu	1.5	1.0	0.6	0.4	0.5	0.5	1.8	1.9	1.9	2.2	2.0
Gd	5.4	2.9	3.0	1.1	1.7	2.5	9.9	6.5	6.2	6.7	9.1
Dy	6.5	3.0	3.5	1.3	2.0	3.0	8.8	5.3	5.0	4.8	8.1
Ho	1.4	0.6	0.7	0.3	0.4	0.6	1.7	1.0	0.9	0.9	1.6
Er	3.7	1.5	2.0	0.8	1.2	1.8	4.0	2.4	2.2	2.0	3.7
Yb	3.8	1.4	2.1	0.8	1.1	1.8	3.7	2.2	2.1	1.7	3.5
Lu	0.6	0.2	0.3	0.1	0.2	0.3	0.6	0.4	0.3	0.3	0.6
Chondrite Normalized											
La	33.1	18.2	30.7	19.5	33.7	20.7	99.4	79.6	78.7	104.3	72.9
Ce	32.0	17.8	30.6	15.0	34.0	19.9	108.1	76.4	75.3	97.4	82.9
Pr	28.2	15.6	24.0	10.2	24.5	16.1	99.8	68.3	67.3	84.0	80.7
Nd	25.9	14.9	19.7	8.1	16.3	14.0	81.1	55.4	55.6	69.0	69.8
Sm	20.0	10.8	12.6	4.8	7.2	9.4	52.5	33.9	33.6	37.3	47.0
Eu	19.5	12.9	7.4	5.5	6.9	5.8	23.5	24.0	24.4	29.1	25.6
Gd	19.6	10.3	10.8	4.0	6.2	8.9	35.9	23.4	22.5	24.2	33.0
Dy	18.9	8.7	10.3	3.9	5.7	8.6	25.7	15.4	14.5	13.9	23.6
Ho	17.6	7.3	9.2	3.3	5.3	7.8	21.7	12.8	11.9	11.3	20.0
Er	16.4	6.8	8.9	3.4	5.1	7.8	17.9	10.7	9.7	9.0	16.4
Yb	17.1	6.2	9.3	3.6	5.0	8.0	17.0	9.9	9.4	7.6	15.9
Lu	17.7	6.2	9.7	3.5	5.6	8.0	16.8	10.3	9.1	7.4	16.2
$(Ce/Yb)_N$	1.9	2.9	3.3	4.2	6.9	2.5	6.4	7.7	8.0	12.8	5.2
Eu/Eu*	1.0	1.2	0.6	1.2	1.0	0.6	0.5	0.9	0.9	1.0	0.6

Sample	VH404	VH405	VH406	VH407	VH14	VH18	VH20	VH33	VH35	VH179	VH262
Suite	LAS	LAS	LAS	LAS	def MD	MoG	post-D2 MD	syn-D2 MD	GrLG	D2-GS	EMG
La	22.0	31.5	39.9	73.3	43.6	24.7	55.7	7.4	23.4	49.8	33.8
Ce	58.5	77.1	95.5	157.0	127.3	59.7	138.5	20.9	40.4	106.0	74.4
Pr	7.8	9.9	12.1	17.4	17.7	7.1	17.0	2.9	3.9	12.3	8.1
Nd	36.2	39.5	48.9	66.0	79.7	28.4	66.5	15.6	11.8	46.9	30.2
Sm	7.9	6.9	8.8	13.1	17.0	6.1	12.0	4.6	1.5	8.3	5.4
Eu	2.0	2.1	2.3	2.6	4.4	1.4	2.7	1.8	1.3	2.5	1.1
Gd	7.6	6.1	7.9	13.7	15.3	6.4	10.1	5.7	1.1	7.0	4.6
Dy	6.2	4.3	5.8	12.1	9.6	6.1	7.4	5.3	0.8	5.0	3.4
Ho	1.2	0.8	1.1	2.3	1.7	1.2	1.4	1.0	0.1	0.9	0.6
Er	2.8	1.7	2.4	5.0	3.5	3.0	3.0	2.3	0.4	2.0	1.5
Yb	2.5	1.5	2.0	3.8	2.9	2.7	2.5	2.0	0.4	1.7	1.5
Lu	0.4	0.2	0.3	0.6	0.5	0.4	0.4	0.3	0.1	0.2	0.2
Chondrite Normalized											
La	66.9	95.7	121.3	222.8	132.5	75.1	169.3	22.5	71.1	151.4	102.7
Ce	67.7	89.1	110.3	181.5	147.2	69.0	160.1	24.1	46.8	122.5	86.0
Pr	64.2	81.5	99.0	142.5	144.7	58.4	139.4	24.0	31.8	101.1	66.6
Nd	57.5	62.7	77.6	104.8	126.5	45.1	105.6	24.8	18.7	74.4	47.9
Sm	38.7	34.1	43.2	64.4	83.5	29.8	59.3	22.9	7.5	41.0	26.7
Eu	25.7	27.8	30.4	33.4	56.8	17.7	34.8	23.4	17.1	32.5	14.5
Gd	27.5	22.2	28.7	49.6	55.4	23.0	36.5	20.6	3.9	25.4	16.6
Dy	18.2	12.4	16.8	35.3	27.9	17.8	21.7	15.3	2.2	14.7	9.9
Ho	15.0	10.0	13.7	29.4	21.7	15.3	17.4	12.3	1.8	11.5	7.9
Er	12.4	7.7	10.7	22.2	15.7	13.1	13.3	10.4	1.8	8.8	6.5
Yb	11.5	6.6	9.3	17.3	13.3	12.0	11.1	9.1	1.9	7.5	6.7
Lu	11.5	6.2	8.8	16.2	14.2	11.8	10.3	8.8	2.1	7.1	6.8
$(Ce/Yb)_N$	5.9	13.4	11.9	10.5	11.1	5.7	14.4	2.7	25.1	16.2	12.9
Eu/Eu*	0.8	1.0	0.9	0.6	0.8	0.7	0.7	1.1	3.2	1.0	0.7

Sample	VH299	SH65141
Suite	D2-GS	Tay EMG
La	19.9	40.0
Ce	29.0	95.2
Pr	2.5	11.6
Nd	7.2	46.6
Sm	0.7	9.0
Eu	1.8	1.9
Gd	0.4	8.2
Dy	0.3	6.8
Ho	0.0	1.3
Er	0.1	3.1
Yb	0.2	2.9
Lu	0.0	0.5
Chondrite Normalized		
La	60.5	121.6
Ce	33.6	110.0
Pr	20.6	95.3
Nd	11.4	74.0
Sm	3.5	44.4
Eu	22.9	24.5
Gd	1.5	29.9
Dy	0.7	19.9
Ho	0.4	16.4
Er	0.5	13.7
Yb	0.8	13.2
Lu	0.9	13.3
$(Ce/Yb)_N$	41.0	8.3
Eu/Eu*	10.0	0.7

Abbreviations

Petrological parameters and model reservoirs

REE	Rare earth elements	**BABI**	Basaltic Achondrite Best Estimate
LREE	Light rare earth elements	**BSE**	Bulk Silicate Earth
MREE	Middle rare earth elements	**CHUR**	Chondrite Uniform Reservoir
HREE	Heavy rare earth elements	**DM**	Depleted mantle
LILE	Large ion lithophile elements	**PM**	Primitive mantle
LFSE	Low field strength elements	**MORB**	Mid-ocean ridge basalt
HFSE	High field strength elements	**N-MORB**	Normal-MORB
CE	Compatible trace elements	**E-MORB**	Enriched-MORB
IE	Incompatible trace elements	**MSWD**	Mean square weighted deviations
FC	Fractional crystallization	**HSZ**	High-strain zone
AFC	Assimilation-fractional crystallization	**TEDD**	Trace-element discrimination diagram
CAB	Continental arc basalts	**LOI**	Loss on ignition
CFB	Continental flood basalts	**SHMB**	Siliceous high-Mg basalt

Phases

Ab	Albite	**Kspar**	K-feldspar
Alm	Almandine	**Mag**	Magnetite
An	Anorthite	**Ol**	Olivine
And	Andradite	**Opx**	Orthopyroxene
Biot	Biotite	**Or**	Orthoclase
Cpx	Clinopyroxene	**Pig**	Pigeonite
Fs	Ferrosilite	**Plag**	Plagioclase
Grs	Grossular	**Pyp**	Pyrope
Grt	Garnet	**Qtz**	Quartz
Hbl	Hornblende	**Sps**	Spessarine
Ilm	Ilmenite	**Wo**	Wollastonite

Commonly used symbols

D	Bulk distribution coefficient (ΣK_d)
ε	Initial isotopic ratio relative to reservoir model
i, or I_x	Initial isotopic ratio
K_d	Mineral-melt distribution coefficient
λ	Decay constant (year^{-1})
m	Measured isotopic ratio
mg	Molecular Mg-number (Mg^{2+} / Mg^{2+} + Fe^{2+}) where Fe^{2+} / Fe^{3+} =0.15
P	Pressure
T	Temperature
t	Time (years)
X	Composition

CIPW norms

Ab	Albite
An	Anorthite
Ap	Apatite
C	Corundum
Di	Diopside
En	Enstatite
Hy	Hypersthene
Ilm	Ilmenite
Mt	Magnetite
Ol	Olivine
Or	Orthoclase
Q	Quartz

Late Archaean - Early Proterozoic Geology of the Vestfold Hills

Pre-D1(ca. 2500 Ma) Gneiss Suites

Early Mafic Gneiss
medium-grained opx-cpx-plag orthogneiss
x cogenetic xenoliths in the Taynaya Suite

Chelnok Paragneiss
dominantly garnetiferous psammitic pelites
c calc-silicate layers and boudins
s skarn horizon

Taynaya Paragneiss
high-magnesium sapphirine granulites

Mossel Gneiss
early layered felsic orthogneiss, mostly tonalites

Pre-D2 (ca. 2480) Crooked Lake Gneiss Suites

Composite Felsic Orthogneiss
early felsic orthogneiss (Mossel Gneiss) intruded by and interlayered with later intermediate to felsic orthogneiss

Ultramafic to Melagabbroic CLG Suites
coarse-grained cpx-opx-hbl-plag cumulates
o spotted cumulates

Gabbroic to Monzodioritic CLG Suites
coarse-grained plag-hbl-cpx-opx orthogneiss

Intermediate CLG Suites
coarse-grained equigranular intermediate orthogneiss mostly qtz- and hbl-bearing monzonites, monzodiorites and diorites

Felsic CLG Suites (gradational with above)
medium- to coarse-grained equigranular felsic orthogneiss mostly quartz monzonites, quartz diorites and tonalites

Feldspar-Phyric Intermediate to Felsic CLG Suite
medium- to coarse-grained porphyritic intermediate orthogneiss, mostly mesoperthite-phyric monzonite to monzodiorite, locally with abundant qtz

Feldspar-Phyric Dioritic CLG Suite
medium-grained diorite commonly with felsdspar phenocrysts

Homogeneous Granodioritic CLG Suite
coarse-grained homogeneous granodioritic orthogneiss

Grace Lake Granodioritic CLG Suite
coarse-grained heterogeneous granodioritic orthogneiss, contains abundant mafic schlieren and leucocratic remobilisate

Late Syn-Deformational (D2) CLG Granites
coarse-grained (pink and white) granite pods and sheets

Intermediate CLG dykes
medium-grained diorite and quartz diorite dykes that are pre-, syn- and post-deformational (D2)
pd post-D2 (2477 Ma) quartz-diorite dyke

Δ Xenolithic assimilation zone
LAS Lake Alice Suite
RLS Rookery Lake Suite
HPS Hbl-phyric suites

Post-Deformational (D2) Norite Dyke Complex

Homogeneous Norite
coarse-grained, dark brown, opx-plag gabbro

Spotted 'Snowflake' Norite
coarse-grained, dark brown, opx-plag gabbro with plag-rich intergranular 'snowflake' texture

Xenolithic 'Rubble Zone' Norite
xenolithic zone with abundant ultramafic and sapphirine-bearing xenoliths

Recent Glacial Cover

Rybnaya Bay
Taynaya Bay
Tryne Fjord
Long Fjord
Broad Peninsula
HPS
LAS
pd

N

Scale(km) 0 1 2 3 4

Key to Symbols

- S_i: graded layering in cumulates, upward facing and overturned respectively
- $S_{0/1/2}$: compositional and gneissic layering, and composite foliation in Chelnok Paragneiss
- $S_{1/2}$: gneissic layering and composite foliation in Early Mafic and Mossel Gneisses
- S_2: gneissic layering and simple foliation in Crooked Lake Gneiss
- F_1: fold axes of intrafolial F_1 folds
- F_2: fold axes of major and parasitic F_2 folds
- F_{3m}: fold axes of minor F_3 open folds
- F_{3r}: fold axes of regional F_3 open warp
- L_2: mineral elongation or mineral aggregate lineation associated with F_2 folds
- Z: parasitic F_2 fold with dextral asymmetry
- S: parasitic F_2 fold with sinistral asymmetry
- Proterozoic mylonitic shear-zones that significantly offset gneissic lithologies

Archaean - Early Proterozoic Geological Evolution of the Vestfold Hills

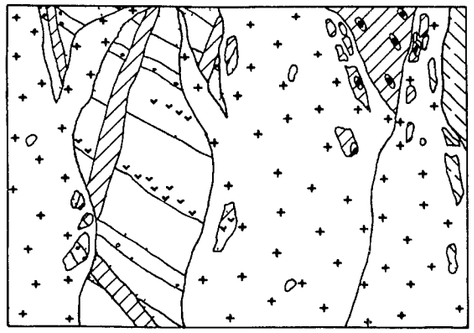

2526 - ~ 2501 Ma Intrusion of Mossel Gneiss protolith

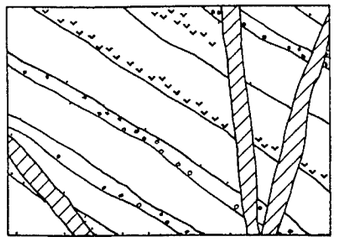

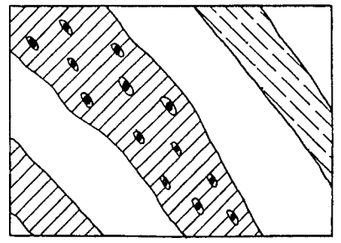

ca 2800? - 2526 Ma Metasedimentary, metavolcanic? and intrusive protoliths High-grade metamorphism?

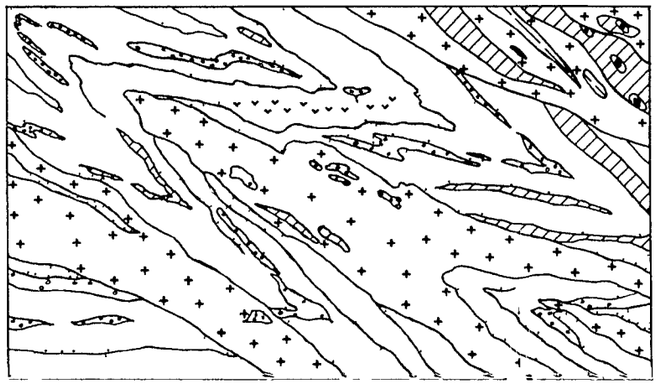

2496 Ma D1-M1 high-grade metamorphism and deformation

Pre D1 (2496 Ma) Gneiss Suites

- Early Mafic Gneiss (EMG)
- Chelnok Paragneiss
- Taynaya Paragneiss
- Mossel Gneiss

Pre-D2 (2475 Ma) Crooked Lake Gneiss

- Ultramafic to melagabbroic suites
- Gabbroic to monzodioritic suites
- Intermediate suites
- Feldspar-phyric suites
- Homogeneous granodiorite suite
- Syn-deformational (D2) granite suites
- Pre- syn and post-deformational (D2) intermediate dykes

2496 - 2475 Ma Crooked Lake magmatic episode Compositionally diverse magmas intruded into heterogeneous gneissic host

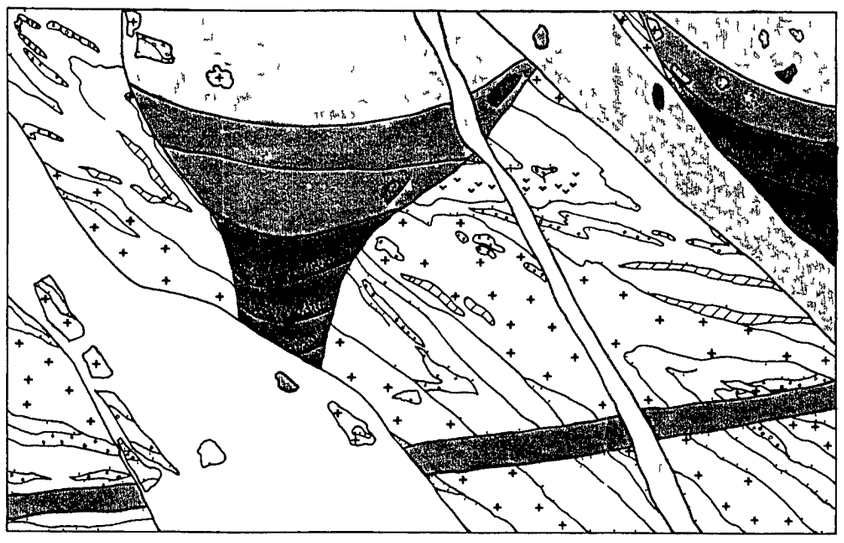

2475 Ma D2-M2 high-grade metamorphism and deformation Intense deformation that refolded earlier structures into <km-scale folds These D2 folds were then deformed by open warping

Late Archaean - Early Proterozoic High-Grade Structural Relations in the Vestfold Hills, East Antarctica

Lithology

Pre D_1 (*ca* 2500 Ma) Gneiss Suites

Chelnok Paragneiss ($S_{0/1/2}$)
Dominantly garnetiferous psammitic pelites

Early Layered Mafic and Minor Paragneiss ($S_{1/2}$)
Mossel Gneiss including Early Mafic Gneiss

Pre D_2 (*ca* 2480 Ma) Gneiss Suites

Crooked Lake Gneiss (S_2)
Includes all CLG suites and deformed mafic dykes

Post D_2/D_3 (*ca* 2480 Ma) Igneous Intrusions

2477 Ma Quartz Diorite Dyke
Important intermediate dyke that cuts F_2 folds and F_3 regional warping

Norite Complex
Extensive *ca* 2240 Ma Norite complex

Glacial Cover

Structure

Lithological Boundary

Schematic outline of F_2 folds

Schematic trend of S_2 showing reorientation by F_3

Major Proterozoic mylonites that significantly offset gneissic lithologies

Equal area stereonets are contoured for poles to planes of simple or composite foliations For the Chelnok Paragneiss (CP) $S_{0/1/2}$ Early Mafic Gneiss (EMG) $S_{1/2}$ Mossel Gneiss (MoG) $S_{1/2}$ Crooked Lake Gneiss (CLG) S_2 Symbols as lithological key above EMG are depicted by small squares

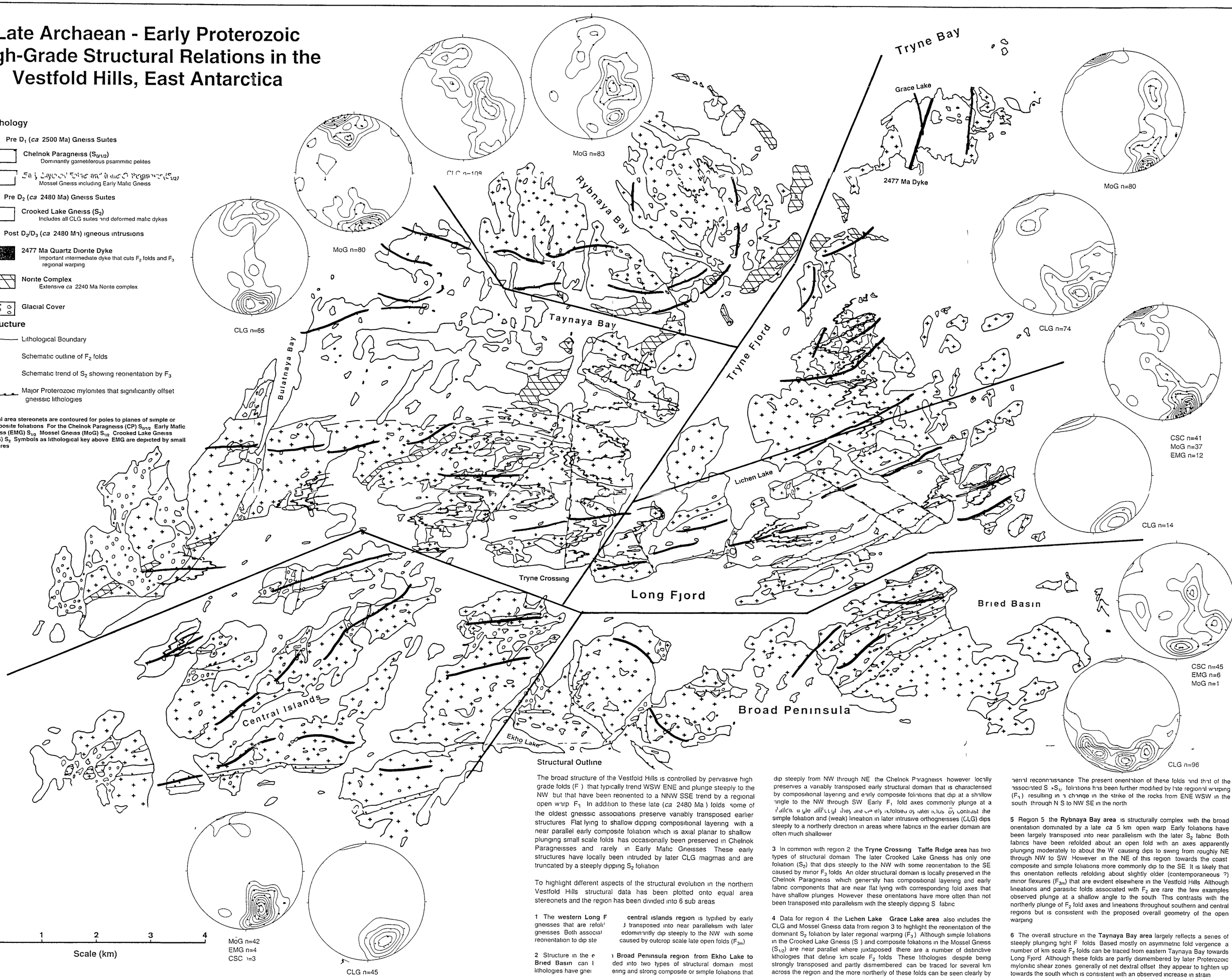

Structural Outline

The broad structure of the Vestfold Hills is controlled by pervasive high grade folds (F_1) that typically trend WSW ENE and plunge steeply to the NW but that have been reoriented to a NNW SSE trend by a regional open warp F_3 In addition to these late (*ca* 2480 Ma) folds some of the oldest gneissic associations preserve variably transposed earlier structures Flat lying to shallow dipping compositional layering with a near parallel early composite foliation which is axial planar to shallow plunging small scale folds has occasionally been preserved in Chelnok Paragneisses and rarely in Early Mafic Gneisses These early structures have locally been intruded by later CLG magmas and are truncated by a steeply dipping S_2 foliation

To highlight different aspects of the structural evolution in the northern Vestfold Hills structural data has been plotted onto equal area stereonets and the region has been divided into 6 sub areas

1 The **western Long F** gneisses that are refold gneisses Both associat reorientation to dip ste

central islands region is typified by early J transposed into near parallelism with later edominantly dip steeply to the NW with some caused by outcrop scale late open folds (F_{3m})

2 Structure in the e **Bried Basin** can l lithologies have gnei

Broad Peninsula region from Ekho Lake to ded into two types of structural domain most ering and strong composite or simple foliations that dip steeply from NW through NE the Chelnok Paragneiss however locally preserves a variably transposed early structural domain that is characterised by compositional layering and early composite foliations that dip at a shallow angle to the NW through SW Early F_1 fold axes commonly plunge at a shallow angle although they are clearly refolded by later folds By contrast the simple foliation and (weak) lineation in later intrusive orthogneisses (CLG) dips steeply to a northerly direction in areas where fabrics in the earlier domain are often much shallower

3 In common with region 2 the **Tryne Crossing Taffe Ridge area** has two types of structural domain The later Crooked Lake Gneiss has only one foliation (S_2) that dips steeply to the NW with some reorientation to the SE caused by minor F_3 folds An older structural domain is locally preserved in the Chelnok Paragneiss which generally has compositional layering and early fabric components that are near flat lying with corresponding fold axes that have shallow plunges However these orientations have more often than not been transposed into parallelism with the steeply dipping S fabric

4 Data for region 4 the **Lichen Lake Grace Lake area** also includes the CLG and Mossel Gneiss data from region 3 to highlight the reorientation of the dominant S_2 foliation by later regional warping (F_3) Although simple foliations in the Crooked Lake Gneiss (S_2) and composite foliations in the Mossel Gneiss ($S_{1/2}$) are near parallel where juxtaposed there are a number of distinctive lithologies that define km scale F_2 folds These lithologies despite being strongly transposed and partly dismembered can be traced for several km across the region and the more northerly of these folds can be seen clearly by aerial reconnaissance The present orientation of these folds and that of the associated $S_2/S_{1/2}$ foliations has been further modified by late regional warping (F_3) resulting in a change in the strike of the rocks from ENE WSW in the south through N S to NW SE in the north

5 Region 5 the **Rybnaya Bay area** is structurally complex with the broad orientation dominated by a late *ca* 5 km open warp Early foliations have been largely transposed into near parallelism with the later S_2 fabric Both fabrics have been refolded about an open fold with an axes apparently plunging moderately to about the W causing dips to swing from roughly NE through NW to SW However in the NE of this region towards the coast composite and simple foliations more commonly dip to the SE It is likely that this orientation reflects refolding about slightly older (contemporaneous ?) minor flexures (F_{3m}) that are evident elsewhere in the Vestfold Hills Although lineations and parasitic folds associated with F_2 are rare the few examples observed plunge at a shallow angle to the south This contrasts with the northerly plunge of F_2 fold axes and lineations throughout southern and central regions but is consistent with the proposed overall geometry of the open warping

6 The overall structure in the **Taynaya Bay area** largely reflects a series of steeply plunging tight F folds Based mostly on asymmetric fold vergence a number of km scale F_2 folds can be traced from eastern Taynaya Bay towards Long Fjord Although these folds are partly dismembered by later Proterozoic mylonitic shear zones generally of net dextral offset they appear to tighten up towards the south which is consistent with an observed increase in strain